Polymerization Catalysis of Rare-Earth Metal Alkylaluminates and Dialkyls – A Systematic Study

Dissertation

der Mathematisch-Naturwissenschaftlichen Fakultät
der Eberhard Karls Universität Tübingen
zur Erlangung des akademischen Grades eines
Doktors der Naturwissenschaften
(Dr. rer. nat)

vorgelegt von
Dipl.-Chem. Christoph Otto Hollfelder
aus Forchheim (Ofr.)

Tübingen 2019

Tag der mündlichen Qualifikation	29.07.2019
Dekan:	Prof. Dr. Wolfgang Rosenstiel
1. Berichterstatter	Prof. Dr. Reiner Anwander
2. Berichterstatter	Prof. Dr. Hermann A. Mayer

Für meine Familie

Once, I had a dream,

And this is it!

[...]

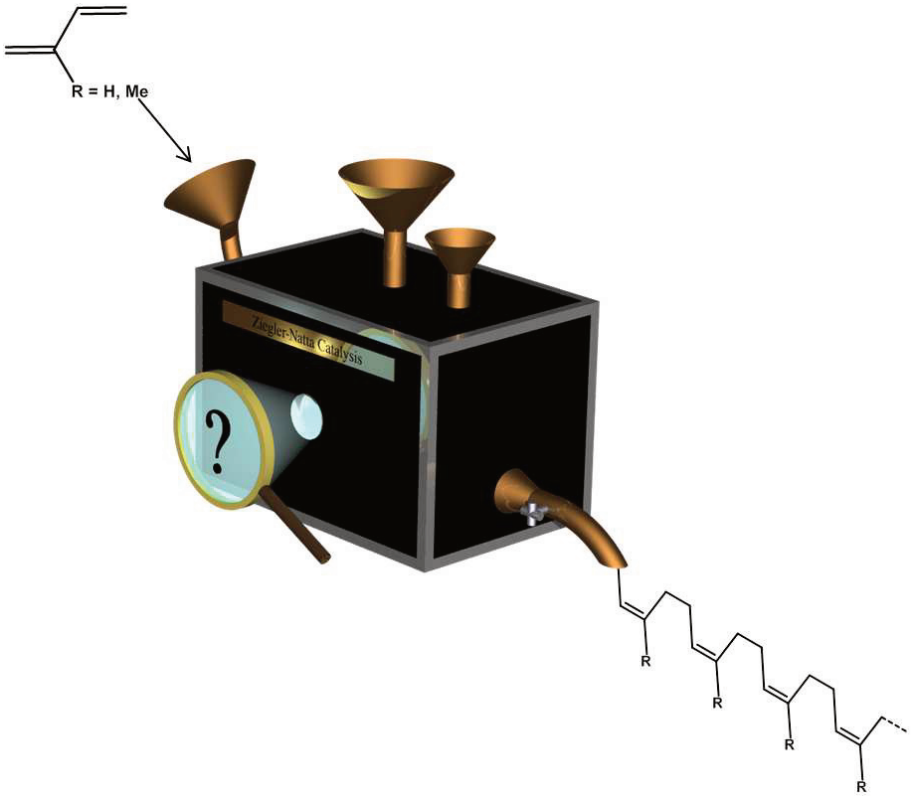

Open the chest once more

Dark chest of wonders

Seen through the eyes

Of the one with pure heart

Once so long ago

Tuomas Holopainen, *Nightwish*

Science is the poetry of reality

Richard Dawson

Preface

The work has been carried out during the period November 2010 to April 2019 under the supervision of Prof. Dr. Reiner Anwander and co-supervision of Prof. Dr. Doris Kunz at the University of Tübingen, Germany. Funding has been gratefully provided by the Deutsche Forschungsgemeinschaft (DFG).

The thesis begins with a review on catalytically active rare-earth-metal species in Ziegler-Natta catalysis and crystallographic evidence regarding their structure and composition. Effects of the coordination environment of the catalytic centers are highlighted. Following this introduction, a summary of the main results, concluding remarks, four manuscripts containing unpublished results and five papers are provided.

Parts of this thesis have been presented on an international conference.

Acknowledgement, Danksagung

In fast acht Jahren der Promotion haben mich auf meinem Weg in die Wissenschaft zahlreiche Menschen begleitet. Ich durfte von vielen großen Geistern lernen und das Feuer der Begeisterung für mein Fach an Jüngere weitergeben. Zudem habe ich viele Menschen erleben dürfen, die mir über die Jahre gute Kollegen waren und zum Teil auch enge Freunde geworden sind. Darüber hinaus waren meine Freunde aus dem Leben vor der Promotion und meine Familie stets für mich da und bereit, Freude und Leid mit mir zu teilen. Ich freue mich, dass mir die Tradition nun die Möglichkeit gibt, einige dieser Personen namentlich zu erwähnen und ihre Beiträge zu würdigen.

Zu allererst ist natürlich Prof. Dr. Reiner Anwander zu nennen, mein Doktorvater, der mich 2010 in seinen Arbeitskreis aufgenommen hat. Obwohl er mich kaum kannte, hat er mir mit einem immensen Vertrauensvorschuss die Möglichkeit gegeben, meinen Weg zu gehen und eigene Erfahrungen zu sammeln. Die Freiheit, die ich durch ihn erleben durfte, lehrte mich nicht nur wissenschaftliches Arbeiten, sondern auch ein großes Maß an Selbstdisziplin. Seine hohen Anforderungen im Bereich der Anorganik, aus Sicht eines Bayreuther Diplomanden, wirkten ausgesprochen motivierend und ließen mich in diesem Bereich über mich hinauswachsen. Damit trieb er mich zu einer Akribie im Bereich der Aufklärung der Polymerisationsmechanismen, die ich mir zu Beginn meiner Doktorarbeit selbst kaum vorstellen konnte. Sein Vertrauen und seine Geduld, auch in schwierigen Phasen der letzen Jahre, erfüllen mich mit Stolz. Mein Dank dafür, dass ich in all dieser Zeit unter seiner Führung so wachsen und reifen durfte wird ihm allzeit gewiss sein.

Neben den Mitgliedern meines Prüfungskomitees Prof. Dr. Hermann A. Mayer, Prof. Dr. Thomas Grösser und Prof. Dr. Doris Kunz gilt mein Dank unter den Tübinger Hochschullehrern selbstverständlich Dr. Peter Sirsch. Er und Prof. Dr. Hermann A. Mayer haben mir im Bereich der Lehre viel Vertrauen entgegengebracht und mir die Möglichkeit gegeben, mich als Betreuer im Grundpraktikum und bei Vertretungsvorlesungsstunden einzubringen und als Prüfungsbeisitzer Erfahrungen zu sammeln. Dr. Cäcilia Maichle-Mößmer begleitete diese Arbeit nicht nur als Kristallographin. Ihrem Management und ihrem stets offenem Ohr ist es zu verdanken, dass im Arbeitskreis so vieles rund läuft. Dr. Yucang Liang verdanke ich neben Fachlichem auch viele Einblicke und lehrreiche Gespräche.

Über die Jahre der Promotion durfte ich viele andere Kollegen besonders schätzen lernen. Menschen, die mich zu dem gemacht haben, der ich heute bin, für meine Sorgen und Nöte immer offene Ohren hatten und die mir ans Herz gewachsen sind.
Chronologisch möchte ich dabei mit Nicole Dettenrieder und Thomas Deschner beginnen, die mir in der Gruppe von Anfang an eine Heimat gegeben haben. Vor allem fachlich war in dieser Zeit Christoph Schädle wichtig, der mir in vielen Aspekten meiner Arbeit vorangegangen ist. Hans-Martin Dietrich bin ich vor allem dafür dankbar, dass er mir Einblick in seine Perspektive gegeben hat, die Natur und Wissenschaft auf eine hochinteressante Weise neu verbindet, und in der immer irgendwo ein Hirsch röhrt. Den größten Anteil an meiner Arbeit fällt im Kollegenkreis Lars Jende zu. Seine Unterstützung und Beiträge in so zahlreichen Diskus-

sionen waren mir über die Jahre ein enorm wichtiger Anker. Von keinem anderen Kollegen habe ich so viel gelernt. Hervorheben möchte ich auch Sonja König, der ich einige extrem spannende Gespräche verdanke und Tatiana Spallek, die mit ihrer Herzlichkeit so viel gutes Klima geschaffen hat. Andrea Sonström kann Arbeitstage in Abenteuer verwandeln und Jochen Friedrich bringt auf seine tiefsinnige Art so vieles einfach auf den Punkt. Alan Crozier und Lena Stoll durfte ich, genauso wie Irene Gust, Isabell Walker und Sophie Wernitz nach Aventurien entführen, wo es phantastische Abenteuer zu bestehen galt. Daniel Werner hervorzuheben fällt mir nicht schwer, denn auch er hat über die Jahre "Haare auf den Füßen" bekommen. Er war einfach immer (für uns Kollegen) da und war für jeden Spaß zu haben. Ein fabelhafter Kollege voller verrückter Ideen.
Doch auch die anderen Kollegen im Arbeitskreis möchte ich nicht vergessen. Olaf Michel, Dorothea Schädle, Damir Barisic, Renita Thim, Martin Bonath, David Schneider, Lorenz Bock, Christoph Stuhl, Benjamin Wolf, Dominic Diether, Verena Birkelbach, Uwe Bayer, Dennis Buschmann, Simon Trzmiel, Georgios Spiridopoulos, Alexandros Mortis, Markus Katzenmeyer, Theresa Rieser, Jakob Lebon, Lars Kuckuk, Eric Moinet und Felix Kracht. Ein besonderer Dank gilt Leilei Luo, Ning Yuan und Shima Hamidi, die ihre einzigartige Perspektive bereitwillig mit mir geteilt haben und die ich regelmäßig mit Fragen löchern durfte, sowie allen Gastdoktoranden und -professoren während meiner Zeit in der Arbeitsgruppe.
Es war mir außerdem eine große Freude, die Leidenschaft für mein Fach an meine Praktikanten Lena Stoll, Mareike Binder, Rita Stauder, Marcel Leonhard und Theresa Zelger weiter zu geben. Für Rita und Theresa

gipfelte das in einer Publikation (Paper IV) und einem außerplanmäßigen Spezialeinsatz, weit jenseits meiner künstlerischen Grenzen. Ebenfalls Teil dieser Publikation ist Dominic Diether, dessen Diplomarbeit ich mitbetreuen durfte und der die Polymere im AK Anwander weiter beackern wird.
Besonders wichtig ist mir, denen für ihre Arbeit zu danken, ohne die nichts laufen würde, allen voran Elke Niquet. Ohne ihren unermüdlichen Einsatz wäre das Meiste nicht möglich gewesen. Ebenso großen Anteil an dieser Arbeit haben Daniela Kauling und Felix Thol, die in unzähligen Stunden die Analytik gestemmt haben. Karlheinz Ableitner und Tobias Wolf sorgten allzeit für die nötige Sicherheit und standen in technischen Fragen stets mit Rat und Tat zur Seite. Ein besonderes Dankeschön verdienen auch die Meister der Metallwerkstatt und insbesondere Eberhard Braun. Sie haben bei unzähligen Problemen beim Reaktorenbau mit angepackt, Hilfe und Rat angeboten und hatten einfach immer den passenden Klemmring oder O-Ring in einer ihrer Schubladen. Walter Schaal war stets zur Stelle, wenn es um technische und elektronische Fragestellungen ging und hat eine Motordatenerfassungssoftware für den ersten Parr-Reaktor beigesteuert. Wolfgang Bock danke ich für die stets zuverlässigen Elementaranalysen. Viele Arbeitsstunden, Problemlösungen und nicht zuletzt die stets einwandfrei funktionierenden NMR-Spektrometer verdanke ich, wie wir alle, Dr. Klaus Eichele und Kristina Strohmaier. Besonders mit den DOSY Messungen durfte ich Aufregendes von ihnen lernen. Paul Schuler und Dr. Dorothée Wistuba haben mich ebenfalls mit Analytik unterstützt. Auch Tanja Kunz ist hier für ihre stets problemfreien DLS Messungen zu nennen.

Wenn ich nun das Fachliche verlasse fällt mir neben den Sekretärinnen Sabine Ehrlich und Irene Gust vor allem Nadja Wettering ein. Sie hat nicht nur mit einem Stückchen Software zu meiner Doktorarbeit beigetragen und mich vor Alpträumen von Datenverlusten gerettet. Sie ist mir über die Jahre auch zu einer guten Freundin geworden und ich freue mich auf noch viele schöne Erlebnisse mir ihr, auch auf dem Wacken Open Air. Für Kameradschaft, Zuverlässigkeit und steten Einsatzwillen danke ich außerdem den Kollegen von der schnellen Eingreiftruppe der chemischen Institute, allen voran deren Leitung, Prof. Dr. Ulrich Nagel, Dr. Markus Kramer und Walter Schaal. Dennis Buschmann, Uwe Bayer, Alexandros Mortis und Lorenz Bock waren und sind herausfordernde Gegner beim Fantasy Football, so wie es Lars Jende und Damir Barisic bei diversen Fußball-Tippspielen waren. Doch auch Mitglieder anderer Arbeitskreise durfte ich privat kennenlernen und nenne sie schon lange meine Freunde. Filiz Kocak, Janina Hirdler, Katrin Gittinger und Tomasz Misztal möchte ich dabei besonders hervorheben und auch die “wohlgelehrten Damen” Sophie Wernitz und Isabell Walker nicht vergessen.

Nun aber ist es Zeit, all jene zu erwähnen, die in mir die Begeisterung für Chemie entfacht und genährt haben. Immer mehr wissen zu wollen, dazu hat mich Dr. Heribert Peter (R.I.P.) stets ermutigt. So hat er mir geistige Grenzen genommen und mir gezeigt, was Bildung bedeutet, und was dadurch alles möglich ist. Meine Grundschullehrerin Angela Gebel hat bereits dem kleinem Christoph in der ersten Klasse prophezeiht, dass er einst promovieren würde und ihn entsprechend mit einer promotionstaug-

lichen Handschrift versorgt. Allen voran aber danke ich Josef Maier, der mir mit seiner Begeisterung für unser Fach und durch seine Menschlichkeit stets ein großes Vorbild war. Unter den Professoren meines Studiums gilt es sicherlich Ola F. Wendt, Aleksander Ostoja-Starszewski und Axel H. E. Müller besonders zu erwähnen, denn sie haben die faszinierendsten, nachhaltigsten und motivierendsten Eindrücke hinterlassen. Ferner möchte ich den Arbeitskreisen Wendt und Maurer in Lund und Schmidt in Bayreuth danken, deren Mitglied ich zeitweise sein durfte, sowie den Arbeitsgruppen bei Siemens Medical Solutions und bei BASF, in denen ich meine Praktika absolvierte. Volker Keppner, Dr. Steffen Seidel, Norbert Gmähle, Tanja Hahn und Hans-Jürgen Conrad sind Namen, die dabei unbedingt fallen müssen.

Aus dem Kreis meiner Freunde, den Wackingern und den Rollenspielern, die stets für mich da und zur Stelle sind, rekrutieren sich auch die Korrekturleser dieser Arbeit: Ralf Stehle, dem ich zusammen mit Stefanie Wunder noch so viel mehr an Meinungen, Rat und Einsatz verdanke, dazu Miriam Reuleaux, Hanno Röttenbacher, Kilian Hollfelder, Philipp Siebenbürger und Johannes Grad.

Meine Familie, Großeltern, Eltern und Geschwister und meine Schwiegerfamilie haben über all die Jahre fest an mich geglaubt und standen mit all ihrer Kraft hinter mir. Ohne sie wäre all das hier undenkbar gewesen. Vielen lieben Dank dafür.

Die letzte Erwähnung in dieser Aufzählung aber gebührt der Frau, die mich seit nunmehr zwölf Jahren in allen Lebenslagen begleitet und erträgt, stützt und anspornt, Hoffnung und Perspektiven schafft und mich bedingungslos liebt, meiner Miriam.

All diese Menschen bilden das Fundament, das diese Arbeit möglich gemacht hat. Jeder hat seinen Anteil und ohne jeden von ihnen hätte ein entscheidendes Stück gefehlt.

Ich danke Euch!

Contents

Preface v
Acknowledgement, Danksagung vi
Contents xiii
Abbreviations xvii
List of Publications xxiii
Personal Contribution to Collaborative Publications xxvii
Summary xxxi
Zusammenfassung xxxiii
Objective of the Thesis xxxv

1 Polymerization Catalysis of Rare-Earth Metal Alkylaluminates and Dialkyls 1

1.1 Introduction 3
1.2 Cationic Lanthanide Species Countered by Tetrakis-(Pentafluorophenyl)-Borato and Tris-(Pentafluorophenyl)-mono-Alkyl-Borato 5

2 Summary of the Main Results 103

2.1 1,3-Diene Polymerization Behavior of Catalysts Derived from Homoleptic Rare-Earth Metal Tetramethylaluminates 105

2.2 Half-Sandwich Rare-Earth Metal Alkylaluminates as Precatalysts in 1,3-Diene Polymerization 114
2.3 Half-Sandwich Rare-Earth-Metal Allyls Bearing a Donor Sidearm as Precatalysts in 1,3-Diene Polymerization 129
2.4 Half-Sandwich Ln^{III} Dimethyls as Precatalysts in 1,3-Diene Polymerization 131
2.5 Hydro-*tris*-(3-*tert*butyl-5-methyl-pyrazolyl)borate Rare-Earth Metal Trimethylaluminates as Precatalysts in 1,3-Diene Polymerization 145
2.6 A Tetrametallic Titanium Catecholate Complex 145
2.7 Overall Comparisons and Outstanding Polymers 146

3 Concluding Remarks 152

4 References 157

5 Unpublished Results 193

Manuscript I: C–H Activation and Isoprene Polymerization Studies Applying Pentamethylcyclopentadienyl-Supported Rare-Earth Metal Dimethyl Complexes 195
Manuscript II: Reactivity Studies of Pentamethylcyclopentadienyl-Supported Rare-Earth-Metal Dimethyl Complexes with Donor Molecules 234
Manuscript III: Polymerization Studies on $Tp^{tBu,\,Me}$ Rare-Earth Metal Dimethyls 254
Manuscript IV: Experiments on Titanium Catecholate Activation 271

6 Publications 279

Paper I: Half-Sandwich Rare-Earth-Metal Alkylaluminate Complexes Bearing Peripheral Boryl Ligands 281
Paper I: Supporting Information 287
Paper II: Rare-Earth-Metal Allyl Complexes Supported by the [2-(*N,N*-Dimethylamino)ethyl]tetramethylcyclopentadienyl Ligand: Structural Characterization, Reactivity, and Isoprene Polymerization 307
Paper II: Supporting Information 319
Paper III: C–H Bond Activation and Isoprene Polymerization by Lutetium Alkylaluminate / gallate Complexes Bearing a Peripheral Boryl and a Bulky Hydrotris(pyrazolyl) Borate Ligand 331
Paper III: Supporting Information 343
Paper IV: 1,3-Diene Polymerization Mediated by Homoleptic Tetramethylaluminates of the Rare-Earth Metals 379
Paper IV: Supplementary Materials 403
Paper V: 1,3-Diene Polymerization Promoted by Half-Sandwich Rare-Earth Metal Dimethyl Complexes: Active Species Clustering and Cationization / Deactivation Processes . . . 433
Paper V: Supporting Information 441

A Curriculum Vitae **496**
Curriculum Vitae 497

Abbreviations

Abbreviation	Meaning
A	Cocatalyst $[CPh_3][B(C_6F_5)_4]$
Å	Ångström, 10^{-10} m
amim	anilidoimine
Ap^*	$[(C_6H_2{}^iPr_3\text{-}2,4,6)\text{-}(o\text{-}C_5H_3N\text{-}o)\text{-}N\text{-}Dipp]$
Ar	Aryl
Ar^F	Perfluorophenyl, (C_6F_5)
atm	atmospheric pressure
B	Cocatalyst $[PhNMe_2H][B(C_6F_5)_4]$
bar	Bar
BAr^F	Anion of the $[B(C_6F_5)_xR_y]$ motif, $x + y = 4$
$BAr^F{}_3R$	$[B(C_6F_5)_3R]$ Anion
$BAr^F{}_4$	$[B(C_6F_5)_4]$ Anion
BD	Butadiene
Bu	Butyl
C	Cocatalyst $[B(C_6F_5)_3]$
cf.	confer
CHO	Cyclohexylen oxide
CL	ε-Caprolactone

Abbreviation	Meaning
Cp^*	1,2,3,4,5-Pentamethyl cyclopentadienyl
Cp'	1,2,3,4-Tetramethyl-5-trimethylsilyl cyclopentadienyl
Cp^A	1,2,3,4-Tetramethyl-5-Dimethylaminoethyl cyclopentadienyl
Cp^R	Cyclopentadienyl decorated with R
Cp^{ttt}	1,2,4-Tris-*tert*butylcyclopentadienyl
CSA	Chain Shuttling Agent
CTA	Chain Transfer Agent
D	Cocatalyst Me_2AlCl
DCM	Dichloromethane
DFT	Density Functional Theory
DiCp	Dicyclopentadiene
Dipp	2,6-Diisopropylphenyl
DME / dme	Dimethoxyethane
DOSY	Diffusion Ordered Spectroscopy
E	Cocatalyst Et_2AlCl
E-PD	E-1,3-Pentadiene
equiv.	Equivalents
Et	Ethyl
Et	Ethylene[1]
and coworkers	*et alii* or *et aliae*, resp.
F	Cocatalyst Me_3SiCl
G	Cocatalyst Me_2GaCl
g	Gramm

Abbreviation	Meaning
GPC	Gel Permeation Chromatography
h	Hour
Heptad	1,6-Heptadiene
Hexad	1,5-Hexadiene
HIBAO	Hexaisobutylalumoxane
HMPA / hmpa / HMPT	Hexamethyl phosphoric triamide
Hz	Hertz
i or ^{i}	*iso*
IP	Isoprene
k	kilo, 10^{3}
L	Ligand
L-LA	*L*-Lactic Acid
Ln	Lanthanide, rare-earth metal
M	Molar
M	Mega, 10^{6}
m	milli, 10^{-3}
m	Meter
m	Meso diade
m	meta
M_n	Number average molecular weight
$M_{n,theo}$	M_n with 100 % active centers at 100 % conversion
M_W	Mass average molecular weight

Abbreviation	Meaning
MAO	Methylaluminoxane
MBL	α-Methyl-γ-Butyrolactone
MC	Monomer Content
Me	Methyl
Me_4-TCAD	1,4,7,10-Tetramethyl-1,4,7,10-Tetraazacyclododecane
min	Minute
MMA	Methylmethacrylate
MMBL	γ-Methyl-α-Methylene-γ-Butyrolactone
mol	Mol, $6.022 \cdot 10^{23}$
MWD	Molecular Weight Distribution
n	Molar amount
n-alkyl	alkyl without branches
nacnac	Diketiminato ligand
$nacnac^{R_2}$	Diketiminato ligand with R in 1- and 3-position
NB	Norbornene
NMR	Nuclear Magnetic Resonance
o	ortho
p	para
PBD	Poly-1,3-butadiene
PD	1,3-Pentadiene
PDI	Polydispersity Index
PE	Polyethylene
Ph	Phenyl
PIP	Polyisoprene

Abbreviation	Meaning
PMAO-IP	Polymethylaluminoxane-Improved Performance
PP	Polypropylene
PS	Polystyrene
psi	Pounds per square inch
Pr	Propyl
Pr	Propylene[1]
QM / MM	Quantum mechanics / Molecular mechanics computational study
r	Racemo diade
RE	Rare-earth metal
Ref.	Reference
resp.	respectively
ROP	Ring Opening Polymerization
rpm	Rounds per minute
r.t. or rt	Room temperature
SEC	Size Exclusion Chromatography
St	Styrene
t or ^{t}	*tert*
THF / thf	Tetrahydrofuran
TMC	Trimethylene Carbonate
TMEDA	N,N,N',N'-Tetramethylethylen diamine
TOF	Turnover frequency

Abbreviation	Meaning
$Tp^{tBu,\ Me}$	Hydro-*tris*-(3-methyl-5-*tert*butyl-pyrazolyl)borato
TREN	*Tris*-(2-aminoethyl)amine
VPDMS	*p*-Vinylphenyl dimethylsilane
w	Weight
1-Hex	1-Hexene
[9]aneS_3	cyclotriethenyltrithioether $[S(CH_2)_2]_3$
η^x	hapto-x coordination
κ^x	x-dental coordination
%	percent, 10^{-2}
°C	degree Celsius

[1] where indicated

List of Publications

This thesis is based on the following scientific papers. In the text, they will be referred to by Roman numerals.

Paper I "Half-Sandwich Rare-Earth-Metal Alkylaluminate Complexes Bearing Peripheral Boryl Ligands"
Nicole Dettenrieder, Christoph O. Hollfelder, Lars N. Jende, Cäcilia Maichle-Mössmer, and Reiner Anwander

Organometallics, **2014**, *33*, 1528–1531
doi: 10.1021/om401163a

Paper II "Rare-Earth-Metal Allyl Complexes Supported by the [2-(*N,N*-Dimethylamino)ethyl]tetramethylcyclopentadienyl Ligand: Structural Characterization, Reactivity, and Isoprene Polymerization"
Lars N. Jende, Christoph O. Hollfelder, Cäcilia Maichle-Mössmer, and Reiner Anwander

Organometallics, **2015**, *34*, 32–41
doi: 10.1021/om500725g

Paper III "C–H Bond Activation and Isoprene Polymerization by Lutetium Alkylaluminate / gallate Complexes Bearing a Peripheral Boryl and a Bulky Hydrotris(pyrazolyl) borate Ligand"
Martin Bonath, Christoph O. Hollfelder, Dorothea Schädle, Cäcilia Maichle-Mössmer, Peter Sirsch, and Reiner Anwander

Eur. J. Inorg. Chem. **2017**, *2017*, 4683–4692
doi: 10.1002/ejic.201700730

Paper IV "1,3-Diene Polymerization Mediated by Homoleptic Tetramethylaluminates of the Rare-Earth Metals"
Christoph O. Hollfelder, Lars N. Jende, Dominic Diether, Theresa Zelger, Rita Stauder, Cäcilia Maichle-Mössmer, and Reiner Anwander

Catalysts, **2018**, *8*, 61
Special Issue: "Catalysts for the Controlled Polymerization of Conjugated Dienes"
doi: 10.3390/catal8020061

Paper V "1,3-Diene Polymerization Promoted by Half-Sandwich Rare-Earth Metal Dimethyl Complexes: Active Species Clustering and Cationization / Deactivation Processes"
Christoph O. Hollfelder, Lars N. Jende, Hans-Martin Dietrich, Klaus Eichele, Cäcilia Maichle-Mössmer, and Reiner Anwander

Chem. Eur. J. **2019**, *25*, 7298-7302.
doi: 10.1002/chem.201901269

By the time of the publication of this thesis, **Manuscript 1** has been published as part of:

> "C–H-Bond Activation and Isoprene Polymerization Studies Applying Pentamethylcyclopentadienyl-Supported Rare-Earth-Metal Bis(Tetramethylaluminate) and Dimethyl Complexes"
> Christoph O. Hollfelder, Melanie Meermann-Zimmermann, Georgios Spiridopoulos, Daniel Werner, Karl W. Törnroos, Cäcilia Maichle-Mössmer, and Reiner Anwander
>
> *Molecules* **2019**, *24*, 3703.
> Special Issue: "Well-Defined Metal Complex Catalysts for Olefin Polymerization"
> doi: 10.3390/molecules24203703

Personal Contribution to Collaborative Publications

Paper I: 5 authors; candidate shared first author

Synthesis and inorganic analyses (except single-crystal-structure analyses, which were aquired by Dr. C. Maichle-Mössmer) and writing were planned and conducted by Dr. N. Dettenrieder. Polymerizations of isoprene, polymer analyses, data acquisition and investigations on the active species of the presented precatalysts were performed by the candidate. Except for the tetramethylaluminates presented for comparison, which were performed by Dr. L. N. Jende. The candidate wrote parts of the article and presented the microstructural data in a new fashion. All authors took part in the scientific discussion and Dr. N. Dettenrieder, Dr. L. N. Jende and the candidate interpreted the active species spectra.

Paper II: 4 authors; candidate second author

The experimental work (except single-crystal-structure analyses, which were aquired by Dr. C. Maichle-Mössmer) and writing were planned and conducted by Dr. L. N. Jende. The candidate contributed to the polymerization experiments, data interpretation and the graphical comparison of the polyisoprene microsturctures. All authors took part in the scientific discussion.

Paper III: 6 authors; candidate shared first author

Inorganic synthesis and analyses were performed by M. Bonath (except single-crystal-structure analyses, which were aquired by

Dr. C. Maichle-Mössmer). Polymerization catalysis, polymer analyses, interpretation and active species determination were carried out by the candidate. M. Bonath and the candidate took equally part in the interpretation of the obtained active species data. Writing was performed by M. Bonath and the candidate in equal collaboration. All authors took part in the scientific discussion.

Paper IV: 7 authors, candidate first author

The experimental work and analyses were planned, performed and carried out by the candidate (except for the polymers by the lutetium species, performed by Dr. L. N. Jende, the ethylene polymerization, investigated by D. Diether and the single crystal structure analyses, aquired by Dr. C. Maichle-Mössmer). The candidate wrote the paper and presented and interpreted the data. T. Zelger and R. Stauder contributed to the polymerization experiments and data presentation as well as to the artwork of the graphical abstract. All authors took part in the scientific discussion.

Paper V: 6 authors, candidate first author

The main part of the experimental work and analyses were planned and carried out by the candidate. Dr. L. N. Jende contributed about 15 % of the polymerization data and the idea to investigate aluminum-free polymerization. Single-crystal-structure analyses was aquired by Dr. C. Maichle-Mössmer. Dr. K. Eichele performed the NMR DOSY spectroscopic experiments. Dr. H.-M. Dietrich

contributed the single-crystal-structure of the degradation product. The candidate wrote the paper and interpreted the data, assisted by Dr. L. N. Jende. All authors took part in the scientific discussion.

Further Unpublished Results: 4 manuscripts

All experimental work, analyses and writing were carried out by the candidate, except for crystallographic contributions by Dr. C. Maichle-Mössmer, Dr. D. Werner, Prof. Dr. K. W. Törnroos and Dr. M. Meermann-Zimmermann. Dr. D. Schädle synthesized the precatalysts in **Manuscript III**. A. Sonström synthesized the precursor in **Manuscript IV**.

Summary

The steric coordination environment of a metal center active in Ziegler-Natta 1,3-diene polymerization catalysis has a major impact on the properties of the polymeric products. Nowadays, polymer characterization allows an easy access to statistical chain data as well as microstructural ratios and material parameters, whereas a direct mechanistic insight into the catalytic process remains a challenging task. Therefore, both strategies have been combined in this work for a maximal output of conclusions regarding sterical effects and active species identifications. Applying this concept, a variety of classes of rare-earth metal alkyls and alkylaluminates ('alkyls in disguise') have been targeted and analyzed systematically as precatalysts.

In a comprehensive study of homoleptic lanthanide tetramethylaluminates as precatalysts ($[Ln(AlMe_4)_3]$, (Ln = La, Ce, Pr, Nd, Gd, Tb, Dy, Ho, Y, Er, Lu), the clusters known to be formed upon activation with dialkyl aluminum chloride were shown to disintegrate upon monomer coordination. In case of pentamethylcyclopentadienyl rare earth metal dimethyl trimers ($[(C_5Me_5LnMe_2]_3$, Ln = Dy, Ho, Y, Lu), strong indications for a multimetallic nature could be found for the active species. Furthermore, a second radical reaction pathway causing polymer crosslinking was detected with these systems. The species were also found to undergo C–H-bond activations releasing methane. Introducing boryl aluminates as sterically bulky group in the alkyl possition it was found that C–H-bond activations play a major role in their catalytic applications. Furthermore, a $Tp^{tBu,\,Me}$ (Hydro-*tris*-(3-methyl-5-*tert*butyl-pyrazolyl)borato) scorpionate ligand was selected as representative bulky spectator ligand. Here, the

polymerizations revealed to depend only on the steric environment of the precatalyst.

With all these findings, this thesis contributes significantly to the understanding of the processes within the ‘black box’ of Ziegler-Natta polymerization catalysis.

Zusammenfassung

Die sterische Koordinationsumgebung eines aktiven Metallzentrums in der Ziegler-Natta-Polymerisationskatalyse der 1,3-Diene hat bedeutenden Einfluss auf die Eigenschaften seiner polymeren Produkte. Mittlerweile ermöglicht die Polymeranalytik einen effizienten Zugang zu statistischen Kettendaten, der mikrostrukturellen Zusammensetzung und den Materialkenngrößen dieser Polymere. Direkte mechanistische Einblicke in den katalytischen Prozess hingegen stellen immer noch eine Herausforderung dar. Deshalb wurden in dieser Arbeit beide Ansätze kombiniert, um den größtmöglichen Erkenntnissgewinn bezüglich Struktur-Wirkungs-Beziehungen und der Aufklärung der aktiven Spezies zu erlangen. Mit diesem Konzept wurde eine Auswahl von Seltenerdmetallalkylen und -aluminaten als Präkatalysatoren eingesetzt und untersucht.

In einer umfassenden Studie homoleptischer Tetramethylaluminate ($[Ln(AlMe_4)_3]$, (Ln = La, Ce, Pr, Nd, Gd, Tb, Dy, Ho, Y, Er, Lu) wurde im Moment der Monomerkoordination ein Abbau der, sich bekanntermaßen bei Aktivierung mittels Dialkylaluminiumchloriden bildenden, Clusterverbindungen beobachtet. Im Falle der Pentamethylcyclopentadienyl-Seltenerdmetalldimethyltrimeren ($[(C_5Me_5LnMe_2]_3$, Ln = Dy, Ho, Y, Lu) wurden starke Anzeichen dafür gefunden, dass auch die aktiven Spezies multimetallisch sind. Darüber hinaus wurde ein zweiter, radikalischer Mechanismus entdeckt, der für die, bei diesen Systemen auftretenden, Polymer-Vernetzungen verantwortlich ist. Außerdem wurde festgestellt, dass diese Katalysatoren zu C–H-Bindungsaktivierungen unter Methanabspaltung neigen. Bei der Einführung von Borylaluminaten als sterisch anspruchsvolle Alternative in der Alkylposition der Präkatalysatoren, tra-

ten ebenfalls C–H-Bindungsaktivierungen auf, die eine bedeutende Rolle in der Polymerisationskatalyse dieser Komplexe spielen. Des Weiteren wurde der $Tp^{tBu,\,Me}$-Skorpionatligand ($Tp^{tBu,\,Me}$ = Hydro-*tris*-(3-methyl-5-*tert*butyl-pyrazolyl)borato) als sterisch anspruchsvoller Zuschauerligand gewählt. Hier zeigen die Polymerisationen lediglich eine Abhängigkeit von der sterischen Umgebung des katalytischen Zentrums und von der Reaktivität des Liganden. Mit all diesen Befunden trägt diese Arbeit signifikant zum Verständnis der Vorgänge in der „Black Box" der Ziegler-Natta-Polymerisationskatalyse bei.

Objective of the Thesis

More than 65 years after Ziegler's discovery of the catalytic effects of metalorganic compounds in olefin polymerization, the actual involved mechanisms have remained unclear. Although several theoretical approaches have been investigated, none of them has been experimentally proven. Over these 65 years, lanthanide complexes have revealed outstanding catalytic performance in this field.

Chapter 1 gives an overview on the rare-earth metal complexes featuring perfluoroarylborato anions known to literature. The chapter is focused on single component polymerization catalysts and model systems for catalytically active species. Besides that, it contains a section on those ion pairs that have not been applied in polymerization catalysis yet.

Chapter 2 states the contribution of this thesis to the field of rare-earth metal based Ziegler-Natta catalysis, focusing both on the application of selected precatalyst / cocatalyst binary systems in 1,3-diene polymerization and the determination of the respective catalytically active species. In order to provide a systematic study, homoleptic tetramethylaluminates were investigated as precatalysts next to complexes bearing 1,2,3,4,5-pentamethylcyclopentadienyl or hydro *tris*-(3-*tert*butyl-5-methylpyrazolyl)borato as spectator ligands. Inorganic and polymer analytic techniques were employed to obtain the data, the conclusions in **Chapter 3** are derived from. All investigations are discussed in detail in **Chapter 5** (unpublished results) and **Chapter 6** (published results), respectively.

Chapter 1

Polymerization Catalysis of Rare-Earth Metal Alkylaluminates and Dialkyls

Chapter 1. Polymerization Catalysis of Rare-Earth Metal Alkylaluminates and Dialkyls

1.1 Introduction[1]

Since the early days of catalytic anionic polymerization[1–3] more and more monomers could be introduced into the field, various polymer micorstructures and tacticities could be achieved and polydispersities between almost monodisperse and extremely polydisperse have been discovered.
But still, despite this enormous diversity of achievable polymer properties and major experimental and theoretical efforts two very essential aspects of the polymerization reactions have remained concealed: the mechanism and the actual active catalyst species.

For example, in case of the mechanism of the lanthanide centered isoprene polymerization, Taube and coworkers[4, 5] have shown conclusive approaches to reveal the mechanism (Scheme 1.1). Nevertheless, the lack of an experimental proof keeps an uncertainty that leaves room for speculations about the various parameters influencing such a reaction and their amplification. Regarding the active species, several groups were able to contribute first discoveries. These will be summarized in this chapter.

[1]Parts of this section are meant to be published as part of a review article.

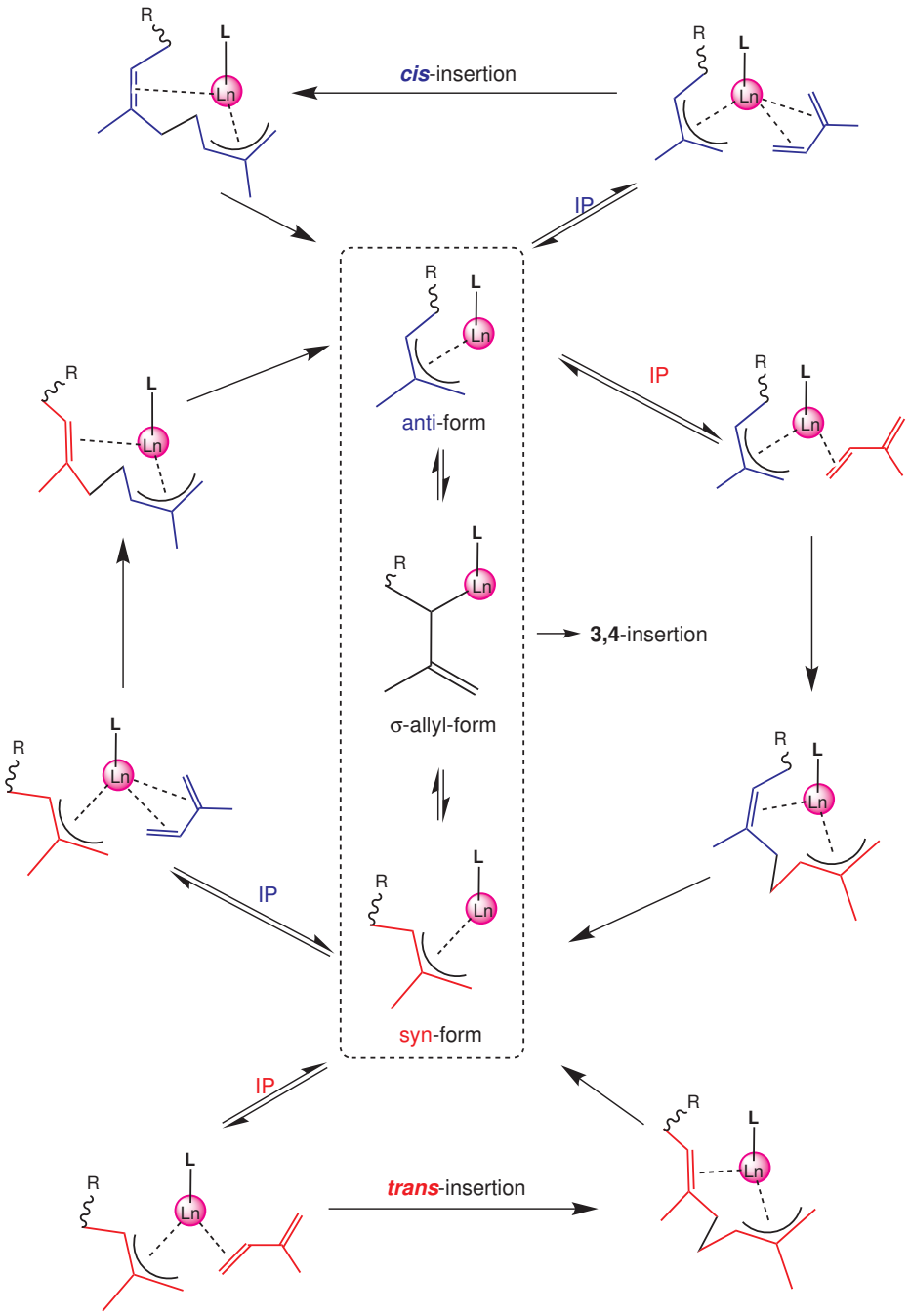

Scheme 1.1: Taube's proposed mechanism of the lanthanide-centered isoprene 1,4-polymerization,[4, 5] Scheme according to Lars Jende.[6] Shown as an example for current mechanistic research in this field.

1.2 Cationic Lanthanide Species Countered by Tetrakis-(Pentafluorophenyl)-Borato and Tris-(Pentafluorophenyl)-mono-Alkyl-Borato

1.2.1 Historic Background

It has been several decades, since the first lanthanide-based catalytic systems for 1,3-diene polymerization were patented in 1965 by Union Carbide Co.[7, 8] and the first published lanthanide-based catalyst active in ethylene polymerization by Ballerd and coworkers.[9] Since then, the scientific community produced a large variety of species not only active in the polymerization of 1,3-dienes and ethylene, but also of other α-olefins and in the ring opening polymerization of various cyclic esters and epoxides. Polymerization performances of lanthanide-based catalytic systems have been reviewed earlier[4, 10–22] and even quite recently,[23–28] but active species determination has rarely been focused in such reviews if even mentioned. Nevertheless, to date little is known about the nature of the active catalytic species and *ergo* the mechanisms of polymerization. In order to obtain new insights into these aspects, and especially to investigate the role and tuneabiltiy of the cationic lanthanide center, new methods beyond the original Ziegler-Natta-Systems[1–3] were envisaged. *Inter alia*, they were adopted from the parallel developing field of Group IV polymerization catalysts.[29]

By treatment with organo borate compounds (e.g. $[Ph_3C][B(C_6F_5)_4]$ (cocatalyst **A**) and $[PhNHMe_2][B(C_6F_5)_4]$ (cocatalyst **B**)) and borane (e.g. $B(C_6F_5)_3$ (cocatalyst **C**)) developed by Massey and coworkers,[30, 31] cationic lanthanide species can be readily obtained by ligand abstraction

or protonolysis.[32] The weakly coordinating perfluorophenyl borate anions ($[B(C_6F_5)_4]^-$ = $[BAr^F{}_4]^-$ and $[B(C_6F_5)_3R]^-$ = $[BAr^F{}_3R]^-$)[33] enable a great variety of monomers to access the cationic lanthanide center. The fluorine atoms provide a further NMR spectroscopic handle to determine the coordination strength of the anions.[34, 35]

In contrast, the characterization of the active species is still a challenging task as these species are typically fugacious, or too reactive to handle under regular conditions.[36–38] Therefore theoretical approaches are becoming more and more important in this field.[39] However, despite recent advances in this area, simplifications and assumptions are still necessary. Thus, due to the complexity of the system, practical evidence is still crucial to affirm accurate theoretical findings.

Investigations by NMR spectroscopy are an appropriate tool to obtain insight into the catalytic process, and are frequently applied.[40] However, complications in spectral interpretation arise as soon as ligand dynamics, beginning decomposition or formation of multiple active species or side products are occurring. For this reason, crystallization and species identification from these reaction mixtures are, unfortunately, highly challenging, as well. Further, the $[BAr^F{}_4]^-$ and $[BAr^F{}_3R]^-$ anions have been reported to show low tendency towards crystallization.[36, 37]

To assist in crystallization of these highly elusive species, model systems with $[BPh_4]$ anions have been introduced[41–43] and are frequently investigated due to their lower solubility.[44,45] Although successful in giving isolatable structures, somewhat ironically the obtained complexes do not catalyze polymerization reactions as their fluorinated counterparts.[46,47] This can be attributed to a dominant η^6-coordination of their aryl rings

to the cationic metal center, which is for steric reasons disadvantageous to the catalytic activity.[48] Besides these two major differences, it is clear, that the tendency towards an interaction with a cationic metal center is much higher for electron rich fluorine than it is for hydrogen or η^6-arenes. This is the reason, why other types of model systems are frequently favored.

Coordination saturation of the Ln-cation by small molecules (e.g. donor solvents or ligands with neutral side arm donors), is another means to initiate crystallization of an active cationic compound and thus discussed within this chapter.

Besides model systems, there are of course rare examples in which the cationic lanthanide active species was crystallized and tested in polymerization as a single-component catalyst. These systems and their capability in polymerization are the main focus of this chapter, followed by some unexpected results in catalyst activation.[49]

1.2.2 Cations Active in the Coordinative Polymerization

1.2.2.1 Ethylene Polymerization

When Evans and coworkers published the first solid state structure of a lanthanide [BAr^F] ion pair ([Cp^*_2Sm][$HBAr^F_3$], **2**) in 1998[50] (see Scheme 1.2), it was synthesized by reacting [Cp^*_3Sm] (**1**) with cocatalyst **C** ($B(C_6F_5)_3$, BAr^F_3). They suggested its applicability in olefin polymerization. Although this was not further investigated, one year prior, they also showed that **1**, as its Sm^{II} analoga,[51] is a single component catalyst for ethylene polymerization, due to its capability to switch one Cp^*-ligand from η^5 to κ^1 coordination.[49,52]

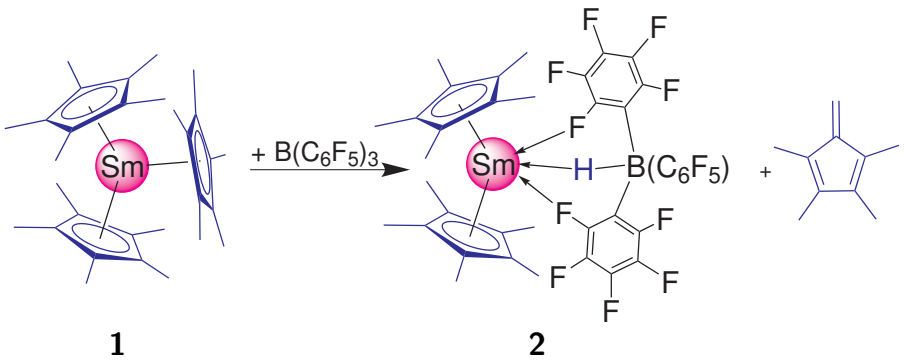

1 **2**

*Scheme 1.2: Synthesis of the first Ln [BAr^F] ion pair, [Cp$^*_2$Sm][B(C$_6$F$_5$)$_3$H] (**2**), from [Cp$^*_3$Sm] (**1**) applying cocatalyst **C**, according to ref. 50.*

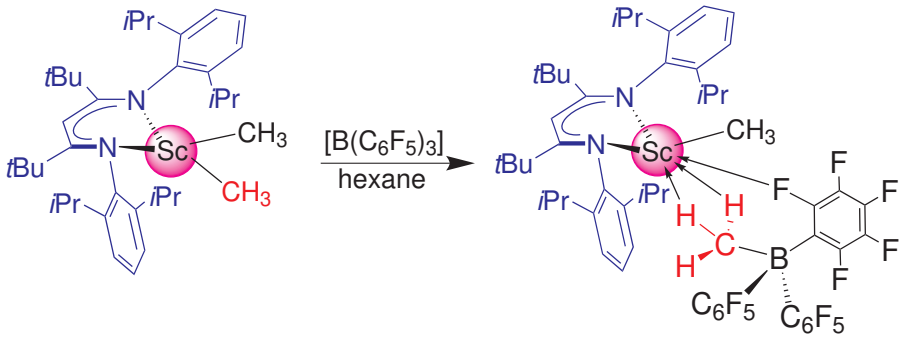

3 **4**

*Scheme 1.3: Synthesis of ion pair ["nacnac"ScMe](μ-F)(μ-H)$_2$[B(C$_6$F$_4$)(C$_6$F$_5$)$_2$CH] (**4**), bridged by one fluorine and two methyl hydrogens, from its dimethyl precursor (**3**) applying cocatalyst **C** in n-hexane according to ref. 53. As **4** was found to be unstable in solution, it was not tested in polymerization.*

So, the field of ethylene polymerization with structurally known active [BAr^F] species begun in 2002, when Piers and coworkers[53] crystallized the activation product (**4**) of a LScMe$_2$-precatalyst (**3**) bearing a bulky "nacnac"-type diketiminato ligand L (L = [{DippN=C(^{t}Bu)}$_2$CH]$^-$, "nacnac$^{t\mathrm{Bu}_2}$") (Scheme 1.3). Applying a relatively high ethlyene pressure

*Table 1.1: Ethylene Hompolymerization by [LScMe$_2$] (**3**), data taken from ref. 53*

Entry[a]	Precatalyst[b]	Cocatalyst[c]	Activity [kg·mol^{-1}·h^{-1}]	M_W [10^{4}g·mol^{-1}]	PDI
1	[LScCl$_2$] **3a**	PMAO-IP	99	135.7	2.2
2	[LScMe$_2$] **3**	PMAO-IP	1200	186.6	1.98
3	[LScMe$_2$] **3**	**C**	300	105.1	1.7
4	[LScMe$_2$] **3**	**A**	480	85.1	2.48

[a] Conditions: 50 °C, 300 psi, cyclohexane/toluene, stirr rate = 3000 rpm, [Sc] = 300μM, [PMAO-IP] = 1mM as scavenger;
[b] L = [(Dipp-N=C(^{t}Bu))$_2$CH]$^-$
[c] **A** = [Ph$_3$C][B(C$_6$F$_5$)$_4$], **B** = [PhNMe$_2$H][B(C$_6$F$_5$)$_4$], **C** = [B(C$_6$F$_5$)$_3$];

of 300 psi (20.7 bar) at 50 °C to prereacted solutions of **3** / **A** and **3** / **C** yielded PE of MWDs implying single-site behavior (see Table 1.1). It is noteworthy that similar polymers were achieved applying PMAO-IP as a cocatalyst and that only in case of PMAO-IP also the chloride complex [LScCl$_2$] (**3a**) yielded polymer. The synthesis of **4**, that yielded the crystal structure mentioned above, is shown in Scheme 1.3 and was obtained from the reaction of the dimethyl precatalyst (**3**) with cocatalyst **C**. Interestingly, it contains a [BAr$^F{}_3$Me] anion, that is coordinated to the Sc center via a fluorine atom from one of the Ar^F groups and two hydrogen atoms of the boryl-transferred methyl group.[54] As **4** was found to be unstable in solution, it was not tested as a single-component catalyst.
Piers and coworkers had published a crystal structure of an activated Ln-BAr^F-species ([("nacnac^{Me_2}")Sc(CH$_2$Ph)][BAr$^F{}_3$CH$_2$Ph] (**6**), obtained from the reaction of the neutral bisbenzyl precursor [("nacnac^{Me_2}")Sc(CH$_2$Ph)$_2$] (**5**) and cocatalyst **C**) earlier as well, but it had shown not to be active in polymerization.[55] The systems differ, as that, published in 2002 (**3**) is bulkier than the earlier inactive species (**5**), and **3** contains methyl moieties instead of the benzyl ligands published in 1999 (**5**).

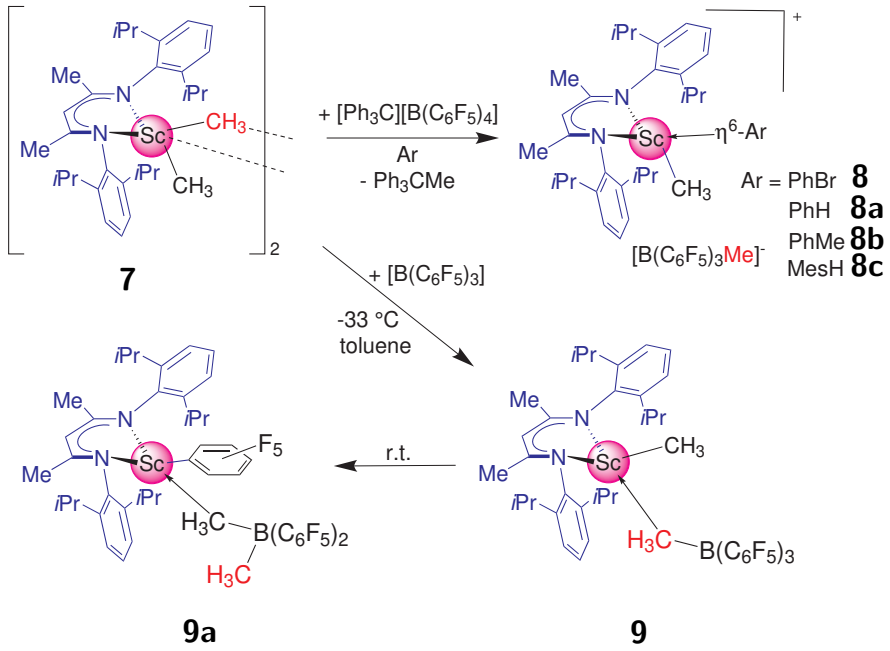

*Scheme 1.4: Synthesis of ion pair ["nacnac^{Me_2}"ScMeAr][B(C_6F_5)$_3$$CH_3$] Ar = (PhBr (**8**), PhH (**8a**), PhMe(**8b**), MesH (**8c**), from its precursor ["nacnac^{Me_2}"ScMe(μMe)]$_2$ **7** applying cocatalyst **A** in the respective aromatic solvent (Ar) according to ref. 56 and synthesis of ion pair ["nacnac^{Me_2}"ScMe][B(C_6F_5)$_3$$CH_3$] **9** at -33°C from **7** applying cocatalyst **C** in toluene and its conversion to **9a** upon heating to r.t. according to ref. 57.*

In 2003, Piers and coworkers[56] investigated an analogue system containing a less bulky methyl substituted "nacnac"-ligand ([{DippN=C(Me)}$_2$CH]$^-$) ("nacnac^{Me_2}") and obtained [("nacnac^{Me_2}")ScMe(η^6-Ar)][BAr$^F{}_4$] (η^6-Ar = bromobenzene (**8**), benzene (**8a**), toluene (**8b**) or mesitylene (**8c**)) from the dimeric precursor [("nacnac^{Me_2}")ScMe$_2$]$_2$ (**7**) upon activation with cocatalyst **A** in the resp. aromatic solvent η^6-Ar (see Scheme 1.4). Next to the three solvent-coordinated ion pairs that were inactive in ethylene polymerization (η^6-Ar = bromobenzene, benzene and toluene (**8**, **8a**,**b**)) they obtained the mesitylene-coordinated species (**8c**) that showed slight activity.

The resulting yield was too little to characterize the polymer. Further unfortunately, only the non-polymerizing species with bromobenzene (**8**) and toluene (**8b**) coordination could be crystallized. Due to the solvent-coordination, the anions do not find enough space to coordinate as well. In 2005,[57] Piers and coworkers published the results of the activation of **7** with cocatalyst **C** in toluene, that yielded no species active in polymerization catalysis (*vide infra*).

Quite recently, Kempe and coworkers[58] reported a nitrogen donor

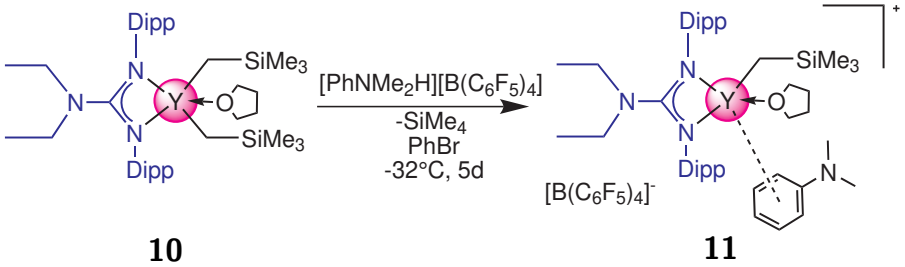

10 **11**

*Scheme 1.5: Synthesis of the ion pair [(Et$_2$NC(NDipp)$_2$)Y(CH$_2$SiMe$_3$)(Me$_2$NPh)][B(C$_6$F$_5$)$_4$] (**11**) from its dimethyl precursor (**10**) applying cocatalyst **B**. Scheme according to ref. 58.*

ligand-stabilized catalyst derived from the yttrium guadinate system ([(Et$_2$NC(NDipp)$_2$)Y(CH$_2$SiMe$_3$)$_2$], **10**). Next to ethylene oligomerization and α-olefin synthesis, **10** showed activity in ethylene polymerization, when activated by cocatalyst **B** (Scheme 1.5). The resulting ion pair [(Et$_2$NC(NDipp)$_2$)Y(CH$_2$SiMe$_3$)(Me$_2$NPh)][B(C$_6$F$_5$)$_4$] (**11**) was reacted with AlEt$_3$ to be active in ethylene chain transfer polymerization. With 9 bar ethylene pressure at 80 °C, an activity of 156 $\frac{kg}{mol \cdot h \cdot bar}$ was achieved. Polyethylene with a PDI of 1.1 and a molecular weight average (M_n) of $0.3 \cdot 10^4 \frac{g}{mol}$ was obtained. The low number average molecular weight emphasizes the large chain transfer capability of the system. It is noteworthy, that although Kempe and coworkers obtained **11** as single-crystals

suitable for x-ray structure analysis and isolated it, a single component catalysis applying this ion pair was not described.

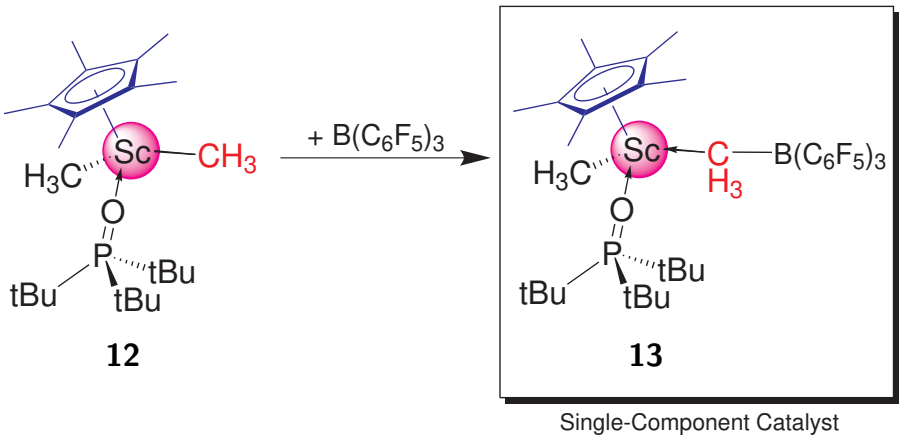

Scheme 1.6: Synthesis of the ion pair [Cp(tBu3P=O)ScMe][B(C6F5)3Me] (**13**) from its dimethyl precursor (**12**) applying cocatalyst **C**. Scheme according to ref. 59.*

The half-sandwich complex [Cp*ScMe$_2$] was investigated by Piers and coworkers in 2004,[59] offering enough steric space for a (^{t}Bu$_3$P=O) donor at the Sc center. Reacting this precatalyst (**12**) with cocatalyst **C** yields **13**, an ion pair, in which only the transferred methyl moiety bridges the ions (see Scheme 1.6). This activated species serves as a single-component catalyst for the polymerization of ethylene at room temperature under 1 atm (ca. 1 bar) with an activity of 130 $\frac{kg}{mol \cdot h}$.[60] In this case, higher temperatures favor the catalysts decomposition, and are therefore non-beneficial to the catalysis.

Hou and coworkers employed an even bulkier Cp ligand and hydride coligands bound to Sc, namely Cp' (Cp' = CpMe$_4$SiMe$_3$) in [{Cp'ScH$_2$}$_4$(thf)$_n$] (n = 0 – 2 (**14**, **14a**, and **14b**)), in the same year.[61] Two (n = 0 (**15**) and n = 2 (**15b**)) of the three clusters resulting from the activation of the

neutral clusters applying cocatalyst **A** (see Scheme 1.7) could be crystallized[62] revealing that a fluorine atom of the [$BAr^F{}_4$] anion is in close contact to the Sc center for n = 0 (**15**). Next to the polymerization of various monomers[23, 61–63] (*vide infra*), the authors mention that for n = 0, 1 (**14**, and **14a**) ethylene polymerizations were achieved with an activity of ca. 1,000 $\frac{kg}{mol \cdot h \cdot bar}$. In case of n = 2 (**14b**) instead, no polymerization was obtained.

Further studies involving the Cp' ligand, such as those of [Cp'Sc(*o*-$CH_2C_6H_4NMe_2$)$_2$] (**25**) in 2007,[64] or [Cp'Sc(CH_2SiMe_3)$_2$(thf)] (**16**) in 2009,[65] did not focus on the homopolymerization of ethylene, but its copolymers with various monomers. The ethylene homopolymer obtained with **16** was published earlier[66] in a study of ethylene-styrene copolymerization.[67] There, an activity of 786 $\frac{kg}{mol \cdot h \cdot bar}$ was found (PDI = 1.72 at 1 atm, ca. 1 bar ethylene pressure in toluene) for the *in situ* generated system with cocatalyst **A**. This focus was also extended to the bulkier ligand $Cp^{Me_4(o\text{-anisole})}$ and its Sc(CH_2SiMe_3)$_2$ complex (**17**).[68]

Nevertheless, there is one more single-component catalyst to report for the polymerization of ethylene. Trifonov and Kempe and coworkers[69, 70] presented a Y-hydrido trimeric complex, that bears one Ap^*-ligand per Y center [(Ap^*Y)$_3$(μ_2H)$_3$(μ_3H)$_2$(thf)$_2$(CH_2SiMe_3)] (**18^Y**) (Ap^* = [($C_6H_2{}^iPr_3$-2,4,6)-(*o*-C_5H_3N-*o*)-N-($C_6H_4{}^iPr_2$-2,6)]) (Scheme 1.8). This neutral single component catalyst produces polyethylene from a toluene solution at 20 °C with 0.5 atm (ca. 0.5 bar) ethylene pressure with an activity of 560 $\frac{kg}{mol \cdot h \cdot bar}$. Applying these conditions an activity of 840 $\frac{kg}{mol \cdot h \cdot bar}$ is achieved for [(Ap^*Y(thf))$_3$(μ_2H)$_3$(μ_3H)$_2$][$BAr^F{}_4$] (**19^Y**), synthesized by the application of cocatalyst **B** on **18^Y**, notably 280 $\frac{kg}{mol \cdot h \cdot bar}$ higher than the productivity of **18^Y** without activation.[49]

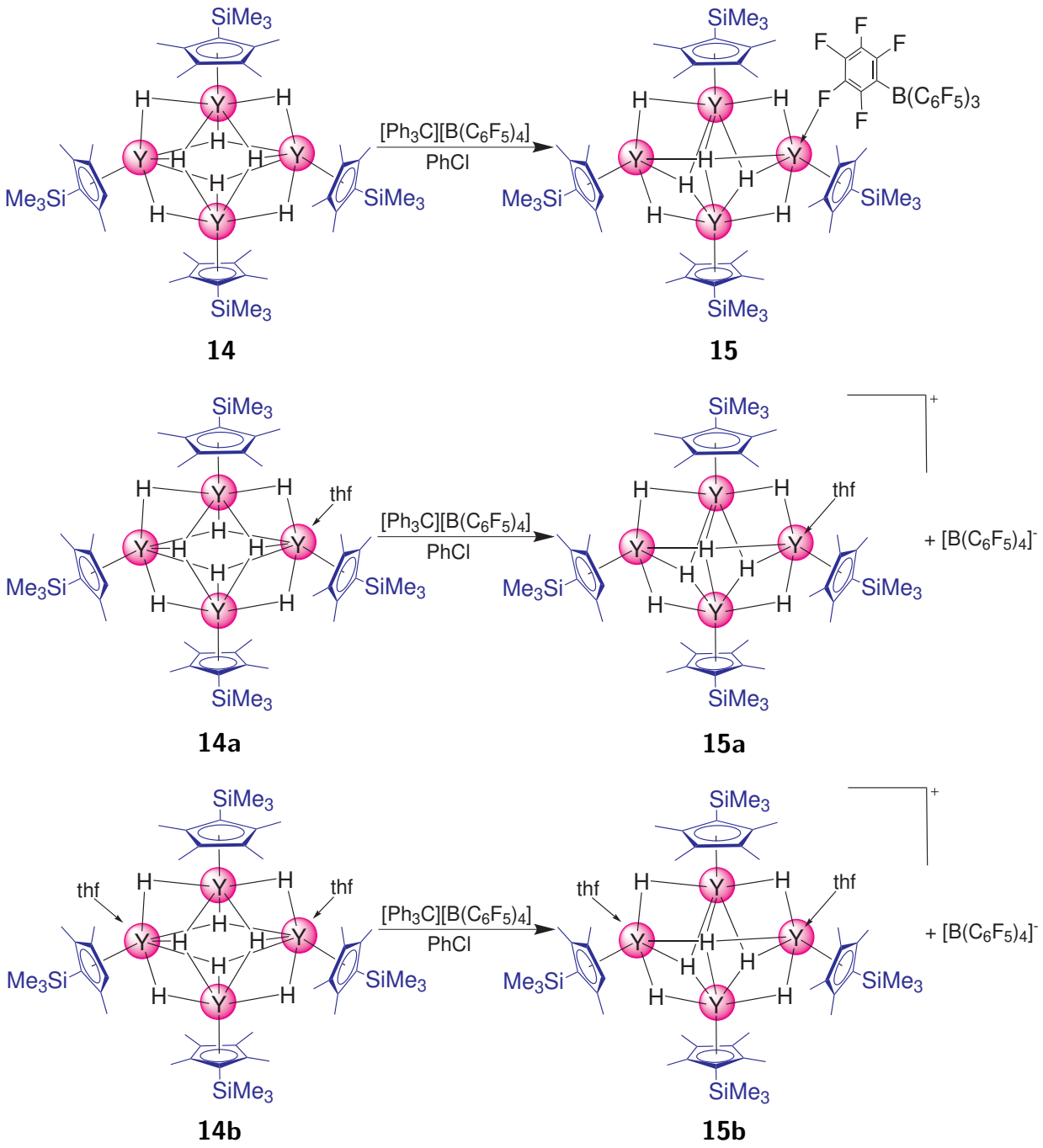

*Scheme 1.7: Synthesis of the ion pairs [{Cp'$_4$Y$_4$H$_7$}(thf)$_n$][B(C$_6$F$_5$)$_4$] (n = 0 – 2 (**15**, **15a** and **15b**)) from the corresponding neutral hydrido clusters (**14**, **14a** and **14b**) applying cocatalyst **A**. Scheme according to ref. 62.*

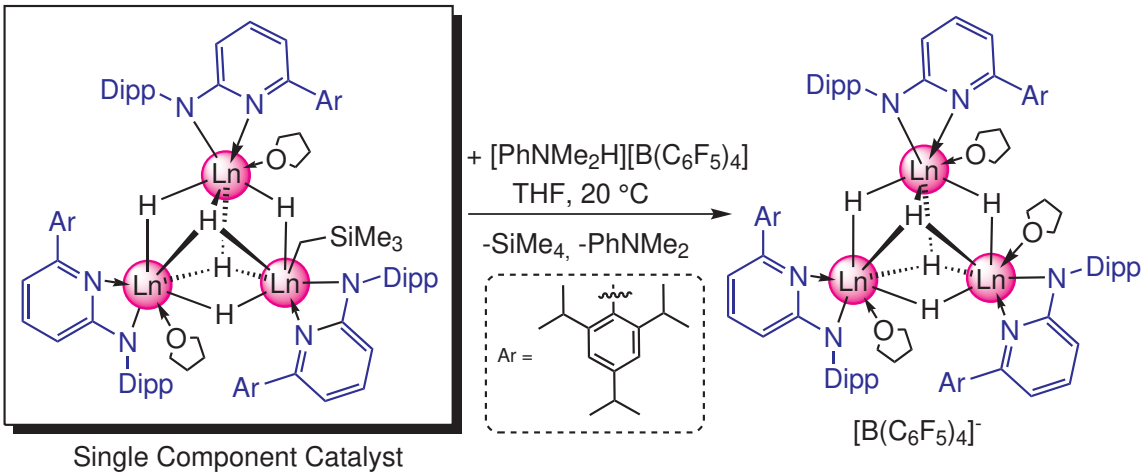

*Scheme 1.8: Synthesis of [{Ap*Ln(thf)}$_3$H$_5$] clusters (Ap* = [(C$_6$H$_3$^{i}Pr$_3$-2,4,6)-(o-C$_5$H$_3$N-o)-N-(C$_6$H$_4$^{i}Pr$_2$-2,6)]; Ln = Y (**19^Y**), Lu (**19^{Lu}**)) from [{Ap*Ln(thf)}$_2${Ap*Ln(CH$_2$SiMe$_3$)}H$_5$] (Ln = Y (**18^Y**), Lu (**18^{Lu}**)). Scheme according to ref. 70.*

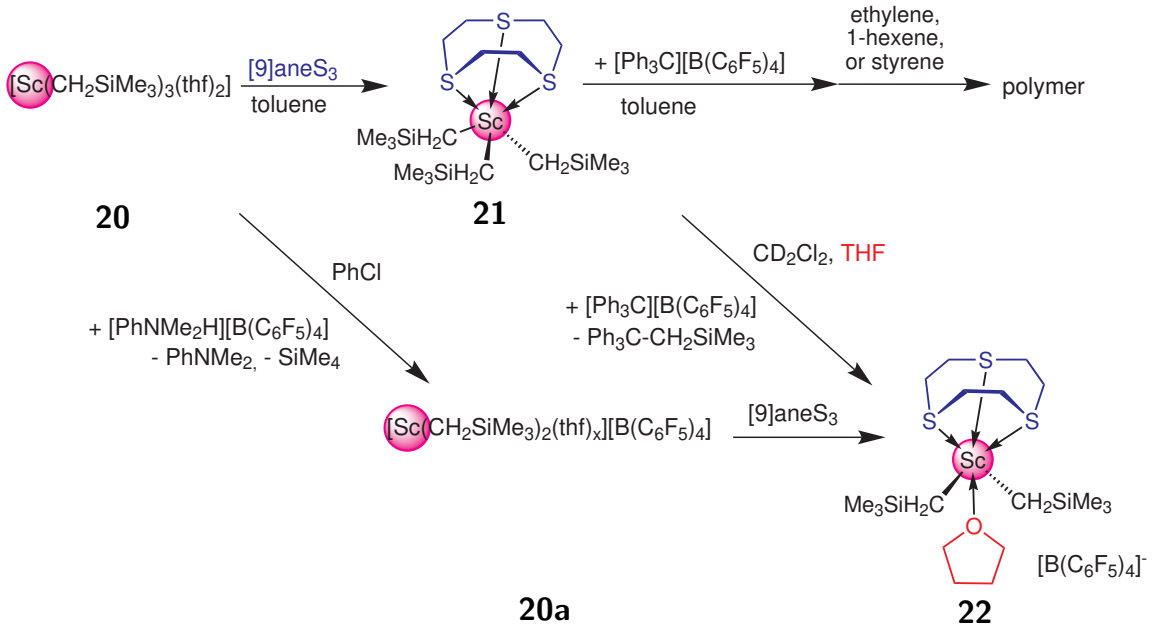

Scheme 1.9: Polymerization of ethylene applying cocatalyst ***A*** *on [{[9]aneS$_3$}Sc(CH$_2$SiMe$_3$)$_3$] (**21**) and its synthesis as well as synthesis of the ion pair [{[9]aneS$_3$}Sc(CH$_2$SiMe$_3$)$_2$(thf)][B(C$_6$F$_5$)$_4$] (**22**) from its bisneosilyl precursor ion pair (**20a**) applying the ligand and synthesis of* ***20a*** *from Sc(CH$_2$SiMe$_3$)$_3$(thf)$_2$ (**20**) applying cocatalyst* ***B****. **22** can also be synthesized from **21** applying cocatalyst* ***A****. Scheme according to refs. 72 and 71.*

Besides all these Cp and Ap* systems, a ligand system investigated by Mountford and coworkers[71, 72] completes the picture. The group synthesized a [Sc(CH$_2$SiMe$_3$)$_3$] complex bearing a facially coordinated neutral [9]aneS$_3$-ligand (**21**), which they applied in *in situ*-cationization in combination with cocatalyst **A**. Furthermore, Al^{i}Bu$_3$ was added as a scavenger for impurities, producing polyethylene at an activity of 860 $\frac{kg}{mol \cdot h \cdot bar}$ and a PDI as high as 83 with 6 bar ethylene pressure at 36 °C. As very broad MWDs were observed, it is likely that several active species are present in the activated system. In addition, Mountford and coworkers reported an uncontrolled homolytic chain transfer process beyond

the well known chain transfer ability of Al^iBu_3 which further enhanced the polydispersity. As no crystals of the active cationic species could be obtained, a non-polymerizing thf-coordinated cationic species (**22**) was synthesized as a model system. It is produced by the addition of the ligand to precationized $[Sc(CH_2SiMe_3)_2(thf)_x]^+$ (**20a**), which is obtained from applying cocatalyst **B** on **20**, the precursor in the synthesis of the actual precatalyst (**21**, see Scheme 1.9) or by direct application of cocatalyst **A** on **21**. Further, the system was also tested in the polymerization of α-olefins (*vide infra*).

1.2.2.2 α-Olefin Polymerization including Styrene Polymerization

The field of α-olfin polymerisation was opened in 1998, when Bochmann and coworkers polymerized isobutylene applying a single component initiator, namely $[(Cp^{H_4SiMe_3})_2Y][(MeBAr^F{}_3)]$ (**24**), as species derived from $[(Cp^{H_4SiMe_3})_2YMe]_2$ (**23**).[73] The crystal structure of the initiator contains an ion pair that shows close contacts of one BAr^F fluorine atom and two methyl hydrogen atoms to the Y center.[54] Although the polymer yields were quite low (2.6 % and 5.8 % resp.) and the obtained PDIs were rather high (>2), these results are remarkable as this initiator is one of the rare Ln centered examples[74–76] that can polymerize isobutylene at all. Interestingly, the polymers were produced below the boiling point of isobutylene (-6.9 °C) at temperatures of -78 and -50 °C.[77]
It is noteworthy, that the authors did not expect the polymerization to be catalytic. Instead, a carbocationic mechanism was suggested, where **24** serves as an initiator. This is also the reason for the high monomer concentration, applied in the polymerization experiments of this study. Lastly, it shall be mentioned that *in situ* generation of the initiator applying **23** and cocatalyst **A** in toluene instead of CH_2Cl_2 led to similar polymers.

The first ion pair that truely qualified as a single-component catalyst in α-olefin polymerization[78] was investigated by the group of Hou and coworkers in 2004.[61] The precatalysts of type Cp'ScR_2 (where Cp' = $C_5Me_4SiMe_3$ and R represents a large variety of different actor ligands) have been studied intensively by Hou and coworkers.[61, 64, 65, 79] Such complexes have been tested with various monomers including α-ole-

fins.[23] The investigations started off, when Hou and his coworker at that time, Cui, investigated tetrameric hydrido clusters of the Cp'Sc-moiety (**14**, **14a** and **14b**).[61] Despite successful reactions with a wide variety of non-α-olefinic monomers, attempts at styrene polymerization only led to an allyl-bonded styrene ligand when a large excess of monomer was used. In keeping with the $CpScR_2$ construct, an aminobenzyl deriviative [Cp'Sc(*o*-$CH_2C_6H_4NMe_2)_2$] (**25**) was synthesized (see Scheme 1.10), and because of its succesful production of the first poly-α-olefin (in the form of poly-1-hexene), it was also patented.[64, 80–87] In the first study utilizing this catalyst both homo-poly-1-hexene and its copolymers with dicyclopentadiene as comonomer were obtained (Table 1.2, runs 2–6). It is unfortunate for the purpose of this chapter, that the poly-1-hexene is only reported for the *in situ* formed catalyst in the reaction of the precatalyst (**25**) with cocatalyst **B**, resulting in a polymer with a PDI of 1.7 (at an activity of 3.1 $\frac{kg}{mol \cdot h}$) and no polymer produced from the isolated active species was published. PDI and activity were found in the same range for the copolymers in which the ratio of found comonomer content nearly equals the ratio of comonomer feed. The copolymer findings with dicyclopentadiene are independent of the use of either the *in situ* generated analogue applying cocatatyst **B** or the preformed catalyst [Cp'Sc(*o*-$CH_2C_6H_4NMe_2$)][$BAr^F{}_4$] (**26**). Besides, the crystal structure of the catalyst contains close contacts between the Sc center and the [$BAr^F{}_4$] anion (*via* two fluorine atoms). Interestingly, the hexene content of the copolymer increased, when cocatalyst **A** was used instead of **B** for the *in situ* catalyst formation.

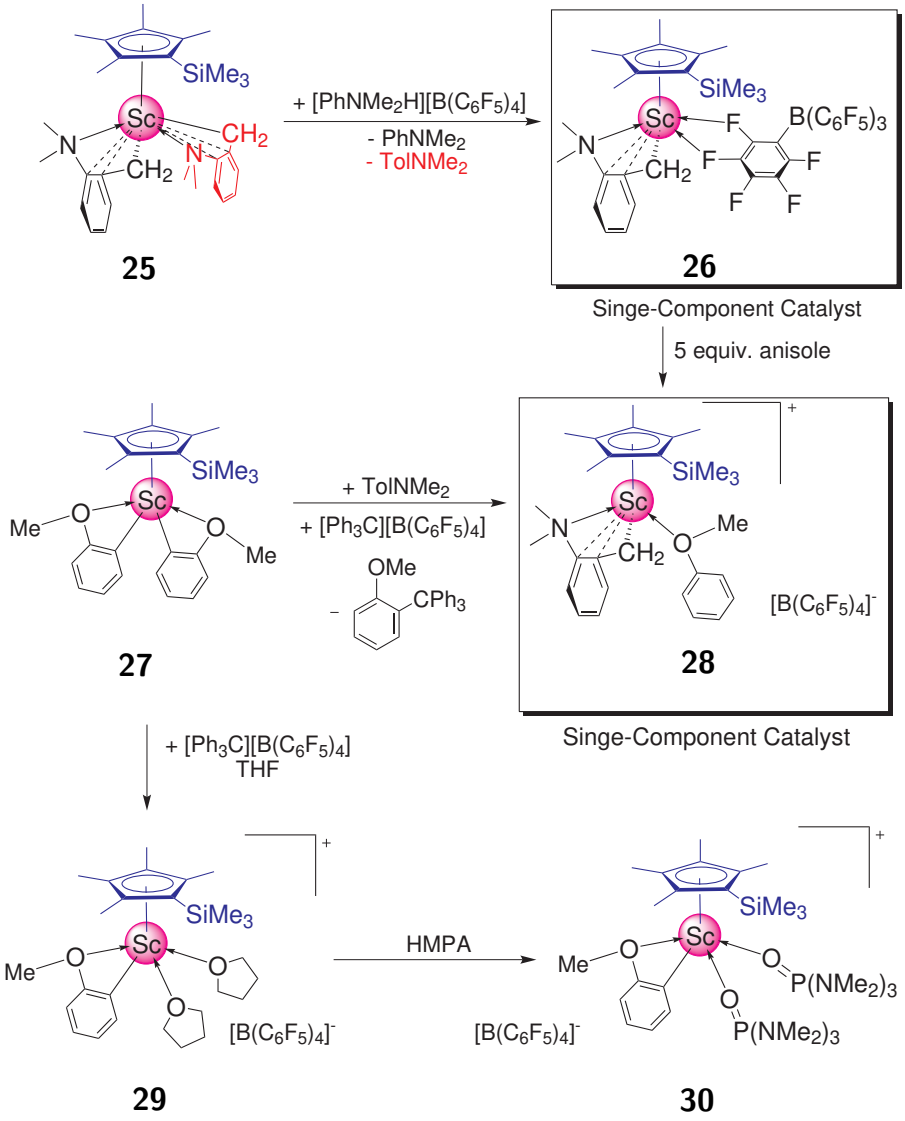

*Scheme 1.10: Synthesis of the ion pair [Cp'Sc(o-$CH_2C_6H_4NMe_2$)][$BAr^F{}_4$] (**26**) from the neutral bisalkyl (**25**) applying cocatalyst **B** and reaction coordinating anisole to form **28**. Second route for the synthesis of **28** from **27** and reaction of **27** to the model species **29** and **30**. Scheme according to refs. 64 and 92.*

*Table 1.2: Comparison of the α-olefin polymers produced with [Cp'Sc(o-$CH_2C_6H_4NMe_2$)$_2$] (**25**) and chain shuttling species [Cp'Sc(o-$CH_2C_6H_4NMe_2$)(anisole)][$BAr^F{}_4$] (**28**) and [Cp'Sc(o-anisyl)$_2$] (**27**).*

Entry[a]	Precatalyst	Cocatalyst[b]	Monomer[c]	Activity [$\frac{kg}{mol \cdot h \cdot bar}$]	M_n[d] [10^4g·mol^{-1}]	PDI[d]	MC 1[e] [%]	MC 2[e] [%]	MC 3[e] [%]	Ref.
1	**25**	**A**	Propylene[k]	5	1.3	2.65	100	—	—-	88
2	**25**	**A**	1-Hexene	3.1	3.5	1.70	100	—	—	64
3	**25**	**A**	DiCp	0.5	—	—	100	—	—	64
4	**25**	**B**	1-Hex, DiCp	2.9	1.5	1.55	46	54	—	64
5	**25**	**A**	1-Hex, DiCp	3.8	1.4	1.60	52	48	—	64
6[f]	**25**	—	1-Hex, DiCp	3.4	1.5	1.62	48	52	—	64
7	**25**	**A**	Styrene	3 125	25.2	1.53	100	—	—	91
8	**28**[l]	—	Styrene	4.6	1.2	2.7	100	—	—	92
9	**27**	**A**	Styrene	3 120	13.9	2.1	100	—	—	92
10	**25**[m]	**A**	Styrene	46.3	0.3	2.6	100	—	—	92
11[g]	**25**	**A**	*p*-MeSt	> 3 540	43.5	1.98	100	—	—	99
12	**25**	**A**	Hexadiene	28.1	1.6	2.56	100	—	—	91
13	**25**	**A**	St, Hexad	59.2	4.1	2.29	74	22/4[h]	—	91
14	**25**	**A**	St, Et, Hexad	1 179	11.0	1.53	32	50	17/1[h]	91
15[g]	**25**	**A**	Heptadiene	123	5.1	2.02	100	—	—	95
16[g]	**25**	**A**	St, Heptad	n. d.	n. d.	n. d.	n. d.	n. d.	n. d.	95
17[g]	**25**	**A**	St, Et, Heptad[i]	1 301	5.4	2.42	49	28	17/6[j]	95
18[g]	**25**	**A**	*p*-MeSt, Et	1 665	16.9	1.75	55	45	—	99
19	**25**	**A**	VPDMS	3 160	11.6	2.16	100	—	—	98
19a[g]	**25**	**A**	VPDMS	> 4 374	57.5	1.48	100	—	—	99
20[g]	**25**	**A**	VPDMS, Et	2 070	16.7	1.53	55	45	—	99
21[g]	**25**	**A**	*p*-ClSt	38	5.0	2.00	100	—	—	100
21a[g,n]	**25**	**A**	*p*-ClSt	505	4.5	3.27	100	—	—	100
22[g]	**25**	**A**	*p*-FSt	4	2.4	2.49	100	—	—	100
23[g]	**25**	**A**	*p*-FSt, Et	4 279	18.4	1.95	81	19	—	101

[a] Conditions: r.t., toluene, [Sc] = [Cocat] = 19 µmol – 40 µmol in 5 mL – 8 mL solvent, equimolar addition of the liquid monomers at ca. 1 bar of the gaseous monomers.;
[b] **A** = [Ph_3C][$B(C_6F_5)_4$], **B** = [$PhNMe_2H$][$B(C_6F_5)_4$], **C** = [$B(C_6F_5)_3$] ;
[c] 1-Hex = 1-hexen; DiCp = dicyclopentadiene; St = styrene; Hexad = 1,5-hexadiene; Heptad = 1,6-heptadiene; Et = ethylene; *p*-MeSt = paramethylstyrene; VPDMS = paradimethylsilystyrene; *p*-ClSt = parachlorostyrene; *p*-FSt = parafluorostyrene;
[d] Determined by GPC against Polystyrene standards;
[e] MC = monomer content; determined by ^{1}H and ^{13}C NMR spectroscopy;
[f] Activated form [Cp'Sc(*o*-$CH_2C_6H_4NMe_2$)][$BAr^F{}_4$] (**26**) is applied;
[g] Solvent PhCl;
[h] 1,5-Addition as a 5-membered ring / vinylic addition;
[i] Feed St / Heptad = 3 / 2;
[j] Methylene-1,3-cyclohexane units / ethylene-1,2-cyclopentane units;
[k] Propylene pressure: 2 bar;
[l] Chain shuttling polymerization, obtaining a molar ratio of anisole / dimethylaminotoluene chain ends of of 62 /38;
[m] Chain transfer polymerization applying 5 mol% of 2-dimethylaminotoluene as chain transfer agent, obtaining triades of mr = 99 %;
[n] Bulk polymerization;

Astonishingly, with **25** and three other precatalysts in combination with cocatalyst **A**, Li and coworkers[88] achieved atactic homopolymerization of propylene (Table 1.2, run 1). Although **25** / **A** belongs to the lesser active systems in their study, activities around 5 $\frac{kg}{mol \cdot h \cdot bar}$ were obtained applying a pressure of 0.2 MPa (approx. 2 bar). The authors ascribe the low activity to a coordination of the solvent (toluene) to the activated species. It must be mentioned, that the systems applied in this study are among few examples of lanthanide-centered catalysts that polymerize propylene at all, instead of forming stable allyl complexes. However, this observation is chronologically the second mention of this remarkable feature as Kempe and coworkers[70] had polymerized propylene already in 2011 with a structurally known catalyst (*vide infra*).[89]

By applying the same *in situ* generated systems (**25** / **A** and **25** / **B**), the homopolymerization of styrene occurred (Table 1.2, run 7).[90, 91] Syndiotactic polystyrene was obtained in nearly full conversion (98 %) after one minute (PDI =1.5 - 1.7; 0.2 chains per Sc center at 3,215 $\frac{kg}{mol \cdot h}$). Recently, **25** / **A** was also applied in a styrene chain transfer polymerization (Table 1.2, run 10).[92] Here, 5 mol% dimethylaminotoluene were added as chain transfer agent (CTA). Purely syndiotactic polystyrene (99 % *rrrr*) was obtained with an activity of 46.30 $\frac{kg}{mol \cdot h}$ and 13.7 chains per Sc center. Furthermore, with this system (**25** / **A**), chain shuttling polymerization was investigated as well, where polystyrene was obtained in lower activity (4.6 $\frac{kg}{mol \cdot h}$) applying anisole as chain shuttling agent (CSA).[93] The active chain shuttling initiation species used for this purpose ([Cp'Sc(*o*-$CH_2C_6H_4NMe_2$)(anisole)][$BAr^F{}_4$] (**28**)), could be crystallized and serves as single-component catalyst (Table 1.2, run 8). Hou and coworkers[92] present

furthermore a second synthetic route yielding **28** *via* [Cp'Sc(*o*-anisyl)$_2$] (**27**). **27** is highly active itself (3,120 $\frac{kg}{mol \cdot h}$ Table 1.2, run 9) when activated by cocatalyst **A** and a model compound for its active species was targeted. [Cp'Sc(C_6H_4OMe-*o*)(hmpa)$_2$][$BAr^F{}_4$] (**30**) could be obtained from the activation reaction in THF and subsequent reaction with of hexamthyl phosphoric triamide (HMPA) in PhCl. Both **30** and the isolated but not crystallized thf-adduct **29** (Scheme 1.10) showed no activity in styrene polymerization.

Li and coworkers[88] applied **25** / **A** in a copolymerization attempt of propylene and styrene in 2017. However, as product, only styrene homopolymer was obtained.

Styrene copolymers with comonomers such as non-conjugated dienes have also been obtained from this catalyst (**25** / **A**) along with their terpolymers with non-conjugated dienes and ethylene (see Table 1.2).[91, 94, 95] Bipolymers with α,ω-dienes, attempted with both hexa- and heptadiene could only be obtained with hexadiene, while in case of heptadiene a blend of the respective homopolymers was the product.[96] The copolymerization with hexadiene shows a clear tendency towards styrene addition to form large syndiotactic polystyrene segments (Table 1.2, run 13). The relatively low activity ($< 100 \frac{kg}{mol \cdot h}$) of the system in this bipolymerization with hexadiene is remarkable, when compared to that occuring in the terpolymerizations (with hexa- or hepatiene), where ethylene is the third monomer ($> 1{,}000 \frac{kg}{mol \cdot h}$) (Table 1.2, run 14). The polyethylene contents in the two terpolymers were quite different, which is probably due to the different solvents used in the polymerizations and their different solubility towards ethylene. While in combination with heptadiene in chlorobenzene

a maximum of 33 % of ethylene content was obtained, applying hexadiene in toluene the lowest ethylene content found was 49 % (maximum = 66 % variing styrene and diene feed at a constant ethylene pressure of 1 bar). Furthermore it shall be mentioned, that the system (**25** / **A**) also polymerizes such styrene derivatives with high syndiotacticity and activity, which contain heteroatoms in the *para*-position to the vinyl-moiety.[97, 98]

Li and coworkers[98] also applied **25** / **A** for syndiotactic homopolymerization of VPDMS (*p*-dimethylsilyl-styrene) (Table 1.2, run 19). In toluene, an activity (3,160 $\frac{kg}{mol \cdot h}$) even slightly higher than with styrene was observed. The polymeric product was applied as educt in a polymer reaction with perylene bisimide. In collaboration with Hou and coworkers,[99] the authors also polymerized further substituted styrenes applying **25** / **A**. While polymerization of α-methylstyrene remained unsuccessful, high activity was achieved with *p*-methylstyrene ($>$ 3,540 $\frac{kg}{mol \cdot h}$) and VPDMS ($>$ 4,374 $\frac{kg}{mol \cdot h}$in PhCl) (Table 1.2, runs 11 and 19a). Homopolymers of divinylbenzene and *p*-butylenylstyrene were achieved with slightly lower activity. With *p*-methylstyrene and VPDMS, Hou and coworkers[99] also performed copolymerization experiments with ethylene. Applying an ethylene pressure of $1.01 \cdot 10^5$ Pa (approx. 1 bar) to their polymerization setup, this was achieved with comonomer loads of 400 equiv. per Sc center in good activities (1,665 $\frac{kg}{mol \cdot h}$ for *p*-methylstyrene and 2,070 $\frac{kg}{mol \cdot h}$ for VPDMS) (Table 1.2, runs 18 and 20).

In the following year, the two groups, Hou and coworkers[100] and Li and coworkers[101] targeted the polymerization of halogenated styrene in two studies. In *para*-position, halogens (F, Cl, Br, I) were tested, while for chlorine the position at the arene ring was varied. In contrast to the other halo-

gens with chlorine only pentades of pure stereoregularity (*rrrr* >99 %) were obtained independent of its position. The activity was influenced both by the monomer concentration and the location of the halogen atom. A maximum of 38 $\frac{kg}{mol \cdot h}$ was reached for chlorine in *para*-position with 500 equiv. monomer per Sc center in the most concentrated case and 505 $\frac{kg}{mol \cdot h}$ in bulk polymerization (see Ref. 100, Table 1 for details and Table 1.2 for examples). Fluorine substituted arenes showed the lowest activity in this study. When copolymerizing the halogenated monomers with unsubstituted styrene, Hou and coworkers[100] obtained comonomer contents that equal the feed rations throughout the study. The activities, however, remained low, if the halogenated monomer was fed in equal ratios or higher to the styrene. Still, polymers with a halogenated styrene content of 25 % could be achieved in good activity for all halogens (Ref. 100, Table 2). A "comonomer effect"[102] allowed high activities (up to 4.279 $\frac{kg}{mol \cdot h}$) in the copolymerization of *p*-fluorostyrene and ethylene, compared to those of the homopolymerization of *p*-fluorostyrene (4 $\frac{kg}{mol \cdot h}$) (Table 1.2, run 22).[101] Interestingly, even comonomer contents of *p*-fluorostyrene far above 50 % were easily achieved in moderate dispersity (see Table 1.2, run 23, as an example).

In the same year, Hou and coworkers[103] presented a study of polymerization of α-olefins containing donor atoms of the motif (H_2C=CH-$(CH_2)_2$-E-Ph_n). Although **25** / **A** revealed not to be efficient in the homopolymerizations of these monomers, copolymerizations with ethylene afforded high yields for three of the tested monomers. Interestingly, the polymerization attempt applying butenyl phenyl ether was not successful at all, but prolonging the monomer by one methylene unit enabled the copolymerization. Due to the

"comonomer effect"[102] also polymers for butenyl phenyl thioether (E = S, n = 1) and butylenyl diphenylphosphane (E = P, n = 2) were achieved in low to moderate activities (3.3 $\frac{kg}{mol \cdot h}$ and 64.4 $\frac{kg}{mol \cdot h}$, respectively). Pentenyl phenyl ether (the prolonged version of E = O, n = 1) showed moderate activity as well (20.5 $\frac{kg}{mol \cdot h}$).
Besides all these polyimerization applications, **25** / **A** has also been shown to be active in α-C–H alkylation catalysis.[104]

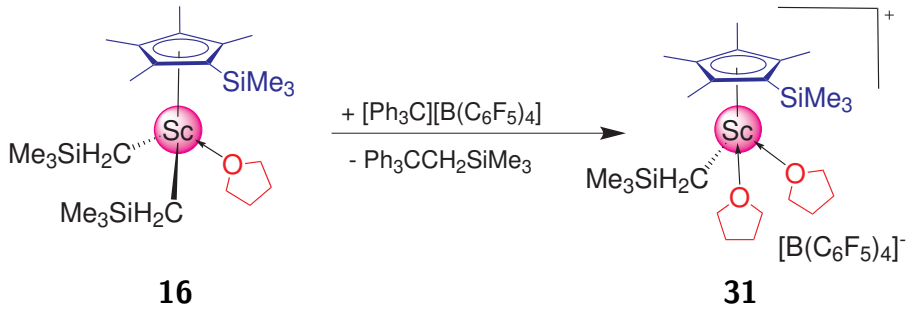

*Scheme 1.11: Synthesis of the ion pair [Cp'Sc(CH_2SiMe_3)(thf)$_2$][$BAr^F{}_4$] (**31**) from the neutral bisneosilyl (**16**) applying cocatalyst **A**. Scheme according to ref. 65.*

A further set of coligands was investigated by Hou and coworkers in 2009.[65] While two neosilyl groups are the respective alkyls of the Cp'ScR_2 motif in this case, a thf ligand is necessary to sterically satisfy the precatalyst **16**. A cationic model complex containing a second THF molecule **31** (see Scheme 1.11) was published together with the results of the isoprene and ethylene polymerization[65] (also see the corresponding patents in refs. 80, 82, 106, 107, 125–127, 309–311). Recently,[88] the system was tested in the polymerization of propylene in combination with cocatalyst **A** (Table 1.3, run 1). Activities as high as 488 $\frac{kg}{mol \cdot h \cdot bar}$ might surprise, as rare-earth metal complexes are known to rather form stable allyls with propylene

*Table 1.3: Comparison of the α-olefin-(co)polymers produced with [Cp'Sc(CH_2SiMe_3)$_2$(thf)] (**16**).*

Entry[a]	Cocatalyst[b]	Monomer[c]	Activity $[\frac{kg}{mol \cdot h \cdot bar}]$	M_n[d] $[10^4 g \cdot mol^{-1}]$	PDI[d]	MC 1[e] [%]	MC 2[e] [%]	MC 3[e] [%]	Ref.
1	**A**	Propylene[k]	488	2.0	2.05	100	—	—	88
2	**A**	Pr, Et[l]	1 148	2.8	1.79	50	50	—	88
3	**A**	Styrene	3 125	8.9	1.38	100	—	—	66
4	**A**	Styrene, Et	2 314	15.1	1.26	87	13	—	66
5	**A**	DiCp	80	n.d.	n.d.	100	—	—	109
6	**A**	Styrene, DiCp	—	—	—	—	—	—	109
7	**A**	St, DiCp, Et	600	51.1	1.45	57	7	36	109
8[f]	**A**	St, DiCp, Et	1 800	38.1	1.42	4	26	70	109
9	**A**	Hexadiene	2 471	n.d.[g]	n.d.	n.d.	n.d.	n.d.	91
10	**A**	St, Hexad	21	1.5	1.70	100	0	—	91
11	**A**	Heptadiene	171	0.3	6.21	100	—	—	174
12[h]	**A**	St, CL	—	2.7	1.32	81	19	—	110
13	**A**[i]	Isobutylene	—	22.1	1.82	100	—	—	108
14	**A**[i]	IB, IP[j]	—	6.3	1.77	98.8	1.2	—	108
15	**A**	Et, Pr, IP	1 400	n.d.	n.d.	84	9	7	105
16	**A**	p-ClSt	> 414	8.1	2.20	100	—	—	100
17	**A**	p-ISt	683	4.5	1.10	100	—	—	100
18	**A**	p-FSt[m]	704	8.3	3.20	100	—	—	101
19	**A**	p-FSt[m]	1 303	18.8	3.03	100	—	—	101
20	**A**	p-FSt, Et	3 568	14.2	1.54	88	12	—	101

[a] Conditions: r.t., 1 atm, toluene, [Sc] = [Cocat] = 19 – 21 μmol in 5.5 mL – 40 mL solvent, equimolar addition of the liquid monomers at ca. 1 bar of the gaseous monomers.;
[b] **A** = $[Ph_3C][B(C_6F_5)_4]$, **B** = $[PhNMe_2H][B(C_6F_5)_4]$, **C** = $[B(C_6F_5)_3]$;
[c] DiCp = dicyclopentadiene; St = styrene; Hexad = 1,5-hexadiene; Et = ethylene; Pr = propylene; IB = isobutylene; CL = ε-caprolactone; *p*-ClSt = parachlorostyrene; *p*-ISt = paraiodostyrene; *p*-FSt = parafluorostyrene;
[d] Determined by GPC against Polystyrene standart;
[e] MC = monomer content; determined by ^1H and ^{13}C NMR spectroscopy;
[f] Feed ratio: St / DiCp = 6 / 1;
[g] Insoluble crosslinked polymers were obtained;
[h] Feed ratio: St / CL = 3 / 1 in subsequent monomer addition resulting in block-copolymer formation;
[i] Reaction temperature: -35 °C;
[j] IP feed: 3 %;
[k] Propylene pressure: 2 bar;
[l] Propylene / ethylene feed ratio: 5 / 1;
[m] Run 18: [p-FSt] / [Sc] = 1000, Run 19: [p-FSt] / [Sc] = 2000;

than to catalyze its polymerization. Nevertheless, the results of this study discover this conclusion to be not true as a general statement. With PDIs around 2 the obtained atactic polypropylene chains are moderately uniform.

The system **16** / **A** does also homopolymerize isobutylene (Table 1.3, run 13),[108] which is a rarely found property among rare-earth metal catalysts as well. The polymerizations were performed at low temperatures (around -35 °C). High yields and moderate polydispersion were obtained. However,

the fact that isobutylene is polymerized at all is the by far most remarkable feature of this study.

Interestingly, copolymerizations applying ethylene and propylene[88] (Table 1.3, run 2) resulted in much higher propylene contents in the polymer than in the feed, suggesting a much higher affinity of the active species to this monomer. The activity though is much higher than in the homopolymerization of propylene (1,148 $\frac{kg}{mol \cdot h \cdot bar}$ for a 5 / 1 feed of propylene / ethylene. Interestingly, the obtained copolymers are amorphous, probably due to the high propylene content.

In 2004, styrene polymerization by applying the precatalyst (**16**) and cocatalyst **A** was investigated[66] and continued in 2005,[109] 2010[110] and 2011[91, 111] where syndiotactic polystyrene (> 99 %) was obtained in quantitative yield after 1 min (PDI = 1.25 – 1.38 at 3,125 $\frac{kg}{mol \cdot h}$, 0.44 – 0.58 chains per Sc center) (Table 1.3, run 3). Styrene copolymers with several comonomers were also examined. Styrene-ethylene-copolymers were already targeted in 2004[66] (Table 1.3, run 4) and investigated in a QM/MM-study[112] in 2011.[113] Applying 1 atm (ca. 1 bar) of ethylene to their standard styrene polymerization procedure on a *in situ* generated system with cocatalyst **A**, the authors obtain multiblock-copolymers with catalytic activities rising with styrene feed up to 2,314 $\frac{kg}{mol \cdot h \cdot bar}$ and narrower MWDs in the copolymer than in the styrene or ethylene homopolymer. The subsequent computational study, where Cp' is simplified to Cp^*, enlightens the energetic preference of the unusual 2,1-insertion of styrene obtained in this context and explains the multiblock nature of the obtained copolymer.[113]

In 2017, styrene propylene copolymerization was targeted by Li and

coworkers.[88] Here, relatively low activities were obtained. Still both comonomers were incorporated into the copolymers in ratios that mirrored the ratios of feed. Compared to the homopolymerization, the PDIs were rather low. In terpolymerization of the two monomers with ethylene, Li and coworkers[88] found much higher activities (up to 465 $\frac{kg}{mol \cdot h \cdot bar}$). The observed polydispersities were lower than in case of propylene homopolymerization or styrene propylene copolymerization and similar to those obtained from styrene ethylene copolymerization. Interestingly, the observation of the affinity for propylene addition in the propylene ethylene copolymerization cannot be confirmed here, as propylene units are by far underrepresented in the terpolymer, compared to the feed.

An attempt by Hou and coworkers to apply the **16** / **A** system in the copolymerization of styrene and dicyclopentadiene failed (Table 1.3, run 6) and even the homopolymerization of styrene was inhibited in the presence of dicyclopentadiene.[109] However, Hou and coworkers obtained activities up to 1,800 $\frac{kg}{mol \cdot h \cdot bar}$ (600 $\frac{kg}{mol \cdot h \cdot bar}$ at equimolar feed (styrene vs. dicyclopentadiene)) by applying an ethylene atmosphere of ca. 1 bar to the styrene / dicyclopentadiene copolymerization reaction mixture. The resulting terpolymers showed low PDIs (1.21–1.45) and surprisingly high styrene contents (see Table 1.3, run 7 for an example). This reactivity toward these terpolymers was ascribed to a "comonomer effect"[102, 114] with a preference of the ethylene chain ends to add styrene as subsequent monomer.

In case of the styrene copolymerization with non-conjugated α,ω-hexadiene, only a styrene homopolymer was obtained, although the system is known to be active in the homopolymerization of the diene[91]

(*vide infra*). With **16 / A**, high yields were also achieved throughout the series of halogenated styrene polymerization.[100, 101] Both the position of the halogen atom at the arene ring and the nature of the halogen element itself have been screened in this study. The position of a chlorine atom *para* to the vinyl moiety is only slightly favored with this catalyst. Only, with the halogen in *meta* position a syndiotactic polymer was obtained, while the polymers remained atactic in all other cases. Studying the nature of the halogen atom itself in *para* position, led to a remarkable uniform polymer when *p*-iodostyrene was applied, which was produced with high activity ($683\,\frac{kg}{mol \cdot h}$) (Table 1.3, run 17). For the *p*-halogenated styrene monomers also a copolymerization with styrene was tested. The contents of comonomer in the polymer almost equaled the feed ratios. High activities were obtained throughout the series, while the PDI increased with increasing halogen radius. So the narrow MWDs obtained in *p*-iodostyrene homopolymerization did not find its expression in these copolymers even at high feed ratios. Due to its highly active performance in *p*-fluorostyrene polymerization (up to $1{,}300\,\frac{kg}{mol \cdot h}$) (Table 1.3, run 19), **16 / A** was also tested in the copolymerization with ethylene. Here, another "comonomer effect"[102] drove the activity up to $3{,}568\,\frac{kg}{mol \cdot h}$, even with a *p*-fluorostyrene incorporation of 88 % (Table 1.3, run 20).

Non-conjugated α,ω-heptadiene was homopolymerized (see Table 1.3, run 11) and copolymerized with isoprene (*vide infra*) with this system (**16 / A**) as well. A block-copolymer with ε-caprolactone could be achieved by subsequent monomer addition. Interestingly, although the system polymerized ε-caprolactone in full yield in 5 min, the comonomer contents in the styrene-ε-caprolactone copolymer did not match the feed

ratio. Instead the ε-caprolactone-blocks remained rather short even after 30 min.[110]

In 2017, Hou and coworkers[103] tested the system **16** / **A** also in the polymerization catalysis of α-olefins incorporating donor atoms. As the homopolymerization of these monomers was ineffectively slow, they decided to make use of the "comonomer effect"[102] once more and tested it in the copolymerization with ethylene. However, both for butenyl phenyl thioether and pentenyl phenyl ether, the activities remained low (2–10 $\frac{kg}{mol \cdot h}$) and so did the incorporation ratios for the donor comonomers as well ($< 40\,\%$).

Finally, in a study from 2011 a styrene-isoprene-copolymer was obtained from a chain shuttling setup.[111] As secondary catalysts serve two species ([CpSc(CH_2SiMe_3)$_2$(thf)] and [(Dipp$_2$-benzimidinate)Sc(CH_2SiMe_3)$_2$(thf)]), which are known for their rapid and selective performance in isoprene polymerization (as [Cp'Sc(CH_2SiMe_3)$_2$(thf)] (**16**) polymerizes isoprene with unselective microstructure and relatively slowly.[65]).

Besides these polymerization applications, the catalytic system **16** / **A** was also tested in the α-C–H-alkylation of methyl sulfides.[104]

In this series of studies Hou and coworkers also investigated an *o*-anisole substituted Cp ligand with [Cp$^{Me_4(o\text{-anilsole})}$Y($CH_2SiMe_3$)$_2$] (**17**) as a precursor.[65] A cationic species was also accessible as a thf-adduct, by applying cocatalyst **B**. Although [Cp$^{Me_4(o\text{-anilsole})}$Y($CH_2SiMe_3$)(thf)$_2$][BAr$^F{}_4$] (**32**) can only serve as a model species as it is not active in polymerization itself, its *in situ* generated analogue polymerizes styrene in 1 min to full conversion (at 3,125 $\frac{kg}{mol \cdot h}$).[91, 110] With this system the block-copolymer

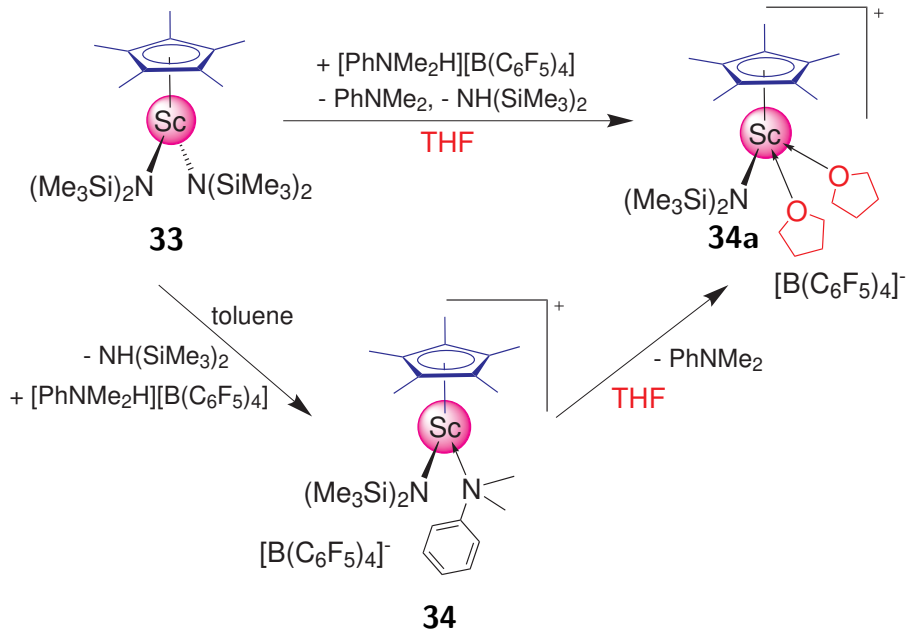

*Scheme 1.12: Synthesis of the model compound $[Cp^*Sc\{N(SiMe_3)_2\}(thf)_2]$ (**34a**) from the neutral bisamide (**33**) applying cocatalyst **B** and synthesis of the intermediate $[Cp^*Sc(N(SiMe_3)_2)(PhNMe_2)]$ (**34**). Scheme according to ref. 115.*

with ε-caprolactone[110] and the styrene-hexadiene-copolymer[91] have been targeted as well. Similar results as in the Cp' case have been achieved. So the styrene-hexadiene copolymerization led to styrene-homopolymer, and the block-copolymer with ε-caprolactone resulted in a significantly higher styrene content than what was fed.

In the cationic species, the steric saturation due to the presence of the thf ligand eliminates the possibility of a direct ion-ion-interaction in the model species for both systems in this study. But as the active, *in situ* generated species are produced in thf free environments, they are not necessarily sterically saturated and therefore, an ion-ion-contact is still possible.

Another Cp-based system, that was published in the context of structu-

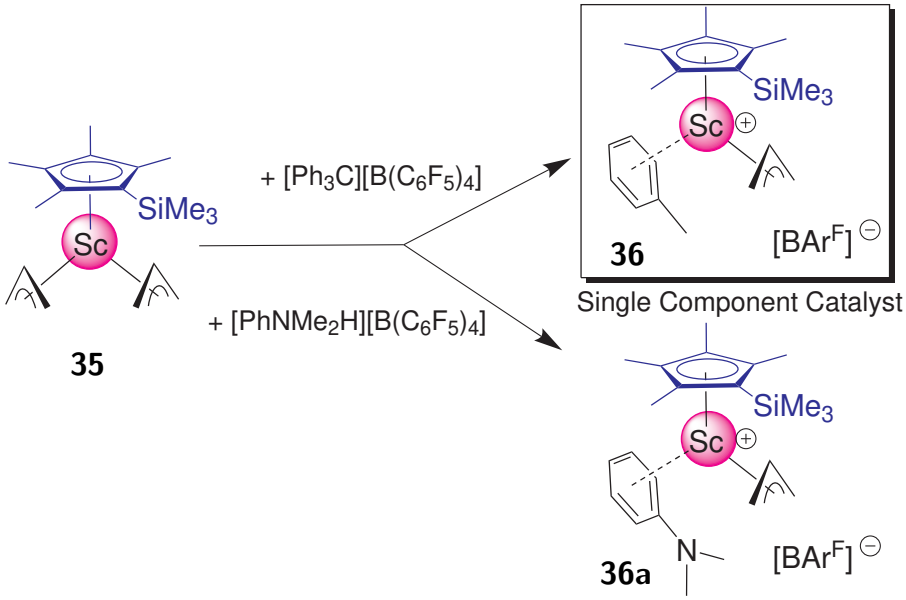

*Scheme 1.13: Synthesis of the two active species (**36** and **36a**) derived from the Cp'Sc bisallylic precursor (**35**) according to ref 79.*

rally proven active Ln-species for α-olefin-polymerization was crystallized by Luo and coworkers in 2014.[115] The $[Cp^*Sc\{N(SiMe_3)_2\}(thf)_2]$ (**34a**) cation, produced by subsequent reactions of the corresponding bisamide (**33**) with cocatalyst **B** in toluene and with THF or with cocatalyst **B** in THF (see Scheme 1.12) serves as another model compound as its thf ligand leads to steric saturation and therefore no driving force towards monomer addition remains. The respective intermediate (**34**) could be obtained, but not crystallized. *In situ* generated **34**, however, showed activity in the syndiotactic homopolymerization of styrene[116] in the presence of 10 equiv. of Al^iBu_3. As Al^iBu_3 is known to be active as a chain transfer agent, the high molecular weight of the resulting polymer can only be explained by a very small amount of active metal centers.

The final Cp-based system to be mentioned in this section, $[Cp'Sc(allyl)_2]$ (**35**), was synthesized by Hou and coworkers[79] in 2008 (Scheme 1.13) and

applied in the catalysis of cyclic norbornene and its copolymerization with isoprene. Recently, Li and coworkers[88] managed to apply this system in propylene polymerization, where it showed little activity (up to 3.4 $\frac{kg}{mol \cdot h \cdot bar}$) at moderate polydispersities (< 2).[117]

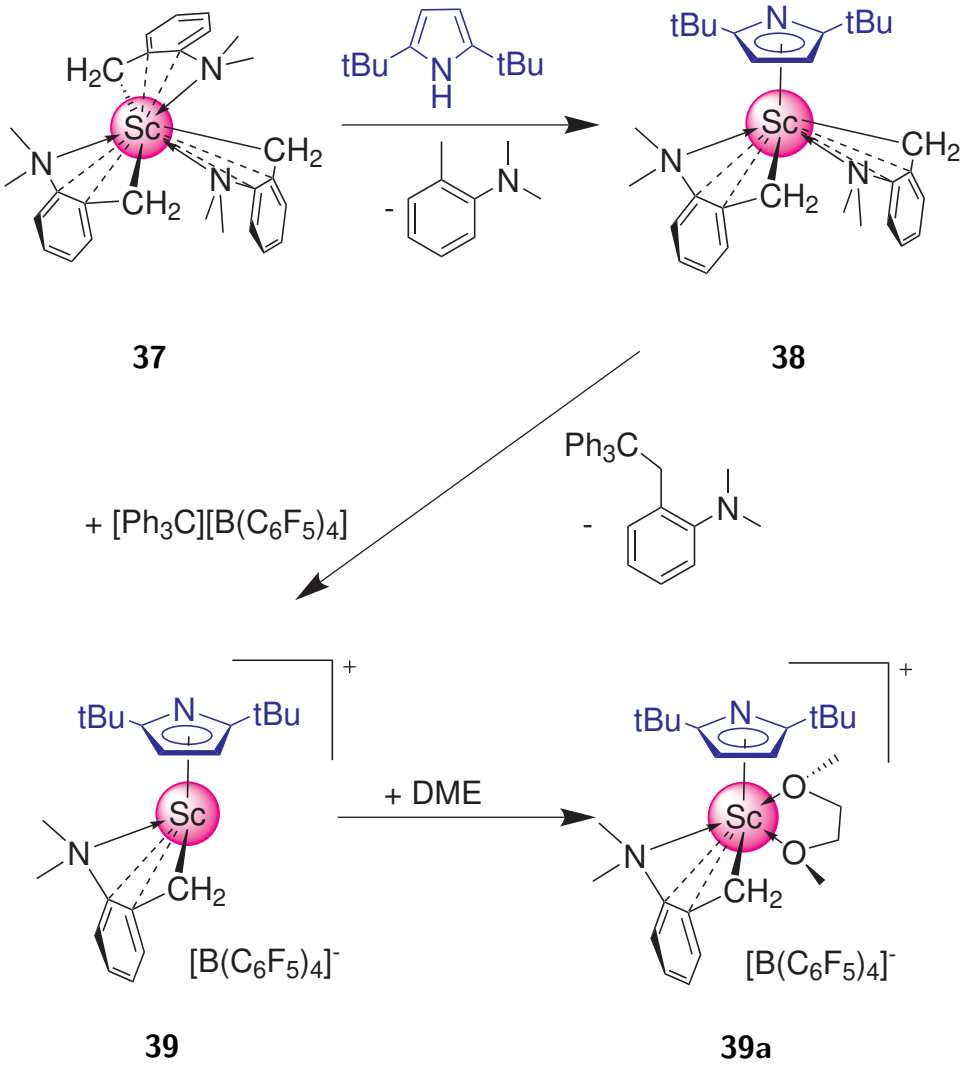

*Scheme 1.14: Synthesis of [(1,4-bistertbutylpyrollyl)Sc($CH_2C_6H_4NMe_2$)][$B(C_6F_5)_4$] (**39**) from the neutral bisaryl (**38**) applying cocatalyst **A** and synthesis of the model compound [(1,4-bistertbutylpyrollyl)Sc($CH_2C_6H_4NMe_2$)(dme)][$B(C_6F_5)_4$] (**39a**). Scheme according to ref. 119.*

The next general group of ligands, whose Ln-bisalkyls and bishydrides are able to polymerize α-olefins by structurally characterized active species are N-donor ligands. Once again, the first representative of this group was published by Hou and coworkers, although the respective species cannot be called a classic N-donor. In 2008,[118, 119] it was shown that [(1,4-bis*tert*butyl-pyrollyl)Sc($CH_2C_6H_4NMe_2$)$_2$] (**38**) forms a cationic species (**39a**) with cocatalyst **A**, further stabilized by dme (see Scheme 1.14). Both the non-stabilized single component catalyst (**39**, not crystallized) and the *in situ* generated active species (**38** / **A**) polymerized styrene in full yield in less than 1 min with high activity ($> 3{,}100\,\frac{kg}{mol \cdot h}$) and full syndiotacticity, while the stabilized compound (**39a**) is inactive. Still, the molecular weight of the polymer was higher than expected, which means that not all Sc centers are active in polymerization (e.g., only every third to fifth is active.). The rather high PDI (of ca. 2) can be seen as indicative of such an initiation deficit, as well.

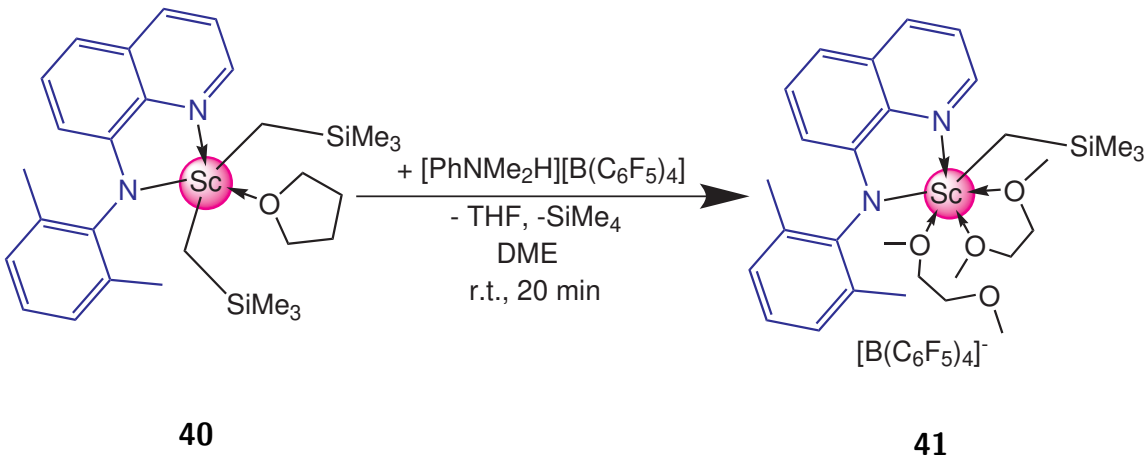

40 **41**

*Scheme 1.15: Synthesis of [LSc(CH_2SiMe_3)(dme)$_2$][B(C_6F_5)$_4$] (**41**) from the corresponding neutral bisneosilyl thf adduct (**40**) applying cocatalyst **B** in DME. Scheme according to ref. 120.*

*Table 1.4: Styrene polymerizations by [(N-o,o-xylyl-amidoquinolyl)Sc(CH_2SiMe_3)$_2$(thf)] (**40**) taken from ref. 120.*

Entry[a]	(Pre)Catalyst[b]	Cocatalyst[c]	Cat / [Al] [equiv.]	Activity $[\frac{kg}{mol \cdot h}]$	M_n[d] $[10^4 g \cdot mol^{-1}]$	PDI[d]
1	[LSc(CH_2SiMe_3)$_2$(thf)] (**40**)	**B**	0	70	2.9	1.70
2	[LSc(CH_2SiMe_3)$_2$(thf)] (**40**)	**B**	5	624	2.8	1.93
3	[LSc(CH_2SiMe_3)(dme)$_2$][$BAr^F{}_4$] (**41**)	—	10	11	1.7	1.96

[a] 10^{-5} mol of Sc complex; in chlorobenzene; monomer / solvent = 5 : 2 (v/v); [Al] = Al^{i}Bu$_3$; 25 °C; [St]/[Sc] = 500; [Sc]/[**B**] = 1 : 1;
[b] L = N-*o*,*o*-xylyl-amidoquinolyl;
[c] **A** = [Ph_3C][$B(C_6F_5)_4$], **B** = [$PhNMe_2H$][$B(C_6F_5)_4$], **C** = [$B(C_6F_5)_3$] ;
[d] Determined by GPC against polystyrene standards;

In 2010, the first classical N-donor system was crystallized and used in polymerization. Cui and coworkers[120] published a Sc-bisneosilyl compound bearing N-*o*,*o*-xylyl-amidoquinolyl as bidentate monoanionic ligand, and a single coordinating THF molecule (**40**). Applying cocatalyst **B** in DME, a bis-dme-adduct ion pair (**41**) could be obtained (Scheme 1.15) that is active in the polymerization of styrene only in the presence of Al^{i}Bu$_3$ (the authors claim this is due to the necessity to remove the dme ligands as Al^{i}Bu$_3$ adducts). The *in situ* generated cationic species, produced in chlorobenzene, and devoid of DME is instead active in styrene polymerization without the addition of any Al^{i}Bu$_3$ as well (see Table 1.4). Comparing the product of the ion pair / Al^{i}Bu$_3$-system with that of the *in situ* generated system with Al^{i}Bu$_3$, it is apparent, that the DME-Al^{i}Bu$_3$-adduct lowers the overal activity and is therefore non-beneficial. Still, comparing the products of the *in situ* generated catalyst with and without Al^{i}Bu$_3$ shows that the activity enhancing effect (next to its chain transfer ability) of the Al^{i}Bu$_3$ cannot be neglected.

The final N-donor system arguably contains the most surprising observation of its time. [{$Ap^*Ln(thf)$}$_2${$Ap^*Ln(CH_2SiMe_3)$}H_5] clusters ($Ap^* = [(C_6H_3{}^iPr_3$-2,4,6)-(*o*-C_5H_3N-*o*)-N-($C_6H_4{}^iPr_2$-2,6)]; Ln = Y (**18**),

Lu (**18^{Lu}**)) as crystallized by Kempe, Trifonov and coworkers in 2011[70] are one of the very rare examples of a lanthanide-centered catalyst for propylene-polymerization. The polymerizations were performed parallel to the corresponding ethylene polymerization[70] (*vide supra*) in toulene at 0 °C and a propylene pressure of 0.5 atm (ca. 0.5 bar).[121] Although the activities[121] of 64 $\frac{kg}{mol \cdot h}$ (Y) and 37 $\frac{kg}{mol \cdot h}$ (Lu) might seem low, the fact that propylene was polymerized instead of forming a stable allyl complex is unexpected and very remarkable. Yet, it must be mentioned, that these results were achieved by the application of the unactivated precatalysts **18** and **18^{Lu}** and not by the corresponding cations **19** and **19^{Lu}** (Scheme 1.8).[49]

The species completing the list of α-olefin polymerizing systems discussed in this chapter consists of the crownether-like [9]aneS$_3$ ligand, bound to [Sc(CH$_2$SiMe$_3$)$_3$] (**21**, see Scheme 1.9) and its corresponding cationic species [{[9]aneS$_3$}Sc(CH$_2$SiMe$_3$)$_2$(thf)]$^+$ (**22**) produced by adding the ligand to the precationized precursor [Sc(CH$_2$SiMe$_3$)$_2$(thf)$_x$]$^+$ (**21a**). This precursor was synthesized by the addition of cocatalyst **B** to the homoleptic Sc-neosilyl bis-thf-adduct (**20**, see Scheme 1.9). Mountford and coworkers[71, 72] reported the activity of the *in situ* generated catalyst applying cocatalyst **A** in the polymerization of 1-hexene with an activity as high as 200 $\frac{kg}{mol \cdot h}$. Adding a second equivalent of the cocatalyst even raises the activity to 3,360 $\frac{kg}{mol \cdot h}$ with 32 % of isotactic *mmmm*-pentads, but a PDI of 32. Furthermore, the system polymerized styrene even faster (13,600 $\frac{kg}{mol \cdot h}$) but the authors did not give any further information about the tacticity and chain properties of the polystyrene.[72]

1.2.2.3 Polymerization of cyclic olefins

In the field of the polymerization of cyclic olefin monomers, four studies involving three cationic systems of the Cp'ScR_2-type with structurally proven active species have been published so far, all three by Hou and coworkers.[38, 64, 79, 109]

The first system, published in 2007 was tested both in the polymerization of dicyclopentadiene and its copolymerization with 1-hexene.[64] The homopolymerization, which was performed by the *in situ* formed catalyst from the reaction of precatalyst [Cp'Sc(o-$CH_2C_6H_4NMe_2$)$_2$] (**25**) with cocatalyst **A**, showed a relatively low activity of 0.5 $\frac{kg}{mol \cdot h}$. Copolymers instead, were produced with higher activity and could be investigated by GPC in contrast to the homopolymers due to their higher solubility. There, both polymers, produced by the single component catalyst [Cp'Sc(o-$CH_2C_6H_4NMe_2$)][$BAr^F{}_4$] (**26**) and the *in situ* generated species, gave similar results (ratio of comonomer feed equals ratio of monomer units in the polymer, activity = 3 $\frac{kg}{mol \cdot h}$, PDI = 1.6, see also Table 1.2 and Scheme 1.10).
In the following year Hou and coworkers published[79] and patented[122–127] a system that polymerized norbornene and copolymerized it with isoprene. [Cp'Sc(allyl)(η^6-Ar)][$BAr^F{}_4$] (**36** and **36a**) was produced from precatalyst [Cp'Sc(allyl)$_2$] (**35**) by applying cocatalyst **A** (Ar = toluene (**36**)) or **B** (Ar = $PhNMe_2$ (**36a**)) (see Scheme 1.13). They both showed a low activity towards homopolymerization of norbornene (ca. 1 $\frac{kg}{mol \cdot h}$) with moderate PDI (1.7 for Ar = $PhNMe_2$ and 1.8 for Ar = toluene) but the copolymers still exhibited a norbornene content of 19 resp. 31 % at equimolar feed after 15 min (see Table 1.8). The latest of the three published systems

*Table 1.5: Comparison of the cyclo-olefin-(co)polymers produced with [Cp'Sc(CH_2SiMe_3)$_2$(thf)] (**16**).*

Entry[a]	Cocatalyst[b]	Monomer[c]	Activity $[\frac{kg}{mol \cdot h \cdot bar}]$	M_n[d] $[10^4 g \cdot mol^{-1}]$	PDI[d]	MC 1[e] [%]	MC 2[e] [%]	Ref.
1	**A**	Norbornene	0.5	n.d.	n.d.	100	—	38
2	**A**	DiCp	80	n.d.	n.d.	100	—	109
3	**A**	NB, Et	8 000	11	1.79	41	59	38
4	**B**	NB, Et	14 200	12	2.78	44	56	38
5	**C**	NB, Et	700	n.d.	n.d.	0	100	38
6	**A**	DiCp, Et	3 000	22	2.28	43	57	109
7[f]	**A**	DiCp, Et	3 100	17	2.38	44	56	109

[a] Conditions: r.t., toluene, [Sc] = [cocat] = 21 µmol (runs 2,6 and 7) and 40 µmol (runs 1, 3 – 5) in 40 mL solvent, equimolar addition of the liquid monomers at ca. 1 bar of the gaseous monomers.;
[b] **A** = $[Ph_3C][B(C_6F_5)_4]$, **B** = $[PhNMe_2H][B(C_6F_5)_4]$, **C** = $[B(C_6F_5)_3]$;
[c] DiCp = dicyclopentadiene; NB = norbornene; Et = ethylene;
[d] Determined by GPC against polystyrene standards;
[e] MC = monomer content; determined by ^{1}H and ^{13}C NMR spectroscopy;
[f] Reaction temperature 50°C;

is [Cp'Sc(CH_2SiMe_3)(thf)$_2$][$BAr^F{}_4$] (**31**),[65] which serves as a model compound for the *in situ* generated cationic species that is formed, when cocatalyst **A** is applied to [Cp'Sc(CH_2SiMe_3)$_2$(thf)] (**16**). Both studies, in which this system polymerized cyclic olefins have been published in 2005 and focus on norbornene and its copolymerization with ethylene[38] and dicyclopentadiene and its copolymerization with styrene and ethylene, as well as the corresponding terpolymerization (see Table 1.5).[109]

Before Hou and coworkers performed the first lanthanide-centered ethylene-norbornene copolymers with this system (a polymer, which has not been structurally accessible yet at that time[38]), they investigated homopolymerizations of both monomers, obtaining low activities (esp. in the case of norbornene: $0.5 \frac{kg}{mol \cdot h}$). However, once more with this system, the activity of the copolymerization with ethylene was much higher, due to a "comonomer effect" (cf. the results involving α-olefins, *vide supra*).[102] Performing the norbornene polymerization in an ethylene atmosphere of ca. 1 bar, led in case of the application of cocatalyst **A** to an activity of

8,000 $\frac{kg}{mol \cdot h \cdot bar}$ and 41 % of norbornene content (PDI = 1.79) in the strictly alternating copolymer (see Table 1.5). By alternation of the norbornene feed, reaction temperature and monomer concentration, the copolymerization conditions were optimized obtaining a maximum in activity of 25,000 $\frac{kg}{mol \cdot h \cdot bar}$ (See Table 2 in ref. 38 for details). Further experiments with a constant ethylene pressure of 1 bar (reacted ethylene was constantly refilled) led to block copolymers consisting of a homopolyethylene and an alternating polyethylene-co-norbornene block. For comparative reasons, cocatalysts **B** and **C** were also tested in standard conditions. In case of cocatalyst **B** an activity of 14,200 $\frac{kg}{mol \cdot h \cdot bar}$ was obtained, which is even higher than under the unoptimized case of cocatalyst **A**. While the norbornene contents were almost identical, for these two polymers, the PDI of the polymer produced by the system with cocatalyst **B** was much higher (2.78). In contrast, in case of cocatalyst **C** pure homo-polyethylene was the product.

Shortly after their norbornene study, Hou and coworkers investigated the system in the polymerization of the larger dicyclopentadiene (see Tables 1.3 and 1.5).[109] Its homopolymerization only resulted in very low conversions of 2 %, but in case of the copolymerizations another "comonomer effect" was observed.[102] While the bipolymerization with styrene was not observed, when attempted, that with ethylene gave high yields within 5 min at high activities up to 3,000 $\frac{kg}{mol \cdot h \cdot bar}$ at 25 °C and even 3,100 $\frac{kg}{mol \cdot h \cdot bar}$ at 50 °C. Compared to the ethylene-norbornene copolymers of the previous study,[38] effects of the larger monomer size of the cycloolefin were observed, especially in terms of a lower activity and a slightly higher PDI. In terpolymerizations[109] of dicyclopentadiene and ethylene with

*Table 1.6: Polar Olefin homopolymerization by **44** and **45**, data taken from ref. 128.*

Entry[a]	Precatalyst	Monomer	Monomer/Kat [equiv.]	Solvent	t [min]	Yield[b] [%]	$M_{n,SEC}$[c] [10^4g·mol^{-1}]	PDI[c]
1	$\mathbf{44^{Sc}}$	MMA	50	toluene	1 440	59	2.09	1.12
1a	$\mathbf{44^{Y}}$	MMA	50	toluene	240	58	1.06	1.03
2	$\mathbf{44^{Sc}}$	MBL	100	PhCl	360	67	1.81	2.91
3	$\mathbf{44^{Sc}}$	MMBL	100	PhCl	60	100	3.54	1.44
3a	$\mathbf{44^{Y}}$	MMBL	100	PhCl	3	100	2.78	1.60
4	$\mathbf{45^{Sc}}$	MMA	50	toluene	1 440	61	1.81	1.11

[a] Conditions: 20 µmol (40 µmol with MMA) of Ln, , 0.4 mL of toluene or 1 mL of PhCl.
[b] Yield of the isolated polymer.
[c] Determined by GPC in DMF against PMMA standards.

styrene, another "comonomer effect" enables the copolymerization of dicyclopentadiene and styrene. There, the high styrene content in the resulting terpolymers is remarkable.[102]

1.2.2.4 Polymerization of Polar Olefinic Monomers

In this section, so far, only one study, by Xu and coworkers[128] has been published. This study features rare-earth metal dineosilyls bearing a "nacnac"-type ligand with a P-donor side arm (Scheme 1.16). After a protonolytic reaction of [(Dipp-"nacnac^{Me_2}"-$(CH_2)_2$)-PPh_2)Ln$(CH_2SiMe_3)_2$] (**42**) with 2,6-di*tert*butylphenol, the mixed alkyl / aryl oxide species [(Dipp-"nacnac^{Me_2}"-$(CH_2)_2$)-PPh_2)Ln(CH_2SiMe_3)(OAr)] (**43**, Ar = 2,6-di*tert*buthylphenyl) was activated by cocatalyst **B** and stable ion pairs (**44**) formed for Ln = Sc, Y, Lu. These single-component catalysts were applied in the polymerization of methylmethacrylate (MMA), α-methyl-γ-butyrolactone (MBL) and γ-methyl-α-methylene-γ-butyrolactone (MMBL) (Table 1.6). For the latter, the systems were most active, showing full conversion after 3 min, while in case of MMA only 60 %

conversion was achieved after 4 h. With this monomer, the PDIs were extremely narrow, reaching even down to 1.03 in case of Ln = Y. For Ln = Sc, that showed slower chain propagation and less uniform polymers in case of MMA and MBL than Ln = Lu, Y, crystals of a species of the first monomer insertion (**45**) could be obtained. To the best of our knowledge, this is the first polymerizing species with a [BAr^F] anion, that was crystallized in that stage of the commencing polymerization (Scheme 1.16). So interestingly, the monomer has inserted into the Ln–P bond forming a nine-membered metallacycle. This insertion product showed to be an active single-component catalyst in the polymerization of MMA. A similar product was achieved, when chalcone [Ph-$(CH_2)_2$-C(O)-Ph] was added to **44**. Crystals suitable for X-ray diffraction were obtained both for the MMA insertion product (**45**) and the chalcone insertion product (**46**), that models the other two monomers.

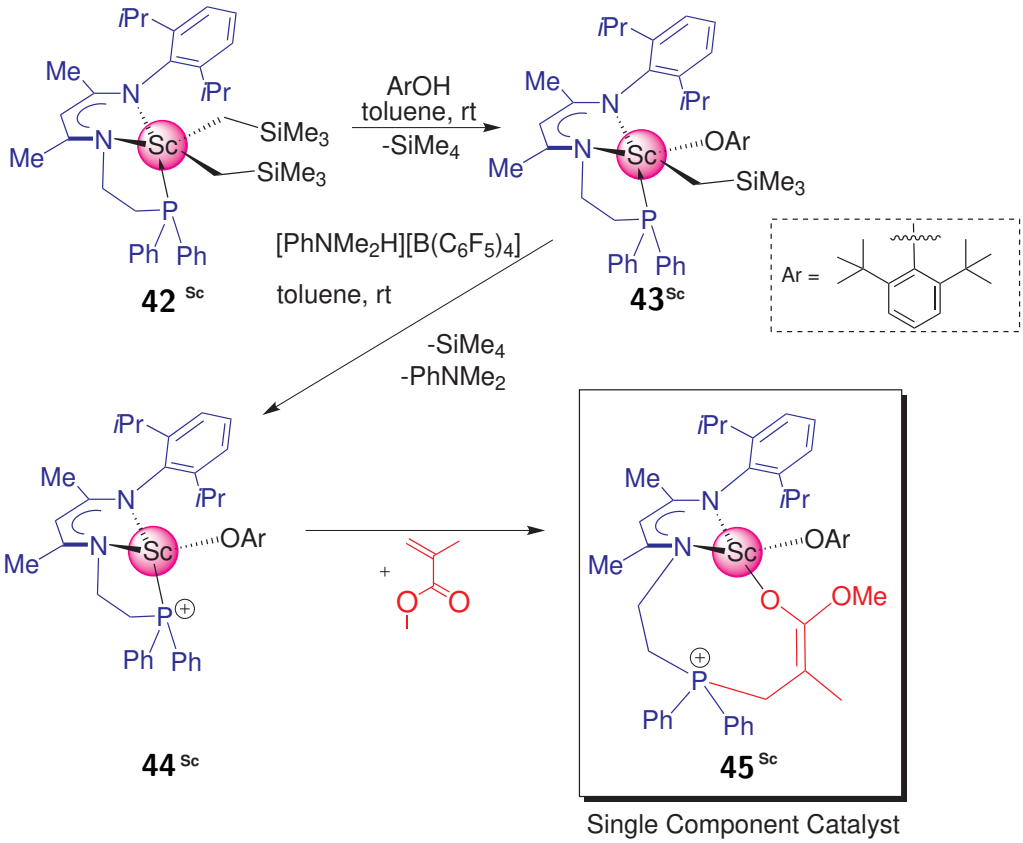

*Scheme 1.16: Synthesis of the active species (**44**) derived from the bis-neosilyl precursor (**42**) according to ref 128.*

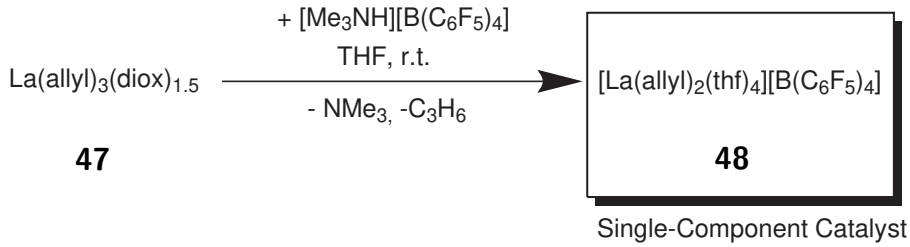

*Scheme 1.17: Synthesis of the single-component catalyst (**48** derived from the dioxane coordinated tris-allyl precursor (**47**) according to ref 4.*

1.2.2.5 1,3-Diene Polymerization

The variety of the crystallized active species polymerizing 1,3-dienes mirrors the diversity of systems proven to be active in catalyzing these reactions.

The first lanthanide-centered single-component catalyst in the field of 1,3-diene polymerization was published, by Taube contributing to a book edited by Kaminsky in 1999.[4] There, Taube reported on $[La(allyl)_2(thf)_4][BAr^F{}_4]$ (**48**), which is produced according to scheme 1.17. The orange-yellow crystals were applied in the polymerization of 1,3-butadiene at 50 °C. When 2,000 equivalents of the monomer were applied to the catalyst a moderate activity was observed (TOF = 1,000 h^{-1}) due to the strongly coordinating thf ligands. A polymer with very narrow MWD (PDI = 1.04) but interestingly unselective microstructure was obtained (*cis* / *trans* / 1,2 = 27 / 68 / 5). Higher *cis* contents and far more efficient catalysis was achieved with the corresponding Nd compound $\mathbf{48^{Nd}}$ and especially applying the dioxane-coordinated analogue $\mathbf{48a^{Nd}}$, which both did not crystallize. Remarkably, also the non-cationized precursors (both La (**47**) and Nd ($\mathbf{47^{Nd}}$)) serve as single-component catalysts for butadiene polymerization.[129] Here, *trans* contents of 83 %

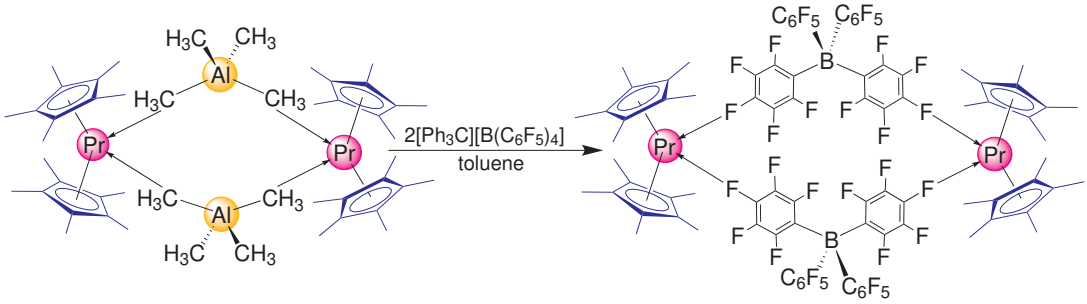

49 **50**

Scheme 1.18: Synthesis of the dimeric ion pair [[Cp$_2$Pr][BAr$^F{}_4$]]$_2$ (**50**) from the tetramethylaluminate bridged precursor (**49**) by application of cocatalyst **A** in toluene. This reaction is given as an example Ln = Pr, due to the fact that only for Pr a full characterization by single-crystal X-ray diffractometry was performed. For Ln = Nd (**50Nd**) structural similarity was confirmed according to ref. 151.*

Table 1.7: Butadiene polymerization by [[Cp$_2$Ln][BAr$^F{}_4$]]$_2$ **50**, **50Nd** and **50^{Gd}**. Taken from ref. 151.*

Entry[a]	Catalyst	T [°C]	t [min]	Yield [%]	*cis*[b] [%]	*trans*[b] [%]	3,4[b] [%]	M_n[c] [10^4g·mol^{-1}]	PDI[c]
1	(**50**)	50	300	95	90.2	6.8	3.0	7.6	1.65
2	(**50Nd**)	50	25	96	91.3	6.3	2.4	13.0	1.37
3	(**50^{Gd}**)	50	3	>99	97.5	1.0	1.5	24.5	1.73
4	(**50^{Gd}**)	-78	720	54	>99.9	0.0	<0.1	30.1	1.45

[a] Conditions: toluene, Ln: 20 µmol, Al^{i}Bu$_3$: 100 µmol, [Ln] / [1,3-Butadiene] = 1 / 500;
[b] Determined by ^{1}H and ^{13}C NMR Sectroscopy;
[c] Determined by GPC against Polystyrene standart;

([La(allyl)$_3$(diox)$_{1.5}$]) **47** and 94 % ([Nd(allyl)$_3$(diox)] **47Nd**) and lower activities were observed. The chain properties of these polymers were not investigated. Addition of MAO, Et_2AlCl or $EtAlCl_2$ led to higher *cis* contents. Furthermore, analogues of the La species with other donors like DME, TMEDA or HMPT were successfully applied as single-component catalysts in the polymerization of 1,3-butadiene, as well as the donor-free homoleptic tris(allyl) neodymium.[130, 131]

Before the next active single-component catalysts were crystallized in

the field of 1,3-diene polymerization, Hou and coworkers obtained three cationic species, which need to be activated with Al^iBu_3 in order to serve as polymerization catalysts.[132–151] $[[Cp^*_2Ln][BAr^F_4]]_2$ (Ln = Pr (**50**), Nd (**50Nd**), Gd (**50^{Gd}**)) was obtained from the cationization reaction of $[Cp^*_2Ln(AlMe_4)]_2$ (Ln = Pr (**49**), Nd (**49Nd**), Gd (**49^{Gd}**)) with cocatalyst **A** (see Scheme 1.18). In these dimeric structures, each Ln center coordinates to one fluorine atom of each of the two BAr^F_4 anions. Due to this sterically crowded environment of the Ln centers a further activation is necessary in order to enable their accessibility for monomer coordination. From such *in situ* activated systems, polybutadienes for all three applied Ln were obtained. As shown in Table 1.7 several remarkable polymer properties were observed. While the PDI was in moderate range (compared to later results in the field of catalyzed 1,3-butadiene polymerization of 1.37–1.73) and the yields were almost quantitative, three important trends are clearly visible in this study. With decreasing size of the Ln center, the catalysts became more active, more *cis*-selective and the polymer chains were much longer (see Table 1.7). So, while for Ln = Pr 0.42 chains per Ln center were produced, this figure shrinks to 0.25 in case of Ln = Nd and to 0.13 for Ln = Gd, which means that only every eighth Gd center grew a polymer chain, while almost every second Pr center did so. Therefore the rate of the initiation reaction comes into focus for this system. Especially in case of Gd, the usual assumption, that the initiation process is much faster, than the chain propagation process seems not to be correct. This is why the monomer is consumed rapidly, by those Gd centers that are activated at an early stage of the polymerization. For Ln = Gd also polymerizations at low temperatures were performed in order to increase the *cis*

content up to almost quantitative level (see Table 1.7, run 4). Kaita and coworkers continued their study in 2006.[152] Here, the authors investigated analogue systems that were not only activated by AlR_3 (R = Me, Et or ^{i}Bu) or $HAl^{i}Bu_2$, but before also cationized by applying cocatalyst **A** in an *in situ* reaction with the polymerization for eleven different Ln, including the above mentioned Pr, Nd and Gd. The results obtained from the experiments with $Al^{i}Bu_3$ were very similar to those produced by the precationized precatalysts three years before. A maximum in activity and the highest *cis* contents were found with Ln of medium size. For Ce, the largest Ln tested in this study, even a *trans*-focused polymer (60 % *trans* content) was the product. The *trans* content decreased with decreasing ionic radii of the Ln centers until it reached 2 % for Gd. For Gd also once more polymerizations at colder temperatures were performed and almost quantitative *cis* contents were obtained in analogy to the precationized precatalyst. Variation of the AlR_3 activator towards shorter alkyls (R) showed that the micorostructure was strongly affected. The shorter the alkyl, the lower are the *cis* contents (For Ln = Gd: 97.3 % ($Al{i}Bu_3$), 96.1 % ($HAl^{i}Bu_2$), 73.9 % ($AlEt_3$) and 59.7 % ($AlMe_3$)). For the *trans* selective large Ln centers this means, that the *trans* contents of the polymers rose up to 93.8 % (Ln = Ce) when $AlMe_3$ was applied as activator.[153,154] The authors further detected living character of some of their polymerizations (Ln = Sm, Nd) where $AlMe_3$ was used for activation.[152, 155] Comparing the molecular weights obtained for the different AlR_3, the lower M_n for $Al^{i}Bu_3$ stood out, caused by the chain transfer ability of this activator. In 2004, the Gd system with $Al^{i}Bu_3$ was also investigated in the polymerization of isoprene and its copolymerization with 1,3-butadiene.[156–169] Regarding

the isoprene homopolymers lower activities than in the butadiene case and unselective microstructures were observed. Only with 20 and more equivalents of Al^iBu_3 and at low temperatures high *cis* contents could be achieved. Interestingly, the system polymerized isoprene even without AlR_3 activator, but still produced polymers with unselective microstructure. The PDIs were moderate and increased at cold temperatures up to 10. From that can be concluded, that once more, especially at -20 °C, the initiation reaction rate is not high enough that all catalyst molecules become initiated before significant amounts of monomer are consumed. In case of the isoprene-butadiene copolymers, good PDIs were achieved (1.42 – 1.51, varying the isoprene feed ratio). The micorstructures of the copolymers were 1,4-selective for the butadiene units and unselective for the isoprene units in the copolymer. In all cases the isoprene contents in the copolymer were much lower than feeded at conversions below 25 %. This mirrors the different activities of the catalytic system towards the two monomers.

The formation of the second active species that was structurally characterized and serves as single-component catalyst in this field is shown in Scheme 1.7 and was published by Hou and coworkers in 2006.[62] Although the resulting poly-cyclohexadienes obtained from polymerization experiments were not published, the authors claim them to be very similar to those produced, if the mono-thf-adduct $[[Cp'YH_2]_4(thf)]$ (**14a**) is used as precatalyst in an *in situ* activation and polymerization applying cocatalysts **A** and **B**. This particular precatalyst did not yield any crystals of the corresponding active species (**15a**) suitable for X-ray

*Table 1.8: Isoprene and Norbornene Hompolymerizations and Copolymerization by [Cp'Sc(allyl)(η^6-Ar)][$BAr^F{}_4$] (**36a**) systems, data taken from ref. 79.*

Entry[a]	Catalyst	NB[b] [mmol]	IP[b] [mmol]	T [°C]	t [min]	Yield[c] [%]	M_n[d] [$10^4 \frac{g}{mol}$]	PDI[d]	IP %[e] [mol%]	T_g[f] [°C]
1	[Cp'Sc(allyl)(η^6-PhNMe$_2$)][$BAr^F{}_4$] (**36a**)	0	5	25	15	85	3.3	1.12	100	-1.9
2	[Cp'Sc(allyl)(η^6-PhNMe$_2$)][$BAr^F{}_4$] (**36a**)	5	0	25	720	59	0.5	1.70	0	380.0
3	[Cp'Sc(allyl)(η^6-PhNMe$_2$)][$BAr^F{}_4$] (**36a**)	5	5	25	15	35	2.5	1.33	81	13.4
4	[Cp'Sc(allyl)(η^6-PhMe)][$BAr^F{}_4$] (**36**)	0	5	25	15	91	2.2	1.12	100	-6.9
5	[Cp'Sc(allyl)(η^6-PhMe)][$BAr^F{}_4$] (**36**)	5	0	25	720	66	0.4	1.81	0	384.7
6	[Cp'Sc(allyl)(η^6-PhMe)][$BAr^F{}_4$] (**36**)	5	5	25	15	44	2.3	1.13	69	20.2

[a] Conditions: 25 µmol of Sc, 25 mL of toluene.
[b] NB = norbornene, IP = isoprene.
[c] Yield of the isolated polymer.
[d] Determined by GPC against polystyrene standards.
[e] Determined by ^{1}H NMR.
[f] Measured by DSC.

diffraction, while the bis-thf-adduct (**14b**), which is inactive as precatalyst, could be structurally elucidated.[62] It is noteworthy, that in case of the sterically unsaturated precursor [Cp'YH$_2$]$_4$ (**14**) a direct Y–F interaction ($d_{Y-F} = 2.405(4)$ Å) was found in the structure of the corresponding active species (**15**). In case of **14b** instead, a separated ion pair (**15b**) was obtained.
Besides being active in cyclohexadiene polymerization the active catalysts also showed high activity in the polymerization of ethylene and styrene (see ref. 61). Furthermore, the authors describe a 1:1 addition of the monomer to the non-activated precatalyst in question.[62]

Two years later, Hou and coworkers presented two activated scandium complexes originating from precatalyst [Cp'Sc(allyl)$_2$] (**35**).[79] 1:1 Conversion with [Ph$_3$C][B(C$_6$F$_5$)$_4$] (**A**) led to the formation of [Cp'Sc(allyl)(η^6-PhMe)][$BAr^F{}_4$] (**36**), while upon activation with cocatalyst [PhNHMe$_2$][B(C$_6$F$_5$)$_4$] (**B**), single crystals of

[Cp'Sc(allyl)(η^6-PhNMe$_2$)][BAr$^F{}_4$] (**36a**) were obtained (see Scheme 1.13). These species are stable enough to be isolated in a scale of 200 mg, possibly due to the η^6-coordinated aryl ring. Therefore it was possible to test these compounds as single-component catalysts in isoprene and norbornene homo- and copolymerization.

Due to the steric encumbrance of the catalysts, a relatively high 3,4-polyisoprene content of approx. 70 % was observed, causing a T_g of the polymer as high as -2 °C (see Table 1.8). Even more remarkable is the fact that Hou and coworkers observed that not all Sc centers were active in the isoprene homopolymerization, as one might expect from a single-component catalyst. In contrast, the homopolymerization of norbornene resulted in the observation of chain transfer and a far less active system (*vide supra*). For the copolymerization of both monomers, the large difference of the catalyst in activity toward isoprene and norbornene, enabled the high polyisoprene contents, which are quite rarely achieved in such copolymers applying non-catalytic polymerization protocols. Besides, *in situ* generation of the catalyst provides a very similar copolymer.

The system was furthermore investigated in the polymerization of 1,3-butadiene (BD) and E-1,3-Pentadiene (E-PD) and their copolymerization by Hou and coworkers five years later.[170] For isoprene, the system of the precatalyst [Cp'Sc(allyl)$_2$] (**35**) activated by cocatalyst **B** showed a low 1,4-polyisoprene content of only 30 % (*cis* + *trans*), in the butadiene case 87 %, and in the pentadiene case, at -40 °C, 90 % *cis*-content were obtained. Still, only every second (BD) and fourth (E-PD) Sc center appeared to be active in polymerization, but the MWDs remain quite narrow (PDI < 1.30). At -60 °C even a quantitative (> 99 %) *cis* content

*Table 1.9: Isoprene homopolymerization of the precatalysts [Cp'Sc(CH_2SiMe_3)$_2$(thf)] (**16**) and [Cp$^{o\text{-}anisol}$Sc(CH_2SiMe_3)$_2$(thf)] (**17**) presented in ref. 65*

Entry[a]	Precatalyst	Cocat.[b]	T [°C]	t [min]	Yield[c] [%]	*cis*[d] [%]	*trans*[d] [%]	3,4[d] [%]	M_n[e] [$10^4 \frac{g}{mol}$]	PDI[e]
1	[Cp'Sc(CH_2SiMe_3)$_2$(thf)] (**16**)	**A**	25	180	100	20	15	65	7.7	1.07
2	[Cp'Sc(CH_2SiMe_3)$_2$(thf)] (**16**)	**B**	25	180	100	17	18	65	6.9	1.07
3	[Cp'Sc(CH_2SiMe_3)$_2$(thf)] (**16**)	**C**	25	180	91	3	57	40	7.7	1.08
4	[Cp$^{o-anisol}$Sc(CH_2SiMe_3)$_2$(thf)] (**17**)	**A**	25	120	100	29	60	11	7.7	1.05
5	[Cp$^{o-anisol}$Sc(CH_2SiMe_3)$_2$(thf)] (**17**)	**B**	25	120	100	28	61	11	6.9	1.08
6	[Cp$^{o-anisol}$Sc(CH_2SiMe_3)$_2$(thf)] (**17**)	**C**	25	120	100	10	79	11	11.4	1.11

[a] Conditions: 25 µmol of Sc, 25 µmol of cocatalyst, 15 mmol of isoprene, 10 mL of PhCl.
[b] **A** = [Ph_3C][$B(C_6F_5)_4$], **B** = [$PhNHMe_2$][$B(C_6F_5)_4$], **C** = $B(C_6F_5)_3$.
[c] Yield of the isolated polymer.
[d] Determined by ^{1}H and ^{13}C NMR spectroscopy
[e] Determined by GPC in THF at 45°C.

could be achieved for the E-PD case, showing a quantitative isotacticity ($> 99\,\%$ (*mm*)). The block-copolymer that resulted from the subsequent addition of both monomers exhibited a high *cis* content for both monomers (86 % BD, 97 % PD) after 120 min.
The system is also part of several patents (see refs. 122–127).

Another comparable Cp'Sc-bisalkyl precatalyst, [Cp'Sc(CH_2SiMe_3)$_2$(thf)] (**16**) was cationized and crystallographically characterized by Hou and coworkers in 2009.[65] The species was obtained in all three reactions, where the precatalyst was treated with one of the three cocatalysts **A**, **B** or **C**. As the cationization reactions are performed in THF, the coordination sphere of the resulting cation can be easily saturated by THF coordination, giving [Cp'Sc(CH_2SiMe_3)(thf)$_2$][$BAr^F{}_4$] (**31**, see Scheme 1.11) or resp. [Cp'Sc(CH_2SiMe_3)(thf)$_2$][$BAr^F{}_3(CH_2SiMe_3)$] (**31a**). The second cation presented by the authors is a derivative of this complex in which the Cp'-ligand is exchanged for C_5Me_4(*o*-anisol) in which the O-donor-sidearm coordinates to the Sc center (**17**). Though

even in this case, the cation ($[Cp^{Me_4(o\text{-anilsole})}Y(CH_2SiMe_3)(thf)_2][BAr^F{}_4]$ (**32**)) is coordinated by two thf molecules. This steric saturation by strongly coordinated ligands becomes the best possible explanation for the inactivity of these species in isoprene polymerization.

Instead, in order to obtain active catalysts, the cationization reaction was performed in PhCl. Applying the resulting species in isoprene homopolymerization produced nearly quantitative yields with all three cocatalysts within 2, resp. 3 h. Interestingly both precatalysts (**16** and **17**) revealed a different polymerization behavior, when either cocatalysts **A** and **B** or cocatalyst **C** was applied (see Table 1.9). Especially concerning the Cp' ligand system (**16**), this difference stands out. Cocatalysts **A** and **B** provided an active species that produced a polymer with a 3,4-focused microstructure, while **C** promoted a remarkable shift toward *trans*-selectivity from 18 % (**A** and **B**) to 57 % (**C**). For the $Cp^{Me_4,o-anisol}$-compound (**17**) this *trans*-shift led from a *trans*-focused polymer (for **A** and **B**) to a far more *trans*-selective polymer if cocatalyst **C** was applied (from 60 % to 79 %). From these findings, the conclusion must be drawn, that the uniformity of the cations produced by all three cocatalysts in THF does not automatically imply uniform cations formed in other solvents like PhCl. Instead interactions with Ph_3CMe or $PhNMe_2$, respectively in the active species formed by **A** and **B** should neither be completely excluded nor can the influence of their slightly different anions (**A** and **B** compared to **C**) be neglected.

Besides that, Hou and coworkers studied the monomer coordination of $[Cp^{Me_4(o\text{-anilsole})}Y(CH_2SiMe_3)(thf)_2][BAr^F{}_4]$ (**32**) to investigate why the catalyst produced such a high 1,4-*trans* selectivity.[171] They concluded,

that the steric bulk of the donor side arm causes a deformation in a *anti*-coordinated monomer (coordination mode, that leads to 1,4-*cis*-addition). So to avoid this deformation, the coordinated monomer underwent a *anti* → *syn* isomerization. As the *syn*-coordination has no steric necessity to deform the monomer in such a significant extent as in the *anti*-case, it is energetically favored. The *syn*-coordination then leads to a 1,4-*trans* addition.

Furthermore both systems and their *in situ* generated analogues were tested in the copolymerization of isoprene in an ethylene atmosphere. The first alternating copolymers of their kind were obtained in reasonable yields with 3,4-focused polyisoprene microstructures (see Table 4 in ref. 65). In 2017, Marks and coworkers[172] used the system **16** / **A** for comparison, in a study, in which they introduced a dimeric version of it, with an alkyl linkage between the $SiMe_3$ groups of the ligands. Besides these results, the precatalyst / cocatalyst binary systems derived from **16** and **17** have been applied in further studies. Especially [Cp'Sc(CH_2SiMe_3)$_2$(thf)] (**16**), which was tested on various monomers[23] such as styrene[173], α,ω-dienes[174] and E-1,3-pentadiene.[170] Additionally styrene-isoprene,[173] styrene-ethylene[66, 113] and α,ω-diene-isoprene-copolymers[170] were obtained from this system. The latter study,[170] that applied cocatalyst **A**, revealed that the isoprene segments in the copolymers are far more 1,4-linked (esp. 1,4-*trans*), than the corresponding homopolymer. The α,ω-diene segments instead show high *cis*-contents ($> 85\%$). As the system **16** / **A** had shown to copolymerize ethylene and propylene earlier,[88] Li and coworkers also targeted its terpolymerization adding isoprene to the copolymerization. Here, once more the affinity to propylene incorporation found for the

copolymerization of ethylene and propylene was not repeated. Instead, ethylene was the by far favored monomer. Narrow MWDs were achieved throughout the study and high activities (up to 1,400 $\frac{kg}{mol \cdot h}$) were obtained, especially with lower concentrations of propylene.

The same group targeted isobutylene polymerization with this system (**16** / **A**) recently.[108] In this study, they also produced isoprene isobutylene copolymers. They applied very low ratios of isoprene (1–3 %) in the feed, which already led to the reduction of the yield by half. Only even smaller ratios of isoprene units were found in the copolymer.

Quite recently as well, Hou and coworkers[175] successfully tested **16** / **A** in the polymerization of myrcene. Moderate activities (49 $\frac{kg}{mol \cdot h}$) and a small focus on 3,4-polymerization were observed. In its copolymerization with ethylene, which was targeted in the same study[175] much higher activities could be achieved (up to 458 $\frac{kg}{mol \cdot h}$). With myrcene, it can be suspected that the usual "comonomer effect"[102] is also supported by a steric effect. Ethylene incorporation increases the distance between two bulky myrcene units. In the process of copolymerization this decreases the steric bulk around the active center significantly, as with an incorporation of ethylene after a myrcene insertion, the energetically unfavorable situation of the simultaneous coordination of a bulky myrcene chain end and a myrcene monomer did not occur. This has also to be taken into account, when discussing the results of their terpolymerization of the two monomers with propylene and the copolymerization of myrcene and propylene. The latter showed moderate activities (59 $\frac{kg}{mol \cdot h}$ with 250 equiv. myrcene and 0.60 MPa, approx. 6 bar of propylene) and only low tendencies to incorporate myrcene at all (< 35 %). Applying ethylene to the reaction

mixture, terpolymers are formed with more than the tenfold activity (up to 711 $\frac{kg}{mol \cdot h}$). Once again, the propylene focused copolymerization of ethylene and propylene was not repeated. Instead, an ethylene focused terpolymer was obtained in all cases, while the incorporation rate of myrcene remained lowest.

The system (**16** / **A**) was also successfully applied in a chain shuttling study[111] together with two systems of higher isoprene polymerization performance. Due to its high activity towards styrene (*vide supra*) block copolymers of styrene and 1,3-dienes were obtained in high yields.

Furthermore, the $Cp^{Me_4, o-anisol}$-compound (**17**) was tested in this study. There, a *cis*-shift of the microstucture (compared to the corresponding homopolymer) was observed and the addition of the α,ω-diene-monomer seemed to be slightly favored against that of isoprene, resulting in a comonomer content above the feed ratio.

Another precatalyst that is part of this study is [Cp'Sc($CH_2C_6H_4$-*o*-NMe_2)$_2$] (**25**). First presented in 2007,[64] it was shown to be active in 1-hexene and dicyclopentadiene homo- and copolymerization (*vide supra*). In 2013[170, 174] and 2015[96] Hou and coworkers then published further studies involving that system, and patented its application in 1,3-diene polymerization.[80–87]

The system (**25** / **A**) is active in the homopolymerization of isoprene,[174] yielding *cis*-centered selectivity (62 %) in good yields with narrow MWD and in that of 1,3-butadiene,[96] where it showed high *cis*-selectivity and rapid conversion (100 % after 5 min with BD / Y = 500 / 1). As a third diene, E-1,3-pentadiene[170] was tested. It also produced a *cis*-centered polymer in a rapid reaction (100 % after 5 min with PD / Y = 150 /1).

Furthermore, copolymerization attempts of isoprene with α,ω-dienes were not successfull (see ref. 174 for details).
In 2018, Hou and coworkers[175] polymerized myrcene with **25** / **A**. The system added myrcene units preferably vinylicly (74 %) and showed a moderate activity of 55 $\frac{kg}{mol \cdot h}$. Copolymerization of myrcene with ethylene was performed applying 1 atm (approx. 1 bar) ethylene pressure to the homopolymerization setup of myrcene. Due to the affinity of the system toward ethylene polymerization, the activity increased to 136 $\frac{kg}{mol \cdot h \cdot bar}$, but an ethylene content of 42 % in the resulting polymer gives room for speculation about another "comonomer effect".[102]
In the article about the Cp'Sc-bisneosilyl catalyst (**16**, *vide supra*),[65] Hou and coworkers mention, that a complex of their previous studies[176] was also tested in copolymerization of isoprene and ethylene, which only resulted in a blend of the homopolymers. Interestingly, this precatalyst (**52**), bearing a bis(phosphinophenyl)amido ligand ($PNP^{Ph} = \{2\text{-}(Ph_2P)C_6H_4\}_2N$) also forms a cationic species ($[(PNP^{Ph})Lu(CH_2SiMe_3)(thf)_2][BAr^F{}_4]$ (**53**), see Scheme 1.19) that can serve as a structure model for the actual active catalyst in both isoprene and butadiene homopolymerization, as well as their copolymerization.

The polyisoprene obtained from the *in situ* generated active species in PhCl shows a high *cis*content and a very low PDI (see Table 1.10) implying living polymerization. Even higher *cis* contents could be achieved when the precatalyst is exchanged for its yttrium-centered analogue (**53^Y**). Although those systems were not as efficient as those published later by the group,[65] they still were the first example of an aluminum-free living isoprene homopolymerization catalyst yielding such high *cis* contents at

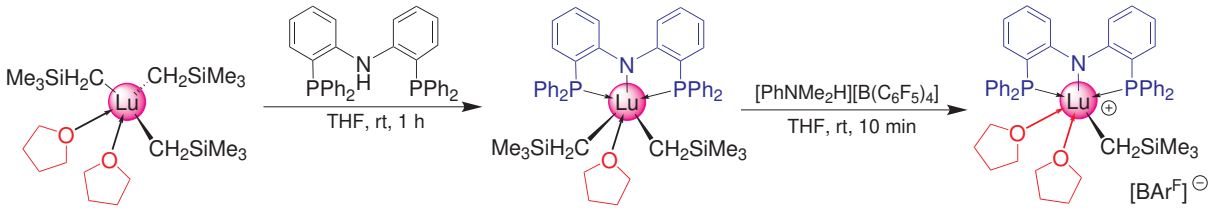

*Scheme 1.19: Synthesis of structure model [(PNP^{Ph})Lu(CH$_2$SiMe$_3$)(thf)$_2$][BAr$^F{}_4$] (**53**) from its bisneosilyl precursor (**52**) applying cocatalyst **B**. **52** is synthesized by the addition of the protonated ligand to [Lu(CH$_2$SiMe$_3$)$_3$(thf)$_2$] (**51**). Scheme according to ref. 176.*

*Table 1.10: Isoprene homopolymerization by [(PNP^{Ph})Ln(CH$_2$SiMe$_3$)$_2$(thf)] (Ln = Lu (**53**), Y (**53^Y**)), data taken from ref. 176.*

Entry[a]	Precatalyst	Cocat.[b]	T [°C]	t [min]	Yield[c] [%]	*cis*[d] [%]	*trans*[d] [%]	3,4[d] [%]	$M_{n,SEC}$[e] [10^4g·mol^{-1}]	PDI[e]
1	[(PNP^{Ph})Lu(CH$_2$SiMe$_3$)$_2$(thf)] (**53**)	**B**	25	60	100	97.1	0.0	2.9	19	1.09
2	[(PNP^{Ph})Y(CH$_2$SiMe$_3$)$_2$(thf)] (**53^Y**)	**B**	25	60	100	99.3	0.0	0.7	23	1.10

[a] Conditions: 25 µmol of Ln, 25 µmol of cocatalyst, 15 mmol of isoprene, 10 mL of PhCl.
b **A** = [Ph$_3$C][B(C$_6$F$_5$)$_4$], **B** = [PhNHMe$_2$][B(C$_6$F$_5$)$_4$], **C** = B(C$_6$F$_5$)$_3$.
[c] Yield of the isolated polymer;
[d] Determined by ^{1}H and ^{13}C NMR spectroscopy.
[e] Determined by GPC in THF at 45°C.

that time.

Furthermore the Y-compound (**53^Y**) was tested in butadiene homopolymerization and isoprene-butadiene-copolymerization activated by cocatalyst **A**, also yielding high *cis* contents (> 99 %) and living (co-)polymers. A further study, mentioned by Hou and coworkers when presenting their bisneosilyls,[65] is their benzamidinate project, published in 2008.[177] Here, very high 3,4-contents (91 % at r.t.) could be achieved by applying [{PhC(NDipp)$_2$}Y(*o*-CH$_2$C$_6$H$_4$NMe$_2$)$_2$] (Dipp = (C$_6$H$_4$^{i}Pr$_2$-2,6), **54^Y**) as a precatalyst, switching the selectivity to high-*cis*, when AlMe$_3$ was added to the active mixture (see Table 1.11, run 1–3).[177] This behavior was explained by the proposal of a mechanism that involves both metal centers (Y

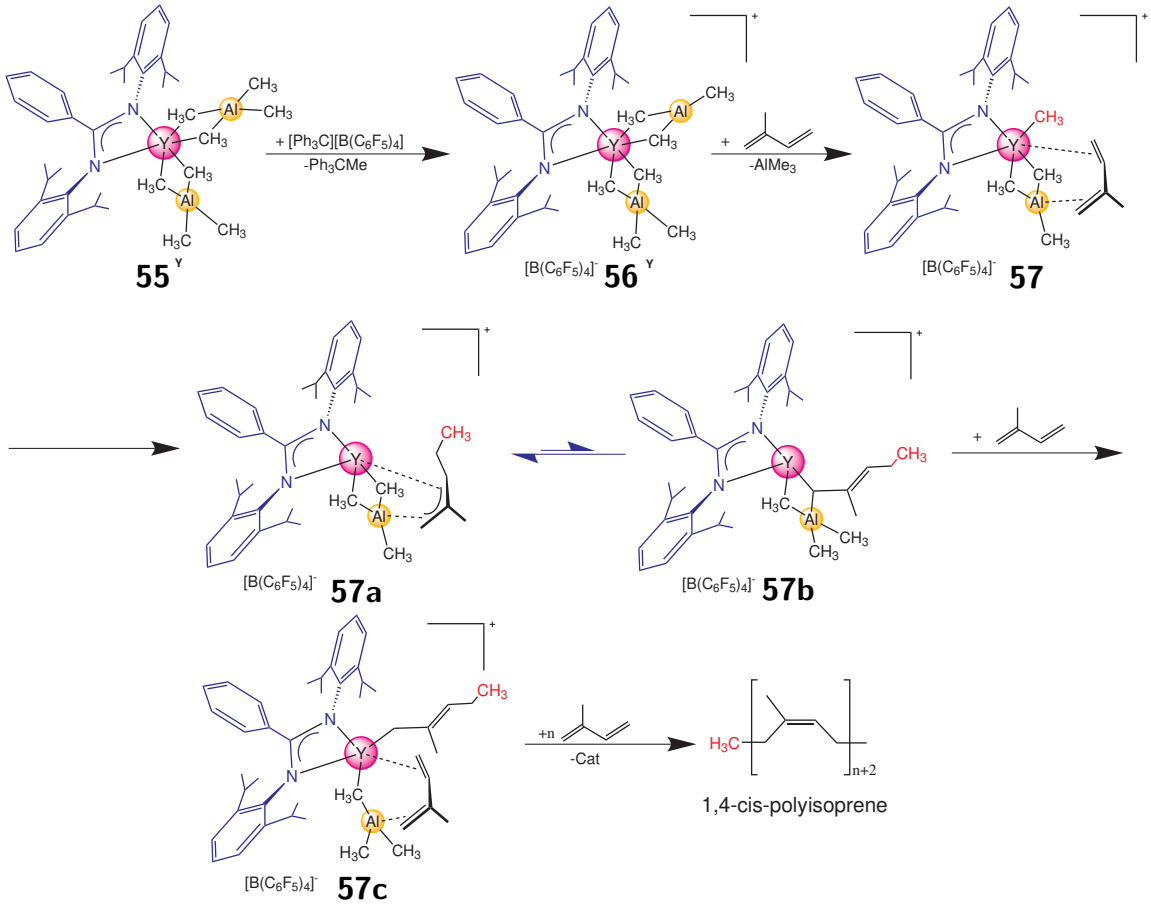

*Scheme 1.20: Suggested mechanism for the 1,4-cis-polymerization of isoprene by [{PhC(NDipp)$_2$}Y(AlMe$_4$)$_2$] (**55^{Y}**) + **A** or [{PhC(NDipp)$_2$}Y(o-CH$_2$C$_6$H$_4$NMe$_2$)$_2$] (**54^{Y}**) + **A** + AlMe$_3$. Scheme according to ref. 177.*

and Al) introducing a [{PhC(NC$_6$H$_4$^{i}Pr$_2$-2,6)$_2$}Y(AlMe$_4$)$_2$] (**55^{Y}**) that the authors expect to be formed in the first place (see Scheme 1.20). This study lacks, due to the instability of the formed cations a structural evidence.

It took until 2012, when a structure model of an active Sc catalyst bearing the identical benzamidinato ligand was presented by Luo and coworkers.[178] Another year later, the Y analogue was published[179] and subsequently patented.[180]

*Table 1.11: Isoprene homopolymerizations applying benzamidinate catalysts (**54**, **58**, **59** and **60**), data taken from refs. 177–179, 182.*

Entry[a]	Precatalyst[b]	Cocat.[c]	$AlMe_3$ [equiv]	t [min]	Yield[d] [%]	*cis*[e] [%]	*trans*[e] [%]	3,4[e] [%]	M_n[f] [$10^4 \frac{g}{mol}$]	PDI[f]	ref.
1	$[LY(o\text{-}CH_2C_6H_4NMe_2)_2]$ (**54**)	**A**	0	2	100	9	0	91	13.7	1.3	177
2	$[LY(o\text{-}CH_2C_6H_4NMe_2)_2]$ (**54**)	**A**	10	10	100	91	6	3	6.3	1.5	177
3	$[LY(AlMe_4)_2]$ ($\mathbf{55^Y}$)	**A**	0	10	100	92	2	6	7.5	1.6	177
4	$[LSc\{N(SiMe_2H)_2\}_2]$ (**58**)	**A**	0	45	100	9	2	89	14.7	1.6	178
5	$[LSc\{N(SiMe_2H)_2\}_2]$ (**58**)	**A**	5	2	100	93	1	6	3.5	1.5	178
6	$[LSc\{Am\}][BAr^F_4]$ (**59**)	—	0	15	56	11	1	88	9.9	1.7	178
7	$[LSc(AlMe_4)_2]$ (**55**)	**A**	0	2	98	94	1	5	8.0	1.6	178
8	$[LY\{N(SiMe_2H)_2\}_2]$ ($\mathbf{58^Y}$)	**A**	0	240	traces	—	—	—	—	—	179
9	$[LY\{N(SiMe_2H)_2\}_2]$ ($\mathbf{58^Y}$)	**A**	5	10	98	90	6	4	5.5	1.6	179
10	$[(Ap^*Sc\{N(SiMe_2H)_2\}]$ (**60**)	**B**	10	1 200	100	96	0.0	4	24.1	2.32	182

[a] Conditions: runs 1-3: 20 µmol of Y, 20 µmol of cocatalyst, 15 mmol of isoprene, 10 mL of PhCl, 25 °C; runs 4-9: 20 µmol of Ln, 20 µmol of cocatalyst, 10 mmol of isoprene, 3 mL of toluene; run 10: 10 µmol of Sc, 10 µmol of cocatalyst, 10 mmol of isoprene, 10 mL of PhCl;
[b] $L = \{PhC(NC_6H_4{}^iPr_2\text{-}2,6)_2\}$, $Ap^* = [(C_6H_3{}^iPr_3\text{-}2,4,6)\text{-}(o\text{-}C_5H_3N\text{-}o)\text{-}N\text{-}(C_6H_4{}^iPr_2\text{-}2,6)]$, $Am = N(SiHMe_2)(SiMe_2N(SiHMe_2)_2)$;
[c] $\mathbf{A} = [Ph_3C][B(C_6F_5)_4]$, $\mathbf{B} = [PhNHMe_2][B(C_6F_5)_4]$, $\mathbf{C} = B(C_6F_5)_3$.
[d] Yield of the isolated polymer;
[e] Determined by ^1H and ^{13}C NMR spectroscopy.
[f] Determined by GPC in THF.

Both model compounds $[\{PhC(NDipp)_2\}Ln\{N(SiMe_2H)_2\}(thf)_2][BAr^F_4]$ (Ln = Sc (**58**), Y ($\mathbf{58^Y}$)) were synthesized in THF in order to model the active species that is produced, when the bis-silylamido precatalysts are activated by cocatalyst **A** in toluene. Here as well, a high 3,4-content was observed in the case of Sc (see Table 1.11, run 4–7). An investigation by NMR spectroscopy showed, that the cationization in toluene takes place at first at the silylamide ligand, giving a bulky $[N(SiHMe_2)(SiMe_2N(SiHMe_2)_2)]^-$ (Am^-) group,[178] and therefore an ion pair $[LScAm][BAr^F_4]$ (**59**). This species was isolated and tested as single-component catalyst in isoprene polymerization (see Table 1.11, run 6), but did not produce crystals suitable for X-ray diffraction. The obtained polyisoprene is in good analogy to that produced by the *in situ* formed catalyst. In the case of the Y compound ($\mathbf{58^Y}$) corresponding to **58**, only traces of polymer were obtained.[179]

For the addition of $AlMe_3$ fast polymerizations and rather high *cis*

contents were found (see Table 1.11, runs 5 and 9), due to the formation of bisaluminates as intermediates (cf., ref. 177 and Scheme 1.20). Direct synthesis of the tetramethylaluminate complex (**55**) and its Y analogue $\mathbf{55^Y}$ by addition of an excess of trimethylaluminium and application of these compounds in isoprene polymerization in combination with cocatalyst **A** led to polymers of analogue properties as the application of the ternary systems **54** / **A** / $AlMe_3$ and **58** / **A** / $AlMe_3$ which confirms the originally intended mechanism given in Scheme 1.20. The respective species have also been proposed by Kempe and coworkers[181, 182] and the resulting highly *cis*-selective polymers (96 %) have been observed for their aminopyridinate systems **60** (see Table 1.11, run 10). Their Y-analogue ($\mathbf{60^Y}$) (that did not crystallize) was tested as a single-component catalyst for the polymerization of isoprene by Trifonov and coworkers in 2014.[121] Interestingly, the obtained polymer showed a bimodal MWD (both modes with individual PDIs > 1.5) and *cis*-regularity up to 63 %.

In 2010 another highly *cis*-selectively isoprene-polymerizing catalytic system was investigated by Cui and coworkers.[183] This study was focused on easily obtained complexes like $LGdCl_2(thf)_2$ (**62**, L = (2,6-$Me_2C_6H_3$)NH=C(Me)CH=C(Me)N(2,6-$Me_2C_6H_3$), a "nacnac^{Me_2}"-derivative.), that can be synthesized just by protonolysis adding the proligand to $[GdCl_3(thf)_2]$ (**61**, see Scheme 1.21). When isoprene polymerizations of $[LGdCl_2(thf)_2$ or its Nd, Dy, Er and Y analogues were performed in the presence of an excess of trialkyl aluminum species, esp. Al^{i}Bu$_3$, *cis*-contents higher than 98 % were achieved in all cases.

The authors point out, that the order of addition of the components of these ternary systems has a dramatic effect in the course of polymerization,

as polymers were obtained only if the trialkyl aluminum was added after the cocatalyst (see Scheme 1.21).

This implies, that only then an active species is formed. The authors investigated this hypothesis by NMR spectroscopy using the Y and the Gd compounds. Doing so, they explored the addition order that had shown to be inactive in terms of isoprene polymerization. Both after the first (Al^iBu_3) and the second addition (cocatalyst **B**), crystals suitable for X-ray diffraction could be obtained, elucidating the inactive trimeric species (see Scheme 1.21).

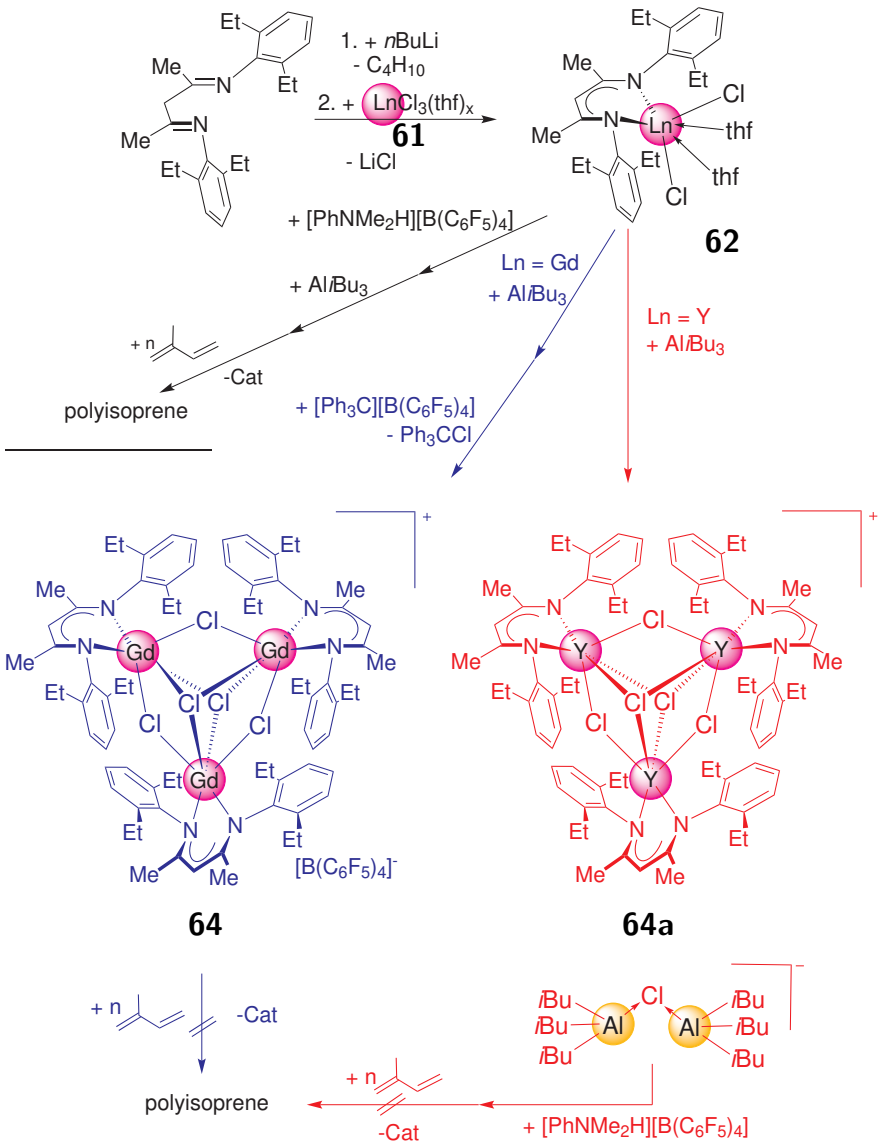

*Scheme 1.21: Synthesis of $[LLnCl_2(thf)_2]$ (**62**) ($L = (2,6\text{-}C_6H_3Me_2)NH{=}C(Me)CH{=}C(Me)N(2,6\text{-}C_6H_3Me_2)$, a "nacnac^{Me_2}"-derivative.) from thf-activated $LnCl_3$ (**61**) and activation attempts applying cocatalyst **B** and Al^iBu_3 in different orders. While in the black case an active species is formed, that polymerizes isoprene (here, byproducts were observed leading to the conlusion shown in Scheme 1.22), following the addition order given in blue and red, no polymerization was observed, but inactive intermediate ion pairs (**64** and **64a**) could be structurally characterized (given in red for $Ln = Gd$ and blue for $Ln = Y$). Scheme according to ref. 183.*

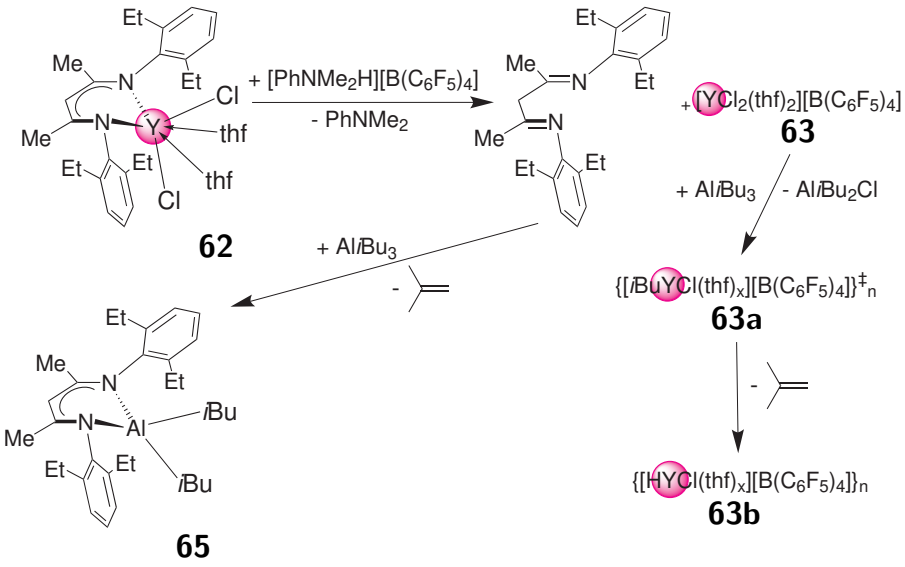

*Scheme 1.22: Synthesis of the intended active species $\{[HYCl(thf)_x][BAr^F_4]\}_n$ (**63b**) by ligand abstraction and via an isobutyl-yttrium intermediate (**63a**) and proposed side reaction toward $[LAl(^iBu)_2]$ (**65**). Indications for this reaction pathway were obtained by observation of the byproducts in NMR spectroscopic experiments. Scheme according to ref. 183.*

*Table 1.12: Isoprene homopolymerization by [Nd(BH$_4$)$_3$(thf)$_3$] (**66**), data taken from ref. 184.*

Entry[a]	Precatalyst	Cocat.[b]	Al^{i}Bu$_3$ [equiv]	T [°C]	t [min]	Yield[c] [%]	*cis*[d] [%]	*trans*[d] [%]	3,4[d] [%]	$M_{n,SEC}$[e] [10^{4}g·mol^{-1}]	PDI[e]
1	Nd(BH$_4$)$_3$(thf)$_3$ (**66**)	**B**	10	20	1 440	66	81	15	4	4.7	1.71
2	Nd(BH$_4$)$_3$(thf)$_3$ (**66**)	**B**	10	20	45	25	92	3	5	5.7	1.34
3	[Nd(BH$_4$)$_2$(thf)$_5$][BAr$^F_4$] (**67**)	—	10	20	30	82	84	10	6	8.5	2.31

[a] Conditions: run 1: 10 µmol of Nd, 10 µmol of cocatalyst, 10 mmol of isoprene, 1 mL of toluene; run 2: 10 µmol of Nd, 10 µmol of cocatalyst, 30 mmol of isoprene, 50 µL + 0.4 mL of toluene; run 3: 9.6 µmol of Nd, 31.25 mmol of isoprene, 50 µL of toluene.
[b] **A** = [Ph$_3$C][B(C$_6$F$_5$)$_4$], **B** = [PhNHMe$_2$][B(C$_6$F$_5$)$_4$], **C** = B(C$_6$F$_5$)$_3$.
[c] Yield of the isolated polymer.
[d] Determined by ^{1}H and ^{13}C NMR spectroscopy.
[e] Determined by GPC in THF against polystyrene standards.

Although successful crystallization of the inactive species was possible, the active species and the intermediates in its synthesis remained structurally uncharacterized. However, NMR spectroscopic studies revealed the formation of [YCl$_2$(thf)$_2$][BAr$^F_4$] (**63**) and free ligand after the addition of cocatalyst **B** to the Y compound. Upon addition of Al^{i}Bu$_3$ to the mixture, the formation of isobutene was recorded, which is believed to originate from a reaction shown in Scheme 1.22. These proposed [HYCl(thf)$_x$]$_n^+$-clusters (**63b**) are in good agreement with the relatively high molecular masses ($> 2 \cdot M_{n,theo}$) and PDI (> 1.5) as several different active clusters are likely to be formed (cf. refs. 14, 15, 20, 277, *vide infra* for further active species degradation studies).

Cui and coworkers[183] also presented a further set of complexes (bearing the aforementioned "nacnac^{Me_2}"-system), the borohydrido derivatives, ["nacnac^{Me_2}"Ln(BH$_4$)$_2$(thf)] (**68**). They reported it to be surprisingly inactive in isoprene polymerization. Two years earlier in 2008, Visseaux and coworkers investigated[184] and patented[185] a homoleptic neodymium borohydride stabilized by three thf ligands, [Nd(BH$_4$)$_3$(thf)$_3$] (**66**, see also ref. 312). It was applied in polymerization in a ternary *in situ* generated

system (with cocatalyst **B** and Al^iBu_3). As well, it was further reacted with cocatalyst **B** to obtain $[Nd(BH_4)_2(thf)_5][BAr^F{}_4]$ (**67**) in yields large enough to allow structural characterization and examination of the polymerization potential of the crystalline material. So they compared its isoprene polymerization behavior in the presence of Al^iBu_3 with that of their ternary system. From these experiments two conclusions were drawn: First, broader MWDs but higher activities are obtained in the case of the preactivated catalyst (**67**), the broader MWDs due to the low solubility of the salt causing slow initiation. Secondly, the isoprene concentration has an enormous effect on the polymerization results. The highest *cis*-content (92 %) was, for example, gained in a run, where the initiation took place almost under bulk conditions (toluene/isoprene = 1/60 v/v) and the concentration was lowered (to 15/100), 10 min after initiation (see Table 1.12, run 2). Similar results applying 2 equiv. of cocatalyst **A** and 10 equiv. of Al^iBu_3 were published in 2013.[186]
For myrcene, this ternary system produced analyzable polymers only at 70 °C and in moderate yields.[187] Applying cocatalysts **B** and **C**, the obtained yields were in the same regime, but compared to cocatalyst **A** high PDIs were found, while the polymerizations favoured *cis*-1,4-addition in all three cocatalyst cases (*cis* content $> 90\%$).

Another very surprising finding is the active species of precatalyst [(2-Me-Ind)$_2$Sc{N(SiMe$_3$)$_2$}] (**69**) reported in 2008 by Tardif and Kaita[188] and patented in the following years.[189–218] Instead of cleaving the amido moiety during the reaction with cocatalysts **A** and **B**, as predicted by earlier studies,[219–223] either activator attacked the complex on one of its indenyl

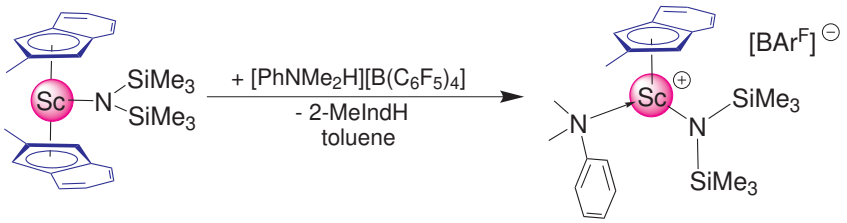

69 **70**

*Scheme 1.23: Synthesis of [(2-Me-Ind)Sc{N(SiMe$_3$)$_2$}][BAr^F$_4$] (**70**) from its sandwich precursor (**69**) applying cocatalyst **B** in toluene. The cleavage of the indenyl ligand instead of the amido moiety is unexpected. Scheme according to ref. 188.*

*Table 1.13: 1,3-Butadiene homopolymerization by [(2-Me-Ind)$_2$Ln{N(SiMe$_3$)$_2$}] (**69** and **69^{Gd}**), data taken from ref. 188.*

Entry[a]	Precatalyst	Cocat.[b]	Al^{i}Bu$_3$ [equiv]	T [°C]	t [min]	Yield[c] [%]	*cis*[d] [%]	*trans*[d] [%]	3,4[d] [%]	$M_{n,SEC}$[e] [10^4g·mol^{-1}]	PDI[e]
1	[L$_2$Sc{N(SiMe$_3$)$_2$}] (**69**)	**B**	10	20	15	100	88	0	12	18.3	1.15
2	[L$_2$Gd{N(SiMe$_3$)$_2$}] (**69(Gd)**)	**B**	10	20	15	95	99	1	0	10.2	1.17
3	[LSc{N(SiMe$_3$)$_2$}][BAr^F$_4$] (**70**)	—	10	20	15	100	88	0	12	35.3	1.22

[a] Conditions: 30 µmol of Ln, 30 µmol of cocatalyst, 10 mmol of isoprene, 19 mL of toluene. L = 2-Methylindenyl.
[b] **A** = [Ph$_3$C][B(C$_6$F$_5$)$_4$], **B** = [PhNHMe$_2$][B(C$_6$F$_5$)$_4$], **C** = B(C$_6$F$_5$)$_3$.
[c] Yield of the isolated polymer.
[d] Determined by ^{1}H and ^{13}C NMR.
[e] Determined by GPC in THF against polystyrene standarts.

ligands producing 2-Me-IndH and [(2-Me-Ind)Sc{N(SiMe$_3$)$_2$}][BAr^F$_4$] (**70**) as an active species (see Scheme 1.23). Its behavior in the polymerization of 1,3-butadiene in the presence of Al^{i}Bu$_3$ mimics that of the *in situ* generated ternary catalyst system (precatalyst, cocatalyst and Al^{i}Bu$_3$) (see Table 1.13). An even higher *cis* content was achieved by application of the Gd-analogue (**69^{Gd}**) as precatalyst (see Table 1.13, run 2).[224]

Finally, there is one more system to be mentioned in this context. It is not a classic BAr^F-structure, but it was synthesized by applying cocatalyst **C** on a lanthanide half sandwich complex. In 2008, our research group[225]

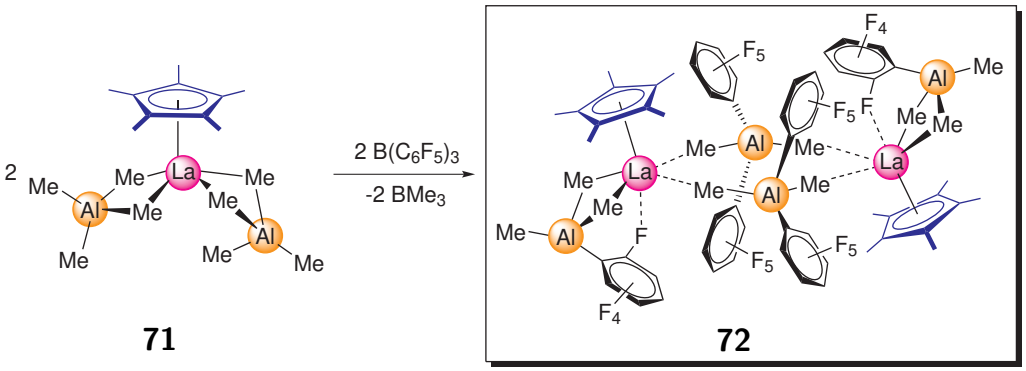

*Scheme 1.24: Surprising finding of $AlAr^F$ species $[Cp^*La(Me_3AlAr^F)(\mu\text{-}Me_2AlAr^F{}_2)]_2$ (**72**), when applying cocatalyst **C** to $[Cp^*La(AlMe_4)_2]$ (**73**). Scheme according to ref. 225.*

*Table 1.14: Isoprene polymerization applying $[Cp^*La(AlMe_4)_2]$ (**71**), data taken from ref. 225.*

Entry[a]	Precatalyst	Cocat.[b]	T [°C]	t [h]	Yield[c] [%]	*cis*[d] [%]	*trans*[d] [%]	3,4[d] [%]	M_n[e] [$10^4 \frac{g}{mol}$]	PDI[e]
1	$[Cp^*La(AlMe_4)_3]$ (**71**)	**C**	40	18	>99	0.0	99.5	0.5	24	1.18
2	$[Cp^*La(Me_3AlAr^F)(\mu\text{-}Me_2AlAr^F{}_2)]_2$ (**72**)	—	40	24	>99	0.2	99.0	0.8	23	1.19

[a] Conditions: 20 µmol of Ln, 20 µmol of cocatalyst, 20 mmol of isoprene, 8 mL of toluene.
[b] **A** = $[Ph_3C][B(C_6F_5)_4]$, **B** = $[PhNHMe_2][B(C_6F_5)_4]$, **C** = $B(C_6F_5)_3$.
[c] Yield of the isolated polymer.
[d] Determined by ^1H and ^{13}C NMR.
[e] Determined by GPC in THF against polystyrene standarts.

applied $[Cp^*La(AlMe_4)_2]$ (**71**) in the polymerization of isoprene and obtained an active species for the case of activation with cocatalysts **A**–**C**: $[Cp^*La(Me_3AlAr^F)(\mu\text{-}Me_2AlAr^F{}_2)]_2$ (**72**, crystallographically verified with cocatalyst **C**, see Scheme 1.24). So, interestingly, the Ar^F-moieties of the cocatalyst were exchanged for methyl groups from the aluminates forming the side product BMe_3. Although this behavior is known for free trialkylaluminum compounds and cocatalyst **C** in solution,[226] the finding of an active species with $AlAr^F$-anions derived from the borane was quite remarkable. The hazardous catalyst[227] did act as a neutral single-component catalyst and showed an almost quantitative *trans*-selectivity

(99.0 %) and a narrow PDI of 1.19, but also high molecular weights of ca. 3.5 · $M_{n,theo}$ (see Table 1.14). This leads to the conclusion that even if the species with bond growing polymer chain is dimeric as well, not all dimeric active catalyst complexes initiate a polymer chain. This is also true for the *in situ* generated analogue, which behaves basically identically in the isoprene polymerization.

1.2.2.6 Ring-opening polymerization of cyclic esters

So far, only one precatalyst active in the ring-opening polymerization (ROP) of cyclic esters has been structurally characterized (three more already crystallized species have been found active in this field, *vide infra*). In 2013, Capentier and coworkers[228] found that the dimeric Yb^{II} species $[\{RO\}Yb]_2[H_2N\{B(C_6F_5)_3\}_2]_2$ (**75**, RO = cyclic aminoether ([15-crown-5] analogue, containing a bridging amine based $CH_2C(CF_3)_2OH$ side arm, see Scheme 1.25) can polymerize both *L*-lactide and trimethylene carbonate (TMC) in a highly active immortal fashion, if $PhCH_2OH$ (BnOH) is applied as a chain transfer agent (terneric system, see Table 1.15).
Although, crystals suitable for X-ray diffraction studies could only be obtained from the Yb derivative (**75a**), similar divalent compounds for Eu, Ca, Sr and Ba were synthesized and tested in the ROP of *L*-lactide, where the alkaline-earth metal compounds proved not to be as active as the rare-earth analogues. In addition, the authors discussed the non-innocent role of the RO-ligand in the polymerization process by proposing a ligand-assisted activated monomer ROP mechanism, which was supported by both experimental kinetic studies and DFT calculations (see Scheme 1.25).
Furthermore, the system was investigated in the hydrophosphination catalysis of styrene by Trifonov and coworkers.[229]

With the exception of the Ln^{II} crown ether system (**75**), only three more species active in the ROP of cyclic esters have been crystallized. It was in 1998, when Greiner and coworkers[230] published the ROP of ε-caprolactam by the first BAr^F-system ever published (**1**, by Evans and coworkers in 1998).[50]

*Table 1.15: Immortal ROP of L-lactide and TMC by [{RO}Yb][$H_2N\{B(C_6F_5)_3\}_2$] **75a** according to ref. 228.*

Entry[a]	Monomer	RE[a]	T [°C]	t [min]	Yield[b] [%]	TOF[c] [mol (mol·h)$^{-1}$]	$M_{n,theor}$[d] [10^4g·mol^{-1}]	$M_{n,SEC}$[e] [g·mol^{-1}]	PDI[e]
1	*L*-lactide	Yb (**75a**)	60	180	70	233	1.0	0.9	1.03
2	*L*-lactide	Eu (**75a^{Eu}**)	60	180	74	247	1.1	1.0	1.05
3	TMC	Yb (**75a**)	30	5	44	5 280	0.5	0.4	1.09

[a] Initial concentration [*L*-lactide]$_0$ = 2.0 M; [TMC]$_0$ = 1.0 M; Solvent: toluene; [Monomer]/[RE][BnOH] = 1 000 : 1 : 10; RE = RE in $[\{RO\}Yb]_2^{2+}$;
[b] Yield of the isolated polymer;
[c] Non-optimized turnover frequency determined at the final reaction time;
[d] $M_{n,theor}$ =[monomer]$_0$/[BnOH$_0$] · yield ·$M_{monomer}$ · M_{BnOH};
[e] Determined by size exclusion chromatography calibrated vs. polystyrene standarts; M_n values were corrected by a factor of 0.58 for P*L*LA and 0.73 for PTMC;

The list of ROP catalysts with crystallographic known active species is completed by the two systems [Cp'Sc(CH_2SiMe_3)$_2$(thf)] (**16**) and [$Cp^{Me_4,o\text{-anisol}}$Sc($CH_2SiMe_3$)$_2$] (**17**) published in ref. 65 (*vide supra*), that were found to be active in the homopolymerization of ε-caprolactone and its block-copolymerization with styrene by subsequent monomer addition in 2010.[110] Full conversion was obtained in all cases by the $Cp^{Me_4,o-anisol}$-system and in case of the homopolymers, the Cp' system. For both precatalysts very narrow PDIs could be achieved. The resulting polymers have in addition been investigated for the mechanical properties of processed samples (see ref. 110 for details).

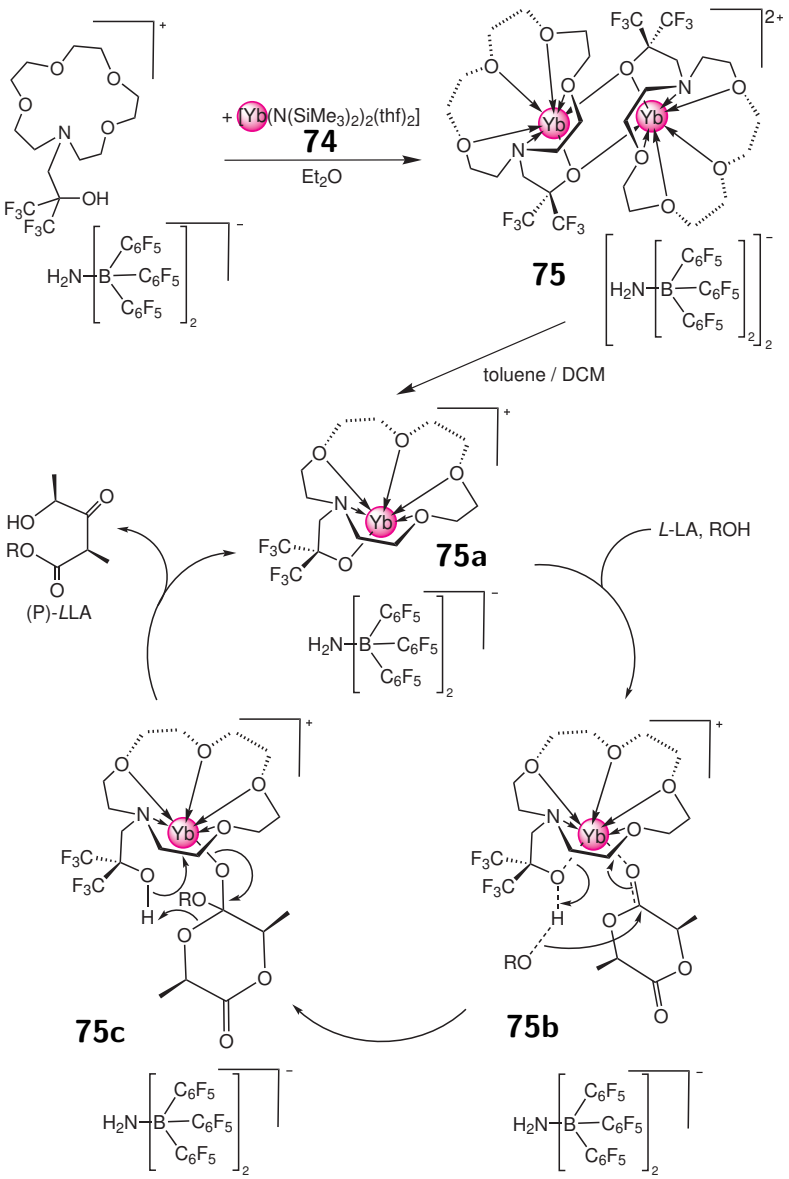

*Scheme 1.25: Catalyst synthesis and proposed ligand-assisted activated monomer mechanism for the iROP of L-LA mediated by $[\{RO\}Yb]_2[H_2N\{B(C_6F_5)_3\}_2]$ (**75a**, RO = cyclic amino-ether ([15-crown-5] analogue) containing an amine based $CH_2C(CF_3)_2OH$ side arm), where ROH = (P)LLA-OH. The active catalyst is synthesized by addition of the $[H_2N\{B(C_6F_5)_3\}_2]^-$ salt of the RO ligand to $[Yb(N(SiMe_3)_2)_2(thf)_2]$ (**74**) in Et_2O, and a solvent exchange to DCM or toluene resp. in order to break up the dimeric solid state structure of **75**. Scheme according to ref. 228.*

*Table 1.16: ROP of cyclohexene oxide and its alternating copolymerization with CO_2 applying Cp'Y-hydride clusters (**14a**) and Cp'Sc-bisneosilyls (**16**). Taken from ref. 63.*[a]

Entry[b]	Catalyst	Solv/Bulk	T [°C]	t [h]	Yield[c] [%]	TOF[d] [g (mol·h)$^{-1}$]	M_n[e] [10^4·g·mol^{-1}]	PDI[e]	CL[f] [%]
1	[{Cp'YH_2}$_4$(thf)] (**14a**)	Tol	rt	6	10	—	5.8	2.60	—
2	[{Cp'YH_2}$_4$(thf)] (**14a**)	Bulk	rt	3	77	—	6.9	2.01	—
3	[Cp'Sc(CH_2SiMe_3)$_2$(thf)] (**16**)	Tol	rt	6	40	—	14.7	2.38	—
4	[Cp'Sc(CH_2SiMe_3)$_2$(thf)] (**16**)	Bulk	rt	3	85	—	5.1	2.89	—
5[g]	[{Cp'YH_2}$_4$(thf)] (**14a**)	Tol	70	24	—	437	3.5	4.39	97
6[g]	[Cp'Sc(CH_2SiMe_3)$_2$(thf)] (**16**)	Tol	70	24	—	567	0.8	3.68	23

[a] Please see ref. 63 for details on the polymerizations involving the Dy, Lu and Y-derivatives of the resp. given complexes.
[b] Conditions: [Ln] = 0.063 mmol; CHO / Ln = 400; toluene (Tol), if any: 2 mL;
[c] Yield of the isolated polymer;
[d] Turn over frequency;
[e] determined by GPC calibrated vs. polystyrene standards;
[f] Carbonate linkage rate; Determined by the integration of the methine resonances in the ^{1}H-NMR spectrum;
[g] Conditions: 12 atm of CO_2; [Ln] = 16.3 mmol/L; [CHO] = 6.5 mol/L;

1.2.2.7 Ring-opening polymerization of epoxides

In 2005, Hou and coworkers[63] published the only study in this field so far in which they investigated the homopolymerization of cyclohexene oxide (CHO) and its copolymerization with CO_2 applying two catalysts.
The first catalyst that was structurally characterized in this study[231] is [{Cp'LnH_2}$_4$(thf)] (Ln = Y (**14a**), Dy (**14a^{Dy}**), Lu (**14a^{Lu}**)), which was active as a single-component catalyst without any addition of borates or Al-compounds in CHO polymerization (cf. polymerizations of other monomers, *vide supra*). For all three tested Ln, yields below 20 % were obtained (CHO / Ln = 400) after 6 h. Only under bulk conditions larger yields were found (up to 77 %) even after 3 h (see Table 1.16, runs 1–2). Interestingly, M_n does not significantly increase, when changing from solution to bulk, even taking the lower polymerization time into account.[232] This means that most of the yield gain is caused by the fact that more Ln centers were involved in the polymerization. A higher exchange rate of the coordinating THF by a CHO molecule and / or a higher reaction

temperature, as no solvent mediates the released thermal energy of the exothermic chain growth reactions, could be the reason.

In contrast to the homopolymerization, the copolymerization of the Ln-hydride clusters with CO_2 were performed at higher temperatures, e.g. 70 °C (at 12 atm, ca. 12 bar CO_2 pressure) resulting in almost perfectly alternating copolymers (carbonate linkage rate $\gg 90\,\%$ in all cases)(see Table 1.16, run 5). Compared to the homopolymers, these polycyclohexylcarbonates show surprisingly high PDIs which was not further commented on by the authors.

Although the activated $BAr^F{}_4$ salt of the Y complex (**14a**) is known as well, it has not been tested in epoxide ring-opening polymerization so far.[62]

The second crystallized complex used in this study was ([Cp'Sc(CH_2SiMe_3)$_2$(thf)]) (**16**).[65] Compared to the other Ln derivatives of this ligand set tested in this study, the Sc compound reveals an extraordinarily high performance in CHO-homopolymerization in toluene, while in bulk it did not differ much from analogue complexes of other Ln except for the much higher PDI (2.89 compared to 2.06 – 2.27 for the analogue complexes of other Ln.[63]) (see Table 1.16, runs 3 – 4). This leads to the question if in case of the Sc derivative, in toluene solution a different initiation or even propagation mechanism causes the deviant behavior. Cause of this discrepancy could possibly be either a lack of toluene coordination due to steric reasons or the higher exchange rate of cyclohexylene oxide vs. toluene. This exchange cannot take place in the bulk case. It is unfortunate that the authors could not obtain further insight into the CHO-polymerization intermediates

despite best efforts. Still it can be assumed that the initiation of this polymerization must follow a completely different pathway as that of the other monomers, as CHO is even more bulky than those, but does not require cationization. It is probable, that the initiation takes place by the exchange of the coordinated thf by CHO which is in high excess at that moment. Speculations about the role of the released THF (mediator of the polymerization, comonomer or just none) could possibly be clarified by an NMR spectroscopic experiment applying a precatalyst bearing a deuterated thf-ligand.

The high tendency of **16** toward CHO-homopolymerization is also the reason for its relatively poor performance in the copolymerization with CO_2 which mainly resulted in polyether (only 23 % carbonate linkages) (see Table 1.16, run 6). As the CHO-polymerization intermediates were not accessable (*vide supra*), the authors attempted to synthesize CO_2 insertion products which they obtained as dimers bridged by the resulting caboxylates. $[Cp'Ln(O_2CCH_2SiMe_3)_2]_2$ is active in the CHO-CO_2-copolymerization as well, as shown for Ln = Y (**16a**), Lu (**16a^{Lu}**). The copolymers produced in this context are similar to those produced by $[Cp'Ln(CH_2SiMe_3)_2(thf)]$ (Ln = Y (**16**), Lu (**16^{Lu}**). As only a cationic model complex is known for the activation of the Sc derivative, which has not shown any polymerization activity yet, it was not tested in this polymerization.[65]

1.2.2.8 Comparison of the single-component catalyst crystal structures

It is a matter of fact, that model systems, e.g. cations stabilized by coordinated donor (solvent) ligands can give hints on the nature of the active catalyst species, but they can also be misleading. This is because the structure in a donor-free environment is likely to differ in case of much lower steric saturation. The systems tend to avoid this energetically suboptimal condition e.g. by aggregation or even ligand activation, reactions that cannot be pictured by donor ligands.
For the purpose of a deeper insight into the "black box" of active species in lanthanide-based catalytic polymerization, the few existing single-component BAr^F-structures shall be compared.
So far, seven general systems with in total nine crystal structures qualify as active catalyst species, as they do not only polymerize the same monomers as their corresponding *in situ* generated analogues, but they also lead to very similar polymers and are produced according to the same procedures as the *in situ* catalysts.[233]
It is remarkable, that five of the seven systems are Sc complexes with three containing the same Cp'-ligand.[64, 79] But besides bearing the same ligand, the complexes are different. Despite of the obvious difference in their alkyl ligands (η^3-allyl in one case and a dimethylamino benzyl in the two other cases, decorated with a anisyl donor in one case), the most significant difference is that these complexes show a completely different behavior concerning steric saturation. This is caused both by the different alkyl ligands and the fact that the three active species are produced in two different solvents (toluene and chlorobenzene). While $[Cp'Sc(o\text{-}CH_2C_6H_4NMe_2)]^+$ (**26**) coordinates the anion *via* two of its

fluorine atoms, $[Cp'Sc(allyl)]^+$ (**36**) coordinates either the arylic solvent (if cocatalyst **A** is applied) or $PhNMe_2$ in case of cocatalyst **B** (see Schemes 1.10 and 1.13) and $[Cp'Sc(o\text{-}CH_2C_6H_4NMe_2)(anisole)][BAr^F{}_4]$ (**28**) is already saturated without further coordination due to its anisyl donor. Although the electronic properties of the Sc centers might be slightly different, this finding can be rather explained by steric effects as the allyl moiety is much smaller than the aminobenzyl group. Still, during polymerization, after a few monomer additions, both alkyl groups and the anion or the resp. η^6-aryl ligand are too far away from the active center to influence the polymerization. This explains the similar microstructures of the polyisoprenes that are obtained with **26** and **36** (cf. refs. 79 and 174). System **28** instead, is active in the polymerization of styrene, where its anisyl moiety serves as chain shuttling agent.

The fourth monomeric and Sc structure $[Cp^*ScMe(O{=}P(^tBu)_3)][BAr^F{}_4]$ (**13**, see Scheme 1.6) was presented several years earlier by Piers and coworkers.[59] It is produced by the neutral cocatalyst **C**, that forms an anion by satisfying its borons electrophility by abstracting a methyl group from the precatalyst. This methyl moiety bound to the boron atom coordinates to scandium in the resulting ion pair to fulfill the steric demand of the Sc center. The ion pair is active as single-component catalyst in the polymerization of ethylene and has not been tested with further monomers (probably due to the steric bulk of the coligand). The catalyst becomes less active with temperatures above r.t. as it decomposes under such conditions.[233]

The final Sc-based single-component catalyst is to the best of our knowledge the first crystallized active species that is a monomer

insertion product.[128] Enolate [(Dipp-"nacnac^{Me_2}"-$(CH_2)_2$)-PPh_2-CH_2-C(Me)=C(OMe)-O)Ln(OAr)]$^+$ (Ar = 2,6-di-*tert*-butylphenyl, **45**) is active in the polymerization of MMA. The monomer is inserted into the Ln-P bond of its precursor that bears a P-donor side arm substituted version of a "nacnac^{Me_2}" ligand. Besides from MMA, the single component catalyst has not been tested in the polymerization of other monomers so far.
Taube's $[La(allyl)_2(thf)_4]^+$ (**48**), synthesized and characterized at rt. is the only example of a structurally characterized single-component catalyst ion pair of a Ln center larger than Y.[4] Due to the large number of donor ligands, a coordination of the anion is not possible here. So far it was only tested in the polymerization of 1,3-butadiene at 50 °C. Although being the historically first published Ln centered cationic single-component catalyst, it did not catch much attention by the comunity yet, as the precursors in its synthesis also serve as single-component catalysts and the activation is therefore not necessary to enable polymerization.[129]

In addition, Hou and coworkers[62] presented the structure of tetrameric Y hydrido clusters (**14**, **14a** and **14b**). These are either coordinated by one or two thf ligands if THF is present in the synthesis, alternatively one fluorine atom of the BAr^F anion is coordinated. Comparing this structure to Kempe's and Trifonov's trimeric hydrido clusters[69, 70] (Y (**18^Y**)), Lu (**18^{Lu}**)), coordinated by the Ap*-ligand (Ap* = [($C_6H_3{}^iPr_3$-2,4,6)-(*o*-C_5H_3N-*o*)-N-($C_6H_4{}^iPr_2$-2,6)]) and one THF molecule per Ln center, the most obvious difference is, that the Hou-system needs cationization to promote polymerization (in all cases except the ROP of the epoxide CHO), while the Kempe / Trifonov-system catalyzes the polymerization of various monomers as the non-cationized precatalyst. To explain this observation

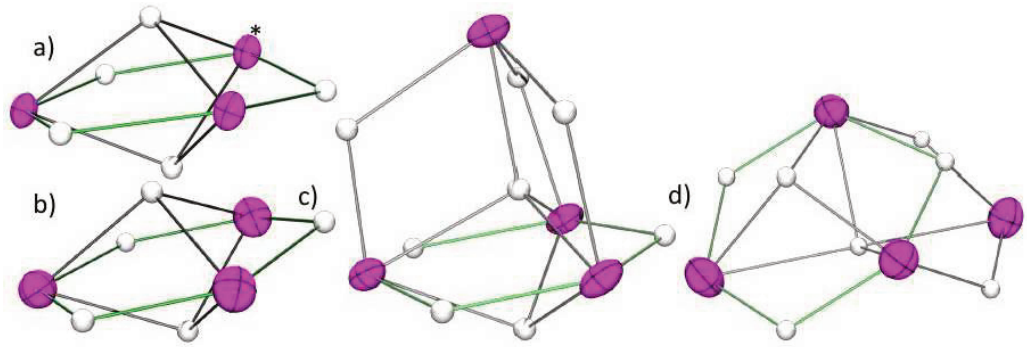

*Figure 1.1: ORTEP drawings of the yttrium hydride cores of four structures. General: Non-hydride-ligands and the $[BAr_4^F]^-$ ion (in figure part b and d) are omitted for clarity. Y atoms are shown in pink, H atoms are white. The Y_3H_3 rings are highlighted in green as they form the common motif of these four structures, together with the hydrides overcapping them on both sides of the ring. All elipsoids are set to 50 % probability. a) Neutral trimeric structure taken from ref. 69. It is active in polymerization of ethylene without further activation. The Y-atom bearing the neosilyl anion is marked with * to explain the slight asymmetry. b) Cationic trimeric structure taken from ref. 70. It is active in polymerization of several monomers. c) Tetrameric structure taken from ref. 231. It serves as the inactive precursor in ref. 62. d) Cationic tetrameric structure taken from ref. 62. In contrast to its precursor it is active in the polymerization of several monomers.*
The similarities in the steric situation of the Y-atoms in figure parts a, b and the outer Y atoms in figure part d are visualized.

a closer look into both structures is necessary.

Independent of the supporting ligand, in both structures, a $\{Ln_3(\mu_2H)_3(\mu_3H)_2\}$ substructure motif is found (see Figure 1.1, marked in green). In case of the tetramer, two of these substructures are anilated sharing one Y-H-Y triangular face (see Figure 1.1d). Its pre-catalyst, the non-activated tetramer, instead shows only one of these substructures capped by a YH_3 unit (see Figure 1.1c). As a matter of fact, this leads to the conclusion, that in the cationic case, at least two Y-atoms are in a sterically saturated situation which is very similar to that of the

Ln in Kempe's and Trifonov's trimer. Instead, the capped non-activated tetranuclear structure does not contain such "terminal" Y centers, but instead far more crowded surroundings at its Y-atoms. In other words, the μ_3H–Y–μ_2H$_{cap}$-angles are above 114 °(see Figure 1.1c), while in case of the polymerizing clusters, the largest HYH-angle perpendicular to the six-membered ring is below 60 °(see Figure 1.1a, b, d). Therefore, the accessibility of the Y centers for the monomers is much higher in the active cases, which might be the reason for their activity. The fact that a radial orientation of the supporting Ap*-ligand in the trimeric clusters is in contrast to the tangential orientation of the Cp'-ligand in the tetrameric clusters might also assist in allowing polymerization even in the non-activated case. Further, the fact that there is a polymerization in the activated case of the Cp' system shows that this cannot be the main steric aspect.

Still it should not be neglected that the polymerization performance of Kempe's and Trifonov's trimer increases when it is activated and cationized.[70] The absence of the neosilyl moiety (which is bulkier than the thf ligand in the activated form), the thereby augmented symmetry[234] and the positive charge will take part in this finding.

In case of the ROP of CHO of the Cp'-systems,[63] the steric accessibility does not play the main role, probably due to the ability of the epoxide monomer to exchange with the thf-ligand, which would then be the initiative step of the polymerization.

Next to these BAr^F-structures stands the AlAr^F structure [Cp*La(Me$_3$AlAr^F)(μ-Me$_2$AlAr$^F{}_2$)]$_2$ (**72**) of our research group.[225] The hazardous[227] catalyst (see Scheme 1.24) shows two types of AlAr^F-

anions. While (μ-$Me_2AlAr^F{}_2$) bridges the two metal centers of the dimer, (Me_3AlAr^F) is bound to a single La and shows a close La–F interaction. Homopolyisoprenes produced by this catalyst are of high *trans*-content and narrow PDI at unexpectedly high molecular weights.

This example also implies that in the large amount of ternary cases where precatalysts activated by BAr^F cocatalysts and a trialkylaluminate or an AlR_3 activator is present $AlAr^F$ species are likely to be the polymerizing catalyst. Crystallized active species of these systems are not currently known, but would probably provide significant insight into what is occurring within this "black box" paradigm.

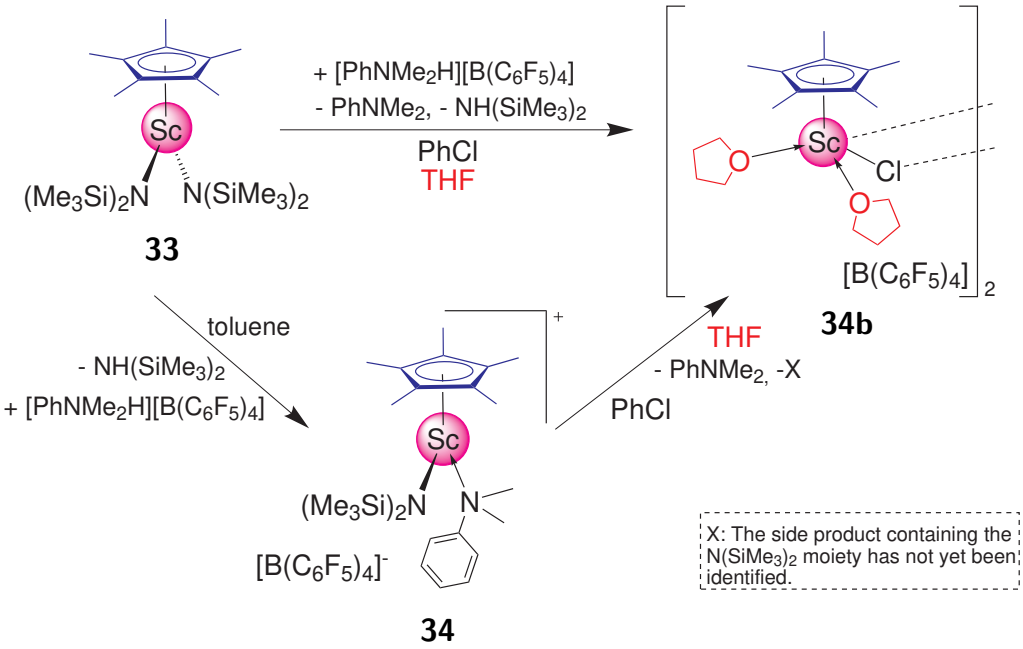

*Scheme 1.26: Instead of stabilizing the cation with thf ligands (see Scheme 1.12), the active catalyst (**34**) published by Luo and coworkers in 2014 can also react with PhCl, that was investigated as a possible solvent for catalysis. Here, again by the addition of THF, a species (**34b**) can be obtained, that has the amido ligand exchanged for a chlorido moiety. Scheme according to ref. 115.*

1.2.2.9 Investigations on Catalyst Degradation Pathways

A catalyticly active species is in most cases not only active, when exposed to a substrate, that it can catalyze, e.g. a monomer. Ageing, inter- or intracompound reactions that decrease the energetic or steric driving force of the reactivity of the species will occur in the course of time. The resulting products of such catalyst degradation reactions or non-polymerization reactivities of active species have been investigated and some of them even crystallized in several studies. Examples of possible pathways are given in this section.

As the solvent is a reactant, that is available in large excess com-

pared to the active species, especially in polar media, reactions between active catalyst and solvent are observed. Luo and coworkers[115] produced dicationic species (with $[Cp^*ScCl(thf)_2]_2[BAr^F{}_4]$ (**34b**)), by addition of a small amount of THF to a solution of their active species $[Cp^*Sc(N(SiMe_3)_2)(PhNMe_2)][BAr^F{}_4]$ (**34**) in PhCl (see Scheme 1.26).

A degradation reaction involving the BAr^F-anion was reported by Piers and coworkers.[235] In their study (Scheme 1.27) they investigated a non-crystallizing Y species bearing an anilido-imine ligand $[(amim)Y(CH_2SiMe_2Ph)_2(thf)]$ (**76**, amim = anilidoimine, Dipp-N=C-(*o*-C_6H_4)-N-Dipp) and its cationized analogue $[(amim)Y(CH_2SiMe_2Ph)(thf)][B(C_6F_5)_3(CH_2SiMe_2Ph)]$ (**77**, see Scheme 1.27). While **77** could only be observed by NMR spectroscopy at temperatures below -20 °C, the species degraded by an Ar^F-shift to neutral $[(anim)Y(Ar^F)_2(thf)]$ (**77a**) at r.t.. Addition of an excess of THF during the cation formation led instead to a temperature stable white powder of $[(amim)Y(CH_2SiMe_2Ph)(thf)_2][B(C_6F_5)_3(CH_2SiMe_2Ph)]$ (**77b**). The same type of anion activation was also found for their "nacnac^{Me_2}" system published in the same year ([("nacnac^{Me_2}")$ScMe_2]_2$, (**7**)) that can be cationized (to give [("nacnac^{Me_2}")ScMe][$MeB(C_6F_5)_3$], (**9**)) by cocatalyst **C** to react on to the Ar^F-shifted [("nacnac^{Me_2}")$Sc(C_6F_5)$][$Me_2B(C_6F_5)_2$] (**9a**) by heating to r.t. (see Scheme 1.4).[56, 57]

Especially, when cocatalyst **B** is applied, side products of the cationization can be activated as well. Beyond coordination[236] toward the active metal center as a N-donor, $PHNMe_2$ has shown reactivities of its *o*-arene hydrogene atoms, which implies potential to serve as a mono-anionic

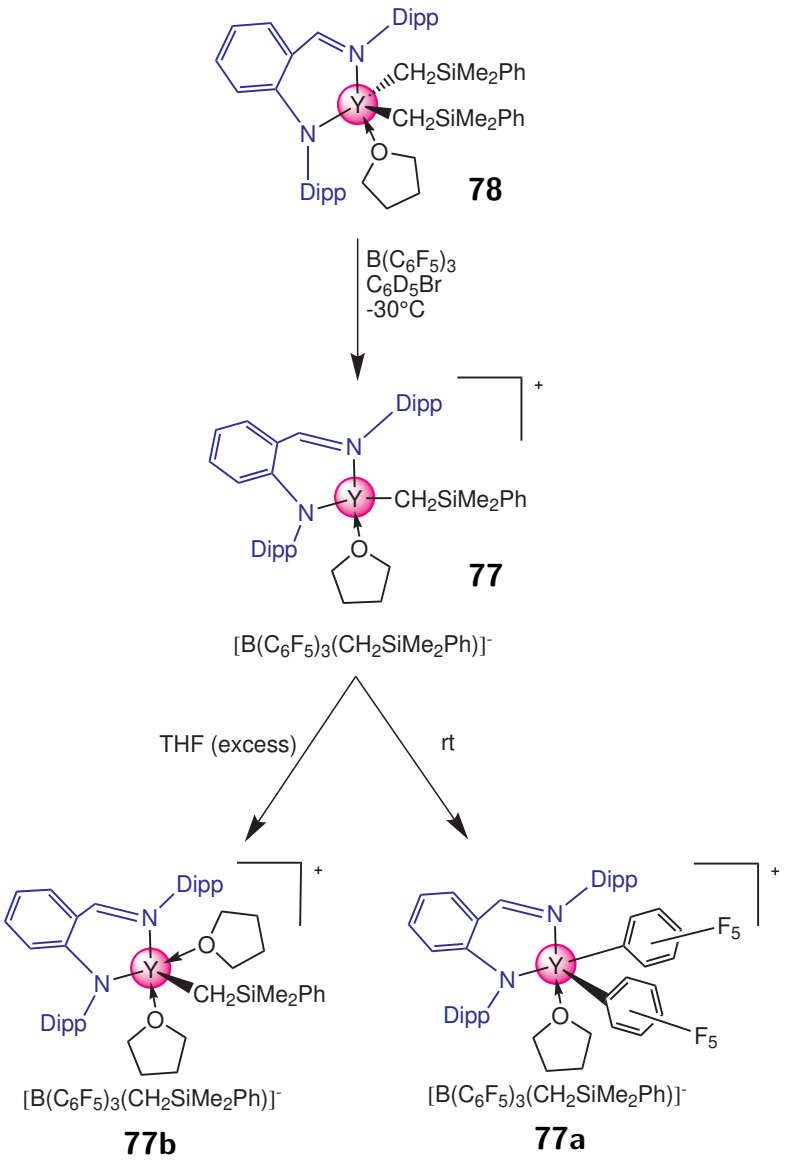

Scheme 1.27: The cationic species ***77****, that is produced below -20 °C by the addition of cocatalyst* ***C*** *to the precoursor [(amim)Y(CH$_2$SiMe$_2$Ph)$_2$(thf)] (****78****) reacts under double Ar^F shift to* ***77a****, when heated to r.t.. Addition of an excess amount of THF to* ***76*** *produces the temperature stable bis-thf-adduct* ***77b****. Scheme according to ref. 235.*

bidentate ligand (Paper V). Here, we observed a polymeric structure of $[Cp^*_2Y_2(Me)_2(C_6H_4NMe_2)]$ cations alternating with a BAr^F_4 anions

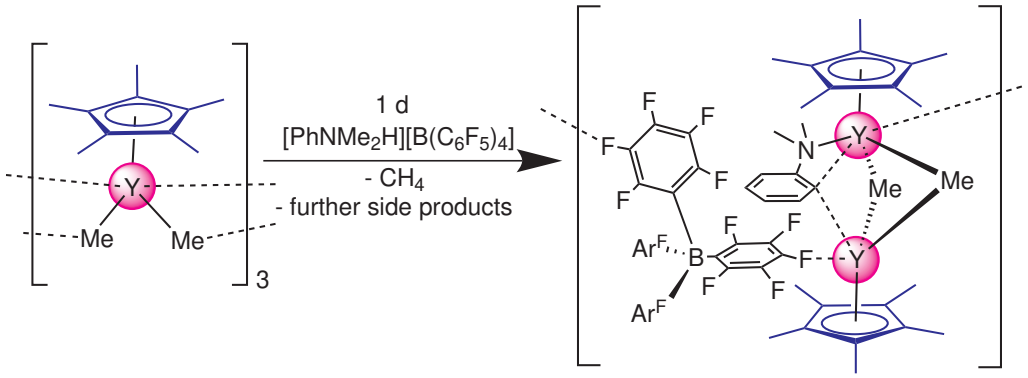

79 **80**

*Scheme 1.28: The polymeric degradation product **80** crystallized from a toluene solution of precatalyst [Cp*YMe$_2$]$_3$ and cocatalyst **B**. Scheme according to Paper V.*

coordinated to both Y centers with two fluorine atoms of different Ar^F moieties (**80**)(s. Scheme 1.28). This finding disproves Hou and coworkers, who suggest a monomeric active species for that system according to DFT calculations at least in parts.[237] A publication discussing our findings on the catalyst system in detail has been accepted (Paper V).

The final frequently observed phenomenon that shall be mentioned in this context is a degradation via C–H bond activation at the ancillary ligand backbone.[238] Interestingly, this degradation pathway does not automatically inactivate the ion pair in terms of polymerization potential.[239] Instead we found by NMR spectroscopy for our trispyrazolylborate system ([Tp$^{t\mathrm{Bu,\,Me}}$Lu(Me)(Me$_3$AlB(CN-C$_6$H$_4$*i*Pr$_2$)$_2$)], **81**), that the active species is altered by C–H activation during the polymerization applying cocatalyst **B** (see Table 1.17, runs 1 and 2). Still, thermolytic C–H activation is also possible without cationization with this system, leading to the second precatalyst presented in our article ([Tp$^{*,t\mathrm{Bu,\,Me}}$Lu(Me$_2$AlB(CN-C$_6$H$_4$*i*Pr$_2$)$_2$)],

*Table 1.17: Isoprene polymerization applying [Tp$^{tBu,\ Me}$Lu(Me)(Me$_3$AlB(CN-C$_6$H$_4$iPr$_2$)$_2$)] (**81**) and [Tp$^{*,tBu,\ Me}$Lu(Me$_2$AlB(CN-C$_6$H$_4$iPr$_2$)$_2$)] (**81a**), data taken from ref. 239.*

Entry[a]	Precatalyst	Cocat.[b]	t [h]	Yield[c] [%]	*cis*[d] [%]	*trans*[d] [%]	3,4[d] [%]	M_n[e] [$10^4 \frac{g}{mol}$]	PDI[e]	T_g[f] [°C]
1	[Tp$^{tBu,\ Me}$Lu(Me)(Me$_3$Al"boryl")] (**81**)	**B**	1	47	72.5	2.6	24.9	11.9	3.72	-47.5
2	[Tp$^{tBu,\ Me}$Lu(Me)(Me$_3$Al"boryl")] (**81**)	**B**	24	89	68.7	7.5	23.9	14.0	2.98	-48.2
3	[Tp$^{*,tBu,\ Me}$Lu(Me$_2$Al"boryl")] (**81a**)	**B**	1	2	70.4	4.0	25.6	36.1[g]	1.81[g]	-46.0
4	[Tp$^{*,tBu,\ Me}$Lu(Me$_2$Al"boryl")] (**81a**)	**B**	24	90	66.7	5.7	27.6	27.9[g]	2.60[g]	-45.9

[a] Conditions: 20 µmol of Ln, 20 µmol of cocatalyst, 20 mmol of isoprene, 8 mL of toluene. * marks C–H-bond activation, "boryl" = B(CN-C$_6$H$_4$iPr$_2$)$_2$).
[b] **A** = [Ph$_3$C][B(C$_6$F$_5$)$_4$], **B** = [PhNHMe$_2$][B(C$_6$F$_5$)$_4$], **C** = B(C$_6$F$_5$)$_3$.
[c] Yield of the isolated polymer.
[d] Determined by ^{1}H and ^{13}C NMR spectroscopy.
[e] Determined by GPC in THF against polystyrene standards.
[f] Determined by a Perkin Elmer DSC 8000; heat rate: 20 K/min, cooling rate: 60 K/min.
[g] MWD contains more than one mode. The data of the main mode is given here. It represents 98 mol% (run 3), and > 99 mol% (run 4) of the polymer.

81a, where "*" indicates, that two *tert*butyl groups of the ligand are C–H activated and bind to the Lu center *via* the resulting CH_2 moieties, see Scheme 1.29). Both systems led to identical presumed chain propagation structures, after C–H activation occuring for species **82** toward **82a**, which is confirmed by the similar obtained polymers for the polymerizations after 24 h (see Table 1.17, runs 2 and 4).

These four examples show inevitably that investigations into degradation structures and species can provide insights into the nature and catalytic behavior of an active catalyst and should be considered, whenever a catalytic mechanism or species is intended to be elucidated.

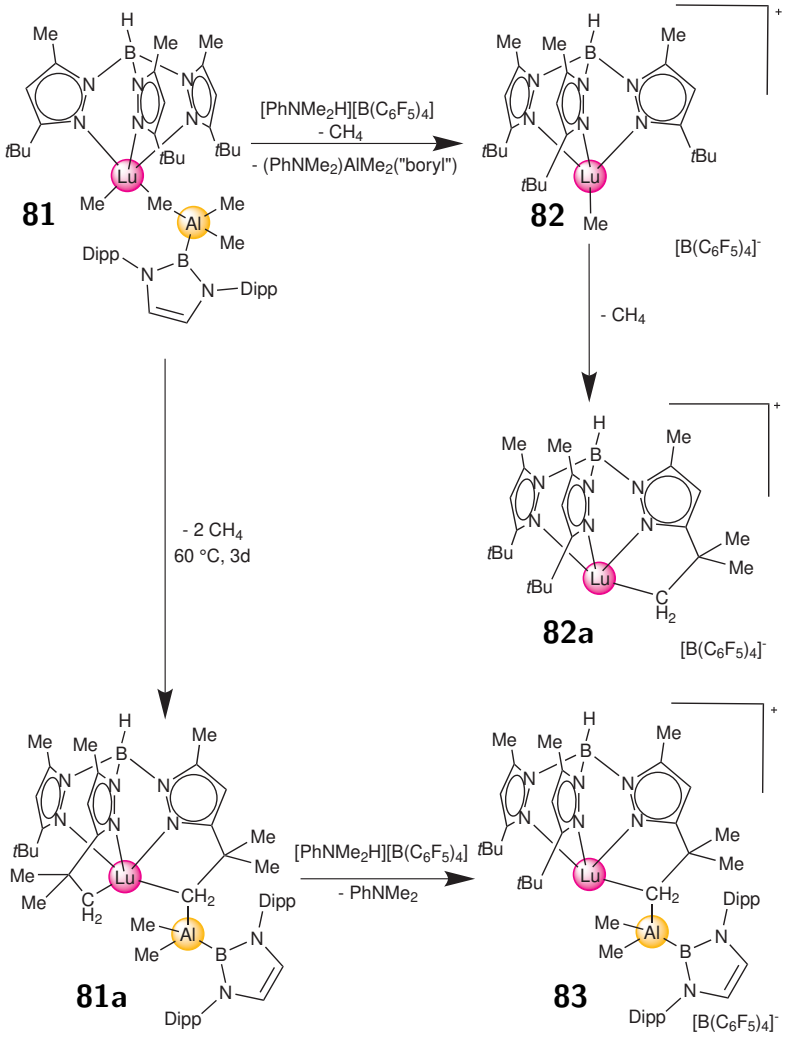

*Scheme 1.29: Catalyst degradation starting out from [Tp$^{tBu,\ Me}$Lu(Me)(Me$_3$AlB(CN-C$_6$H$_4$iPr$_2$)$_2$)] (**81**) leading to [Tp$^{tBu,\ Me}$Lu(Me)][BAr$^F{}_4$] (**82**) upon cationization applying cocatalyst **B**, which reacts on to [Tp$^{\#,tBu,\ Me}$Lu][BAr$^F{}_4$] (**82a**) and the thermal degradation of **81** towards [Tp$^{*,tBu,\ Me}$Lu(Me$_2$AlB(CN-C$_6$H$_4$iPr$_2$)$_2$)] (**81a**), which leads to [Tp$^{\#,tBu,\ Me}$Lu(Me$_2$AlB(CN-C$_6$H$_4$iPr$_2$)$_2$)][BAr$^F{}_4$] (**83**) upon activation with cocatalyst **B**.*[240] *Scheme according to ref. 239 (Paper III).*

1.2.3 Ion Pairs Inactive in the Coordinative Polymerization

Besides those ion pairs investigated due to their polymerization properties mentioned above, some have also been synthesized for other applications like small molecule activation or have not yet been examined for their polymerisation ability. In addition, some of the polymerisation catalyzing species shown earlier in this review are once more mentioned in this section as they were originally intended to be applied for other purposes.
Historically there is a Cp^*_2Sm-system (**1**) to be mentioned first (see Scheme 1.2). Evans and coworkers[50] published the crystal structure in 1998, after it had successfully been used in ethylene polymerization,[52] and suggested its application in α-olefin polymerizations. These were not published till date, but Greiner and coworkers applied this system in the ring-opening polymerization of cyclic esters[230] (*vide supra*). The structure contains a Sm center, that has coordinated two fluorines located at the same Ar^F-ring and one hydrogen of the anions methyl moiety.
One year later, in 1999, Piers and coworkers were the next to contribute to the field.[55] Activating their diketiminato-system [("nacnac^{Me_2}")Sc$(CH_2Ph)_2$(thf)] (**5**) with cocatalyst **C**, they obtained one of the benzyl moieties bound to the boron of the anion, while its phenyl ring coordinated in η^6-mode to the Sc center. Although this system failed to polymerize ethylene, the group was able to apply it successfully in H_2-activation.

In 2001, Taube and coworkers present {[Nd(allyl)Cl$(thf)_5$][$BAr^F{}_4$]·THF} (**87**), an ion pair, that was obtained from a feasability study.[241, 242] The question if such an ion pair was possible to be synthesized arose from 1,3-

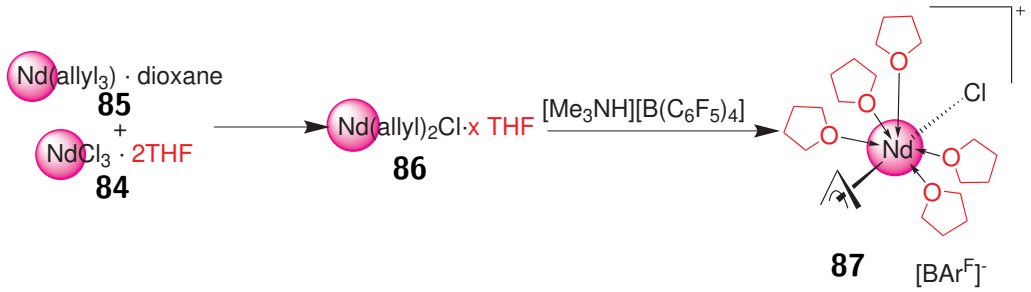

*Scheme 1.30: Synthesis of [Nd(allyl)Cl(thf)$_5$][BAr$^F{}_4$] (**87**) from thf and dioxane adducts of the homoleptic Nd chloride (**84**) and trisallyl (**85**) via [Nd(allyl)$_2$Cl·x THF] (**86**). Scheme according to ref. 242.*

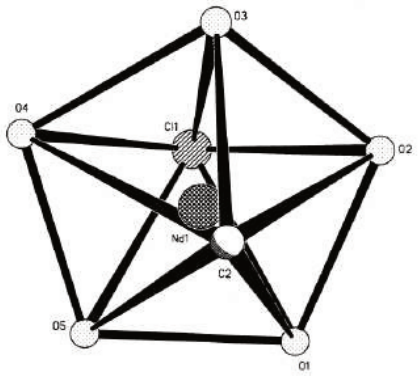

*Figure 1.2: Pentagonal bipyramidal coordination polyeder of [Nd(allyl)Cl(thf)$_5$][BAr$^F{}_4$] (**87**). Taken from ref. 242.*

butadiene polymerization studies applying various catalysts derived from [Nd(allyl)$_2$Cl(thf)$_2$] (**86**) and activated by MAO, HIBAO and several other cocatalysts.[4, 243–245] Although it cannot be seen as a classical model complex for the catalysis, as the cocatalysts applied in the polymerization study were not considered in its preparation (see Scheme 1.30), it is another early example of the attempt to gain insight into lanthanide centered polymerization catalysis by the investigation of a crystal structure of a compound related to the intended active species (cf. the homoleptic al-

lyls in refs. 129–131 and 4, *vide supra*). The cation has the shape of a neodymium-centered pentagonal bipyramide, where the THF-oxgens are located at the verteces of the pentagonal plane and allyl and chloride form the tips. A coordination of the anion is not possible in this compound, due to the high saturation of the cationic Nd center, by the five thf-ligands (see Figure 1.2).

After a another gap of two years in which no activity in the field can be reported in terms of non-polymerizing systems, Shore and coworkers[246] synthesized a divalent Yb center only surrounded by thf-ligands (**88**), and applied it in the systhesis of various Yb^{II}-species (e.g. $Yb(BH_4)_2$). In the cation, the steric saturation of the Yb center by the thf-ligands rules out the coordination of the anion.[247]

Then, two years later Hessen and coworkers[248] observed the active species Bercaw and coworkers had applied in ethylene polymerization earlier.[249] They showed, that $[Cp^*ScMe]^+$ (**89**) coordinates to two neighboring fluorines of an Ar^F ring of the anion (*vide supra*).

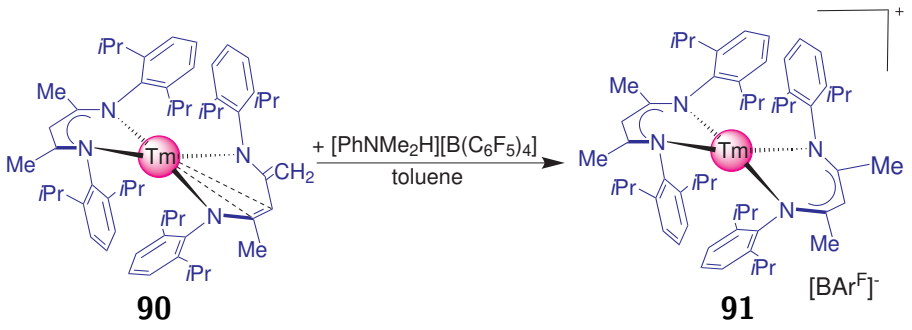

Scheme 1.31: Synthesis of the first bisdiketiminato Tm cation (L = anionic diketiminato-ligand). Scheme according to ref. 250.

The first bisdiketiminato ("bisnacnac") ion pair (**91**) was published in the same year by Lappert and coworkers[250] by applying cocatalyst **B** to a Tm-complex containing both the anionic diketiminato-ligand and a protonated neutral ligand (**90**) (see Scheme 1.31). No direct interaction between anion and metal center was obtained, due to the steric bulk of the two "nacnac^{Me_2}"-ligands. Lappert and coworkers do not suggest any application for their system as their project was meant as a feasibility study concerning the "bisnacnac"-motif.

The next two structures that were published in this field, both in 2005, were once again "nacnac"-systems of scandium and were investigated by Piers and coworkers.[57] In both cases cocatalyst **C** was applied to the resp. precursor, which was either [("nacnac^{Me_2}")$ScMe_2]_2$ (**7**) or [("nacnac$^{t\mathrm{Bu}}$")$Sc(CH_2SiMe_3)_2$] (**92**). While in case of the neosilyl-system only the methyl-moiety in the resulting anion is bridging to the metal center, for the methyl-derivative, the situation is remarkably different. Here, a whole Ar^F-ring is transferred to the metal center at r.t., and the remaining $MeBAr^F{}_2$ binds to the second methyl moiety resulting in a methyl-bridged $Me_2BAr^F{}_2$-anion (see Scheme 1.4, *vide supra*). This shows furthermore, how much the substituend in the "nacnac" backbone influences the steric situation of the complex and therefore its reactivity (cf. the monomeric [("nacnac$^{t\mathrm{Bu}}$")$ScMe_2$] (**3**), *vide supra*).

Although different ligand binding occurs for the neosilyl derivative, it holds its own remarkable characteristics. There, only a methyl moiety is found attached to the $BAr^F{}_3$-anion while the remaining Me_2SiCH_2 inserts into the remaining Sc-neosilyl bond forming a $(CH_2Si(Me)_2CH_2SiMe_3)$-anion. This insertion leads to the conclusion that this system is likely to polyme-

rize isobuthylene, due to the structural similarity of these compounds.
This study was continued in 2007, when Piers and coworkers[251] applied larger "nacnac"-ligands to the bismethyl system. Thus, through the introduction of more steric bulk, η^6-arene stabilized cations in seperated ion pairs could be obtained.
One year earlier, the group had cationized [("nacnac$^{t\mathrm{Bu}}$")ScMe-amide (**93**) in order to perform ligand exchange reactions.[252] Once more, the resulting motif was a MeBAr$^{\mathrm{F}}{}_3$-anion interacting with the metal center *via* its methyl moiety.

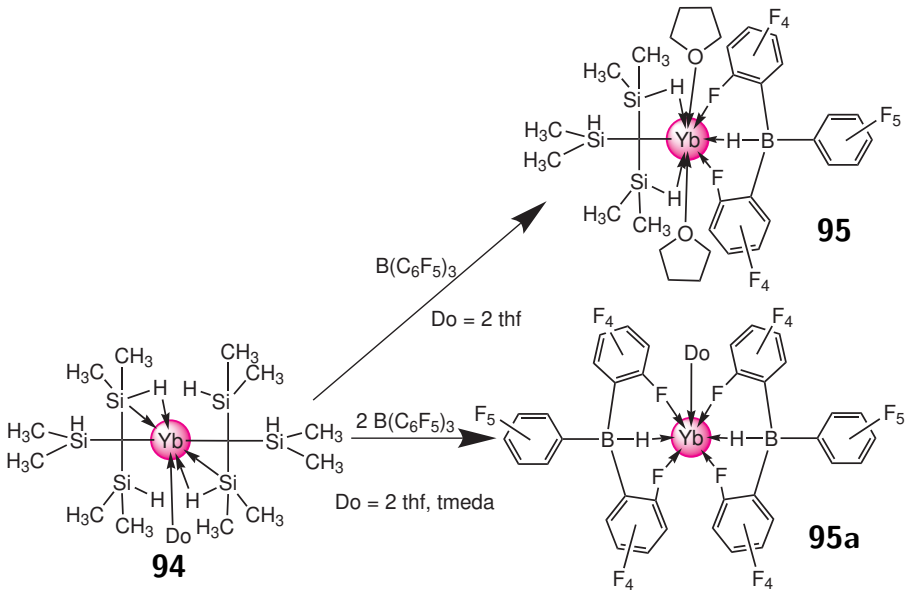

*Scheme 1.32: Synthesis of [Yb(C(SiHMe$_2$)$_3$)(thf)$_2$(μH)(μF-C$_6$F$_4$)$_2$BAr^F] (**95**) and [Yb{κ^3-HBAr$^F{}_3$}$_2$(Do)] (Do = tmeda (**95a(tmeda)**), Do = 2 thf (**95a(2 thf)**)) from [Yb(C(SiHMe$_2$)$_3$)$_2$(Do)] (**94**) applying one and two resp. equivalents of cocatalyst **C**. Scheme according to refs. 253, 254.*

In 2009, Sadow and coworkers begun Yb^{2+}-stabilization studies, which they continued in 2013.[253, 254] Starting with [(Yb(C(SiMe$_2$H)$_3$)$_2$(thf)$_2$] (**94**) they

obtained the dimerized dehydrogenated alkyl ligand, a Yb^{2+} complex bearing one alkyl ligand and a $HBAr^F{}_3$-anion upon activation with cocatalyst **C**. Here, the anion is coordinated via the hydride and two *ortho*-fluorines of different Ar^F-rings. The structures they obtained four years later contain two individuals of the same anionic motif (see Scheme 1.32). Steric saturation is achieved by the addition of either THF or TMEDA, which is found in the crystal structures in 2 (thf) or 1 (tmeda) coordinating equivalents.
For the purpose of hydrogen activation, Okuda and coworkers contributed to the field in 2011, and further in 2013.[255, 256] In both studies they present cationic Lu species bearing bulky multidentate N-donor ligands. Although both studies focus on structures containing the $[B(C_6H_3\text{-}3,5\text{-}(CF_3)_2)_4]^-$-ion, one $BAr^F{}_4$-structure is published for comparitive reasons in each of them. $[(Me_5\text{-TREN})CH_2)Lu(CH_2SiMe_3)][BAr^F{}_4]$ (**96**) ($(Me_5\text{-TREN})CH_2 = N(CH_2CH_2NMe_2)_2(CH_2CH_2N(Me)CH_2)$) and the dimeric $[(Me_4\text{-TCAD})LuH_2]_2{}^{2+}$ (**97**) (Me_4-TCAD = (NMe) analogue of crownether (4-crown-12)) are both produced in a reaction of cocatalyst **B** with the respective precursors. Their anions do not show any direct coordination to the Lu center.
Small molecule activation has also been a goal for other studies that led to BAr^F-structures of the lanthanides. The studies of Piers, Berkefeld and coworkers[257, 258] are one example in which small molecule activation is targeted. In order to activate CO, the group produced both $[Cp^*{}_2Sc][BAr^F{}_3H]$ (**98**) and its CO insertion product $[Cp^*{}_2Sc][BAr^F{}_2(C_6F_4CHO)]$ (**99**). In both cases the anions coordinate to the Sc center. The insertion precursor (**98**) shows that the direct interactions between the ions via two neighboring fluorines of one of the Ar^F-rings. Further, the insertion product (**99**)

coordinates only one fluorine and the oxygen atom of the incorporated CO.[257] In the case of CO_2, the same insertion precursor (**98**) leads to CO_2 insertion into the B–H bond, and therefore generation of ions (**100**) that are formally bridged by a formate moiety, without further fluorine coordination. (see Scheme 1.33).[258]

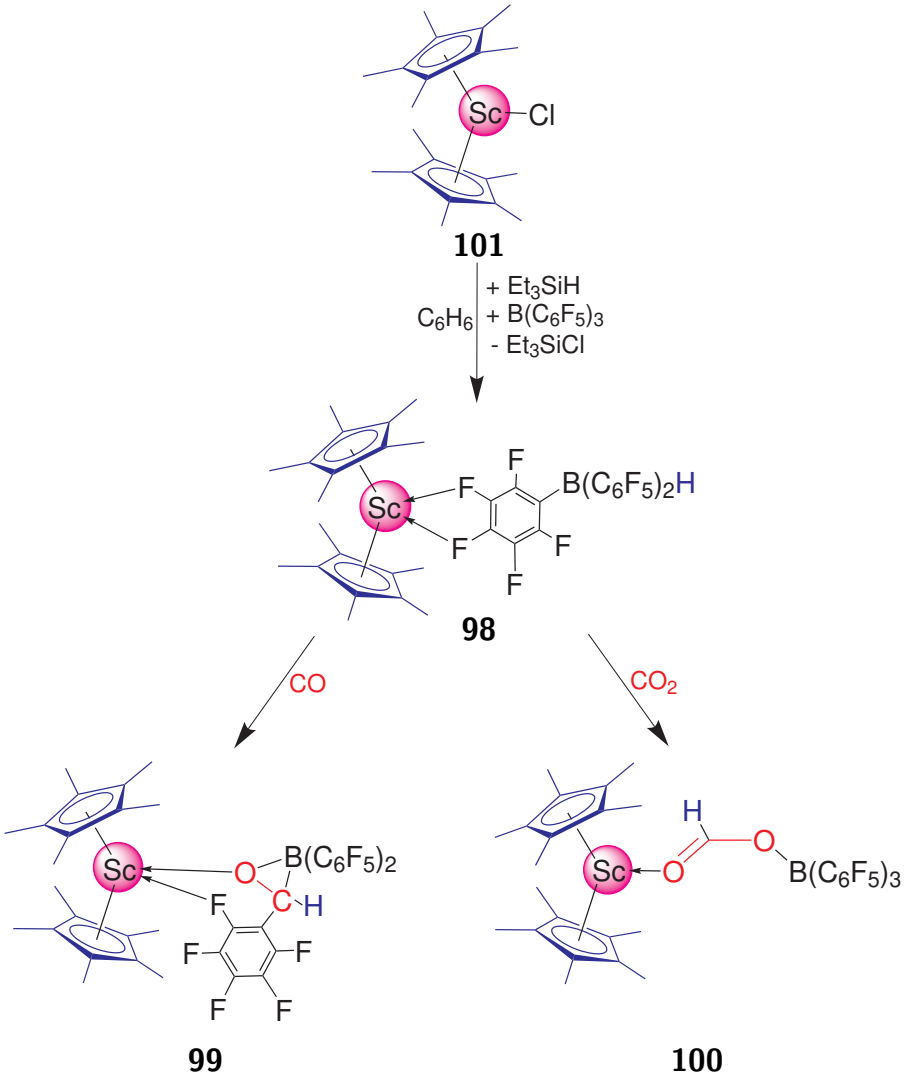

*Scheme 1.33: Synthesis and small molecule activation of $[Cp^*_2Sc][BAr^F_3H]$ (**98**). Scheme according to refs. 257 and 258.*

A further interesting ion pair was reported in 2013. Hou and coworkers[259] show, that a cubane type complex $[Cp'_4Lu_4(CH_2)_4]$ (**102**) can be protonated by cocatalyst **B** which simply results in $[Cp'_4Lu_4(CH_2)_3(Me)]^+$ (**103**) and a non-coordinating $BAr^F{}_4$-anion.
In 2014, Luo and coworkers[115] investigated Cp^*Sc-systems, and the group published $BAr^F{}_4$ ion pairs of both the monochlorido-cation-mono(thf), and the mono(bistrimethylsilylamido)-bis(thf)-cation (**34a**). The lack of steric bulk in the chlorido-case necessitates the dimerization, forming a $[Cp^*{}_2Sc_2Cl_2]^{2+}$ dication (**34b**, *vide supra* in Section 1.2.2.9). Both ion pairs are not directly linked to their anion *via* a coordinating moiety. These two systems were investigated in terms of reactivity and were successfully applied in the activation of C–Cl bonds. Furthermore, in the case of the chloride derivative, it was shown to be effective in styrene polymerization (*vide supra*).[116]
Two of the more recent ion pairs that are mentioned in this context were published by the groups of Hayes[260] and his mentor Piers.[261] Both examples contain N-donor ligands. The pincer type motif of the Bis-phosphinoimine-pyrrole ligand of the Lu-cation (**104**) Hayes and coworkers present provides enough steric protection to the Lu center (especially when two ligands are coordinating), that no anion coordination is feasible (also see ref. 313 for further details).

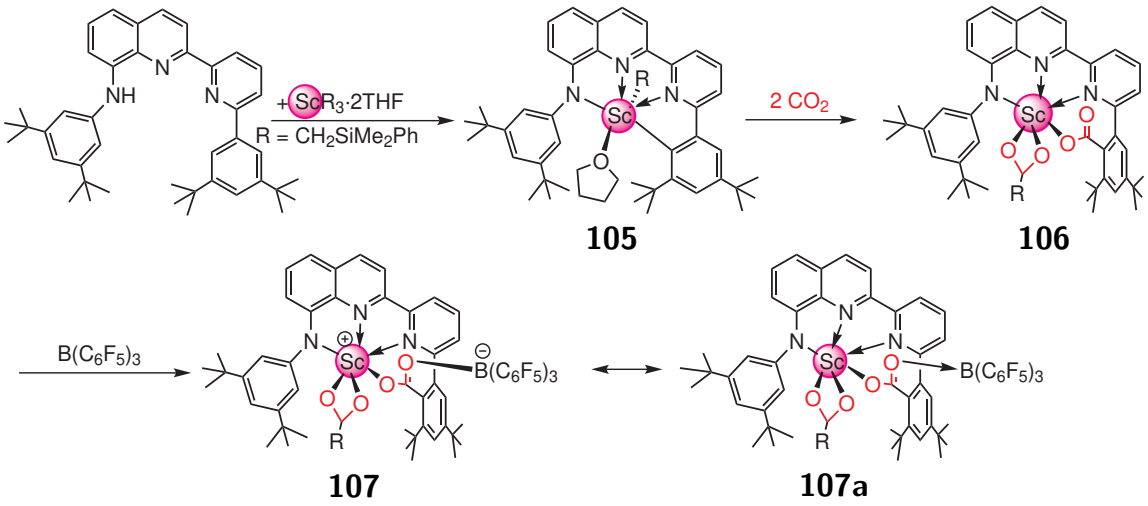

*Scheme 1.34: Synthesis of [{anilidobipyridyl-CO_2-($B(C_6F_5)_3$)}Sc(OOC-CH_2SiMe_2Ph)] (**107** and **107a**) by addition of cocatalyst **C** to the CO_2 insertion product (**106**) of [{anilidobipyridyl}Sc(CH_2SiMe_2Ph)(thf)] (**105**) according to ref. 261.*

Instead, Piers and coworkers observed a coordination of the anion in their neutral compound. They present the addition compound (**107**) of neutral cocatalyst **C** to a neutral precursor (**106**) formed by the insertion of two CO_2 molecules into Sc–C bonds in a bulky Sc anilidobipyridyl complex (see Scheme 1.34). There, one of the oxygens of the previously formed carboxylates coordinates to the $BAr^F{}_3$-boron. Interestingly, although this complex is neutral, Piers and coworkers observed catalytic activity in the hydrosilylation of CO.

In a collaboration study from three groups of the Hong Kong University of Science and Technology with Arnold,[262] the reactivity of the Ce=O bond was probed in 2016. Reacting such a bond, found in an aquo-complex of Ce^{IV} bearing Käulis tripodal ligand (which is a metalorganic compound itself: $CpCo^{III}$(diethylphosphite)$_3$) twice and the targeted C=O bond associated by (Me-C(O)NH_2) (**108**) with two equivalents of cocatalyst **C** yields a dicationic $[(käuli)_2Ce(Me\text{-}C(O)NH_2)]^{2+}$ (**109**) countered by two $[HOBAr^F{}_3]$ monoanions. **109** is a rare example of cationic Ce^{IV} complexes. A cationic complex of Ce^{III} was published in the following year by Sadow and coworkers.[263] Here, a bulky homoleptic Ce^{III} alkyl $[Ce(C(SiMe_3)_3]$ (**110**) was reacted with cocatalyst **C**. $[Ce(C(SiMe_3)_2][HBAr^F{}_3]$ (**111**) was yielded, in which the anion is coordinating to the Ce center *via* two *o*-aryl fluorines and the hydrogen bond to the boron. The complex was found to be active in the hydrosilylation of acrylates and methacrylates.

In the same year, two groups researching single molecule magnets contributed a disprosocenium cation (**113**), obtained by reaction of the respective $[Cp^{ttt}{}_2DyCl]$ (Cp^{ttt} = 1,2,4-tris-*tert*butylcyclopentadienyl) with

$[(Et_3Si)_3H][BAr^F{}_4]$. Mills and coworkers[264] and Layfield and coworkers[265] simultaneously reported the discovery. Mills and coworkers[266] reproted several rare earth metallocenium cations of the Cp^{ttt} ligand in the same year for the same purpose. So $[Cp^{ttt}{}_2Ln]^+$ ions for Ln = Gd, Ho, Er, Tm, Yb, Lu were introduced to the field.

Still in 2017, Cloke and coworkers[267] synthesized $[Cp^*Yb(OEt_2)_3][BAr^F{}_4]$ (**115**) from a pentalene (Pn) tripledecker complex $[(Cp^*Yb)_2Pn]$ (**114**) in diethyl ether at low temperatures. In the process of the sythesis of bimetallic pentalene complexes the cation serves as an intermediate.

The final example and latest addition to the field of non-polymerizing Ln-BAr^F ion pairs was published by Hou and coworkers.[268] For 1,5-diene cyclisation catalysis, they apply a mono(phosphinimido)-ligated scandium dimethylaminotoluidine (**117**) that they produce from its neutral *bis*-dimethylaminotoluidine precursor (**116**) by reaction with cocatalysts **A** and **C**.

1.2.4 Introductional Essentials

In this chapter, insight into the "black box" of lanthanide centered polymerization catalysis applying perfluorophenylborate anions has been provided. Till date, a large variety of crystallized model systems containing additional donor ligands that stabilize the active systems both sterically and electronicly are known. Next to these, seven cases (nine species) are known in which the catalytically active cationic species has successfully been crystallized and investigated.

The tetramethyl(trimethylsilyl)cyclopentadiene scandium (Cp'Sc) systems presented by Hou and coworkers are monomeric and a good example for the independence of the polymerization ability from the existance and strength of an anion coordination in the active species. Another monomeric system crystallized so far is a Sc centered cation bearing a "nacnac"-type ligand presented by Piers and coworkers. This species only polymerizes ethylene, probably due to the steric bulk of the supporting ligand. Xu and coworkers present a Sc-species bearing a "nacnac" type system equipped with a P-donor side arm. To the best of our knowledge this is the first structure, that, next to being an active single component catalyst shows the insertion of the first monomer molecule. Taube presented the first system in this context. His thf-stabillized lanthanum bisallyl cation was so far only tested in the polymerization of butadiene. As its precursor also serves as a single component catalyst in this field, it was not further investigated.

Hydrido clusters such as those presented by Hou and coworkers and Kempe and Trifonov and coworkers are the second type of system, where active catalyst species could be crystallized. Here cationization changes

the geometry of the clusters and therefore the steric environment. A trimeric cluster like in Kempe's and Trifonov's case is therefore able to polymerize without activation or ionization, while in the tetrameric case the geometry rearrangement must be induced to obtain an active catalyst. From the amount of Scandium based structural chemistry, it appears to be the most suitable metal center in lanthanide based polymerization catalysis. But a rough overview on the polymerising systems that have been published in this field easily proves, that the ratio of active scandium centers in the total amount of catalysts is far smaller. Therefore it seems likely, that this over-representance is either caused by good crystallization properties of the metal center or the focus of the active structure investigating community is shifted towards this metal. This favoritism could have been inspired by the success of the catalysts presented by the group of Hou.

Despite of that we can state that although only few catalyst systems have been crystallized so far, the way of sterical saturation of the active catalyst plays a minor role towards its activity as long as provided the degree of donor dissociation is high (e.g. coordination of the anion or solvent molecules, switch of a ligand into a higher chelating coordination mode or the formation of higher aggregates (clusters)). Still, even with crystallized single component catalysts, the initiation ratios do not reach 100 % of the metal centers by far. Therefore, in order to obtain further insight into the "black box", this fact should be a focus of the investigations.

Furthermore, it is shown, that investigations on degradation structures can provide insight into the nature and catalytic behavior of an active catalyst and should be therefore be considered, whenever a catalytic

mechanism or species is intended to be elucidated, as well.

Chapter 2

Summary of the Main Results

In general, catalytic 1,3-diene polymerization is achieved by a complex[1] bearing an alkyl moiety and a coordinated monomer molecule. The monomer will insert into the Ln–alkyl bond by allowing migration of the alkyl to the monomer and the resulting moiety switches from an η^2 or η^4 to a terminal bonding mode. This liberates a coordination site for the next monomer molecule to coordinate and the chain reaction continues. Regarding this anionic alkyl / growing polymer chain ligand and the fact that the free coordination site is mostly obtained by cationization of the respective precatalyst complex, two valencies of the active metal center are occupied. In case of the trivalent lanthanides, this enables the possibility of the presence / introduction of an anionic spectator ligand. In this thesis, both two types of systems with such a bulky ligand (half-sandwich complexes and scorpionate systems), as well as homoleptic systems without such a ligand have been investigated. As already mentioned, in order to enable a neutral complex (precatalyst) for coordination of a monomer molecule, a coordination site needs to be liberated, which is e.g. achieved by cationization in a pre-reaction with cationization agents (cocatalysts). Here, borates ($[Ph_3C][B(C_6F_5)_4]$ (**A**) and $[PhNHMe_2][B(C_6F_5)_4]$ (**B**)), a borane ($[B(C_6F_5)_3]$ (**C**)) and cluster-forming halogenation agents (Me_2AlCl (**D**), Et_2AlCl (**E**) and Me_2GaCl (**G**)) are applied. Performing these polymerizations, both structure-reactivity-relationships and the nature of active catalyst species are targeted.

In this chapter the main results of this thesis are addressed in an order of scientific logic, rather than the chronological order of the publications.

[1] In this theses a complex of a lanthanide metal.

2.1 1,3-Diene Polymerization Behavior of Catalysts Derived from Homoleptic Rare-Earth Metal Tetramethylaluminates

With all these prerequisites for catalytic polymerizations listed (*vide supra*), the simplest potential precatalyst would be a homoleptic trimethyl lanthanide. But these have not yet proven to be active in polymerization.[269] However, homoleptic tetramethylaluminates of the lanthanides ([Ln(AlMe$_4$)$_3$, $\mathbf{I^{Ln}}$), 'methyls in disguise', were chosen, as they have already been shown to polymerize 1,3-dienes.[15, 270–277] A full overview on the polymerization behavior of $\mathbf{I^{Ln}}$ is provided, featuring eleven different lanthanide centers (Ln = La, Ce, Pr, Nd, Gd, Tb, Dy, Ho, Y, Er, Lu) (Paper IV).[278] The respective study applies both borane / borate cocatalysts (**A**–**C**), as well as cluster-forming R$_2$AlCl (R = Me, Et) type halogenating cocatalysts (**D** and **E**).

The differing activation mechanisms (Scheme 2.1) show a large impact on the obtained polymers, as expected from literature.[15, 279] The general trend for isoprene polymerization in this study (Paper IV), observed for the borate / borane cocatalysts is that the amount of 1,4-linkages within the polymer increases with smaller ion size of the lanthanide center.

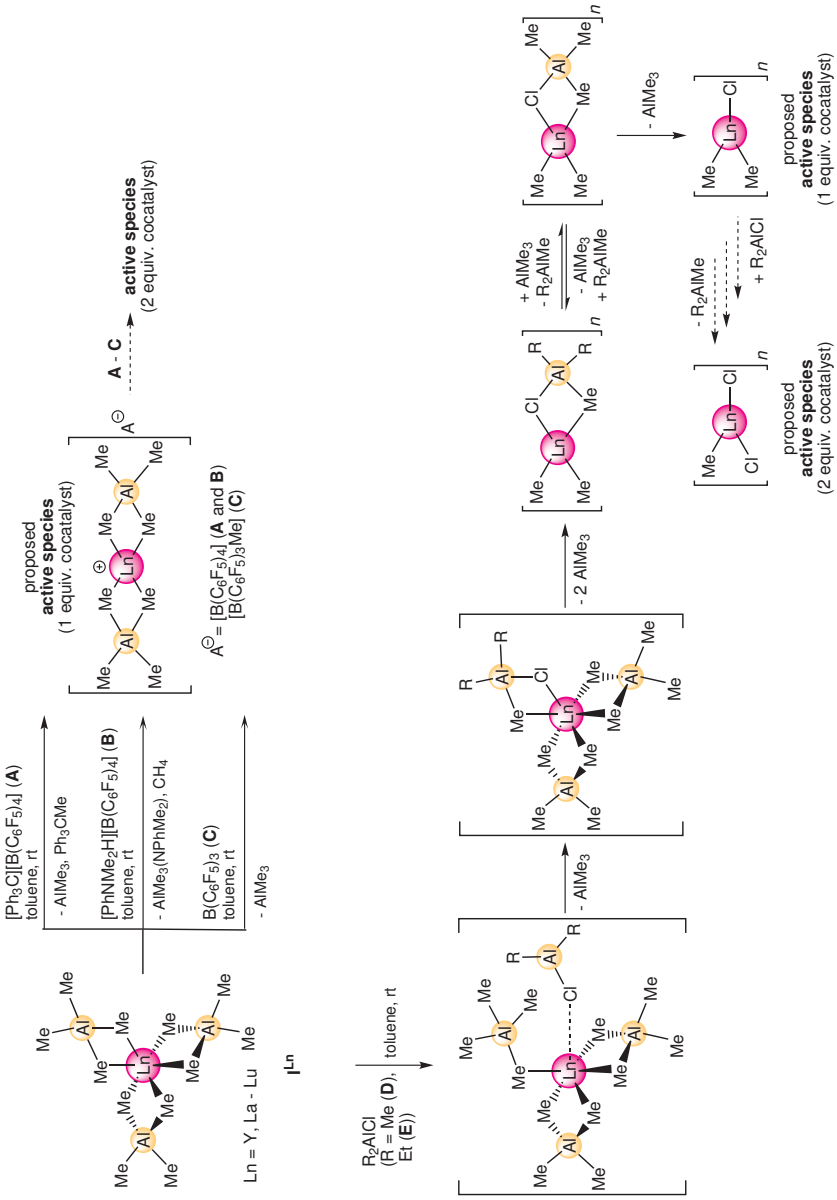

*Scheme 2.1: Two activation mechanisms of homoleptic rare-earth metal tetramethylaluminates with borate / borane (**A**–**C**) and R_2AlCl type (**D**, **E**) cocatalysts. In analogy to Paper IV, see there for further details.*

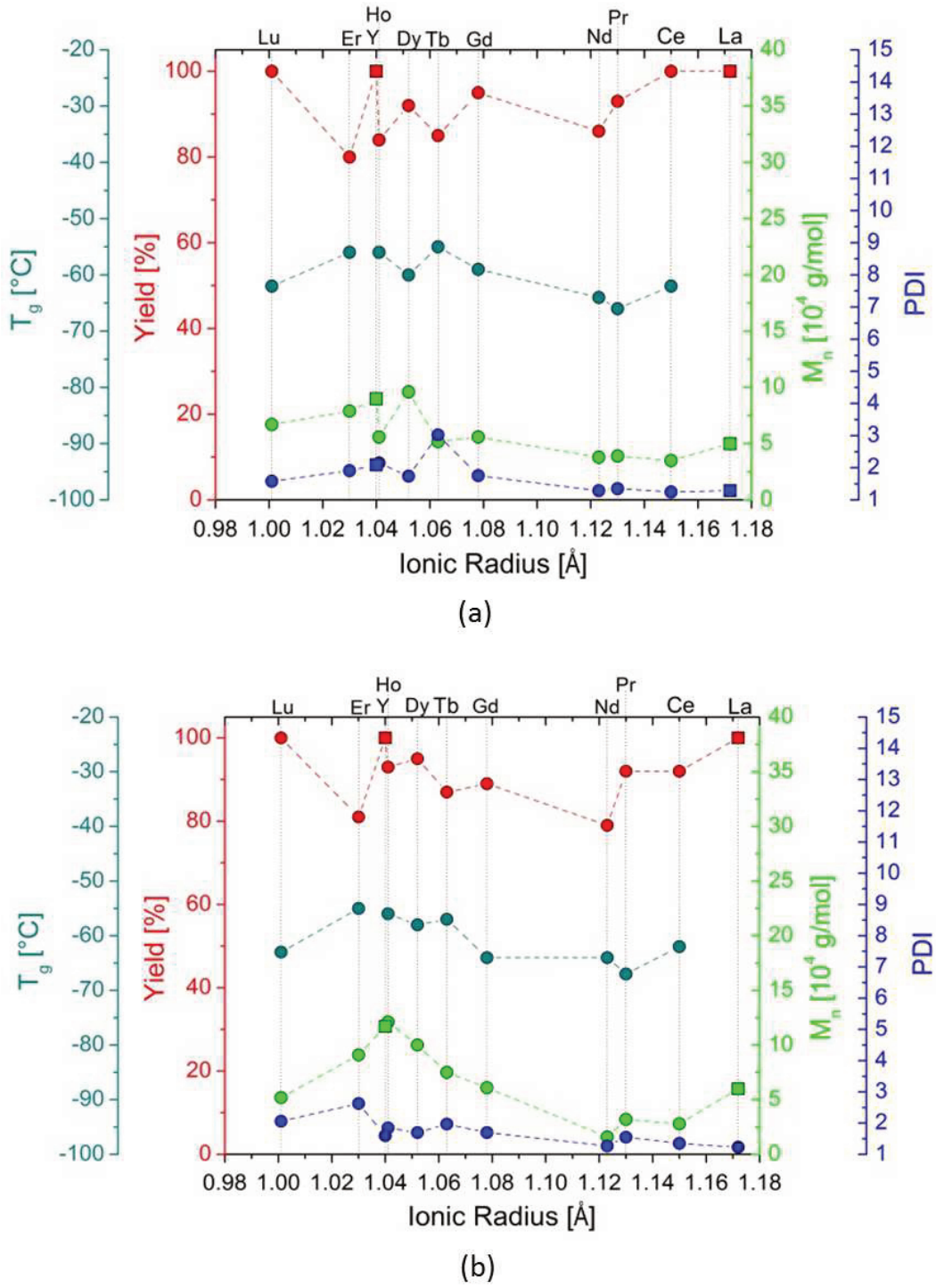

Chart 2.1: (See page 109 for caption.)

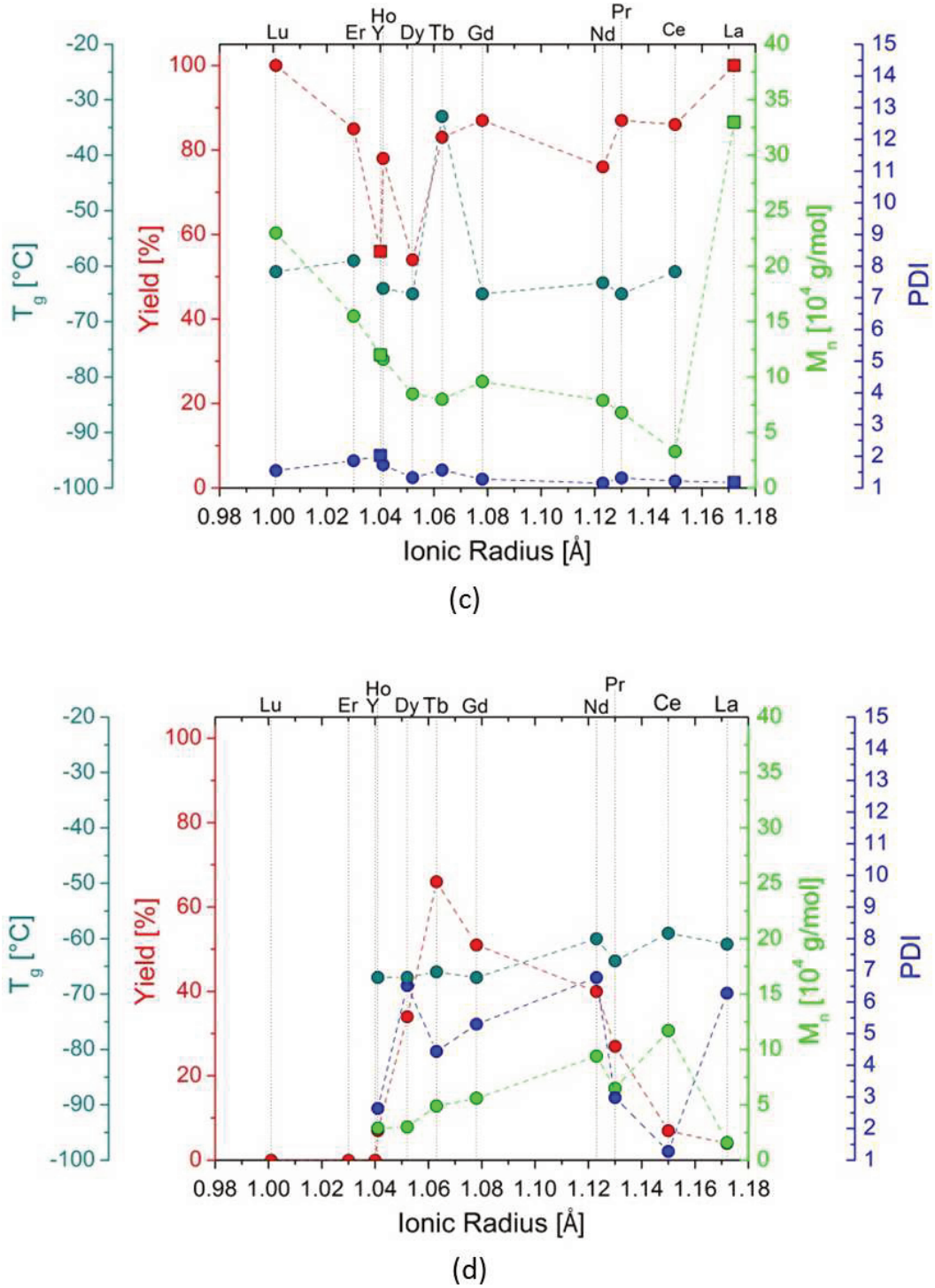

Chart 2.1: (See page 109 for caption.)

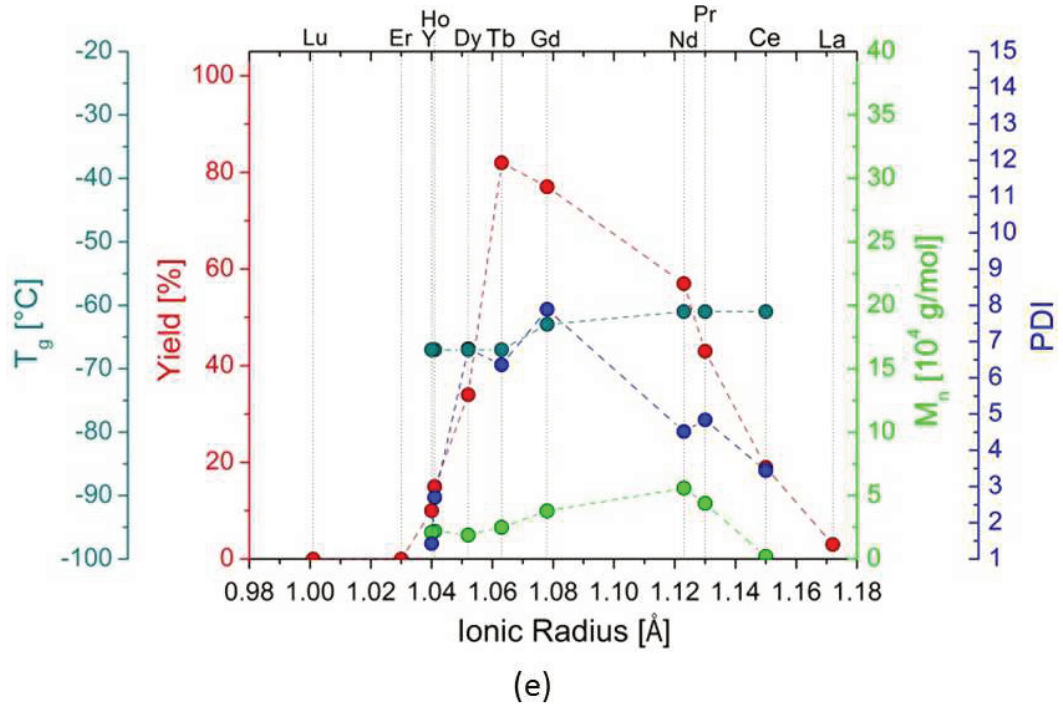

*Chart 2.1: (On this and previous pages) Overview charts representing the chain properties, yield and glass transition temperature of the polyisoprenes obtained from the homoleptic rare-earth metal tetramethylaluminates (**I**^{Ln}). Panels (a-e) give details on the data obtained from the application of a certain cocatalyst (**A**-**E**; **A** = $[Ph_3C][B(C_6F_5)_4]$, **B** = $[PhNMe_2H][B(C_6F_5)_4]$, **C** = $B(C_6F_5)_3$, **D** = Me_2AlCl, **E** = Et_2AlCl). Results for the addition of 1 equiv. of cocatalyst per alkylaluminate precatalyst after 1 h are shown by circles (dashed lines) If such results were not available, data of reaction times of 24 h marked with squares. The lanthanide precatalysts $Ln(AlMe_4)_3$ (**I**^{Ln}) are shown in the order of increasing ionic radii (x-axis); the corresponding data are shown referring to four different y-axes: red (yield), green (M_n), blue (PDI) and teal (T_g). In all panels lines are meant to assist the reader to follow the certain curves within the plot and not to indicate linear behavior of the curves in between the points of measurement. For a more traditional compilation of the polymer data in table form, sorted by precatalyst, see Tables S1.2.1 – S1.2.11, Paper IV, Supporting Information. Panels (a-e) are in analogy to Figure 3 in Paper IV.*

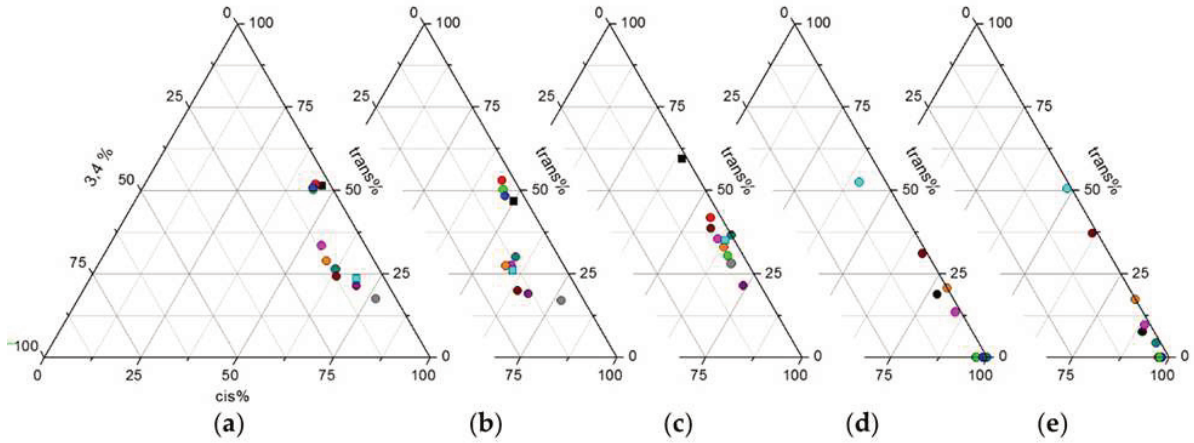

*Chart 2.2: Ternary plots of the microstructures of the polyisoprenes obtained from the homoleptic tetramethylaluminates (**I**^{Ln}) tested in this thesis applying one equivalent of cocatalyst each. The symbols in the plots are color-coded throughout the entire chart regarding the lanthanide center as follows: black (La), red (Ce), green (Pr), blue (Nd), teal (Gd), pink (Tb), orange (Dy), brown (Ho), cyan (Y), violet (Er) and grey (Lu). Parts a) to e) represent polymers obtained from systems of the respective homoleptic lanthanide tetramethylaluminate precatalysts ([Ln(AlMe$_4$)$_3$], **I**) with cocatalysts [Ph$_3$C][B(C$_6$F$_5$)$_4$] (**A** in part a), [PhNHMe$_2$][B(C$_6$F$_5$)$_4$] (**B** in part b), [B(C$_6$F$_5$)$_3$] (**C** in part c), [Me$_2$AlCl] (**D** in part d) and [Et$_2$AlCl] (**E** in part e). Circles mark reaction times of 1 h, while squares represent those of 24 h. These plots contain data from refs. 280 and 342 for comparison. Taken from Paper IV.*

This can be explained by a more likely increased steric encumbrance for the larger ion sizes. Reversible coordination of a further, neutral ligand, such as a solvent molecule or an activation side product would be a possible explanation. Alternatively, the coordination of the borate anion or dimerization could be the reason for the enhanced steric bulk. A possibly reversible switch from η^2 to η^3 coordination for the remaining alkylaluminates as observed for complexes of the larger lanthanides with the cyclopentadienyl *bis*-alkylaluminates (**II**, *vide infra*) can also not fully be ruled out.[273] Through the whole series of lanthanide centers, the yields

of the obtained polymers remain high (Chart 2.1).
For the chlorinating cocatalysts instead, the yield decreases with lanthanide ion size. Nevertheless, the most remarkable feature of these polymers is their microstructure (Chart 2.2). For the larger ions, the polymerization is highly 1,4-*cis*-selective, reaching even '> 99.9 %' for Ln = Gd with cocatalyst Me_2AlCl (**D**). From Ln = Ho on, the *cis*-content drops to give way to an increasing *trans*-content, due to steric reasons.

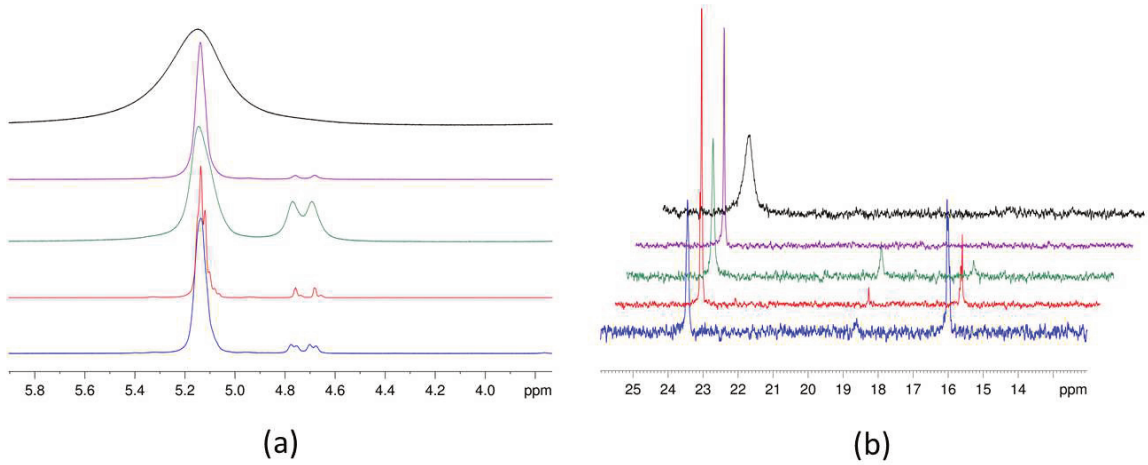

*Figure 2.1: Comparison of ^{1}H NMR (a) and ^{13}C NMR spectra (b) of selected polyisoprene samples (sorted by microstructure: decreasing trans-content bottom to top) produced by the systems $Nd(AlMe_4)_3$ (**I**Nd) / $[PhNMe_2H][B(C_6F_5)_4]$ (**B**) (blue; cis / trans / vinylic = 47 / 48 / 5 %), $La(AlMe_4)_3$ (**I**^{La}) / 2 $B(C_6F_5)_3$ (**C**) (red; 78 / 19 / 4 %), $Dy(AlMe_4)_3$ (**I**^{Dy}) / 2 $[Ph_3C][B(C_6F_5)_4]$ (**A**) (green; 72 / 10 / 18 %), $Nd(AlMe_4)_3$ (**I**Nd) / Me_2AlCl (**D**) (violet, 99 / 0 / 1 %) and $Gd(AlMe_4)_3$ (**I**^{Gd}) / Me_2AlCl (**D**) (black; > 99 / 0 / 0 %). Inclusion of the quenching products into the polymer cannot be fully avoided. In case of polymers produced by paramagnetic catalyst systems this causes a broadening of the signals that increases the error of microstructure determination. Taken from Paper IV. there for details.*

It is noteworthy that due to the paramagnetic nature of some of the lanthanides and their quenching products being included in the polymers, line

broadening was observed in the NMR spectra applied for micorstructure determination (Figure 2.1). In order to bypass that, ATR-IR has successfully been established as a second microstructure determinating method in this study.

$\mathbf{I^{Nd}}$, $\mathbf{I^{Pr}}$ and $\mathbf{I^{Y}}$ were also tested as precatalysts in the polymerization of 1,3-butadiene, where similar results were obtained. In general, the ratios of the vinylic addition remained slightly smaller. Furthermore, the yields were lower, probably due to shear induced gelation.

For both monomers (isoprene and 1,3-butadiene), two sets of screening experiments were performed to gain deeper insight into the polymerization reactions and the involved active species. As a model system $\mathbf{I^{Nd}}$ / **E** was chosen.

At first, the prereaction time (time between cocatalyst and monomer addition) was varied. While the microstructure remained constant at 98 / 0 / 2 % (*cis* / *trans* / 3,4 linkages) for isoprene, yields were higher for shorter pre-reaction times if a minimum of 10 min was allowed. Another interesting result is that the ratio of polymer chains per yttrium center is astonishingly high, for a system presumed to involve multimetallic clusters (reaching a value of 1 at a prereaction time of 22 min, see Paper IV for further details). As a possible explanation for this result a break-up of the multimetallic entities upon first monomer coordination is suggested. This would imply large structural differences between the activated catalyst and the chain propagation structure. Both are considered to be multimetallic regarding the obtained polymer data, but the sizes of the cluster cations are presumed to vary. Most interestingly, the data obtained from the identical study applying 1,3-butadiene as monomer indicates that this break-up

does occur to a much lesser extent, if at all, for the less bulky monomer. As a second screening parameter, the cocatalyst concentration was chosen. Increasing this concentration frees more and more aluminum trialkyls and therefore enables chain transfer reactions leading to lower average molecular weights, but an increased number of polymer chains.

2.2 Half-Sandwich Rare-Earth Metal Alkylaluminates as Precatalysts in 1,3-Diene Polymerization

As already mentioned at the beginning of this chapter, the trivalent nature of the lanthanide cations allows one anionic spectator ligand to be present during the polymerization. In this thesis, 1,2,3,4,5-pentamethylcyclopentadienyl (Cp^*) is applied as a model cyclopentadienyl half-sandwich ligand and hydro-*tris*-(3-*tert*butyl-5-methylpyrazolyl)borato ($Tp^{tBu,\,Me}$) is the model scorpionate ligand of choice.

2.2.1 Tetramethylaluminato Complexes

2.2.1.1 Synthesis and Application of Pentamethylcyclopentadienyl Lanthanide *Bis*-(tetramethylaluminate) Precatalysts

In this thesis, two studies contain polymerization results applying $[Cp^*Ln(AlMe_4)_2]$ ($\mathbf{II^{Ln}}$). In Paper I, the lutetium compound is presented for comparison reasons, while Manuscript I covers the analogues of holmium, dysprosium, terbium and gadolinium. Polymerizations applying the respective neodymium, lanthanum and yttrium complexes have been shown in the previous literature.[281, 282]

*Table 2.1: Isoprene homopolymerization by [Cp*Ln(AlMe4)2] (**II**^{Ln})*

Entry[a]	Precatalyst	Cocat.[b]	T^c [°C]	t^c [h]	Yield[d] [%]	*cis*[e] [%]	*trans*[e] [%]	3,4[e] [%]	$M_{n,SEC}$[f] [10^4 g·mol^{-1}]	PDI[f]	T_g[g] [°C]
1[i]	[Cp*La(AlMe$_4$)$_2$] (**II**^{La})	**A**	40	24	> 99	4	87	9	7	1.28	n.d.
2[i]	[Cp*La(AlMe$_4$)$_2$] (**II**^{La})	**B**	40	24	> 99	3	80	17	6	1.22	n.d.
3[i]	[Cp*La(AlMe$_4$)$_2$] (**II**^{La}	**C**	40	24	> 99	0	99.5	0.5	24	1.18	n.d.
4[i]	[Cp*Nd(AlMe$_4$)$_2$] (**II**Nd)	**A**	40	24	> 99	14	70	16	3	2.87	n.d.
5[i]	[Cp*Nd(AlMe$_4$)$_2$] (**II**Nd)	**B**	40	24	> 99	7	80	13	4	1.16	n.d.
6[i]	[Cp*Nd(AlMe$_4$)$_2$] (**II**Nd)	**C**	40	24	> 99	4	92	4	13	1.35	n.d.
7	[Cp*Gd(AlMe$_4$)$_2$] (**II**^{Gd})	**A**	25	1	93	16	68	16	10.6	1.33	-57
8	[Cp*Gd(AlMe$_4$)$_2$] (**II**^{Gd})	**B**	25	1	87	22	45	33	4.3	1.19	-43
9	[Cp*Gd(AlMe$_4$)$_2$] (**II**^{Gd})	**C**	25	1	traces[h]	_[h]	_[h]	_[h]	_[h]	_[h]	_[h]
10	[Cp*Gd(AlMe$_4$)$_2$] (**II**^{Gd})	**C**	25	24	94	6	87	7	19.4	1.30	-64
11	[Cp*Dy(AlMe$_4$)$_2$] (**II**^{Dy})	**A**	25	1	94	20	43	37	12.7	1.31	-52
12	[Cp*Dy(AlMe$_4$)$_2$] (**II**^{Dy})	**B**	25	1	83	14	63	23	5.0	1.28	-43
13	[Cp*Dy(AlMe$_4$)$_2$] (**II**^{Dy})	**C**	25	1	11	39	52	9	3.7	1.54	-65
14	[Cp*Ho(AlMe$_4$)$_2$] (**II**^{Ho})	**A**	25	1	54	23	50	27	11.0	1.50	-38
15	[Cp*Ho(AlMe$_4$)$_2$] (**II**^{Ho})	**B**	25	1	81	29	24	47	4.1	1.48	-23
16	[Cp*Ho(AlMe$_4$)$_2$] (**II**^{Ho})	**C**	25	1	traces[h]	_[h]	_[h]	_[h]	_[h]	_[h]	_[h]
16a	[Cp*Ho(AlMe$_4$)$_2$] (**II**^{Ho})	**C**	25	24	85	9	79	12	6.6	1.62	-62
17[i]	[Cp*Y(AlMe$_4$)$_2$] (**II**^{Y})	**A**	40	24	> 99	61	21	19	2	8.95	n.d.
18[i]	[Cp*Y(AlMe$_4$)$_2$] (**II**^{Y})	**B**	40	24	> 99	44	29	28	6	1.59	n.d.
19[i]	[Cp*Y(AlMe$_4$)$_2$] (**II**^{Y})	**C**	40	24	> 99	2	94	4	9	1.59	n.d.
20[j]	[Cp*Lu(AlMe$_4$)$_2$] (**II**^{Lu})	**A**	40	0.25	> 99	74	20	6	10	1.49	n.d.
21[j]	[Cp*Lu(AlMe$_4$)$_2$] (**II**^{Lu})	**B**	40	0.25	> 99	70	20	10	9.5	1.48	n.d.
22[j]	[Cp*Lu(AlMe$_4$)$_2$] (**II**^{Lu})	**C**	40	0.25	> 99	74	21	5	11.0	1.39	n.d.

[a] Conditions: 20 µmol of precatalyst, 20 µmol of cocatalyst, 20 mmol of isoprene, 8 mL of toluene.
[b] **A** = [Ph$_3$C][B(C$_6$F$_5$)$_4$], **B** = [PhNHMe$_2$][B(C$_6$F$_5$)$_4$], **C** = B(C$_6$F$_5$)$_3$.
[c] T = polymerization temperature, t = reaction time.
[d] Yield of the isolated polymer.
[e] Determined by ^{1}H and ^{13}C NMR spectroscopy.
[f] Determined by GPC in THF at 35 °C.
[g] Determined on a Perkin Elmer DSC 8000; Heat rate: 20 K/min, Cooling rate: 60 K/min.
[h] Evaluation impossible due to low yield.
[i] Taken from ref. 282 for comparison.
[j] Taken from Paper V.

The presence of the Cp^* ligand completely inhibits the halogenation activation protocol (*cf.* the lower part of Scheme 2.1). The necessity for an active catalyst of one lanthanide-alkyl bond is no longer fulfilled with a spectator ligand, probably due to the fact that stable, halogenido bridged dimers are formed in the process.[6, 283] The borate / borane cocatalysts instead are able to activate $[Cp^*Ln(AlMe_4)_2]$ ($\mathbf{II^{Ln}}$) for polymerization. Here, the obtained results for Ln = Gd, Dy, Ho fit well into the pattern published for lanthanum and neodymium, while the polymers of the yttrium and lutetium compounds stick out. Especially in case of yttrium, due to the similar ion size, a polymer in alignment with that of holmium would be expected, but significant deviations have been observed. However, an absolute comparison of the polymerizations of the three smaller lanthanides (Lu, Y and Ho) with those of the La and Nd complexes needs to take the reaction temperatures for both setups into account. As these differ, the trimehtylaluminum coordination equilibria are probably slightly shifted. Verification by experiments with the holmium compound at augmented temperatures, searching for a polymerization behavior in analogy to that of the yttrium compound, are subject to further research.
Despite of that, with these polymers, the high 1,4-*trans*-contents must be emphasized. Although lower than in case of lanthanum (99.5 %, Table 2.1, run 3), the polymers of gadolinium, dysprosium, and holmium still show some remarkable selectivity (Table 2.1) that will serve as a signature microstructure to identify active species behaving similarly, when discussing the further studies (*vide infra*).

2.2.1.2 Hydro-*tris*-(3-*tert*butyl-5-methyl-pyrazolyl)borato as an ancillary ligand

For the second spectator ligand, scorpionate hydro-*tris*-(3-*tert*butyl-5-methyl-pyrazolyl)borate ($Tp^{tBu,\,Me}$, Manuscript III), *bis*-alkylaluminate species are not isolable due to the steric demand of the ligand.[284–286] Instead, monomethyl-mono-tetramethylaluminates [$Tp^{tBu,\,Me}LnMe(AlMe_4)$] (**III^{Ln}**) are accessible for this ligand. These complexes were investigated in isoprene polymerization for holmium, yttrium, and lutetium (Table 2.2 and Manuscript III for further details). Interestingly, the lack of a second alkylaluminate enables higher 1,4-*cis*-selectivity than in the Cp^* case at higher temperatures (Paper I, Manuscript I).[281, 282, 287] This can be interpreted as another indication for the temperature-induced release of $AlMe_3$, presumed to cause the augmented 1,4-*cis* linkage observed for [$Cp^*Ln(AlMe_4)_2$] (**II^{Ln}**, Section 2.2.1.1) by decreasing the steric encumbrance around the lanthanide center.

The effect that only *mono*-tetramethylaluminates are accessible furthermore implies that in case of the $Tp^{tBu,\,Me}$-supported methyl-tetramethylaluminates an activation without release of $AlMe_3$ is theoretically possible. According to the obtained polymer data, it is most likely only realized for the system **III^{Y} / B**.

Table 2.2: Isoprene homopolymerization by $Tp^{tBu,\ Me}$ rare-earth metal tetramethylaluminates ***III^{Ln}***

Entry[a]	Precatalyst	Cocatalyst[b]	T [°C]	t [min]	Method[c]	Yield[d] [%]	*cis*[e] [%]	*trans*[e] [%]	3,4[e] [%]	$M_{n,SEC}$[f] [10^4g·mol^{-1}]	PDI[f]	T_g [°C]
23	$Tp^{tBu,\ Me}$YMe(AlMe$_4$) (**III^{Y}**)	**A**	25	60	1	97	78	10	12	17.3	1.94	-60
23a	$Tp^{tBu,\ Me}$YMe(AlMe$_4$) (**III^{Y}**)	**A**	25	60	2	34	75	7	18	19.1	2.20	-54
24	$Tp^{tBu,\ Me}$YMe(AlMe$_4$) (**III^{Y}**)	**B**	25	60	1	96	32	42	26	24.4	2.94	-49
24a	$Tp^{tBu,\ Me}$YMe(AlMe$_4$) (**III^{Y}**)	**B**	25	60	2	88	68	6	26	46.7	2.44	-47
25	$Tp^{tBu,\ Me}$YMe(AlMe$_4$) (**III^{Y}**)	**C**	25	60	1	none[h]	-[h]	-[h]	-[h]	-[h]	-[h]	-[h]
25a	$Tp^{tBu,\ Me}$YMe(AlMe$_4$) (**III^{Y}**)	**C**	25	60	2	none[h]	-[h]	-[h]	-[h]	-[h]	-[h]	-[h]
26	$Tp^{tBu,\ Me}$HoMe(AlMe$_4$) (**III^{Ho}**)	**A**	25	60	1	93	87	0	13	28.3	1.75	-54
27	$Tp^{tBu,\ Me}$HoMe(AlMe$_4$) (**III^{Ho}**)	**B**	25	60	1	92	72	0	28	23.5	3.33	-44
28	$Tp^{tBu,\ Me}$HoMe(AlMe$_4$) (**III^{Ho}**)	**C**	25	60	1	none[h]	-[h]	-[h]	-[h]	-[h]	-[h]	-[h]
29[i]	$Tp^{tBu,\ Me}$LuMe(AlMe$_4$) (**III^{Lu}**)	**A**	25	60	1	none[h]	-[h]	-[h]	-[h]	-[h]	-[h]	-[h]
30[i]	$Tp^{tBu,\ Me}$LuMe(AlMe$_4$) (**III^{Lu}**)	**B**	25	60	1	90	64	16	20	15.3	2.40	-52
30a	$Tp^{tBu,\ Me}$LuMe(AlMe$_4$) (**III^{Lu}**)	**B**	25	60	2	81	66	9	25	26.6	1.98	-49
31	$Tp^{tBu,\ Me}$LuMe(AlMe$_4$) (**III^{Lu}**)	**C**	25	60	1	none[h]	-[h]	-[h]	-[h]	-[h]	-[h]	-[h]

[a] Conditions: 20 µmol of precatalyst, 20 µmol of cocatalyst, 20 mmol of isoprene, 8 mL of toluene.
[b] **A** = $[Ph_3C][B(C_6F_5)_4]$, **B** = $[PhNHMe_2][B(C_6F_5)_4]$, **C** = $B(C_6F_5)_3$.
[c] see Supporting Information for details: 1 = Standard procedure applying 5 min of pre-reaction time. 2 = the method inspired by Hou and coworkers.[288]
[d] Yield of the isolated polymer.
[e] Determined by ^{1}H and ^{13}C NMR spectroscopy.
[f] Determined by GPC in THF at 35 °C.
[g] Determined by DSC.
[h] Evaluation impossible due to low yield.
[i] These polymers have been presented in Paper III, ref. 239 and are shown here for comparison.

In this study, an alternative activation protocol inspired by Hou and coworkers[288] was additionally tested. Here, without a prereaction period of precatalyst and cocatalyst before monomer addition, the system $\mathbf{III^Y}$ / **B** does as well as the other systems (with both this and the originally applied protocol with a prereaction time of 5 min) produce a polymer with a microstructure focused on 1,4-*cis* addition.

Interestingly in all cases the rate of initiation (amount of lanthanide centers / amount of polymer chains) is significantly smaller than 1, and in most cases even smaller than 0.5. As cluster formation upon activation does not seem likely due to the bulky ligand, this is ascribed to a deficient initiation, occuring for the same steric reasons.

The effect that $\mathbf{III^{Lu}}$ is not activated by methyl abstraction from the sterically demanding trityl cation of cocatalyst **A** is explained by the crowded environment around the metal center.

Next to the tetramethylaluminates, for Ln = Ho, Y, tetramethylgallates [Tp$^{t\mathrm{Bu,\,Me}}$LnMe(GaMe$_4$)] ($\mathbf{IV^{Ln}}$) have been investigated in this study. The main difference of the polymers produced by the gallates to those produced by the alkylaluminates (Table 2.3) is the reduction of the 1,4-*cis* selectivity in the polymerization process, due to the enhance steric bulk which is the consequence of the larger ionic radius of gallium compared to aluminum (with exception of $\mathbf{IV^Y}$ / **B**).

Table 2.3: Isoprene homopolymerization by $Tp^{tBu,\ Me}$ rare earth metal tetramethylgallates $\boldsymbol{IV^{Ln}}$

Entry[a]	Precatalyst	Cocatalyst[b]	T [°C]	t [min]	Method[c]	Yield[d] [%]	*cis*[e] [%]	*trans*[e] [%]	3,4[e] [%]	$M_{n,SEC}$[f] [10^4g·mol^{-1}]	PDI[f]	T_g [°C]
32	$Tp^{tBu,\ Me}$YMe($GaMe_4$) (**IV^{Y}**)	**A**	25	60	1	89	62	19	19	16.9	2.53	-53
32a	$Tp^{tBu,\ Me}$YMe($GaMe_4$) (**IV^{Y}**)	**A**	25	60	2	92	67	9	24	19.8	2.39	-49
33	$Tp^{tBu,\ Me}$YMe($GaMe_4$) (**IV^{Y}**)	**B**	25	60	1	87	61	17	22	10.8	2.91	-49
33a	$Tp^{tBu,\ Me}$YMe($GaMe_4$) (**IV^{Y}**)	**B**	25	60	2	88	62	14	24	17.9	2.40	-48
33b	$Tp^{tBu,\ Me}$YMe($GaMe_4$) (**IV^{Y}**)	**B**	25	60	3	59	62	16	23	24.4	2.48	-49
34	$Tp^{tBu,\ Me}$YMe($GaMe_4$) (**IV^{Y}**)	**C**	25	60	1	none[h]	-[h]	-[h]	-[h]	-[h]	-[h]	-[h]
34a	$Tp^{tBu,\ Me}$YMe($GaMe_4$) (**IV^{Y}**)	**C**	25	60	2	none[h]	-[h]	-[h]	-[h]	-[h]	-[h]	-[h]
35	$Tp^{tBu,\ Me}$HoMe($GaMe_4$) (**IV^{Ho}**)	**A**	25	60	1	95	58	19	23	18.1	2.81	-51
36	$Tp^{tBu,\ Me}$HoMe($GaMe_4$) (**IV^{Ho}**)	**B**	25	60	1	96	64	11	25	17.0	2.44	-51
37	$Tp^{tBu,\ Me}$HoMe($GaMe_4$) (**IV^{Ho}**)	**C**	25	60	1	traces[h]	-[h]	-[h]	-[h]	-[h]	-[h]	-[h]

[a] Conditions: 20 µmol of precatalyst, 20 µmol of cocatalyst, 20 mmol of isoprene, 8 mL of toluene.
[b] **A** = $[Ph_3C][B(C_6F_5)_4]$, **B** = $[PhNHMe_2][B(C_6F_5)_4]$, **C** = $B(C_6F_5)_3$.
[c] see Supporting Information for details: 1 = Standard procedure applying 5 min of prereaction time. 2 = the method inspired by Hou and coworkers.[288] 3 = Standart procedure applying no pre-reaction time.
[d] Yield of the isolated polymer.
[e] Determined by ^{1}H and ^{13}C NMR spectroscopy.
[f] Determined by GPC in THF at 35 °C.
[g] Determined by DSC.
[h] Evaluation impossible due to low yield.

2.2.2 Borylaluminate Complexes

In order to investigate the effects of peripheral steric bulk in the alkylaluminate position, borylaluminates have been tested as precatalysts in 1,3-diene polymerization. In analogy to the case of the tetramethylaluminates, for Cp^* as spectator ligand the *bis*-borylaluminate $[Cp^*Ln(AlMe_3\{B(NDippCH)_2\})_2]$ ($\mathbf{V^{Ln}}$, Dipp = di*iso*propylphenyl) is realized, while with $Tp^{tBu,\,Me}$, only the *mono*-borylaluminate $[Tp^{tBu,\,Me}Ln(AlMe_3\{B(NDippCH)_2\})Me]$ ($\mathbf{VI^{Ln}}$) is accessible.

2.2.2.1 Pentamethylcyclopentadienyl as ancillary ligand

Table 2.4: Isoprene homopolymerization by $[Cp^*Ln(AlMe_3\{B(NDippCH)_2\})_2]$ ($\boldsymbol{V^{Ln}}$)

Entry[a]	Precatalyst	Cocat.[b]	t[c] [h]	Yield[d] [%]	*cis*[e] [%]	*trans*[e] [%]	3,4[e] [%]	$M_{n,SEC}$[f] [10^4g·mol^{-1}]	PDI[f]
38	$[Cp^*Y(AlMe_3\{B(NDippCH)_2\})_2]$ ($\mathbf{V^Y}$)	**A**	1	8.7	21.3	12.7	66.0	2.4	1.41
39	$[Cp^*Y(AlMe_3\{B(NDippCH)_2\})_2]$ ($\mathbf{V^Y}$)	**A**	24	> 99	49.4	5.3	45.3	9.6	1.45
40	$[Cp^*Y(AlMe_3\{B(NDippCH)_2\})_2]$ ($\mathbf{V^Y}$)	**B**	1	11.2	30.7	3.3	66.8	3.8	1.22
41	$[Cp^*Y(AlMe_3\{B(NDippCH)_2\})_2]$ ($\mathbf{V^Y}$)	**B**	24	> 99	34.1	15.5	50.4	7.4	1.29
42	$[Cp^*Y(AlMe_3\{B(NDippCH)_2\})_2]$ ($\mathbf{V^Y}$)	**C**	1	traces	—[g]	—[g]	—[g]	—[g]	—[g]
43	$[Cp^*Y(AlMe_3\{B(NDippCH)_2\})_2]$ ($\mathbf{V^Y}$)	**C**	24	71.8	1.9	84.1	11.2	5.4	2.02
44	$[Cp^*Lu(AlMe_3\{B(NDippCH)_2\})_2]$ ($\mathbf{V^{Lu}}$)	**A**	1	> 99	21.5	17.7	60.8	4.7	1.44
45	$[Cp^*Lu(AlMe_3\{B(NDippCH)_2\})_2]$ ($\mathbf{V^{Lu}}$)	**B**	1	5.5	38.6	3.2	58.2	—[g]	—[g]
46	$[Cp^*Lu(AlMe_3\{B(NDippCH)_2\})_2]$ ($\mathbf{V^{Lu}}$)	**B**	24	> 99	21.4	14.7	63.9	6.0	1.23
47	$[Cp^*Lu(AlMe_3\{B(NDippCH)_2\})_2]$ ($\mathbf{V^{Lu}}$)	**C**	1	traces	—[g]	—[g]	—[g]	—[g]	—[g]
48	$[Cp^*Lu(AlMe_3\{B(NDippCH)_2\})_2]$ ($\mathbf{V^{Lu}}$)	**C**	24	34.1	21.2	68.4	10.4	3.0	1.97
49	$[Cp^*Lu(AlMe_3\{B(NDippCH)_2\})_2]$ ($\mathbf{V^{Lu}}$)	**C**	48	65.9	38.3	52.6	9.1	3.2	2.07

[a] Conditions: 20 µmol of precatalyst, 20 µmol of cocatalyst, 20 mmol of isoprene, 7 mL of toluene, r.t. Data has been presented in Paper I.
[b] Aged with cocatalyst at ambient temperature for 30 min: **A** = $[Ph_3C][B(C_6F_5)_4]$, **B** = $[PhNHMe_2][B(C_6F_5)_4]$, **C** = $B(C_6F_5)_3$.
[c] t = reaction time.
[d] Yield of the isolated polymer.
[e] Determined by ^{1}H and ^{13}C NMR spectroscopy.
[f] Determined by GPC in THF at 35 °C against polystyrene standarts
[g] Not determined due to low yield.

With introduction of the boryl-aluminato moieties, the sterical space for monomer coordination is further limited. Therefore, the enhanced selectivity toward vinylic addition with $[Cp^*Ln(AlMe_3\{B(NDippCH)_2\})_2]$ ($\mathbf{V^{Ln}}$, Dipp = di*iso*propylphenyl), compared to the tetramethylaluminates does

not come as a surprise (Table 2.4 and Paper I for further details) at first sight. Besides some minor initiation deficits (initation rates above 0.5 but below 1) and a low chain propagation rate, these polymers show a low PDI. Therefore, the active species was presumed to be of manageable complexity and targeted by NMR spectroscopy, which revealed an important second reason, for the obtained microstructure.

This NMR spectroscopic study (Figure 2.2), revealed that one of the Dipp moieties interacts with the cationic lanthanides. This contact hampers the release of the second dimethylborylaluminum moiety, which further stabilizes the bulky environment around the active center. Besides that, Horton analysis[34, 35] showed that the coordination strength of the anion is in the medium range between strong and loose. In conclusion, the rigidity of the situation with low sterical space around the active metal center is experimentally proven, which is known to cause η^2 coordination of the monomer and therefore 3,4-addition.[4–6]

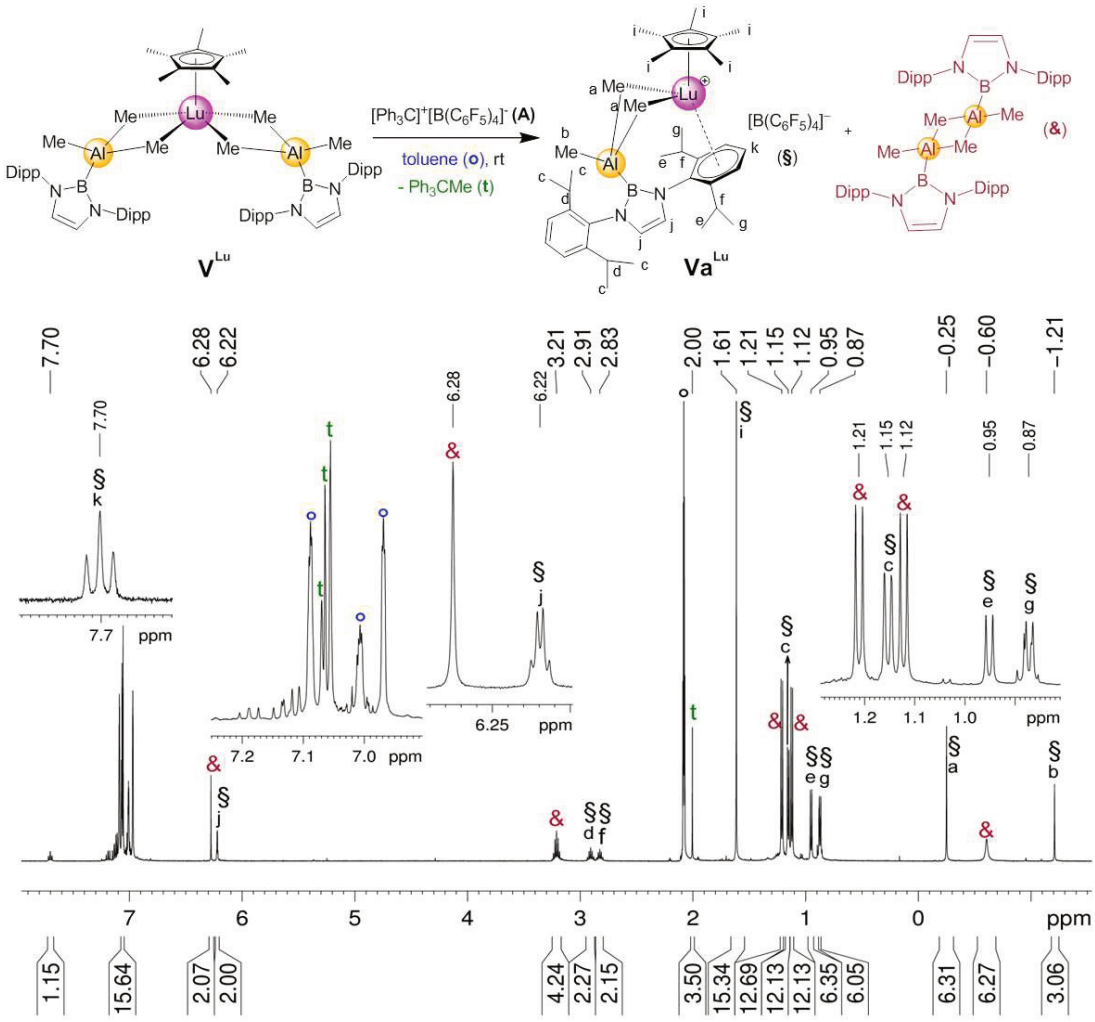

*Figure 2.2: NMR spectroscopic study verifying the active species (**Va^{Lu}**) formed from [Cp*Lu(AlMe$_3${B(NDippCH)$_2$}$_2$)$_2$] **V^{Lu}**, Dipp = diisopropylphenyl) by activation with cocatalyst **A**. An interaction between an aryl ring of one of the Dipp moieties with the cationic center was observed. Tags for the identifaction of peaks in the ^{1}H NMR spectrum are given with the reaction scheme. Figure according to Paper I, see there for further details.*

2.2.2.2 Hydro-*tris*-(3-*tert*butyl-5-methyl-pyrazolyl)borato as an ancillary ligand

For the $Tp^{tBu,\,Me}$-supported Ln^{III} borylaluminates, only the smallest lanthanide, lutetium was targeted (Paper III). As mentioned above, for sterical reasons, only a mono-borylaluminato complex [$Tp^{tBu,\,Me}$LuMe($AlMe_3${B(NDippCH)$_2$})] (**VI^{Lu}**) is accessible, bearing a remaining methyl anion as second non-spectator ligand. This complex was found to react on the application of thermal energy by liberation of methane *via* C–H-bond activation (Scheme 2.2), forming a tuck-in product (**VIa^{Lu}**). This second stable complex was together with its precursor, the original mono-borylaluminate (**VI^{Lu}**) assessed in the polymerization of isoprene.

In this study (Table 2.5), microstructures of moderate 1,4-*cis*-selectivity were obtained in low yields after one hour with cocatalysts **A** and **B**. The neutral cocatalyst (**C**) afforded a polymer with a rather unselective microstructure. Applying cocatalysts **A** and **C**, multimodal MWDs were obtained. In combination with the average molecular weights and the PDI, this indicates an ongoing reaction that alternates the active species during polymerization. In case of cocatalysts **A** and **C**, the products of this degradation reaction are active polymerization catalysts as well causing the multimodality. In order to target the responsible active species, the activation reaction was followed by NMR spectroscopy over time with all three cocatalysts. Therby, with cocatalyst **B** a single tuck-in C–H bond activation under methane release was tracked (Scheme 2.2). The product, **VIIa^{Lu}**, is inactive in diene polymerization.

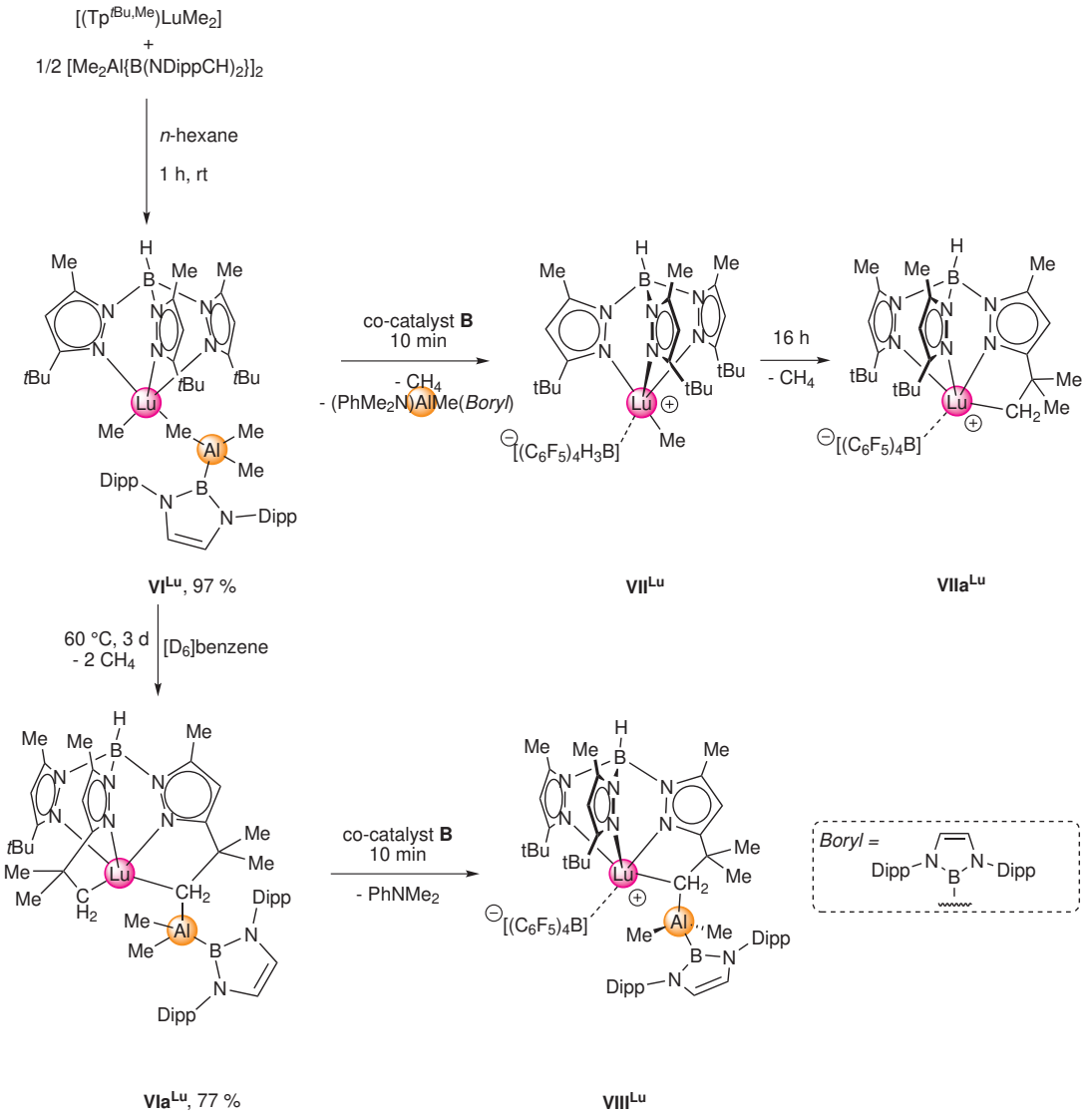

*Scheme 2.2: Upon heating to 60 °C of [Tp$^{tBu,\ Me}$LuMe(AlMe$_3${B(NDippCH)$_2$})] (**VI^{Lu}**) C–H bond activation occurs and with release of methane, the double tuck-in complex **VIa^{Lu}** is formed. Both complexes are activated for polymerization applying [PhNMe$_2$H][B(C$_6$F$_5$)$_4$] (**B**). The respective active species are identified by NMR spectroscopy and shown in this scheme: **VI^{Lu}** produces a cation (**VII^{Lu}**) under formation of methane and (PhMe$_2$N)AlMe{B(NDippCH)$_2$}. Thereafter **VII^{Lu}** undergoes C–H bond activation and forms a tuck-in cation (**VIIa^{Lu}**), releasing another equivalent of methane. In case of the double tuck-in complex **VIa^{Lu}**, **B** protonates one of the tuck-in tert-butyl groups to produce a single-tuck-in cation (**VIII^{Lu}**). Scheme according to Paper III, see there for further details.*

*Table 2.5: Isoprene homopolymerization by [Tp$^{tBu,\ Me}$LuMe(AlMe$_3${B(NDippCH)$_2$})] (**VI^{Lu}**) and its thermolytic product [(Tp$^{(tBu\text{-}H)_2/tBu,Me)}$Lu(AlMe$_2$B(NDippCH)$_2$)] (**VIa^{Lu}**)*

Entry[a]	Precatalyst	Cocat.[b]	t[c] [h]	Yield[d] [%]	*cis*[e] [%]	*trans*[e] [%]	3,4[e] [%]	$M_{n,SEC}$[f] [10^4 g·mol^{-1}]	PDI[f]	T_g[g] [°C]
50	[Tp$^{tBu,\ Me}$LuMe(AlMe$_3${B(NDippCH)$_2$})] (**VI^{Lu}**)	**A**	1	14	80.6	7.7	11.8	6.7[h]	1.91[h]	-56.9
51	[Tp$^{tBu,\ Me}$LuMe(AlMe$_3${B(NDippCH)$_2$})] (**VI^{Lu}**)	**A**	24	90	70.3	17.8	11.9	14.0	2.63	-56.1
52	[Tp$^{tBu,\ Me}$LuMe(AlMe$_3${B(NDippCH)$_2$})] (**VI^{Lu}**)	**B**	1	47	72.5	2.6	24.9	11.9	3.72	-47.5
53	[Tp$^{tBu,\ Me}$LuMe(AlMe$_3${B(NDippCH)$_2$})] (**VI^{Lu}**)	**B**	24	89	68.7	7.5	23.9	14.0	2.98	-48.2
54	[Tp$^{tBu,\ Me}$LuMe(AlMe$_3${B(NDippCH)$_2$})] (**VI^{Lu}**)	**C**	1	31	31.4	44.4	24.2	3.3[h]	1.80[h]	-38.6
55	[(Tp$^{(tBu\text{-}H)_2/tBu,Me)}$Lu(AlMe$_2$B(NDippCH)$_2$)] (**VIa^{Lu}**)	**A**	1	32	80.8	0.0	19.2	26.4	1.77	-52.8
56	[(Tp$^{(tBu\text{-}H)_2/tBu,Me)}$Lu(AlMe$_2$B(NDippCH)$_2$)] (**VIa^{Lu}**)	**A**	24	>99	88.4	0.0	11.6	5.6[i]	2.41[i]	-54.6
57	[(Tp$^{(tBu\text{-}H)_2/tBu,Me)}$Lu(AlMe$_2$B(NDippCH)$_2$)] (**VIa^{Lu}**)	**B**	1	2	70.4	4.0	25.6	36.1[h]	1.81[h]	-46.0
58	[(Tp$^{(tBu\text{-}H)_2/tBu,Me)}$Lu(AlMe$_2$B(NDippCH)$_2$)] (**VIa^{Lu}**)	**B**	24	90	66.7	5.7	27.6	27.9[h]	2.60[h]	-45.9

[a] Conditions: 20 µmol of precatalyst, 20 µmol of cocatalyst, 20 mmol of isoprene, 8 mL of toluene. Data taken from Paper III.
[b] Aged with cocatalyst at ambient temperature for 5 min: **A** = [Ph$_3$C][B(C$_6$F$_5$)$_4$], **B** = [PhNHMe$_2$][B(C$_6$F$_5$)$_4$], **C** = B(C$_6$F$_5$)$_3$.
[c] t = reaction time.
[d] Yield of the isolated polymer.
[e] Determined by ^{1}H and ^{13}C NMR spectroscopy.
[f] Determined by GPC in THF at 35 °C against polystyrene standarts
[g] Determined on a Perkin Elmer DSC 8000; Heat rate: 20 K/min, Cooling rate: 60 K/min.
[h] MWD contains more than one mode. The data of the main mode is given here; it represents 85 mol-% (run 1), 78 mol-% (run 5), 98 mol-% (run 8), and >99 mol-% (run 9) of the polymer.
[i] The polymers are not fully soluble in THF. The data of the soluble part is given here; it represents 24 mol-% of the actual polymer mixture.

The thermolytic product ($\mathbf{VIa^{Lu}}$) yields polymers only with **A** and **B**. The majority of the polymer product of **A** is insoluble in THF. The polymerizations are more (**A**) and likewise (**B**) 1,4-*cis*-selective than those applying $\mathbf{VI^{Lu}}$. Both polymers produced by $\mathbf{VIa^{Lu}}$ show multimodal / broad MWDs. For $\mathbf{VIa^{Lu}}$ / **A**, another catalyst alternation reaction is suspected, while with $\mathbf{VIa^{Lu}}$ / **B**, the broad MWD is due to a very slow initiation reaction. The active species ($\mathbf{VIII^{Lu}}$, Scheme 2.2) was investigated by NMR spectroscopy over time. Thereby, cationization by reformation of an originally C–H-bond activated and tucked-in *tert*butyl moiety of the non-innocent spectator ligand (Scheme 2.2) was revealed.

Comparison of the polymerization results to those obtained from tetramethylaluminates shows, that in analogy to the corresponding Cp^*-derived catalysts a shift from 1,4-*cis* to 1,4-*trans*-selectivity is observed upon borylaluminate introduction. Contrary to the Cp^*-supported Lu^{III} heteroaluminates, no arene interaction is found as in the presumed active species arene is absent (Scheme 2.2). Instead, the boryl moiety was discovered to be part of the side product $[(NMe_2Ph)Me_2Al\{B(NDippCH)_2\}]$. Therefore it can be concluded, that the activation of the $Tp^{tBu,\,Me}$-supported Lu^{III} borylaluminate precatalysts forms active species that differ significantly from those of the Cp^* analoga.

Another deeper look into the obtained polymer data of this study is worthwhile. Although the obtained polymers for precatalysts $\mathbf{VI^{Lu}}$ and its thermolytic product $\mathbf{VIa^{Lu}}$ differ significantly after a reaction time of 1 hour, similarities occur after 24 hours. This can be explained regarding the presumed active species (Scheme 2.2): the respective Ln–CH_2 bond is in both cases the position, where the insertion of the monomer units is

supposed to take place. Therefore, the borylaluminato moiety of $\mathbf{VIII^{Lu}}$ migrates off the catalytic center over time, which leaves the steric situation for incoming monomer molecules more and more similar to that of $\mathbf{VIIa^{Lu}}$ with each step of chain propagation.

2.3 Half-Sandwich Rare-Earth-Metal Allyls Bearing a Donor Sidearm as Precatalysts in 1,3-Diene Polymerization

Cyclopentadienyl complexes bearing a donor sidearm have been studied intensively by Cui and coworkers[289–292] and our group[293, 294] as catalysts in 1,3-diene polymerization. With the study of $[Cp^{NMe_2}Ln(allyl)_2]$ ($Cp^{NMe_2} = C_5Me_4(CH_2CH_2NMe_2)$, $\mathbf{IX^{Ln}}$) complexes as precatalyst in the polymerization of 1,3-dienes, a flexible ancillary ligand[295] is applied to the allyl motif investigated by Cui and coworkers[290–292, 296] and Taube and coworkers.[4, 129–131, 297] The sterically crowded systems produced polymers of moderate vinylic selectivity in low yield but living fashion (Paper II). The yield increased, when trialkylaluminum additives (AlR_3) were applied. Besides chain transfer, that occured especially with R = *i*Bu, the microstructures were shifted to an extreme extent, probably due to the allyl → aluminate exchange described by Evans and coworkers.[298] Furthermore, the ability of $AlMe_3$ to coordinate to the donor sidearm was investigated, as $AlMe_3$ had been added to the reactive mixture in excess. With the $AlMe_3$ coordinated sidearm pointing away from the catalytic center, into open space, and the exchanged allyl ligands toward alkylaluminates (**IXa**, Scheme 2.3), microstructures were obtained, that pictured the 1,4-*trans*-selectivity obtained upon $AlMe_3$ addition and that is wellknown for the Cp^*-derived half-sandwich bisaluminates of the larger rare-earth metals (*vide supra*, Section 2.2.1.1). In addition, the coordinative abilities of the donor sidearm are probably the main reason for the unexpected high sensitivity toward impurities, examined in this study.

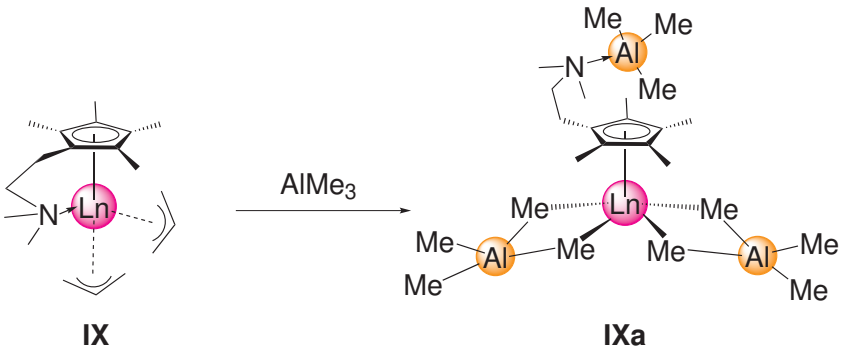

IX **IXa**

Scheme 2.3: Reaction of $[Cp^{NMe_2}Ln(allyl)_2]$ *(*$Cp^{NMe_2} = C_5Me_4(CH_2\text{-}CH_2NMe_2)$*,* $\boldsymbol{IX^{Ln}}$*) with an access of* $AlMe_3$ *resulting in a full allyl→ aluminate exchange and a coordination of* $AlMe_3$ *to the N-donor side arm of the ligand. Scheme according to Paper II, see there for further details.*

2.4 Half-Sandwich Ln^{III} Dimethyls as Precatalysts in 1,3-Diene Polymerization

Alkylaluminate-promoted polymerizations have shown to be influenced by $AlMe_3$ (TMA), that is set free during the cationization of the precatalyst. Without the possibility of TMA release and as they are the simplest possible alkyls, Ln^{III} dimethyl complexes have been investigated for complexes of both, the cyclopentadienyl (Cp^*), as well as the scorpionate ligand ($Tp^{tBu,\,Me}$).

2.4.1 Pentamethylcyclopentadienyl as Ancillary Ligand

Pentamethylcyclopentadienyl rare-earth metal dimethyl complexes are stable as trimeric clusters $[Cp^*LnMe_2]_3$ ($\mathbf{X^{Ln}}$). Their synthesis has only been reported for Ln = Y so far.[299, 300, 301] These clusters are highly symmetric and their trimeric nature influences their polymerization properties significantly.

2.4.1.1 Synthesis

In general, complexes $[Cp^*LnMe_2]_3$ ($\mathbf{X^{Ln}}$) are accessible up to the ion size of Tb^{3+} (Scheme 2.4). Therefore, the library was extended in this work to Ln = Lu, Ho, Dy and Tb (Paper V, Manuscript I). The synthesis protocol as published for yttrium[299, 300] is feasible for the lutetium, holmium and dysprosium compound, as well (Scheme 2.4). When this synthesis route is applied for terbium and gadolinium, pyramidal pentametallic clusters are the only identified species of the obtained product mixture. While in case of

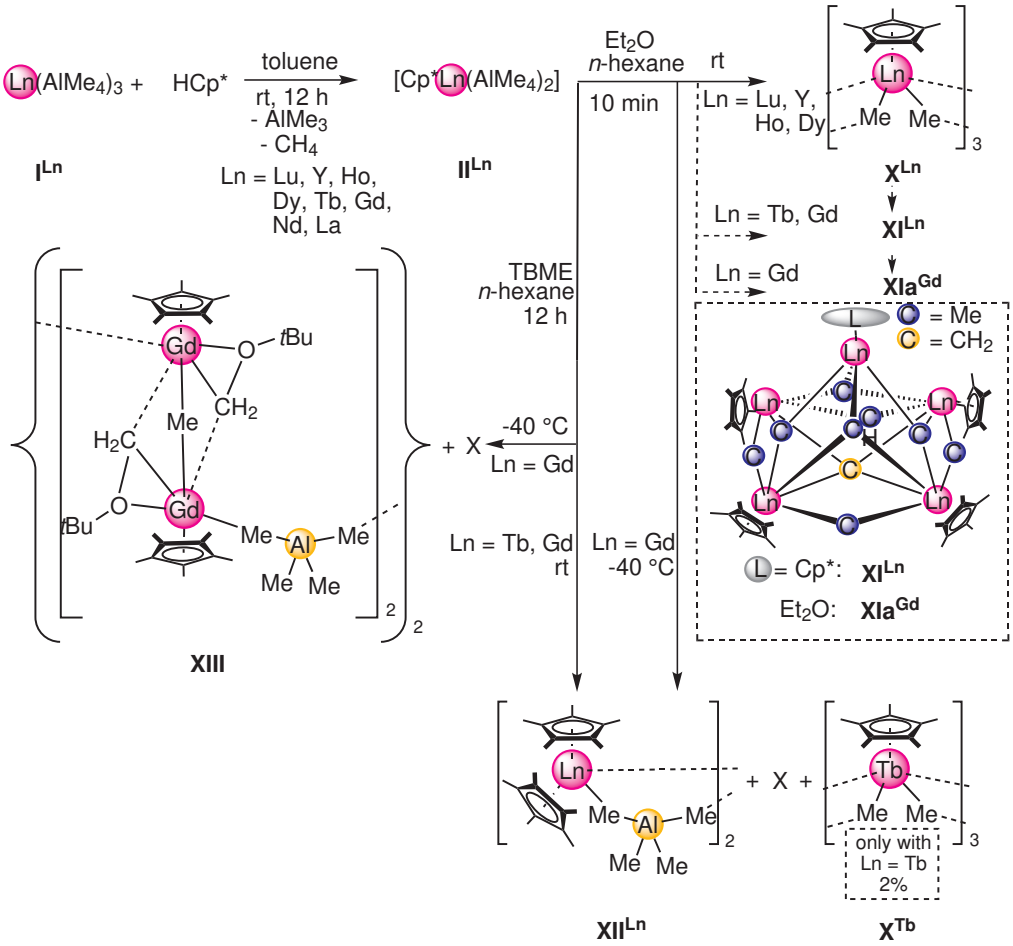

*Scheme 2.4: Protolytic synthesis of [Cp*Ln(AlMe$_4$)$_2$] (**II^{Ln}**) from the homoleptic tetramethylaluminate **I^{Ln}** and cleavage reaction with diethyl ether toward [Cp*LnMe$_2$]$_3$ (**X^{Ln}**), which could only be isolated for Ln = Lu, Y, Ho, Dy. As main product in this reaction with Ln = Tb, Gd, the square pyramidal complex **XI^{Ln}** is obtained, together with a product of extended C–H bond activation (**XIa^{Gd}**) in case of Ln = Gd. It is assumed, that (**X^{Ln}**) is an intermediate in the formation of the pyramidal pentamers. Upon the activation attempt using tert-butyl methyl ether (TBME), a metallocene alkylaluminate (**XII^{Ln}**) is obtained by ligand redistribution for Ln = Tb, Gd, in case of terbium, **X^{Tb}** is observed as a side product here. The metallocene product **XII^{Gd}** is also obtained, when the activation with diethyl ether is performed at -40 °C, but only for Ln = Gd. When the activation by TBME is performed at these conditions (Ln = Gd), an octameric macrocycle (**XIII**) was observed as product. Scheme according to Manuscript I, which has been published with ref. 304 by the time, this thesis is published. See there for further details.*

terbium only a pyramidal cluster bearing five Cp^* ligands ($[(Cp^*Tb)_5(CH_2)(Me)_8]$, $\mathbf{XI^{Tb}}$) was isolated (Figure 2.3), for Ln = Gd simultaneously to $\mathbf{XI^{Gd}}$ a similar complex bearing a diethyl ether donor ligand instead of one Cp^* ($\mathbf{XIa^{Gd}}$) was obtained as well (Scheme 2.4).

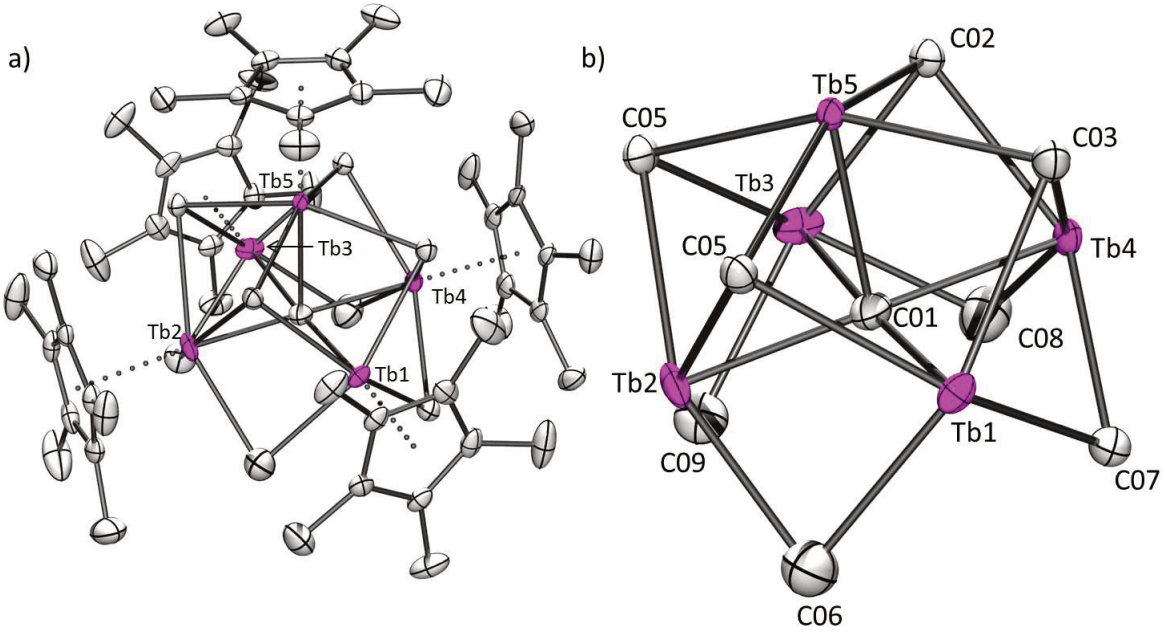

Figure 2.3: a) ORTEP view of the molecular structure of $[(Cp^*Tb)_5(CH_2)(Me)_8]$ ($\boldsymbol{XI^{Tb}}$). Atomic displacement parameters are set at the 50 % probability level. Hydrogen atoms and one molecule of n-hexane per asymmetric unit are omitted for clarity. b) Detailed view on the bonding situation in the pyramidal motif of the structure presented in figure part a, furthermore omitting the Cp^* ligands for enhanced clarity. The figures are shown as an example for the pyramidal motif of the obtained pentameric clusters $\boldsymbol{XI^{Ln}}$ and $\boldsymbol{XIa^{Gd}}$. Figure according to Manuscript I, which has been published with ref. 304 by the time, this thesis is published. See there for further details.

In contrast to a lozange shaped base tetragon of the pyramid obtained by Zimmermann,[302] the tetragon present in case of $\mathbf{XI^{Ln}}$ and $\mathbf{XIa^{Gd}}$ is significantly more square shaped and bears a CH_2^{2-} ion in its center. The presence of this carbon and at least one hydrogen is (crystallographically)

proven in all three pyramids obtained in this study. In case of $\mathbf{XIa^{Gd}}$ the ion is suspected to be a CH^{3-} for charge balance reasons. Figure 2.3 shows the pyramidal cage of $\mathbf{XI^{Tb}}$ as an example. These pyramidal clusters are presumed to form from the (by this method non-isolable) trimeric dimethyl clusters, $[Cp^*LnMe_2]_3$ ($\mathbf{X^{Ln}}$) (Ln = Tb, Gd), by C–H bond activation and release of methane.

For Ln =Tb and Gd the alkylaluminate cleavage reaction,[303] *tert*butyl-methyl-ether (TBME) has also been applied as cleaving agent (Scheme 2.4). For both metals the metallocene alkylaluminate dimer $[Cp^*_2Ln(AlMe_4)]_2$ ($\mathbf{XII^{Ln}}$) was the main product. Only in case of terbium, the dimethyl ($[Cp^*TbMe_2]_3$ ($\mathbf{X^{Tb}}$)) was obtained as an isolable byproduct (2 % crystallized yield). In case of Ln = Gd, the cleavage reactions have also been investigated at lower temperatures. Here, with diethyl ether, $\mathbf{XII^{Gd}}$ was formed as well. In contrast, indications for an dodecametallic cluster, forming a 24-membered ring (**XIII**), were found (Scheme 2.4 and Figure 2.4), when applying TBME instead.

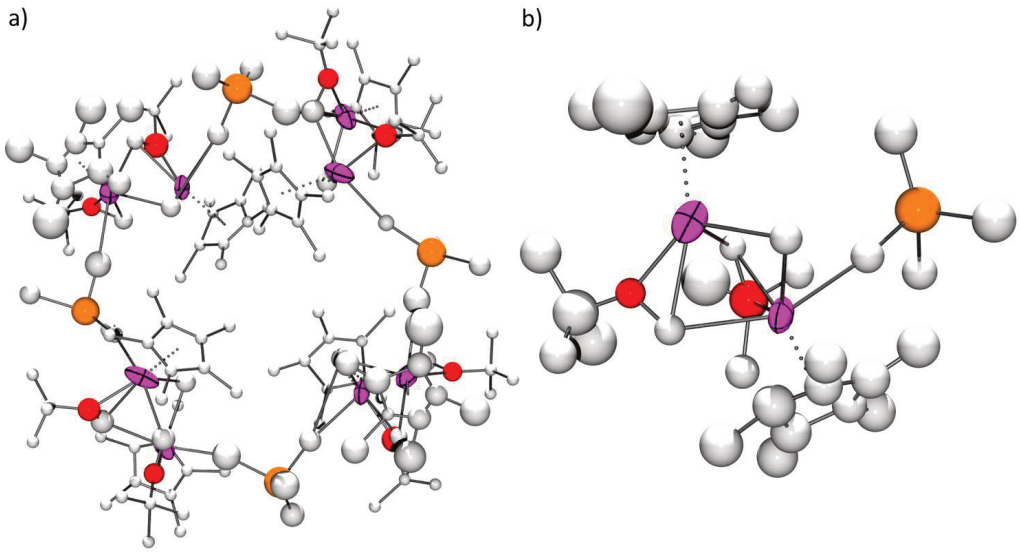

*Figure 2.4: a) Connectivity structures of the product **XIII** of the activation of [Cp*Gd($AlMe_4$)$_2$] (**II^{Gd}**) using TBME to cleave the alkylaluminates at -40°C. b) Zoom into the dimeric repetition unit of the structure presented in figure part a. In both ball and stick models, grey balls represent carbon atoms, the magenta ones represent gadolinium atoms, orange balls represent aluminum and the red depict the location of oxygen atoms. Hydrogen atoms are omitted for clarity. Due to high R-values of the measurement no further detailed figure is possible. Figure according to Manuscript I, which has been published with ref. 304 by the time, this thesis is published. See there for further details.*

2.4.1.2 Polymerization Catalysis

*Table 2.6: 1,3-Butadiene homopolymerization by [Cp*LnMe$_2$]$_3$ ($\mathbf{X^{Ln}}$)*

Entry[a]	Precatalyst	Cocat.[b]	T[c] [°C]	t[c] [h]	Yield[d] [%]	*cis*[e] [%]	*trans*[e] [%]	3,4[e] [%]	$M_{n,SEC}$[f] [10^4g·mol^{-1}]	PDI[f]	T_g[g] [°C]
67	[Cp*DyMe$_2$]$_3$ ($\mathbf{X^{Dy}}$)	**A**	25	1	99	97	0	3	16.2	1.63	-102
68	[Cp*DyMe$_2$]$_3$ ($\mathbf{X^{Dy}}$)	**B**	25	1	92	96	0	4	20.4	1.64	-102
69	[Cp*HoMe$_2$]$_3$ ($\mathbf{X^{Ho}}$)	**A**	25	1	90	91	4	5	5.5	1.52	-102
70	[Cp*HoMe$_2$]$_3$ ($\mathbf{X^{Ho}}$)	**B**	25	1	59	94	2	4	32.8	1.35	-101
71	[Cp*YMe$_2$]$_3$ ($\mathbf{X^{Y}}$)	**A**	25	1	21	91	4	5	76.4	1.58	-97
72	[Cp*YMe$_2$]$_3$ ($\mathbf{X^{Y}}$)	**B**	25	1	48	95	2	3	49.6	1.20	-97
73	[Cp*LuMe$_2$]$_3$ ($\mathbf{X^{Lu}}$)	**A**	25	1	> 99	85	8	7	39.7	1.84	-94
74	[Cp*LuMe$_2$]$_3$ ($\mathbf{X^{Lu}}$)	**B**	25	1	95	85	8	7	33.0	1.77	-93

[a] Conditions: 20 µmol of precatalyst, 20 µmol of cocatalyst, 20 mmol of isoprene, 8 mL of toluene. Data taken from Paper V, and Mauscript I.[304]
[b] **A** = [Ph$_3$C][B(C$_6$F$_5$)$_4$], **B** = [PhNHMe$_2$][B(C$_6$F$_5$)$_4$], **C** = B(C$_6$F$_5$)$_3$.
[c] T = polymerization temperature, t = reaction time.
[d] Yield of the isolated polymer.
[e] Determined by ^{1}H and ^{13}C NMR spectroscopy.
[f] Determined by GPC in THF at 35 °C.
[g] Determined on a Perkin Elmer DSC 8000; Heat rate: 20 K/min, Cooling rate: 60 K/min.
[h] Evaluation impossible due to low yield.

1,3-Diene polymerization was investigated for [Cp*LnMe$_2$]$_3$ ($\mathbf{X^{Ln}}$, Ln = Lu, Y, Ho, Dy). The set of polymers obtained from 1,3-butadiene (Table 2.6, and Manuscript I and Paper V for details) shows an uniform and highly 1,4-*cis*-selective microstructure for all tested lanthanides. A tendency towards even higher selectivity was observed with increasing ionic radius, reaching 97 / 0 / 3 % (*cis* / *trans* / 3,4 addition) with $\mathbf{X^{Dy}}$ as a maximum. Remarkable differences between these butadienes exist in yield and chain properties, depending on the lanthanide metal center used. Reproducibly, the initiation rates of the yttrium analogue are significantly lower, than for the other Ln, resulting in lower yield and higher molecular weight averages.

The polyisoprenes (Table 2.7 and Manuscript I[304] and Paper V for details) are produced in much more uniform yields, while the micorstructures vary significantly. The dimethyl derivative of the smallest lanthanide (Lu)

Table 2.7: Isoprene homopolymerization by [Cp^*LnMe_2]$_3$ ($\mathbf{X^{Ln}}$)

Entry[a]	Precatalyst	Cocat.[b]	T[c] [°C]	t[c] [h]	Yield[d] [%]	*cis*[e] [%]	*trans*[e] [%]	3,4[e] [%]	$M_{n,SEC}$[f] [10^4g·mol^{-1}]	PDI[f]	T_g[g] [°C]
59	[Cp^*DyMe_2]$_3$ ($\mathbf{X^{Dy}}$)	**A**	25	1	90	53	13	34	6.3	3.15	-36
60	[Cp^*DyMe_2]$_3$ ($\mathbf{X^{Dy}}$)	**B**	25	1	89	33	25	43	14.6	1.38	-24
61	[Cp^*HoMe_2]$_3$ ($\mathbf{X^{Ho}}$)	**A**	25	1	96	36	18	46	15.5	1.27	-20
62	[Cp^*HoMe_2]$_3$ ($\mathbf{X^{Ho}}$)	**B**	25	1	87	33	16	51	12.0	1.13	-20
63[j]	[Cp^*YMe_2]$_3$ ($\mathbf{X^{Y}}$)	**A**	25	1	> 99	51	17	32	8.4	2.33	-47
64[j]	[Cp^*YMe_2]$_3$ ($\mathbf{X^{Y}}$)	**B**	25	1	90	36	11	53	14.1	1.16	-27
65[j]	[Cp^*LuMe_2]$_3$ ($\mathbf{X^{Lu}}$)	**A**	25	1	> 99	21	21	58	26.8	2.00	-16
66[j]	[Cp^*LuMe_2]$_3$ ($\mathbf{X^{Lu}}$)	**B**	25	1	> 99	21	22	57	29.2	1.38	-17

[a] Conditions: 20 µmol of precatalyst, 20 µmol of cocatalyst, 20 mmol of isoprene, 8 mL of toluene. Data taken from Paper V, and Mauscript I.[304]
[b] **A** = [Ph_3C][$B(C_6F_5)_4$], **B** = [$PhNHMe_2$][$B(C_6F_5)_4$], **C** = $B(C_6F_5)_3$.
[c] T = polymerization temperature, t = reaction time.
[d] Yield of the isolated polymer.
[e] Determined by ^{1}H and ^{13}C NMR spectroscopy.
[f] Determined by GPC in THF at 35 °C.
[g] Determined on a Perkin Elmer DSC 8000; Heat rate: 20 K/min, Cooling rate: 60 K/min.
[h] Evaluation impossible due to low yield.
[j] Taken from Paper V.

affords a polymer with focus on the vinylic addition for both cocatalysts, **A** and **B**. Interestingly, this behavior is in accordance with that of the holmium analogue, where the focus is present to a lesser extent for ion size reasons. In contrast, the yttrium and dysprosium analogues both produce 1,4-*cis*-focused polymers with cocatalyst **A**. Applying **B**, similar polymers to those formed with holmium for both cocatalysts, are obtained.

The system $\mathbf{X^{Ho}}$ / **A** is the exception also in terms of polydispersity, producing the lowest in this series with cocatalyst **A**. For the other tested lanthanides, the PDIs are significantly higher with this cocatalyst. The reason for all these phenomena is a second reaction mechanism, present in all polymers of $\mathbf{X^{Ln}}$ / **A**. For $\mathbf{X^{Y}}$ / **A**, this behavior was further investigated (Paper V).

With $\mathbf{X^{Y}}$ / **A**, at lower temperatures, crosslinked polymers were observed, according to swelling experiments based on the Flory-Rehner equation (Paper V).[305–307] This behavior is ascribed to radicals being present

during the polymerization, causing this second reaction pathway. The reactivity of these presumed radicals was investigated performing post-polymerization modification, e.g. attempting crosslinking on a quenched polymer. It was confirmed, that this crosslinking behavior occurs only, when both the precatalyst and the cocatalyst as well as further monomer are added to the polymer solution. These results triggered the interest for the study of stabilizer addition (Details in Manuscript II, *vide infra*).
In 2014, Hou and coworkers[237] predicted a polymerization behavior involving a monomeric active species. However, such a species was not observed during all studies with that system. Therefore, investigations to find the active catalytic species were performed. As the high molecular weight averages and low ratios of chains per yttrium center imply, the active species is suspected to be multimetallic. Further indication was obtained from an experiment, where $\mathbf{X^Y}$ / **B** polymerizes in the presence of $AlMe_3$. There, polymers different from those of $[Cp^*Ln(AlMe_4)_2]$ ($\mathbf{II^Y}$) / **B** and $\mathbf{II^Y}$ / **B** / $AlMe_3$ with an equal excess of $AlMe_3$ are obtained. Therefore a reaction of $\mathbf{X^Y}$ with $AlMe_3$ to form three equivalents of $\mathbf{II^Y}$ can be excluded to happen in a significant extent within the given prereaction time. Due to high symmetry, classic NMR spectroscopic approaches are not sucessful in the determination of the active species. Nevertheless, some hints of the structure of the active species are found in combination with a study of polymerization at lower cocatalyst concentrations. Prior to the active catalyst, an inactive species of the composition '$Cp^*_3Y_3Me_{4-5}$' is formed. This implies an ongoing C–H bond activation reaction during the cationization and probably also during polymerization. In ^{1}H DOSY NMR spectroscopic experiments, evidence for the clusterlike nature of

the active species is found, as they reveal large molecular weights for the active species (Paper V).
When '$Cp^*_3Y_3Me_{4-5}$' is brought to reaction with further cocatalyst, a single molecule of borate statistically activates 4–6 catalytic yttrium centers. This implies degradation into smaller units that are either not monometallic or not all equally active, according to the obtained polymer chain properties.
With $\mathbf{X^Y / B}$ a coordination polymeric degradation product $[(Cp^*Y)_2Me_2(N(Me)_2(C_6H_4)]_n[B(C_6F_5)_4]_n$ (**XIV**) is obtained after 1 h. Its existence highlights the possibility of the coordination of the activation side product $PhNMe_2$ in case of the active species (likely as a coordination equilibrium) and the non-innocence of this potential neutral donor ligand.

2.4.1.3 Reactivity

With knowledge about the multimetallic nature of the catalytically active species of $\mathbf{X^{Ln}}$, the idea, that a slightly decreased steric bulk could be sufficient to reach 1,4-*cis*-selectivity as in case of the less bulky monomer 1,3-butadiene was established. It was intended to achieve such an environment for the active metal center by breaking up the trimeric clusters and introducing neutral donor ligands, to stabilize the complex. Therefore, a selection of five monodentate, six bidentate and two tridentate frequently applied ligands has been screened with the system $\mathbf{X^{Ln} / B}$ (Manuscript II).
All additives show individual influences on the polymerization:

- With a single equivalent of **THF** a polymer different from that of the THF-induced C–H bond activation product $[(Cp^*Y)_3Me_4(CH_2)(thf)_2]$

($\mathbf{XV^Y}$) (Paper V) was obtained. While the microstructure is not affected by the presence of THF at all, the activity is low, as in case of $\mathbf{XV^Y}$.

- **Diethyl ether** produces a rather unselective microstructure with chain properties that are close to livingness.

- **TBME** has only little effect on the resulting polymer after a pre-reaction time of 5 min prior to cocatalyst addition.

- The frequently applied stabilizer **BHT** inhibits the polymerization completely.

- **Benzophenone** hampers the initiation reaction. Besides that, it has little influence on the polymerization. When added after the cocatalyst it furthermore slows down the chain propagation.

- **Benzoquinone** produces few, long and very uniform polymer chains. A multimodal MWD is obtained, when it reacts directly with the active species of $\mathbf{X^{Ln}\,/\,B}$.

- This is the only polymerization condition for **4,4'-bipyridine** allowing polymerization, as well. The obtained polymer differs from that produced by $\mathbf{X^{Ln}\,/\,B}$ by its multimodal MWD.

- With **DMAP**, a ratio of chains per yttrium center of approximately 1 can be achieved.

- **Aminoquinoline** once more decreases the initiation rate.

- **Phenanthroline** hampers the polymerization significantly, but affords crystals of a coordination structure (**XVI**) suitable for X-ray diffractometry (Scheme 2.5 left and Manuscript II for details).
- The last bidentate donor, **(DippNC(H))$_2$** (Dipp = 2,4-diisopropylphenyl), produced a highly 3,4-selective microstructure.
- **Tetramethylguanidine** reacted under C–H-bond activation and the corresponding anion is found in a bridging mode (crystallographically verified, Scheme 2.5 right and Manuscript II for details) in a dimeric structure (**XVII**). With this system less chains than with pure $\mathbf{X^Y}$ / **B** are initiated, but high yields are achieved with unaffected microstructure.
- **Thiourea** finally inhibits the activation, when added to the precatalyst. With the pre-activated system, it does not affect the polymerization.

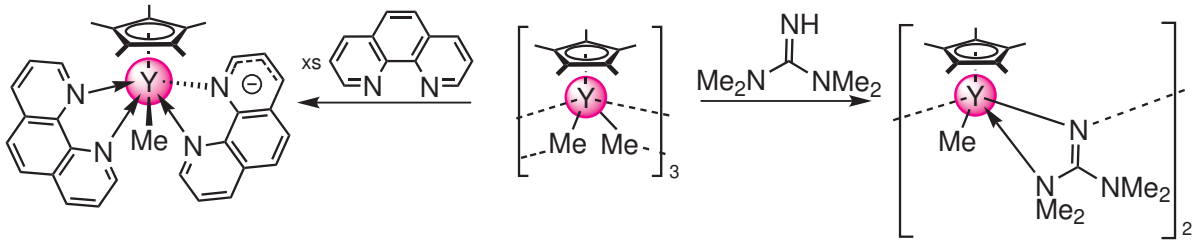

XVI^Y **X^Y** **XVII^Y**

*Scheme 2.5: Reactivity of $[Cp^*YMe_2]_3$ (**X^Y**) with phenanthroline toward $[Cp^*YMe(phenanthroline)(phenanthrolide)]$ (**XVI^Y**) and with tetramethylguanidine toward $[Cp^*YMe(tetramethylguadinide)]_2$ (**$XVII^Y$**). See Manuscript II for details and single crystal structures / connectivities.*

The three donors in this list, known as stabilizers to prevent radical reactions, were tested in a second study with cocatalyst **A**. The aim was suppression of the crosslinking obtained with $\mathbf{X}^{\mathbf{Y}}$ / **A** at low temperatures.

- **Benzophenone** inhibits the polymerization in most of the tested setups. The only polymers obtained in its presence (1 equivalent of benzophenone prior to activation) are crosslinked.
- With **BHT**, crosslinking did not occur for all tested systems. For most of them, multiple effects on the polymer are observed. Nevertheless, if a single equivalent is added prior to the activation, an almost unaffected polymer is obtained. Interestingly, with ten equivalents of the additive, a microstructural shift to high 1,4-*trans*-selectivity of 97 % is observed. Both polymerization reactions are relatively slow yielding full conversion only after 24 h.
- **Benzoquinone** produces a highly 1,4-*trans*-selective microstructure (96 %) as well, when applied in high excess (10 equiv.). With lower concentration it caused multimodal MWDs, but no crosslinking. Reactions with benzoquinone addition after the pre-reaction with the cocatalyst inhibited the polymerization.

2.4.2 Hydro-*tris*-(3-*tert*butyl-5-methyl-pyrazolyl)borato as an ancillary ligand

In contrast to the Cp^*-supported Ln^{III} dimethyls, with the larger scorpionate ligand ($Tp^{tBu,\,Me}$) monomeric precatalyst complexes ($\mathbf{XVIII^{Ln}}$) are accessible for holmium, yttrium, and lutetium. However a monomeric precatalyst does not automatically afford a monomeric active species, but the obtained polymerization results point in that direction (Manuscript III for details). Significantly higher contents of 1,4-*cis* linkages (Table 2.8) imply an enhanced steric space around the active metal center. Interestingly, cocatalyst **C** is able to activate the precatalyst for these systems (in contrast to the Cp* dimethyl precatalysts $\mathbf{X^{Ln}}$). However, the obtained catalyst is less active than those produced by **A** and **B**, with exception for $\mathbf{XVIII^{Y}}$ / **B**. Further noteworthy is the low overall yield with this system and its lutetium analog. Evidence for a suggested protonation of the spectator ligand remains a matter of research. In case of $\mathbf{XVIII^{Lu}}$ / **A** crosslinking cannot be excluded.

Table 2.8: Isoprene homopolymerization by $Tp^{tBu,\ Me}$ rare-earth metal dimethyls ***XVIII*** ^{Ln}

Entry[a]	Precatalyst	Cocatalyst[b]	T [°C]	t [min]	Method	Yield[d] [%]	*cis*[e] [%]	*trans*[e] [%]	3,4[e] [%]	$M_{n,SEC}$[f] [10^4g·mol^{-1}]	PDI[f]	T_g [°C]
61	$Tp^{tBu,\ Me}YMe_2$ (**XVIII**$^{\mathbf{Y}}$)	**A**	25	60	1	93	71	2	27	37.2	2.07	-46
62	$Tp^{tBu,\ Me}YMe_2$ (**XVIII**$^{\mathbf{Y}}$)	**B**	25	60	1	5	71	0	29	81.1	1.52	-44
63	$Tp^{tBu,\ Me}YMe_2$ (**XVIII**$^{\mathbf{Y}}$)	**C**	25	60	1	traces[h]	91	0	9	-[h]	-[h]	-[h]
64	$Tp^{tBu,\ Me}HoMe_2$ (**XVIII**$^{\mathbf{Ho}}$)	**A**	25	60	1	97	71	0	29	27.6	2.85	-45
65	$Tp^{tBu,\ Me}HoMe_2$ (**XVIII**$^{\mathbf{Ho}}$)	**B**	25	60	1	93	71	0	29	26.7	2.96	-43
66	$Tp^{tBu,\ Me}HoMe_2$ (**XVIII**$^{\mathbf{Ho}}$)	**C**	25	60	1	4	92	0	8	41.3	1.72	-57
67	$Tp^{tBu,\ Me}LuMe_2$ (**XVIII**$^{\mathbf{Lu}}$)	**A**	25	60	1	90	73	0	27	-[i]	-[i]	-43
68	$Tp^{tBu,\ Me}LuMe_2$ (**XVIII**$^{\mathbf{Lu}}$)	**B**	25	60	1	6	67	5	29	42.5	1.99	-47
69	$Tp^{tBu,\ Me}LuMe_2$ (**XVIII**$^{\mathbf{Lu}}$)	**C**	25	60	1	none[h]	-[h]	-[h]	-[h]	-[h]	-[h]	-[h]

[a] Conditions: 20 µmol of precatalyst, 20 µmol of cocatalyst, 20 mmol of isoprene, 8 mL of toluene.
[b] **A** = $[Ph_3C][B(C_6F_5)_4]$, **B** = $[PhNHMe_2][B(C_6F_5)_4]$, **C** = $B(C_6F_5)_3$.
[c] see Supporting Information for details: 1 = Standard procedure applying 5 min of pre-reaction time.
[d] Yield of the isolated polymer.
[e] Determined by ^{1}H and ^{13}C NMR spectroscopy.
[f] Determined by GPC in THF at 35 °C.
[g] Determined by DSC.
[h] Evaluation impossible due to low yield.
[i] Product polymer was insoluble in THF.

2.5 Hydro-*tris*-(3-*tert*butyl-5-methyl-pyrazolyl)borate Rare-Earth Metal Trimethylaluminates as Precatalysts in 1,3-Diene Polymerization

The smaller steric bulk of trimethylaluminates (Manuscript III) compared to the tetramethylaluminates allows coordination of this moiety twice, next to $Tp^{tBu,\,Me}$ and forms $[Tp^{tBu,\,Me}Ln(HAlMe_3)_2]$ (**XIX^{Ln}**).[284–286] With this second alkylaluminate present, $AlMe_3$ has to be released upon cationization. Like the Cp^*-supported Ln^{III} tetramethylaluminates, these precatalysts (investigated for Ln = Y, Lu) produce significant amounts of 1,4-*trans* linkages, due to $AlMe_3$ presence and steric bulk of the presumed active species with one aluminato moiety remaining after cationization.

2.6 A Tetrametallic Titanium Catecholate Complex

Besides all these lanthanide precatalysts, a titanium catecholate amido complex[308] ($[Ti(Cct)(NMe_2)_2]_2$, **XX**) has been studied as well (Manuscript IV). Upon activation attempts of **XX** with cocatalyst **C**, a stable reaction product could be crystallized. The obtained tetrameric cluster, $[Ti_4(Cct)_4(NMe_2)_7][HB(C_6F_5)_3]$ (**XXI**), shows two different motifs of bridging catecholato ligands and is inactive in 1,3-diene polymerization.

2.7 Overall Comparisons and Outstanding Polymers

2.7.1 Yttrium and Holmium Precatalysts

Comparing all data obtained in this thesis, it is striking that for several investigated Cp^*-derived and homoleptic species the polymerization behavior, studied vs. the lanthanide ion size, undergoes dramatic changes around the ion size of Ho^{III} and Y^{III}. Catalyst pollution by salt coordination is a reasonable interpretation, when ligands bearing donor atoms are present (Paper II), but cannot be responsible for the observed phenomena, when non-donor spectator ligands or no ancillary ligands at all are present. Furthermore, as these observations occur reproducibly and with holmium species synthesized from starting materials originating from several sources and suppliers a pollution seems unlikely but cannot be fully excluded. In these cases it seems reasonable, that the steric environment might play a major role. Still, due to the crosslinking behavior observed for the $[Cp^*LnMe_2]_3$ ($\mathbf{X^{Ln}}$) precatalysts, the actual electronic situation in the respective catalyst activation processes and chain propagation reactions seem to be a promising target to further investigation.

2.7.2 Accessible Polymers Applying Rare-Earth Metal Methyls and Those in Disguise

Although this thesis features mainly polymers of rather unselective microstructure to enable determination of diviations in all possible directions, in the respective screening studies, several remarkable polymers were produced.

The highest 1,4-*cis* selectivity in polyisoprene microstructures were

achieved with the homoleptic tetramethylaluminates ($\mathbf{I^{Ln}}$). With Ln = Gd ($Gd(AlMe_4)_3$, $\mathbf{I^{Gd}}$) activated by Me_2AlCl (**D**), both 1,4-*trans* and 3,4-linkages could not be observed in the polymer at all, leading to a nominal *cis*-selectivity of "> 99 %" (Chart 2.3d and Paper IV for details). The highest 1,4-*cis* content in a poly-1,3-butadiene in this thesis (99.7 %) was obtained in the same study, investigating the system of $\mathbf{I^{Nd}}$ / **D**.

The highest 1,4-*trans* selectivities of polyisoprene were obtained from systems containing the $[Cp^*Ln(AlMe_4)_3]$ ($\mathbf{II^{Ln}}$) and $[Cp^*LnMe_2]_3$ ($\mathbf{X^{Ln}}$) precatalysts. While the highest ever published 1,4-*trans*-content mentioned in this thesis for comparison was published by Zimmermannand coworkers[225, 282] with the $\mathbf{II^{La}}$ derivative and cocatalyst $[B(C_6F_5)_3]$ (**C**, 99.5 % 1,4-*trans*, Chart 2.3f and Table 2.1, run 3). The highest 1,4-*trans* selectivity found in the course of this thesis was obtained applying system $[Cp^*YMe_2]_3$ ($\mathbf{X^{Y}}$) in the presence of an equivalent of benzoquinone and cocatalyst $[Ph_3C][B(C_6F_5)_4]$ (**A**, 96 % 1,4-*trans*).

Polyisoprenes of the highest selectivity regarding vinylic (3,4) linkage was obtained from a system of $[Cp^*YMe_2]_3$ ($\mathbf{X^{Y}}$) prereacted with an equivalent of diisopropylphenyldiimine (DiIm) before addition of cocatalyst $[PhNHMe_2][B(C_6F_5)_4]$ (**B**). Here, probably due to the large steric bulk of the coligand, 88 % of the linkages were found to be vinylic (Paper V and Manuscript II for details).

The overall lowest PDI presented in this thesis and living polymerization was obtained from systems produced by coauthor Lars Jende of Paper II (System: $[Cp^{NMe_2}Lu(allyl)_2]$ ($Cp^{NMe_2} = C_5Me_4(CH_2CH_2NMe_2)$, $\mathbf{IX^{Lu}}$), both cocatalysts **A** and **B**. PDI: 1.04). The lowest PDI of a polymer produced by the author of this thesis was observed for one component of a poly-

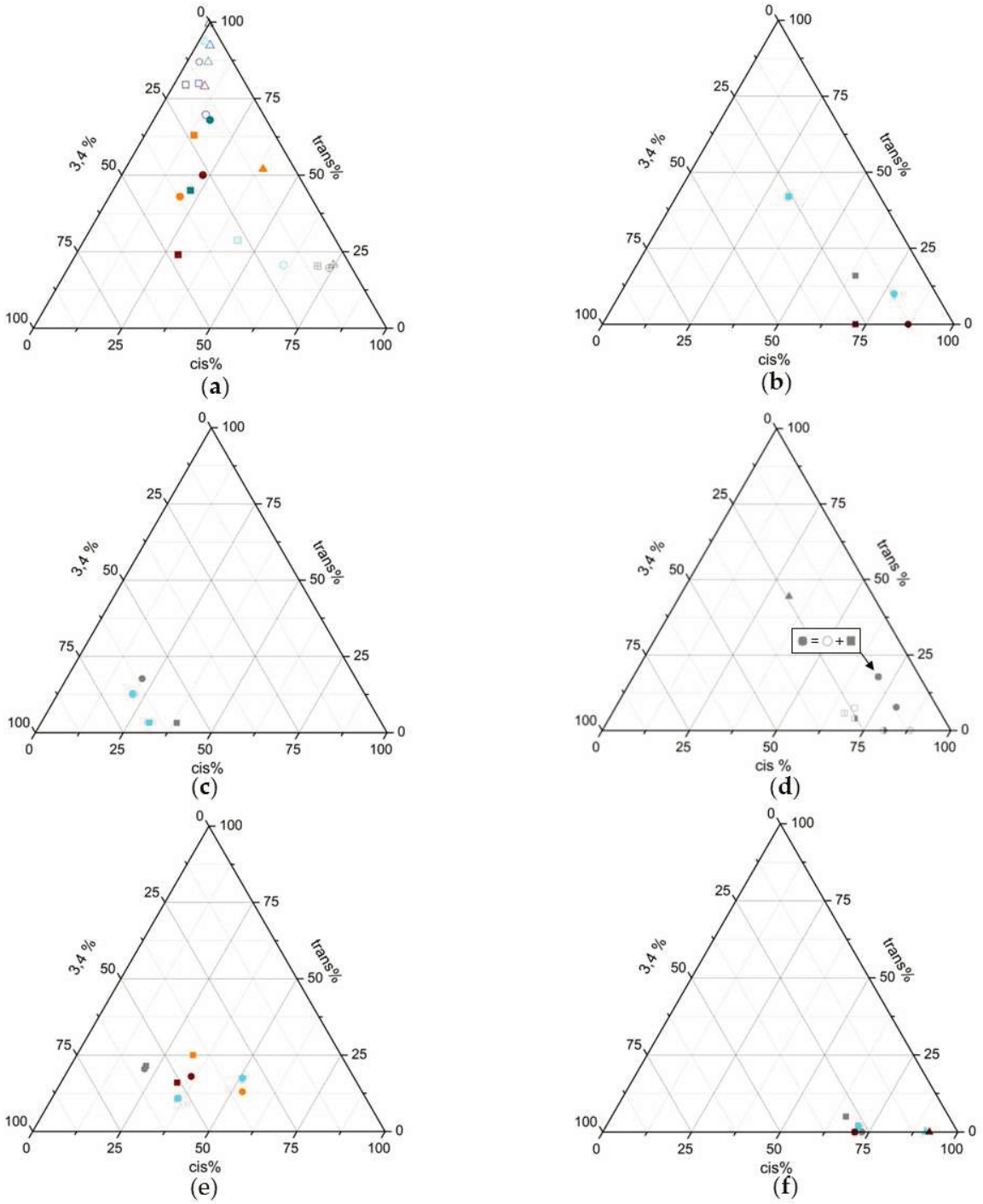

Chart 2.3: (See next page for caption.)

mer blend (two polyisoprenes of different properties). It was obtained from a study in which system $\mathbf{X^Y}$ / **B** was prereacted at ambient temperature followed by a polymerization of isoprene at -20 °C (PDI = 1.05). Lowest PDIs of a monomodal polyisoprene were obtained from both the system $\mathbf{X^Y}$ / **B** and $\mathbf{X^Y}$ /benzoquinone / **B** at ambient temperature (PDI = 1.09). The polymers produced by system $\mathbf{X^Y}$ / **B** or its derivatives cannot be considered to be living as the criterion of an initiation ratio of 1 is not fulfilled (Paper V and Manuscript II for details).

*Chart 2.3: (On previous page) This chart is meant to complement Chart 2.2. Ternary plots of the microstructures of the polyisoprenes obtained from the various catalysts tested in this thesis applying one equivalent of cocatalyst each, shown for comparison purposes. The symbols in the plots are color-coded throughout the entire chart regarding the lanthanide center as follows: black (La), red (Ce), green (Pr), blue (Nd), teal (Gd), pink (Tb), orange (Dy), brown (Ho), cyan (Y), violet (Er) and grey (Lu). The cocatalysts are represented by circles ($[Ph_3C][B(C_6F_5)_4]$, **A**), squares ($[PhNMe_2H][B(C_6F_5)_4]$, **B**) and triangles ($[B(C_6F_5)_3]$, **C**), while the reaction time is marked by crossed (15 min), solid (1 h) and hollow (24 h) symbols. Part a) represents polymerizations applying the respective Cp^* lanthanide bisaluminates ($[Cp^*Ln(AlMe_4)_2]$, **II**). Data is taken from Paper I and V and ManuscriptI[304], polymer data obtained from refs. 282 and 287 is shown for comparison. Part b) shows the microstructure of polymers obtained with $Tp^{tBu,\ Me}$ lanthanide monoaluminates ($[Tp^{tBu,\ Me}LnMe(AlMe_4)]$, **III**) Data is taken from Manuscript III. Part c) represents polymers obtained in a study applying Cp^* lanthanide bis-borylaluminates. ($[Cp^*Ln(AlMe_3\{B(NDippCH)_2\})_2]$, **V**) Data is taken from Paper I. Part d) represents polymers obtained from $Tp^{tBu,\ Me}$ lanthanide mono-borylaluminate systems ($[Tp^{tBu,\ Me}LnMe(AlMe_3\{B(NDippCH)_2\})]$, **VI**). Here, halfened symbols mark runs applying the thermolytic degradation product ($[(Tp^{(tBu\text{-}H)_2/tBu,Me)}Lu(AlMe_2B(NDippCH)_2)]$, **VIa**). Data is taken from Paper III. Part e) represents polymers obtained applying Cp^*Ln dimethyls ($[Cp^*LnMe_2]_3$, **X**) with one equiv. of cocatalyst per Ln center. Data is taken from Paper V and Manuscript I.[304] Part f) represents polymers produced by systems of $Tp^{tBu,\ Me}$ lanthanide dimethyls ($[Tp^{tBu,\ Me}LnMe_2]$, **XVI**). Data is taken from Manuscript III.*

Chapter 3

Concluding Remarks

The polymerization properties of a certain catalytically active center depend strongly on its steric environment. These environments and their effects have been studied in this thesis by polymerization experiments and direct analytic approaches. It was found that not only the steric bulk of a certain (ancillary) ligand influences the polymers, produced by an active species. Coordination of donors (additives, heteroatoms in ligands or side products of the activation reaction), cluster formation and degradation as well as side reactions (e.g. causing radical crosslinking) have been shown to have a major impact on the obtained polymers in this thesis.

Although the actual processes in the 'black box' of Ziegler-Natta 1,3-diene polymerization catalysis are challenging to determine, some new insights into the investigated mechanisms could be provided. A systematic survey from homoleptic rare-earth metal tetramethylaluminates *via* half-sandwich and scorpionate tetraalkylaluminates to cyclopentadienyl and *tris*pyrazolylborate alkyls is presented in this thesis. In the process, 1,3-diene polymers of significant microstructures and chain properties are featured, leading to conclusions regarding catalyst substrate interactions, activation and disactivation mechanisms and side reactions.

Overviewing the polymerization of homoleptic rare-earth metal tetramethylaluminates provided new insight into an "old" class of precatalysts and depicted trends within the series of eleven different lanthanide centers, highlighted by a polyisoprene with a 1,4-*cis*-selectivity beyond 99.9 %.

With pentamethylcyclopentadienyl (Cp^*) as an ancillary ligand rare-earth metal dimethyl trimers, rare aluminum-free catalytic systems, were tested in polymerization. The complex cluster nature of its active species could be illuminated and studies of its manipulation were performed. A crosslinking

side reaction was discovered and the synthetic limits of the precatalyst formation have been targeted. Nevertheless, the microstructural highlight of this study are the highly 1,4-*cis*-selective polybutadienes, that were obtained.

In a study on the polymerization properties of dimethyl complexes bearing hydro-*tris*-(3-methyl-5-*tert*butyl-pyrazolyl)borato ($Tp^{tBu,\,Me}$) as the ancillary ligand the monomeric equivalent of the abovementioned cyclopentadienyl study is presented. These catalysts produce polyisoprene with a high focus on 1,4-linkages. Here, the influence of the addition order of the catalyst components was also investigated. Furthermore, $Tp^{tBu,\,Me}$ rare-earth metal tetramethylaluminates and tetramethylgallates were also part of this study for comparison. In presence of these moieties, slight shifts towards 1,4-*trans* and 3,4-selectivity are observed, respectively.

With both of these spectator ligands (Cp^* and $Tp^{tBu,\,Me}$), studies applying borylalkylaluminates were performed. Special insight into the degradation of the active species could be obtained in the $Tp^{tBu,\,Me}$ case, while with Cp^* a coordination of an aryl ring at the boryl moiety influenced the microstructure to a focus on vinylic addition.

Moreover, a cyclopentadienyl system set bearing a donor side arm was investigated and found to be significantly more impurity sensitive than systems without sidearm. Besides that the obtained poylmerizations are living and moderately selective on vinylic linkages.

With all these data and studies rich in detail, a foundation is laid that allows future investigators to bring even more light into the ‘black box’ of Ziegler-Natta polymerization catalysis.

Chapter 4

References

References

[1] Ziegler, K. *Patent*, BE 533362, **1955**.

[2] Ziegler, K.; Holzkamp, E.; Breil, H.; Martin, H. *Angew. Chem.* **1955**, *67*, 426–426.

[3] Natta, G.; Pino, P.; Corradini, P.; Danusso, F.; Mantica, E.; Mazzanti, G.; Moraglio, G. *J. Am. Chem. Soc.* **1955**, *77*, 1708–1710.

[4] Taube, R. In *Catalytic reaction mechanisms and structur-reactivity-relationships in the stereospecific butadiene polymerization*; Kaminsky, W., Ed.; Springer Berlin, 1999; Chapter Metalorganic Catalysts for Synthesis and Polymerization, pp 531–547.

[5] Tobisch, S.; Bögel, H.; Taube, R. *Organometallics* **1996**, *15*, 3563–3571.

[6] Jende, L. N. Ph.D. Thesis, Eberhard Karls Universität Tübingen, **2015**.

[7] von Dohlen, W. C.; Wilson, T. P.; Caflisch, E. G. *Patent*, BE 644291, **1964**.

[8] von Dohlen, W. C.; Wilson, T. P.; Caflisch, E. G. *Patent*, US 3297667, **1967**.

[9] Ballard, D. G. H.; Courtis, A.; Holton, J.; McMeeking, J.; Pearce, R. *Chem. Commun.* **1978**, *1978*, 994–995.

[10] Margl, P.; Deng, L. Q.; Ziegler, T. *J. Am. Chem. Soc.* **1999**, *121*, 154–162.

[11] Arndt, S.; Okuda, J. *Chem. Rev.* **2002**, *102*, 1953–1976.

[12] Hou, Z. *Bull. Chem. Soc. Japan* **2003**, *76*, 2253–2266.

[13] Gromada, J.; Carpentier, J. F.; Montreux, A. *Coord. Chem. Rev.* **2004**, *248*, 397–410.

[14] Arndt, S.; Okuda, J. *Adv. Synth. Chem.* **2005**, *347*, 339–354.

[15] Fischbach, A.; Anwander, R. *Adv. Polym. Sci.* **2006**, *204*, 155–281.

[16] Friebe, L.; Nuyken, O.; Obrecht, W. In *Neodymium-Based Ziegler/Natta Catalysts and their Application in Diene Polymerization*; Nuyken, O., Ed.; Springer Berlin / Heidelberg, 2006; Vol. 204, Chapter Neodymium-Based Ziegler/Natta Catalysts and their Application in Diene Polymerization, pp 1–154.

[17] Hou, Z.; Luo, Y.; Li, X. *J. Organomet. Chem.* **2006**, *691*, 3114 – 3121.

[18] Rodrigues, A.-S.; Kirillov, E.; Carpentier, J.-F. *Coord. Chem. Rev.* **2008**, *252*, 2115 – 2136.

[19] Rodrigues, A.-S.; Carpentier, J.-F. *Coord. Chem. Rev.* **2008**, *252*, 2137 – 2154.

[20] Robert, D.; Spaniol, T. P.; Okuda, J. *Eur. J. Inorg. Chem.* **2008**, *2008*, 2801–2809.

[21] Nishiura, M.; Hou, Z. *Nat. Chem.* **2010**, *2*, 257–268.

[22] Zhang, Z.; Cui, D.; Wang, B.; Liu, B.; Yang, Y. In *Polymerization of 1,3-Conjugated Dienes with Rare-Earth Metal Precursors*; Roesky, P. W., Ed.; Springer Berlin Heidelberg, 2010; Vol. 137, Chapter 16, pp 49–108.

[23] Nishiura, M.; Guo, F.; Hou, Z. *Acc. Chem. Res.* **2015**, *48*, 2209–2220.

[24] Kelly, R. P.; Roesky, P. W. In *Catalytic Sigma-Bond Metathesis and the Polymerization of 1,3-Dienes by Rare-Earth Metal Complexes*; Michael, D.; Mingos, P., Eds.; Springer International Publishing Switzerland, 2015; Vol. 172, Chapter Structure and Bonding, pp 85–117.

[25] Trifonov, A. A.; Lyubov, D. M. *Coord. Chem. Rev.* **2017**, *340*, 10 – 61, Chemistry and Applications of the Lanthanides.

[26] Yang, F.; Li, X. *J. Polym. Sci. Part A1* **2017**, *55*, 2271–2280.

[27] Jothieswaran, J.; Fadlallah, S.; Bonnet, F.; Visseaux, M. *Catalysts* **2017**, *7*, 378.

[28] Huang, J.; Liu, Z.; Cui, D.; Li, X. *ChemCatChem* **2018**, *10*, 42 – 61.

[29] For examples of early group IV polymerization catalysts containing BAr^F-anions see refs. 37, 314–324.

[30] Massey, A.; Park, A. *J. Organomet. Chem.* **1964**, *2*, 245–250.

[31] Massey, A.; Park, A. *J. Organomet. Chem.* **1966**, *5*, 218–225.

[32] For early examples for early lanthanide-centered polymerization catalysts cationized by BAr^F-cocatalysts see refs. 249, 325–328 and 329.

[33] For an overview on less frequently applied borate anions see refs. 37 and 330.

[34] Horton, A. D. *Organometallics* **1996**, *15*, 2675–2677.

[35] Horton, A. D.; de With, J.; van der Linden, A. J.; van de Weg, H. *Organometallics* **1996**, *15*, 2672–2674.

[36] Jia, L.; Yang, X.; Ishihara, A.; Marks, T. J. *Organometallics* **1995**, *14*, 3135–3137.

[37] Chen, E. Y.-X.; Marks, T. J. *Chem. Rev.* **2000**, *100*, 1391–1434.

[38] Li, X.; Baldamus, J.; Hou, Z. *Angew. Chem. Int. Edit.* **2005**, *44*, 962–965.

[39] For examples of theoretical studies in this field see refs. 113, 237, 331, 332 and 333.

[40] For examples of active species investigated by NMR, see refs. 38, 183, 225, 326 and 287.

[41] Sauro, L.; Moeller, T. *J. Inorg. Nuc. Chem.* **1968**, *30*, 953 – 960.

[42] Pneumaticakis, G. A. *Chem. Ind.* **1968**, *24*, 770.

[43] Pneumaticakis, G. A. *Chem. Ind.* **1968**, *26*, 882.

[44] Schaverien, C. J. *Organometallics* **1992**, *11*, 3476–3478.

[45] For further, more recent, examples of BPh_4-anions with lanthanide centered cations in the context of polymerization catalysis see refs. 14, 20, 174, 182, 334–342 and 259.

[46] For examples of BPh_4 single component catalysts see refs. 343 and 242.

[47] In case of ROP of cyclic esters catalytic polymerizations even with BPh_4 are known, for example see ref. 344.

[48] For further information on Ln-F interactions see refs. 330 and 345.

[49] Further neutral single component catalysts, esp. for the polymerization of ethylene, e.g. metallocene methyl or hydride dimers have also been observed. For examples see chapter 2 in ref. 13 and literature cited therein.

[50] Evans, W. J.; Forrestal, K. J.; Ansari, M. A.; Ziller, J. W. *J. Am. Chem. Soc.* **1998**, *120*, 2180–2181.

[51] Evans, W. J.; DeCoster, D. M.; Greaves, J. *Macromolecules* **1995**, *28*, 7929–7936.

[52] Evans, W. J.; Forrestal, K. J.; Ziller, J. W. *Angew. Chem. Int. Edit.* **1997**, *36*, 774–776.

[53] Hayes, P. G.; Piers, W. E.; McDonald, R. *J. Am. Chem. Soc.* **2002**, *124*, 2132–2133.

[54] The coordination motif of one fluorine an fluorine atom from one of the Ar^F groups and two hydrogens of the boryl-transferred methyl

group occurs frequently for methyl species activated by cocatalyst **C**. For examples see refs. 53, 73.

[55] Lee , L. W. M.; Piers , W. E.; Elsegood, M. R. J.; Clegg, W.; Parvez, M. *Organometallics* **1999**, *18*, 2947–2949.

[56] Hayes, P. G.; Piers, W. E.; Parvez, M. *J. Am. Chem. Soc.* **2003**, *125*, 5622–5623.

[57] Hayes, P. G.; Piers, W. E.; Parvez, M. *Organometallics* **2005**, *24*, 1173–1183.

[58] Gollwitzer, A.; Dietel, T.; Kretschmer, W. P.; Kempe, R. *Nat. Comm.* **2017**, *8*, 1226.

[59] Henderson, L. D.; MacInnis, G. D.; Piers, W. E.; Parvez, M. *Canad. J. Chem.* **2004**, *82*, 162–165.

[60] Further information about MWDs or M_n is not given in ref. 59.

[61] Cui, D.; Tardif, O.; Hou, Z. *J. Am. Chem. Soc.* **2004**, *126*, 1312–1313.

[62] Li, X.; Baldamus, J.; Nishiura, M.; Tardif, O.; Hou, Z. *Angew. Chem. Int. Edit.* **2006**, *45*, 8184–8188.

[63] Cui, D.; Nishiura, M.; Hou, Z. *Macromolecules* **2005**, *38*, 4089–4095.

[64] Li, X.; Nishiura, M.; Mori, K.; Mashiko, T.; Hou, Z. *Chem. Commun.* **2007**, *2007*, 4137–4139.

[65] Li, X.; Nishiura, M.; Hu, L.; Mori, K.; Hou, Z. *J. Am. Chem. Soc.* **2009**, *131*, 13870–13882.

[66] Luo, Y.; Baldamus, J.; Hou, Z. *J. Am. Chem. Soc.* **2004**, *126*, 13910–13911.

[67] The data has also been published as reference in studies of ethylene-norbornene copolymerization[38] and ethylene-styrene-dicyclopentadiene terpolymerization.[109].

[68] The copolymers of these precatalysts will be discussed in detail with their comonomers, as the properties of these copolymers are far more comparable to the properties of the homopolymers of the comonomers than they are to homopolyethylene (*vide infra*).

[69] Lyubov, D. M.; Döring, C.; Fukin, G. K.; Cherkasov, A. V.; Shavyrin, A. S.; Kempe, R.; Trifonov, A. A. *Organometallics* **2008**, *27*, 2905–2907.

[70] Lyubov, D. M.; Döring, C.; Ketkov, S. Y.; Kempe, R.; Trifonov, A. A. *Chem. Eur. J.* **2011**, *17*, 3824–3826.

[71] Tredget, C. S.; Clot, E.; Mountford, P. *Organometallics* **2008**, *27*, 3458–3479.

[72] Tredget, C. S.; Bonnet, F.; Cowley, A. R.; Mountford, P. *Chem. Commun.* **2005**, *2005*, 3301–3303.

[73] Song, X.; Thornton-Pett, M.; Bochmann, M. *Organometallics* **1998**, *17*, 1004–1006.

[74] Touchard, V.; Spitz, R.; Boisson, C.; Llauro, M.-F. *Macromol. Rapid Comm.* **2004**, *25*, 1953–1957.

[75] Bochmann, M. *Acc. Chem. Res.* **2010**, *43*, 1267–1278.

[76] Li, Y.; Cokoja, M.; Kühn, F. E. *Coord. Chem. Rev.* **2011**, *255*, 1541–1557.

[77] These low temperatures both keep the monomer accessible due to its low vapor pressure under these conditions and the exothermic polymerization under control, which is beneficial to the polydispersity of the resulting polymers.

[78] Earlier examples of lanthanide-centered single-component catalysts for α-olefin polymerization were neurtral (*cf.* ref. 346).

[79] Yu, N.; Nishiura, M.; Li, X.; Xi, Z.; Hou, Z. *Chem. Asian J.* **2008**, *3*, 1406–1414.

[80] Li, Y.; Guo, F.; Shi, Z.; Ma, H.; Wang, B.; Li, T.; Wang, Y. *Patent*, CN 103819593 A 20140528, **2014**.

[81] Li, Y.; Shi, Z.; Guo, F.; Shen, K.; Li, T.; Wang, Y. *Patent*, CN 103772566 A 20140507, **2014**.

[82] Hou, Z.; Nishiura, M.; Nishii, K. *Patent*, JP 2014025043 A 20140206, **2014**.

[83] Nishiura, M.; Guo, F.; Hou, Z. *Patent*, WO 2011111656 A1 20110915, **2011**.

[84] Urakawa, N.; Uekusa, T.; Saito, J.; Todo, A.; Hou, Z.; Nishiura, M. *Patent*, JP 2011084641 A 20110428, **2011**.

[85] Kizu, K.; Todo, A.; Nishiura, M.; Hou, Z. *Patent*, JP 2010235719 A 20101021, **2010**.

[86] Hou, Z.; Li, X. F.; Yu, N. *Patent*, JP 2008095008 A 20080424, **2008**.

[87] Senda, T.; Hanaoka, H. *Patent*, WO 2008004628 A1 20080110, **2008**.

[88] Tan, R.; Guo, F.; Li, Y. *Polym. Chem.* **2017**, *8*, 615–623.

[89] For some of the rare examples of propylene polymerization catalyzed without structurally characterized catalyst see refs. 347–350 and 351.

[90] Yamamoto, A.; Nishiura, M.; Oyamada, J.; Koshino, H.; Hou, Z. *Macromolecules* **2016**, *49*, 2458–2466.

[91] Guo, F.; Nishiura, M.; Koshino, H.; Hou, Z. *Macromolecules* **2011**, *44*, 6335–6344.

[92] Yamamoto, A.; Nishiura, M.; Yang, Y.; Hou, Z. *Organometallics* **2017**, *36*, 4635–4642.

[93] Furthermore several derivatives of anisole have been tested as transfer agent in the styrene polymerization[90].

[94] Guo, F.; Nishiura, M.; Hou, Z. *Kidorui* **2010**, *56*, 28–29.

[95] Guo, F.; Nishiura, M.; Koshino, H.; Hou, Z. *Macromolecules* **2011**, *44*, 2400–2403.

[96] Guo, F.; Meng, R.; Li, Y.; Hou, Z. *Polymer* **2015**, *76*, 159–167.

[97] Shi, Z.; Guo, F.; Li, Y.; Hou, Z. *J. Polym. Sci. Part A1* **2015**, *53*, 5–9.

[98] Guo, F.; Wang, B.; Ma, H.; Li, T.; Li, Y. *J. Polym. Sci. Part A1* **2016**, *54*, 735–739.

[99] Qui, C.-Y.; Guo, F.; Li, Y.; Hou, Z. *Acta Polym. Sin.* **2016**, *12*, 1662–1668.

[100] Guo, F.; Jiao, N.; Jiang, L.; Li, Y.; Hou, Z. *Macromolecules* **2017**, *50*, 8398–8405.

[101] Jiao, N.; Guo, F.; Li, Y. *Acta Polym Sin.* **2017**, *12*, 1922–1929.

[102] This means in theory, that the reactivity of all possible chain ends of a copolymerization is low in means of addition of both of two comonomers, but at least one of them has a high affinity towards addition of a third comonomer. Due to the fact that the chain ends produced by this third monomer are active towards all three monomers a copolymerization takes place.

[103] Wang, C.; Luo, G.; Nishiura, M.; Song, G.; Yamamoto, A.; Luo, Y.; Hou, Z. *Sci. Adv.* **2017**, *3*, e1701011.

[104] Luo, Y.; Ma, Y.; Hou, Z. *J. Am. Chem. Soc.* **2018**, *140*, 114–117, PMID: 29261308.

[105] Tan, R.; Shi, Z.; Guo, F.; He, L.; Han, L.; Li, Y. *Polym. Chem.* **2017**, *8*, 4651–4658.

[106] Hou, Z.; Han, R. *Patent*, JP 2011190288, **2011**.

[107] Hou, Z.; Han, R. *Patent*, JP 5713380, **2011**.

[108] Yang, K.; Li, T.; Tan, R.; Shen, K.; Li, Y. *J. Polym. Sci. Part A1* **2018**, *56*, 467–470.

[109] Li, X.; Hou, Z. *Macromolecules* **2005**, *38*, 6767–6769.

[110] Pan, L.; Zhang, K.; Nishiura, M.; Hou, Z. *Macromolecules* **2010**, *43*, 9591–9593.

[111] Pan, L.; Zhang, K.; Nishiura, M.; Hou, Z. *Angew. Chem. Int. Edit.* **2011**, *50*, 12012–12015.

[112] Quantum mechanics/Molecular mechanics computational study.

[113] Luo, Y.; Luo, Y.; Qu, J.; Hou, Z. *Organometallics* **2011**, *30*, 2908–2919.

[114] In reality, the exception that styrene showed to form syndiotactic polystyrene blocks within the copolymer, due to the high activity of the system towards styrene homopolymerization, must be made. However, as no direct styrene-dicyclopentadiene links are found in the copolymer, ethylene remains still the key educt to enable this copolymerization.

[115] Lei, Y.; Su, Q.; Chen, J.; Luo, Y. *J. Organomet. Chem.* **2014**, *769*, 119–123.

[116] Luo, Y.; Feng, X.; Wang, Y.; Fan, S.; Chen, J.; Lei, Y.; Liang, H. *Organometallics* **2011**, *30*, 3270–3274.

[117] The fact that the system polymerized propylene at all is a remarkable feature, as it remains one of very few group III metal examples to do so. Ironically, a stable allyl complex is formed usually on propylene application to a rare-earth metal complex. And **35** is nothing else than such a stable allyl complex.

[118] Nishiura, M.; Masuko, T.; Hou, Z. *Patent*, JP2008222780, **2008**.

[119] Nishiura, M.; Mashiko, T.; Hou, Z. *Chem. Commun.* **2008**, *2008*, 2019–2021.

[120] Liu, D.; Luo, Y.; Gao, W.; Cui, D. *Organometallics* **2010**, *29*, 1916–1923.

[121] Lyubov, D. M.; Cherkasov, A. V.; Fukin, G. K.; Ketkov, S. Y.; Shavyrin, A. S.; Trifonov, A. A. *Dalton Trans.* **2014**, *43*, 14450–14460.

[122] Hou, Z.; Nishiura, M.; Niishi, K. *Patent*, JP 2014025043, **2014**.

[123] Hou, Z.; Li, X.; Yu, N. *Patent*, JP 2008095008, **2008**.

[124] Hou, Z.; Li, X.; Yu, N. *Patent*, JP 5013402, **2008**.

[125] Cui, D.; Liu, D. *Patent*, WO 2016023503, **2016**.

[126] Cui, D.; Liu, D. *Patent*, CN 105440187, **2016**.

[127] Cui, D.; Liu, D.; Wang, Z. *Patent*, CN 105330779, **2016**.

[128] Xu, P.; Yao, Y.; Xu, X. *Chem. Eur. J.* **2017**, *23*, 1263–1267.

[129] Taube, R.; Windisch, H.; Maiwald, S.; Hemling, H.; Schumann, H. *J. Organomet. Chem.* **1996**, *513*, 49 – 61.

[130] Taube, R.; Windisch, H.; enborn, H. W.; Hemling, H.; Schumann, H. *J. Organomet. Chem.* **1997**, *548*, 229 – 236.

[131] Maiwald, S.; Weißenborn, H.; Sommer, C.; Müller, G.; Taube, R. *J. Organomet. Chem.* **2001**, *640*, 1 – 9.

[132] Kaita, S.; Hou, Z.; Wakatsuki, Y. *Patent*, US 20020119889, **2002**.

[133] Kaita, S.; Hou, Z.; Wakatsuki, Y. *Patent*, US 6683140, **2004**.

[134] Kaita, S.; Hou, Z.; Wakatsuki, Y. *Patent*, JP 2002256012, **2002**.

[135] Suzuki, E.; Ozawa, Y.; Kaita, S.; Wakatsuki, Y. *Patent*, JP 4651921, **2011**.

[136] Suzuki, E.; Ozawa, Y.; Kaita, S.; Wakatsuki, Y. *Patent*, JP 2005036063, **2005**.

[137] Suzuki, E.; Ozawa, Y.; Kaita, S.; Wakatsuki, Y. *Patent*, WO 2005007740, **2011**.

[138] Suzuki, E.; Ozawa, Y.; Kaita, S.; Wakatsuki, Y. *Patent*, EP 1647571, **2011**.

[139] Suzuki, E.; Ozawa, Y.; Kaita, S.; Wakatsuki, Y. *Patent*, CN 1839180, **2006**.

[140] Suzuki, E.; Ozawa, Y.; Kaita, S.; Wakatsuki, Y. *Patent*, CN 100469831, **2009**.

[141] Suzuki, E.; Ozawa, Y.; Kaita, S.; Wakatsuki, Y. *Patent*, ES 2366631, **2011**.

[142] Suzuki, E.; Ozawa, Y.; Kaita, S.; Wakatsuki, Y. *Patent*, US 20070179267, **2007**.

[143] Suzuki, E.; Ozawa, Y.; Kaita, S.; Wakatsuki, Y. *Patent*, US 7511108, **2009**.

[144] Kaita, S.; Hou, Z.; Wakatsuki, Y.; Doi, Y. *Patent*, WO 20035503, **2003**.

[145] Kaita, S.; Hou, Z.; Wakatsuki, Y.; Doi, Y. *Patent*, JP 2004027179, **2004**.

[146] Kaita, S.; Hou, Z.; Wakatsuki, Y.; Doi, Y. *Patent*, JP 3624290, **2005**.

[147] Kaita, S.; Hou, Z.; Wakatsuki, Y.; Doi, Y. *Patent*, JP 2004238637, **2005**.

[148] Kaita, S.; Hou, Z.; Wakatsuki, Y.; Doi, Y. *Patent*, EP 1512700, **2005**.

[149] Kaita, S.; Hou, Z.; Wakatsuki, Y.; Doi, Y. *Patent*, US 20050233894, **2005**.

[150] Kaita, S.; Hou, Z.; Wakatsuki, Y.; Doi, Y. *Patent*, US 7148299, **2005**.

[151] Kaita, S.; Hou, Z.; Nishiura, M.; Doi, Y.; Kurazumi, J.; Horiuchi, A. C.; Wakatsuki, Y. *Macromol. Rapid Comm.* **2003**, *24*, 179–184.

[152] Kaita, S.; Yamanaka, M.; Horiuchi, A. C.; Wakatsuki, Y. *Macromolecules* **2006**, *39*, 1359–1363.

[153] For studies investigating the effect of AlR_3 alkyl length in lanthanide-centered polymerization catalysts see also refs. 352–354 and 355 as examples.

[154] The trend towards high *trans*-contents with large Ln centers is also found in studies investigating the corresponding Cp^*Ln bisalumiate half-sandwich complexes.[225, 282].

[155] Kaita, S.; Hou, Z.; Wakatsuki, Y. *Macromolecules* **2001**, *34*, 1539–1541.

[156] Kaita, S.; Doi, Y.; Kaneko, K.; Horiuchi, A. C.; Wakatsuki, Y. *Macromolecules* **2004**, *37*, 5860–5862.

[157] Masushita, J.; Kaita, S.; Tamaki, S. *Patent*, WO 2013132849, **2013**.

[158] Masushita, J.; Kaita, S.; Tamaki, S. *Patent*, JP 2013185058, **2013**.

[159] Masushita, J.; Kaita, S.; Tamaki, S. *Patent*, JP 5941302, **2016**.

[160] Masushita, J.; Kaita, S.; Tamaki, S. *Patent*, CN 104159930, **2014**.

[161] Masushita, J.; Kaita, S.; Tamaki, S. *Patent*, EP 2824118, **2015**.

[162] Masushita, J.; Kaita, S.; Tamaki, S. *Patent*, RU 2578566, **2016**.

[163] Masushita, J.; Kaita, S.; Tamaki, S. *Patent*, US 20150080525, **2015**.

[164] Masushita, J.; Kaita, S.; Tamaki, S. *Patent*, WO 2013132848, **2013**.

[165] Masushita, J.; Kaita, S.; Tamaki, S. *Patent*, JP 2013185059, **2013**.

[166] Masushita, J.; Kaita, S.; Tamaki, S. *Patent*, CN 104159932, **2014**.

[167] Masushita, J.; Kaita, S.; Tamaki, S. *Patent*, EP 2824119, **2015**.

[168] Masushita, J.; Kaita, S.; Tamaki, S. *Patent*, RU 2567756, **2015**.

[169] Masushita, J.; Kaita, S.; Tamaki, S. *Patent*, US 20150011701, **2015**.

[170] Nishii, K.; Kang, X.; Nishiura, M.; Luo, Y.; Hou, Z. *Dalton Trans.* **2013**, *42*, 9030–9032.

[171] Zhou, G.; Kang, X.; Wang, X.; Hou, Z.; Luo, Y. *Organometallics* **2018**, *37*, 551–558.

[172] Chen, J.; Gao, Y.; Xiong, S.; Delferro, M.; Lohr, T. L.; Marks, T. J. *ACS Catal.* **2017**, *7*, 5214–5219.

[173] Nishiura, M.; Li, X.; Mori, K.; Hou, Z. *Kidorui* **2009**, *54*, 192.

[174] Guo, F.; Nishiura, M.; Li, Y.; Hou, Z. *Chem. Asian J.* **2013**, *8*, 2471–2482.

[175] Ren, X.; Guo, F.; Fu, H.; Song, Y.; Li, Y.; Hou, Z. *Polymer Chemistry* **2018**, *9*, 1223–1233.

[176] Zhang, L.; Suzuki, T.; Luo, Y.; Nishiura, M.; Hou, Z. *Angew. Chem. Int. Edit.* **2007**, *46*, 1909–1913.

[177] Zhang, L.; Nishiura, M.; Yuki, M.; Luo, Y.; Hou, Z. *Angew. Chem. Int. Edit.* **2008**, *47*, 2642–2645.

[178] Chen, F.; Fan, S.; Wang, Y.; Chen, J.; Luo, Y. *Organometallics* **2012**, *31*, 3730–3735.

[179] Luo, Y.; Lei, Y.; Fan, S.; Wang, Y.; Chen, J. *Dalton Trans.* **2013**, *42*, 4040–4051.

[180] Luo, Y.; Chen, Q.; Chen, J. *Patent*, CN 103130941, **2013**.

[181] Döring, C.; Kempe, R. *Eur. J. Inorg. Chem.* **2009**, *2009*, 412–418.

[182] Döring, C.; Kretschmer, W. P.; Bauer, T.; Kempe, R. *Eur. J. Inorg. Chem.* **2009**, *2009*, 4255–4264.

[183] Li, D.; Li, S.; Cui, D.; Zhang, X. *Organometallics* **2010**, *29*, 2186–2193.

[184] Visseaux, M.; Mainil, M.; Terrier, M.; Mortreux, A.; Roussel, P.; Mathivet, T.; Destarac, M. *Dalton Trans.* **2008**, *2008*, 4558–4561.

[185] Destarac, M.; Mathivet, T.; Mainil, M.; Montreux, A.; Visseaux, M. *Patent*, FR 2906534, **2008**.

[186] Bonnet, F.; Jones, C. E.; Semlali, S.; Bria, M.; Roussel, P.; Visseaux, M.; Arnold, P. L. *Dalton Trans.* **2013**, *42*, 790–801.

[187] Loughmari, S.; Hafid, A.; Bouazza, A.; El Bouadili, A.; Zinck, P.; Visseaux, M. *J. Polym. Sci. Part A1* **2012**, *50*, 2898–2905.

[188] Tardif, O.; Kaita, S. *Dalton Trans.* **2008**, *2008*, 2531–2533.

[189] Ishikawa, S. *Patent*, JP 2011225650, **2011**.

[190] Miyazaki, Y. *Patent*, JP 2011148935, **2011**.

[191] Nukii, N. *Patent*, JP 2011148925, **2011**.

[192] Nakagawa, R. *Patent*, JP 2011111510, **2011**.

[193] Kimura, T. *Patent*, JP 2011111497, **2011**.

[194] Yamagashi, Y. *Patent*, JP 2011099026, **2011**.

[195] Iida, K. *Patent*, JP 2011094031, **2011**.

[196] Maeda, K. *Patent*, JP 2011084635, **2011**.

[197] Akaishi, K. *Patent*, JP 2011084634, **2011**.

[198] Yamagishi, Y. *Patent*, JP 2011079876, **2011**.

[199] Nakagawa, R.; Matsushita, J.; Ozawa, Y.; Kaita, S.; Tardif, O. *Patent*, WO 2009148140, **2009**.

[200] Nakagawa, R.; Matsushita, J.; Ozawa, Y.; Kaita, S.; Tardif, O. *Patent*, CN 102112508, **2009**.

[201] Nakagawa, R.; Matsushita, J.; Ozawa, Y.; Kaita, S.; Tardif, O. *Patent*, EP 2284206, **2009**.

[202] Nakagawa, R.; Matsushita, J.; Ozawa, Y.; Kaita, S.; Tardif, O. *Patent*, KR 2011028488, **2011**.

[203] Nakagawa, R.; Matsushita, J.; Ozawa, Y.; Kaita, S.; Tardif, O. *Patent*, KR 1259275, **2011**.

[204] Nakagawa, R.; Matsushita, J.; Ozawa, Y.; Kaita, S.; Tardif, O. *Patent*, JP 5649117, **2009**.

[205] Nakagawa, R.; Matsushita, J.; Ozawa, Y.; Kaita, S.; Tardif, O. *Patent*, US 20110136995, **2011**.

[206] Nakagawa, R.; Matsushita, J.; Ozawa, Y.; Kaita, S.; Tardif, O. *Patent*, US 8507627, **2011**.

[207] Aida, S.; Tardif, O. *Patent*, JP 2008266523, **2008**.

[208] Kaita, S.; Tardif, O. *Patent*, WO 2007129670, **2007**.

[209] Kaita, S.; Tardif, O. *Patent*, BR 2007011436, **2007**.

[210] Kaita, S.; Tardif, O. *Patent*, CN 101443343, **2007**.

[211] Kaita, S.; Tardif, O. *Patent*, EP 2017280, **2007**.

[212] Kaita, S.; Tardif, O. *Patent*, JP 5325575, **2007**.

[213] Kaita, S.; Tardif, O. *Patent*, KR 2009024144, **2009**.

[214] Kaita, S.; Tardif, O. *Patent*, KR 1457885, **2009**.

[215] Kaita, S.; Tardif, O. *Patent*, KR 2014097561, **2014**.

[216] Kaita, S.; Tardif, O. *Patent*, KR 1538625, **2014**.

[217] Kaita, S.; Tardif, O. *Patent*, US 20090264604, **2009**.

[218] Kaita, S.; Tardif, O. *Patent*, US 8653290, **2009**.

[219] Kim, I.; Zhou, J.-M. *J. Polym. Sci. Part A1* **1999**, *37*, 1071–1082.

[220] Kim, I.; Choi, C.-S. *J. Polym. Sci. Part A1* **1999**, *37*, 1523–1539.

[221] Deacon, G. B.; Forsyth, C. M. *Chem. Commun.* **2002**, *2002*, 2522–2523.

[222] Evans, W. J.; Johnston, M. A.; Greci, M. A.; Gummersheimer, T. S.; Ziller, J. W. *Polyhedron* **2003**, *22*, 119 – 126.

[223] Monteil, V.; Spitz, R.; Boisson, C. *Polym. Int.* **2004**, *53*, 576–581.

[224] This leads to the conclusion that even with the by far larger ionic radius of the Gd-cation, it is the indene that is cleaved off, which is even more unexpected.

[225] Zimmermann, M.; Törnroos, K. W.; Anwander, R. *Angew. Chem. Int. Edit.* **2008**, *47*, 775–778.

[226] Bochmann, M.; Sarsfield, M. J. *Organometallics* **1998**, *17*, 5908–5912.

[227] $[Cp^*La(Me_3AlAr^F)(\mu\text{-}Me_2AlAr^F{}_2)]_2$ reacts in a violent explosion on thermal treatment or shock.[226, 360].

[228] Liu, B.; Roisnel, T.; Maron, L.; Carpentier, J.-F.; Sarazin, Y. *Chem. Eur. J.* **2013**, *19*, 3986–3994.

[229] Basalov, I. V.; Dorcet, V.; Fukin, G. K.; Carpentier, J.-F.; Sarazin, Y.; Trifonov, A. A. *Chem. Eur. J.* **2015**, *21*, 6033–6036.

[230] Agarwal, S.; Mast, C.; Anfang, S.; Karl, M.; Dehnicke, K.; Greiner, A. *Polym. Prep.* **1998**, *39*, 414.

[231] Tardif, O.; Nishiura, M.; Hou, Z. *Organometallics* **2003**, *22*, 1171–1173.

[232] cf. Figure 1 in ref. 63 for a yield / time diagram.

[233] The "nacnac^{Me_2}" system published by Piers and coworkers in 2003[56] is therefore neglected here. The assumingly active species produced so little amount of polymer, that characterization was impossible.

[234] Due to the asymmetric ligand situation in the non-activated case of Kempe's and Trifonov's trimer (see Figure 1.1a) both μ_3-hydrogens are shifted away from the neosilyl moiety and one μ_2-hydrogen is rotated out of the plane of the six-membered Y_3H_3-ring.

[235] Hayes, P. G.; Welch, G. C.; Emslie, D. J. H.; Noack, C. L.; Piers, W. E.; Parvez, M. *Organometallics* **2003**, *22*, 1577–1579.

[236] For an example see ref. 79, 115.

[237] Kang, X.; Luo, Y.; Zhou, G.; Wang, X.; Yu, X.; Hou, Z.; Qu, J. *Macromolecules* **2014**, *47*, 4596–4606.

[238] For examples of C–H activation active species degradations see refs. 239, for examples of C–H activation before catalyst activation see refs. 65, 293, 356–358, and 239 as well.

[239] Bonath, M.; Hollfelder, C. O.; Schädle, D.; Maichle-Mössmer, C.; Anwander, R. *Chem. Eur. J.* **2017**, *23*, 4683 –4693.

[240] Here "#" indicates, that one *t*Bu group of the ligand is C–H activated and binds to the Lu center *via* the resulting CH_2-moiety. "*" indicates, that this C–H activation happened twice.

[241] Windisch, H.; G.Sylvester,; Taube, R.; Maiwald, S. *Patent*, DE 19720171 A1, **1997**.

[242] Taube, R.; Maiwald, S.; Sieler, J. *J. Organomet. Chem.* **2001**, *621*, 327 – 336.

[243] Maiwald, S.; Taube, R.; Hemling, H.; Schumann, H. *J. Organomet. Chem.* **1998**, *552*, 195–204.

[244] Maiwald, S.; Sommer, C.; Müller, G.; Taube, R. *Macromol. Chem. Phys.* **2001**, *202*, 1446–1456.

[245] Maiwald, S.; Sommer, C.; Müller, G.; Taube, R. *Macromol. Chem. Phys.* **2002**, *203*, 1029–1039.

[246] Chen, X.; Lim, S.; Plečnik, C. E.; Liu, S.; Du, B.; Meyers, E. A.; Shore, S. G. *Inorg. Chem.* **2004**, *43*, 692–698.

[247] An analogue complex of a Sm^{II} cation surrounded by six thf ligands countered by a BPh_4 anion was published in the same year (2003) by Evansand coworkers.[361].

[248] Bouwkamp, M. W.; Budzelaar, P. H. M.; Gercama, J.; Del Hierro Morales, I.; de Wolf, J.; Meetsma, A.; Troyanov, S. I.; Teuben, J. H.; Hessen, B. *J. Am. Chem. Soc.* **2005**, *127*, 14310–14319.

[249] Burger, B. J.; Thompson, M. E.; Cotter, W. D.; Bercaw, J. E. *J. Am. Chem. Soc.* **1990**, *112*, 1566–1577.

[250] Hitchcock, P. B.; Lappert, M. F.; Protchenko, A. V. *Chem. Commun.* **2005**, *2005*, 951–953.

[251] Hayes, P. G.; Piers, W. E.; Parvez, M. *Chem. Eur. J.* **2007**, *13*, 2632–2640.

[252] Knight, L. K.; Piers , W. E.; McDonald, R. *Organometallics* **2006**, *25*, 3289–3292.

[253] Yan, K.; Upton, B. M.; Ellern, A.; Sadow, A. D. *J. Am. Chem. Soc.* **2009**, *131*, 15110–15111.

[254] Yan, K.; Schoendorff, G.; Upton, B. M.; Ellern, A.; Windus, T. L.; Sadow, A. D. *Organometallics* **2013**, *32*, 1300–1316.

[255] Venugopal, A.; Fegler, W.; Spaniol, T. P.; Maron, L.; Okuda, J. *J. Am. Chem. Soc.* **2011**, *133*, 17574–17577.

[256] Fegler, W.; Venugopal, A.; Spaniol, T. P.; Maron, L.; Okuda, J. *Angew. Chem. Int. Edit.* **2013**, *52*, 7976–7980.

[257] Berkefeld, A.; Piers, W. E.; Parvez, M.; Castro, L.; Maron, L.; Eisenstein, O. *J. Am. Chem. Soc.* **2012**, *134*, 10843–10851.

[258] Berkefeld, A.; Piers, W. E.; Parvez, M.; Castro, L.; Maron, L.; Eisenstein, O. *Chem. Sci.* **2013**, *4*, 2152–2162.

[259] Li, T.; Nishiura, M.; Cheng, J.; Zhang, W.; Li, Y.; Hou, Z. *Organometallics* **2013**, *32*, 4142–4148.

[260] Zamora, M. T.; Johnson, K. R. D.; Hänninen, M. M.; Hayes, P. G. *Dalton Trans.* **2014**, *43*, 10739–10750.

[261] LeBlanc, F. A.; Piers, W. E.; Parvez, M. *Angew. Chem. Int. Edit.* **2014**, *53*, 789–792.

[262] So, Y.-M.; Li, Y.; Au-Yeung, K.-C.; Wang, G.-C.; Wong, K.-L.; Sung, H. H. Y.; Arnold, P. L.; Williams, I. D.; Lin, Z.; Leung, W.-H. *Inorg. Chem.* **2016**, *55*, 10003–10012, PMID: 27196506.

[263] Pindwal, A.; Patnaik, S.; Everett, W. C.; Ellern, A.; Windus, T. L.; Sadow, A. D. *Angew. Chem. Int. Edit.* **2017**, *56*, 628–631.

[264] Goodwin, C. A. P.; Ortu, F.; Reta, D.; Chilton, N. F.; Mills, D. P. *Nature* **2017**, *548*, 439–442.

[265] Guo, F.-S.; Day, B. M.; Chen, Y.-C.; Tong, M.-L.; Mansikkamäki, A.; Layfield, R. A. *Angew. Chem. Int. Edit.* **2017**, *56*, 11445–11449.

[266] Goodwin, C. A. P.; Reta, D.; Ortu, F.; Chilton, N. F.; Mills, D. P. *J. Am. Chem. Soc.* **2017**, *139*, 18714–18724, PMID: 29182861.

[267] Kilpatrick, A. F. R.; Cloke, F. G. N. *Dalton Trans.* **2017**, *46*, 5587–5597.

[268] Chen, Y.; Song, D.; Li, J.; Hu, X.; Bi, X.; Jiang, T.; Hou, Z. *ChemCatChem* **2018**, *10*, 159–164.

[269] Dietrich, H. M.; Raudaschl-Sieber, G.; Anwander, R. *Angew. Chem. Int. Edit.* **2005**, *44*, 5303–5306.

[270] Zimmermann, M.; Anwander, R. *Chem. Rev.* **2010**, *110*, 6194–6259.

[271] Evans, W. J.; Anwander, R.; Ziller, J. W. *Organometallics* **1995**, *14*, 1107–1109.

[272] Klooster, W. T.; Lu, R. S.; Anwander, R.; Evans, W. J.; Koetzle, T. F.; Bau, R. *Angew. Chem. Int. Edit.* **1998**, *37*, 1268–1270.

[273] Zimmermann, M.; Frøystein, N.-Å.; Fischbach, A.; Sirsch, P.; Dietrich, H. M.; Törnroos, K. W.; Herdtweck, E.; Anwander, R. *Chem. Eur. J.* **2007**, *13*, 8784–8800.

[274] Meermann, C.; Törnroos, K. W.; Nerdal, W.; Anwander, R. *Angew. Chem. Int. Edit.* **2007**, *46*, 6508–6513.

[275] Nieland, A.; Mix, A.; Neumann, B.; Stammler, H.-G.; Mitzel, N. W. *Eur. J. Inorg. Chem.* **2014**, *2014*, 51–57.

[276] König, S. N.; Chilton, N. F.; Maichle-Mössmer, C.; Pineda, E. M.; Pugh, T.; Anwander, R.; Layfield, R. A. *Dalton Trans.* **2014**, *43*, 3035–3038.

[277] Fischbach, A.; Klimpel, M. G.; Widenmeyer, M.; Herdtweck, E.; Scherer, W.; Anwander, R. *Angew. Chem. Int. Edit.* **2004**, *43*, 2234–2239.

[278] Hollfelder, C. O.; Jende, L. N.; Diether, D.; Zelger, T.; Stauder, R.; Maichle-Mössmer, C.; Anwander, R. *Catalysts* **2018**, *8*, 61.

[279] Zimmermann, M.; Anwander, R. *Chem. Rev.* **2010**, *110*, 6194–6259.

[280] Litlabø, R.; Lee, H. S.; Niemeyer, M.; Törnroos, K. W.; Anwander, R. *Dalton Trans.* **2010**, *39*, 6815–6825.

[281] Zimmermann, M.; Törnroos, K. W.; Anwander, R. *Angew. Chem. Int. Edit.* **2008**, *47*, 775–778.

[282] Zimmermann, M.; Törnroos, K. W.; Sitzmann, H.; Anwander, R. *Chem. Eur. J.* **2008**, *14*, 7266–7277.

[283] Dietrich, H. M.; Schuster, O.; Törnroos, K. W.; Anwander, R. *Angew. Chem. Int. Edit.* **2006**, *45*, 4858–4863.

[284] Litlabø, R.; Zimmermann, M.; Saliu, K.; Takats, J.; Törnroos, K. W.; Anwander, R. *Angew. Chem. Int. Edit.* **2008**, *47*, 9560–9564.

[285] Schädle, C.; Schädle, D.; Eichele, K.; Anwander, R. *Angew. Chem. Int. Edit.* **2013**, *52*, 13238–13242.

[286] Dorothea, S.; Cäcilia, M.-M.; Christoph, S.; Reiner, A. *Chem. Eur. J.* **2015**, *21*, 662–670.

[287] Dettenrieder, N.; Hollfelder, C. O.; Jende, L. N.; Maichle-Mössmer, C.; Anwander, R. *Organometallics* **2014**, *33*, 1528–1531.

[288] Du, G.; Wei, Y.; Ai, L.; Chen, Y.; Xu, Q.; Liu, X.; Zhang, S.; Hou, Z.; Li, X. *Organometallics* **2010**, *30*, 160–170.

[289] Wang, B.; Cui, D.; Lv, K. *Macromolecules* **2008**, *41*, 1983–1988.

[290] Jian, Z.; Tang, S.; Cui, D. *Chem. Eur. J.* **2010**, *16*, 14007–14015.

[291] Jian, Z.; Cui, D.; Hou, Z.; Li, X. *Chem. Commun.* **2010**, *46*, 3022–3024.

[292] Jian, Z.; Tang, S.; Cui, D. *Macromolecules* **2011**, *44*, 7675–7681.

[293] Litlabø, R.; Enders, M.; Törnroos, K. W.; Anwander, R. *Organometallics* **2010**, *29*, 2588–2595.

[294] Jende, L. N.; Maichle-Mössmer, C.; Anwander, R. *Chem. Eur. J.* **2013**, *19*, 16321–16333.

[295] Jutzi, P.; Dahlhaus, J.; Bangel, M. *J. Organomet. Chem.* **1993**, *460*, C13–C15.

[296] Jian, Z.; Cui, D.; Hou, Z. *Chem. Eur. J.* **2012**, *18*, 2674–2684.

[297] Taube, R.; Maiwald, S.; Sieler, J. *J. Organomet. Chem.* **2001**, *621*, 327 – 336.

[298] Evans, W. J.; Kozimor, S. A.; Brady, J. C.; Davis, B. L.; Nyce, G. W.; Seibel, C. A.; Ziller, J. W.; Doedens, R. J. *Organometallics* **2005**, *24*, 2269–2278.

[299] Dietrich, H. M.; Zapilko, C.; Herdtweck, E.; Anwander, R. *Organometallics* **2005**, *24*, 5767–5771.

[300] Dietrich, H. M.; Grove, H.; Törnroos, K. W.; Anwander, R. *J. Am. Chem. Soc.* **2006**, *128*, 1458–1459.

[301] The Cp' analogue of Tm ([Cp'$TmMe_2$]) has been synthesized and investigated by Houand coworkers[359] in 2011.

[302] Zimmermann, M. Ph.D. Thesis, Universitetet i Bergen, **2007**.

[303] Holton, J.; Lappert, M. F.; Ballard, D. G. H.; Pearce, R.; Atwood, J. L.; Hunter, W. E. *Dalton Trans.* **1979**, *1979*, 54 –61.

[304] Hollfelder, C. O.; Meermann-Zimmermann, M.; Spiridopoulos, G.; Werner, D.; Törnroos, K. W.; Maichle-Mössmer, C.; Anwander, R. *Molecules* **2019**, *24*, 3703.

[305] Flory, P. J.; Rehner, J. *J. Chem. Phys.* **1943**, *11*, 521–526.

[306] Fernández-Barbero, A.; Fernández-Nieves, A.; Grillo, I.; López-Cabarcos, E. *Phys. Rev. E* **2002**, *66*, 051803.

[307] Crassous, J. J.; Wittemann, A.; Siebenbürger, M.; Schrinner, M.; Drechsler, M.; Ballauff, M. *Coll. Pol. Sci.* **2008**, *286*, 805–812.

[308] Sonström, A.; Schneider, D.; Cäcilia, M.-M.; Anwander, R. *Eur. J. Inorg. Chem.* **2019**, *2019*, 682 – 692.

[309] Hou, Z.; Pan, L. *Patent*, WO 2012153786, **2012**.

[310] Hou, Z.; Pan, L. *Patent*, EP 2708562, **2012**.

[311] Hou, Z.; Pan, L. *Patent*, US 20140088276, **2012**.

[312] Cui, D.; Jian, Z. *Patent*, CN 101906187, **2010**.

[313] Johnson, K. R. D.; Hannon, M. A.; Ritch, J. S.; Hayes, P. G. *Dalton Trans.* **2012**, *41*, 7873–7875.

[314] Yang, X.; Stern, C. L.; Marks, T. J. *J. Am. Chem. Soc.* **1991**, *113*, 3623–3625.

[315] Chien, J. C. W.; Tsai, W. M.; Rausch, M. D. *J. Am. Chem. Soc.* **1991**, *113*, 8570–8571.

[316] Bochmann, M.; Lancaster, S. J. *J. Organomet. Chem.* **1992**, *434*, C1 – C5.

[317] Marks, T. J. *Acc. Chem. Res.* **1992**, *25*, 57–65.

[318] Yang, X.; Stern, C. L.; Marks, T. J. *J. Am. Chem. Soc.* **1994**, *116*, 10015–10031.

[319] Erker, G. *Dalton Trans.* **2005**, *2005*, 1883–1890.

[320] Turner, H. W. *Patent*, EP 0277004 A1, **1988**.

[321] Hlatky, G. G.; Upton, D. J.; Turner, H. W. *Patent*, WO 91/09882, **1991**.

[322] Ewen, J. A.; Elder, M. J. *Patent*, EU 0426637, **1991**.

[323] Ewen, J. A.; Elder, M. J. *Patent*, EU 0427697, **1991**.

[324] Ewen, J. A.; Elder, M. J. *Patent*, US 5561092, **1996**.

[325] Hajela, S.; Schaefer, W. P.; Bercaw, J. E. *J. Organomet. Chem.* **1997**, *532*, 45 – 53.

[326] Bambirra, S.; van Leusen, D.; Meetsma, A.; Hessen, B.; H. Teuben, J. *Chem. Commun.* **2001**, *2001*, 637–638.

[327] Bambirra, S.; van Leusen, D.; Meetsma, A.; Hessen, B.; Teuben, J. H. *Chem. Commun.* **2003**, *2003*, 522–523.

[328] Lawrence, S. C.; Ward, B. D.; Dubberley, S. R.; Kozak, C. M.; Mountford, P. *Chem. Commun.* **2003**, *2003*, 2880–2881.

[329] Arndt, S.; Spaniol, T. P.; Okuda, J. *Angew. Chem. Int. Edit.* **2003**, *42*, 5075–5079.

[330] Krossing, I.; Raabe, I. *Angew. Chem. Int. Edit.* **2004**, *43*, 2066–2090.

[331] Perrin, L.; Bonnet, F.; Visseaux, M.; Maron, L. *Chem. Commun.* **2010**, *46*, 2965–2967.

[332] Perrin, L.; Bonnet, F.; Chenal, T.; Visseaux, M.; Maron, L. *Chem. Eur. J.* **2010**, *16*, 11376–11385.

[333] Wang, X.; Lin, F.; Qu, J.; Hou, Z.; Luo, Y. *Organometallics* **2016**, *35*, 3205–3214.

[334] Döring, C.; Kretschmer, W. P.; Kempe, R. *Eur. J. Inorg. Chem.* **2010**, *2010*, 2853–2860.

[335] Miyake, G. M.; Newton, S. E.; Mariott, W. R.; Chen, E. Y.-X. *Dalton Trans.* **2010**, *39*, 6710–6718.

[336] Liu, D.; Yao, C.; Wang, R.; Wang, M.; Wang, Z.; Wu, C.; Lin, F.; Li, S.; Wan, X.; Cui, D. *Angew. Chem. Int. Edit.* **2015**, *54*, 5205–5209.

[337] Liu, B.; Li, L.; Sun, G.; Liu, J.; Wang, M.; Li, S.; Cui, D. *Macromolecules* **2014**, *47*, 4971–4978.

[338] Du, G.; Long, Y.; Xue, J.; Zhang, S.; Dong, Y.; Li, X. *Macromolecules* **2015**, *48*, 1627–1635.

[339] Du, G.; Xue, J.; Peng, D.; Yu, C.; Wang, H.; Zhou, Y.; Bi, J.; Zhang, S.; Dong, Y.; Li, X. *J. Polym. Sci. Part A1* **2015**, *53*, 2898–2907.

[340] Robert, D.; Abinet, E.; Spaniol, T. P.; Okuda, J. *Chem. Eur. J.* **2009**, *15*, 11937–11947.

[341] Standfuss, S.; Abinet, E.; Spaniol, T. P.; Okuda, J. *Chem. Commun.* **2011**, *47*, 11441–11443.

[342] Arndt, S.; Beckerle, K.; Zeimentz, P. M.; Spaniol, T. P.; Okuda, J. *Angew. Chem. Int. Edit.* **2005**, *44*, 7473–7477.

[343] Bambirra, S.; Bouwkamp, M. W.; Meetsma, A.; Hessen, B. *J. Am. Chem. Soc.* **2004**, *126*, 9182–9183.

[344] Clark, L.; Cushion, M. G.; Dyer, H. E.; Schwarz, A. D.; Duchateau, R.; Mountford, P. *Chem. Commun.* **2010**, *46*, 273–275.

[345] Yin, H.; Zabula, A. V.; Schelter, E. J. *Dalton Trans.* **2016**, *45*, 6313–6323.

[346] Schaverien, C. J. *Organometallics* **1994**, *13*, 69–82.

[347] Coughlin, E. B.; Bercaw, J. E. *J. Am. Chem. Soc.* **1992**, *114*, 7606–7607.

[348] Evans, W. J.; DeCoster, D. M.; Greaves, J. *Organometallics* **1996**, *15*, 3210–3221.

[349] Kirillov, E. N.; Fedorova, E. A.; Trifonov, A. A.; Bochkarev, M. N. *Appl. Organomet. Chem.* **2001**, *15*, 151–156.

[350] Ward, B. D.; Lukešová, L.; Wadepohl, H.; Bellemin-Laponnaz, S.; Gade, L. H. *Eur. J. Inorg. Chem.* **2009**, *2009*, 866–871.

[351] Li, L.; Wu, C.; Liu, D.; Li, S.; Cui, D. *Organometallics* **2013**, *32*, 3203–3209.

[352] Anwander, R.; Klimpel, M. G.; Martin Dietrich, H.; Shorokhov, D. J.; Scherer, W. *Chem. Commun.* **2003**, *2003*, 1008–1009.

[353] Hitzbleck, J.; Okuda, J. *Z. Anorg. Allg. Chem.* **2006**, *632*, 1947–1949.

[354] Hitzbleck, J.; Okuda, J. *Organometallics* **2007**, *26*, 3227.

[355] Kaita, S.; Hou, Z.; Wakatsuki, Y. *Macromolecules* **1999**, *32*, 9078–9079.

[356] Jian, Z.; Cui, D.; Hou, Z. *Chem. Eur. J.* **2012**, *18*, 2674–2684.

[357] Jende, L. N.; Maichle-Mössmer, C.; Anwander, R. *Chem. Eur. J.* **2013**, *19*, 16321–16333.

[358] Jende, L. N.; Maichle-Mössmer, C.; Schädle, C.; Anwander, R. *J. Organomet. Chem.* **2013**, *744*, 74–81.

[359] Zhang, W.-X.; Wang, Z.; Nishiura, M.; Xi, Z.; Hou, Z. *J. Am. Chem. Soc* **2011**, *133*, 5712 – 5715.

[360] Pohlmann, J. L. W.; Brinckmann, F. E. *Z. Naturforsch. B* **1965**, *20b*, 5.

[361] Evans, W. J.; Johnston, M. A.; Greci, M. A.; Gummersheimer, T. S.; Ziller, J. W. *Polyhedron* **2003**, *22*, 119 – 126.

Chapter 5

Unpublished Results

Manuscript I: C–H Activation and Isoprene Polymerization Studies Applying Pentamethylcyclopentadienyl-Supported Rare-Earth Metal Dimethyl Complexes[1]

5.1.1 Introduction

The polymerization properties and active species of cyclopentadienyl rare-earth metal dimethyl trimers $[Cp^*LnMe_2]_3$ (Ln = Y, Lu) have been investigated recently (Paper V). Especially their isoprene polymerization is focused on a vinylic addition of the monomer, while in case of slightly less bulky 1,3-butadiene a much higher *cis*-selectivity was observed. Therefore, their synthesis, based on the earlier findings by our group,[1,2] shall now be applied to further rare-earth metals with larger ionic radii. Applying lanthanides with larger ion sizes is intended to increase the steric space around the potential catalytic centers and thereby simplify the coordination of isoprene in *cis*-conformation. Obtained trimers and precursors are therefore tested in the polymerization of isoprene.

5.1.2 Results and Discussion

The first synthesis approach for $[Cp^*LnMe_2]_3$ (**79**) for lanthanides with ionic radii larger than that of yttrium (1.04 Å for a coordination number of 6[3,4]), starts from the respective homoleptic tetramethylaluminate (**118**) (*cf.* Paper IV).[5–14] A protonolysis protocol is chosen to synthesize the respective pentmethylcyclopentadienyl *bis*-alkylaluminates (**119**)(*cf.* Paper I) from **118**.[1,6,15–21] These *bis*-alkylaluminates are then cleaved by the application of an ether (e.g. diethyl ether)[22] to form the respective dimethyl trimers (**79**) (*cf.* Paper V).[1,2]

In case of lanthanides larger than dysprosium, C–H bond activation occurs directly upon cleavage. This is known to happen with the yttrium analogue as well, when the cleavage reaction is performed above 40 °C (Paper V),[23] only one equivalent of diethyl ether is applied,[2] or in the presence of an aromatic solvent. In these cases, cleavage reactions

[1] By the time of the publication of this thesis, Manuscript I will have been published as main part of ref. 304.

applying another ether (*tert*-butyl methyl ether, TBME) are performed as well, and their products are crystallographically investigated.

5.1.2.1 Pentamethylcyclopentadienyl Lanthanide *Bis*-alkylaluminates

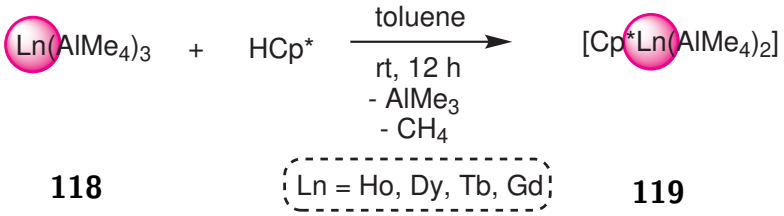

*Scheme 5.1: Protolytic synthesis of [Cp*Ln(AlMe$_4$)$_2$] (**119^{Ln}**) from the homoleptic tetramethylaluminate **118^{Ln}**.*

As known for lanthanum,[1] samarium,[21] yttrium,[17] ytterbium[21] and lutetium,[24] pentamethylcyclopentadienyl *bis*-alkylaluminates (**119^{Ln}**) of holmium, dysprosium, terbium, and gadolinum can be synthesized applying a similar protonolysis protocol as shown in Scheme 5.1. Reacting pentamethylcyclopentadiene with the respective homoleptic tris-tetramethylaluminate (**118**) results in quantitative yields for all four tested rare-earth metals. Crystals suitable for X-ray diffraction could be achieved by simple recrystallization in pure *n*-hexane (Figures 5.1 – 5.4). Their specific bond lengths and angles are given in Table 5.1.

In contrast to the dimethyl trimers (**79^{Ln}**, Table 5.3, *vide infra*), the *bis*-alkylaluminates (**119^{Ln}**, Table 5.1) show clear tendencies to decreasing angles and elongated bonds with increasing ionic radii of the lanthanide center. Due to the monomeric nature of these complexes, the absence of cluster constraints allows the full display of this direct result of the variation of the ionic radius of the lanthanide center. In all cases, one of the two tetramethylaluminate moieties is tucked in, so that a third methyl unit of the tetramethylaluminate is located in relatively close proximity to the lanthanide center. This is more and more favored with larger ionic radii, which results in decreasing bond length towards the respective carbon atom (labeled by C^{far} in Table 5.1) and an increasing torsion angle. The tuck-in shows clearly the influence of the rare-earth metal size on the ligand environment, which is a key to understand the polymerization behavior.

The results obtained in this study fit well to the series of data gained in previous studies for the other rare-earth metals.[1,17,21,24]

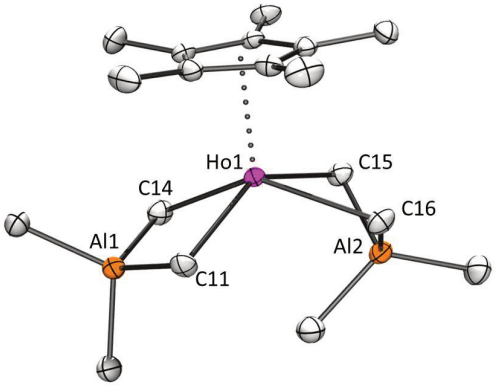

*Figure 5.1: ORTEP view of the molecular structure of [Cp*Ho(AlMe$_4$)$_2$] (**119^{Ho}**). Atomic displacement parameters are set at the 50 % probability level. Hydrogen atoms are omitted for clarity. See Table 5.1 for significant bond lengths and angles.*

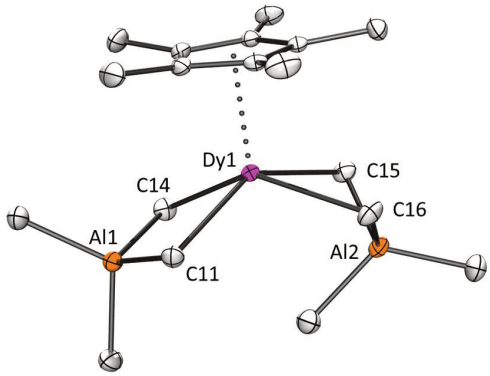

*Figure 5.2: ORTEP view of the molecular structure of [Cp*Dy(AlMe$_4$)$_2$] (**119^{Dy}**). Atomic displacement parameters are set at the 50 % probability level. Hydrogen atoms are omitted for clarity. See Table 5.1 for significant bond lengths and angles.*

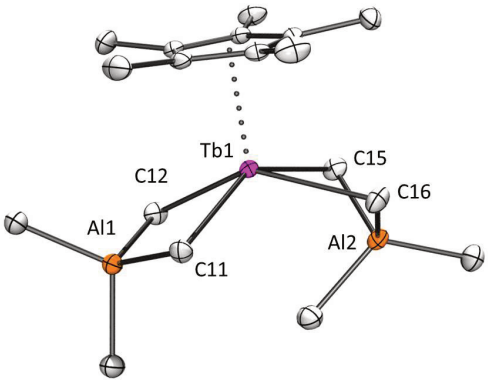

*Figure 5.3: ORTEP view of the molecular structure of [Cp*Tb(AlMe$_4$)$_2$] (**119^{Tb}**). Atomic displacement parameters are set at the 50 % probability level. Hydrogen atoms are omitted for clarity. See Table 5.1 for significant bond lengths and angles.*

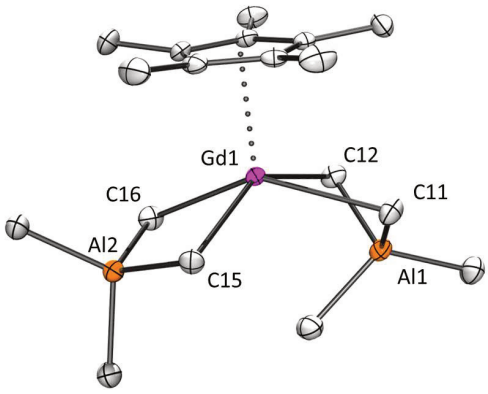

*Figure 5.4: ORTEP view of the molecular structure of [Cp*Gd(AlMe$_4$)$_2$] (**119^{Gd}**). Atomic displacement parameters are set at the 50 % probability level. Hydrogen atoms are omitted for clarity. See Table 5.1 for significant bond lengths and angles.*

*Table 5.1: Comparison of the Crystal structures of the Cp^* rare earth metal bisaluminate species **119**.*

Ln	⌀(Ln–C^{Al})[a] [Å]	Ln–Ct [Å]	⌀(∠ Ct–Ln–C^{Al})[a] [Å]	Ln–C^{far} [a] [°]	⌀(∠ C^{Al1}–Ln–C^{Al1}) [°]	⌀(∠ C^{Al1}–Ln–C^{Al2}) [°]	T: C^{Al1}–Ln–C^{Al1}–Al1)[a]	T: C^{Al2}–Ln–C^{Al2}–Al2)[a]
La[b]	2.749(4)	2.503	106.9	3.140	75.74(10)	94.38(11)	2.2	32.5
Sm[c]	2.6680(19)	2.404	106.9	3.1128(19)	78.19(6)	91.41(6)	3.5	31.3
Gd	2.637(2)	2.376	107.4	3.163	79.59(7)	90.05(7)	4.1	30.7
Tb	2.625(2)	2.362	107.4	3.169	80.15(7)	89.27(7)	4.4	30.6
Dy	2.6079(17)	2.344	107.7	3.186	80.46(5)	88.78(6)	4.7	30.2
Ho	2.602(4)	2.334	108.1	3.248	80.80(12)	87.96(12)	5.1	29.9
Y[d]	2.601(3)	2.340	108.6	3.304	80.49(10)	87.66(10)	5.4	29.4
Yb[c]	2.5632(16)	2.293	109.1	3.3541(18)	81.92(5)	85.63(5)	6.1	28.9
Lu[e]	2.545(3)	2.286	109.6	3.447	82.19(11)	84.73(10)	6.4	28.3

[a] C^{Al} = Carbon of a bridging methyl unit of an alkylaluminate moiety. C^{far} = Tilt in methyl carbon of the tilt alkylaluminate moiety. T = Torsion
[b] Taken From ref. 1.
[c] Taken From ref. 21.
[d] Taken From ref. 17.
[e] Taken From ref. 24.

*Table 5.2: Isoprene homopolymerization by [Cp*Ln(AlMe$_4$)$_2$] (**119^{Ln}**)*

Entry[a]	Precatalyst	Cocat.[b]	T[c] [°C]	t[c] [h]	Yield[d] [%]	*cis*[e] [%]	*trans*[e] [%]	3,4[e] [%]	$M_{n,SEC}$[f] [10^4g·mol^{-1}]	PDI[f]	T_g[g] [°C]
1[i]	[Cp*La(AlMe$_4$)$_2$] (**119^{La}**)	**A**	40	24	> 99	4	87	9	7	1.28	n.d.
2[i]	[Cp*La(AlMe$_4$)$_2$] (**119^{La}**)	**B**	40	24	> 99	3	80	17	6	1.22	n.d.
3[i]	[Cp*La(AlMe$_4$)$_2$] (**119^{La}**)	**C**	40	24	> 99	0	99.5	0.5	24	1.18	n.d.
4[i]	[Cp*Nd(AlMe$_4$)$_2$] (**119Nd**)	**A**	40	24	> 99	14	70	16	3	2.87	n.d.
5[i]	[Cp*Nd(AlMe$_4$)$_2$] (**119Nd**)	**B**	40	24	> 99	7	80	13	4	1.16	n.d.
6[i]	[Cp*Nd(AlMe$_4$)$_2$] (**119Nd**)	**C**	40	24	> 99	4	92	4	13	1.35	n.d.
7	[Cp*Gd(AlMe$_4$)$_2$] (**119^{Gd}**)	**A**	25	1	93	16	68	16	10.6	1.33	-57
8	[Cp*Gd(AlMe$_4$)$_2$] (**119^{Gd}**)	**B**	25	1	87	22	45	33	4.3	1.19	-43
9	[Cp*Gd(AlMe$_4$)$_2$] (**119^{Gd}**)	**C**	25	1	traces[h]	_[h]	_[h]	_[h]	_[h]	_[h]	_[h]
10	[Cp*Gd(AlMe$_4$)$_2$] (**119^{Gd}**)	**C**	25	24	94	6	87	7	19.4	1.30	-64
11	[Cp*Dy(AlMe$_4$)$_2$] (**119^{Dy}**)	**A**	25	1	94	20	43	37	12.7	1.31	-52
12	[Cp*Dy(AlMe$_4$)$_2$] (**119^{Dy}**)	**B**	25	1	83	14	63	23	5.0	1.28	-43
13	[Cp*Dy(AlMe$_4$)$_2$] (**119^{Dy}**)	**C**	25	1	11	39	52	9	3.7	1.54	-65
14	[Cp*Ho(AlMe$_4$)$_2$] (**119^{Ho}**)	**A**	25	1	54	23	50	27	11.0	1.50	-38
15	[Cp*Ho(AlMe$_4$)$_2$] (**119^{Ho}**)	**B**	25	1	81	29	24	47	4.1	1.48	-23
16	[Cp*Ho(AlMe$_4$)$_2$] (**119^{Ho}**)	**C**	25	1	traces[h]	_[h]	_[h]	_[h]	_[h]	_[h]	_[h]
8	[Cp*Ho(AlMe$_4$)$_2$] (**119^{Ho}**)	**C**	25	24	85	9	79	12	6.6	1.62	-62
17[i]	[Cp*Y(AlMe$_4$)$_2$] (**119^{Y}**)	**A**	40	24	> 99	61	21	19	2	8.95	n.d.
18[i]	[Cp*Y(AlMe$_4$)$_2$] (**119^{Y}**)	**B**	40	24	> 99	44	29	28	6	1.59	n.d.
19[i]	[Cp*Y(AlMe$_4$)$_2$] (**119^{Y}**)	**C**	40	24	> 99	2	94	4	9	1.59	n.d.
20[j]	[Cp*Lu(AlMe$_4$)$_2$] (**119^{Lu}**)	**A**	40	0.25	> 99	74	20	6	10	1.49	n.d.
21[j]	[Cp*Lu(AlMe$_4$)$_2$] (**119^{Lu}**)	**B**	40	0.25	> 99	70	20	10	9.5	1.48	n.d.
22[j]	[Cp*Lu(AlMe$_4$)$_2$] (**119^{Lu}**)	**C**	40	0.25	> 99	74	21	5	11.0	1.39	n.d.

[a] Conditions: 20 µmol of precatalyst, 20 µmol of cocatalyst, 20 mmol of isoprene, 8 mL of toluene.
[b] **A** = [Ph$_3$C][B(C$_6$F$_5$)$_4$], **B** = [PhNHMe$_2$][B(C$_6$F$_5$)$_4$], **C** = B(C$_6$F$_5$)$_3$.
[c] T = polymerization temperature, t = reaction time.
[d] Yield of the isolated polymer.
[e] Determined by ^{1}H and ^{13}C NMR spectroscopy.
[f] Determined by GPC in THF at 35 °C.
[g] Determined on a Perkin Elmer DSC 8000; Heat rate: 20 K/min, Cooling rate: 60 K/min.
[h] Evaluation impossible due to low yield.
[i] Taken from ref. 16.
[j] Taken from Paper V.

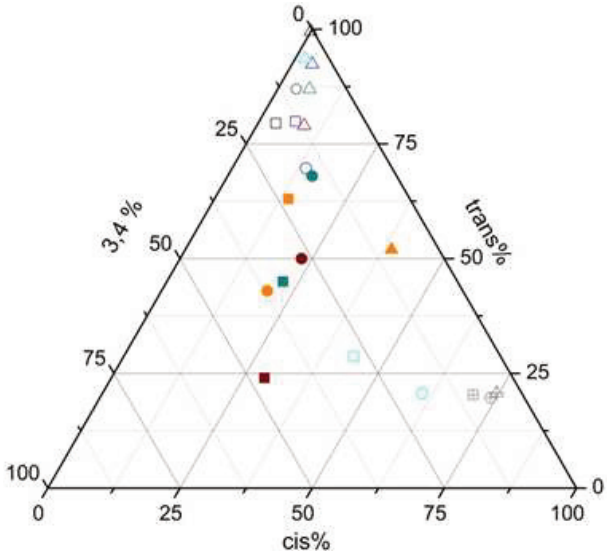

*Chart 5.4: Ternary plot of the microstructures of the polyisoprenes obtained from of [Cp*Ln(AlMe$_4$)$_2$] (**119^{Ln}**). Polymers produced applying cocatalyst **A** are represented by circles, those produced with cocatalyst **B** by squares and products of activations with cocatalyst **C** are represented by triangles. Solid symbols mark reaction times of 1 h, hollow symbols mark reaction times of 24 h and hollow and crossed symbols mark reaction times of 15 min. The metal centers of the precatalyst is color-coded as follows: black (La), blue (Nd), teal (Gd), orange (Dy), brown (Ho), cyan (Y), and grey (Lu). Data of the La, Nd, and Y analogues are shown for comparison and taken from ref. 16.*

The pentamethylcyclopentadienyl rare-earth metal *bis*-tetramethylaluminates (**119**) have been tested in the polymerization of isoprene (Table 5.2, Chart 5.4). Roughly, for polymerizations cocatalyzed by **A** and **B** a decrease of *trans*-selectivity with decreasing ion size is observed. As already shown in Zimmermanns study[16] and Paper I,[20] while for the smaller lanthanides (Ln < Ho) with cocatalyst **A** and **B** relatively unselective microstructures with a slight tendency to 1,4-*cis* focused monomer addition are realized, a trend towards 1,4-*trans*-selectivity occurs with increasing ionic radii of the lanthanide. Besides the steric situation around the lanthanide center, a second possible influence has to be discussed in this context: In the process of activation by cationization, $AlMe_3$ is likely to be set free with these precatalysts. Trimethylaluminum is known to cause slight *trans*-shifts of microstructures, when added to catalytically active mixtures in diene polymerization (see Papers II and V for examples).[25] Although it has not been

reported so far to the best of our knowledge, this property of $AlMe_3$ is dependent on the accessible steric space. So a second indirect *trans*-shifting influence of the ionic radii is also possible, due to the presumed activation side product ($AlMe_3$).
As exceptions, polymers produced by the dysprosium and yttrium systems have to be further mentioned. Next to the microstructures not being fully in line with the observed general trend, the low molecular weight average observed, when cocatalyst **B** is applied to $\mathbf{119^{Dy}}$ stands out slightly and implies a high initiation efficiency. As yttrium and holmium are almost identical in ion size, much more similar polymers would be expected for these two metal centers. The difference implies the possibility of a change in selectivity over the reaction time as the yttrium system was reacted over 24 h, while the holmium centered polymerizations were quenched after 1 h in order to obtain an impression of the polymerization rate. Verification of this theory by polymerization applying the yttrium system with a reaction time of 1 h is a subject to future research.
It is also surprising, that the small lutetium polymerizes much faster than the other systems, producing quantitative yields even after 15 min. As the obtained polymers are relatively similar for the smallest lanthanide in contrast to all other systems, a different active species has to be considered. Chart 5.4 also shows a high agglomeration of hollow symbols, marking the polymerizations run for 24 h in the high-*trans* area of the chart. This is most significant, for polymers produced applying cocatalyst $[B(C_6F_5)_3]$ (**C**, shown as triangles in Chart 5.4). The throughout high *trans*-contents applying cocatalyst **C** can be reasoned, regarding earlier reactions of the cocatalyst with alkylaluminates resulted in perfluoroaryl alkylaluminate anionic species,[15] which then provided an active species that differed from that obtained by the application of cocatalysts **A** and **B**. Such an alternation of the active species, taking place over a longer period during polymerization catalysis explains, why the microstructure produced by $\mathbf{119^{Dy}}$ / **C** after 1 h (Table 5.2, run 13) has a much lower *trans*-content, than the polymerizations by the other systems, that reacted for 24 h. Once again, verification by polymerization applying $\mathbf{119^{Dy}}$ for 24 h is a subject to research. The results for Ln = Lu (Table 5.2, run 22), obtained with the much faster polymerization observed in general for $\mathbf{119^{Lu}}$, would not interfere with the presence of this alternation reaction.

5.1.2.2 Ether Cleavage Reactions

5.1.2.2.1 Holmium and Dysprosium

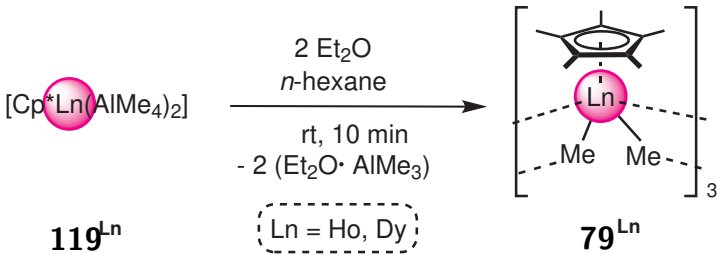

*Scheme 5.2: Synthesis of [Cp*LnMe$_2$]$_3$ (**79^{Ln}**) from the bis-alkylaluminate (**119^{Ln}**) by cleavage reaction with diethyl ether.*[22]

Following the tetramethylaluminate cleavage protocol[22] that has been applied successfully in case of yttrium and lutetium, trimeric [Cp*LnMe$_2$]$_3$ is obtained for holmium and dysprosium as well (Scheme 5.2). While the cleavage with diethyl ether is quantitative with Ln = Ho, a yield of only 19 % could be achieved for Ln = Dy at ambient temperature. In this step, for Dy, the reaction mixture turned into a much deeper yellow color, than the pale yellow typical for dysprosium salts. Empirically this color change has shown to be an indication for ongoing C–H-activation in these cleavage reactions. Here, as explained in Paper V and by Jende[23] multiple products are formed, which can explain why none of the degradation products could be isolated in the case of dysprosium.
Crystals of **79^{Ho}** and **79^{Dy}** suitable for X-ray diffraction could be obtained from simple recrystallization in pure *n*-hexane (Figures 5.5 and 5.6). The specific bond lengths and angles are given in Table 5.3.

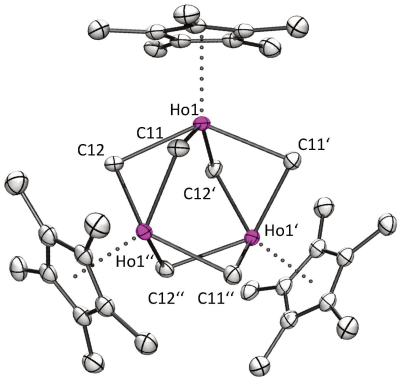

*Figure 5.5: ORTEP view of the molecular structure of [Cp*HoMe$_2$]$_3$ (**79^{Ho}**). Atomic displacement parameters are set at the 50 % probability level. Hydrogen atoms are omitted for clarity. See Table 5.3 for significant bond lengths and angles.*

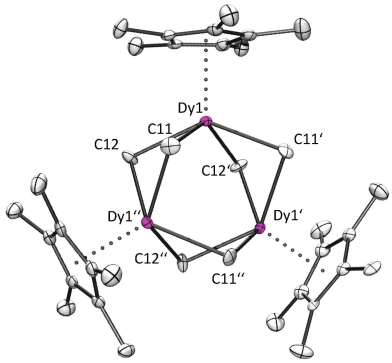

*Figure 5.6: ORTEP view of the molecular structure of [Cp*DyMe$_2$]$_3$ (**79^{Dy}**). Atomic displacement parameters are set at the 50 % probability level. Hydrogen atoms are omitted for clarity. See Table 5.3 for significant bond lengths and angles.*

*Table 5.3: Comparison of the crystal structures of the Cp* rare-earth metal dimethyl trimeric species **79^{Ln}**.*

Ln	Ln–C11 [Å]	Ln–C12 [Å]	Ln–Ct [Å]	⌀(∠ Ct–Ln–C^{Al}) [°]	∠ C11–Ln–C12 [°]	∠ C11–Ln–C11" [°]
Tb	2.54(2)	2.565(19)	2.389	114.0	79.8(3)	82.7(10)
Dy	2.63(3)	2.49(3)	2.360	111.6	80.3(4)	85.1(9)
Ho	2.581(18)	2.58(2)	2.399	112.7	80.7(3)	77.5(7)
Y[a]	2.539	—[a]	2.359	112.9	80.0	82.8
Lu[b]	2.45(2)	2.53(3)	2.317	111.9	80.4(3)	87.8(11)

[a] Taken From ref. 2, centrosymmetric space group.
[b] Taken from Paper V.

*Table 5.4: 1,3-Butadiene homopolymerization by [Cp*LnMe$_2$]$_3$ (**79^{Ln}**)*

Entry[a]	Precatalyst	Cocat.[b]	T[c] [°C]	t[c] [h]	Yield[d] [%]	*cis*[e] [%]	*trans*[e] [%]	3,4[e] [%]	$M_{n,SEC}$[f] [10^4g·mol^{-1}]	PDI[f]	T_g[g] [°C]
23	[Cp*DyMe$_2$]$_3$ (**79^{Dy}**)	**A**	25	60	99	97	0	3	16.2	1.63	-102
24	[Cp*DyMe$_2$]$_3$ (**79^{Dy}**)	**B**	25	60	92	96	0	4	20.4	1.64	-102
25	[Cp*HoMe$_2$]$_3$ (**79^{Ho}**)	**A**	25	60	90	91	4	5	5.5	1.52	-102
26	[Cp*HoMe$_2$]$_3$ (**79^{Ho}**)	**B**	25	60	59	94	2	4	32.8	1.35	-101
27[j]	[Cp*YMe$_2$]$_3$ (**79^{Y}**)	**A**	25	60	21	91	4	5	76	1.58	-97
28[j]	[Cp*YMe$_2$]$_3$ (**79^{Y}**)	**B**	25	60	48	95	2	3	50	1.20	-94
29[j]	[Cp*LuMe$_2$]$_3$ (**79^{Lu}**)	**A**	25	60	>99	85	8	7	40	1.84	-94
30[j]	[Cp*LuMe$_2$]$_3$ (**79^{Lu}**)	**B**	25	60	95	85	8	7	33	1.77	-93

[a] Conditions: 20 µmol of precatalyst, 20 µmol of cocatalyst, 20 mmol of isoprene, 8 mL of toluene.
[b] **A** = [Ph$_3$C][B(C$_6$F$_5$)$_4$], **B** = [PhNHMe$_2$][B(C$_6$F$_5$)$_4$].
[c] T = polymerization temperature, t = reaction time.
[d] Yield of the isolated polymer.
[e] Determined by ^{1}H and ^{13}C NMR spectroscopy.
[f] Determined by GPC in THF at 35 °C.
[g] Determined on a Perkin Elmer DSC 8000; Heat rate: 20 K/min, Cooling rate: 60 K/min.
[h] Evaluation impossible due to low yield.
[j] Taken from Paper V.

Interestingly, the comparison of selected bond lengths and angles of the dimethyl trimers **79^{Ln}** in Table 5.3 does not show a clear dependency on the ionic radius of the respective lanthanide center. It is assumed, that the geometry of the trimeric clusters does simply not provide the freedom for ideal ligand arrangement. This causes the lowering of stability of the trimers, empirically observed with increasing ionic radius, which then results in a higher tendency to undergo side reactions, e.g. C–H-activation reactions or ligand redistribution.

Both the holmium and the dysprosium dimethyl trimer have been tested in the polymerization of 1,3-dienes. Due to the similarity of holmium and yttrium in ion size, the reactivity and polymeric results with 1,3-butadiene in case of the dimethyls differ only slightly (Table 5.4, runs 25 – 28, Chart 5.5a, also *cf.* to Paper V) regarding the microstructure. The isoprene polymerization results of **79^{Ho}** with cocatalyst **B** ([PhNHMe$_2$][B(C$_6$F$_5$)$_4$]) show a silimar analogy (Table 5.5, runs 34 and 36). Only when cocatalyst **A** ([Ph$_3$C][B(C$_6$F$_5$)$_4$]) is applied, the microstructure differs. An active species, behaving much more similar to that produced by **B**, is formed in case of Ln = Ho. In contrast to **79^{Y}** / **A** (Table 5.5, Chart 5.5b and *cf.* to Paper V), this leads reproducibly to only little variance between the **A** and **B** runs (Table 5.5, runs 33 and 34). Regarding the chain properties, once again the polymers produced by activation with **79^{Ho}** and cocatalyst **A**, differ from the yttrium results. Hence, in contrast to the

*Table 5.5: Isoprene homopolymerization by [Cp*LnMe$_2$]$_3$ (**79^{Ln}**)*

Entry[a]	Precatalyst	Cocat.[b]	T[c] [°C]	t[c] [h]	Yield[d] [%]	*cis*[e] [%]	*trans*[e] [%]	3,4[e] [%]	$M_{n,SEC}$[f] [10^4g·mol^{-1}]	PDI[f]	T_g[g] [°C]
31	[Cp*DyMe$_2$]$_3$ (**79^{Dy}**)	**A**	25	60	90	53	13	34	6.3	3.15	-36
32	[Cp*DyMe$_2$]$_3$ (**79^{Dy}**)	**B**	25	60	89	33	25	43	14.6	1.38	-24
33	[Cp*HoMe$_2$]$_3$ (**79^{Ho}**)	**A**	25	60	96	36	18	46	15.5	1.27	-20
34	[Cp*HoMe$_2$]$_3$ (**79^{Ho}**)	**B**	25	60	87	33	16	51	12.0	1.13	-20
35[j]	[Cp*YMe$_2$]$_3$ (**79^{Y}**)	**A**	25	60	> 99	51	17	32	8.4	2.33	-47
36[j]	[Cp*YMe$_2$]$_3$ (**79^{Y}**)	**B**	25	60	90	36	11	53	14.1	1.16	-27
37[j]	[Cp*LuMe$_2$]$_3$ (**79^{Lu}**)	**A**	25	60	> 99	21	21	58	26.8	2.00	-16
38[j]	[Cp*LuMe$_2$]$_3$ (**79^{Lu}**)	**B**	25	60	> 99	21	22	57	29.2	1.38	-17

[a] Conditions: 20 µmol of precatalyst, 20 µmol of cocatalyst, 20 mmol of isoprene, 8 mL of toluene.
[b] **A** = [Ph$_3$C][B(C$_6$F$_5$)$_4$], **B** = [PhNHMe$_2$][B(C$_6$F$_5$)$_4$].
[c] T = polymerization temperature, t = reaction time.
[d] Yield of the isolated polymer.
[e] Determined by ^{1}H and ^{13}C NMR spectroscopy.
[f] Determined by GPC in THF at 35 °C.
[g] Determined on a Perkin Elmer DSC 8000; Heat rate: 20 K/min, Cooling rate: 60 K/min.
[h] Evaluation impossible due to low yield.
[j] Taken from Paper V.

catalysis performed by **79^{Y}** (Paper V), with **79^{Ho}**, no indication of a second, underlying crosslinking reactivity is found. With both monomers, yields, PDI and molecular weight averages imply a much more uniform and simultaneous activation for holmium. However, in case of holmium it has to be pointed out, that except for the polybutadiene obtained from the system **79^{Ho}** / **A** all observed molecular weight averages are high enough to imply ratios of chains per catalytic center far smaller than 1. Therefore the active species are supposed to consist of more than one holmium center, as observed for yttrium (Paper V).

1,3-Butadiene polymerization applying **79^{Dy}** (Table 5.4, runs 23 and 24) leads to very *cis*-selective microstructures as observed for the holmium and yttrium as well. Here, high yields were obtained, that were not achieved in the case of yttrium and only for cocatalyst **A** with holmium. Next to these, differences to the smaller metals occur regarding the chain properties. For dysprosium with both cocatalysts **A** and **B** molecular weights are observed that imply ratios of chains per lanthanide center much smaller than 1. This means that in case of dysprosium far less than every metal center grows a polymer chain independent of the selected cocatalyst. Therefore, an interpretation as indication for active species with more than one lanthanide atom is possible. The PDI seem, although increased, compared to the smaller lanthanides yet too low to ascribe the increased molecular weight averages to only an initiation deficiency.

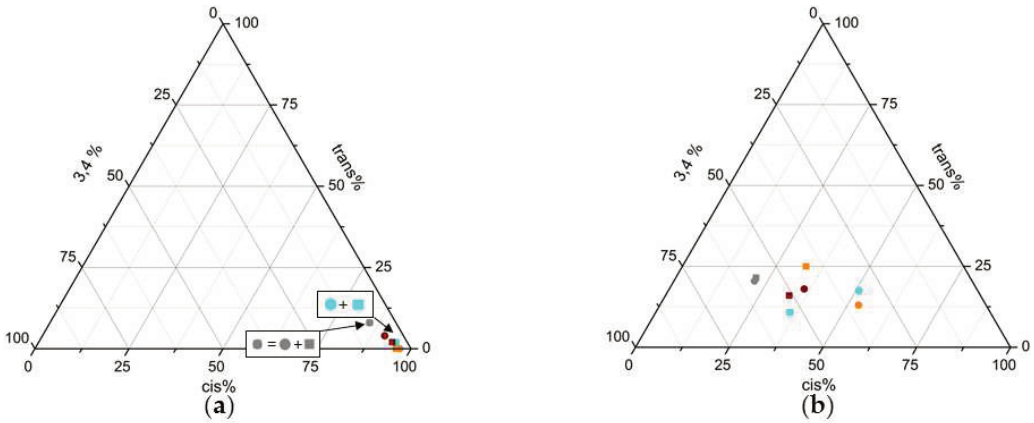

*Chart 5.5: Ternary plot of the microstructures of the poly-1,3-butadienes (a) and polyisoprenes (b) obtained from of $[Cp^*LnMe_2]_3$ (**79^{Ln}**). Polymers produced applying cocatalyst **A** are represented by circles, those produced with cocatalyst **B** by squares. The metal centers of the precatalyst is color-coded as follows: orange (Dy), brown (Ho), cyan (Y), and grey (Lu). Data for the reactions applying the Y and Lu analogue precatalysts is taken from Paper V.*

In case of the isoprene polymerization (Table 5.5, runs 31 and 32), the uniformity of the microstructure, as observed for holmium, is not found in case of dysprosium. While cocatalyst **B** produces a polymer in good analogy to those obtained from holmium, in case of cocatalyst **A** a much higher *cis*-content is obtained. Its comparably small molecular weight average of the polymer with **A** is in the vague region of 1 chain per Dy center and a significantly increased PDI put it in a much closer relation to the polymer produced by the system **79^{Y}** / **A** (Table 5.5, run 35 and Paper V). Furthermore, THF insoluble parts of the polymer are observed, which is in agreement with the yttrium result as well. There, an underlying second mechanism is most likely to cause crosslinking of the polymer chains.

5.1.2.2.2 Terbium

In case of terbium (Scheme 5.3), the cleavage reaction applying diethyl ether produced a brown slurry, that showed to be a mixture of several (in solution) non-isolable C–H-activation products. Only one of those, a pyramidal shaped cluster could be crystallized (**121^{Tb}**, *vide infra*). Applying *tert*-butyl methyl ether (TBME), an ether that does not possess reactive hydrogens which excludes one possible C–H-activation

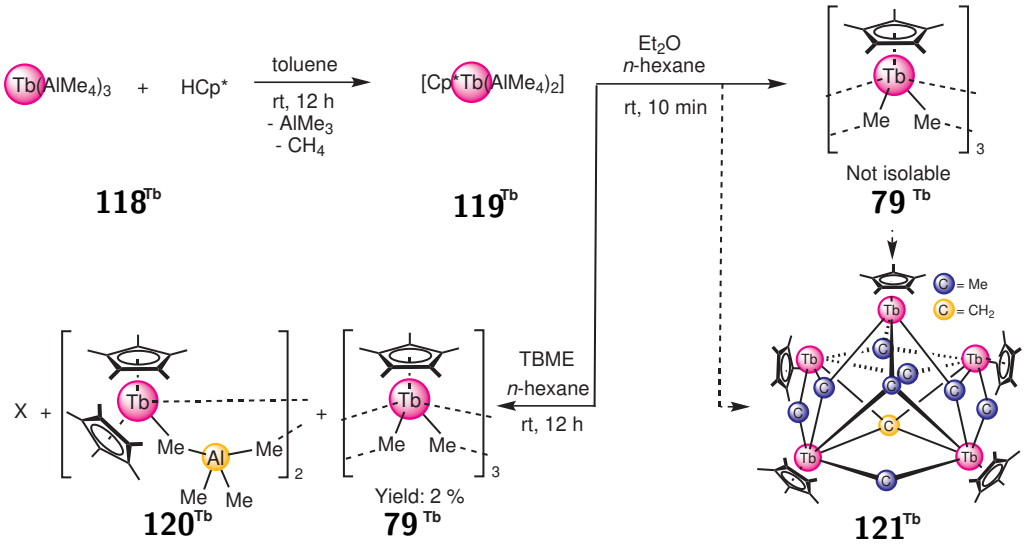

*Scheme 5.3: Protolytic synthesis of [Cp*Tb(AlMe$_4$)$_2$] (**119^{Tb}**) from the homoleptic tetramethylaluminate **118^{Tb}** and cleavage reaction with diethyl ether. The pyramidal complex **121^{Tb}** is obtained. Upon the activation attempt using tert-butyl methyl ether, a metallocene alkylaluminate (**120^{Tb}**) is obtained by ligand redistribution and [Cp*TbMe$_2$]$_3$ (**79^{Tb}**)is fount to be a side product in this reaction.*

pathway, surprisingly leads to the metallocene alkylaluminate **120^{Tb}**[28] crystallizing from the reaction solution as a main product (Figure 5.7). The ligand redistribution leading to a metallocene implies the existance of a second product formed from **119^{Tb}** or *in situ* formed **79^{Tb}**, that has served as a source for the second Cp* ligand, as the stoichiometry of terbium and the Cp* ligand deviates from the original 1 : 1. So far, this second product has not been identified and remains a subject to research. Instead, the originally intended dimethyl trimer **79^{Tb}** was found to be a byproduct of this reaction with a low yield (2 % crystallized yield, see Figure 5.8). Crystals of **79^{Tb}** suitable for X-ray diffractometry could be obtained from recrystallization in pure *n*-hexane (Figure 5.8). Specific bond lengths and angles can be found in Tables 5.3.

In case of the originally performed cleavage reaction with diethyl ether, another product could be identified in yields smaller than 5 %. It is assumed to be one of many formed C–H-activation products. But as it was possible to investigate this species crystallographically (and further structures of this motif of Gd as well, *vide infra*),

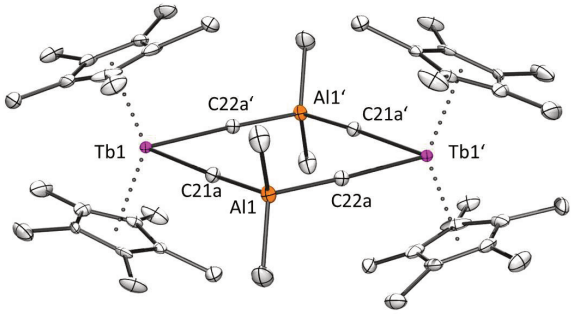

Figure 5.7: ORTEP view of the molecular structure of [Cp$_2$Tb(AlMe$_4$)]$_2$ (**120^{Tb}**). Atomic displacement parameters are set at the 50 % probability level. Hydrogen atoms and one molecule of n-hexane per asymmetric unit are omitted for clarity. See Table 5.6 for significant bond lengths and angles.*

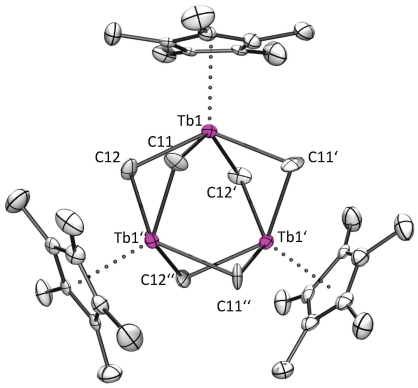

*Figure 5.8: ORTEP view of the molecular structure of [Cp*TbMe$_2$]$_3$ (**79^{Tb}**). Atomic displacement parameters are set at the 50 % probability level. Hydrogen atoms are omitted for clarity. See Table 5.3 for significant bond lengths and angles.*

further details on it shall be provided here.

The observed product (**121^{Tb}**) of several C–H-activation processes in the reaction mixture (Figure 5.9) contains five Cp*Tb fragments, that are positioned in a square pyramidal motif. In the center of the basic face of the pyramid, a CH_2^{2-} anion is located (Figure 5.10). The other eight remaining negative charges are found in eight methyl moieties that both bond bridgingly the four vertex terbium atoms of the pyramid base and overcap its triangular faces. This structure differs significantly from the C–H-activation product found earlier for Ln = Y by Zimmermann[29] by the existence of the central methylene dianion. It is proven not to be present in this position in the yttrium case. Besides that, the terbium and yttrium pyramid differ by the shape of the tetragonal face of the pyramid as well. In case of yttrium, it does not show rectangular vertices and forms a much more lozenge-like tetragon. Furthermore, for yttrium, no hydrogens were crystallographicaly found in the structure at all, which allows the speculation of a composition of $[(Cp^*Y)_5(Me)_6(CH_2)_2]$ to compensate the missing anionic charges.

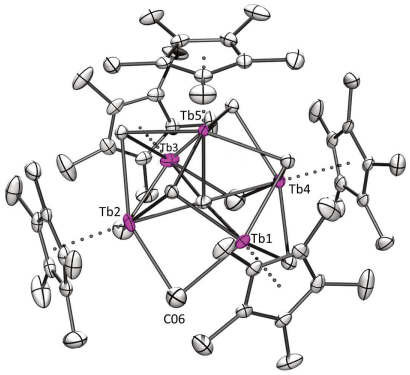

*Figure 5.9: ORTEP view of the molecular structure of $[(Cp^*Tb)_5(CH_2)(Me)_8]$ (**121^{Tb}**). Atomic displacement parameters are set at the 50 % probability level. Hydrogen atoms and one molecule of n-hexane per asymmetric unit are omitted for clarity.*

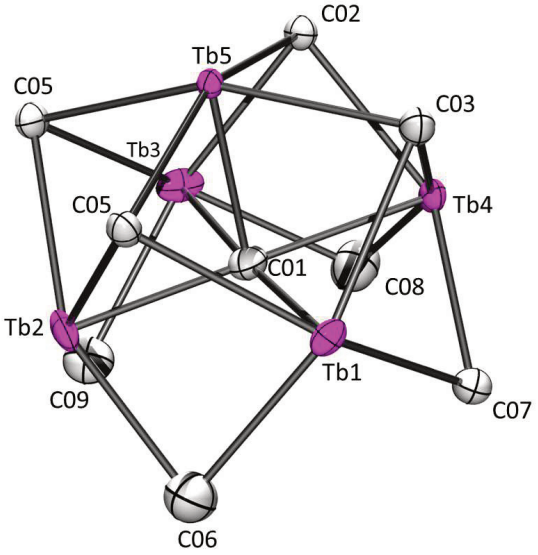

*Figure 5.10: Detailed view of the bonding situation in the structure of $[(Cp^*Tb)_5(CH_2)(Me)_8]$ (**121^{Tb}**). Atomic displacement parameters are set at the 50 % probability level. Hydrogen atoms, Cp^* ligands and one molecule of n-hexane per asymmetric unit are omitted for clarity.*

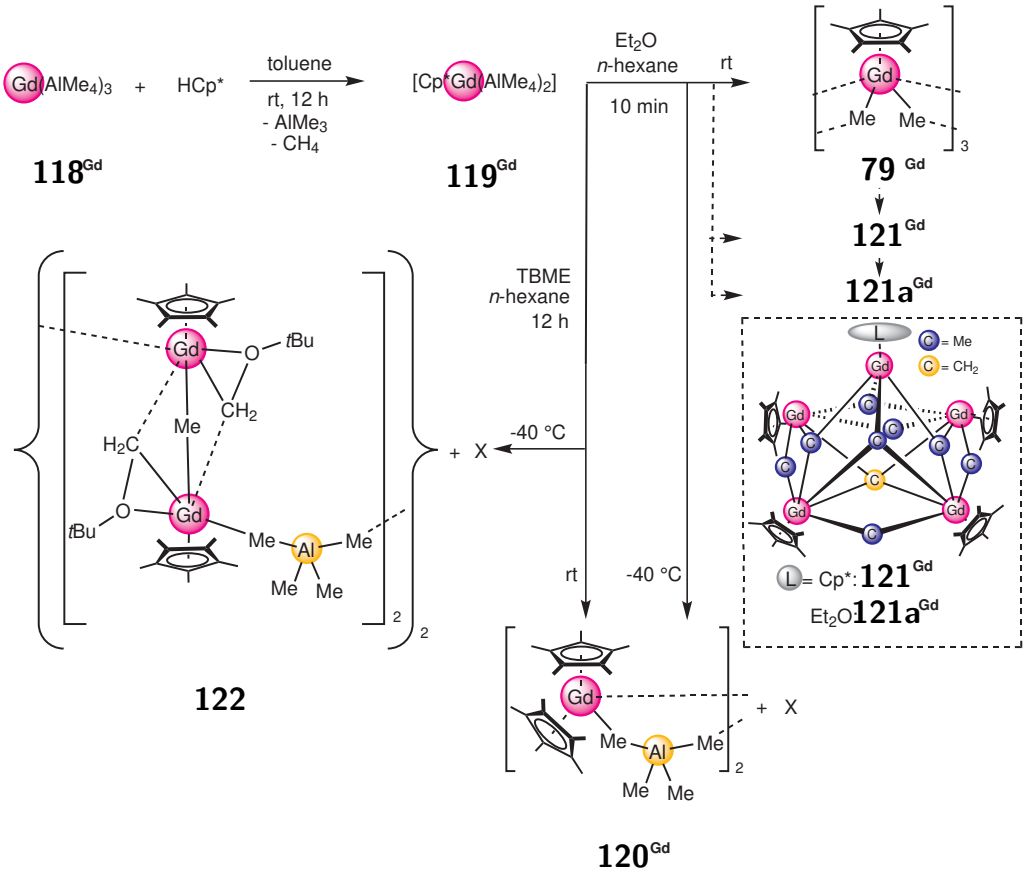

*Scheme 5.4: Protolytic synthesis of [Cp*Gd(AlMe$_4$)$_2$] (**119^{Gd}**) from the homoleptic tetramethylaluminate **118^{Gd}** and attempted cleavage reaction with diethyl ether toward [Cp*GdMe$_2$]$_3$ (**79^{Gd}**), which could not be isolated. As main product in this reaction the pyramidal complex **121^{Gd}** is obtained, together with a product of ligand exchange (**121a^{Gd}**). It is assumed, that (**79^{Gd}**) is an intermediate in this formation. Upon the activation attempt using tert-butyl methyl ether (TBME), a metallocene alkylaluminate (**120^{Gd}**) is obtained by ligand redistribution. This product is also obtained, when the activation with diethyl ether is performed at -40 °C. When the activation by TBME is performed at these conditions, an octameric macrocycle (**122**) was observed as product.*

5.1.2.2.3 Gadolinum

Concluding from the results obtained from the synthesis approaches with terbium precursors, gadolinium with its even larger ionic radius should even more favor C–H-

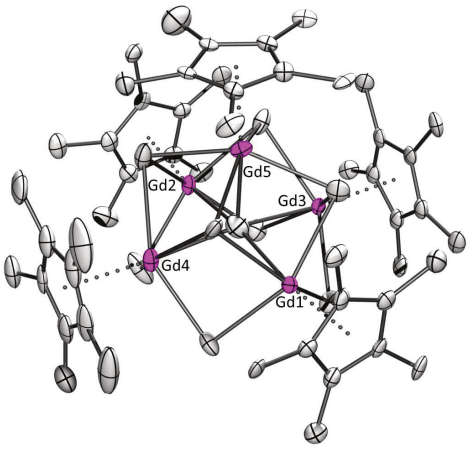

*Figure 5.11: ORTEP view of the molecular structure of [(Cp*Gd)$_5$(CH$_2$)(Me)$_8$] (**121^{Gd}**). Atomic displacement parameters are set at the 50 % probability level. Hydrogen atoms are omitted for clarity.*

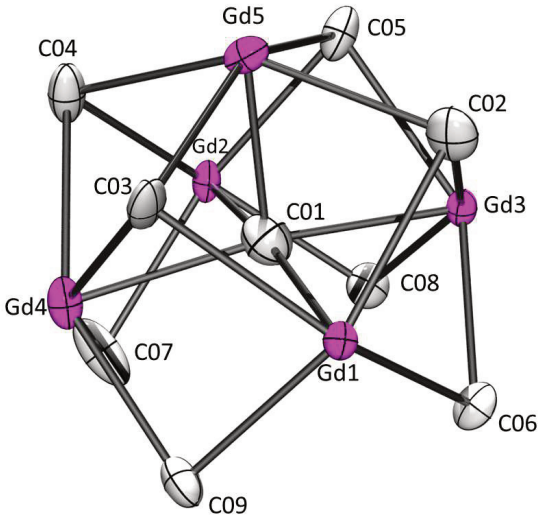

*Figure 5.12: Detailed view of the bonding situation in the structure of [(Cp*Gd)$_5$(CH$_2$)(Me)$_8$] (**121^{Gd}**). Atomic displacement parameters are set at the 50 % probability level. Hydrogen atoms are omitted for clarity.*

activation reactions. Therefore, similar but not identical behavior as in case of terbium was found (Scheme 5.4). Here, no dimethyl trimeric complex was obtained, for both ethers (diethyl ether and TBME) tested in the attempt to cleave the alkylaluminate. Instead, once more products of C–H-activation reactions and ligand redistributions are found.

As in case of terbium, with gadolinium pyramidal structures (**121^{Gd}**, **121a^{Gd}**) are isolated as products of the cleavage attempt applying diethyl ether. Here, two different species of this type crystallize next to each other. The apparently by far dominating amount of crystals reveals to be the analogous pyramidal C–H-activation product (Figures 5.11 and 5.12) as found for terbium (Figure 5.9). Interestingly in the second pyramidal structure, one Cp* ligand is replaced by a diethyl ether donor ligand (**121a^{Gd}**, Figures 5.13 and 5.14). Here, the ion in the center of the tetragonal face of

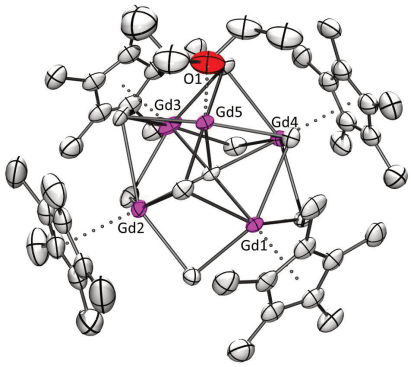

*Figure 5.13: ORTEP view of the molecular structure of [(Cp*Gd)$_4$((Et$_2$O)Gd)(CH)(Me)$_8$] (**121a^{Gd}**). Atomic displacement parameters are set at the 50 % probability level. Hydrogen atoms are omitted for clarity.*

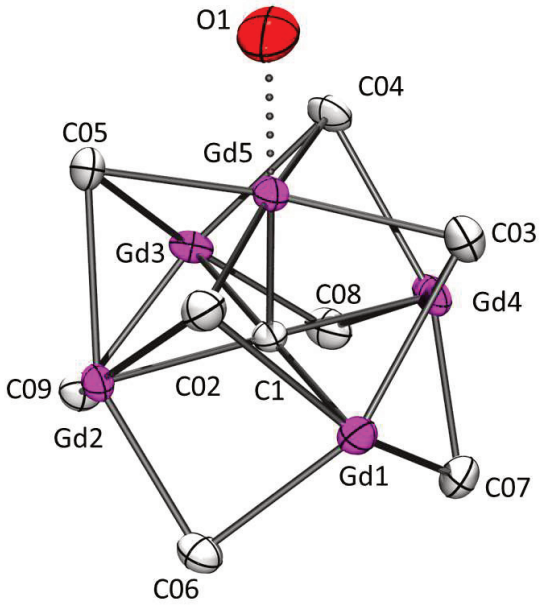

*Figure 5.14: Detailed view of the bonding situation in the structure of [(Cp*Gd)$_4$((Et$_2$O)Gd)(CH)(Me)$_8$] (**121a^{Gd}**). Atomic displacement parameters are set at the 50 % probability level. Hydrogen atoms are omitted for clarity.*

the pyramid is suspected to be a methine trianion to compensate the missing anionic charge of the replaced Cp*. The cleavage of Cp* ligands has not been observed in this type of reactions before and gives an indication, of the possible nature of the second product of the metallocene alkylaluminate dimer (**120**) producing reactions (*vide infra* for Tb, *vide supra* for Gd). However it is to mention, that the yields of the metallocene alkylaluminate dimers seem to be too high to allow a second product that contains five lanthanide atoms per released Cp* ligand.
The gadolinium analogue[28] (**120^{Gd}**) of the terbocene alkylaluminate (**120^{Tb}**) was obtained as main product of the attempted cleavage reaction with TBME as well, when the reaction was performed at ambient temperature (Figure 5.15).

Comparing the selected bond lengths and angles for the known [Cp$^*{}_2$Ln(AlMe$_4$)]$_2$

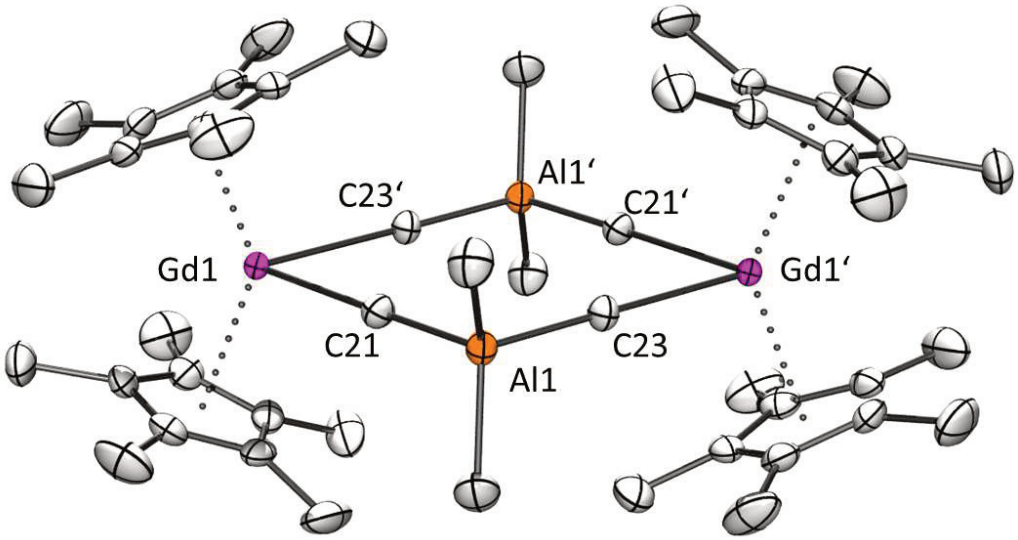

*Figure 5.15: ORTEP view of the molecular structure of $[Cp^*_2Gd(AlMe_4)]_2$ (**120**^{Gd}).[28] Atomic displacement parameters are set at the 50 % probability level. Hydrogen atoms are omitted for clarity. See Table 5.6 for significant lengths and angles.*

(Table 5.6), indicates, that only the bond lengths adjust to the ionic radii of the lanthanide centers, while the angles remain relatively constant. Therefore, the potential tension built up seems, even in cases of large lanthanides, not to be high enough to cause subsequent consecutive reactions. This is probably due to the lack of possibilities to form more stable products *via* C–H-activation (e.g. by release of methane).

The attempt to avoid C–H-activation reactions by choosing lower reaction temperatures (e.g. -40 °C) did not lead to the expected dimethyl trimers. Instead, for the cleavage with diethyl ether, here the metallocene ligand distribution product $[Cp^*_2Gd(AlMe_4)]_2$ (**120**^{Gd}) is obtained as well.
When TBME is applied as cleaving agent, an octameric ether activation product is formed. $[\{(Cp^*Gd)_2(Me)(CH_2OtBu)_2(AlMe_4)\}_2]_2$ (**122**, Figure 5.16) is shaped in form of a macrocycle (Figure 5.17) containing four symmetrically identical tetrameric building blocks (Figure 5.18). Each of them is built up from two chemically identical dimeric parts (Figure 5.19). In these parts the two gadolinium centers are bridged by one methyl group and two TBME units, activated at the former methyl moiety of the ether, which is

Table 5.6: Comparison of the crystal structures of the bis-Cp rare-earth metal alkylaluminate dimeric species **120**.*

Ln[a]	⌀(Ln–C^{Al})[a] [Å]	Ln–Ct1 [Å]	Ln–Ct2 [Å]	⌀(∠ Ct–Ln–C^{Al})[a] [°]	∠ Ct1–Ln–Ct2 [°]	∠ C^{Al1}–Ln–$C^{Al1'}$ [°]
La[b]	2.848(2)	2.522	2.516	104.5	139.62	87.36(4)
La^{Tolbc}	2.867(4)	2.527	2.513	104.3	140.04	87.70(10)
Sm[d]	2.747(16)	2.414	2.419	105.1	138.6	85.0(5)
Sm^{Tolce}	2.749(4)	2.421	2.424	105.8	135.7	87.69(13)
Gd	2.7123(19)	2.399	2.400	104.9	138.5	86.95(6)
Tb	2.690(2)	2.385	2.380	104.4	139.7	86.9
Y[f]	2.66	n.d.	n.d.	n.d.	n.d.	84.9(7)
Yb^{Tole}	2.634(2)	2.314	2.326	105.0	138.1	87.12(6)

[a] Ln^{Tol} = Unit cell contains one molecule of toluene; C^{Al} = Carbon of a methyl unit of an alkylaluminate moiety.
[b] Taken From ref. 17.
[c] Structure contains one toluene molecule.
[d] Taken From ref. 30.
[e] Taken From ref. 21.
[f] Taken From ref. 31.

necessary for charge balance. This macrocycle formed reproducibly, but due to the sheer size of the unit cell, structure elucidation by X-ray diffraction turned out to be rather challenging. Up until now, only conectivity pictures can be given here (Figures 5.16–5.19).

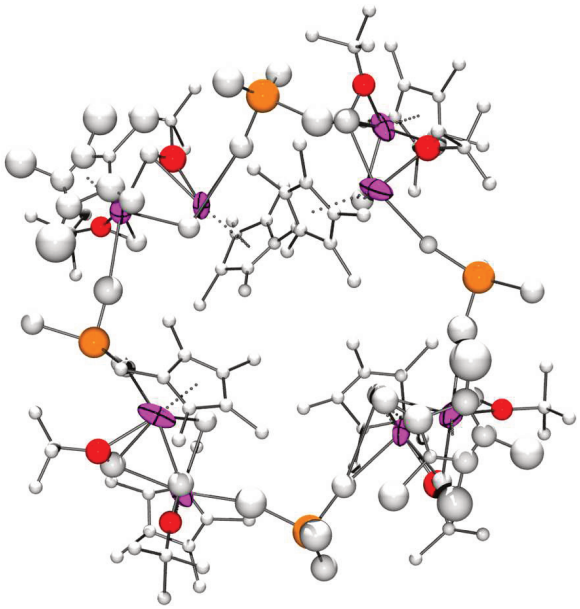

*Figure 5.16: Connectivity study on the product (**122**) of the activation of [Cp*Gd($AlMe_4$)$_2$] (**119^{Gd}**) using TBME to cleave the alkylaluminates. In the ball and stick model, grey balls represent carbon atoms, the magenta ones represent gadolinum atoms, orange balls represent aluminum and the red ones, depict the location of oxygen atoms. Hydrogen atoms are omitted for clarity. Due to high R-values of the measurement no further detailed figure is possible. Please see Figures 5.17, 5.18 and 5.19 for details.*

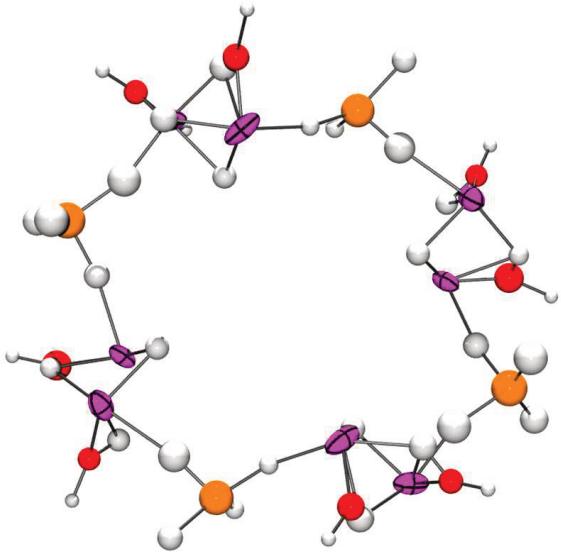

*Figure 5.17: More focused view of the connectivity of the product (**122**) of the activation of [Cp*Gd($AlMe_4$)$_2$] (**119^{Gd}**) using TBME to cleave the alkylaluminates. In the ball and stick model, grey balls represent carbon atoms, the magenta ones represent gadolinum atoms, orange balls represent aluminum and the red ones depict the location of oxygen atoms. Hydrogen atoms, the ^{t}Bu groups and the Cp^{*} ligands are omitted for clarity. Due to high R-values of the measurement no further detailed figure is possible. Please see Figures 5.18 and 5.19 for details.*

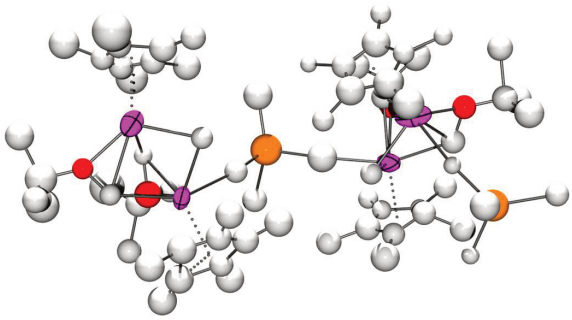

*Figure 5.18: View on the connectivity of the asymmetric repetition unit of the product (**122**) of the activation of [Cp*Gd(AlMe$_4$)$_2$] (**119^{Gd}**) using TBME to cleave the alkylaluminates. In the ball and stick model, grey balls represent carbon atoms, the magenta ones represent gadolinum atoms, orange balls represent aluminum and the red ones depict the location of oxygen atoms. Hydrogen atoms are omitted for clarity. Due to high R-values of the measurement no further detailed figure is possible. Please see Figure 5.19 for details.*

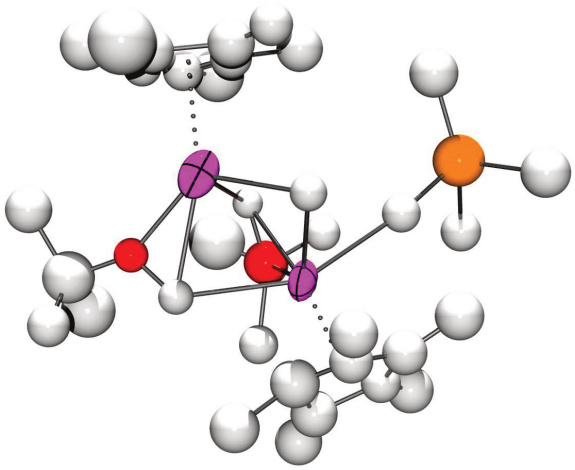

*Figure 5.19: View on the connectivity of one half of the asymmetric repetition unit of the product (**122**) of the activation of [Cp*Gd(AlMe$_4$)$_2$] (**119^{Gd}**) using TBME to cleave the alkylaluminates. In the ball and stick model, grey balls represent carbon atoms, the magenta ones represent gadolinum atoms, orange balls represent aluminum and the red ones depict the location of oxygen atoms. Hydrogen atoms are omitted for clarity. Due to high R-values of the measurement no further detailed figure is possible.*

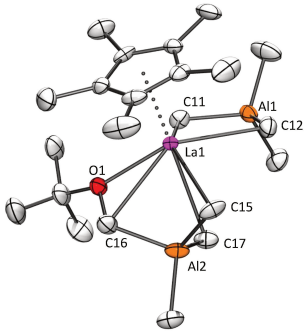

*Figure 5.20: ORTEP view of the molecular structure of [Cp*La(AlMe$_4$)(Me$_3$Al(CH$_2$)O^{t}Bu)] (**123**). Atomic displacement parameters are set at the 50 % probability level. Hydrogen atoms are omitted for clarity.*

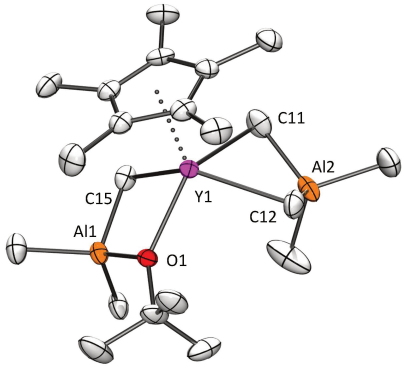

*Figure 5.21: ORTEP view of the molecular structure of [Cp*Y(AlMe$_4$)(Me$_3$AlO^{t}Bu)] (**124**). Atomic displacement parameters are set at the 50 % probability level. Hydrogen atoms are omitted for clarity.*

5.1.2.2.4 Yttrium and Lanthanum

Although the dodecametallic macrocycle is the largest example, there are further activations of TBME by other rare earth metals in this study. Activation of [Cp*La(AlMe$_4$)$_2$] (**119^{La}**) with TBME at -40 °C yielded a complex (**123**) bearing a multidentate (Me$_3$Al(CH$_2$)O^{t}Bu)$^-$ ligand that can be formed by C–H-activation from an alkylaluminate and TBME under release of methane (Figure 5.20). Interestingly, the second alkylaluminate stays intact. For yttrium, a bidentate ligand is formed. Here, probably under ethane release, a direct Al–O-bond is built (Figure 5.21), resulting in a TMA adduct of an *tert*-butanolate (**124**). This ligand has been produced by the addition of AlMe$_3$ to *tert*-butoxides before (See ref. 32 as an example). Interestingly, applying TBME to [Cp*Y(AlMe$_4$)$_2$] (**119^{Y}**) at -40 °C leads to a cleavage reaction resulting in [Cp*YMe$_2$]$_3$ (**79^{Y}**). When TBME is applied to the holmium analogue [Cp*Ho(AlMe$_4$)$_2$] (**119^{Ho}**), both at ambient temperature and at -40 °C, the trimeric dimethyl (**79^{Ho}**) is obtained.

5.1.2.3 C–H-bond activation of $[Cp^*HoMe_2]_3$ upon reaction with THF

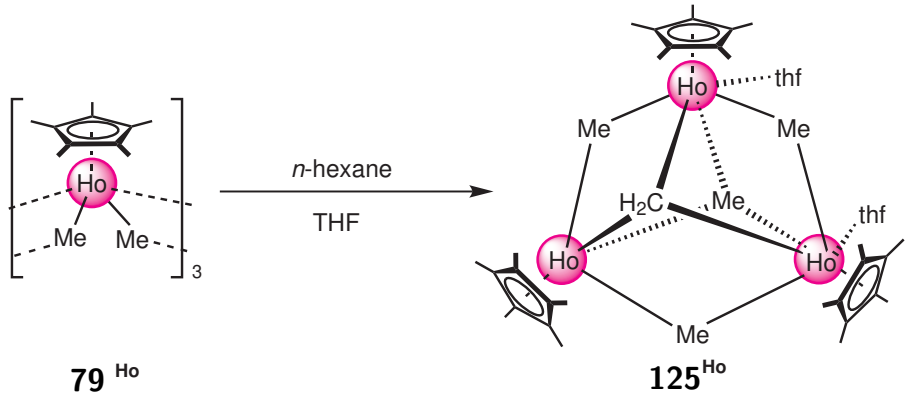

*Scheme 5.5: Synthesis of $[(Cp^*Ho)_3Me_4(CH_2)(thf)_2]$ (**125^{Ho}**) from $[Cp^*HoMe_2]_3$ (**79^{Ho}**) in analogy to the reaction applying the respective yttrium compound in Paper V.*

As for yttrium, the reaction of the dimethyl trimer with an excess of THF leads to a stable C–H-activation product, $[(Cp^*Ho)_3Me_4(CH_2)(thf)_2]$ (**125^{Ho}**, Schemes 5.1 and 5.5 and Figure 5.22). While its activation with cocatalyst **B** only results in a small amount of active holmium centers (as likewise observed in the yttrium study, Paper V), with cocatalyst **A**, two main species are formed that are both active in the polymerization of isoprene. These two species differ significantly in polymerization activity. The main catalyst (61 mol% of the catalytically active mixture) produces a polymer, with chain properties similar to that of **125^{Y}**(Paper V), while the second active species (39 mol%) is much more active and converting over five times more monomer. As the yield does not reach 100 % (in fact it is 71 %, see Table 5.7, run 39) within one hour of reaction time, it can be stated that none of these results can be due to a lack of monomer accessibility.

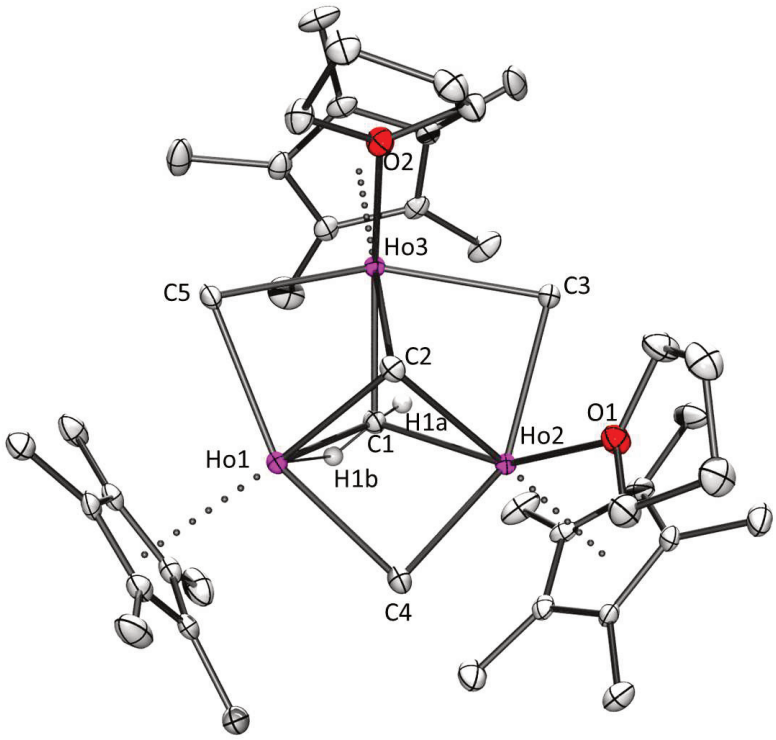

Figure 5.22: ORTEP view of the molecular structure of $[(Cp^*Ho)_3Me_4(CH_2)(thf)_2]$ (***125*** ^{Ho}). *Atomic displacement parameters are set at the 50 % probability level. Hydrogen atoms are omitted for clarity except for H1a and H1b.*

*Table 5.7: Isoprene homopolymerization by [(Cp*Ho)$_3$Me$_4$(CH$_2$)(thf)$_2$] (**125^{Ho}**)*

Entry[a]	Precatalyst	Cocatalyst[b]	T [°C]	t [min]	Monomer	Yield[d] [%]	*cis*[e] [%]	*trans*[e] [%]	3,4[e] [%]	$M_{n,SEC}$[f] [10^4 g·mol^{-1}]	PDI[f]	T_g[g] [°C]
39	[(Cp*Ho)$_3$Me$_4$(CH$_2$)(thf)$_2$] (**125^{Ho}**)	**A**	25	60	IP	71[h]	48[h]	16[h]	36[h]	13.2[h]	1.34[h]	-36[h]
40	[(Cp*Ho)$_3$Me$_4$(CH$_2$)(thf)$_2$] (**125^{Ho}**)	**B**	25	60	IP	9	74	1	25	22.0	1.60	-49

[a] Conditions: 20 µmol of precatalyst (7 µmol, 20 µmol of Ho centers), 20 µmol of cocatalyst, 20 mmol of isoprene, 8 mL of toluene.
[b] **A** = [Ph$_3$C][B(C$_6$F$_5$)$_4$], **B** = [PhNHMe$_2$][B(C$_6$F$_5$)$_4$], **C** = B(C$_6$F$_5$)$_3$.
[d] Yield of the isolated polymer.
[e] Determined by ^{1}H and ^{13}C NMR spectroscopy.
[f] Determined by GPC in THF at 35 °C.
[g] Determined on a Perkin Elmer DSC 8000; Heat rate: 20 K/min, Cooling rate: 60 K/min.
[h] The product (run 39) was identified as a blend of two polymers. This cannot be resolved by NMR spectroscopy or DSC, so the averages are given for the microstructure and glass transition temperature. GPC results instead are given for the main component of the blend (61 mol% of the blend). The smaller part (39 mol%) contains chains of a M_n of $85.0 \cdot 10^4 \frac{g}{mol}$ with a PDI of 1.39.

5.1.3 Experimental

5.1.3.1 General remarks

All operations were performed with rigorous exclusion of air and water, using standard Schlenk, high-vacuum, and argon glovebox techniques (MBraun MB 200B; < 1 ppm O_2, < 1 ppm H_2O). *n*-Hexane, toluene, and THF were purified by using Grubbs type columns (MBraun SPS-800, solvent purification system) and stored in a glovebox. $CDCl_3$ was purchased from Aldrich and used as received. Isoprene was obtained from Aldrich, dried over trioctylaluminum (Aldrich), and vacuum transferred prior to use. $[Ph_3C][B(C_6F_5)_4]$, $[PhNMe_2H][B(C_6F_5)_4]$, and $B(C_6F_5)_3$ were purchased from Boulder Scientific Company and used without any further purification. The NMR spectra for polymer microstructure determination were recorded at 26 °C on a Bruker AVII+ 400 Avance (^{1}H: 400.11 MHz; ^{13}C: 100.61 MHz). ^{1}H and ^{13}C shifts are referenced to internal solvent resonances and reported in parts per million (ppm) relative to TMS. The molar masses (M_W and M_n) of the polymers were determined by size-exclusion chromatography (SEC). Sample solutions (1.0 mg polymer per mL THF) were filtered through a 0.45 µm syringe filter (PTFE) prior to injection. SEC was performed with a pump supplied by Viscotek (GPCmax VE 2001), employing ViscoGEL columns. Signals were detected by means of a triple detection array (TDA 305) and calibrated against polystyrene standards ($M_W/\ M_n < 1.15$). The flowrate was set to 1.0 mL min^{-1}. The microstructures of the polydienes were examined by means of ^{1}H and ^{13}C NMR experiments on the AVII+ 400 Avance spectrometer at ambient temperature, using $CDCl_3$ as a solvent. Glass transition temperatures of the polymers (T_g) were obtained applying a Perkin-Elmer DSC 8000 calibrated with indium and cyclohexane standards, scanning from -100 °C up to +100 °C with heating rates of 20 K/min and cooling rates of 60 K/min in N_2 atmosphere. Precursors $[Ln(AlMe_4)_3]$ were synthesized according to literature methods (Paper IV and literature cited therein).
Single crystals were selected, coated with Parabar 10312 (previously known as Paratone N) and fixed on a microloop. Data were collected on a Bruker APEX DUO instrument equipped with an IμS microfocus sealed tube and QUAZAR optics for MoK_α radiation ($\lambda = 0.71073$ Å). The data collection strategy was determined using COSMO[33] employing ω- and φ scans. Raw data were processed using APEX[34] and SAINT[35], corrections for absorption effects were applied using SADABS[36]. The structures were solved by direct

methods and refined against all data by full-matrix least-squares methods on F^2 using SHELXTL[37,38] and Shelxle.[39]

5.1.3.2 Synthesis of [Cp*Ho(AlMe$_4$)$_2$] (**119^{Ho}**)

In analogy to the literature[1,6,15–21], in a glovebox, 500 mg (1.17 mmol) of [Ho(AlMe$_4$)$_3$] (**118^{Ho}**) were dissolved in 12 mL of toluene and 1,2,3,4,5-pentamethycyclopentadiene (161 mg, 191 µL, 1.17 mmol) was added. The reaction mixture was stirred overnight and the toluene was evaporated. The product was recrystallized from *n*-hexane solution.
Elemental Analysis (%) for $C_{18}H_{39}Al_2Ho$ (474.4 g / mol): Calcd: C 45.57, H 8.29. Found: C 45.62, H 8.15.

5.1.3.3 Synthesis of [Cp*Dy(AlMe$_4$)$_2$] (**119^{Dy}**)

In analogy to the literature,[1,6,15–21] in a glovebox, 500 mg (1.18 mmol) of [Dy(AlMe$_4$)$_3$] (**118^{Dy}**) were dissolved in 12 mL of toluene and 1,2,3,4,5-pentamethycyclopentadiene (162 mg, 193 µL, 1.18 mmol) was added. The reaction mixture was stirred overnight and the toluene was evaporated. The product was recrystallized from *n*-hexane solution.
Elemental Analysis (%) for $C_{18}H_{39}Al_2Dy$ (472.0 g / mol): Calcd: C 45.81, H 8.33. Found: C 45.70, H 8.43.

5.1.3.4 Synthesis of [Cp*Tb(AlMe$_4$)$_2$] (**119^{Tb}**)

In analogy to the literature,[1,6,15–21] in a glovebox, 500 mg (1.19 mmol) of [Tb(AlMe$_4$)$_3$] (**118^{Tb}**) were dissolved in 12 mL of toluene and 1,2,3,4,5-pentamethycyclopentadiene (163 mg, 194 µL, 1.19 mmol) was added. The reaction mixture was stirred overnight and the toluene was evaporated. The product was recrystallized from *n*-hexane solution.
Elemental Analysis (%) for $C_{18}H_{39}Al_2Tb$ (469.4 g / mol): Calcd: C 46.16, H 8.39. Found: C 46.09, H 8.52.

5.1.3.5 Synthesis of [Cp*Gd($AlMe_4$)$_2$] (**119^{Gd}**)

In analogy to the literature,[1,6,15–21] in a glovebox, 500 mg (1.19 mmol) of [Gd($AlMe_4$)$_3$] (**118^{Gd}**) were dissolved in 12 mL of toluene and 1,2,3,4,5-pentamethycyclopentadiene (163 mg, 194 µL, 1.19 mmol) was added. The reaction mixture was stirred overnight and the toluene was evaporated. The product was recrystallized from *n*-hexane solution.
Elemental Analysis (%) for $C_{18}H_{39}Al_2Gd$ (466.7 g / mol): Calcd: C 46.32, H 8.42. Found: C 46.45, H 8.25.

5.1.3.6 Synthesis of [Cp*HoMe$_2$]$_3$ (**79^{Ho}**)

Following the procedure published previously[1,2] complex **119^{Ho}** (474 mg, 1.00 mmol) was dissolved in *n*-hexane (5 mL) and diethyl ether (148 mg, 2.00 mmol) was added under vigorous stirring. The white / bright pink (in artificial light) and bright yellow (in sunlight) precipitate was separated via centrifugation and washed three times with *n*-hexane. Drying in vacuo yielded **79^{Ho}** (330 mg, > 99 %) as powder. Single crystals were obtained through recrystallization from a solution in a 1 / 20 mixture (mol / mol) of toluene in *n*-hexane at -35 °C.
Elemental Analysis (%) for $C_{36}H_{63}Ho$ (990.2 g / mol): Calcd: C 43.65, H 6.41. Found: C 43.34, H 6.17.

5.1.3.7 Synthesis of [Cp*DyMe$_2$]$_3$ (**79^{Dy}**)

Following the procedure published previously[1,2] complex **119^{Dy}** (472 mg, 1.00 mmol) was dissolved in *n*-hexane (5 mL) and diethyl ether (148 mg, 2.00 mmol) was added under vigorous stirring. The white precipitate was separated via centrifugation and washed three times with *n*-hexane. Drying in vacuo yielded **79^{Dy}** (62 mg, > 19 %) as powder. Single crystals were obtained through recrystallization from a solution in a 1 / 20 mixture (mol / mol) of toluene in *n*-hexane at -35 °C.
Elemental Analysis (%) for $C_{36}H_{63}Dy$ (983.4 g / mol): Calcd: C 43.97, H 6.46. Found: C 43.68, H 7.08.

5.1.3.8 Synthesis of [Cp*TbMe$_2$]$_3$ (**79^{Tb}**) and [(Cp*Tb)$_5$(CH$_2$)(Me)$_8$] (**121^{Tb}**)

Following the procedure published previously[1,2] complex **119^{Tb}** (468 mg, 1.00 mmol) was dissolved in *n*-hexane (5 mL) and diethyl ether (148 mg, 2.00 mmol) was added under vigorous stirring. The brownish precipitate was separated via centrifugation and washed three times with *n*-hexane. Drying in vacuo yielded **79^{Tb}** (6.5 mg, $>2\,\%$) as powder. Single crystals were obtained through recrystallization from a solution in a 1 / 20 mixture (mol / mol) of toluene in *n*-hexane at -35 °C. The remaining reaction mixture was dried *in vacuo* as well and an amorphous solid was obtained, re-crystallization from toluene (as the solvation in pure *n*-hexane and the mixture with toluene in 1 / 20 (mol / mol) failed) yielded few single crystals of **121^{Tb}**.
Elemental Analysis (%) for $C_{36}H_{63}Tb$ (972.7 g / mol) (**79^{Tb}**): Calcd: C 44.45, H 6.53. Found: C 45.01, H 6.50. Due to the low yield of **79^{Tb}**, the elemental analysis was performed using the lowest possible amount of compound, which increases the errors. The calced elemental analysis for **121^{Tb}** $C_{59}H_{100}Tb_5$ (1604.1 g / mol) is C 44.18, H 6.28. Found: C 43.47, H 6.15. The carbon value was found to be slightly out of range for both compounds, which is probably due to increased measurement errors reasoned in the low quantity of sample compounds.

5.1.3.9 Synthesis of[(Cp*Ho)$_3$Me$_4$(CH$_2$)(thf)$_2$] (**125^{Ho}**)

Complex **79^{Ho}** (40 mg, 0.04 mmol) was dissolved in 10 mL of THF. Instant gas formation was observed. The clear solution was layered with toluene and stored at -35 °C. Crystals suitable for X-ray diffraction were obtained after 14 d.
Elemental Analysis (%) for $C_{43}H_{75}Ho_3O_2$ (1118.8 g / mol): Calcd: C 46.16, H 6.76. Found: 45.87, H 6.79.

5.1.3.10 Synthesis of [Cp*$_2$Tb(AlMe$_4$)]$_2$ (**120^{Tb}**)

In analogy to the procedure published previously[1,2] complex **119^{Tb}** (117 mg, 0.25 mmol) was dissolved in *n*-hexane (5 mL) and *tert*-butyl methyl ether (TBME, 176 mg, 2.00 mmol) was added under vigorous stirring. After 12 h at ambient temperature, the solvent was

removed *in vacuo* and the brown solid was recrystallized in *n*-hexane. Single crystals were obtained at -35 °C.

5.1.3.11 Synthesis of $[Cp^*_2Gd(AlMe_4)]_2$ ($\mathbf{120^{Gd}}$)

$[Cp^*_2Gd(AlMe_4)]_2$ ($\mathbf{120^{Gd}}$) was obtained from two different reactions.

5.1.3.11.1 Method 1

In analogy to the procedure published previously[1,2] complex $\mathbf{119^{Gd}}$ (117 mg, 0.25 mmol) was dissolved in *n*-hexane (5 mL) and *tert*-butyl methyl ether (TBME, 176 mg, 2.00 mmol) was added under vigorous stirring. After 12 h at ambient temperature, the solvent was removed *in vacuo* and the apricot solid was recrystallized in *n*-hexane. Single crystals were obtained at -35 °C.

5.1.3.11.2 Method 2

Following the procedure published previously[1,2] complex $\mathbf{119^{Gd}}$ (117 mg, 0.25 mmol) was dissolved in precooled (-40 °C) *n*-hexane (5 mL) and precooled (-40 °C) diethyl ether (148 mg, 2.00 mmol) was added under vigorous stirring. After 10 min at -40 °C the solvent was removed *in vacuo* and the apricot solid was recrystallized in *n*-hexane. Single crystals were obtained at -35 °C.

5.1.3.12 Synthesis of $[(Cp^*Gd)_5(CH_2)(Me)_8]$ ($\mathbf{121^{Gd}}$) and $[(Cp^*Gd)_4((Et_2O)Gd)(CH)(Me)_8]$ ($\mathbf{121a^{Gd}}$)

Following the procedure published previously[1,2] complex $\mathbf{119^{Gd}}$ (117 mg, 0.25 mmol) was dissolved in *n*-hexane (5 mL) and diethyl ether (148 mg, 2.00 mmol) was added under vigorous stirring at r.t.. After 10 min the solvent was removed in vacuo and the apricot solid was recrystallized in *n*-hexane. Two different types of single crystals were obtained at -35 °C. The by far larger amount was identified as $[(Cp^*Gd)_5(CH_2)(Me)_8]$ ($\mathbf{121^{Gd}}$), the side product as $[(Cp^*Gd)_4((Et_2O)Gd)(CH)(Me)_8]$ ($\mathbf{121a^{Gd}}$).

5.1.3.13 Synthesis of [{(Cp*Gd)$_2$(Me)(CH$_2$O*t*Bu)$_2$(AlMe$_4$)}$_2$]$_2$ (122)

In analogy to the procedure published previously[1,2] complex **119^{Gd}** (117 mg, 0.25 mmol) was dissolved in precooled (-40 °C) *n*-hexane (5 mL) and precooled (-40 °C) *tert*-butyl methyl ether (TBME, 176 mg, 2.00 mmol) was added under vigorous stirring. After 12 h at -40 °C single crystals suitable for X-ray diffraction were obtained, revealing to be [{(Cp*Gd)$_2$(Me)(CH$_2$O*t*Bu)$_2$(AlMe$_4$)}$_2$]$_2$ (**122**).

5.1.3.14 Synthesis of [Cp*Y(AlMe$_4$)(Me$_3$AlO^{t}Bu)] (124)

In analogy to the procedure published previously[1,2] complex **119^{Y}** (100 mg, 0.25 mmol) was dissolved in precooled (-40 °C) *n*-hexane (5 mL) and precooled (-40 °C) *tert*-butyl methyl ether (TBME, 176 mg, 2.00 mmol) was added under vigorous stirring. After 12 h at -40 °C single crystals suitable for X-ray diffraction were obtained, revealing to be [Cp*Y(AlMe$_4$)(Me$_3$AlO^{t}Bu)] (**124**).

5.1.3.15 Synthesis of [Cp*La(AlMe$_4$)(Me$_3$Al(CH$_2$)O^{t}Bu)] (123)

In analogy to the procedure published previously[1,2] complex **119^{La}** (112 mg, 0.25 mmol) was dissolved in precooled (-40 °C) *n*-hexane (5 mL) and precooled (-40 °C) *tert*-butyl methyl ether (TBME, 176 mg, 2.00 mmol) was added under vigorous stirring. After 12 h at -40 °C single crystals suitable for X-ray diffraction were obtained, revealing to be [Cp*La(AlMe$_4$)(Me$_3$Al(CH$_2$)O^{t}Bu)] (**123**).

5.1.4 Crystal Structures

Table 5.8: Crystal data and structure refinement for ***119^{Ln}***

	119^{Ho}	**119^{Dy}**	**119^{Tb}**	**119^{Gd}**
Empirical formula	$C_{18}H_{39}Al_2Ho$	$C_{18}H_{39}Al_2Dy$	$C_{18}H_{39}Al_2Tb$	$C_{18}H_{39}Al_2Gd$
M_W [g $cdot$ mol^{-1}]	474.38	471.95	468.37	466.70
T [K]	100(2)	100(2)	100(2)	100(2)
Wavelength [Å]	0.71073	0.71073	0.71073	0.71073
Crystal System	Orthorhombic	Orthorhombic	Orthorhombic	Orthorhombic
Space Group	Pbca	Pbca	Pbca	Pbca
a [Å]	17.122(3)	17.1114(6)	17.1031(8)	17.0985(3)
b [Å]	14.301(3)	14.2885(5)	14.3081(7)	14.3377(3)
c [Å]	17.950(3)	17.9364(6)	17.9791(10)	17.9667(4)
α [°]	90	90	90	90
β [°]	90	90	90	90
γ [°]	90	90	90	90
Volume [Å^3]	4395.3(15)	4385.4(3)	4399.7(4)	4404.59(16)
Z	8	8	8	8
Density (calc) [mg ·mm^{-3}]	1.434	1.430	1.414	1.408
Absorption coefficient	3.675	3.482	3.289	3.086
Theta range [°]	2.174 to 28.52	2.564 to 28.70	2.265 to 23.76	2.561 to 30.122
Reflections	41352	83800	37471	63637
Independent reflections	5607 ($R_{int} = 0.0819$)	4845 ($R_{int} = 0.0280$)	4857 ($R_{int} = 0.0304$)	4863 ($R_{int} = 0.0307$)
Data / Restraints / Parameters	5607 / 0 / 247	4845 / 0 / 247	4857 / 3 / 255	4863 / 0 / 313
R_1(obs)[a]	0.0317	0.0125	0.0162	0.0241
wR_2(all)[b]	0.0834	0.0301	0.0377	0.0325

[a] Final R indices [I > 2σ (I)];
[b] R indices (all data).

Table 5.9: Crystal data and structure refinement for $\mathbf{79^{Ln}}$

	$\mathbf{79^{Ho}}$	$\mathbf{79^{Dy}}$	$\mathbf{79^{Tb}}$
Empirical formula	$C_{36}H_{63}Ho_3$	$C_{36}H_{63}Dy_3$	$C_{36}H_{63}Tb_3$
M_W [g *cdot* mol^{-1}]	990.65	983.36	972.62
T [K]	190(2)	100(2)	170(2)
Wavelength [Å]	0.71073	0.71073	0.71073
Crystal System	Hexagonal	Hexagonal	Hexagonal
Space Group	$P6_3$	$P6_3$	$P6_3$
a [Å]	12.25400(10)	12.2235(13)	12.323(2)
b [Å]	12.25400(10)	12.2235(13)	12.323(2)
c [Å]	14.5911(2)	14.4643(16)	14.512(2)
α [°]	90	90	90
β [°]	90	90	90
γ [°]	120	120	120
Volume [Å^3]	1897.47(4)	1871.6(4)	1908.5(7)
Z	2	2	2
Density (calc) [mg ·mm^{-3}]	1.734	1.745	1.693
Absorption coefficient	6.214	5.947	5.518
Theta range [°]	2.373 to 28.265	4.320 to 27.195	2.211 to 28.55
Reflections	14472	41262	11852
Independent reflections	3140 ($R_{int} = 0.0284$)	2469 ($R_{int} = 0.0463$)	3131 ($R_{int} = 0.0349$)
Data / Restraints / Parameters	3140 / 652 / 168	2469 / 811 / 238	3131 / 622 / 238
R_1(obs)[a]	0.0335	0.0270	0.0258
wR_2(all)[b]	0.0913	0.0596	0.0494

[a] Final R indices [I > 2σ (I)];
[b] R indices (all data).

Table 5.10: Crystal data and structure refinement for $\mathbf{120^{Ln}}$

	$\mathbf{120^{Tb}}$	$\mathbf{120^{Gd}}$
Empirical formula	$C_{54}H_{98}Al_2Tb_2$	$C_{54}H_{98}Al_2Gd_2$
M_W [g *cdot* mol^{-1}]	1119.12	1029.61
T [K]	100.15	190(2)
Wavelength [Å]	0.71073	0.71073
Crystal System	Triclinic	Monoclinic
Space Group	$P\bar{1}$	$P2_1/n$
a [Å]	10.6342(2)	10.4209(2)
b [Å]	11.7105(2)	17.2205(3)
c [Å]	12.4893(2)	17.2205(3)
α [°]	70.2974(6)	90
β [°]	72.7174(7)	91.1529(11)
γ [°]	86.0505(7)	90
Volume [Å^3]	1397.30(4)	2537.44(8)
Z	1	2
Density (calc) [mg ·mm^{-3}]	1.330	1.348
Absorption coefficient	2.572	2.653
Theta range [°]	2.28 to 30.02	2.421 to 26.11
Reflections	53230	69851
Independent reflections	8125 ($R_{int} = 0.0265$)	6297 ($R_{int} = 0.0305$)
Data / Restraints / Parameters	8125 / 12 / 466	6297 / 0 / 272
R_1(obs)[a]	0.0172	0.0175
wR_2(all)[b]	0.0411	0.0437

[a] Final R indices [I > 2σ (I)];
[b] R indices (all data).

Table 5.11: Crystal data and structure refinement for ***121^{Ln}***

	121^{Tb}	**121^{Gd}**	**121a^{Gd}**
Empirical formula	$C_{65}H_{114}Tb_5$	$C_{59}H_{100}Gd_5$	$C_{55.5}H_{101}Gd_5O$
M_W [g *cdot* mol^{-1}]	1690.16	1595.63	1570.61
T [K]	100(2)	100(2)	180(2)
Wavelength [Å]	0.71073	0.71073	0.71073
Crystal System	Triclinic	Triclinic	Triclinic
Space Group	$P\bar{1}$	$P\bar{1}$	$P\bar{1}$
a [Å]	13.8572(5)	13.8814(11)	13.882(2)
b [Å]	13.9346(5)	13.9407(12)	21.176(3)
c [Å]	17.9257(6)	17.4653(14)	23.125(4)
α [°]	70.9640(10)	101.1150(10)	85.953(4)
β [°]	75.233(2)	107.0640(10)	72.925(2)
γ [°]	89.4320(10)	91.6700(10)	84.468(4)
Volume [Å^3]	3153.82(19)	3157.2(4)	6461.5(18)
Z	2	2	4
Density (calc) [mg ·mm^{-3}]	1.780	1.678	1.615
Absorption coefficient	5.569	5.210	5.091
Theta range [°]	2.440 to 26.430	2.243 to 28.755	2.940 to 26.430
Reflections	85368	57956	110580
Independent reflections	16286 (R_{int} = 0.0397)	15577 (R_{int} = 0.0760)	28444 (R_{int} = 0.0437)
Data / Restraints / Parameters	16286 / 459 / 829	15577 / 2490 / 946	28444 / 4793 / 1451
R_1(obs)[a]	0.0346	0.0364	0.0486
wR_2(all)[b]	0.0644	0.0876	0.1335

[a] Final R indices [I > 2σ (I)];
[b] R indices (all data).

Table 5.12: Crystal data and structure refinement for ***123****,* ***124*** *and* ***125^{Ho}***

	123	**124**	**125^{Ho}**
Empirical formula	$C_{22}H_{47}Al_2LaO$	$C_{21}H_{45}Al_2OY$	$C_{43}H_{75}Ho_3O_2$
M_W [g *cdot* mol^{-1}]	520.46	456.44	1118.82
T [K]	123(2)	100(2)	100(2)
Wavelength [Å]	0.71073	0.71073	0.71073
Crystal System	Triclinic	Monoclinic	Orthorhombic
Space Group	$P\bar{1}$	$P2_1/c$	$P2_12_12_1$
a [Å]	9.433(3)	11.212(2)	12.8540(12)
b [Å]	17.696(6)	16.416(3)	14.3860(13)
c [Å]	19.017(7)	28.329(6)	22.921(2)
α [°]	109.815(8)	90	90
β [°]	102.367(7)	90.18(3)	90
γ [°]	103.789(8)	90	90
Volume [Å^3]	2745.2(17)	5214.0(19)	4238.5(7)
Z	4	8	4
Density (calc) [mg ·mm^{-3}]	1.259	1.163	1.753
Absorption coefficient	1.628	2.311	5.578
Theta range [°]	2.2122 to 25.5193	2.591 to 26.78	2.272 to 29.14
Reflections	80210	31101	53672
Independent reflections	13275 (R_{int} = 0.1042)	11212 (R_{int} = 0.0424)	11427 (R_{int} = 0.0445)
Data / Restraints / Parameters	13275 / 0 / 551	11212 / 0 / 482	11427 / 0 / 493
R_1(obs)[a]	0.0469	0.0376	0.0416
wR_2(all)[b]	0.0871	0.0814	0.0421

[a] Final R indices [I > 2σ (I)];
[b] R indices (all data).

5.1.5 Conclusion

The pentamethylcyclopentadienyl rare earth metal dimethyl trimers are accessible from the monomeric *bis*-tetramethylaluminates *via* an ether cleavage reaction for an ion size of $Lu^{3+} \leq Tb^{3+}$. The yields of these syntheses decrease with increasing ion size, as ligand redistribution and C–H-bond activation reactions become more favored with larger ions. The ligand redistribution pathway led to *bis*-pentamethylcyclopentadienyl rare-earth metal alkylaluminate dimers (metallocene alkylaluminate dimers), while the C–H-bond activation resulted in the build-up of a large variety of clusters. In case of terbium and gadolinium, square pyramidal shaped clusters of five lanthanide atoms could be crystallographically identified.
Utilization of *tert*-butyl methyl ether instead of the frequently applied diethyl ether was the only procedure that led to the formation of the dimethyl trimer in the terbium case. The ether was activated to form a multidentate ligand together with an alkylaluminate moiety in case of lanthanum, while for gadolinium a dodecametallic macrocyclic cluster was formed *via* C–H bond activation. For yttrium, a direct Al–O-bond was formed.
The isoprene and 1,3-butadiene polymers obtained from the dimethyl trimers are similar to those obtained for yttrium in Paper V. For isoprene, the fact that the second underlying and possibly radicalic crosslinking process observed with cocatalyst $[Ph_3C][B(C_6F_5)_4]$ only in case of yttrium and dysprosium, marks the main difference. Such polymers obtained from the *bis*-alkylaluminate precursors follow the trends known from other representatives of that motive in literature.

References

[1] Dietrich, H. M.; Zapilko, C.; Herdtweck, E.; Anwander, R. *Organometallics* **2005**, *24*, 5767–5771.

[2] Dietrich, H. M.; Grove, H.; Törnroos, K. W.; Anwander, R. *J. Am. Chem. Soc.* **2006**, *128*, 1458–1459.

[3] Shannon, R. D.; Prewitt, C. T. *Acta Cryst. B* **1969**, *25*, 925–946.

[4] Shannon, R. D. *Acta Cryst. A* **1976**, *32*, 751–767.

[5] Fischbach, A.; Anwander, R. *Adv. Polym. Sci.* **2006**, *204*, 155–281.

[6] Zimmermann, M.; Anwander, R. *Chem. Rev.* **2010**, *110*, 6194–6259.

[7] Evans, W. J.; Anwander, R.; Ziller, J. W. *Organometallics* **1995**, *14*, 1107–1109.

[8] Klooster, W. T.; Lu, R. S.; Anwander, R.; Evans, W. J.; Koetzle, T. F.; Bau, R. *Angew. Chem. Int. Edit.* **1998**, *37*, 1268–1270.

[9] Fischbach, A.; Klimpel, M. G.; Widenmeyer, M.; Herdtweck, E.; Scherer, W.; Anwander, R. *Angew. Chem. Int. Edit.* **2004**, *43*, 2234–2239.

[10] Zimmermann, M.; Frøystein, N.-Å.; Fischbach, A.; Sirsch, P.; Dietrich, H. M.; Törnroos, K. W.; Herdtweck, E.; Anwander, R. *Chem. Eur. J.* **2007**, *13*, 8784–8800.

[11] Meermann, C.; Törnroos, K. W.; Nerdal, W.; Anwander, R. *Angew. Chem. Int. Edit.* **2007**, *46*, 6508–6513.

[12] Nieland, A.; Mix, A.; Neumann, B.; Stammler, H.-G.; Mitzel, N. W. *Eur. J. Inorg. Chem.* **2014**, *2014*, 51–57.

[13] König, S. N.; Chilton, N. F.; Maichle-Mössmer, C.; Pineda, E. M.; Pugh, T.; Anwander, R.; Layfield, R. A. *Dalton Trans.* **2014**, *43*, 3035–3038.

[14] Hollfelder, C. O.; Jende, L. N.; Diether, D.; Zelger, T.; Stauder, R.; Maichle-Mössmer, C.; Anwander, R. *Catalysts* **2018**, *8*, 61.

[15] Zimmermann, M.; Törnroos, K. W.; Anwander, R. *Angew. Chem. Int. Edit.* **2008**, *47*, 775–778.

[16] Zimmermann, M.; Törnroos, K. W.; Sitzmann, H.; Anwander, R. *Chem. Eur. J.* **2008**, *14*, 7266–7277.

[17] Dietrich, H. M.; Törnroos, K. W.; Herdtweck, E.; Anwander, R. *Organometallics* **2009**, *28*, 6739–6749.

[18] Litlabø, R.; Enders, M.; Törnroos, K. W.; Anwander, R. *Organometallics* **2010**, *29*, 2588–2595.

[19] Zimmermann, M.; Volbeda, J.; Törnroos, K. W.; Anwander, R. *C. R. Chim.* **2010**, *13*, 651–660.

[20] Dettenrieder, N.; Hollfelder, C. O.; Jende, L. N.; Maichle-Mössmer, C.; Anwander, R. *Organometallics* **2014**, *33*, 1528–1531.

[21] Bienfait, A. M.; Wolf, B. M.; Törnroos, K. W.; Anwander, R. *Organometallics* **2015**, *34*, 5734–5744.

[22] Holton, J.; Lappert, M. F.; Ballard, D. G. H.; Pearce, R.; Atwood, J. L.; Hunter, W. E. *Dalton Trans.* **1979**, *0*, 54 –61.

[23] Jende, L. N. Ph.D. Thesis, Eberhard Karls Universität Tübingen, **2015**.

[24] Anwander, R.; Klimpel, M. G.; Martin Dietrich, H.; Shorokhov, D. J.; Scherer, W. *Chem. Commun.* **2003**, 1008–1009.

[25] Jende, L. N.; Hollfelder, C. O.; Maichle-Mössmer, C.; Anwander, R. *Organometallics* **2015**, *34*, 32–41.

[26] Kaita, S.; Hou, Z.; Nishiura, M.; Doi, Y.; Kurazumi, J.; Horiuchi, A. C.; Wakatsuki, Y. *Macromol. Rapid Comm.* **2003**, *24*, 179–184.

[27] Kaita, S.; Yamanaka, M.; Horiuchi, A. C.; Wakatsuki, Y. *Macromolecules* **2006**, *39*, 1359–1363.

[28] Complexes of this type were originally synthesized by Kaita and coworkers[26,27] and tested in 1,3-diene polymerization. *Cf.* to chapter 1. Crystal structures were only obtained for the cationized species for Ln = Pr and Nd.

[29] Zimmermann, M. Ph.D. Thesis, Universitetet i Bergen, **2007**.

[30] Evans, W. J.; Chamberlain, L. R.; Ulibarri, T. A.; Ziller, J. W. *J. Am. Chem. Soc.* **1988**, *110*, 6423–6432.

[31] Busch, M. A.; Harlow, R.; Watson, P. L. *Inorg. Chim. Acta* **1987**, *140*, 15 – 20.

[32] Evans, W. J.; Boyle, T. J.; Ziller, J. W. *J. Organomet. Chem.* **1993**, *462*, 141–148.

[33] Bruker AXS Inc, Madison, WI, 2012.

[34] Bruker AXS Inc., Madison, WI, 2016.

[35] Bruker AXS Inc., Madison, WI, 2015.

[36] Krause, L.; Herbst-Irmer, R.; Sheldrick, G. M.; D., S. *J. Appl. Cryst.* **2015**, *48*, 3.

[37] SHELXTL, *Acta Cryst.* **2015**, *A71*, 3–8.

[38] Scheldrick, G. M. *Program for crystal structure refinement*; SHELXL-97, 1997.

[39] Hübschle, C. B.; Sheldrick, G. M.; Dittrich, B. *J. Appl. Cryst.* **2011**, *44*, 1281–1284.

5.1.6 Acknowledgement

Coauthors in case of publication: Daniel Werner, Cäcilia Maichle-Mössmer, Reiner Anwander and possibly Melanie Meermann-Zimmermann and Karl W. Törnroos if the lozange-pyramidal yttrium complex is presented in further detail.
The authors thank Deutsche Forschungsgemeinschaft for funding this work.

Manuscript II: Reactivity Studies of Pentamethylcyclopentadienyl-Supported Rare-Earth-Metal Dimethyl Complexes with Donor Molecules

5.2.1 Introduction

The polymerization properties and active species of cyclopentadienyl rare earth metal dimethyl trimers $[Cp^*LnMe_2]_3$ (Ln = Dy, Ho, Y, Lu) have been investigated recently (Manuscript I and Paper V). Especially their isoprene polymerization is focused on a vinylic addition of the monomer, while in case of slightly less bulky 1,3-butadiene a much higher *cis*-selectivity is observed. Therefore, $[Cp^*YMe_2]_3$ is reacted with further donor spectator ligands to break up the trimeric cluster and thereby increase the steric space around the potential catalytic centers. This is intended to enhance the ratio of coordination of isoprene in *cis*-conformation and thereby the 1,4-*cis*-content of the resulting polymers.[1–3] Reactions of $[Cp^*YMe_2]_3$ and a selection of donor molecules containing one or more, possibly chelating donor atoms are produced *in situ*, both prior and after cocatalyst addition in the prereaction of an isoprene polymerization. Furthermore, isolable reaction products of $[Cp^*YMe_2]_3$ and the donors are investigated by single crystal X-ray diffraction.

5.2.2 Results and Discussion

In this study, the influence of donor addition to the polymerization of the system of $[Cp^*YMe_2]_3$ ($\mathbf{79^Y}$) with $[PhNHMe_2][B(C_6F_5)_4]$ (**B**) in a ratio of one equivalent cocatalyst per yttrium center ($\mathbf{79^Y}$ / **B**) is investigated. Furthermore, $\mathbf{79^Y}$ / **A** (**A** = $[Ph_3C][B(C_6F_5)_4]$) is tested with a selection of oxygen donors, known for their stabilizing properties, to supress the crosslinkage behavior found with that system (Paper V).

*Table 5.13: Isoprene homopolymerization of [Cp*YMe$_2$]$_3$] (**79^{Y}**) applying monodentate donors.*

Entry[a]	Donor[b] [equiv]	Cocatalyst[c]	Add. order[d]	t[e] [h]	Yield[e] [%]	*cis*[f] [%]	*trans*[f] [%]	3,4[f] [%]	$M_{n,SEC}$[g] [10^4g·mol^{-1}]	PDI[g]	T_g[h] [°C]
I[i]	none	**B**	—	1	90	36	11	53	14.1	1.16	-27
II[i]	none	**B**	—	1	7	76	0	24	55.1	1.97	-48
III[i]	none	**A**	—	1	> 99	51	18	31	8.4	2.33	-47
1	1 THF	**B**	a	1	5	27	23	50	2.3	1.88	-29
2	1 Et_2O	**B**	a	1	> 99	24	33	43	8.2	1.12	-35
3	1 TBME	**B**	a	1	93	36	10	54	13.4[k]	1.12[k]	-30[l]
4	1 BHT	**A**	a	1	traces[m]	—[m]	—[m]	—[m]	—[m]	—[m]	—[m]
5	1 BHT	**A**	a	24	> 99	45	26	29	25.6	1.78	n.d.
6	1 BHT	**A**	b	1	8	67	20	13	59.7	1.68	-46
7	10 BHT	**A**	a	1	traces[m]	—[m]	—[m]	—[m]	—[m]	—[m]	—[m]
8	10 BHT	**A**	a	24	> 99	0	97	3	23.5[k]	1.39[k]	-25
9	10 BHT	**A**	b	1	none[m]	—[m]	—[m]	—[m]	—[m]	—[m]	—[m]
10	1 BHT	**B**	a	1	none[m]	—[m]	—[m]	—[m]	—[m]	—[m]	—[m]
11	1 BHT	**B**	b	1	none[m]	—[m]	—[m]	—[m]	—[m]	—[m]	—[m]
12	1 BzPh	**A**	a	1	97	36	8	56	—[n]	—[n]	-15
13	1 BzPh	**A**	b	1	none[m]	—[m]	—[m]	—[m]	—[m]	—[m]	—[m]
14	10 BzPh	**A**	a	1	none[m]	—[m]	—[m]	—[m]	—[m]	—[m]	—[m]
15	10 BzPh	**A**	b	1	none[m]	—[m]	—[m]	—[m]	—[m]	—[m]	—[m]
16	1 BzPh	**B**	a	1	65	36	4	60	59.1	1.37	-11
17	1 BzPh	**B**	b	1	14	35	3	62	13.6	2.28	-11

[a] Conditions: 7 µmol of precatalyst (20 µmol of Y centers), 20 µmol of cocatalyst, 20 mmol of isoprene, 8 mL of toluene.
[b] THF = Tetrahydrofuran, Et_2O = Diethyl ether, TBME = *Tert*-butyl methyl ether, BHT = *Bis-tert*-butyl hydroxytoluene (2,6 Di-*tert*-butyl-4-methyl-phenole), BzPh = Benzophenone.
[c] **A** = $[Ph_3C][B(C_6F_5)_4]$, **B** = $[PhNHMe_2][B(C_6F_5)_4]$.
[d] a = Donor was added 5 min prior to the cocatalyst addition. b = Donor was added after a pre-reaction of precatalyst and cocatalyst of 30 min. The mixture was stirred for another 5 min, before isoprene was added.
[e] t = reaction time, Yield of the isolated polymer.
[f] Determined by ^{1}H and ^{13}C NMR spectroscopy.
[g] Determined by GPC in THF at 35 °C.
[h] Determined on a Perkin Elmer DSC 8000; Heat rate: 20 K/min, Cooling rate: 60 K/min
[i] Taken from Paper V for comparison purposes. Runs I and III: Precatalyst $[Cp^*YMe_2]_3]$ (**79^{Y}**), Run II: Precatalyst $[(Cp^*Y)_3Me_4(CH_2)(thf)_2]$ (**125^{Y}**)
[k] Multimodal MWD.
[l] Determined on a Perkin-Elmer DSC 8000; Heat rate: 10 K/min, Cooling rate: 100 K/min for reasons of low ΔC_p at original settings.
[m] Evaluation impossible due to low yield.
[n] Insoluable in THF, specimen swells, probably crosslinked.

5.2.2.1 Monodentate donors as additive: Polymerizations with $[PhNHMe_2][B(C_6F_5)_4]$

The addition of monodentate donors is investigated from relatively small THF to the sterically much more demanding benzophenone. Furthermore, for *bis-tert*-butyl hydroxytoluene (2,6 Di-*tert*-butyl-4-methyl-phenole, BHT) and benzophenone, an addition directly to the preformed active species of **79^{Y}** / **B** is tested (labeled as addition order 'b' in Table 5.13).

THF addition in excess to **79^{Y}** is known to cause C–H-bond activation over night, forming the stable product $[(Cp^*Y)_3Me_4(CH_2)(thf)_2]$ (**125^{Y}**). In this study only one

equivalent of THF is added per yttrium center, and the cocatalyst is added only 5 min after the THF. Polymerization of isoprene (Table 5.13, run 1) shows that, while the yields drop as in case of $\mathbf{125^Y}$ (Table 5.13, run II), the achieved polymer is more similar to that obtained without any donor (Table 5.13, run I) than to that of $\mathbf{125^Y}$. The microstructure is similar to that produced without a donor addition, despite a significantly higher 1,4-*trans*-content, but the polymer chains are almost as non-uniform as with the C–H-bond activated stable thf adduct. The ratio of chains per yttrium center indicates an efficiency of the initiation reaction, that is higher than without THF, but much lower, than with $\mathbf{125^Y}$. As the MWD remains monomodal, a blend of the two polymers produced by $\mathbf{79^Y}$ and $\mathbf{125^Y}$ without further donor addition can be excluded. So an incomplete formation of $\mathbf{125^Y}$ with low yield due to the low concentration of THF can be ruled out, as well.

Replacing the THF by diethyl ether (Table 5.13, run 2) changes the polymerization completely. Instead of the slow polymerization with THF, here an almost quantitative yield is obtained after 1 h. The polymer shows a very low PDI (1.12) and an extrapolated ratio of chains per yttrium center of only 1.2, which brings it close to living polymerization. Unfortunately for possible application, the microstructure is almost perfectly unselective.

Once again, only a slight variation of the added ether towards *tert*-butyl methyl ether (TBME) gives totally different results. Here, the additive does not interact significantly with the catalytic species, as the obtained polymer is very similar to that produced by $\mathbf{79^Y}$ without donor addition, despite the fact, that the MWD shows a small second mode. This indicates the presence of a second catalytic species in the system, that is either much less active or much lower concentrated than the species producing the polymer of the main mode. So it remains a subject to research, if after 5 min, the prereaction is simply incomplete and whether this second mode would become more pronounced, if the prereaction time of precatalyst and donor would be longer.

The first monodentate donor tested in this context, that is significantly bulkier is *bis-tert*-butyl hydroxytoluene (2,6 Di-*tert*-butyl-4-methyl-phenole, BHT). BHT is frequently applied as a stabilizer in both commercially available monomers and for polymer products (as in this study, see Experimental Section 5.2.3). With cocatalyst **B**, this stabilizer works well and does not allow polymerization, both when added to the precatalyst and when added to the already activated species (Table 5.13, runs 10 and 11). Interestingly

this is not true, when cocatalyst **A** is applied (*vide infra*).
The last and bulkiest monodentate donor tested here is benzophenone (labeled 'BzPh' in Table 5.13). The steric bulk brought into the system does not reduce the 1,4-*cis*-content as could be expected. Instead the 1,4-*trans*-content is shifted to vinylic addition and the initiation is hindered (lower yield, higher PDI and molecular weight averages) (Table 5.13, run 16). If the addition of benzophenone takes place after precatalyst activation (Table 5.13, run 17), even lower yield and the highest PDI observed so far in this study are obtained. This indicates a slower and less uniform chain propagation.
So it can be stated that all tested monodentate donors have an individual impact on the polymerization, without any outstanding trends.

5.2.2.2 Donors as stabilizers: Polymerizations with $[Ph_3C][B(C_6F_5)_4]$

Benzophenone and BHT are tested in the polymerization applying cocatalyst **A**, in order to supress the crosslinking observed with the system $\mathbf{79^Y}$ / **A** (Paper V). This approach implies, that the crosslinking observed is induced by a process involving radicals. Scavenging the radicals by these additives would provide non-crosslinked polymers and validation to the assumed nature of the crosslinking process. As these scavengers bear donor atoms, they can serve as donor ligands as well. Their impact on the sterical environment is expressed by their influence on the microstructure of the obtained polymers (Chart 5.6).
In case of benzophenone, the polymerization is hindered by the additive (Table 5.13, runs 12–15). Only if a single equivalent of benzophenone is added prior to the activation of the precatalyst, polymerization takes place. Although a high yield is achieved and the microstructure is altered toward a higher vinylic content in the presence of benzophenone, the resulting polymeric product is still crosslinked (Table 5.13, run 12).
If BHT is applied instead, no crosslinking is found. The terneric system $\mathbf{79^Y}$ / **A** / BHT yields only small amounts of polymer and only traces, if BHT is added before the cocatalyst, after 1 h. Here (Table 5.13, run 6), the microstructure is shifted towards 1,4-addition, esp. towards *cis*-conformation. The initiation efficiency drops significantly. As there is no crosslinking observed, the polymer is more uniform than without the addition of BHT. If BHT is added before the cocatalyst instead and the reaction time is prolonged to 24 h, quantitative yields are produced, even with high concentrations (ten equivalents) of BHT

per yttrium center. And most interestingly, this increase of BHT concentration has an enormous impact on the polymers obtained (Table 5.13, runs 5 and 8). Here, multiple modes are visible in the MWD and the observed microstructure consists of 97 % 1,4-*trans* linkages. This is probably due to one or even more molecules of BHT binding directly to the yttrium center and therefore altering the steric environment to cause the observed result. Furthermore, an addition of ten equivalents per yttrium center after activation of the precatalyst does not produce a species active in isoprene polymerization (Table 5.13, run 9).

Benzoquinone is tested for its capability to supress the crosslinking side reaction occuring in polymerizations with cocatalyst **A** as well. Next to being a wellknown radical scavenger, benzoquinone can serve as bidentate ligand due to its two donor atoms (oxygens). Therefore, more complex results can be expected.

When benzoquinone is added before cocatalyst **A**, only traces of polyisoprene can be isolated after 1 h both with one and ten equivalents of benzoquinone. After 24 h, similar to BHT, two very different polymers are obtained for the two tested concentrations of the scavenger (Table 5.14, runs 19 and 22). A large excess of the additive, leads to a highly 1,4-*trans*-selective polyisoprene in high yield, that still shows crosslinking. With an addition equimolar to the yttrium centers of the trimeric precatalyst, the polymer has a much less pronounced focus on 1,4-*trans* linkages, shows a multimodal MWD and a more deficient initiation than without benzoquinone, but no crosslinking. If benzoquinone is added after precatalyst activation, no yield for high concentrations of the additive is achieved (as in case of BHT, *vide supra*). For the equimolar addition (Table 5.14, run 20), crosslinking is once more avoided, which leads to a more uniform polymer. Although, statistically only one out of 7.2 yttrium centers grows a polymer chain. Interestingly, this polymer is insoluble in chloroform, thus no information about the microstructure can be provided by NMR-spectroscopic analytics. In summary, BHT remains the most sucessfully tested crosslinking supressor in this study. Its application at low temperatures, where the crosslinkikg process was observed with $\mathbf{79^Y}$ / **A** to significantly larger extent (Paper V) is subject to further research.

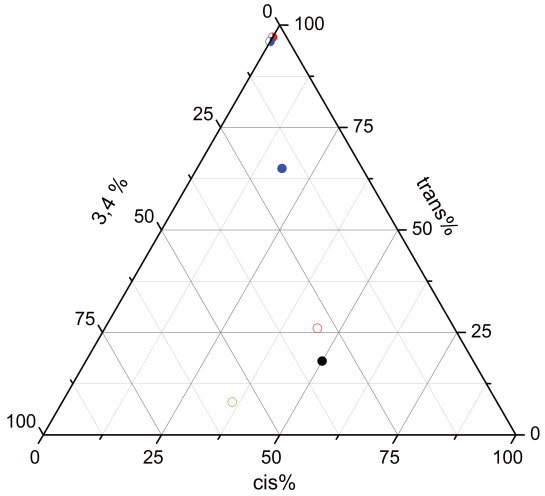

*Chart 5.6: Ternary plot of the microstructures of the polyisoprenes obtained from of [Cp*YMe$_2$]$_3$ (**79^Y**) applying cocatalyst **A** and additives. Solid symbols mark reaction times of 1 h, hollow symbols mark reaction times of 24 h. The additives are color-coded as follows: black (reaction without additive), red (BHT), green (Benzophenone), and blue (Benzoquinone). Vertically half-whitened symbols represent experiments in which 10 equiv. of the additive were applied.*

5.2.2.3 Multidentate donors as additive: Polymerizations with $[\mathbf{PhNHMe_2}][\mathbf{B(C_6F_5)_4}]$

Bidentate and multidentate donors have been investigated in this study with three major intentions. First, as for some of the monodentate ligands, the supression of the crosslinking in the polymerization with the system $\mathbf{79^Y}$ / **A** was targeted with benzoquinone (*vide supra*). Second, bidentate ligands with seperated donor atoms are tested with $\mathbf{79^Y}$ / **B** in order to obtain larger yttrium-yttrium distances in the cluster active species by providing lager bridging ligands and thereby increasing the steric space. And third, chelating multidentate ligands are investigated with the same system, intending to stabilize monomeric Cp^* rare earth methyl species. Alternations of the sterical environment of the active species influence the microstructures of the resulting polymers (Chart 5.7 for an overview).
Next to its application as scavenger, benzoquinone is also tested as one of the multidentate donor additives implied to break up the trimeric precatalyst structure of $\mathbf{79^Y}$ and its active species, that is supposedly multimeric as well (Paper V). It is worth to mention, that due to the location of the donor atoms in benzoquinone in *para* position to one another, it is unlikely that this potential bidentate ligand would bind in a chelating manner. Therefore, the intended steric freedom is rather realized by monodentate binding modes or by benzoquinones bridging yttrium centers over a longer distance than the originally bridging methyl moieties. With the same intention, 4,4'-bipyridine and dimethylaminopyridine (DMAP) are tested.
If benzoquinone is added to the unactivated precatalyst (Table 5.14, run 24), a low yield of only 14 % after 1 h and an extremely low rate of initiation is observed, resulting in an enormous average molecular weight ($M_n > 1.6 \cdot 10^6\,\mathrm{g \cdot mol^{-1}}$). This polymer is very uniform and shows a large focus on 1,4-*cis* linkage (79 %). A similar polymer is found, when the additive is reacted directly with the active polymerization catalyst of $\mathbf{79^Y}$ / **B** (Table 5.14, run 25). The main difference between the results obtained with the two orders of educt addition (Table 5.14, runs 24 and 25), is a multimodal MWD, obtained for 'b', that causes a higher overall PDI.
With 4,4'-bipyridine only addition to the preformed active species of $\mathbf{79^Y}$ / **B** resulted in a species active in isoprene polymerization. The effect of this ligand is mostly focused on the chain properties of the resulting polymer: A multimodal MWD with a relatively high overall PDI (> 3) is observed (Table 5.14, runs 26 and 27).

DMAP, the last, probably non-chelating bidentate donor ligand is investigated (Table 5.14, runs 28 and 29). Both addition orders result in polymers of a microstructure that matches the 36 / 11 / 53 (*cis*% / *trans*% / 3,4%) of the pure bineric system **79$^{\mathbf{Y}}$ / B** (Table 5.14, run I) to close proximity. It is to highlight that a ratio of chains per yttrium centers close to 1 is achieved, if DMAP is added before activation.

*Table 5.14: Isoprene homopolymerization of [Cp*YMe$_2$]$_3$] (**79$^{\mathbf{Y}}$**) applying multidentate donors.*

Entry[a]	Donor[b] [equiv]	Cocatalyst[c]	Add. order[d]	t[e] [h]	Yield[e] [%]	*cis*[f] [%]	*trans*[f] [%]	3,4[f] [%]	$M_{n,SEC}$[g] [10^4g·mol^{-1}]	PDI[g]	T_g[h] [°C]
I[i]	none	**B**	—	1	90	36	11	53	14.1	1.16	-27
III[i]	none	**A**	—	1	> 99	51	18	31	8.4	2.33	-47
18	1 BzQ	**A**	a	1	traces[m]	—[m]	—[m]	—[m]	—[m]	—[m]	—[m]
19	1 BzQ	**A**	a	24	82	18	65	16	12.8[k]	1.40[k]	-8
20	1 BzQ	**A**	b	1	65	—[l]	—[l]	—[l]	32.0	1.76	n.d.
21	10 BzQ	**A**	a	1	traces[m]	—[m]	—[m]	—[m]	—[m]	—[m]	—[m]
22	10 BzQ	**A**	a	24	98	0	96	4	—[n]	—[n]	-4
23	10 BzQ	**A**	b	1	none[m]	—[m]	—[m]	—[m]	—[m]	—[m]	—[m]
24	1 BzQ	**B**	a	1	14	79	0	21	162.3	1.09	n.d.
25	1 BzQ	**B**	b	1	5	72	0	27	49.0[k]	2.05[k]	
26	1 BiPy	**B**	a	1	none[m]	—[m]	—[m]	—[m]	—[m]	—[m]	—[m]
27	1 BiPy	**B**	b	1	75	34	11	56	20.0[k]	3.37[k]	-16
28	1 DMAP	**B**	a	1	46	32	10	58	6.4	1.57	-21
29	1 DMAP	**B**	b	1	29	35	7	58	11.9	1.73	-15
30	1 AmQ	**B**	a	1	85	33	9	58	47.8	1.13	-17
31	1 AmQ	**B**	b	1	> 99	34	10	56	81.6	1.32	-16
32	1 Phen	**B**	a	1	traces[m]	—[m]	—[m]	—[m]	—[m]	—[m]	—[m]
33	1 Phen	**B**	a	36	> 99	33	12	55	33.4[k]	1.49[k]	-27
34	1 Phen	**B**	b	1	none[m]	—[m]	—[m]	—[m]	—[m]	—[m]	—[m]
IV[i]	1 DiIm	**B**	a	1	44	9	3	88	20.2[k]	1.97[k]	-3.5[p]
35	1 DiIm	**B**	b	1	3	15	4	82	20.1[k]	2.16[k]	-4
36	1 Gua	**B**	a	1	98	33	11	56	39.8	1.54	-22
37	1 Gua	**B**	b	1	99	32	13	55	21.3	1.22	-19
38	1 ThioU	**B**	a	1	none[m]	—[m]	—[m]	—[m]	—[m]	—[m]	—[m]
39	1 ThioU	**B**	b	1	87	33	12	55	11.4	1.23	-20

[a] Conditions: 7 µmol of precatalyst (20 µmol of Y centers), 20 µmol of cocatalyst, 20 mmol of isoprene, 8 mL of toluene.
[b] BzQ = Benzoquinone, BiPy = 4,4'-Bipyridine, DMAP = Dimethylaminopyridine, AmQ = Aminoquinoline, Phen = Phenanthroline, DiIm = [dipp-N=CH]$_2$ (Diisopropylphenyldiimine), Gua = Tetramethylguanidine, ThioU = Thiourea.
[c] **A** = [Ph$_3$C][B(C$_6$F$_5$)$_4$], **B** = [PhNHMe$_2$][B(C$_6$F$_5$)$_4$].
[d] a = Donor was added 5 min prior to the co-catalyst addition. b = Donor was added after a pre-reaction of precatalyst and cocatalyst of 30 min. The solution was stirred for another 5 min, before isoprene was added.
[e] t = reaction time. Yield of the isolated polymer.
[f] Determined by ^{1}H and ^{13}C NMR spectroscopy.
[g] Determined by GPC in THF at 35 °C.
[h] Determined on a Perkin Elmer DSC 8000; Heat rate: 20 K/min, Cooling rate: 60 K/min
[i] Taken from Paper V for comparison purposes. Run I, III and IV: Precatalyst [Cp*YMe$_2$]$_3$](**79$^{\mathbf{Y}}$**).
[k] Multimodal MWD.
[l] Polymer is insoluable in CDCl$_3$.
[m] Evaluation impossible due to low yield.
[n] Insoluable in THF, specimen swells, probably crosslinked.
[p] determined by DSC 8000; Heat rate: 10 K/min, Cooling rate: 100 K/min for reasons of low ΔC_p at original settings.

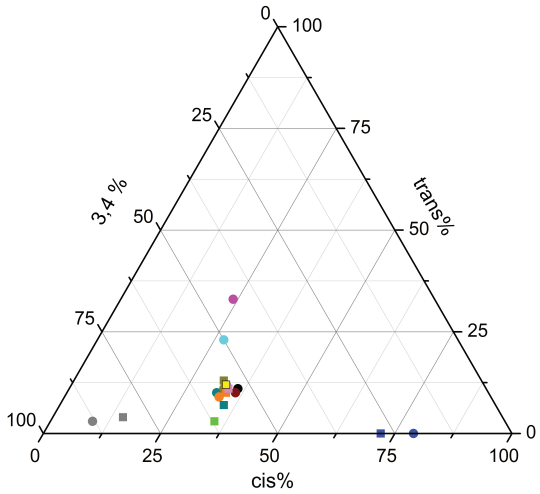

*Chart 5.7: Ternary plot of the microstructures of the polyisoprenes obtained from of [Cp*YMe$_2$]$_3$ (**79^Y**) applying cocatalyst **B** and additives. The additives are color-coded as follows: black (reaction without additive), red (BHT), green (Benzophenone), blue (Benzoquinone), pink (Et_2O), brown (TBME), cyan (THF), teal (DMAP), orange (Aminoquinoline), grey (DippNCH)$_2$), gold (Tetramethylguanidine), rose (4,4'-Bipyridine), yellow (Thiourea). Polymers represented by circular symbols were produced applying addition order a, those produced with addition order b are marked as squares.*

Furthermore, five potentially chelating multidentate ligands are investigated as additive to the catalysis. Their coordination is supposed to break down the multimeric active species into monomeric units allowing access to further yttrium centers.
Aminoquinoline is the first donor tested in this series. Both, when added before and after the catalyst activation, it does not interfere much with the polymerization, but it decreases the initiation rate significantly (Table 5.14, runs 30 and 31) as only one yttrium center out of seven or twelve grows a polymer chain, respectively. Therefore it seems likely, that yttrium centers become inactive in polymerization upon aminoquinoline coordination.
In case of phenanthroline a coordination species (**126**) could be crystallized (Figures 5.23 and 5.24, *vide infra*). Its addition hampers the polymerization significantly. Polyisoprene is only produced, when phenanthroline is added before activation, and even then with a small reaction rate. After 36 h full conversion is obtained. The resulting polymer (Table 5.14, run 33) matches that produced by the system without donor addition (Table 5.14, run I), except for the fact that the initiation deficiency is even higher and the MWD is multimodal. This observed ununiformity of the active species is in good agreement with the species, that has been crystallized as it cannot be the only product of the activation, due to stochiometric reasons (*vide infra*).
The final chelating bidentate ligand tested in this study is a bulky diimine: $(DippNCH)_2$ (Dipp = 2,4-diisopropylphenyl), referred as 'DiIm' in Table 5.14, runs IV and 35 (see Paper V as well). It was chosen in order to provide a more flexible ligand with a slightly less rigid distance between the donor atoms. The thereby applied steric bulk forces the terneric system to produce a highly 3,4-selective polyisoprene with both addition modes. The MWDs are multimodal and the polymerization rate is lower (esp., if DiIm is added after cocatalyst **B**).
A triangular set of donor atoms on a planar tridentate ligand is the last investigated motif. For this study, tetramethyl guanidine and thiourea are chosen. These ligands are intended to combine the coordination properties of the two ligand groups described so far and coordinate in a chelating and bridging fashion at the same time. For the guanidine, this coordination is confirmed, although only two of the three donor atoms coordinate to metal centers. A coordination structure could be crystallized and investigated by x-ray diffraction (Figure 5.25, *vide infra*). Independent of the addition order, the polymers

obtained from the terneric systems containing tetramethyl guanidine show unaffected microstructures with high yields (Table 5.14, runs 36 and 37) compared to the binary system $\mathbf{79^Y}$ / **B**. The terneric system initiates less chains, which results in a larger molecular weight average and a slightly increased PDI.
Polymerization in the presence of thiourea only takes place, when the additive is applied after the cocatalyst. Then a polymer in close proximity to that of the donor-free polymerization is obtained with slightly more active metal centers.

For the multidentate donors no small influences (as in some cases with monodentate donors) are observed. Ligands that interfere with the catalysis (benzoquinone and the investigated diimine) do affect the product to a large extent, while multimodal MWDs are frequently observed. Total disactivation occurs less often with the multidentate ligands than with the monodentate selection.

5.2.2.4 Crystal structures

Twice in this study, crystals suitable for x-ray diffractometry could be obtained from solutions of $\mathbf{79^Y}$ and the respective donor in a mixture of toluene and n-hexane, mimicking the situation before activation by the cocatalyst.
For phenanthroline, an excess of the donor was necessary to force crystallization. In that specific case, a monomeric complex (**126**) is obtained, bearing one remaining methyl moiety, but in total three phenanthroline derivatives, of which one is not coordinated to the metal center. For charge balance reasons, one of them must carry a negative charge. Although the quality of the structure is low and only connectivity pictures can be shown here (Figures 5.23 and 5.24), we suggest the moiety bound *via* N1 and N2 standing perpendicular to the Cp^* to be the phenanthrolid. It has lost its planarity (Figure 5.24), which aligns with losing its aromaticity by adopting a negative charge. Further lengths and angles cannot be discussed due to the low quality of the crystals. Such a complex is assumed to be a possible product of the reaction between $\mathbf{79^Y}$ and phenanthroline, when less of the additive is present (e.g. 1 equiv.). This could explain the ununiform polymeric outcome, as several different species would have to be formed besides this species, to provide it with three equivalents of the bidentate donor. Still,

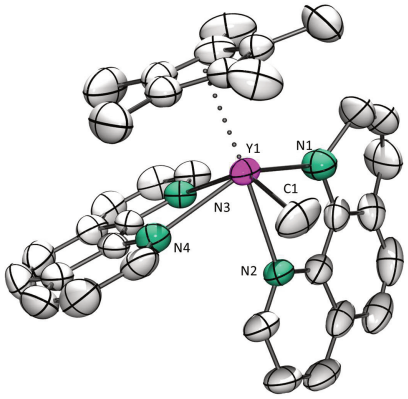

*Figure 5.23: ORTEP view of the connectivity of [Cp*Y(phtr)Me(phenanthrolid)] (**126**). Atomic displacement parameters are set at the 50 % probability level. Hydrogen atoms, one molecule of phenathroline and one molecule of toluene are omitted for clarity.*

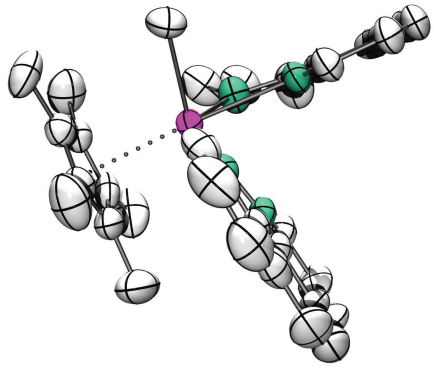

*Figure 5.24: ORTEP view of the molecular structure of [Cp*Y(phtr)Me(phenanthrolid)] (**126**). Atomic displacement parameters are set at the 50 % probability level. Hydrogen atoms, one molecule of phenathroline and one molecule of toluene are omitted for clarity. The structure has been turned to allow an impression of the non-planarity of the phenanthrolid ion.*

the high presence of phenanthroline derived moieties in this species can be due to the excess of the donor during synthesis. This would imply, that **126** is not present in the polymerization experiments.

For the application of a single equivalent of tetramethyl guanidine a dimeric complex is obtained (Figure 5.25). Again only one methyl moiety remains per yttrium atom, implying a negative charge for the guanidine, which bridges the two yttrium atoms with its immidic nitrogen (N2) and coordinates to one of the yttriums, with one of its dimethylamino units, while the other one points into open space. Due to the non-bridging binding mode of the methyl moiety, the distance between metal center and the methyl carbon is much smaller in this guanidine bridged dimer than in $\mathbf{79^{Y}}$ (and even smaller than in $\mathbf{79^{Lu}}$, Paper V). Furthermore, due to the bridging nitrogen, the interspace distance between the two yttrium centers of the dimer is enlarged by 0.4 Å. Surprisingly,

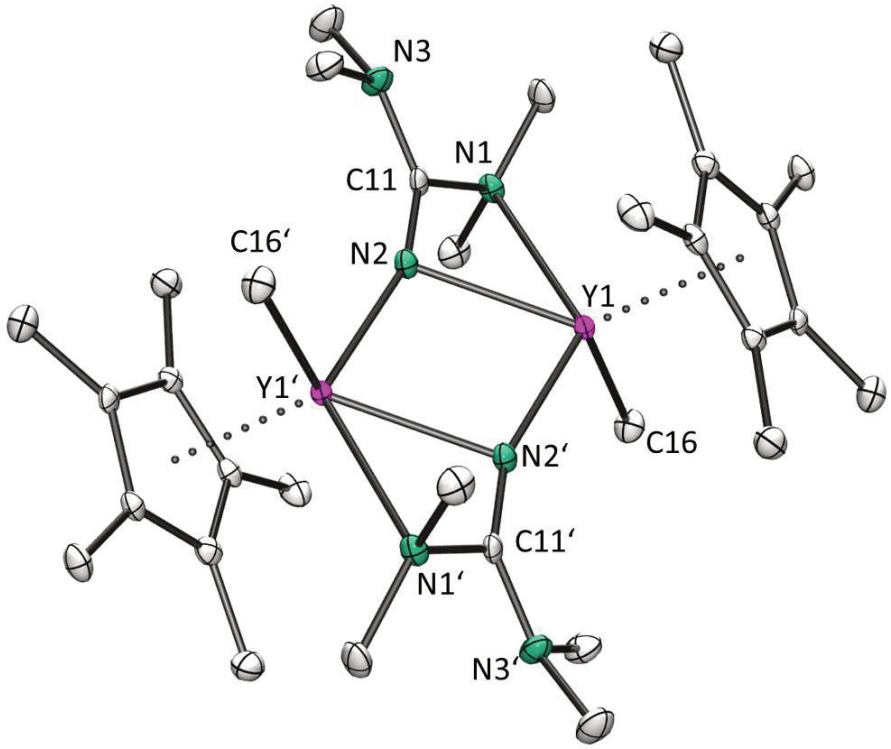

*Figure 5.25: ORTEP view of the molecular structure of [Cp*YMe(gua)]$_2$ (**127**). Atomic displacement parameters are set at the 50 % probability level. Hydrogen atoms are omitted for clarity. Selected lengths (Å) and angles (°): Y1-C16 2.422(3), Y1-Ct 2.395, N1-Y1 2.719(3), N1-C11 1.465(3), N2-Y1 2.278(2), N2-Y1' 2.372(2), N2-C11 1.277(3), ∠(N2-Y1-N2') 77.36(9), ∠(N2-Y1-N1) 54.42(7), ∠(N1-Y1-C16) 88.81(8), ∠(Ct-Y1-C16) 110.91, ∠(Ct-Y1-N1) 112.66.*

this does not affect the microstructure of the polymer produced by the terneric system **79$^{\mathbf{Y}}$ / B /** tetramethyl guanidine. It remains a subject to research if this would change with a longer prereaction time beween precatalyst and the additive.

5.2.3 Experimental Section

5.2.3.1 General Remarks

All operations were performed with rigorous exclusion of air and water, using standard Schlenk, high-vacuum, and argon glovebox techniques (MBraun MB 200B; < 1 ppm O_2, < 1 ppm H_2O). *n*-Hexane, toluene, diethyl ether and THF were purified by using Grubbs type columns (MBraun SPS-800, solvent purification system) and stored in a glovebox. $CDCl_3$ was purchased from Aldrich and used as received. Isoprene was obtained from Aldrich, dried over trioctylaluminum (Aldrich), and vacuum transferred prior to use. $[Ph_3C][B(C_6F_5)_4]$ and $[PhNMe_2H][B(C_6F_5)_4]$ were purchased from Boulder Scientific Company and used without any further purification. TBME was allowed to pump-freeze/thaw cycles prior to use. All other additives were purchased from Aldrich and used as received. The NMR spectra for polymer microstructure determination were recorded at 26 °C on a Bruker AVII+ 400 Avance (^{1}H: 400.11 MHz; ^{13}C: 100.61 MHz). ^{1}H and ^{13}C shifts are referenced to internal solvent resonances and reported in parts per million (ppm) relative to TMS. The molar masses (M_W and M_n) of the polymers were determined by size-exclusion chromatography (SEC). Sample solutions (1.0 mg polymer per mL THF) were filtered through a 0.45 µm syringe filter (PTFE) prior to injection. SEC was performed with a pump supplied by Viscotek (GPCmax VE 2001), employing ViscoGEL columns. Signals were detected by means of a triple detection array (TDA 305) and calibrated against polystyrene standards ($M_W/\ M_n < 1.15$). The flowrate was set to 1.0 mL min^{-1}. The microstructures of the polydienes were examined by means of ^{1}H and ^{13}C NMR experiments on the AVII+ 400 Avance spectrometers at ambient temperature, using $CDCl_3$ as a solvent. Glass transition temperatures of the polymers (T_g) were obtained applying a Perkin-Elmer DSC 8000 calibrated with indium and cyclohexane standards, scanning from -100 °C up to +100 °C with heating rates of 20 K/min and cooling rates of 60 K/min in N_2 atmosphere, if not mentioned otherwise. Precursor $[Cp^*LnlMe_2)]_3$ was synthesized according to literature methods.[4,5]

Single crystals were selected, coated with Parabar 10312 (previously known as Paratone N) and fixed on a microloop. Data were collected on a Bruker APEX DUO instrument equipped with an IμS microfocus sealed tube and QUAZAR optics for MoK_α radiation ($\lambda = 0.71073$ Å). The Data collection strategy was determined using COSMO[6] employing

ω- and φ scans. Raw data were processed using APEX[7] and SAINT[8], corrections for absorption effects were applied using SADABS.[9] The structures were solved by direct methods and refined against all data by full-matrix least-squares methods on F^2 using SHELXTL[10,11] and Shelxle.[12]

5.2.3.2 Polymerization of isoprene

5.2.3.2.1 Method 1

This method is referred as addition order 'a' in Tables 5.13 and 5.14.
A detailed polymerization procedure is described as a typical example. (Table 5.13, run 1) 0.02 mmol (1 equiv. per Y center) of the additive (here 1.6 µL of THF) were added to a solution of **79$^{\mathbf{Y}}$** (5 mg, 0.007 mmol, 0.020 mmol of Y centers)) in toluene (8 mL) and the mixture was aged at ambient temperature for 5 min. Then, $[PhNMe_2H][B(C_6F_5)_4]$ (**B**) (16 mg, 0.02 mmol 1 equiv. per Y center) was added and the mixture was aged for further 30 min. After the addition of isoprene (1.36 g, 20 mmol), the polymerization was carried out at 25 °C for 1 h. The reaction was terminated by pouring the polymerization mixture into 25 mL of methanol containing 0.1 % (w/w) 2,6-di-*tert*-butyl-4-methylphenole (BHT) as a stabilizer and stirred for 1 h. The polymer was washed with methanol and dried under vacuum at ambient temperature to constant weight.

5.2.3.2.2 Method 2

This method is referred as addition order 'b' in Tables 5.13 and 5.14.
A detailed polymerization procedure is described as a typical example. (Table 5.13, run 6) $[Ph_3C][B(C_6F_5)_4]$ (**A**) (18 mg, 0.02 mmol 1 equiv. per Y center) was added to a solution of **79$^{\mathbf{Y}}$** (5 mg, 0.007 mmol, 0.020 mmol of Y centers)) in toluene (8 mL) and the mixture was aged for 25 min (prereaction) at ambient temperature. 5 min after the addition of 0.02 mmol (1 equiv. per Y center) of the additive (here 4.4 mg of 2,6-di-*tert*-butyl-4-methylphenole (BHT)), isoprene (1.36 g, 20 mmol), was added, and the polymerization was carried out at 25 °C for 1 h. The reaction was terminated by pouring the polymerization mixture into 25 mL of methanol containing 0.1 % (w/w) 2,6-di-*tert*-butyl-4-methylphenole (BHT) as a stabilizer and stirred for 1 h. The polymer

was washed with methanol and dried under vacuum at ambient temperature to constant weight.

5.2.3.3 Synthesis of [Cp*Y(phtr)Me(phenanthrolid)] (126)

In a glovebox, 288 mg of phenathroline (1.6 mmol) were added to a solution of 40 mg (0.053 mmol) of **79$^{\mathbf{Y}}$** in 8 mL of toluene. The reaction mixture was stirred for 5 min. The product was crystallized from a mixture of toluene and few drops of *n*-hexane at -40 °C.

5.2.3.4 Synthesis of [Cp*YMe(gua)]$_2$ (127)

In a glovebox, 18.4 mg of phenathroline (0.16 mmol) were added to a solution of 40 mg (0.053 mmol) of **79$^{\mathbf{Y}}$** in 8 mL of toluene. The reaction mixture was stirred for 5 min. The product was crystallized from a mixture of toluene and few drops of *n*-hexane at -40 °C. The product decomposed upon removal of the solvent in *vacuo*.

5.2.3.5 Crystal Structure

*Table 5.15: Crystal data and structure refinement for **127**.*

	127
CCDC	
Empirical formula	$C_{32}H_{60}N_6Y_2$
M_W [g *cdot* mol^{-1}]	706.68
T [K]	173(2)
Wavelength [Å]	0.71073
Crystal System	Monoclinic
Space Group	$P2_1/n$
a [Å]	10.295(6)
b [Å]	11.080(6)
c [Å]	15.591(9)
α [°]	90
β [°]	100.704(11)
γ [°]	90
Volume [Å^3]	1747.5(17)
Z	2
Density (calc) [mg ·mm^{-3}]	1.343
Absorption coefficient	3.333
Theta range [°]	2.279 to 27.24
Reflections	37893
Independent reflections	4341 (R_{int} = 0.0944)
Data / Restraints / Parameters	4341 / 0 / 191
R_1(obs)[a]	0.0319
wR_2(all)[b]	0.0741

[a] Final R indices [I > 2σ (I)];
[b] R indices (all data).

5.2.4 Conclusion

Both monodentate and multidentate donor ligands have been tested as additives to the isoprene polymerization of $[Cp^*YMe_2]_3$ and $[PhNHMe_2][B(C_6F_5)_4]$. All donors show individual influences, if any, on the polymerization without clear trends. In terms of microstructure, benzoquinone and $(DippNC(H))_2$ (Dipp = 2,4-diisopropylphenyl) have the highest impact, shifting toward 1,4-*cis* and 3,4-addition respectively, but cause low initiation rates and multimodal molecular weight distributions.

Supressing the known crosslinking behavior for the system $[Cp^*YMe_2]_3$ / $[Ph_3C][B(C_6F_5)_4]$ is most likely to be successful, when BHT is added to the precatalyst before activation although the polymerization rates decrease enormously. Interestingly, addition of ten equivalents (per yttrium center) of the radical scavengers BHT and benzoquinone results in highly 1,4-*trans*-selective microstructures.

Crystal structures / connectivities of a tetramethyl guanidine and a phenanthroline addition product have been obtained and are provided.

References

[1] Tobisch, S.; Bögel, H.; Taube, R. *Organometallics* **1996**, *15*, 3563–3571.

[2] Taube, R. In *Catalytic reaction mechanisms and structur-reactivity-relationships in the stereospecific butadiene polymerization*; Kaminsky, W., Ed.; Springer Berlin, 1999; Chapter Metalorganic Catalysts for Synthesis and Polymerization, pp 531–547.

[3] Jende, L. N. Ph.D. Thesis, Eberhard Karls Universität Tübingen, **2015**.

[4] Dietrich, H. M.; Zapilko, C.; Herdtweck, E.; Anwander, R. *Organometallics* **2005**, *24*, 5767–5771.

[5] Dietrich, H. M.; Grove, H.; Törnroos, K. W.; Anwander, R. *J. Am. Chem. Soc.* **2006**, *128*, 1458–1459.

[6] Bruker AXS Inc, Madison, WI, 2012.

[7] Bruker AXS Inc., Madison, WI, 2016.

[8] Bruker AXS Inc., Madison, WI, 2015.

[9] Krause, L.; Herbst-Irmer, R.; Sheldrick, G. M.; D., S. *J. Appl. Cryst.* **2015**, *48*, 3.

[10] SHELXTL, *Acta Cryst.* **2015**, *A71*, 3–8.

[11] Scheldrick, G. M. *Program for crystal structure refinement*; SHELXL-97, 1997.

[12] Hübschle, C. B.; Sheldrick, G. M.; Dittrich, B. *J. Appl. Cryst.* **2011**, *44*, 1281–1284.

5.2.5 Acknowledgement

Coauthors in case of publication: Daniel Werner, Cäcilia Maichle-Mössmer, Reiner Anwander. The authors thank Deutsche Forschungsgemeinschaft for funding this work.

Manuscript III: Polymerization Studies on $Tp^{tBu,\,Me}$ Rare-Earth Metal Dimethyls

5.3.1 Introduction

Rare earth metal dialkyls bearing a pentamethylcyclopentadienyl (Cp^*) ligand have been tested for their 1,3-diene polymerization properties recently (Paper V). In order to compare their performance with analogue complexes bearing larger spectator ligands, as previously investigated for the rare earth boryl alkylaluminates (Papers I and III),[1,2] hydro-*tris*-(3-*tert*butyl-5-methyl-pyrazolyl)borate scorpionate systems ($Tp^{tBu,\,Me}LnMe_2$, Ln = Y, Ho, Lu), as well as mono-tetramethylaluminate and tetramethylgallate complexes ($Tp^{tBu,\,Me}LnMe(EMe_4)$, Ln = Y, Ho, Lu, E = Al, Ga) and *bis*-trimethylaluminate complexes ($Tp^{tBu,\,Me}Ln(HAlMe_3)_2$, Ln = Y, Ho) are applied as precatalysts in isoprene polymerization.

5.3.2 Results and Discussion

The hydro-*tris*-(3-*tert*butyl-5-methyl-pyrazolyl)borate ($Tp^{tBu,\,Me}$) systems ($Tp^{tBu,\,Me}LnMe_2$, Ln = Y, Ho, Lu, (**128**)), their mono-tetramethylaluminate and tetramethylgallate analoga ($Tp^{tBu,\,Me}LnMe(EMe_4)$, Ln = Y, Ho, Lu; E = Al, Ga (**129** and **130**) and $Tp^{tBu,\,Me}Ln(HAlMe_3)_2$, (Ln = Y, Lu (**131**)) (Scheme 5.6) have been synthesized according to literature procedures[3–5] and applied in the polymerization of isoprene. As the $Tp^{tBu,\,Me}$ ligand is known to undergo degradation reactions in toluene,[2,6] special precautions have to be taken to minimize pollution of the active polymerization catalyst species by side products. Therefore, three approaches were investigated. Firstly, the prereaction time was reduced (compared to the 30 min applied in the studies Cp^* ligands, *vide supra*) to 5 min. Secondly, inspired by the work of Zhaomin Hou (see ref. 11 as an example), the addition order was changed in case of the mono-tetramethylaluminates. Here, the co-catalyst is added to a solution of the respective $Tp^{tBu,\,Me}$ precatalyst and the monomer in toluene. The precatalysts were tested as single component catalysts and showed no polymerization activity. Thus, this method is applicable, as no polymerization before cocatalyst addition has to be expected. Finally, in one case, (Run 30b) a polymerization without any prereaction time was attempted. Hereby it is assumed that the active catalyst formed *in situ*.

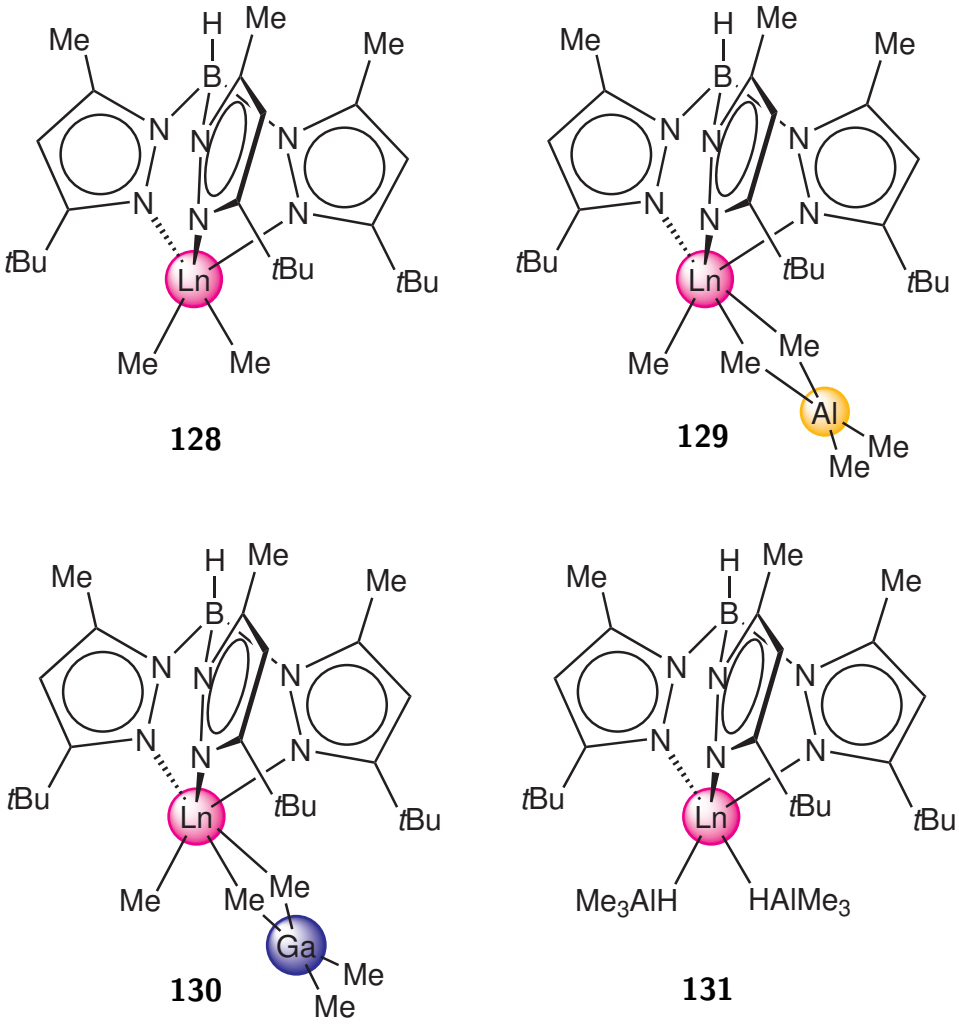

*Scheme 5.6: Hydro-tris-(3-tertbutyl-5-methyl-pyrazolyl)borate ($Tp^{tBu,\ Me}$) precatalysts applied in this study: [$Tp^{tBu,\ Me}LnMe_2$], (Ln = Y, Ho, Lu; (**128**)), [$Tp^{tBu,\ Me}LnMe(AlMe_4)$], (Ln = Y, Ho, Lu; (**129**)), [$Tp^{tBu,\ Me}LnMe(GaMe_4)$] (Ln = Y, Ho; (**130**)) and [$Tp^{tBu,\ Me}Ln(HAlMe_3)_2$] (Ln = Y, Ho; (**131**)).*

5.3.2.1 Polymerizations by $Tp^{tBu,\ Me}$ Rare Earth Metal Dimethyls

*Table 5.16: Isoprene homopolymerization by $Tp^{tBu,\ Me}$ rare earth dimethyls **128**.*

Entry[a]	Precatalyst	Cocatalyst[b]	T [°C]	t [min]	Method	Yield[d] [%]	*cis*[e] [%]	*trans*[e] [%]	3,4[e] [%]	$M_{n,SEC}$[f] [10^4g·mol^{-1}]	PDI[f]	T_g [°C]
1	$Tp^{tBu,\ Me}YMe_2$ (**128^{Y}**)	**A**	25	60	1	93	71	2	27	37.2	2.07	-46
2	$Tp^{tBu,\ Me}YMe_2$ (**128^{Y}**)	**B**	25	60	1	5	71	0	29	81.1	1.52	-44
3	$Tp^{tBu,\ Me}YMe_2$ (**128^{Y}**)	**C**	25	60	1	traces[h]	91	0	9	-[h]	-[h]	-[h]
4	$Tp^{tBu,\ Me}HoMe_2$ (**128^{Ho}**)	**A**	25	60	1	97	71	0	29	27.6	2.85	-45
5	$Tp^{tBu,\ Me}HoMe_2$ (**128^{Ho}**)	**B**	25	60	1	93	71	0	29	26.7	2.96	-43
6	$Tp^{tBu,\ Me}HoMe_2$ (**128^{Ho}**)	**C**	25	60	1	4	92	0	8	41.3	1.72	-57
7	$Tp^{tBu,\ Me}LuMe_2$ (**128^{Lu}**)	**A**	25	60	1	90	73	0	27	-[i]	-[i]	-43
8	$Tp^{tBu,\ Me}LuMe_2$ (**128^{Lu}**)	**B**	25	60	1	6	67	5	29	42.5	1.99	-47
9	$Tp^{tBu,\ Me}LuMe_2$ (**128^{Lu}**)	**C**	25	60	1	none[h]	-[h]	-[h]	-[h]	-[h]	-[h]	-[h]

[a] Conditions: 20 µmol of precatalyst, 20 µmol of cocatalyst, 20 mmol of isoprene, 8 mL of toluene.
[b] **A** = $[Ph_3C][B(C_6F_5)_4]$, **B** = $[PhNHMe_2][B(C_6F_5)_4]$, **C** = $B(C_6F_5)_3$.
[c] see Supporting Information for details: 1 = Standard procedure applying 5 min of prereaction time.
[d] Yield of the isolated polymer.
[e] Determined by ^{1}H and ^{13}C NMR spectroscopy.
[f] Determined by GPC in THF at 35 °C.
[g] Determined by DSC.
[h] Evaluation impossible due to low yield.
[i] Product polymer was insoluble in THF.

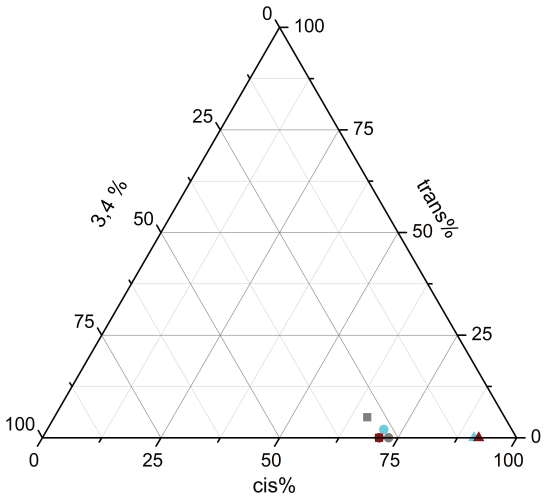

*Chart 5.8: Ternary plot of the microstructures of the polyisoprenes obtained from [Tp$^{tBu,\ Me}$LnMe$_2$] (**128^{Ln}**). Polymers produced applying cocatalyst **A** are represented by circles, those produced with cocatalyst **B** by squares and products of activations with cocatalyst **C** are represented by triangles. The metal centers of the precatalyst is color-coded as follows: brown (Ho), cyan (Y), and grey (Lu).*

The isoprene polymerization catalyzed by Tp$^{tBu,\ Me}$ rare earth dimethyls (**128**) is tested for the respective yttrium, holmium and lutetium derivatives (Table 5.16, Chart 5.8). The application of both borate cocatalysts [Ph$_3$C][B(C$_6$F$_5$)$_4$] (**A**) and [PhNHMe$_2$][B(C$_6$F$_5$)$_4$] (**B**) leads to similar and non-metal-dependent microstructures (*cis* / *trans* / 3,4 ≈ 70 / 0 / 30 %) after 1 h. This indicates similar species as active catalyst for all three lanthanides.

Instead, the main influence of the respective rare earth metal lies within the initiation process. Here, the polymers vary significantly. Especially the reproducibly occuring difference between the Y and the Ho derivative stands out. The polymers of catalysts of these metals are expected to be almost identical due to their similar ion size. Surprisingly, the obtained polymeric results vary significantly. The MWDs obtained from the holmium derivative are broader and initiate more chains to grow than the yttrium analogue. Besides that, the system **128^{Y} / B** does barely produce any polymer. So far, the respective reasons must remain a matter of research. Besides this result a decreasing initiation efficiency with decreasing ion size is observed, as well as a decreasing polydispersity. The insolubility of the polymer produced by the system **128^{Lu} / A** is

ascribed to potential crosslinking (*cf.* Paper V).
The application of the neutral cocatalyst $[B(C_6F_5)_3]$ (**C**) produces only much slower active systems. Only in case of Ln = Ho, after 1 h enough polymer for microstructural analysis by NMR spectroscopy was obtained. Interestingly, a very *cis*-selective polymer is observed, which leads to the conclusion that the nature of the prefluoroarylborate anion ($[RB(C_6F_5)_3]^-$, less bulky in case of cocatalyst **C** compared to **A** and **B**) and its properties regarding interaction with the catalytically active cation play another major role in the polymerization with these systems. A further possible explanation for these findings would suggest a κ^2 binding mode of the $Tp^{tBu,\,Me}$ ligand with the remaining pyrazolyl moiety binding to the boron of $[B(C_6F_5)_3]$ (**C**) (Scheme 5.7, Supporting Information). This would then cause much less steric bulk around the catalytically active lanthanide center and therefore favor the 1,4-*cis*-addition.
The relatively high PDI are presumed to be caused by the degradation reactions, the $Tp^{tBu,\,Me}$ ligands of the active catalysts undergo (*vide supra*). They imply both the possibility of a simultanious presence of several active species as well as an ongoing destruction of active catalysts. In contrast to the Cp^* analoga (Paper V and Manuscript I) the $Tp^{tBu,\,Me}$ dimethyls do not form multimeric complexes, apparently due to the bulkier ligand. Interestingly, this monomeric nature leads to active species that demand less space than in the Cp^* case, which is indicated by the production of much more 1,4-*cis*-selective isoprene polymers. Theoretical studies by Hou and coworkers predicted such 1,4-cis-selective polymerizations for Cp^* systems as well, if they were accessible as monomers.[7]
This steric bulk of the $Tp^{tBu,\,Me}$-ligand is also the reason, why in contrast to Cp^*, only one of the two methyl ligands of the dimethyls (**128**) can react with $AlMe_3$ to form a tetramethylaluminate anion. Therefore, cationization of $Tp^{tBu,\,Me}LnMe(AlMe_4)$, (Ln = Y, Ho, Lu; **129**) by simple abstraction of the remaining methyl moiety (without release of $AlMe_3$) is possible. This would lead to a relatively bulky active species and therefore disable or at least impede the space-demanding *cis*-addition.[8–10]

5.3.2.2 Polymerizations by $Tp^{tBu,\ Me}$ Rare Earth Metal Tetramethylaluminates

*Table 5.17: Isoprene homopolymerization by $Tp^{tBu,\ Me}$ rare earth tetramethylaluminates **129**.*

Entry[a]	Precatalyst	Cocatalyst[b]	T [°C]	t [min]	Method[c]	Yield[d] [%]	*cis*[e] [%]	*trans*[e] [%]	3,4[e] [%]	$M_{n,SEC}$[f] [10^4g·mol^{-1}]	PDI[f]	T_g [°C]
10	$Tp^{tBu,\ Me}$YMe($AlMe_4$) (**129^{Y}**)	**A**	25	60	1	97	78	10	12	17.3	1.94	-60
10a	$Tp^{tBu,\ Me}$YMe($AlMe_4$) (**129^{Y}**)	**A**	25	60	2	34	75	7	18	19.1	2.20	-54
11	$Tp^{tBu,\ Me}$YMe($AlMe_4$) (**129^{Y}**)	**B**	25	60	1	96	32	42	26	24.4	2.94	-49
11a	$Tp^{tBu,\ Me}$YMe($AlMe_4$) (**129^{Y}**)	**B**	25	60	2	88	68	6	26	46.7	2.44	-47
12	$Tp^{tBu,\ Me}$YMe($AlMe_4$) (**129^{Y}**)	**C**	25	60	1	none[h]	-[h]	-[h]	-[h]	-[h]	-[h]	-[h]
12a	$Tp^{tBu,\ Me}$YMe($AlMe_4$) (**129^{Y}**)	**C**	25	60	2	none[h]	-[h]	-[h]	-[h]	-[h]	-[h]	-[h]
13	$Tp^{tBu,\ Me}$HoMe($AlMe_4$) (**129^{Ho}**)	**A**	25	60	1	93	87	0	13	28.3	1.75	-54
14	$Tp^{tBu,\ Me}$HoMe($AlMe_4$) (**129^{Ho}**)	**B**	25	60	1	92	72	0	28	23.5	3.33	-44
15	$Tp^{tBu,\ Me}$HoMe($AlMe_4$) (**129^{Ho}**)	**C**	25	60	1	none[h]	-[h]	-[h]	-[h]	-[h]	-[h]	-[h]
16[i]	$Tp^{tBu,\ Me}$LuMe($AlMe_4$) (**129^{Lu}**)	**A**	25	60	1	none[h]	-[h]	-[h]	-[h]	-[h]	-[h]	-[h]
17[i]	$Tp^{tBu,\ Me}$LuMe($AlMe_4$) (**129^{Lu}**)	**B**	25	60	1	90	64	16	20	15.3	2.40	-52
17a	$Tp^{tBu,\ Me}$LuMe($AlMe_4$) (**129^{Lu}**)	**B**	25	60	2	81	66	9	25	26.6	1.98	-49
18	$Tp^{tBu,\ Me}$LuMe($AlMe_4$) (**129^{Lu}**)	**C**	25	60	1	none[h]	-[h]	-[h]	-[h]	-[h]	-[h]	-[h]

[a] Conditions: 20 µmol of precatalyst, 20 µmol of cocatalyst, 20 mmol of isoprene, 8 mL of toluene.
[b] ẽxtbfA = $[Ph_3C][B(C_6F_5)_4]$, **B** = $[PhNHMe_2][B(C_6F_5)_4]$, **C** = $B(C_6F_5)_3$.
[c] see Supporting Information for details: 1 = Standard procedure applying 5 min of prereaction time. 2 = the method inspired by Hou and coworkers.[11]
[d] Yield of the isolated polymer.
[e] Determined by ^{1}H and ^{13}C NMR spectroscopy.
[f] Determined by GPC in THF at 35 °C.
[g] Determined by DSC.
[h] Evaluation impossible due to low yield.
[i] These polymers have been presented in Section , paper III, ref. 2 and are shown here for comparison.

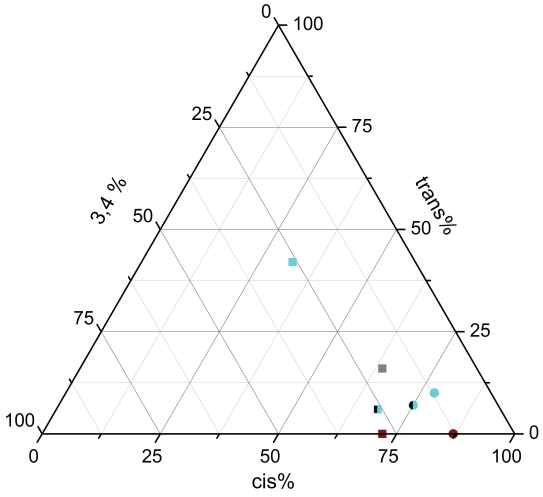

*Chart 5.9: Ternary plot of the microstructures of the polyisoprenes obtained from [Tp$^{tBu,\ Me}$LnMe(AlMe$_4$)] (**129^{Ln}**). Polymers produced applying cocatalyst **A** are represented by circles, those produced with cocatalyst **B** by squares and products of activations with cocatalyst **C** are represented by triangles. The metal centers of the precatalyst is color-coded as follows: brown (Ho), cyan (Y), and grey (Lu). Non-blackened symbols were produced applying Method 1, half-blackened symbols mark runs, performed according to method 2 (see Table 5.17, Tablenote c).*

Indeed, regarding the polymerization results (Table 5.17, Chart 5.9), the system **129^{Y} / B** reproducibly forms a polymer standing out from the series by a relatively high 1,4-*trans* content (Table 5.17, run 11). The other polymers show a much smaller shift towards 1,4-*trans* addition, as well, when compared to the dimethyls (Table 5.16). Free $AlMe_3$ is known to cause such behavior (*cf.* Paper V). So there it seems likely, that the $AlMe_3$ is released during the activation process. In case of **129^{Y} / B** instead, an activation without release of $AlMe_3$ is assumed.

In general, the *cis*-content still slightly decreases with decreasing ion size. For Ln = Ho, Lu with **B**, the shift towards 1,4-*trans* linkages as mentioned above does reproducibly not occur. Notably, **129^{Lu} / A** does not yield any polymer. This is assumed to be due to steric hinderence. Bulky $[Ph_3C]^+$ can probably not interact with the methyl moiety, it would need to abstract for cationization, due to the metal center being located to deep in the pocket created by Tp$^{tBu,\ Me}$ ligand.[2]

With these systems, the alternate activation procedure introduced by Hou and cowor-

kers[11] was tested. Here, precatalyst activation is intended to happen in the presence of the monomer. Comparing the obtained polymer data, to that resulting from the 'classic' activation approach reveals only slight differences for **129^{Lu} / B** (Table 5.17, runs 17 and 17a). With **129^{Y}** instead, two major influences of the addition order become visible: In case of activation by cocatalyst **A**, the yield is reduced drastically, when activated in the presence of monomer, while the degree of polymerization remains rather constant. This implies a much lower initiation efficiency, which can be explained by monomer molecules coordinating to the metal center prior to cationization. Interaction (activation) with the trityl cation would then be less likely, due to steric hindrance. In case of cocatalyst **B** the 1,4-*trans* shift observed with the original activation procedure does not take place. Monomer coordination prior to cationization here is assumed to cause the sterical necessity to release $AlMe_3$ either in the process of cationization or in the formation of the propagation species.

In all cases, the application of cocatalyst **C** did not yield any polymer.

The steric bulk of trimethylaluminate moieties is in contrast to that of the tetramethylaluminates small enough to allow the coordination of two such ligands to the Ln center (Ln = Y, Lu) in the presence of $Tp^{tBu,\,Me}$ forming $[Tp^{tBu,\,Me}Ln(HAlMe_3)_2]$ (**131^{Ln}**).[4] When tetramethylaluminates are seen as 'methyls in disguise' these trimethylaluminates should react as 'hydrids in disguise' likewise. Upon activation by cationization, next to the formation of the respective activation side product (Ph_3CH in case of cocatalyst **A**, H_2 in case of cocatalyst **B** and none in case of cocatalyst **C**), the precatalysts (**131**) necessarily releases at least one equivalent of $AlMe_3$. Both the steric bulk of the remaining cation $[Tp^{tBu,\,Me}Ln(HAlMe_3)]^+$ and the presence of $AlMe_3$ in the polymerization reaction mixture cause a more 1,4-*trans*-selective microstructure (compared to the dimethyls (**128**) and tetramethylaluminates (**129**) as obtained with these catalysts (Table 5.18, Chart 5.10). Hence, the microstructural selectivities are similar to those known from Cp^* *bis*-tetramethylaluminates,[1,12] except for **131^{Y} / B** and its counterpart.

5.3.2.3 Polymerization by $Tp^{tBu,\ Me}$ Rare Earth Metal Trimethylaluminates

*Table 5.18: Isoprene homopolymerization by $Tp^{tBu,\ Me}$ rare earth trimethylaluminates **131**.*

Entry[a]	Precatalyst	Cocatalyst[b]	T [°C]	t [min]	Method[c]	Yield[d] [%]	*cis*[e] [%]	*trans*[e] [%]	3,4[e] [%]	$M_{n,SEC}$[f] [10^4g·mol^{-1}]	PDI[f]	T_g [°C]
19	$Tp^{tBu,\ Me}Y(HAlMe_3)_2$ (**131^{Y}**)	**A**	25	60	1	72	60	31	9	13.6	1.56	-58
19a	$Tp^{tBu,\ Me}Y(HAlMe_3)_2$ (**131^{Y}**)	**A**	25	60	2	48	56	34	10	8.9	1.35	-58
20	$Tp^{tBu,\ Me}Y(HAlMe_3)_2$ (**131^{Y}**)	**B**	25	60	1	70	58	28	14	9.3	1.38	-55
20a	$Tp^{tBu,\ Me}Y(HAlMe_3)_2$ (**131^{Y}**)	**B**	25	60	2	52	59	27	14	6.4	1.56	-57
21	$Tp^{tBu,\ Me}Y(HAlMe_3)_2$ (**131^{Y}**)	**C**	25	60	1	traces[h]	-[h]	-[h]	-[h]	-[h]	-[h]	-[h]
21a	$Tp^{tBu,\ Me}Y(HAlMe_3)_2$ (**131^{Y}**)	**C**	25	60	2	traces[h]	-[h]	-[h]	-[h]	-[h]	-[h]	-[h]
22	$Tp^{tBu,\ Me}Y(HAlMe_3)_2$ (**131^{Y}**)	**C**	25	720	1	27	62	29	9	9.4	1.77	-59
22a	$Tp^{tBu,\ Me}Y(HAlMe_3)_2$ (**131^{Y}**)	**C**	25	720	2	2	71	21	8	1.3	2.73	-61
23	$Tp^{tBu,\ Me}Y(HAlMe_3)_2$ (**131^{Y}**)	**A**	80	60	2	79	50	40	10	14.3	1.68	-59
24	$Tp^{tBu,\ Me}Y(HAlMe_3)_2$ (**131^{Y}**)	**B**	80	60	2	29	53	35	12	7.0	1.59	-57
25	$Tp^{tBu,\ Me}Y(HAlMe_3)_2$ (**131^{Y}**)	**C**	80	60	2	none[h]	-[h]	-[h]	-[h]	-[h]	-[h]	-[h]
26	$Tp^{tBu,\ Me}Lu(HAlMe_3)_2$ (**131^{Lu}**)	**A**	25	60	1	5	77	16	7	2.8	1.43	-62
27	$Tp^{tBu,\ Me}Lu(HAlMe_3)_2$ (**131^{Lu}**)	**B**	25	60	1	20	70	16	14	3.3	1.40	-58
28	$Tp^{tBu,\ Me}Lu(HAlMe_3)_2$ (**131^{Lu}**)	**C**	25	60	1	none[h]	-[h]	-[h]	-[h]	-[h]	-[h]	-[h]

[a] Conditions: 20 µmol of precatalyst, 20 µmol of cocatalyst, 20 mmol of isoprene, 8 mL of toluene.
[b] **A** = $[Ph_3C][B(C_6F_5)_4]$, **B** = $[PhNHMe_2][B(C_6F_5)_4]$, **C** = $B(C_6F_5)_3$.
[c] see Supporting Information for details: 1 = Standard procedure applying 5 min of prereaction time. 2 = the method inspired by Hou and coworkers.[11]
[d] Yield of the isolated polymer.
[e] Determined by ^{1}H and ^{13}C NMR spectroscopy.
[f] Determined by GPC in THF at 35 °C.
[g] Determined by DSC.
[h] Evaluation impossible due to low yield.

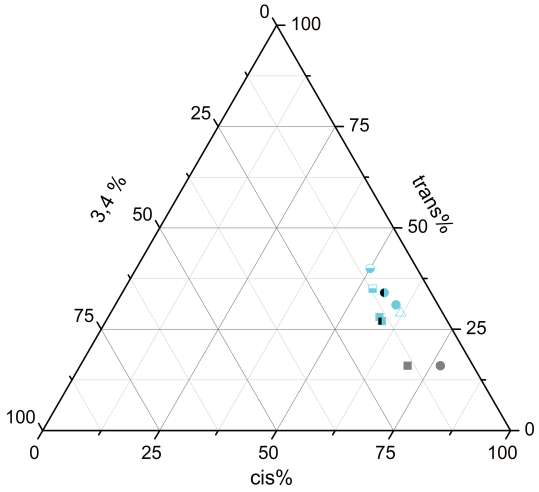

*Chart 5.10: Ternary plot of the microstructures of the polyisoprenes obtained from [Tp$^{tBu,\ Me}$Ln(HAlMe$_3$)$_2$] (**131^{Ln}**). Polymers produced applying cocatalyst **A** are represented by circles, those produced with cocatalyst **B** by squares and products of activations with cocatalyst **C** are represented by triangles. The metal centers of the precatalyst is color-coded as follows: cyan (Y), and grey (Lu). Polymers represented by non-blackened symbols were produced applying Method 1, vertically half-blackened symbols mark runs, performed according to method 2 (see Table 5.18, Tablenote c). Horizontally half-whitened symbols mark polymers produced at a reaction temperature of 80 °C. Solid symbols mark reaction times of 1 h, hollow symbols mark reaction times of 24 h.*

Once again cocatalsyt **C** shows to be much less reactive, but a slightly higher 1,4-*cis*-content (Table 5.18, run 22). Interestingly, polymers produced by **131^{Lu}** (Table 5.18, runs 26–28) show a higher 1,4-*cis*-content as those obtained from the yttrium centered analogue. So, although the ion size of lutetium is significantly smaller, the active species must provide more steric space for monomer coordination. A possible explanation is the release of the second $AlMe_3$ with the first monomer coordination.
Regarding those polymers produced by applying the procedure inspired by Hou and coworkers, no significant differences in microstructure can be observed, besides a smaller overall yield. Again, monomer coordination is assumed to lower the rate of initiation. Attempts to overcome this potential flaw by polymerization at higher temperature (80 °C, Table 5.18, runs 23–25) are only successful, for cocatalyst **A**. Cocatalyst **B** produces an even lower yield. For both cocatalysts the microstructure is slightly less 1,4-*cis*-selective.

5.3.2.4 Polymerization by $Tp^{tBu,\ Me}$ Rare Earth Metal Tetramethylgallates

*Table 5.19: Isoprene homopolymerization by $Tp^{tBu,\ Me}$ rare earth tetramethylgallates **130**.*

Entry[a]	Precatalyst	Cocatalyst[b]	T [°C]	t [min]	Method[c]	Yield[d] [%]	*cis*[e] [%]	*trans*[e] [%]	3,4[e] [%]	$M_{n,SEC}$[f] [10^4 g·mol^{-1}]	PDI[f]	T_g [°C]
29	$Tp^{tBu,\ Me}$YMe($GaMe_4$) (**130^{Y}**)	**A**	25	60	1	89	62	19	19	16.9	2.53	-53
29a	$Tp^{tBu,\ Me}$YMe($GaMe_4$) (**130^{Y}**)	**A**	25	60	2	92	67	9	24	19.8	2.39	-49
30	$Tp^{tBu,\ Me}$YMe($GaMe_4$) (**130^{Y}**)	**B**	25	60	1	87	61	17	22	10.8	2.91	-49
30a	$Tp^{tBu,\ Me}$YMe($GaMe_4$) (**130^{Y}**)	**B**	25	60	2	88	62	14	24	17.9	2.40	-48
30b	$Tp^{tBu,\ Me}$YMe($GaMe_4$) (**130^{Y}**)	**B**	25	60	3	59	62	16	23	24.4	2.48	-49
31	$Tp^{tBu,\ Me}$YMe($GaMe_4$) (**130^{Y}**)	**C**	25	60	1	none[h]	-[h]	-[h]	-[h]	-[h]	-[h]	-[h]
31a	$Tp^{tBu,\ Me}$YMe($GaMe_4$) (**130^{Y}**)	**C**	25	60	2	none[h]	-[h]	-[h]	-[h]	-[h]	-[h]	-[h]
32	$Tp^{tBu,\ Me}$HoMe($GaMe_4$) (**130^{Ho}**)	**A**	25	60	1	95	58	19	23	18.1	2.81	-51
33	$Tp^{tBu,\ Me}$HoMe($GaMe_4$) (**130^{Ho}**)	**B**	25	60	1	96	64	11	25	17.0	2.44	-51
34	$Tp^{tBu,\ Me}$HoMe($GaMe_4$) (**130^{Ho}**)	**C**	25	60	1	traces[h]	-[h]	-[h]	-[h]	-[h]	-[h]	-[h]

[a] Conditions: 20 µmol of precatalyst, 20 µmol of cocatalyst, 20 mmol of isoprene, 8 mL of toluene.
[b] **A** = $[Ph_3C][B(C_6F_5)_4]$, **B** = $[PhNHMe_2][B(C_6F_5)_4]$, **C** = $B(C_6F_5)_3$.
[c] see Supporting Information for details: 1 = Standard procedure applying 5 min of prereaction time. 2 = the method inspired by Hou and coworkers.[11] 3 = Standart procedure applying no prereaction time.
[d] Yield of the isolated polymer.
[e] Determined by ^{1}H and ^{13}C NMR spectroscopy.
[f] Determined by GPC in THF at 35 °C.
[g] Determined by DSC.
[h] Evaluation impossible due to low yield.

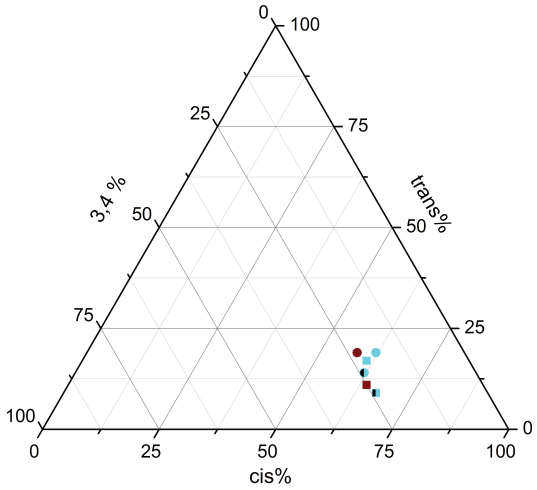

*Chart 5.11: Ternary plot of the microstructures of the polyisoprenes obtained from [Tp$^{tBu,\ Me}$LnMe(GaMe$_4$)] (**130^{Ln}**). Polymers produced applying cocatalyst **A** are represented by circles, those produced with cocatalyst **B** by squares and products of activations with cocatalyst **C** are represented by triangles. The metal centers of the precatalyst is color-coded as follows: brown (Ho), and cyan (Y). Polymers represented by non-blackened symbols were produced applying Method 1, half-blackened symbols mark runs, performed according to method 2 (see Table 5.18, Tablenote c).*

The final ligand set investigated in this study are mono-tetramethylgallates Tp$^{t\mathrm{Bu,\ Me}}$LnMe(GaMe$_4$) (Ln = Y, Ho, **130**). The larger steric bulk of the GaMe$_3$ compared to the AlMe$_3$ causes the smaller *cis*-content of the polymer products obtained in this series (Table 5.19, Chart 5.11). The augmented 1,4-*trans* contents realized with **129$^{\mathbf{Y}}$ / B** do not find their counterpart in the product of **130$^{\mathbf{Y}}$ / B**. Instead the micorstructure of this system fits to the other microstructures produced in this series. In accordance with the tetramethylaluminates (**129**, this behavior implys a release of GaMe$_3$ during the activation and an interaction of trimethylgallium with the propagation species. The simultaneous addition of monomer and cocatalyst to the precatalyst solution was tested with this system (**130$^{\mathbf{Y}}$ / B**, Table 5.19, run 30b). The microstructure does not differ from the polymer obtained with a prereaction time of 5 min (Table 5.19, run 30), but the chain properties of the respective polymers indicate the expected initiation deficit. Approximately only one out of six yttrium centers grows a polymer chain without prereaction, compared to one out of 1.8 for a prereaction time of 5 min. Applying the

order of educt addition inspired by Hou and coworkers does not lead to a loss of yield with the alkylgallates, as observed for the alkylaluminates. Instead less, but longer and more uniform polymer chains are obtained.

Furthermore, the tetramethylaluminates **129** and gallates **130** have been treated with Me_2AlCl and Me_2GaCl respectively to initiate cationization by cluster formation in analogy to Paper IV[13] and previous studies on homoleptic tetramethylaluminates.[14–19] Potential reaction products did not show any activity in isoprene polymerization and could not be isolated.

5.3.3 Conclusion

Hydro-*tris*-(3-*tert*butyl-5-methyl-pyrazolyl)borate ($Tp^{tBu,\,Me}$) scorpionate complexes of the small rare earth metals bearing methyl, tetramethylaluminate, tetramethylgallate or trimethylaluminate ligands have been investigated in the catalyzed polymerization of isoprene. Indication of a monomeric nature of the active species even in case of the dimethyls was found by relatively high 1,4-*cis*-contents, compared to the (multimeric) pentamethylcyclopentadienyl dimethyls. In case of the mono-tetramethylaluminates and gallates, the large steric bulk of the $Tp^{tBu,\,Me}$ ligand causes the release of the respective trimethyl aluminum / gallium and provides therefore enough steric space for a *cis*-focused monomer addition to the growing polymer chain. Trimethylaluminates react as 'hydrides in disguise' and polymerize isoprene less 1,4-*cis*-selectively .

So far, evidence for the suggestions concerning the active species in this manuscript by NMR spectroscopy or even crystallography must remain a subject of research.

5.3.4 Experimental Section

5.3.4.1 General Remarks

All operations were performed with rigorous exclusion of air and water, using standard Schlenk, high-vacuum, and argon glovebox techniques (MBraun MB 200B; < 1 ppm O_2,

< 1 ppm H_2O). *n*-Hexane, toluene, and THF were purified by using Grubbs type columns (MBraun SPS-800, solvent purification system) and stored in a glovebox. $CDCl_3$ was purchased from Aldrich and used as received. Isoprene was obtained from Aldrich, dried over trioctylaluminum (Aldrich), and vacuum transferred prior to use. $[Ph_3C][B(C_6F_5)_4]$, $[PhNMe_2H][B(C_6F_5)_4]$, and $B(C_6F_5)_3$ were purchased from Boulder Scientific Company and used without any further purification. The NMR spectra were recorded at 26 °C on a Bruker AVII+ 400 Avance (^{1}H: 400.11 MHz; ^{13}C: 100.61 MHz). ^{1}H and ^{13}C shifts are referenced to internal solvent resonances and reported in parts per million (ppm) relative to TMS. The molar masses (M_W and M_n) of the polymers were determined by size-exclusion chromatography (SEC). Sample solutions (1.0 mg polymer per mL THF) were filtered through a 0.45 µm syringe filter (PTFE) prior to injection. SEC was performed with a pump supplied by Viscotek (GPCmax VE 2001), employing ViscoGEL columns. Signals were detected by means of a triple detection array (TDA 305) and calibrated against polystyrene standards ($M_W/\ M_n < 1.15$). The flowrate was set to 1.0 mL min^{-1}. The microstructures of the polydienes were examined by means of ^{1}H and ^{13}C NMR experiments on the AVII+ 400 Avance spectrometers at ambient temperature, using $CDCl_3$ as a solvent. Glass transition temperatures of the polymers (T_g) were obtained applying a Perkin-Elmer DSC 8000 calibrated with indium and cyclohexane standards, scanning from -100 °C up to +100 °C with heating rates of 20 K/min and cooling rates of 60 K/min in N_2 atmosphere. All precatalysts ($[Tp^{tBu,\ Me}LnMe_2]$ Ln = Y, Ho, Lu (**128**), $[Tp^{tBu,\ Me}LnMe(EMe_4)]$, Ln = Y, Ho, Lu, E = Al, Ga (**129** and **130**) and $[Tp^{tBu,\ Me}Ln(HAlMe_3)_2]$, Ln = Y, Lu (**131**)) were synthesized according to literature methods.[3–5]

5.3.4.2 Polymerization of Isoprene

5.3.4.2.1 Method 1

A detailed polymerization procedure is described as a typical example (Table 5.16, run 1). $[Ph_3C][B(C_6F_5)_4]$ (**A**) (18 mg, 0.02 mmol 1 equiv.) was added to a solution of **128^{Y}** (10.8 mg, 0.02 mmol) in toluene (8 mL) and the mixture was aged (prereaction) at ambient temperature for 5 min. After the addition of isoprene (1.36 g, 20 mmol), the polymerization was carried out at 25 °C for 1 h. The reaction was terminated by

pouring the polymerization mixture into 25 mL of methanol containing 0.1 % (w/w) 2,6-di-*tert*-butyl-4-methylphenole as a stabilizer and stirred for 1 h. The polymer was washed with methanol and dried under vacuum at ambient temperature to constant weight.

5.3.4.2.2 Method 2

A detailed polymerization procedure is described as a typical example (Table 5.17, run 10a). $[Ph_3C][B(C_6F_5)_4]$ (**A**) (18 mg, 0.02 mmol 1 equiv.) was added to a solution of **129^{Y}** (12.0 mg, 0.02 mmol) in a mixture of toluene (8 mL) and isoprene (1.36 g, 20 mmol). The polymerization was carried out at 25 °C for 1 h. The reaction was terminated by pouring the polymerization mixture into 25 mL of methanol containing 0.1 % (w/w) 2,6-di-*tert*-butyl-4-methylphenole as a stabilizer and stirred for 1 h. The polymer was washed with methanol and dried under vacuum at ambient temperature to constant weight.

5.3.4.2.3 Method 3

Method 3 equals method 1, except for a reduction of the prereaction time to zero.

5.3.5 Additional Schemes and Figures

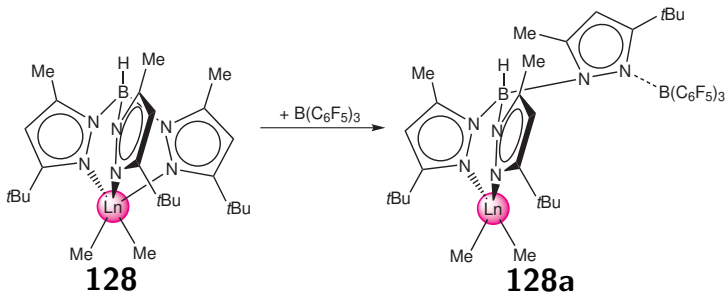

*Scheme 5.7: Potential activation of $Tp^{tBu,\ Me}LnMe_2$ (**128** by cocatalyst $[B(C_6F_5)_3]$ (**C**), decreasing the steric bulk around the Ln center without methyl abstraction.*

References

[1] Dettenrieder, N.; Hollfelder, C. O.; Jende, L. N.; Maichle-Mössmer, C.; Anwander, R. *Organometallics* **2014**, *33*, 1528–1531.

[2] Bonath, M.; Hollfelder, C. O.; Schädle, D.; Maichle-Mössmer, C.; Anwander, R. *Chem. Eur. J.* **2017**, *23*, 4683 –4693.

[3] Litlabø, R.; Zimmermann, M.; Saliu, K.; Takats, J.; Törnroos, K. W.; Anwander, R. *Angew. Chem. Int. Edit.* **2008**, *47*, 9560–9564.

[4] Schädle, C.; Schädle, D.; Eichele, K.; Anwander, R. *Angew. Chem. Int. Edit.* **2013**, *52*, 13238–13242.

[5] Dorothea, S.; Cäcilia, M.-M.; Christoph, S.; Reiner, A. *Chem. Eur. J.* **2015**, *21*, 662–670.

[6] Litlabø, R. Ph.D. Thesis, University of Bergen, **2010**.

[7] Kang, X.; Luo, Y.; Zhou, G.; Wang, X.; Yu, X.; Hou, Z.; Qu, J. *Macromolecules* **2014**, *47*, 4596–4606.

[8] Tobisch, S.; Bögel, H.; Taube, R. *Organometallics* **1996**, *15*, 3563–3571.

[9] Taube, R. In *Catalytic reaction mechanisms and structur-reactivity-relationships in the stereospecific butadiene polymerization*; Kaminsky, W., Ed.; Springer Berlin, 1999; Chapter Metalorganic Catalysts for Synthesis and Polymerization, pp 531–547.

[10] Jende, L. N. Ph.D. Thesis, Eberhard Karls Universität Tübingen, **2015**.

[11] Du, G.; Wei, Y.; Ai, L.; Chen, Y.; Xu, Q.; Liu, X.; Zhang, S.; Hou, Z.; Li, X. *Organometallics* **2010**, *30*, 160–170.

[12] Zimmermann, M.; Törnroos, K. W.; Sitzmann, H.; Anwander, R. *Chem. Eur. J.* **2008**, *14*, 7266–7277.

[13] Hollfelder, C. O.; Jende, L. N.; Diether, D.; Zelger, T.; Stauder, R.; Maichle-Mössmer, C.; Anwander, R. *Catalysts* **2018**, *8*, 61.

[14] Fischbach, A.; Klimpel, M. G.; Widenmeyer, M.; Herdtweck, E.; Scherer, W.; Anwander, R. *Angew. Chem. Int. Edit.* **2004**, *43*, 2234–2239.

[15] Arndt, S.; Beckerle, K.; Zeimentz, P. M.; Spaniol, T. P.; Okuda, J. *Angew. Chem. Int. Edit.* **2005**, *44*, 7473–7477.

[16] Zimmermann, M.; Frøystein, N.-Å.; Fischbach, A.; Sirsch, P.; Dietrich, H. M.; Törnroos, K. W.; Herdtweck, E.; Anwander, R. *Chem. Eur. J.* **2007**, *13*, 8784–8800.

[17] Meermann, C.; Törnroos, K. W.; Nerdal, W.; Anwander, R. *Angew. Chem. Int. Edit.* **2007**, *46*, 6508–6513.

[18] Robert, D.; Spaniol, T. P.; Okuda, J. *Eur. J. Inorg. Chem.* **2008**, , 2801–2809.

[19] Litlabø, R.; Lee, H. S.; Niemeyer, M.; Törnroos, K. W.; Anwander, R. *Dalton Trans.* **2010**, *39*, 6815–6825.

5.3.6 Acknowledgement

Coauthors in case of publication: Dorothea Schädle and Reiner Anwander.
The authors thank Lars N. Jende and Christoph Schädle for sharing their thoughts on the polymerization results, Renita Thim for providing the $Tp^{tBu,\,Me}$ ligand and Deutsche Forschungsgemeinschaft for funding this work.

Manuscript IV: Experiments on Titanium Catecholate Activation

5.4.1 Introduction

Group IV complexes are frequently used as precatalysts in Ziegler-Natta Catalysis.[1,2] In this context, a diamido titanium catecholate[3] ($[Ti(Cct)(NMe_2)_2]_2$) is investigated as precatalyst in the in the polymerization of isoprene.

5.4.2 Results and Discussion

Activation of $[Ti(Cct)(NMe_2)_2]_2$ (**132**) with the borate cocatalysts $[Ph_3C][B(C_6F_5)_4]$ (**A**), $[PhNHMe_2][B(C_6F_5)_4]$ (**B**), borane cocatalyst $B(C_6F_5)_3$ (**C**), and haloginating agents Me_2AlCl (**D**) and Et_2AlCl (**E**) does not yield any cationic species that is active in the polymerization of isoprene, even if $AlMe_3$ is added prior to the cationization. Still the reaction mixtures show a color change towards a dark brown color upon cocatalyst addition. In case of cocatalyst **C** an immediate crystal formation is observed and these crystals are further investigated. After recrystallization small amounts of crystals suitable for X-ray diffractometry are obtained.

By applying cocatalyst **C**, the *bis*-amido titanium catecholate dimer $[Ti(Cct)(NMe_2)_2]_2$ (**132**) is cationized due to the abstraction of a dimethyl amido moiety. The thereby generated *mono*-amido titanium catecholate dimer then reacts with another neutral complex of **132** to form the tetrameric cation **133** (Scheme 5.8). Interestingly, in the crystal structure (Figure 5.26), the anion resulting from this reaction does not bear the expected amido moiety. Instead a simple hydride has anionized the borane. Analytic evidence of a potential side product like N-methylmethanimine (H_3C-N=CH_2) or products of further degradation has not been obtained so far.

The obtained cation $[Ti_4(Cct)_4(NMe_2)_7]^+$ (**133**) shows the bridging catecholate motif analogue to its educt **132** by two catecholates. Another two catecholates bridge three titanium centers. Furthermore, the inner titanium atoms, Ti2 and Ti3 are bridged by an

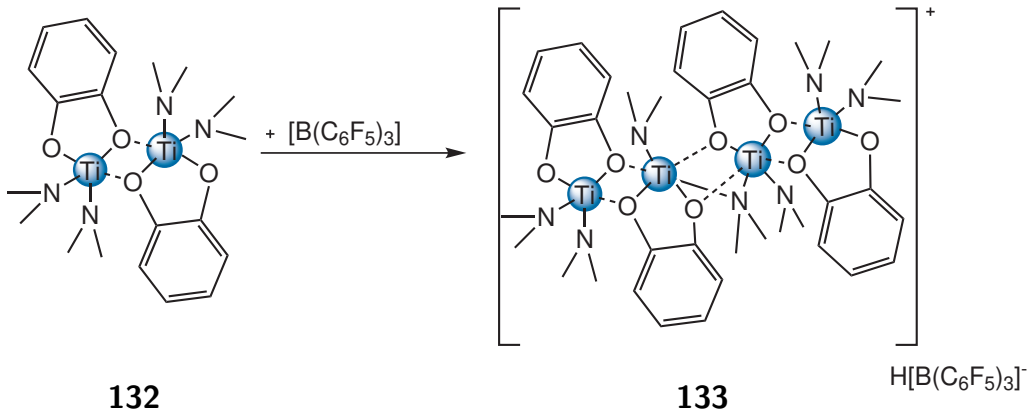

132 **133**

*Scheme 5.8: Synthesis of the cationic $[Ti_4(Cct)_4(NMe_2)_7]$ (**133**) from the neutral precursor **132**, applying $B(C_6F_5)_3$ (**C**).*

amido moiety (N4), while all six further amides are only bond to a single titanium. Due to a low scattering intensity, no angles and bond length could be determined accurately enough to be discussed in this context.

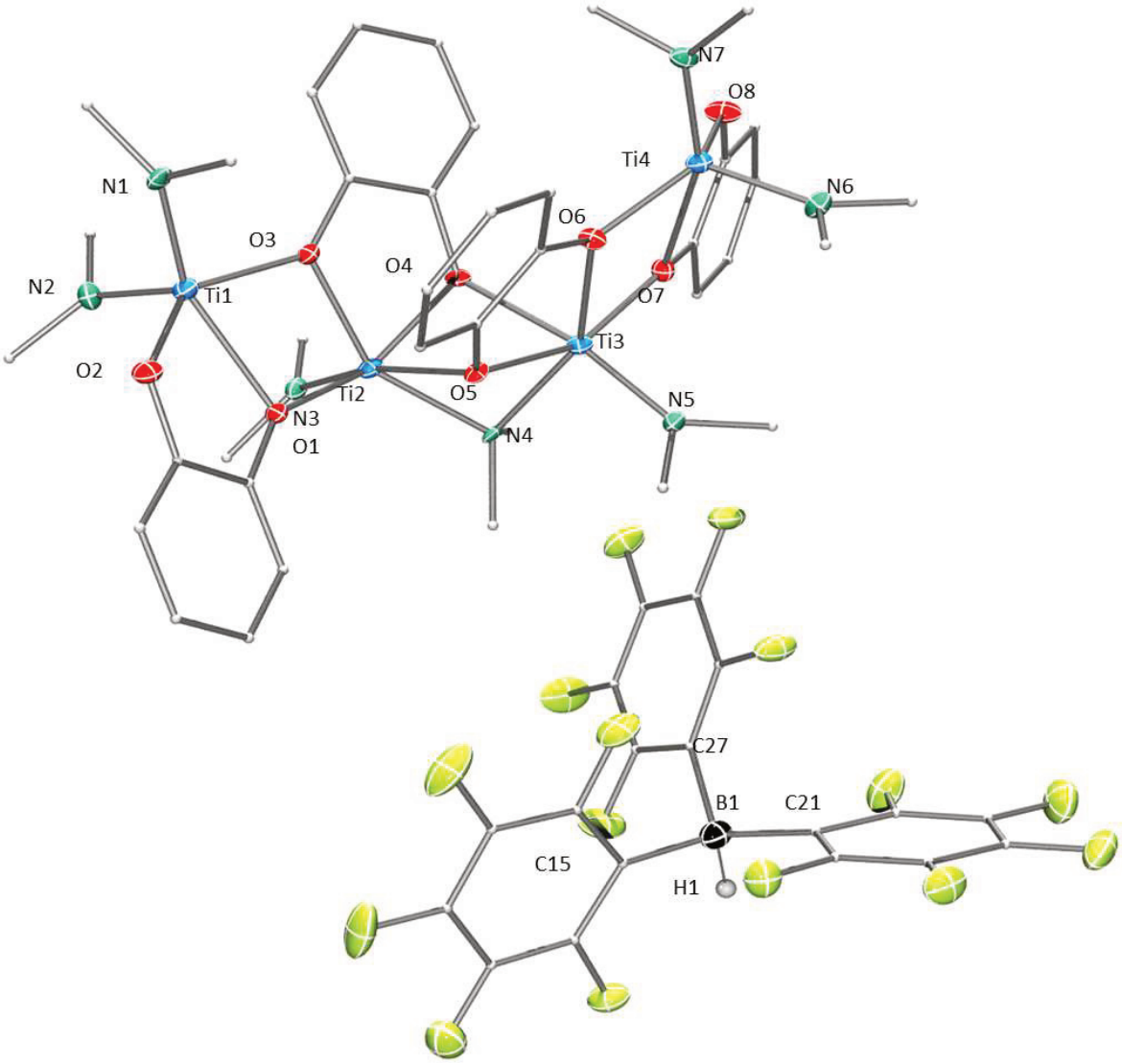

Figure 5.26: ORTEP view of the molecular structure of $[Ti_4(Cct)_4(NMe_2)_7][HB(C_6F_5)_3]$ (***133***). *Atomic displacement parameters are set at the 50 % probability level. Hydrogen atoms except for H1 and one molecule of toluene are omitted for clarity.*

5.4.3 Experimental Section

5.4.3.1 General Remarks

All operations were performed with rigorous exclusion of air and water, using argon glovebox techniques (MBraun MB 200B; $<$ 1 ppm O_2, $<$ 1 ppm H_2O). *n*-Hexane and toluene were purified by using Grubbs type columns (MBraun SPS-800, solvent purification system) and stored in a glovebox. Isoprene was obtained from Aldrich, dried over trioctylaluminum (Aldrich), and vacuum transferred prior to use. $[Ph_3C][B(C_6F_5)_4]$, $[PhNMe_2H][B(C_6F_5)_4]$, and $B(C_6F_5)_3$ were purchased from Boulder Scientific Company and used without any further purification. Me_2AlCl and Et_2AlCl were purchased from Aldrich and used without any further purification. Single crystals of **133** were selected, coated with Parabar 10312 (previously known as Paratone N) and fixed on a microloop. Data were collected on a Bruker APEX DUO instrument equipped with an IμS microfocus sealed tube and QUAZAR optics for MoK_α radiation ($\lambda = 0.71073$ Å). The Data collection strategy was determined using COSMO[4] employing ω- and φ scans. Raw data were processed using APEX[5] and SAINT[6], corrections for absorption effects were applied using SADABS[7]. The structures were solved by direct methods and refined against all data by full-matrix least-squares methods on F2 using SHELXTL[8,9] and Shelxle.[10]

5.4.3.2 Synthesis of $[Ti_4(Cct)_4(NMe_2)_7][HB(C_6F_5)_3]$ (133)

In a glovebox, 20 mg (41 µmol) of **132**[3] and 21 mg (41 µmol) of $B(C_6F_5)_3$ (cocatalyst **C**) were dissolved in 12 mL of toluene. The amber solution changed color towards a very deep brown and immediate crystal formation was observed. After a reaction time of 5 min of stirring at ambient temperature, reaction mixture was removed and the crystals of **133** were washed with toluene and recrystallized from a mixture of toluene and *n*-hexane at -40 °C. The crystals were suitable for X-ray diffraction but showed low scattering intensity.

5.4.4 Conclusion

Reaction of diamido titanium catecholate with borate, borane and halogenating co-catalysts does not yield species active in the polymerization of isoprene. In case of tri-pentafluorophenyl borane, a stable tetrameric cation is produced.

References

[1] Marks, T. J. *Acc. Chem. Res.* **1992**, *25*, 57–65.

[2] Chen, E. Y.-X.; Marks, T. J. *Chem. Rev.* **2000**, *100*, 1391–1434.

[3] Sonström, A.; Schneider, D.; Cäcilia, M.-M.; Anwander, R. *Eur. J. Inorg. Chem.* **2019**, *2019*, 682 – 692.

[4] Bruker AXS Inc, Madison, WI, 2012.

[5] Bruker AXS Inc., Madison, WI, 2016.

[6] Bruker AXS Inc., Madison, WI, 2015.

[7] Krause, L.; Herbst-Irmer, R.; Sheldrick, G. M.; D., S. *J. Appl. Cryst.* **2015**, *48*, 3.

[8] SHELXTL, *Acta Cryst.* **2015**, *A71*, 3–8.

[9] Scheldrick, G. M. *Program for crystal structure refinement*; SHELXL-97, 1997.

[10] Hübschle, C. B.; Sheldrick, G. M.; Dittrich, B. *J. Appl. Cryst.* **2011**, *44*, 1281–1284.

5.4.5 Acknowledgement

Coauthors in case of publication: Andrea Sonström, Daniel Werner, Cäcilia Maichle-Mössmer, Reiner Anwander.
The authors thank Deutsche Forschungsgemeinschaft for funding this work.

Chapter 6

Publications

Paper I: Half-Sandwich Rare-Earth-Metal Alkylaluminate Complexes Bearing Peripheral Boryl Ligands

This aricle is reprinted with permission from:

"Half-Sandwich Rare-Earth-Metal Alkylaluminate Complexes Bearing Peripheral Boryl Ligands"

by
Nicole Dettenrieder, Christoph O. Hollfelder, Lars N. Jende, Cäcilia Maichle-Mössmer, and Reiner Anwander

published in:
Organometallics, **2014**, *33*, 1528–1531
doi: 10.1021/om401163a

Copyright (2014) American Chemical Society.

ORGANOMETALLICS

Communication

pubs.acs.org/Organometallics

Half-Sandwich Rare-Earth-Metal Alkylaluminate Complexes Bearing Peripheral Boryl Ligands

Nicole Dettenrieder, Christoph O. Hollfelder, Lars N. Jende, Cäcilia Maichle-Mössmer, and Reiner Anwander*

Institut für Anorganische Chemie, Eberhard Karls Universität Tübingen, Auf der Morgenstelle 18, 72076 Tübingen, Germany

Supporting Information

ABSTRACT: $[(C_5Me_5)LnMe_2]_3$ (Ln = Y, Lu) dissolve readily in a *n*-hexane/toluene mixture upon addition of 3 equiv of the organoaluminum boryl compound $[Me_2Al\{B(NDippCH)_2\}]_2$ (Dipp = $C_6H_3iPr_2$-2,6). The half-sandwich complexes $(C_5Me_5)Ln[(AlMe_3)\{B(NDippCH)_2\}]_2$ thus formed display unsymmetrical heteroaluminate coordination not only in the solid state but also at lower temperatures in solution, which is distinct from the behavior of the homoaluminate congeners $(C_5Me_5)Ln(AlMe_4)_2$. The effect of homo- versus heteroaluminate coordination is assessed in the coordinative polymerization of isoprene.

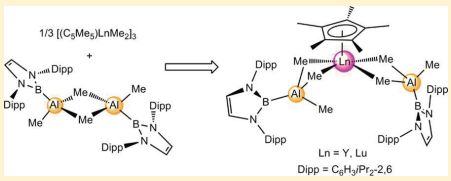

Monocyclopentadienyl rare-earth-metal alkyl complexes continue to reveal unique performance in stereospecific (co)polymerization catalysis.[1] As a consequence, much effort has been devoted to catalyst design by assessing cyclopentadienyl ring and peripheral substitution as well as type of alkyl actor ligand[2] and cocatalyst(s).[1] We and others have embarked on a strategy utilizing tetramethylaluminate ligands (Chart 1, **I**) as

Chart 1. Known Half-Sandwich Bis(alkylaluminates) I and III and Proposed Active Species II for Polymerization Reactions

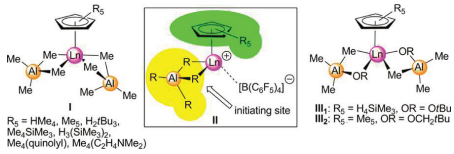

alkyls in disguise, ensuring not only thermal robustness and steric saturation but also high dynamic behavior.[3] While activation (=cationization) of complexes **I** is routinely achieved by reaction with borane/borate cocatalysts, the remaining $[AlMe_4]^-$ moiety features the initiating site (**II**): e.g., for 1,3-diene polymerization.[3d,e,h,i] It can be anticipated that the composition of the aluminate actor ligand will significantly affect the polymerization performance, which is why we set out to implement heteroatom-substituted aluminate ligands ("heteroaluminates"). For monoanionic moieties X featuring either strongly electronegative donor atoms (OR (**III**),[2,4] NR_2,[5] Cl[6]) or hydrido[7] and alkynyl ligands,[8] X is found in the bridging position exclusively: that is, $Ln(\mu\text{-}X)(\mu\text{-}Me)_xAlMe_{1+y}$ ($x + y = 2$). In the case of heteroaluminates with different alkyl groups, the bulkier X is found in the peripheral position: that is, $Ln(\mu\text{-}Me)_{1+x}AlMe_yX$ ($x + y = 2$).[9]

We have recently described homoleptic heteroaluminate complexes of the type $Ln[(AlMe_3)\{B(NDippCH)_2\}]_3$ (Ln = Y, Lu; Dipp = $C_6H_3iPr_2$-2,6),[10] featuring the bulky carbanion-like boryl ligand[11] in the peripheral position. Herein we extend this study to the synthesis and characterization of the first half-sandwich complexes bearing such peripheral boryl ligands and the suitability of the resulting complexes for the polymerization of isoprene.

Half-sandwich heteroaluminate complexes $(C_5Me_5)Ln[(AlMe_3)\{B(NDippCH)_2\}]_2$ (**2** (Ln = Y), **3** (Ln = Lu)) can be obtained by applying a strategy which had previously been successful for the synthesis of the respective homoleptic derivatives. Accordingly, addition of stoichiometric amounts of $[Me_2Al\{B(NDippCH)_2\}]_2$ (**1**) to $[(C_5Me_5)LnMe_2]_3$ (Ln = Y, Lu)[12] gave complexes **2** and **3** in quantitative yields (Scheme 1). Complexes **2** and **3** were examined by X-ray crystallography and found to be isomorphous.[13] However, due to a low-quality data set collected for yttrium complex **2**, only the molecular structure of **3** will be discussed in the following. Figure 1 shows one out of two molecules $(C_5Me_5)Lu[(AlMe_3)\{B(NDippCH)_2\}]_2$ detected in the asymmetric unit. As anticipated, the two $[B(NDippCH)_2]$ moieties are terminally bonded to the aluminum atoms and are oriented nearly perpendicular to each other (∠N1B1N2−N3B2N4 = 87.1°; ∠N5B3N6−N7B4N8 = 89.3°). The $AlMe_3$ moieties, which connect the boryl entities to the lutetium center, each have two bridging methyl groups and a terminal methyl group. The terminal methyl groups are positioned in opposite directions, probably because of steric hindrance. One of the $[AlMe_2Lu]$ units is nearly planar (∠C32Lu1C33−C32Al2C33 = 13.7°; ∠C78Lu2C79−C78Al3C79 = 13.1°), while the other is remarkably bent (∠C35Lu1C36−C35Al1C36 = 51.2°;

Received: November 29, 2013
Published: March 19, 2014

ACS Publications © 2014 American Chemical Society

Organometallics Communication

Scheme 1. Synthesis of $(C_5Me_5)Ln[(AlMe_3)\{B(NDippCH)_2\}]_2$ (Ln = Y (2), Lu (3)) and Reactivity toward Tetrahydrofuran

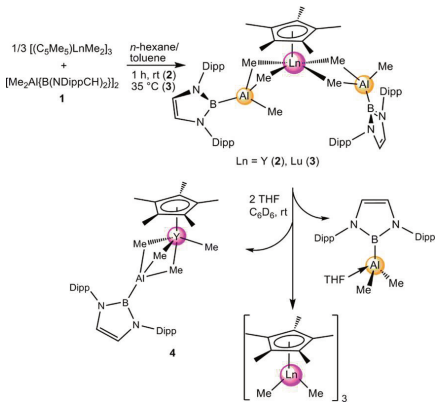

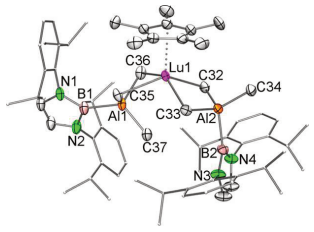

Figure 1. Molecular structure of $(C_5Me_5)Lu[(AlMe_3)\{B(NDippCH)_2\}]_2$ (**3**) with atomic displacement parameters set at the 50% level. The carbon atoms of the aromatic parts are shown with reduced radii. Hydrogen atoms, cocrystallized hexane, and the second molecule of the asymmetric unit have been omitted for clarity. Selected interatomic distances (Å) and angles (deg): Lu1−C32, 2.506(4); Lu1−C33, 2.504(3); Lu1−C35, 2.605(4); Lu1−C36, 2.590(4); Lu···C37, 3.381(4); Lu1···Al1, 2.917(2); Lu1···Al2, 3.059(2); ∠C32Lu1C33−C32Al2C33, 13.7; ∠C35Lu1C36−C35Al1C36, 51.2; B1−Al1, 2.137(5); B2−Al2, 2.135(5); Lu2−C78, 2.507(4); Lu2−C79, 2.509(4); Lu2−C81, 2.622(4); Lu2−C82, 2.591(4); Lu2···C83, 3.351(4); Lu2···Al3, 3.062(2); Lu2···Al4, 2.913(2); ∠C78Lu2C79−C78Al3C79, 13.1; ∠C81Lu2C82−C81Al4C82, 51.6; B3−Al4, 2.137(4); B4−Al3, 2.137(4).

∠C81Lu2C82−C81Al4C82 = 51.6°). This distinct Ln−alkylaluminate bonding is a well-known structural motif of half-sandwich rare-earth-metal bis(tetramethylaluminate), as previously revealed by $(C_5Me_5)Lu(AlMe_4)_2$,[3a] $(C_5Me_5)La(AlMe_4)_2$,[3b] $[1,3\text{-}(Me_3Si)_2C_5H_3]Ln(AlMe_4)_2$ (Ln = Y, Nd, Lu), $(C_5Me_4SiMe_3)Y(AlMe_4)_2$, and $[1,2,4\text{-}(Me_3C)_3C_5H_2]Ln(AlMe_4)_2$ (Ln = La, Nd, Sm).[3e] Moreover, the bent $[AlMe_2Lu]$ moiety in complex **3** displays further literature-known characteristics:[3] elongated Lu−(μ-CH_3) distances (Δ_{Lu-C} = 0.08−0.11 Å), a shortened Lu−Al distance (Δ_{Lu-Al} = 0.14−0.15 Å), and an additional short Lu−C(Me) contact (Lu1···C37 = 3.381(4); Lu2···C83 = 3.351(4) Å). The last observation is probably caused by steric unsaturation and is also reflected in the different angles Lu−Al−C_{term} of the two $[(AlMe_3)\{B(NDippCH)_2\}]$ ligands[3b] (∠Lu1−Al1−C37 = 84.9(2)°; ∠Lu1−Al2−C34 = 117.5(2)°; ∠Lu2−Al4−C83 = 84.0(2)°; ∠Lu2−Al3−C80 = 117.3(2)°). The B−Al distances in complex **3** (average 2.137 Å) are slightly shorter than those in our recently published homoleptic Lu complex $Lu[(AlMe_3)\{B(NDippCH)_2\}]_3$ (average 2.153 Å).[10]

$^{11}B\{^1H\}$ NMR spectra were measured for both **2** and **3**, as well as a $^1H-^{89}Y$ HSQC NMR spectrum of **2**. The boron signals appear in the expected region of 31.4 (**2**) and 31.0 (**3**) ppm (see Figures S6 and S11, Supporting Information) and are comparable to those of educt **1** (27.9 ppm) and $(THF)Me_2Al[B(NDippCH)_2]$ (31.9 ppm) (all recorded in C_6D_6).[10] The yttrium resonance of complex **2** at 144.5 ppm (see Figure S5, Supporting Information) appears at relatively low field in comparison to the published values of other(C_5Me_5)-substituted yttrium complexes,[14] which can be attributed to poor electron donation of the $Me_2Al[B(NDippCH)_2]$ ligands.[14]

Low-temperature ^1H NMR spectroscopic studies were performed both for $(C_5Me_5)Y[(AlMe_3)\{B(NDippCH)_2\}]_2$ (**2**) and $(C_5Me_5)Lu[(AlMe_3)\{B(NDippCH)_2\}]_2$ (**3**). Interestingly, the asymmetric bonding of the $[(AlMe_3)\{B(NDippCH)_2\}]$ entities as featured by the solid-state structure (Figure 1) gets nicely resolved through decoalescing methyl groups at lower temperatures. These observations are in contrast to those made for homoleptic $Ln[(AlMe_3)\{B(NDippCH)_2\}]_3$ (Ln = Y, Lu).[10] For the latter, the methyl group signal splits up at lower temperatures into two peaks with an integral ratio of 2:1 and further into three peaks with a 1:1:1 ratio, which can be explained by an intitial separation into bridging and terminal methyl groups (2:1 ratio), with a further decoalescence of the bridging methyl moieties (1:1:1).[10]

At ambient temperature, lutetium complex **3** shows a broad singlet in the high-field region, which accounts for a high fluxionality of bridging and terminal methyl groups. An analogous observation is made for the yttrium complex **2**; however, due to yttrium coupling, a doublet with a $^2J_{YH}$ coupling constant of 2.9 Hz is observed. In complex **2**, the methyl resonance of 18 protons splits up into 2 signals at about −40 °C with a ratio of 15:3, followed by a decoalescence of the larger resonance into 2 signals with a ratio of 9:6 at ca. −50 °C. The signal that corresponds to 9 protons decoalesces further at about −70 to −80 °C (ratio 3:6). At −80 °C, there are then 4 separate signals for the aluminum methyl groups, with proton ratios of 3:6:6:3. The initial splitting of the signal (15:3) at −40 °C already documents the separation of a single (terminal) methyl group from the others and shows the inequivalency of the terminal methyl groups on the $(AlMe_3)[B(NDippCH)_2]$ ligands. The final signal splitting at −80 °C with 4 signals in the ratio 3:6:6:3 indicates separate resonances for the bridging and terminal methyl groups on each ligand. Despite a different signal ordering/shifting in the low-temperature ^1H NMR spectra of Lu complex **3**, qualitatively similar observations were made as for **2** (Figure 2). For the smaller Lu(III) metal center, all decoalescence phenomena are observed at higher temperature because of enhanced steric hindrance. The single methyl resonance starts splitting up at around −20 °C with separation of one methyl group (15:3). Further splitting of the larger signal into 2 signals of 12 and 3 protons, respectively, is observed at about −25 °C. Between −30 and −40 °C, the decoalescence of the bridging methyl groups takes place to produce the final 4-signal pattern with an integral ratio of 6:6:3:3. For comparison, the low-temperature ^1H NMR spectra of half-sandwich rare-earth-metal tetramethylaluminate complexes $(C_5Me_5)Ln(AlMe_4)_2$ (**I**, Chart 1) revealed high methyl group mobility even at −85 °C, meaning that any decoalescence into bridging and terminal $AlMe_3$ signals could not be observed at all.[3] The heteroaluminate complex $(C_5Me_5)Y[(\mu\text{-}OCH_2CMe_3)(\mu\text{-}Me)AlMe_2]_2$ (**III$_2$**, Chart 1)

dx.doi.org/10.1021/om401163a | *Organometallics* 2014, 33, 1528−1531

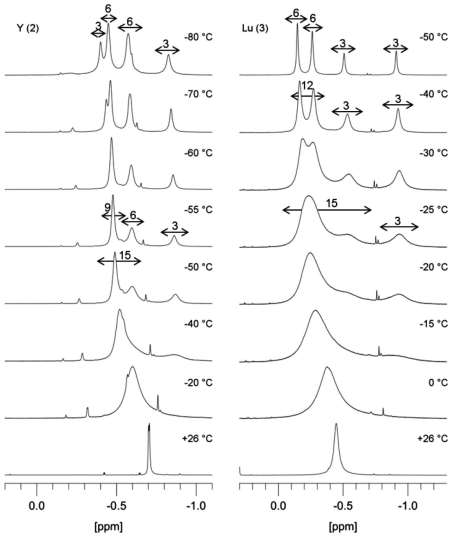

Figure 2. Low-temperature NMR spectra of $(C_5Me_5)Ln[(AlMe_3)\{B(NDippCH)_2\}]_2$ (**2**, left; **3**, right).

gave one broad $AlMe_3$ signal at ambient temperature as well but displayed a 3-signal pattern with an integral ratio of 6:6:6 in the range −30 to −80 °C, indicative of two separate signals for the terminal methyl groups and one signal for the bridging methyl groups.[2b]

The reactivity of half-sandwich complexes **2** and **3** toward THF was exploited by NMR-scale experiments in deuterated benzene as solvent. The envisaged donor-induced cleavage should proceed via separation of $(THF)Me_2Al[B(NDippCH)_2]$ and re-formation of complexes $[(C_5Me_5)LnMe_2]_3$ (Ln = Y, Lu), when using 2 equiv of THF (Scheme 1). For lutetium complex **3**, the formation of both expected products was observed without detection of any significant byproducts (see Figure S14, Supporting Information). For yttrium complex **2**, a similar cleavage reaction took place but one byproduct could be identified as well (ca. 31%). The ^{1}H NMR spectrum of this byproduct showed an integral signal ratio of about 2:15:12:12:3:9 (see also Figure S13, Supporting Information), which can be assigned to the partially donor-cleaved species $[(C_5Me_5)YMe(Me_3Al)\{B(NDippCH)_2\}]$ (**4**, Scheme 1). The signals of the metal-bonded methyl groups appear as two doublets ($^2J_{YH}$ = 2.2 and 2.0 Hz) in a 3:9 ratio. A control NMR measurement, which was performed after 3 days at ambient temperature, revealed decomposition of this species as well as of $[(C_5Me_5)YMe_2]_3$, in contrast to the case for $(THF)Me_2Al[B(NDippCH)_2]$.

Complexes **2** (Ln = Y) and **3** (Ln = Lu) were successfully tested in the polymerization of isoprene (Table 1), upon addition of borates $[Ph_3C][B(C_6F_5)_4]$ (**A**) and $[PhNMe_2H][B(C_6F_5)_4]$ (**B**) as cationizing cocatalysts (for activation with borane $B(C_6F_5)_3$ (**C**), see Table S1 in the Supporting Information). The combination **3**/**A** (run 5 in Table 1) displayed the highest activity and gave quantitative polymerization after 1 h. Exemplarily, this polymer was investigated by differential scanning calorimetry (DSC), revealing a single glass transition at −20.8 °C.

Surveying runs 1−7, in terms of microstructure, it is apparent that there is a strong tendency toward the formation of 3,4-polyisoprene if cocatalysts **A** and **B** are involved. As both cocatalysts are intended to produce a similar active species,[3h,i] the formation of similar polymers is not unexpected. However, the quite different activity situations for **3**/**A** (run 5) and **3**/**B** (run 6) are remarkable. Furthermore, the molecular weight distributions seem to be significantly cocatalyst dependent: PDI(**A**) = 1.4−1.5; PDI(**B**) = 1.2−1.3. On comparison of the obtained polymer data with our earlier results,[3e] applying $(C_5Me_5)Ln(AlMe_4)_2$ (Ln = Y, Lu) precatalysts (run 8−11 in Table 1) shows that the microstructure develops differently. In contrast to the present study, the homoaluminate-supported catalysts tend to form mainly *cis*-polyisoprene. It is striking that especially the combination $(C_5Me_5)Lu(AlMe_4)_2$/**B** is far more active than the corresponding boryl-substituted species.

For a better understanding of the cationization reaction and the involved high 3,4-polyisoprene content, the formation of the most active catalyst/cocatalyst mixture, **3**/**A**, was examined by NMR spectroscopy. The cationization reaction as depicted in eq 1 was complete after 7 min. In addition to the expected formation of 0.5 equiv of **1** and 1 equiv of Ph_3CMe as byproducts, the active species $[(C_5Me_5)Lu[(AlMe_3)\{B(NDippCH)_2\}]]^+[B(C_6F_5)_4]^-$ (**4**) gave clean and well-resolved NMR spectra.

Table 1. Selected Examples of Isoprene Polymerization at Ambient Temperature

entry[a]	precatalyst	cocatalyst[b]	*t* (h)	yield (%)	*cis*-1,4[c]	*trans*-1,4[c]	3,4[c]	M_n[d] (×10^4)	M_w/M_n[d]	ref
1	**2**	**A**	1	8.7	21.3	12.7	66.0	2.4	1.41	*g*
2	**2**	**A**	24	>99	49.4	5.3	45.3	9.6	1.45	*g*
3	**2**	**B**	1	11.2	30.7	3.3	66.8	3.8	1.22	*g*
4	**2**	**B**	24	>99	34.1	15.5	50.4	7.4	1.29	*g*
5	**3**	**A**	1	>99	21.5	17.7	60.8	4.7	1.44	*g*
6	**3**	**B**	1	5.5	38.6	3.2	58.2	–[e]	–[e]	*g*
7	**3**	**B**	24	>99	21.4	14.7	63.9	6.0	1.23	*g*
8[f]	$Cp^*Y(AlMe_4)_2$	**A**	24	>99	60.5	20.6	18.9	2.0	8.95	3e
9[f]	$Cp^*Y(AlMe_4)_2$	**B**	24	>99	43.5	28.7	27.8	6.0	1.59	3e
10[f]	$Cp^*Lu(AlMe_4)_2$	**A**	0.25	>99	73.9	19.7	6.4	10.0	1.49	*g*
11[f]	$Cp^*Lu(AlMe_4)_2$	**B**	0.25	>99	70.3	20.3	9.4	9.5	1.45	*g*

[a]Conditions: 0.02 mmol of precatalyst, [Ln]/[cocat] = 1/1, 7 mL of toluene, 20 mmol of isoprene, room temperature. [b]Cocatalyst: $[Ph_3C][B(C_6F_5)_4]$ (**A**); $[PhNMe_2H][B(C_6F_5)_4]$ (**B**). Polymerizations applying $B(C_6F_5)_3$ (**C**) can be found in the Supporting Information (Table S1). [c]Determined by ^{1}H and ^{13}C NMR spectroscopy in $CDCl_3$. [d]Determined by means of size-exclusion chromatography (SEC) against polystyrene standards. [e]Not determined due to low yield. [f]Polymerizations at 40 °C. [g]This work.

$$(C_5Me_5)Lu[(AlMe_3)_3\{B(NDippCH)_2\}]_2 + \mathbf{A} \rightarrow 0.5\ \mathbf{1} + [(C_5Me_5)Lu[(AlMe_3)_4\{B(NDippCH)_2\}]]^+[B(C_6F_5)_4]^- + Ph_3CMe \quad (1)$$

In comparison to the spectra of nonactivated **3**, the integrals of the signals assigned to the $(AlMe_3)[B(NDippCH)_2]$ ligands were cut in half, which proves complete separation of one of these ligands. The signals assigned to the remaining $(AlMe_3)$-$[B(NDippCH)_2]$ ligand split up, implying hindered rotation. The latter phenomenon might reflect the coordination of one of the aryl moieties to the cationized metal center in **4**, which would also explain a decreased polymerization rate and a 3,4-selectivity (see Figure S15 in the Supporting Information). In addition, the ^{19}F chemical shift difference of the *p*- and *m*-F atoms of the borate anions in **3**/**A** is found to be 4.1 ppm, which implies a very weak interaction with the cationic entity (tight ion pairs, ca. 5.4 ppm; none, 2.7 ppm).[15]

In conclusion, half-sandwich complexes $(C_5Me_5)Ln[(AlMe_3)$-$\{B(NDippCH)_2\}]_2$ can be accessed in high yields via addition of $[(Me_2Al)\{B(NDippCH)_2\}]_2$ to $[(C_5Me_5)LnMe_2]_3$ (Ln = Y, Lu; Dipp = $C_6H_3iPr_2$-2,6). The bulky boryl ligand $[B(NDippCH)_2]$ favors an unsymmetrical peripheral coordination (=terminal at aluminum), which markedly affects the fluxional behavior of the metal-bonded methyl groups. With respect to isoprene polymerization, the implementation of heteroaluminate ligands does not affect the cationization reaction with borate activators but bears on the microstructure of polyisoprene (switch from *cis*-1,4 to 3,4).

■ ASSOCIATED CONTENT

Supporting Information

Text, figures, tables, and a CIF file giving experimental details for the syntheses and characterization of complexes **2** and **3** as well as of the polymerization study, NMR spectra, and crystallographic data for **2**. This material is available free of charge via the Internet at http://pubs.acs.org.

■ AUTHOR INFORMATION

Corresponding Author

*E-mail for R.A.: reiner.anwander@uni-tuebingen.de.

Notes

The authors declare no competing financial interest.

■ ACKNOWLEDGMENTS

We thank the German science foundation for funding (Grant AN 238/14-2) and Jürgen Koch (THASS GmbH) for kindly providing the DSC measurements.

■ REFERENCES

(1) (a) Arndt, S.; Okuda, J. *Chem. Rev.* **2002**, *102*, 1953. (b) Fischbach, A.; Anwander, R. *Adv. Polym. Sci.* **2006**, *204*, 155. (c) Hou, Z. *Bull. Chem. Soc. Jpn.* **2003**, *76*, 2253. (d) Okuda, J. *Dalton Trans.* **2003**, 2367. (e) Zimmermann, M.; Anwander, R. *Chem. Rev.* **2010**, *110*, 6194. (f) Nishiura, M.; Hou, Z. *Nat. Chem.* **2010**, *2*, 257.

(2) (a) Evans, W. J.; Boyle, T. J.; Ziller, J. W. *J. Organomet. Chem.* **1993**, *462*, 141. (b) Fischbach, A.; Herdtweck, E.; Anwander, R. *Inorg. Chim. Acta* **2006**, *359*, 4855.

(3) (a) Anwander, R.; Klimpel, M. G.; Dietrich, H. M.; Shorokhov, D. J.; Scherer, W. *Chem. Commun.* **2003**, 1008. (b) Dietrich, H. M.; Zapilko, C.; Herdtweck, E.; Anwander, R. *Organometallics* **2005**, *24*, 5767. (c) Le Roux, E.; Nief, F.; Jaroschik, F.; Törnroos, K. W.; Anwander, R. *Dalton Trans.* **2007**, 4866. (d) Zimmermann, M.; Törnroos, K. W.; Anwander, R. *Angew. Chem., Int. Ed.* **2008**, *47*, 775. (e) Zimmermann, M.; Törnroos, K. W.; Sitzmann, H.; Anwander, R. *Chem. Eur. J.* **2008**, *14*, 7266. (f) Robert, D.; Spaniol, T. P.; Okuda, J. *Eur. J. Inorg. Chem.* **2008**, 2801. (g) Dietrich, H. M.; Törnroos, K. W.; Herdtweck, E.; Anwander, R. *Organometallics* **2009**, *28*, 6739. (h) Zimmermann, M.; Volbeda, J.; Törnroos, K. W.; Anwander, R. *Compt. Rend. Chim.* **2010**, *13*, 651. (i) Litlabø, R.; Enders, M.; Törnroos, K. W.; Anwander, R. *Organometallics* **2010**, *29*, 2588. (j) Jende, L. N.; Maichle-Mössmer, C.; Anwander, R. *Chem. Eur. J.* **2013**, *19*, 16321.

(4) For Ln(III) examples, see: (a) Evans, W. J.; Boyle, T. J.; Ziller, J. W. *J. Am. Chem. Soc.* **1993**, *115*, 5084. (b) Biagini, P.; Lugli, G.; Abis, L.; Millini, R. *J. Organomet. Chem.* **1994**, *474*, C16. (c) Giesbrecht, G. R.; Gordon, J. C.; Brady, J. T.; Clark, D. L.; Keogh, D. W.; Michalczyk, R.; Scott, B. L.; Watkin, J. G. *Eur. J. Inorg. Chem.* **2002**, 723. (d) Gordon, J. C.; Giesbrecht, G. R.; Brady, J. T.; Clark, D. L.; Keogh, D. W.; Scott, B. L.; Watkin, J. G. *Organometallics* **2002**, *21*, 127. (e) Fischbach, A.; Herdtweck, E.; Anwander, R.; Eickerling, G.; Scherer, W. *Organometallics* **2003**, *22*, 499. (f) Fischbach, A.; Klimpel, M. G.; Widenmeyer, M.; Herdtweck, E.; Scherer, W.; Anwander, R. *Angew. Chem., Int. Ed.* **2004**, *43*, 2234. (g) Fischbach, A.; Eickerling, G.; Scherer, W.; Herdtweck, E.; Anwander, R. *Z. Naturforsch., B* **2004**, *59b*, 1353. (h) Fischbach, A.; Meermann, C.; Eickerling, G.; Scherer, W.; Anwander, R. *Macromolecules* **2006**, *39*, 6811. (i) Occhipinti, G.; Meermann, C.; Dietrich, H. M.; Litlabø, R.; Auras, F.; Törnroos, K. W.; Maichle-Mössmer, C.; Jensen, V. R.; Anwander, R. *J. Am. Chem. Soc.* **2011**, *133*, 6323.

(5) For Ln(III) examples, see: (a) Evans, W. J.; Anwander, R.; Doedens, R. J.; Ziller, J. W. *Angew. Chem., Int. Ed.* **1994**, *33*, 1641. (b) Evans, W. J.; Anwander, R.; Ziller, J. W. *Inorg. Chem.* **1995**, *34*, 5927. (c) Evans, W. J.; Ansari, M. A.; Ziller, J. W.; Khan, S. I. *Inorg. Chem.* **1996**, *35*, 5435. (d) Gordon, J. C.; Giesbrecht, G. R.; Clark, D. L.; Hay, P. J.; Keogh, D. W.; Poli, R.; Scott, B. L.; Watkin, J. G. *Organometallics* **2002**, *21*, 4726. (e) Zimmermann, M.; Törnroos, K. W.; Anwander, R. *Organometallics* **2006**, *25*, 3644. (f) Zimmermann, M.; Estler, F.; Herdtweck, E.; Törnroos, K. W.; Anwander, R. *Organometallics* **2007**, *26*, 6029.

(6) (a) Evans, W. J.; Champagne, T. M.; Giarikos, D. G.; Ziller, J. W. *Organometallics* **2005**, *24*, 570. (b) Evans, W. J.; Champagne, T. M.; Ziller, J. W. *Organometallics* **2005**, *24*, 4882.

(7) Schädle, C.; Schädle, D.; Eichele, K.; Anwander, R. *Angew. Chem., Int. Ed.* **2013**, *52*, 13238.

(8) Nieland, A.; Mix, A.; Neumann, B.; Stammler, H.-G.; Mitzel, N. W. *Chem. Eur. J.* **2013**, *19*, 8268.

(9) Klimpel, M. G.; Eppinger, J.; Sirsch, P.; Scherer, W.; Anwander, R. *Organometallics* **2002**, *21*, 4021.

(10) Dettenrieder, N.; Dietrich, H. M.; Schädle, C.; Maichle-Mössmer, C.; Törnroos, K. W.; Anwander, R. *Angew. Chem., Int. Ed.* **2012**, *51*, 4461.

(11) (a) Segawa, Y.; Yamashita, M.; Nozaki, K. *Science* **2006**, *314*, 113. (b) Segawa, Y.; Suzuki, Y.; Yamashita, M.; Nozaki, K. *J. Am. Chem. Soc.* **2008**, *130*, 16069.

(12) The complexes $[(C_5Me_5)LnMe_2]_3$ can be obtained from the bis(tetramethylaluminates) $(C_5Me_5)Ln(AlMe_4)_2$[3b,g] via donor-induced cleavage with THF or diethyl ether: Dietrich, H. M.; Grove, H.; Törnroos, K. W.; Anwander, R. *J. Am. Chem. Soc.* **2006**, *128*, 1458.

(13) Crystal data for compound **2** ($C_{77}H_{126}Al_2B_2YN_4$, M_r = 1272.298): $P\bar{1}$, a = 13.5337 Å, b = 18.6533 Å, c = 33.0015 Å, α = 82.371°, β = 83.305°, γ = 78.392°. Because of the poor quality of the crystal, data were not deposited. Crystal data for compound **3** ($C_{77}H_{126}Al_2B_2LuN_4$, M_r= 1358.37): $P\bar{1}$, a = 13.4966(3) Å, b = 18.6094(5) Å, c = 32.8876(9) Å, α = 82.408(2)°, β = 83.663(1)°, γ = 79.017(2)°, V = 8006.9(4) Å^3, and d_{calcd} = 1.127 g cm^{-3} for Z = 4. CCDC 972153 contains supplementary crystallographic data for compound **3**. These data can be obtained free of charge from The Cambridge Crystallographic Data Centre via www.ccdc.cam.ac.uk/data_request/cif.

(14) Schaverien, C. J. *Organometallics* **1994**, *13*, 69.

(15) (a) Horton, A. D. *Organometallics* **1996**, *15*, 2675. (b) Horton, A. D.; de With, J.; van der Linden, A. J.; van de Weg, H. *Organometallics* **1996**, *15*, 2672.

Paper I: Supporting Information

This Supporting Information is reprinted with permission from the Supporting Information of:

"Half-Sandwich Rare-Earth-Metal Alkylaluminate Complexes Bearing Peripheral Boryl Ligands"

by
Nicole Dettenrieder, Christoph O. Hollfelder, Lars N. Jende, Cäcilia Maichle-Mössmer, and Reiner Anwander

published in:
Organometallics, **2014**, *33*, 1528–1531
doi: 10.1021/om401163a

Copyright (2014) American Chemical Society.

Supporting Information

Half-Sandwich Rare-Earth Metal Alkylaluminate Complexes Bearing Peripheral Boryl Ligands

Nicole Dettenrieder, Christoph O. Hollfelder, Lars N. Jende, Cäcilia Maichle-Mössmer, and Reiner Anwander

Institut für Anorganische Chemie, Universität Tübingen, Auf der Morgenstelle 18, D-72076 Tübingen, (Germany)

Table of Contents:

S2 Experimental data including NMR spectra

S17 Crystallographic data

S18 References

General Considerations. All operations were performed with rigorous exclusion of air and water, using standard Schlenk, high-vacuum, and glovebox techniques (MBraun 200B; <0.1 ppm O_2, <0.1 ppm H_2O). *n*-Hexane and toluene were purified by using Grubbs columns (MBraun SPS-800, solvent purification system) and stored in a glovebox. Benzene-*d*6 (99.5 %) was received from Deutero GmbH, toluene-*d*8 (99.5%) from euriso-top. Both NMR solvents were dried over NaK for a minimum of 48 h, and filtered through a filter pipette (Whatman) before use. $[(C_5Me_5)YMe_2]_3$ was synthesized from $(C_5Me_5)Y(AlMe_4)_2$,[1] which was made according to the literature (route a).[2] $[(C_5Me_5)LuMe_2]_3$ was obtained from $(C_5Me_5)Lu(AlMe_4)_2$.[3] $(C_5Me_5)Lu(AlMe_4)_2$ was synthesized slightly modified to the literature synthesis,[3] with 4 equiv. of HC_5Me_5 and 6 days reaction time at 35 °C. $[Me_2Al\{B(NDippCH)_2\}]_2$ was also synthesized according to the literature.[4] NMR spectra were recorded by using *J. Young* valve NMR tubes and obtained on a Bruker AVII+400 (^{1}H: 400.11 MHz, ^{13}C: 100.61 MHz) and on a Bruker AVII+500 spectrometer (^{1}H: 500.13 MHz, ^{13}C: 125.76 MHz, ^{11}B: 160.46 MHz, ^{19}F: 376.43 MHz , ^{89}Y: 24.51 MHz). ^{1}H and ^{13}C shifts are referenced to internal solvent resonances and reported in parts per million relative to TMS. IR spectra were recorded on a NICOLET Impact 410 FTIR spectrometer using a DRIFT chamber with dry KBr/sample mixtures and KBr windows. For the latter the collected data were converted using the Kubelka-Munk refinement. Elemental analyses were performed on an Elementar Vario MICRO cube.
The molar masses (M_w and M_n) of the polymers were determined by size-exclusion chromatography (SEC). Sample solutions (1.0 mg polymer per mL THF) were filtered through a 0.45 mm syringe filter prior to injection. SEC was performed with a GPCmax VE2001 pump (Viscotek) by employing ViscoGEL columns. Signals were detected by using a triple detection array (TDA 305) and calibrated against polystyrene standards (M_w/M_n<1.15). The flow rate was set to 1.0 mL min^{-1}. The microstructure of the polyisoprenes was examined by ^{1}H NMR and ^{13}C NMR spectroscopy on an AV400 spectrometer in $CDCl_3$ at ambient temperature. The DSC measurement was performed applying a X-DSC 7000 by Hitachi attached with an electric cooling unit. The sample of 12.8 mg of the investigated polymer was measured within a temperature range from -80°C to 140°C applying a heating rate of 10 K min^{-1}.

The abbreviation Dipp denotes 2,6-di*iso*propylphenyl.

$(C_5Me_5)Y[(AlMe_3)\{B(NDippCH)_2\}]_2$ (2)

To a suspension of $[(C_5Me_5)YMe_2]_3$ (48 mg, 0.063 mmol) was added dropwise a solution of $[Me_2Al\{B(NDippCH)_2\}]_2$ (168 mg, 0.189 mmol) in a mixture of *n*-hexane/toluene. The resulting, nearly clear solution was stirred for 1 h at ambient temperature and dried in vacuo. To the resulting sticky, white residue, *n*-hexane was added, the mixture filtered through a filter pipette, its volume reduced and recrystallized at -40 °C to yield 150 mg (69%) of pure product. ^{1}H NMR (C_6D_6, 500.13 MHz, 26 °C): $\delta = 7.28$ (4 H, *p*-C_6H_3-*i*Pr_2, unresolved t from AB_2 spin system, ^3J = 7.8 Hz), 7.23 (8 H, *m*-C_6H_3-*i*Pr_2, unresolved d from AB_2 spin system, ^3J = 7.8 Hz), 6.36 (s, 4 H, NC*H*), 3.40 (sep, 8 H, ^3J = 6.9 Hz, C*H*Me_2), 1.54 (s, 15 H, C_5Me_5), 1.36 (d, 24 H, ^3J = 6.9 Hz, CH*Me*$_2$), 1.25 (d, 24 H, ^3J = 6.8 Hz, CH*Me*$_2$), -0.63 (d, ^1J (Y-H) = 2.6 Hz, 18 H, $AlMe_3$) ppm. ^{13}C {^{1}H} NMR (C_6D_6, 125.77 MHz, 26 °C): $\delta = 146.6$ (*o*-C_6H_3-*i*Pr_2), 142.6 (*i*-C_6H_3-*i*Pr_2), 127.4 (*p*-C_6H_3-*i*Pr_2), 123.4 (*m*-C_6H_3-*i*Pr_2), 121.9 (or 121.8) (N*C*H), 121.8(or 121.9) (C_5Me_5), 28.6 (*C*HMe_2), 26.5 (CH*Me*$_2$), 23.6 (CH*Me*$_2$), 12.0 (C_5Me_5) ppm. For the C atoms of the $AlMe_3$ groups, no signal could be detected at 26 °C. However, when lowering the temperature to -55 °C in toluene-d_8, two coupling signals for the bridging methyl groups could be located at 6.6 and 8.7 ppm, respectively, in the HSQC NMR spectrum. ^{11}B {^{1}H} NMR (C_6D_6, 160.46 MHz, 26 °C): $\delta = 31.4$ ppm. ^{89}Y−^{1}H HSQC (C_6D_6, 24.51 MHz, 26 °C): δ (^{89}Y) = 144.5 ppm. IR (DRIFT, cm^{-1}): 3061 (w), 3023 (w), 2958 (vs), 2925 (s), 2862 (s),

2782 (w), 1456 (vs), 1442 (s), 1379 (s), 1323 (m), 1264 (m), 1255 (m), 1236 (m), 1206 (w), 1175 (w), 1150 (w), 1117 (m), 1058 (m), 936 (w), 894 (w), 803 (m), 761 (vs), 695 (vs), 615 (s), 552 (m), 512 (w), 459 (w). Elemental analysis (%) calcd. for $C_{68}H_{105}Al_2B_2N_4Y$ (1143.040 g mol^{-1}): C 71.45; H 9.26; N 4.90; found: C 72.19; H 8.91; N 4.53. Although these results are outside the range viewed as establishing analytical purity, they are provided to illustrate the best values obtained to date.

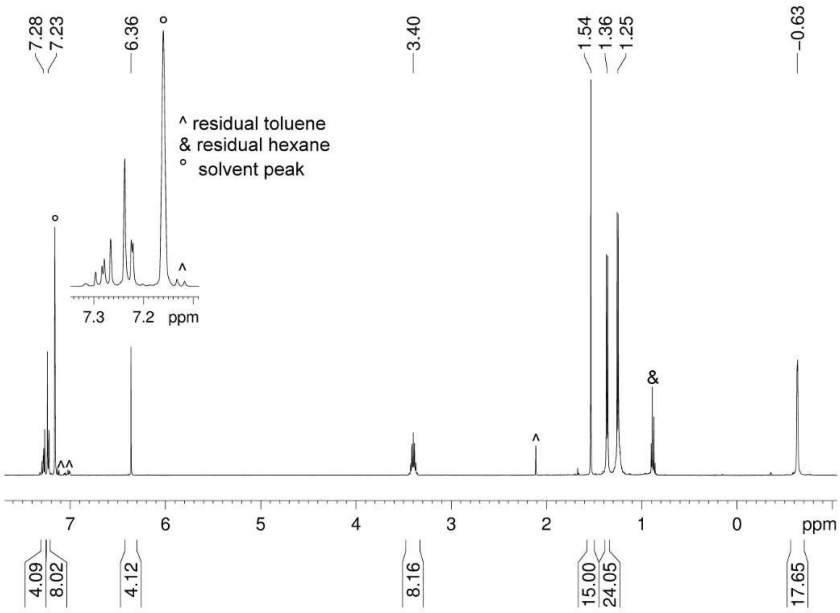

Figure S1. ^{1}H NMR spectrum of $(C_5Me_5)Y[(AlMe_3)\{B(NDippCH)_2\}]_2$ (**2**) in C_6D_6 at 26 °C.

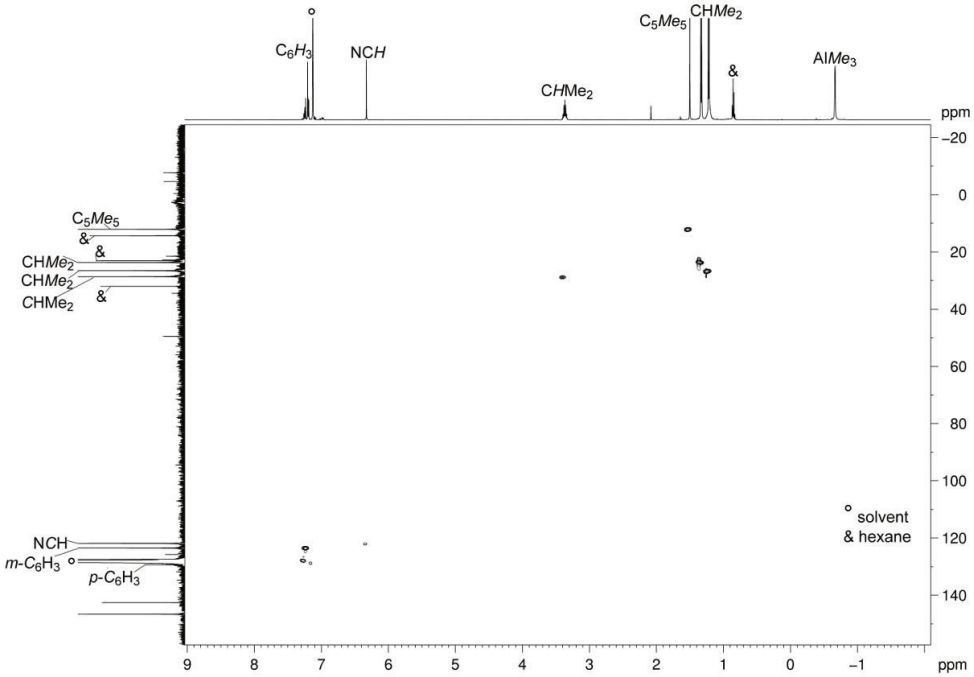

Figure S2. $^{1}H-^{13}C$-HSQC NMR spectrum of **2** in C_6D_6 at 26 °C.

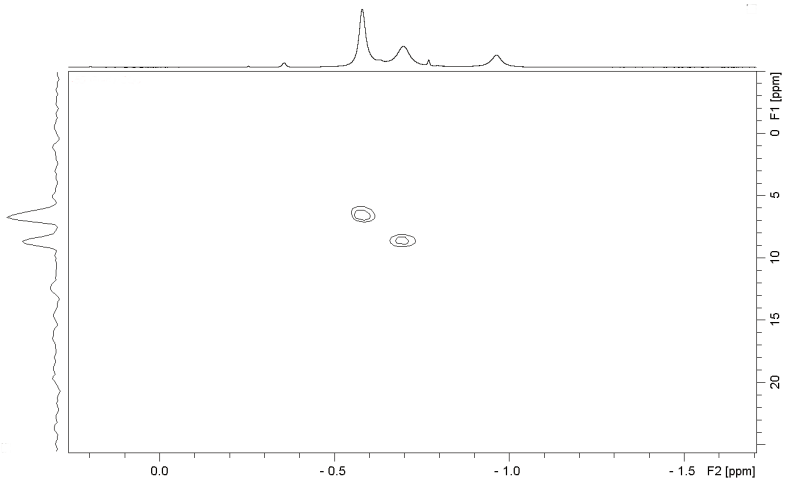

Figure S3. Cutout from a $^{1}H-^{13}C$-HSQC NMR spectrum of **2** at -55 °C in toluene- d_8 to detect the ^{13}C signals of the $AlMe_3$ units.

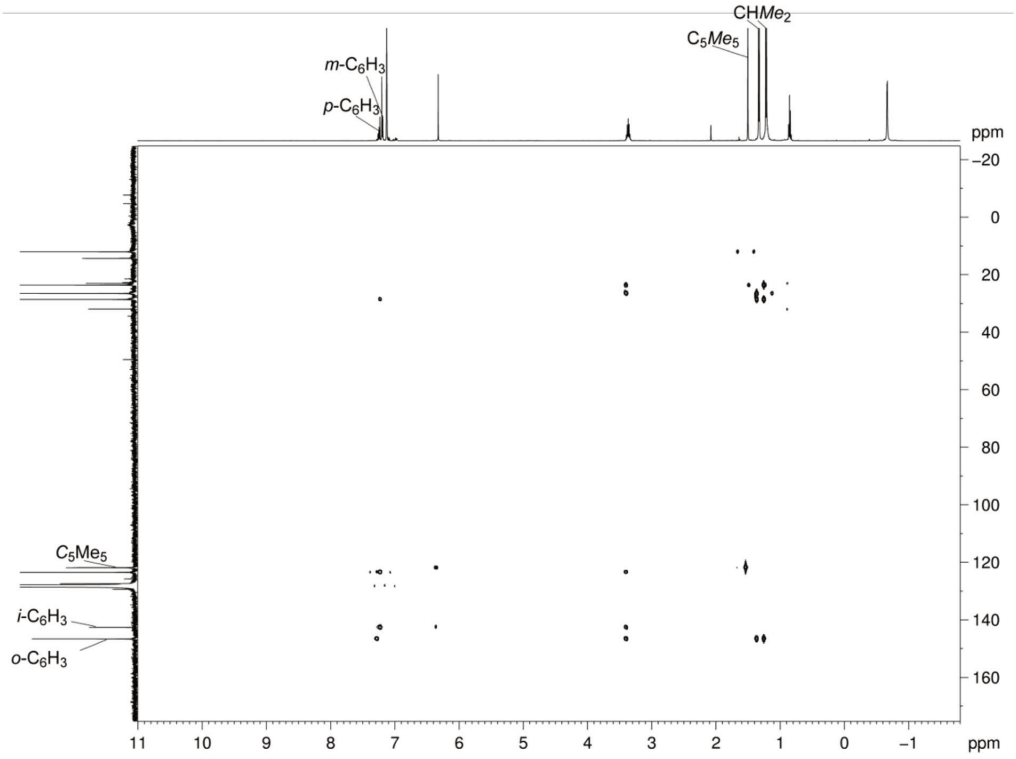

Figure S4. ^{1}H-^{13}C-HMBC NMR spectrum of **2** in C_6D_6 at 26 °C to detect quaternary C atoms.

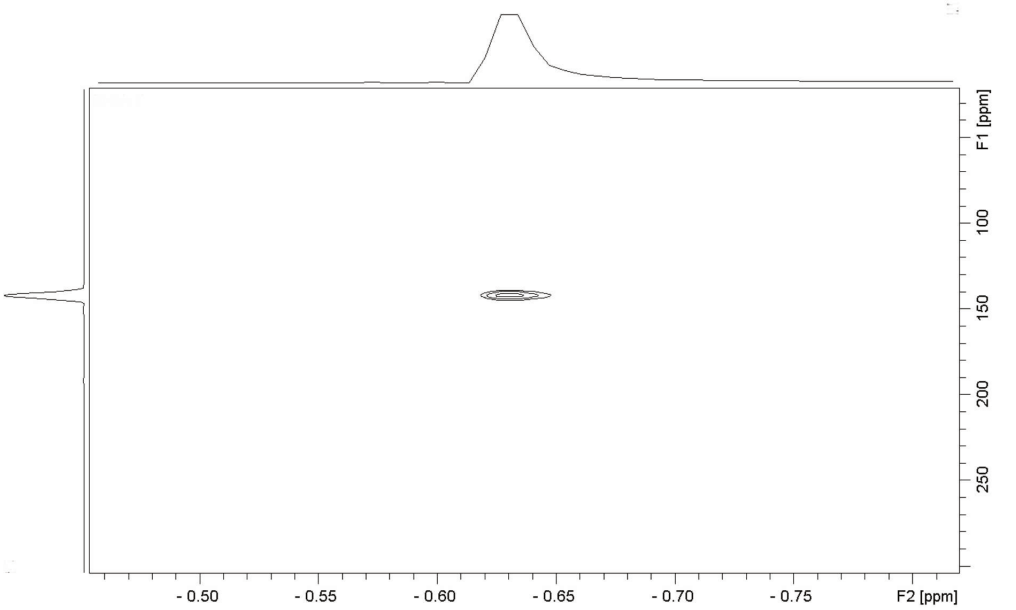

Figure S5. $^{1}H-^{89}Y$-HSQC NMR spectrum of **2** in C_6D_6 at 26 °C.

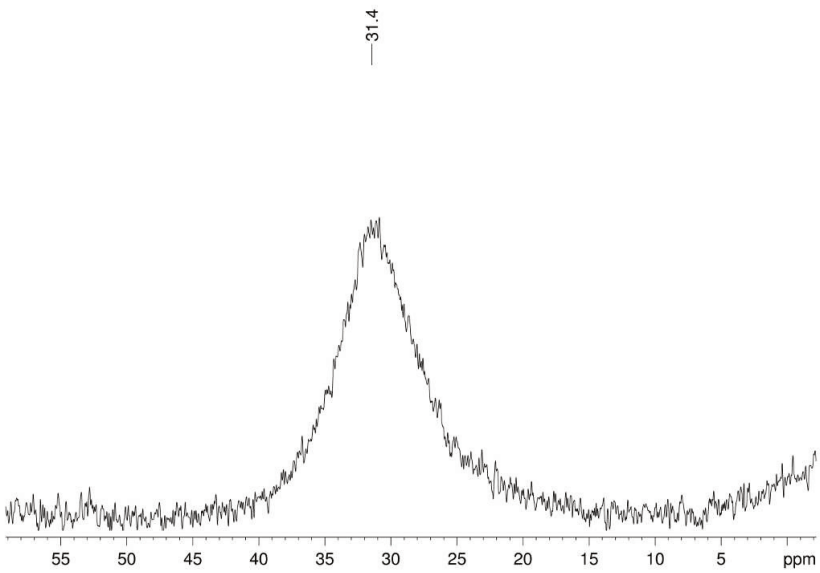

Figure S6. $^{11}B\{^{1}H\}$ NMR spectrum of **2** in C_6D_6 at 26 °C.

$(C_5Me_5)Lu[(AlMe_3)\{B(NDippCH)_2\}]_2$ (3)

To a solution of $\{Me_2Al[B(NDippCH)_2]\}_2$ (163 mg, 0.183 mmol) in 3 mL of *n*-hexane, $[(C_5Me_5)LuMe_2]_3$ (62 mg, 0.061 mmol) was added together with some drops of toluene. The resulting yellow suspension was stirred at +35 °C for one hour. The solvents were removed in vacuo and the sticky residue was recrystallized from *n*-hexane to yield colorless crystals with a yield of 148 mg (67%). ^{1}H NMR (C_6D_6, 400.11 MHz, 26 °C): $\delta = 7.26$ (4 H, *p*-C_6H_3-*i*Pr_2, m, A part of AB_2 spin system, ^{3}J = 7.9 Hz), 7.23 (8 H, *m*-C_6H_3-*i*Pr_2, m, B_2 part of AB_2 spin system, ^{3}J = 7.9 Hz), 6.36 (s, 4 H, NC*H*), 3.40 (sep, 8 H, ^{3}J = 6.8 Hz, C*H*Me_2), 1.56 (s, 15 H, (C_5Me_5)), 1.37 (d, 24 H, ^{3}J = 6.9 Hz, CH*Me*$_2$), 1.25 (d, 24 H, ^{3}J = 6.8 Hz, CH*Me*$_2$), -0.41 (s, 18 H, $AlMe_3$) ppm. $^{13}C\{^{1}H\}$ NMR (C_6D_6, 100.62 MHz, 26 °C): $\delta = 146.6$ (*o*-C_6H_3-*i*Pr_2), 142.5 (*i*-C_6H_3-*i*Pr_2), 127.4 (*p*-C_6H_3-*i*Pr_2), 123.4 (*m*-C_6H_3-*i*Pr_2), 121.9 (N*C*H), 120.4 (*C*$_5$Me$_5$), 28.6 (*C*HMe_2), 26.6 (CH*Me*$_2$), 23.6 (CH*Me*$_2$), 12.0 (C_5Me_5) ppm. For the C atoms of the $AlMe_3$ groups, no signal could be detected at 26 °C. However, when lowering the temperature to -40 °C in toluene-d_8, two C signals for the bridging methyl groups were located at 10.2 and 8.4 ppm, respectively. $^{11}B\{^{1}H\}$ NMR (C_6D_6, 160.46 MHz, 26 °C): $\delta = 31.0$ ppm. IR (DRIFT, cm^{-1}): 3065 (w), 3026 (w), 2958 (vs), 2937 (s), 2887 (m), 2866 (s), 1461 (s), 1442 (s), 1370 (vs), 1323 (m), 1267 (m), 1255 (m), 1239 (m), 1217 (w), 1182 (w), 1053 (w), 1112 (w), 939 (w), 897 (w), 803 (s), 761 (vs), 697 (s), 618 (m), 548 (w), 456 (w). Elemental analysis (%) calcd. for $C_{68}H_{105}Al_2B_2N_4Lu$ (1229.101 g mol^{-1}): C 66.45; H 8.61; N 4.56; found: C 65.87; H 8.62; N. 3.96. Although these results are outside the range viewed as establishing analytical purity, they are provided to illustrate the best values obtained to date.

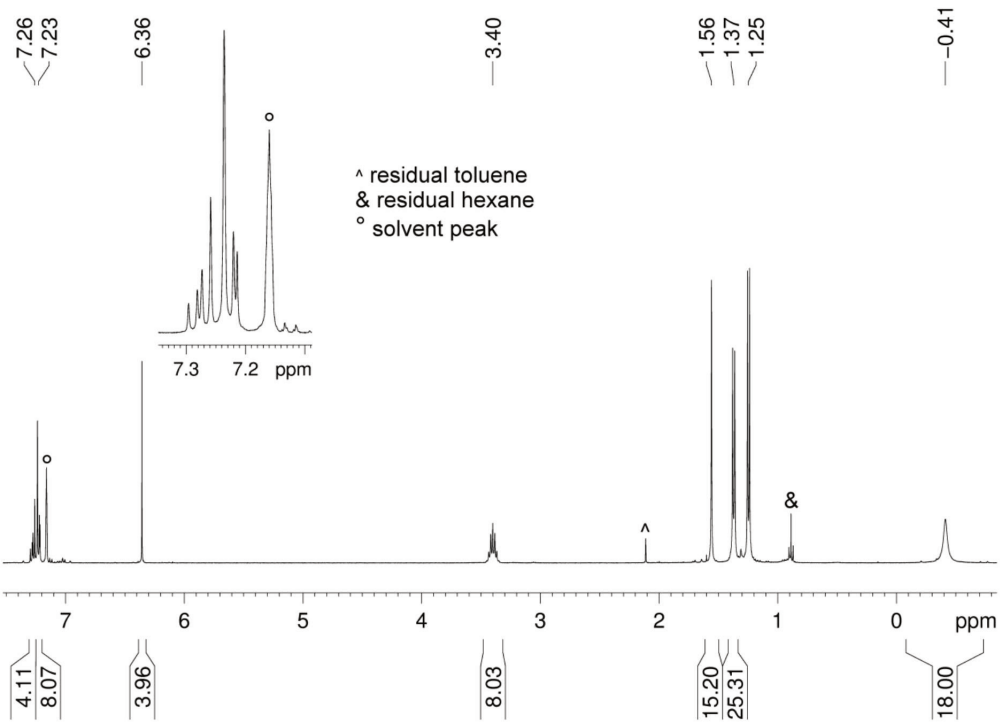

Figure S7. ^{1}H NMR spectrum of $(C_5Me_5)Lu[(AlMe_3)\{B(NDippCH)_2\}]_2$ (**3**) in C_6D_6 at 26 °C.

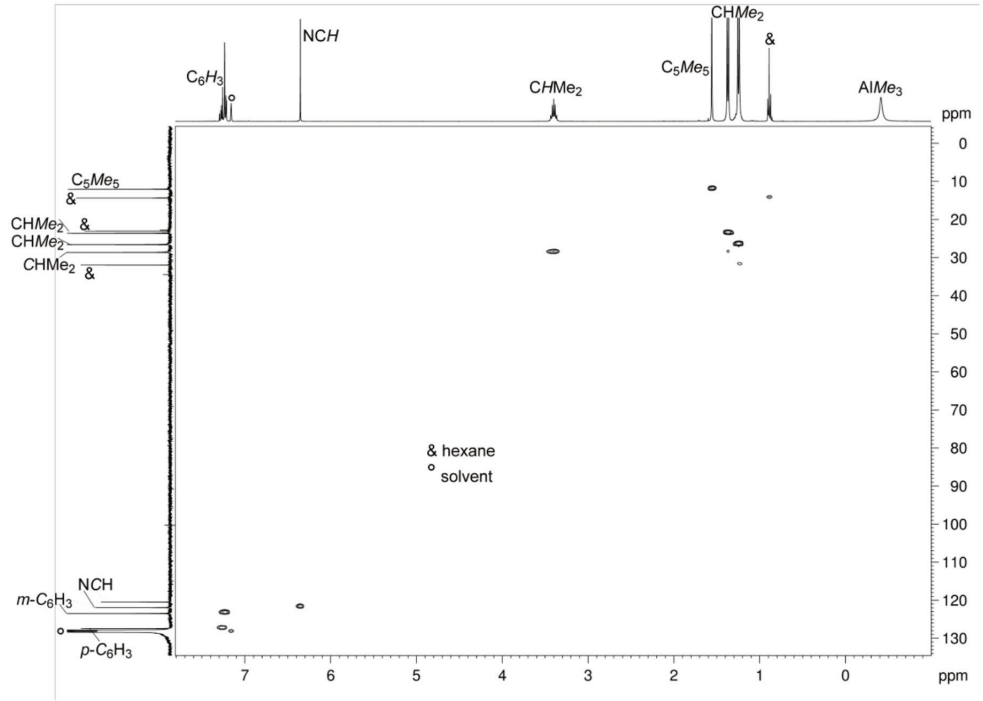

Figure S8. ^{1}H−^{13}C-HSQC NMR spectrum of **3** in C_6D_6 at 26 °C.

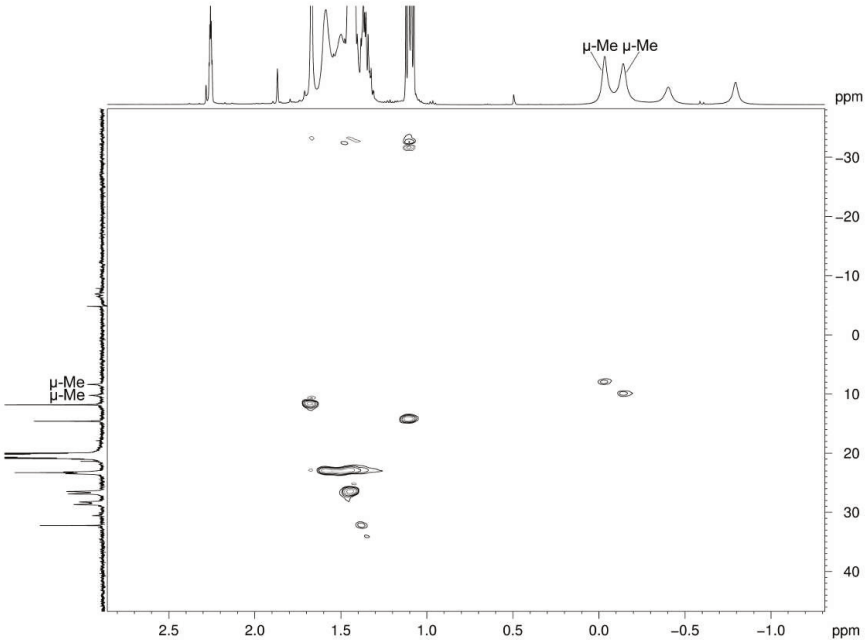

Figure S9. Cutout from a $^{1}H-^{13}C$-HSQC NMR spectrum of **3** at -40 ℃ in toluene-d_8 to detect ^{13}C signals of the $AlMe_3$ units.

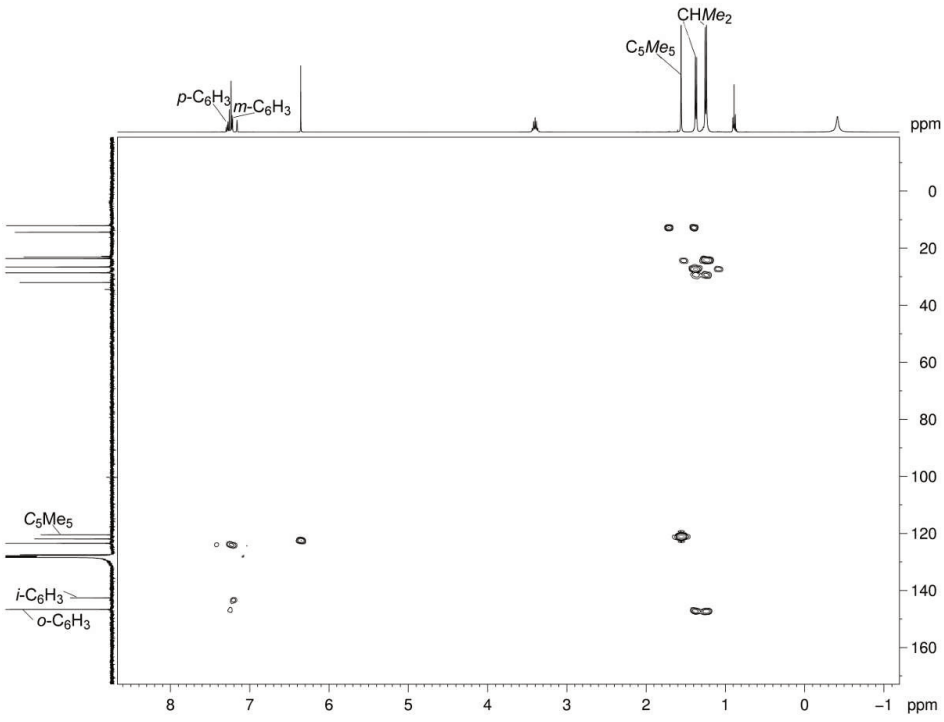

Figure S10. $^{1}H-^{13}C$-HMBC NMR spectrum of **3** in C_6D_6 at 26 ℃ to detect quaternary C atoms.

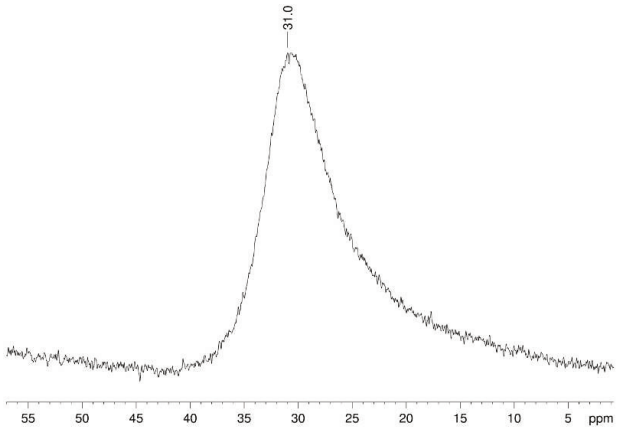

Figure S11. $^{11}B\{^{1}H\}$ NMR spectrum of **3** in C_6D_6 at 26 °C.

NMR reaction of $(C_5Me_5)Y[(AlMe_3)\{B(NDippCH)_2\}]_2$ (2) with two equivalents of THF

For the reaction, a stock solution of THF in C_6D_6 was prepared. Therefore, 6.5 mg (0.09 mmol) of THF were dissolved in 2.5 mL of C_6D_6. In a J. Young-valved NMR tube, 0.5 mL of the stock solution were added to 10.5 mg ($9.2 \cdot 10^{-3}$ mmol) of **2**. The reaction was monitored as shown in Figure S12.

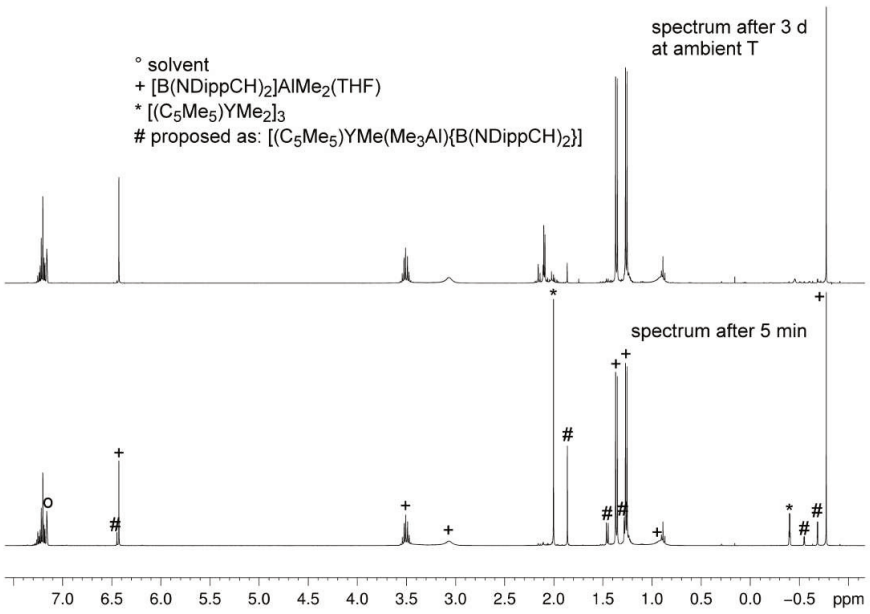

Figure S12. Reaction of $(C_5Me_5)Y[(AlMe_3)\{B(NDippCH)_2\}]_2$ (**2**) with 2 equiv of THF. C_6D_6 was used as a solvent. A cutout from the NMR spectrum is shown in Figure S13.

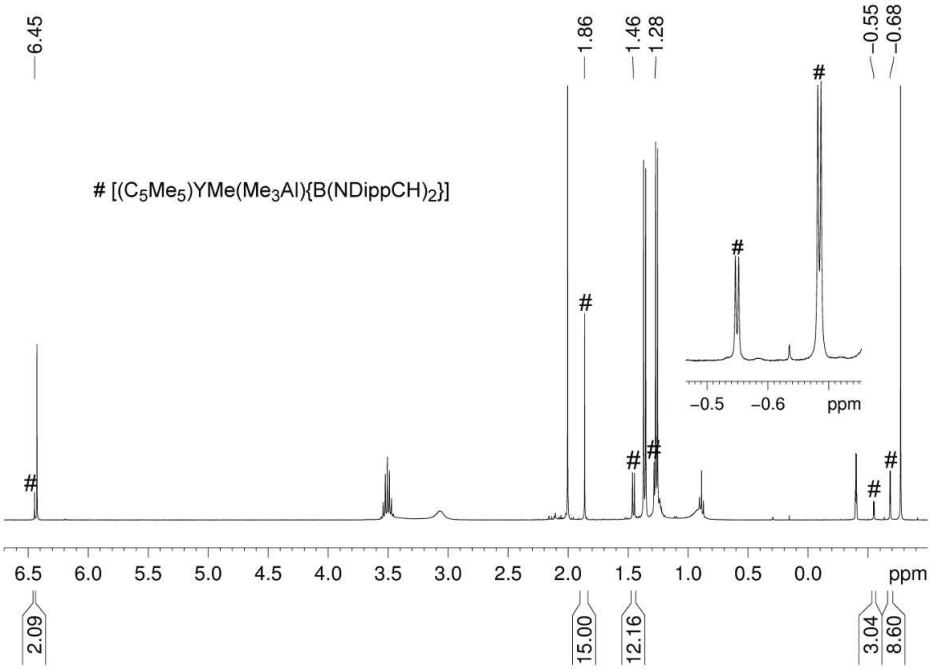

Figure S13. Cutout from Figure S12. The integrated and marked ^{1}H resonances belong to a species that is proposed to be $[(C_5Me_5)YMe(Me_3Al)\{B(NDippCH)_2\}]$ (**4**) by NMR.

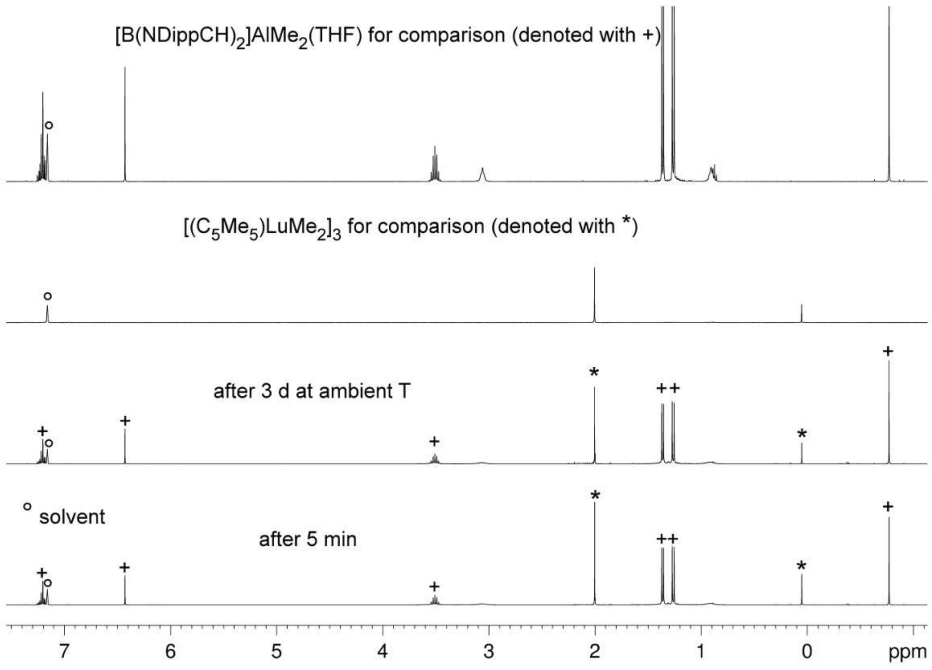

Figure S14. NMR-monitored reaction of $(C_5Me_5)Lu[(AlMe_3)\{B(NDippCH)_2\}]_2$ (**3**) with THF to form 2 $(THF)Me_2Al[B(NDippCH)_2]$ and 1/3 $[(C_5Me_5)LuMe_2]_3$. C_6D_6 was used as a solvent.

Polymerization of isoprene

A detailed polymerization procedure (run 5, Table 1 in the main publication) is described as a typical example. $[Ph_3C][B(C_6F_5)_4]$ (**A**, 18 mg, 0.02 mmol, 1 equiv) was added to a solution of compound **3** (24 mg, 0.02 mmol) in toluene (7 mL) and the mixture was aged under ambient temperature for 30 min. After the addition of isoprene (1.36 g, 20 mmol), the polymerization reaction was carried out at ambient temperature for 1 h. The reaction was terminated by pouring the polymerization mixture into methanol (200 mL) that contained 2,6-di-*tert*-butyl-4-methylphenol (0.1%, w/w) as a stabilizer and stirred for several minutes. The polymer was washed with methanol and dried under vacuum at ambient temperature to constant weight.

Table S1. Selected Examples of Isoprene Polymerization at ambient temperature.

entry[a]	precatalyst	cocatalyst[b]	t (h)	yield (%)	*cis*-1,4[c]	*trans*-1,4[c]	3,4[c]	M_n[d] (x 10^4)	M_w/M_n[d]	ref.
12	**2**	**C**	1	traces	---[e]	---[e]	---[e]	---[e]	---[e]	
13	**2**	**C**	24	71.8	1,9	84,1	11.2	5.4	2.02	
14	**3**	**C**	1	traces	---[e]	---[e]	---[e]	---[e]	---[e]	
15	**3**	**C**	24	34.1	21.2	68.4	10.4	3.0	1.97	
16	**3**	**C**	48	65.9	38.3	52.6	9.1	3.2	2.07	
17[f]	$Cp^*Y(AlMe_4)_2$	**C**	24	>99	1.9	93.6	4.5	9.0	1.78	5
18[f]	$Cp^*Lu(AlMe_4)_2$	**C**	0.5	26	74.6	20.7	4.7	11.0	1.39	

[a]Conditions: 0.02 mmol precatalyst, [Ln]/[cocat] = 1:1, 7 mL toluene, 20 mmol isoprene, r.t.. [b]Co-catalyst: **C** = $B(C_6F_5)_3$; [c]Determined by ^1H and ^{13}C NMR spectroscopy in $CDCl_3$. [d]Determined by means of size-exclusion chromatography (SEC) against polystyrene standards. [e]Not determined due to low yield. [f]Polymerizations at 40°C.

NMR-spectroscopic investigation on the active species

In order to investigate the active species of the polymerization run 5 of Table 1, 0.007 mmol (9 mg) of **3** were dissolved in 0.6 mL of toluene-d_8 and an equimolar amount of $[Ph_3C][B(C_6F_5)_4]$ (6.7 mg) was added as a solution in 0.3 mL of toluene-d_8. ^1H-NMR-Spectra were taken after 7, 10, 15, 20, 25 and 30 min. As no difference in the spectra was detected, only the first ^1H NMR spectrum is depicted (Figure S15). After 30 min, ^{19}F, ^{11}B, and ^{13}C NMR spectra were taken, as well as the 2D NMR spectra ^1H-^1H-COSY, ^{13}C-^1H-HSQC, and ^{13}C-^1H-HMBC.

The formation of three species is assumed: $[\{B(NDippCH)_2\}AlMe_2]_2$ (in the following denoted with the symbol &), $[\{B(NDippCH)_2\}(AlMe_3)Lu(C_5Me_5)]^+$ $[B(C_6F_5)_4]^-$ (in the following denoted with the symbol §), and Ph_3CMe (denoted as "t" in the spectra).

^1H NMR (toluene-*d*8, 500 MHz, 26 °C): δ = 7.70 (t, 1 H, ^3J = 7.7 Hz, *p*-$C_6H_3(iPr)_2$, §), 6.28 (s, 2 H, NC*H*, &), 6.22 (two overlapping doublets, 2 H, NC*H*, §), 3.21 (sep, ^3J = 6.9 Hz, 4 H, C*H*Me_2, &), 2.91 (sep, 2 H, ^3J = 7.0 Hz, C*H*Me_2, §), 2.83 (sep, 2 H, ^3J = 6.9 Hz, C*H*Me_2, §), 2.00 (s, 3 H, Ph_3CMe), 1.61 (s, 15 H, C_5Me_5), 1.21 (d, 12 H, CHMe_2, &), 1.15 (d, 12 H, CHMe_2, §), 1.12 (d, 12 H, CHMe_2, &), 0.95 (d, 6 H, CHMe_2, §), 0.87 (d, 6 H, CHMe_2, §), -0.25 (s, 6 H, μ-$AlMe_2$, §), -0.60 (s, 6 H, $AlMe_2$, &), -1.21 (s, 3 H, AlMe, §) ppm.

^{13}C {^1H} NMR (toluene-*d*8, 126 MHz, 26 °C) (incomplete and partly assigned on the basis of HSQC (see Figure S17) and HMBC spectra (see Figure S18)): δ = 158 (*o*-C_6H_3, §), 149 (*i*-$(C_6H_5)_3CMe$), 123 (C_5Me_5, §), 52 (Ph_3CMe), 28.6 (*C*HMe_2, &), 22.9 (μ-$AlMe_2$, §), 17.6 (CHMe_2, §), 11.4 (C_5Me_5, §) ppm.

^{11}B{^1H} NMR (toluene-*d*8, 160 MHz, 26 °C): δ = 16.0 ppm.

^{19}F{^1H} NMR (toluene-*d*8, 376 MHz, 26 °C): δ = -131.7 (br s, 2 F, *o*- C_6F_5), -162.5 (t, 1 F, ^3J = 20 Hz, *p*-C_6F_5), -166.4 (br s, 2 F, *m*- C_6F_5) ppm.

a)

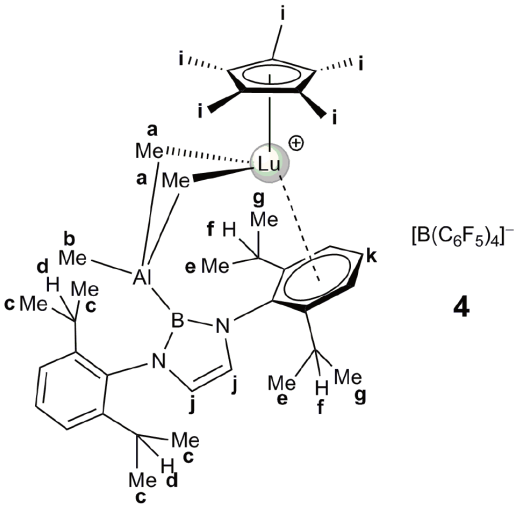

b)

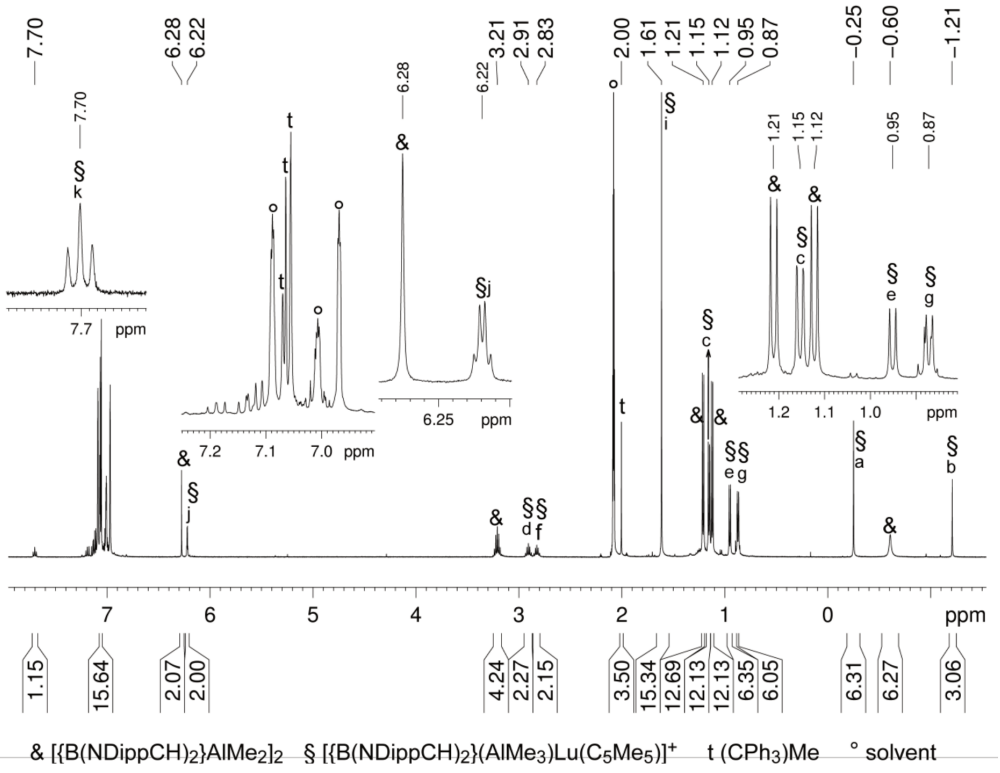

Figure S15. a) Suggested active species **4**; b) ^{1}H NMR spectrum (toluene-*d*8) of the equimolar reaction of $(C_5Me_5)Lu[(Me_3Al)\{B(NDippCH)_2\}]_2$ (**3**) and $[Ph_3C][B(C_6F_5)_4]$ measured 7 min after addition of the compounds.

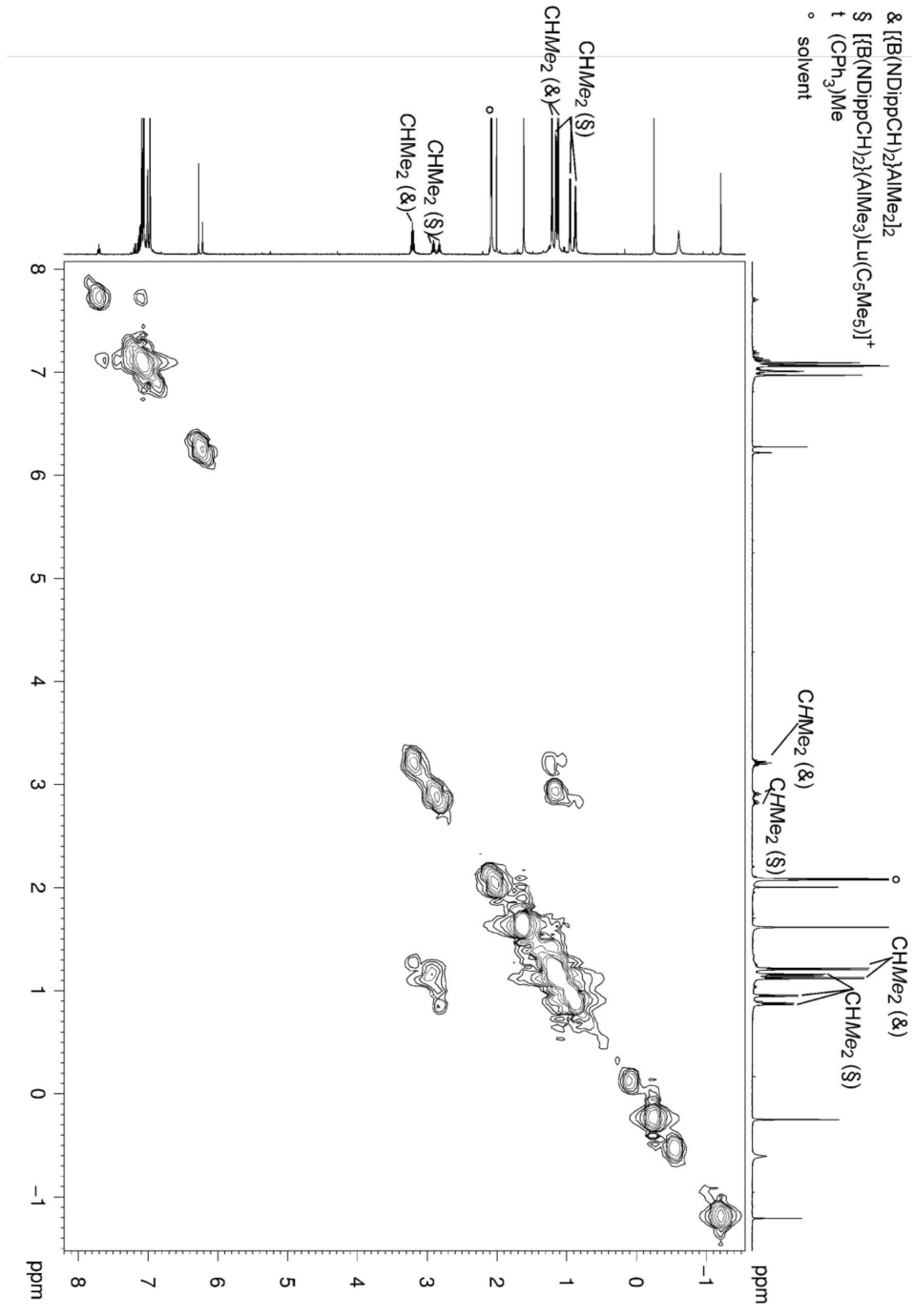

Figure S16. ^{1}H-^{1}H COSY NMR spectrum (toluene-*d*8) of the equimolar reaction of $(C_5Me_5)Lu[(Me_3Al)\{B(NDippCH)_2\}]_2$ (**3**) and $[Ph_3C][B(C_6F_5)_4]$. The cross-coupling peaks help for the assignment of the methyl signals of the isopropyl groups to the septet of the corresponding methine proton.

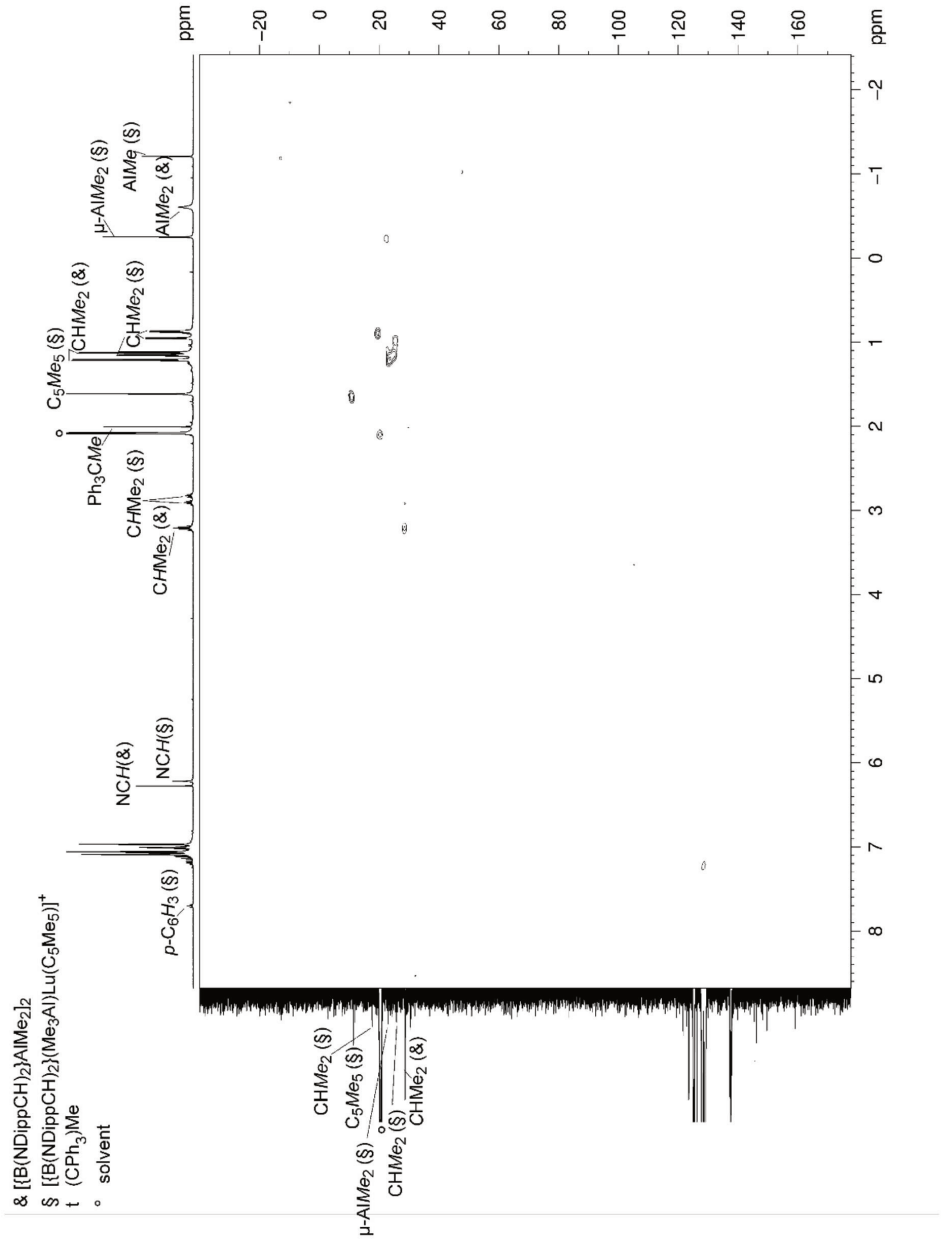

Figure S17. ^{1}H-^{13}C HSQC NMR spectrum (toluene-*d*8) of the equimolar reaction of $(C_5Me_5)Lu[(Me_3Al)\{B(NDippCH)_2\}]_2$ (**3**) and $[Ph_3C][B(C_6F_5)_4]$.

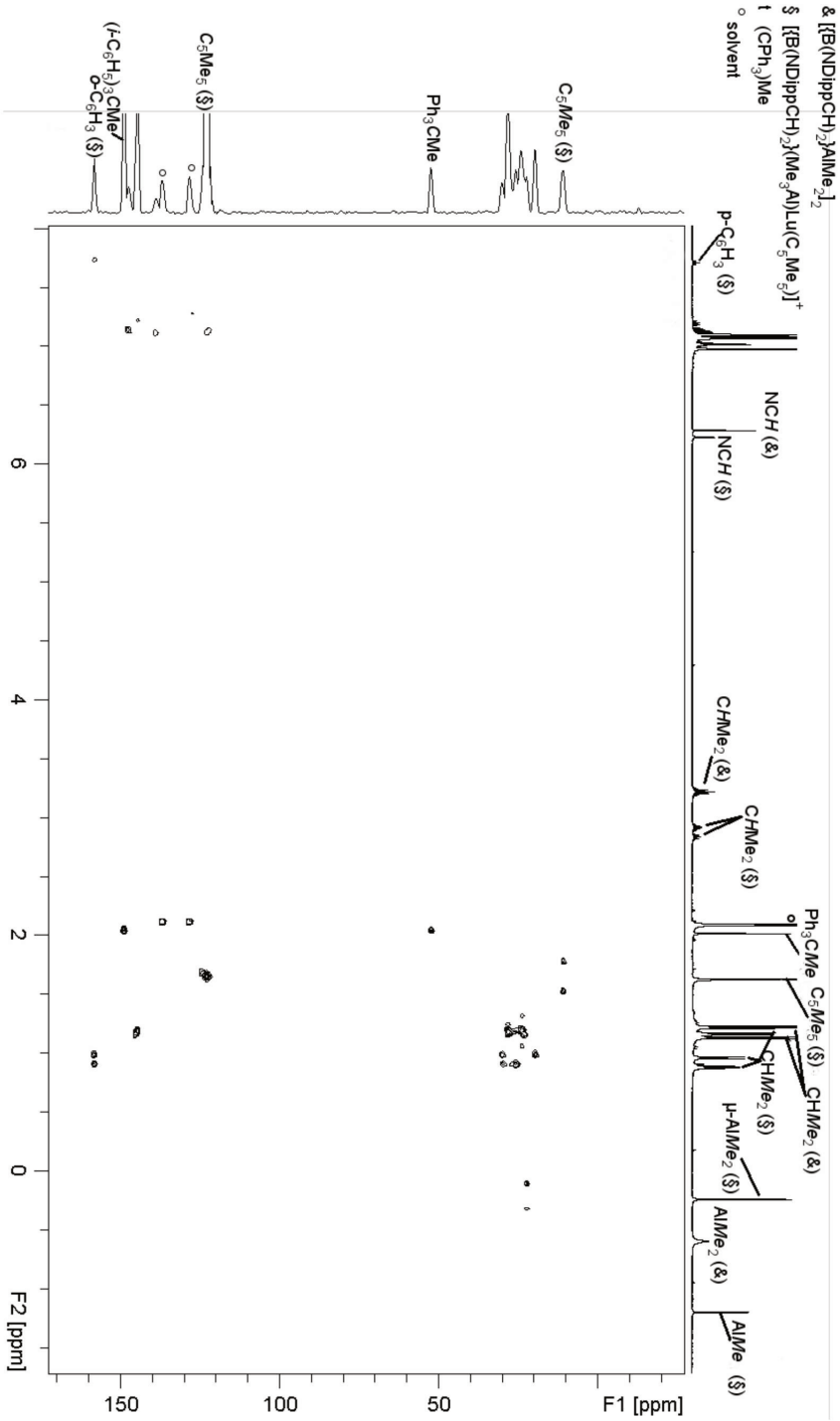

Figure S18. . ^{1}H-^{13}C HMBC spectrum (toluene-*d*8) of the equimolar reaction of $(C_5Me_5)Lu[(Me_3Al)\{B(NDippCH)_2\}]_2$ (**3**) and $[Ph_3C][B(C_6F_5)_4]$.

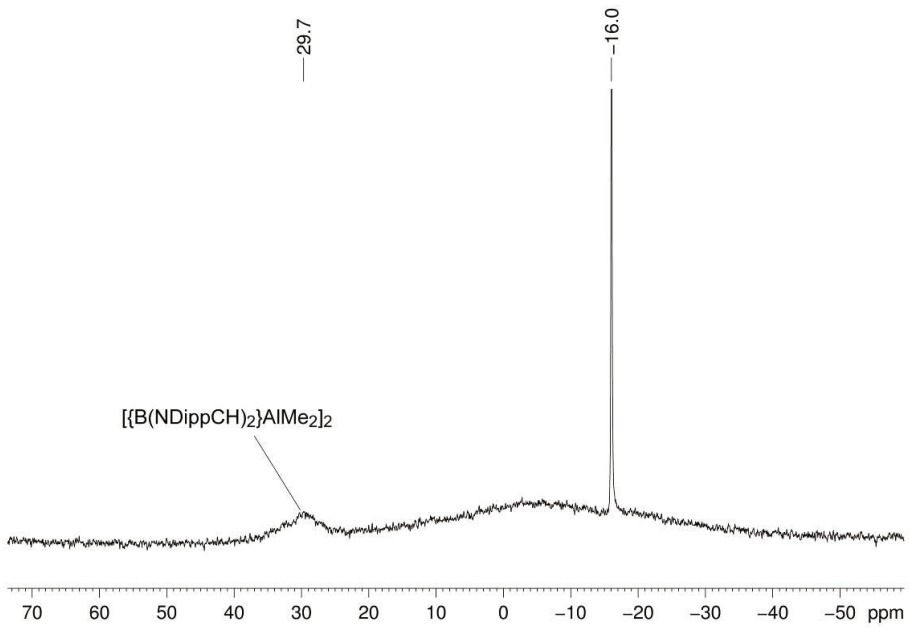

Figure S19. $^{11}B\{^{1}H\}$ NMR spectrum (toluene-*d*8) of the equimolar reaction of $(C_5Me_5)Lu[(Me_3Al)\{B(NDippCH)_2\}]_2$ (**3**) and $[Ph_3C][B(C_6F_5)_4]$.

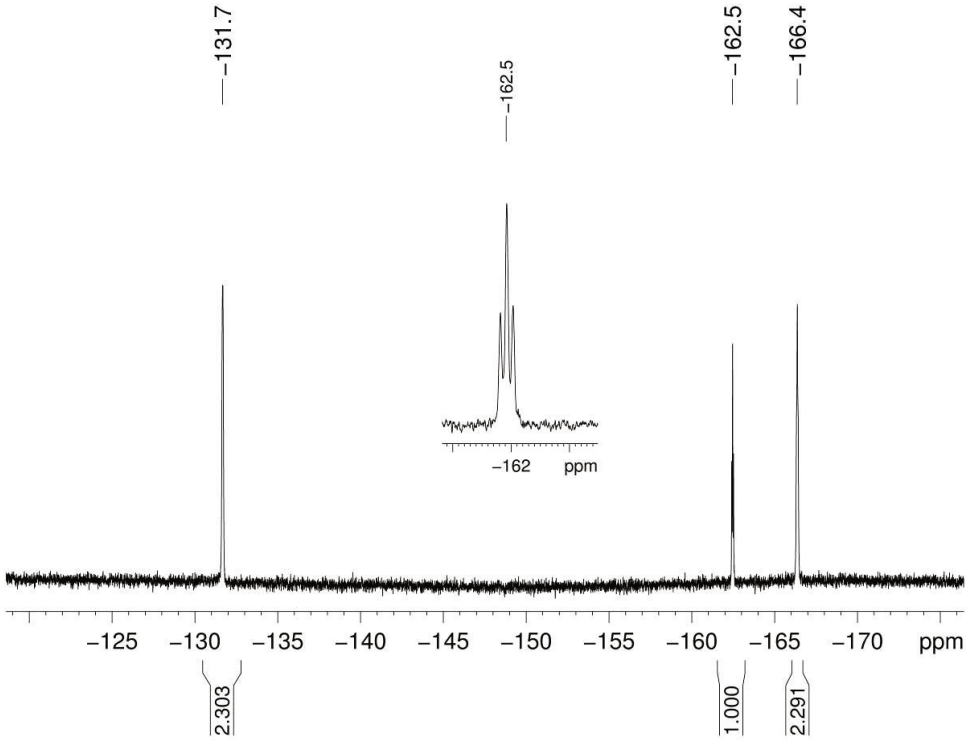

Figure S20. $^{19}F\{^{1}H\}$ NMR spectrum (toluene-*d*8) of the equimolar reaction of $(C_5Me_5)Lu[(AlMe_3)\{B(NDippCH)_2\}]_2$ (**3**) and $[Ph_3C][B(C_6F_5)_4]$.

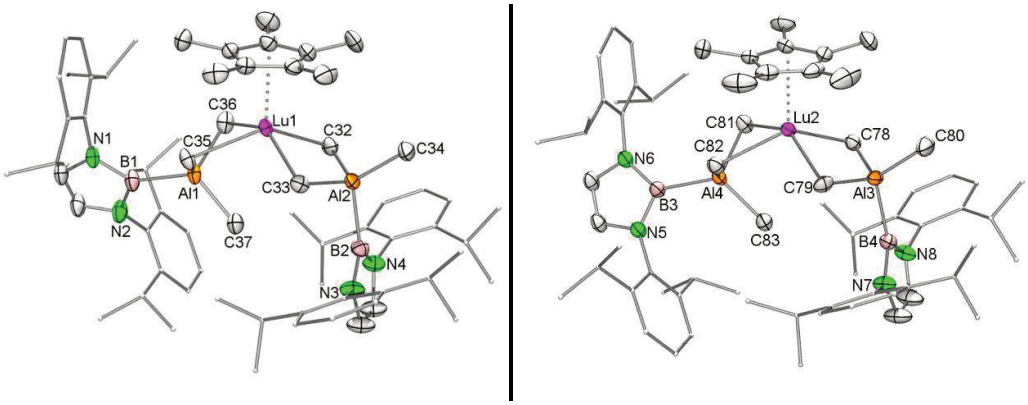

Figure S21. Solid-state structure of the two molecules in the asymmetric unit of $(C_5Me_5)Lu[(AlMe_3)\{B(NDippCH)_2\}]_2$ (**3**) with atomic displacement parameters set at the 50% level. The carbon atoms of the aromatic parts are shown with reduced radii. Hydrogen atoms and co-crystallized *n*-hexane have been omitted for clarity. Disorder in the aromatic parts has been removed. Selected bond lengths and angles are listed below in Table1.

Table S2. Relevant distances [Å] and angles [°] for the two molecules in the asymmetr ic unit of **3**.

Lu1−C32	2.506(4)	Lu2−C78	2.507(4)
Lu1−C33	2.504(3)	Lu2−C79	2.509(4)
Lu1−C35	2.605(4)	Lu2−C81	2.622(4)
Lu1−C36	2.590(4)	Lu2−C82	2.591(4)
Lu1···C37	3.381(4)	Lu2···C83	3.351(4)
Lu1···Al1	2.917(2)	Lu2···Al3	3.062(2)
Lu1···Al2	3.059(2)	Lu2···Al4	2.913(2)
Al1−C35	2.067(4)	Al4−C82	2.067(4)
Al1−C36	2.068(4)	Al4−C81	2.073(4)
Al1−C37	1.989(4)	Al4−C83	1.986(4)
Al2−C32	2.077(4)	Al3−C78	2.086(4)
Al2−C33	2.088(4)	Al3−C79	2.087(4)
Al2−C34	1.987(4)	Al3−C80	1.982(4)
B1−Al1	2.137(5)	B3−Al4	2.137(4)
B2−Al2	2.135(5)	B4−Al3	2.137(4)
C32Lu1C33−C32Al2C33	13.7	C78CLu2C79−C78Al3C79	13.1
C35Lu1C36−C35Al1C36	51.2	C81Lu2C82−C81Al4C82	51.6

Table S3. Crystallographic data information for **3**.

	3
Formula	$C_{77}H_{126}Al_2B_2LuN_4$
Fw	1358.37
temp (K)	100(2)
cryst syst	triclinic
space group	P-1
a (Å)	13.4966(3)
b (Å)	18.6094(5)
c (Å)	32.8876(9)
α (deg)	82.408(2)
β (deg)	83.6630(10)
γ (deg)	79.017(2)
vol (Å^3)	8006.9(4)
Z	4
ρ_{calcd} (mg/mm^3)	1.127
μ (mm^{-1})	1.295
R1[a] ($I > 2.0\sigma(I)$)	0.0423
wR2[b] (all data)	0.1148
diffractometer system	APEX II DUO

[a] $R1 = \Sigma(||F_0|-|F_c||)/\Sigma|F_0|$. [b] $wR2 = \{\Sigma[w(F_0^2-F_c^2)^2/\Sigma[w(F_0^2)^2]\}^{1/2}$

Because of poor crystal quality, data collection for complex **2** was not completed and hence not deposited. Due to the nearly identical cell parameters (a = 13.5337; b = 18.6533; c = 33.0015; α = 82.371; β = 83.305; γ = 78.392), crystals of complex **2** are assumed to be isomorphous to the ones of **3**. Crystals of compounds **2** and **3** are colorless and were crystallized from a mixture of toluene/ *n*-hexane at -40 °C. Data for **2** and **3** were collected on a Bruker APEX DUO instrument by using QUAZAR optics and MoK_α radiation (λ = 0.71073 Å), with ω and ϕ scans. The raw data was processed by using APEX2[6] and SAINT software;[7] structure solution and final model refinement were performed by using SHELXTL.[8] Corrections for absorption effects were applied by using SADABS.[9] All graphics were produced by using ORTEP-3[10] and POV-Ray.[11]

References

(1) Dietrich, H. M.; Grove, H.; Törnroos, K. W.; Anwander, R. *J. Am. Chem. Soc.* **2006**, *128*, 1458.
(2) Dietrich, H. M.; Törnroos, K. W.; Herdtweck, E.; Anwander, R. *Organometallics* **2009**, *28*, 6739.
(3) Dietrich, H. M; Zapilko, C.; Herdtweck, E.; Anwander, R. Organometallics **2005**, *24*, 5767.
(4) Dettenrieder, N.; Dietrich, H. M.; Schädle, C.; Maichle-Mössmer, C.; Törnroos, K. W.; Anwander, R. *Angew. Chem., Int. Ed.* **2012**, *51*, 4461.
(5) Zimmermann, M.; Törnroos, K. W.; Sitzmann, H.; Anwander, R. *Chem. Eur. J.* **2008**, *14*, 7266.
(6) APEX v. 2012.10_0 Madison, WI, **2010**.
(7) Saint v. 7.99A Madison, WI, **2010**.
(8) Sheldrick, G. M., SHELXTL v. 2012.10_2, Madison, WI, **2012**.
(9) Sheldrick, G. M., SADABS v. 2012/1, Madison, WI, **2012**.
(10) L. J. Farrugia *J. Appl. Crystallogr.* **1997**, 565.
(11) POV-Ray v. 3.6 Williamstown, Victoria, Australia, **2004**, (http://www.povray.org).

Paper II: Rare-Earth-Metal Allyl Complexes Supported by the [2-(*N*,*N*-Dimethylamino)ethyl]tetramethylcyclopentadienyl Ligand: Structural Characterization, Reactivity, and Isoprene Polymerization

This aricle is reprinted with permission from:

"Rare-Earth-Metal Allyl Complexes Supported by the [2-(*N*,*N*-Dimethylamino)ethyl]tetramethylcyclopentadienyl Ligand: Structural Characterization, Reactivity, and Isoprene Polymerization"

by
Lars N. Jende, Christoph O. Hollfelder, Cäcilia Maichle-Mössmer, and Reiner Anwander

published in:
Organometallics, **2015**, *34*, 32–41
doi: 10.1021/om500725g

Copyright (2015) American Chemical Society.

ORGANOMETALLICS

Article

pubs.acs.org/Organometallics

Rare-Earth-Metal Allyl Complexes Supported by the [2-(*N*,*N*-Dimethylamino)ethyl]tetramethylcyclopentadienyl Ligand: Structural Characterization, Reactivity, and Isoprene Polymerization

Lars N. Jende, Christoph O. Hollfelder, Cäcilia Maichle-Mössmer, and Reiner Anwander*

Institut für Anorganische Chemie, Universität Tübingen, Auf der Morgenstelle 18, D-72076 Tübingen, Germany

Supporting Information

ABSTRACT: Rare-earth-metal half-sandwich allyl complexes bearing an amino-functionalized cyclopentadienyl ligand (Cp^{NMe2} = 1-[2-(*N*,*N*-dimethylamino)ethyl]-2,3,4,5-tetramethylcyclopentadienyl) were synthesized in a two-step salt-metathesis reaction. Treatment of $LnCl_3(THF)_x$ with $LiCp^{NMe2}$, followed by an in situ reaction with the Grignard reagent C_3H_5MgCl, generated the bis(allyl) half-sandwich complexes $Cp^{NMe2}Ln(\eta^3\text{-}C_3H_5)_2$ only for the smaller rare-earth metals (Ln = Y, Ho, Lu) in good yields (82−88%). In case of the larger neodymium, the dimeric mono(allyl) chlorido half-sandwich complex $[Cp^{NMe2}Nd(\eta^3\text{-}C_3H_5)(\mu\text{-}Cl)]_2$ was obtained in 68% yield. All complexes show moderate to high activity in isoprene polymerization upon cationization with organoborates $[Ph_3C][B(C_6F_5)_4]$ and $[PhNMe_2H][B(C_6F_5)_4]$, the yttrium, holmium, and neodymium metal centers yielding mainly 3,4-microstructures (maximum 79%). Addition of 10 equiv of $AlMe_3$ to the catalyst systems $Cp^{NMe2}Ln(\eta^3\text{-}C_3H_5)_2$ (Ln = Y, Ho)/$[PhNMe_2H][B(C_6F_5)_4]$ and $[Cp^{NMe2}Nd(\eta^3\text{-}C_3H_5)(\mu\text{-}Cl)]_2$/$[PhNMe_2H][B(C_6F_5)_4]$ switched the polyisoprene stereoregularity from 3,4-specific to trans-1,4-selective (maximum 85%). The use of $AliBu_3$ instead led to polymers with mainly cis-1,4-microstructure for the monomeric yttrium and holmium complexes (maximum 74%). Treatment of the bis(allyl) complexes with Et_2AlCl (as cocatalyst) did not provide active species for isoprene polymerization but led to [allyl] → [Cl] exchange and isolation of the hexameric rare-earth-metal clusters $[\{(Cp^{NMe2AlEt3})_2(Cp^{NMe2})Ln_3(\mu_2\text{-}Cl)_3(\mu_3\text{-}Cl)_2\}(\mu_2\text{-}Cl)]_2$ (Ln = Y, Ho). The complexes $Cp^{NMe2}Ln(\eta^3\text{-}C_3H_5)_2$ (Ln = Y, Ho, Lu), $[Cp^{NMe2}Nd(\eta^3\text{-}C_3H_5)(\mu\text{-}Cl)]_2$, and $[\{(Cp^{NMe2AlEt3})_2(Cp^{NMe2})Ln_3(\mu_2\text{-}Cl)_3(\mu_3\text{-}Cl)_2\}(\mu_2\text{-}Cl)]_2$ (Ln = Y, Ho) were analyzed by X-ray crystallography.

INTRODUCTION

The development of rare-earth-metal (Ln) based single-site initiators for polymerization reactions has been closely related to the progress in group 4 metal based homogeneous Ziegler−Natta catalysis.[1] Most striking was the discovery by Marks and Schumann et al. that lanthanidocene complexes revealed high catalytic activity in ethylene polymerization without further activation by cocatalysts (so-called single-component catalysts).[2,3] The introduction of dianionic bidentate amido-cyclopentadienyl ligands by Bercaw and Shapiro, such as in scandium complexes $[(C_5Me_4SiMe_2NCMe_3)Sc(PMe_3)_2(\mu\text{-}R)]_2$ (R = H, alkyl), marked another milestone.[4] This approach, which implies enhanced reactivity through electronically and sterically less saturated metal centers, was adopted by the Dow and Exxon Chemical Cos. for group 4 metal centers as the first "constrained geometry" catalysts (CGC).[5,6] Since then, a series of rare-earth-metal(III) complexes of this type have been reported,[7] but as they exist by nature only as mono(alkyl) or -(hydride) species, these complexes generally display no activity in 1,3-diene polymerization. The rare examples that can polymerize 1,3-butadiene and isoprene are limited to the dimeric complexes $[(C_5Me_4)_2Ln(\mu\text{-}Me)_2AlMe_2]_2$[8−11] and $[(C_5Me_4)SiMe_2P(Cy)Ln(CH_2SiMe_3)]_2$[12] (Ln = Y, Lu; Cy = cyclohexyl), requiring activation with 1 equiv of cocatalyst, thus forming a dimeric mono(alkyl) monocation as the active species, and the *ansa*-neodymocene complex $[(CpCMe_2Flu)Nd(\mu^3\text{-}C_3H_5)(thf)]$ (Cp = cyclopentadienyl, Flu = fluorenyl),[13,14] representing a single-component catalyst which also terpolymerizes conjugated dienes with styrene and ethylene. The need for a remaining reactive metal−carbon bond upon activation led to extensive investigations of half-sandwich rare-earth-metal bis(hydrocarbyl) complexes of the $[(\mathbf{L})Ln^{III}R_2(Do)_x]$ type, bearing a monoanionic ancillary ligand (**L**) and σ-bonded alkyl groups (R = Me, CH_2SiMe_3, CH_2Ph, $CH_2C_6H_4$-*o*-NMe_2), as versatile polymerization initiators.[15,16] Due to the sterically unsaturated Ln(III) centers, incorporation of neutral donor ligands (Do) was frequently observed.[15,16]

In contrast, donor side arm substituted cyclopentadienyls, fluorenyls, and indenyls as monoanionic ancillary ligands can mimic a constrained geometry configuration, thus accomplishing "solvent free", highly stable precatalysts with well-defined reaction sites.[17−33] Very recently, Cui et al. reported on the synthesis and characterization of a series of linked-half-sandwich rare-earth-metal bis(allyl) complexes and demonstrated their excellent catalytic performance in the polymerization of 1,3-diene and styrene, following cationization with organoborate activators in the presence or absence of

Received: July 15, 2014
Published: December 24, 2014

ACS Publications © 2014 American Chemical Society

DOI: 10.1021/om500725g
Organometallics 2015, 34, 32−41

trialkylaluminum.[17,18,20,24] Worth emphasizing is a comprehensive study on isoprene polymerization promoted by the *N*,*N*-dimethylanilinyl-substituted half-sandwich rare-earth-metal complexes $[(C_5Me_4C_6H_4$-*o*-$NMe_2)Ln(\eta^3$-$C_3H_5)_2]$ (Ln = Y, Nd, Gd, Dy) back in 2010.[24] Activation of the respective gadolinium complex with $[PhNMe_2H][B(C_6F_5)_4]$ and 10 equiv of $AlMe_3$ produced the first rare-earth-metal bis(allyl) system that polymerizes isoprene in a living fashion (PDI = 1.11). While the moderate cis-1,4 selectivity of 83% could be increased to 99% via addition of Al^iBu_3, the capability of the organoaluminum compound to act as a chain-transfer agent was revealed by up to eight growing polymer chains per gadolinium center (800% catalytic efficiency). In the same year, the group of Cui reported the bis(allyl) lutetium complex $[(C_5Me_4C_6H_4N)Lu(\eta^3$-$C_3H_5)_2]$, bearing a pyridyl-substituted cyclopentadienyl ancillary ligand, to initiate highly cis-1,4-selective (99%) butadiene and purely syndiotactic (*rrrr* >99%) styrene polymerization on activation with the trityl borate agent $[Ph_3C][B(C_6F_5)_4]$.[17] The latter cationic lutetium CGC catalyst was also employed for the terpolymerization of styrene with 1,3-butadiene and isoprene, allowing outstanding control over regio- and stereoregularity as well as block copolymer formation.[20] Previous studies on bis(allyl) rare-earth-metal half-sandwich complexes also feature Taube's complex $[(C_5Me_5)Nd(\eta^3$-$C_3H_5)_2(C_4H_8O_2)_{0.7}]$, which upon activation with MAO (Al/Nd = 30) produced polybutadiene with cis contents as high as 66%.[34] The latter dioxane complex was obtained via protonolysis employing $[Nd(\eta^3$-$C_3H_5)_3(C_4H_8O_2)]$ and HC_5Me_5.

Recently, our group developed a bis(tetramethylaluminate)-based library of $[(\mathbf{L})Ln^{III}(AlMe_4)_2]$-type complexes, particularly to be exploited for 1,3-diene polymerization. The respective monoanionic ancillary ligands **L** also comprise N-donor-functionalized quinolyl-,[35] aminophenyl-,[35] and dimethylaminoethyl-cyclopentadienyl ligands[36] (Cp^Q, Cp^{ANMe2}, and Cp^{NMe2}).[37−41] Triggered by the interesting catalytic properties of the bis(allyl) complexes presented by Cui, we set out to examine Cp^{NMe2}-supported rare-earth-metal bis(allyl) complexes. Here, we focused on the implications of a flexible C_2 spacer between the cyclopentadienyl and N-donor moieties, and whether [allyl] → [organoaluminum] exchanges under formation of identifiable alkylaluminate species can be observed as Evans reported for $[\{C_5Me_4SiMe_2(CH_2CH{=}CH_2)\}_2Y(\eta^3$-$C_3H_5)]$.[42] In addition, the performance in isoprene polymerization upon activation with perfluorated organoborate compounds was tested and compared with the performance of half-sandwich bis(aluminate) complexes.

■ RESULTS AND DISCUSSION

The salt-metathesis reaction of $LnCl_3(THF)_x$ with $[C_5Me_4C_2H_4NMe_2]Li$ at ambient temperature for 4 h, followed by an in situ reaction with the Grignard reagent C_3H_5MgCl for another 16 h, generated the bis(allyl) half-sandwich complexes $[Cp^{NMe2}Ln(\eta^3$-$C_3H_5)_2]$ (**1**) in high yields (82−88%) for the smaller rare-earth metals (Ln = Y (**1a**), Ho (**1b**), Lu (**1c**)) (Scheme 1). In the case of the larger neodymium, only the dimeric mono(allyl) chlorido half-sandwich complex $[Cp^{NMe2}Nd(\eta^3$-$C_3H_5)(\mu$-$Cl)]_2$ (**2**) was obtained under identical reaction conditions. We assume that the presence of two bridging chlorido ligands sterically disfavors any complete displacement by allyl moieties. Although the elemental analyses of samples, obtained from the reaction of isolated complex **2** with another 1 equiv of C_3H_5MgCl, showed increased

Scheme 1. Synthesis of Rare-Earth-Metal Bis(allyl) Complexes 1 and the Dimeric Neodymium Mono(allyl) Chlorido Half-Sandwich Complex 2

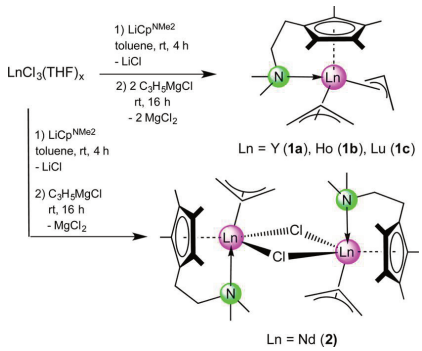

hydrogen and carbon values indicative of further chlorido allyl exchange, no crystalline products could be obtained. Attempts to isolate the respective complexes with the largest rare-earth-metal, lanthanum, failed.

The ^{1}H NMR spectra of the diamagnetic complexes **1a** (Y) and **1b** (Lu) show the expected sets of signals for the cyclopentadienyl ligand. In particular, three singlets for the methyl groups and two multiplets for the ethyl spacer were detected. The methine proton of the allyl group in compound **1a** gave a doublet of quintets at 6.31 ppm. The signal splitting of the quintet ($^3J_{HH}$ = 12.36 Hz) is clearly attributable to a two-bond ^{1}H−^{89}Y scalar coupling ($^2J_{YH}$ = 1.36 Hz). The resonance of the corresponding methylene protons appeared at 3.04 ppm as a rather broad doublet, implying fast exchange of the terminal allylic protons (H_{syn} and H_{anti}). The allyl groups of the lutetium complex **1c** gave a quintet at 6.37 ppm ($^3J_{HH}$ = 12.36 Hz) and a sharp doublet at 3.07 ppm ($^3J_{HH}$ = 12.36 Hz) for the methine and methylene protons, respectively.

Single crystals of complexes **1** suitable for X-ray crystallography were grown from saturated toluene/*n*-hexane solutions at −35 °C. The complexes are isostructural and crystallize in the monoclinic space group $P2_1$. The representative molecular structure of **1a** is shown in Figure 1, and selected bond distances and angles for complexes **1** are given in Table 1. The ancillary ligand coordinates to the Ln^{III} center in a η^5/κ^1 fashion

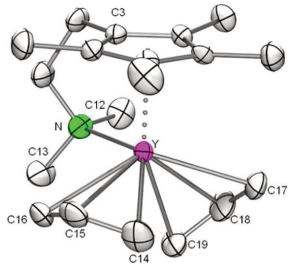

Figure 1. Molecular structure of $[Cp^{NMe2}Y(C_3H_5)_2]$ (**1a**), representative of isostructural complexes **1**. Atomic displacement parameters are set at the 50% probability level; hydrogen atoms are omitted for clarity.

DOI: 10.1021/om500725g
Organometallics 2015, 34, 32−41

Table 1. Selected Bond Lengths (Å) and Angles (deg) of 1a, 1b, 1c, and 2

	1a (Y)	1b (Ho)	1c (Lu)	2 (Nd)
Ln−C14	2.609(4)	2.604(6)	2.575(4)	2.666(5)
Ln−C15	2.625(5)	2.617(7)	2.581(4)	2.702(4)
Ln−C16	2.610(5)	2.604(6)	2.572(4)	2.685(5)
Ln−C17	2.590(5)	2.587(7)	2.534(4)	
Ln−C18	2.614(7)	2.615(14)	2.545(8)	
Ln−C19	2.663(7)	2.660(13)	2.633(9)	
Ln−Cl				2.796(1)
Ln−Cl′				2.874(1)
Ln−N	2.583(4)	2.566(6)	2.550(4)	2.666(3)
Ln−Cp	2.593(4)−2.705(6)	2.589(6)−2.70(1)	2.557(3)−2.669(7)	2.686(4)−2.801(4)
$Ln-Cp_{av}$	2.653	2.645	2.627	2.738
$Ln-Ct_1$	2.363	2.353	2.322	2.459
$Ct_1-Ln-Ct_2$	109.93	109.64	109.53	106.89
$Ct_1-Ln-Ct_3$	131.81	131.36	131.62	
$Ct_2-Ln-Ct_3$	108.40	108.64	108.12	
Ct_1-Ln-N	96.99	97.43	98.21	94.02
Ct_2-Ln-N	109.77	109.69	110.2	112.45
Ct_3-Ln-N	96.47	96.82	96.34	
$Ct_1-Ln-Cl$				101.44
$Ct_1-Ln-Cl'$				166.54
$Ct_2-Ln-Cl$				118.11
$Ct_2-Ln-Cl'$				86.30
N−Ln−Cl				119.09(8)
N−Ln−Cl′				78.04(8)
Cl−Ln−Cl′				73.75(3)

via the Cp ring and the nitrogen atom of the amino group, generating a constrained geometry, while the two allyl moieties bind the rare-earth-metal atom in π-η^3 modes. Due to the constrained geometry the Cp ring is slightly tilted, with the shortest Ln−C distance involving the C3 carbon atom (**1a**, 2.593(4) Å; **1b**, 2.589(6) Å; **1c**, 2.557(3) Å). The two allyl ligands show distinct bonding toward the Ln^{III} centers. While the terminal (C_{AT}) and central (C_{AC}) carbon atoms of one allyl ligand (C14−C16) reveal similar Ln−C_{AT} and Ln−C_{AC} bond lengths (**1a**, average 2.615 Å; **1b**, average 2.608 Å; **1c**, average 2.576 Å), the second allyl ligand features one significantly elongated Ln−C_{AT} distance (C19: **1a**, 2.663(7) Å, **1b**, 2.660(13) Å; **1c**, 2.633(9) Å). The overall ligand arrangement is comparable with that of the *N*,*N*-dimethylanilinyl-substituted half-sandwich rare-earth complexes [($C_5Me_4C_6H_4$-*o*-NMe_2)Ln-(η^3-C_3H_5)$_2$] (Ln = Y, Lu).[24]

The bond angles Ct_2−Ln−Ct_3 involving the allyl centroids (**1a**, 108.40°; **1b**, 108.64°; **1c**, 108.12°) are smaller than in the nonfunctionalized rare-earth-metal bis(allyl) complexes [(C_5Me_4R)Sc(η^3-C_3H_5)$_2$] (R = $SiMe_3$, 119.11°; R = Me, 115.09)[43] but somewhat elongated in comparison to [($C_5Me_4C_6H_4$-*o*-NMe_2)Ln(η^3-C_3H_5)$_2$] (Y, 106.9°; Lu, 106.0°).[24] Furthermore, the bite angles between the cyclopentadienyl centroid and the nitrogen atom Ct_1−Ln−N (**1a**, 96.99°; **1b**, 97.43°; **1c**, 98.21°) are slightly wider than in the anilinyl-functionalized complexes (Y, 95.4°; Lu, 96.7°).[24]

Single crystals of the neodymium complex **2** were also grown from a saturated toluene/*n*-hexane mixture at −35 °C. The complex crystallizes in the triclinic space group $P\bar{1}$ with one molecule of toluene in the unit cell. An X-ray structure analysis of **2** revealed the dimeric structure [Cp^{NMe2}Nd(η^3-C_3H_5)(μ-Cl)]$_2$ with bridging chlorido ligands (Figure 2, Table 1). The N-donor-functionalized cyclopentadienyl ligand and the allyl

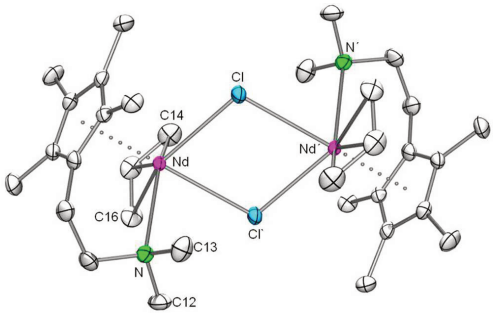

Figure 2. Molecular structure of [Cp^{NMe2}Nd(η^3-C_3H_5)(μ_2-Cl)]$_2$ (**2**). Atomic displacement parameters are set at the 50% probability level; hydrogen atoms are omitted for clarity.

group display the expected η^5/κ^1 and π-η^3 coordination modes, respectively, with a Ct_1−Nd−N bite angle of 94.02° and Nd−C_A distances ranging from 2.666(5) to 2.702(4) Å. The coordination geometry of the neodymium centers is best described as distorted trigonal bipyramidal, with the Cp centroid and one chlorine atom in the apical positions, while the other chlorine atom, the allyl group, and the nitrogen atom span the equatorial plane. The bond length between the neodymium atom and the chlorine atom trans to the Cp ring, Nd−Cl′ (2.874(1) Å), is markedly longer than the neodymium−chlorine bond in the trigonal plane (Nd−Cl = 2.796(1) Å). Comparable Nd−Cl distances were found in [{Nd(η^3-C_3H_5)$_2$(μ-Cl)(THF)$_2$}$_2$][44] (2.822(1)/2.874(1) Å) and [{Nd($AlMe_4$)(μ-Cl){1,2,4-(Me_3C)$_3C_5H_2$}}$_2$][38] (2.7807(6)/2.8077(6) Å).

DOI: 10.1021/om500725g
Organometallics 2015, 34, 32−41

Reactivity toward Et_2AlCl. Activation of rare-earth-metal alkyl or hydride complexes with Lewis acidic diethylaluminum chloride as a "weakly cationizing" cocatalyst is known to form promising catalysts for stereoregular 1,3-diene polymerization.[45,46] In particular, Ln/Al heterobimetallic complexes such as $[Ln(AlMe_4)_3]$,[47,48] $[LnAl_3Me_8(O_2CC_6H_2iPr_3\text{-}2,4,6)_4]$,[49] and $[Ln(AlMe_3)_n(OR)_3]$[50] (R = neopentyl, $C_6H_3iPr_2$-2,6) activated with chlorination reagents such as Et_2AlCl and Ph_3CCl give catalysts for highly cis selective isoprene polymerization. However, active species for the polymerization of isoprene were not formed upon treatment of complexes **1** with Et_2AlCl in 1:0.5, 1:1, 1:1.5, and 1:2 molar ratios.

Addition of 2 equiv of Et_2AlCl to a solution of **1a,b** in deuterated benzene led to full [allyl] → [Cl] exchange under the formation of $[\{(Cp^{NMe2AlEt3})_2(Cp^{NMe2})Ln_3(\mu_2\text{-}Cl)_3(\mu_3\text{-}Cl)_2\}(\mu_2\text{-}Cl)]_2$ (Ln = Y (**3a**), Ho (**3b**); Scheme 2). ^{1}H NMR

Scheme 2. Allyl−Chlorido Exchange: Synthesis of Complexes $[\{(Cp^{NMe2AlEt3})_2(Cp^{NMe2})Ln_3(\mu_2\text{-}Cl)_3(\mu_3\text{-}Cl)_2\}(\mu_2\text{-}Cl)]_2$ (3)

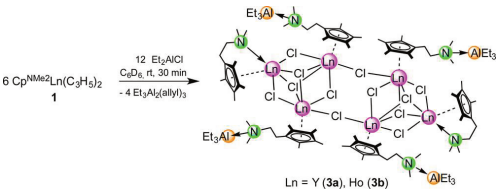

spectroscopic investigations were not conclusive, probably due to cluster rearrangements and coordination switch of the hemilabile donor function of the cyclopentadienyl ligand at the Lewis acidic Ln(III) and Al(III) centers. Single crystals of **3** suitable for X-ray structure analysis were obtained when pentane was added to a benzene solution which was then cooled to −35 °C. Complexes **3** crystallize in the triclinic space group $P\bar{1}$ with varying amounts of solvent molecules. Since the crystallographic data of the yttrium complex **3a** were of low quality (only allowing the assignment of a connectivity structure; see the Supporting Information), ORTEP drawings of the holmium structure **3b** are shown in Figure 3. Both complexes share the same core structure, which can be best described as two distorted hexagonal bipyramids $[Ln_3Cl_5]$ linked by two chlorido (C16) ligands (Figure 3A).[51] The resulting hexalanthanide cluster $[Ln_6Cl_{12}]$ adopts a chairlike geometry (Figure 3B). Each $[Ln_3Cl_5]$ unit implements three μ_2- and two μ_3-chlorido ligands with Ln−Cl distances of 2.6672(2)−2.7048(2) and 2.7639(2)−2.8486(2) Å, respectively. With regard to the μ_3-chlorido ligands, the contacts involving Cl1 are significantly shorter (2.7639(2)−2.8018(3) Å). Similar cluster arrangements were found previously for the earlier ("larger") lanthanides in the presence of small anions (X) such as halo, cyano, borohydro, and hydroxy, which favorably act as bridging ligands.[52] Examples include $[Nd_6(2,4\text{-}C_7H_{11})_6Cl_{12}(thf)_2]$,[51] $[Ln_6(C_5Me_5)_6Cl_{12}(thf)_2]$ (Ln = Nd, Sm),[53] $[Ln_6(C_5Me_4nPr)_6(BH_4)_{12-x}Cl_x(thf)_2]$ (Ln = Sm, Nd; x = 0, 5, 10),[54] and $[Sm_6(C_5Me_5)_6Cl_{10}(OH)_2(thf)_2]$.[55] The yttrium complex $[Y_6(L)_6Cl_6(OH)_6(thf)_2]$ (L = 2-phenyl-1,4,5,6,7,8-hexahydroazulenyl) represents a rare example of a $[Ln_6X_{12}]$ cluster with a smaller rare-earth-metal center.[56] Herein the hydroxo ligands occupy the two μ_3 and one μ_2 position in the trimeric subunit. In addition to the η^5-coordinated cyclopentadienyl ligand, two of the metal centers in each triangle accommodate five anionic ligands X, while the third has only contact to four X. The latter metal center is additionally coordinated by one thf donor ligand to achieve steric saturation. This way, each metal center has a coordination number of 8. In contrast, the vacant position at Ho3 in complex **3b** is occupied by the nitrogen donor functionality of the cyclopentadienyl ligand, accomplishing a chelating η^5/κ^1 coordination mode (Ho3−N3 = 2.5162(3) Å). The other metal centers (Ho1/Ho2) are η^5 coordinated by the Cp^{NMe2} ligand, while their donor functions are attached to triethylaluminum (N1/2−Al1/2 = 2.0683(2)/2.0612(2) Å). This coordination mode of the Cp^{NMe2} ligand was previously detected in the half-sandwich bis(tetramethylaluminate) complexes $[\{Cp^{NMe2AlMe3}\}Ln(AlMe_4)_2]$ (Ln = Y, La, Nd).[57]

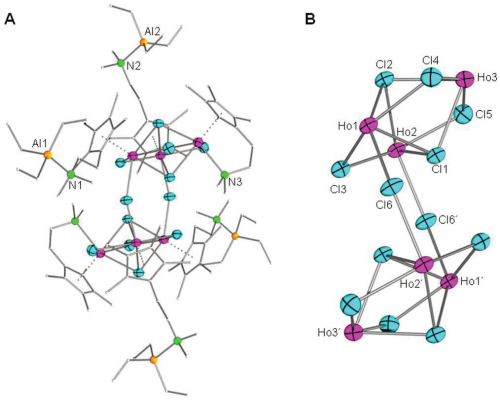

Figure 3. (A) Molecular structure of complex **3b**. Atomic displacement parameters are set at the 50% probability level; hydrogen atoms are omitted for clarity. Aluminum, carbon, and nitrogen atoms are shown with a ball and stick representation. The disorders of the ethyl groups at the aluminum atoms and in the side arm functionality are not shown. (B) Core structure of the hexameric complex. Atomic displacement parameters are set at the 50% probability level. Selected bond distances (Å) and angles (deg): Ho1/2/3−Cl1 2.7885(2)/2.8018(3)/2.7639(2), Ho1/2/3−Cl2 2.8406(3)/2.8486(2)/2.8004(3), Ho1−Cl3/4 2.6672(2)/2.6998(2), Ho2−Cl3/5 2.6771(2)/2.6839(2), Ho3−Cl4/5 2.7048(2)/2.7022(2), Ho1−Cl6 2.6951(3), Ho2−Cl6′ 2.7007(2), Ho3−N3 2.5162(3), Al1/2−N1/2 2.0683(2)/2.0612(2), Cl3/4/5−Ho1/3/2−Cl4/5/3 145.037(14)/145.330(13)/145.330(13), Ho1/2/3−Cl3/5/4−Ho2/3/1 90.298(11)/90.298(11)/ 90.616(13), Ho1/2/3−Cl3/5/4−Ho2/3/1 95.732(13)/94.209(16)/93.830(14), Ho1/2/3−Cl2−Ho2/3/1 88.314(12)/88.611(13)/88.810(11), Ho1−Cl6−Ho2′ 140.437(17), N3−Ho3−Cl1/2/4/5 82.62(4)/154.55(4)/93.98(5)/96.38(5).

Polymerization of Isoprene. The bis(allyl) complexes **1** and the dimeric mono(allyl) chlorido complex **2** were tested as precatalysts in the polymerization of isoprene. Upon cationization with the organoborate reagents $[Ph_3C][B(C_6F_5)_4]$ (**A**) and $[PhNMe_2H][B(C_6F_5)_4]$ (**B**) as cocatalysts, the monomeric complexes **1** displayed moderate to high activity, producing polyisoprenes with microstructures that were affected by the rare-earth-metal center rather than the cocatalyst (Table 2, Figure 4). The yttrium- and holmium-based catalyst systems **1a/A**, **1a/B**, **1b/A**, and **1b/B** produced polymers with dominant 3,4 -sequences, as detected by ^{1}H NMR spectroscopy (Table 2, runs 1, 2, 5, and 6). Determination of the accurate cis

DOI: 10.1021/om500725g
Organometallics 2015, 34, 32−41

Table 2. Selected Examples of Isoprene Polymerization at 40 °C

entry[a]	precat.	cocat.[b]	time (min)	yield (%)	*cis*-1,4[c]	*trans*-1,4[c]	3,4[c]	$10^4 M_n$[d]	M_w/M_n[d]
1	$(Cp^{NMe2})Y(C_3H_5)_2$ (**1a**)	**A**	120	19	6	15	79	0.9	1.15
2	$(Cp^{NMe2})Y(C_3H_5)_2$ (**1a**)	**B**	120	20	4	21	75	1.0	1.09
3	$(Cp^{NMe2})Y(C_3H_5)_2$ (**1a**)	**B**/$AlMe_3$	30	>99	<1	71	29	5.4	1.24
4	$(Cp^{NMe2})Y(C_3H_5)_2$ (**1a**)	**B**/Al*i*Bu$_3$	60	>99	74	<1	26	1.5	1.19
5	$(Cp^{NMe2})Ho(C_3H_5)_2$ (**1b**)	**A**	120	16	11	12	77	1.23	1.17
6	$(Cp^{NMe2})Ho(C_3H_5)_2$ (**1b**)	**B**	120	17	7	17	76	1.23	1.13
7	$(Cp^{NMe2})Ho(C_3H_5)_2$ (**1b**)	**B**/$AlMe_3$	30	>99	<1	72	28	4.0	1.24
8	$(Cp^{NMe2})Ho(C_3H_5)_2$ (**1b**)	**B**/Al*i*Bu$_3$	60	>99	74	<1	26	1.0	1.25
9	$(Cp^{NMe2})Lu(C_3H_5)_2$ (**1c**)	**A**	120	97	27	34	39	2.4	1.04
10	$(Cp^{NMe2})Lu(C_3H_5)_2$ (**1c**)	**B**	120	81	32	31	37	2.6	1.04
11	$(Cp^{NMe2})Lu(C_3H_5)_2$ (**1c**)	**B**/$AlMe_3$	30	>99	4	51	45	3.3	1.39
12	$(Cp^{NMe2})Lu(C_3H_5)_2$ (**1c**)	**B**/Al*i*Bu$_3$	60	>99	40	25	35	1.0	1.72
13	$[(Cp^{NMe2})Nd(\mu\text{-}Cl)(C_3H_5)]_2$ (**2**)	**A**	120	>99	5	29	66	4.3	1.10
14	$[(Cp^{NMe2})Nd(\mu\text{-}Cl)(C_3H_5)]_2$ (**2**)	**B**	120	>99	6	30	64	4.7	1.11
15	$[(Cp^{NMe2})Nd(\mu\text{-}Cl)(C_3H_5)]_2$ (**2**)	**B**/$AlMe_3$	30	>99	<1	85	15	4.3	1.06
16	$[(Cp^{NMe2})Nd(\mu\text{-}Cl)(C_3H_5)]_2$ (**2**)	**B**/Al*i*Bu$_3$	60	>99	5	10	85	1.2	1.29
17[e]	$(Cp^{NMe2AlMe3})Y(AlMe_4)_2$ (**4**)	**A**	120	>99	<1	77	23	2.7	1.11
18[e]	$(Cp^{NMe2AlMe3})Y(AlMe_4)_2$ (**4**)	**B**	120	>99	4	75	21	2.7	1.22

[a]Conditions: 0.02 mmol of catalyst, [complex]/[cocat] = 1/1, 8 mL of solvent, 20 mmol of isoprene. [b]Cocatalyst: **A**, $[Ph_3C][B(C_6F_5)_4]$; **B**, $[PhNMe_2H][B(C_6F_5)_4]$. [c]Determined by ^1H and ^{13}C NMR spectroscopy in $CDCl_3$. [d]Determined by means of size-exclusion chromatography (SEC) against polystyrene standards. [e][Ln]/[cocat]/[isoprene] = 1/1/500, 4 mL of solvent.

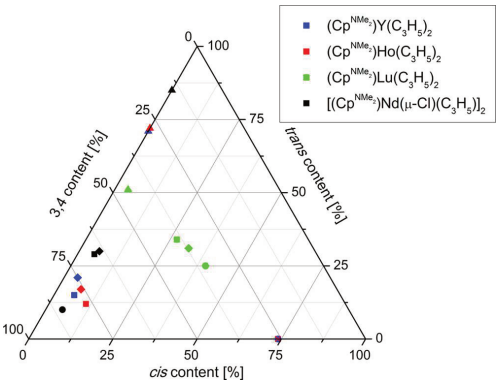

Figure 4. Ternary plot of the microstructures of the polyisoprenes obtainend from precatalysts **1** and **2** upon activation with **A** (■), **B** (◆), **B**/$AlMe_3$ (▲), and **B**/Al^{i}Bu$_3$ (●) (see Table 2).

and trans contents of the 1,4-units by ^{13}C NMR spectroscopy is hampered by the high contents of atactic 3,4-polyisoprene, leading to broad signals (Figure S14, Supporting Information). Furthermore, in contrast to our intensely studied aluminate precatalysts,[37−39] the selectivity of the allyl complexes is very sensitive toward small (salt) impurities. The lutetium complex **1c** gave polymers with almost equal amounts of *cis*-1,4-, *trans*-1,4-, and 3,4-polyisoprene units (Table 2, runs 9 and 10). The dimeric neodymium complex **2** did not display any activity when a [Ln]:[cocat.] ratio of 1:1 was applied, indicating the displacement of both allyl moieties. However, upon activation of complex **2** with 1 equiv of **A** or **B**, polyisoprenes with a dominant 3,4-microstructure were produced (Table 2, runs 13 and 14). The high 3,4-content is proposed to result from an enhanced steric encumbrance at the CGC metal center in comparison to donor side arm free half-sandwich complexes, which produce predominantly *trans*-1,4-polyisoprene.[37−39] The molecular weight distributions of all obtained polyisoprenes are very narrow (1.04−1.17), suggesting polymerization in a living fashion.

In this context it is worth mentioning that the rare-earth-metal CGC $[(C_5Me_4)SiMe_2(NCMe_3)Sc(PMe_3)_2(\mu_2\text{-}H)_2]$ polymerizes not only ethylene but also higher α-olefins[4] and that the first isospecific 3,4-polymerization (100% 3,4; *mmmm* >99%) of isoprene was achieved by applying the binuclear complexes $[(C_5Me_4)SiMe_2P(Cy)Ln(CH_2SiMe_3)]_2$ (Ln = Y, Lu; Cy = cyclohexyl) bearing a dianionic phosphido-substituted cyclopentadienyl ligand.[12] Furthermore, the rare-earth-metal postmetallocene bis(alkyl) complexes $[\{PhC(NC_6H_4iPr_2\text{-}2,6)_2\}Y(o\text{-}CH_2C_6H_4NMe_2)_2]$,[58] $[L^{1/2}Sc(CH_2SiMe_3)_2]$[59] ($L^1$ = 2,5-bis((pyrrolidin-1-yl)methylene)-pyrrolyl, L^2 = 2,5-bis-((piperidino)methylene)-pyrrolyl), and $[\{2,6\text{-}R_2C_6H_3NCH_2C\text{-}(CH_2\text{−}SiMe_3)=NC_6H_3R_2\text{-}2,6\}Ln(CH_2SiMe_3)_2(THF)]$[60] (Ln = Sc, Y, Lu; R = Me, *i*Pr) were reported to polymerize isoprene in high 3,4-regioselectivity on activation with cocatalyst **A**. For the latter complexes, DFT calculations demonstrated a favorable η^2 coordination of the monomer to the metal center, leading to the 3,4-insertion product. The tendency for 3,4-polyisoprene formation in the presence of sterically demanding ligands was also presented in an investigation of the structure−reactivity relationship of half-sandwich bis(alkyl) scandium complexes, bearing nonfunctionalized and heteroatom-substituted cyclopentadienyl ligands.[33]

It has been shown earlier that the addition of trialkylaluminum compounds to binary catalyst systems has a drastic effect on the activity as well as the regio- and stereoselectivity.[24,58,61] Hence, in subsequent reactions, 10 equiv of each of the trialkylaluminum compounds AlR_3 (R = Me, ^{i}Bu) was added to the catalyst systems utilizing cocatalyst $[PhNMe_2H][B(C_6F_5)_4]$ (**B**), in order to investigate the implications for activity and selectivity. In case of the lutetium complex **1c** and addition of $AlMe_3$, a decrease in the cis-1,4-content to 4% in the resulting polymer was observed, while the trans-1,4- and the 3,4-microstructure contents increased to 51% and 45%, respectively. The use of Al*i*Bu$_3$ instead caused only minor changes in

DOI: 10.1021/om500725g
Organometallics 2015, 34, 32−41

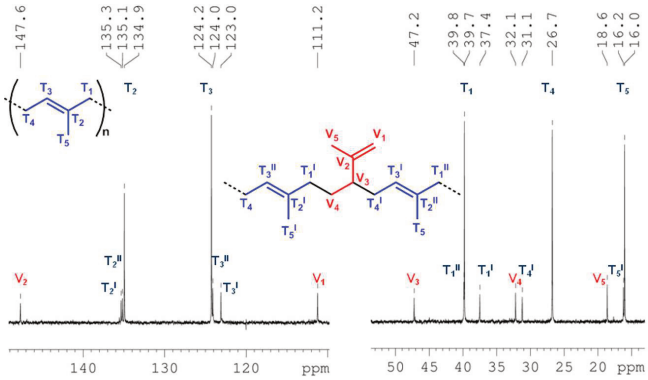

Figure 5. Olefinic and aliphatic regions of the ^{13}C NMR spectrum (101 MHz, 25 °C, $CDCl_3$, σ 77.0 ppm) of polyisoprene obtained with the catalyst system **2**/**B**/$AlMe_3$ (Table 2, run 15).

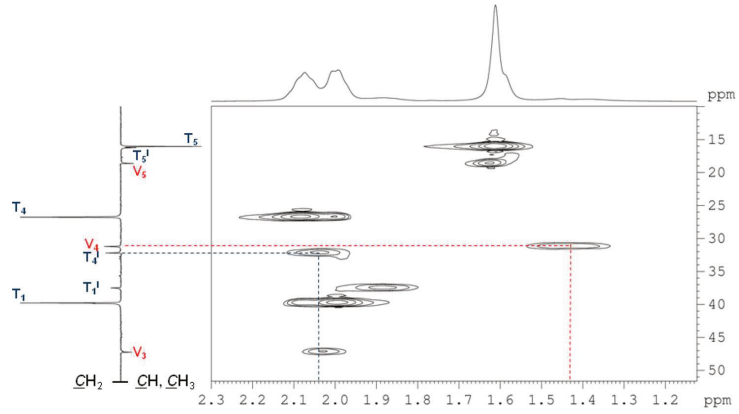

Figure 6. Aliphatic region of the $^1H-^{13}C$ HSQC NMR spectrum (25 °C, $CDCl_3$, σ 77.0 ppm/7.26 ppm) of polyisoprene obtained with the catalyst system **2**/**B**/$AlMe_3$ (run 15). The ^{13}C (DEPT 135) NMR spectrum is shown on the left edge of the contour plot, while the ^1H NMR spectrum is shown at the top.

the stereoregularity, while in both cases a broadening of the molecular weight distribution was found (Table 2, runs 11 and 12). In contrast, the yttrium-based (**1a**) and holmium-based (**1b**) systems were dramatically influenced by the choice of trialkylaluminum reagent. While addition of $AlMe_3$ resulted in moderate trans-1,4-selectivity of 71% (**1a**) and 72% (**1b**) (runs 3 and 7), the use of Al*i*Bu_3 provided polyisoprene with moderate contents of cis-1,4-microstructure in both cases (74%, runs 4 and 8). This is in agreement with the findings on $[(C_5Me_4C_6H_4$-*o*-$NMe_2)Y(\eta^3$-$C_3H_5)_2]$/**A** based catalyst systems, where the addition of $AlMe_3$ led to 70% *trans*-1,4-polyisoprene and Al*i*Bu_3 produced 75% *cis*-1,4-polyisoprene.[24] Furthermore, the decrease of the polymer molecular weights with consistently low molecular weight distributions in the presence of Al*i*Bu_3 (runs 4, 8, 12, and 16) are in agreement with its chain-transfer capability,[24] ideally leading to a so-called "immortal" polymerization.[62,63] Interestingly, for the catalyst system **2**/**B** only a shift toward 1,4-selectivity was observed upon addition of $AlMe_3$ (85% trans, Table 2, run 15), while Al*i*Bu_3 increased the 3,4-selectivity up to 85% (Table 2, run 16).

In contrast to the case for natural rubber (*Hevea*; 100% *cis*-1,4-PIP) and gutta-percha (100% *trans*-1,4-PIP), synthetic rubbers often not only reveal a mixture of 1,4-units but also incorporate 3,4-microstructures. Depending on the amount and tacticity of the 3,4-units, distinct NMR shifts of adjacent isoprene units are observed, making structure analysis a challenging task.[64] On the other hand, systematic incorporation of 3,4-units has been proven to influence the physicochemical properties of such rubbers, as has been shown for the increase in wet skid resistance coupled with balanced abrasion and rolling resistance properties of produced tire treads.[65] However, the majority of publications on the structural NMR analysis of polyisoprenes have dealt with the incorporation of 3,4-units in polymers with pronounced cis-1,4-microstructure.[66−69] The catalytic system **2**/**B**/$AlMe_3$ (Table 2, run 15) produced polyisoprene with predominant trans-1,4-regularity but also featured 15% of 3,4-units as determined by ^1H NMR spectroscopy. The ^{13}C NMR gave sharp resonances for both the trans-1,4- (**T**) and the 3,4-units (**V**) but no indication of

DOI: 10.1021/om500725g
Organometallics 2015, 34, 32−41

any cis-1,4-microstructures (signals at 23.4, 26.4, and 32.2 ppm in the aliphatic region) (Figure 5).

The integral ratio of the peaks assigned to the 3,4-units at 18.6, 47.2, 111.2, and 147.6 fits the presence of single isolated 3,4-units incorporated into the trans-1,4-polymer chain, as shown in Figure 5. To correlate the remaining signals, a two-dimensional $^{1}H-^{13}C$ HSQC NMR spectrum was recorded (Figure 6). This allowed us to verify that the ^{13}C NMR signal at 32.1 ppm is the $\mathbf{V}_4$ carbon of the 3,4-unit correlating with the broad doublet at 1.43 ppm in the ^{1}H NMR spectrum and that the peak at 31.1 ppm belongs to the $\mathbf{T}_4^{\mathbf{I}}$ carbon. As far as we are aware, this type of polyisoprene microstructure and its corresponding NMR data have not been described in detail to date. Such polymers might open up interesting avenues for selective functionalization of the pendant vinylic groups.

With the aim of gaining more knowledge about the effect of the trialkylaluminum compounds, the reaction of the diamagnetic yttrium bis(allyl) complex $[Cp^{NMe2}Y(\eta^3\text{-}C_3H_5)_2]$ (**1a**) with $AlMe_3$ was investigated by NMR experiments (see the Supporting Information). To this end, **1a** was charged into an NMR tube fitted with a J. Young valve, dissolved in C_6D_6, and blended with 10 equiv of trimethylaluminum (Scheme 3, **I**). Disappearance of the quintet at 6.31 ppm and the doublet at 3.04 ppm in the ^{1}H NMR spectrum indicated a rapid displacement of the η^3-coordinated allyl ligands (**i**, Figure 7a). After evaporation of the volatiles, a clean spectrum of the reaction products was obtained, suggesting the formation of two different species (Figure 7b). A closer examination of the obtained data unambiguously verified one of the species as the yttrium half-sandwich bis(tetramethylaluminate) complex $[Cp^{NMe2AlMe3}Y(AlMe_4)_2]$ (**4**) reported recently (Figure 7c).[57,70]

Scheme 3. Allyl–Alkyl Exchange: Synthesis of the Rare-Earth-Metal Bis(aluminate) Half-Sandwich Complex $[Cp^{NMe2AlMe3}Y(AlMe_4)_2]$ (4)[70]

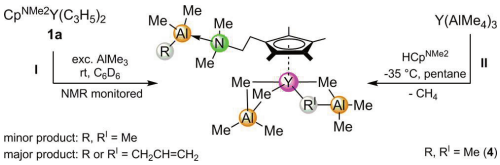

The second reaction product could not be isolated. It is likely that the nitrogen-functionalized side arm coordinates to a trialkylaluminum instead of the rare-earth-metal center, as indicated by the separation of the ethylene-linker proton signals (**ii**) in the ^{1}H NMR spectra. Furthermore, the appearance of two multiplets at 5.66 and 5.10 ppm (**iii**) with a proton integral ratio of 1:2 may belong to one remaining allyl ligand σ-bonded to a metal center either as $AlMe_2R$ ($R = CH_2CHCH_2$) coordinated by the nitrogen atom or as a bridging anion of a $[AlMe_3R]^-$ moiety (Scheme 3).[71,72]

In order to work out if a half-sandwich bis(aluminate) species represents the real precatalyst, the complex $[Cp^{NMe2AlMe3}Y(AlMe_4)_2]$ (**4**) was synthesized by applying the protonolysis protocol with the homoleptic tetramethylaluminate yttrium complex as the precursor (Scheme 3, **II**) and tested in isoprene polymerization after cationization with the borate reagents **A** and **B**. Both polymerization reactions produced polyisoprene with moderate trans-1,4-microstructures of 77% and 75%, while the cis-1,4-contents were very low (Table 2, runs 17 and 18), which is comparable to those for the catalyst systems **1**/**B**/$AlMe_3$ of yttrium and holmium. It is important to note that none of the cationized species could be unambiguously identified and that the excess amount of trimethylaluminum in the ternary catalyst systems might have further implications for the activation sequence.

CONCLUSIONS

Linked half-sandwich rare-earth-metal bis(allyl) complexes $Cp^{NMe2}Ln(\eta^3\text{-}C_3H_5)_2$, bearing an amino-functionalized tetramethylcyclopentadienyl ancillary ligand, are accessible in a straightforward one-pot synthesis by using a two-step salt-metathesis protocol for the smaller rare-earth metals yttrium, holmium, and lutetium. When the same reaction sequence was employed, the larger neodymium metal led to the mono(allyl)

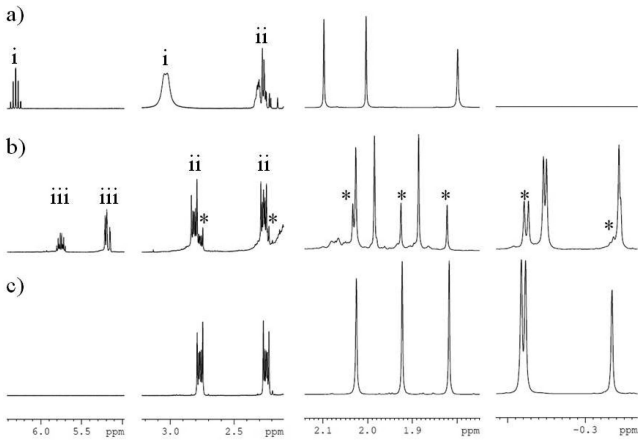

Figure 7. Regions of the ^{1}H NMR spectra (400 MHz, 25 °C, C_6D_6) of (a) pure $[Cp^{NMe2}Y(\eta^3\text{-}C_3H_5)_2]$ (**1a**), (b) reaction product of $[Cp^{NMe2}Y(\eta^3\text{-}C_3H_5)_2]$ with 10 equiv of $AlMe_3$ after evaporation of volatiles, and (c) $[Cp^{NMe2AlMe3}Y(AlMe_4)_2]$ (**4**).

DOI: 10.1021/om500725g
Organometallics 2015, 34, 32–41

chlorido complex $[Cp^{NMe2}Nd(\eta^3\text{-}C_3H_5)(\mu\text{-}Cl)]_2$. Upon activation with $[PhNMe_2H][B(C_6F_5)_4]$, the yttrium and holmium bis(allyl) complexes showed moderate activity for mainly 3,4-selective isoprene polymerization. In the presence of 10 equiv of AlR_3, the activities increased and dramatic shifts toward 1,4-selectivity were observed. The addition of an excess of $AliBu_3$ led to mainly cis-1,4-regulated polyisoprene, while the use of $AlMe_3$ produced polymers with dominant trans-1,4-microstructure. NMR spectroscopic studies of the mixture $Cp^{NMe2}Y(\eta^3\text{-}C_3H_5)_2/AlMe_3$ revealed rapid [allyl] → [aluminate] exchange (allyl/methyl scrambling) with loss of the constrained geometry conformation involving the formation of complexes such as $Cp^{NMe2AlMe3}Y(AlMe_4)_2$.[70] In accordance with the NMR study, the catalyst systems $Cp^{NMe2}Y(\eta^3\text{-}C_3H_5)_2/[PhNMe_2H][B(C_6F_5)_4]/AlMe_3$ and $Cp^{NMe2AlMe3}Y(AlMe_4)_2/[PhNMe_2H][B(C_6F_5)_4]$ showed similar performance. Apparently, trialkylaluminum reagents are less prone to disrupt the chelate coordination of more rigid CG complexes such as Cui's anilinyl-type complexes $[(C_5Me_4C_6H_4\text{-}o\text{-}NMe_2)Ln(\eta^3\text{-}C_3H_5)_2]$, which afford high cis-1,4 selectivtiy.[24] Treatment of the bis(allyl) complexes with dialkylaluminum chloride as a cocatalyst did not afford initiators for isoprene polymerization but complete [allyl] → [Cl] exchange. As revealed by the X-ray diffraction analyses of the hexameric clusters $[\{(Cp^{NMe2AlEt3})_2(Cp^{NMe2})Ln_3Cl_5\}(\mu_2\text{-}Cl)]_2$ (Ln = Y, Ho), the donor functionality of the ancillary ligand Cp^{NMe} exhibits hemilability in the presence of Lewis acids (here $AlEt_3$): four of the Cp^{NMe} groups coordinate in a η^5 mode to the metal center with a dangling amine group attached to triethylaluminum (formed from $ClAlEt_2$), while the remaining two groups are bonded to the rare-earth-metal center in a chelating η^5/κ^1 fashion.

EXPERIMENTAL SECTION

General Remarks. All operations were performed with rigorous exclusion of air and water, using standard Schlenk, high-vacuum, and argon glovebox techniques (MBraun MB 200B; <1 ppm of O_2, <1 ppm of H_2O). *n*-Hexane, toluene, and THF were purified by using Grubbs columns (MBraun SPS-800, solvent purification system) and stored in a glovebox. C_6D_6 and toluene-d_8 were obtained from Aldrich, dried over Na for 24 h, and filtered. $CDCl_3$ and $AlMe_3$ were purchased from Aldrich and used as received. Homoleptic $Y(AlMe_4)_3$ was prepared according to literature methods.[73] HCp^{NMe2} (Cp^{NMe2} = 1-[2-(*N*,*N*-dimethylamino)ethyl]-2,3,4,5-tetramethylcyclopentadienyl) was synthesized as described in the literature.[36] Isoprene was obtained from Aldrich, dried over trioctylaluminum, and vacuum-transferred prior to use. $[Ph_3C][B(C_6F_5)_4]$ (**A**) and $[PhNMe_2H][B(C_6F_5)_4]$ (**B**) were purchased from Boulder Scientific Co. and used without any further purification. C_3H_5MgCl (1.7 M solution in THF) was purchased from Aldrich and used as received. The NMR spectra of air- and moisture-sensitive compounds were recorded by using J. Young valve NMR tubes at 25 °C on a Bruker AVII+400 (^1H, 400.13 Hz; ^{13}C, 100.61 MHz). ^1H and ^{13}C shifts are referenced to internal solvent resonances and reported in parts per million relative to TMS. IR spectra were recorded between 4000 and 400 cm^{-1} on a NICOLET 6700 FTIR spectrometer using a DRIFT chamber with dry KBr/sample mixtures and KBr windows. The collected data were converted using the Kubelka–Munk refinement. Elemental analyses were performed on an Elementar Vario MICRO cube. The crystalline materials were dried under vacuum for several hours before analysis; however, the solvent molecules incorporated into the crystal lattice of complexes **2** and **3** could not be removed under these conditions and hence were allowed for the calculation of the theoretical values. The molar masses (M_w and M_n) of the polymers were determined by size-exclusion chromatography (SEC). Sample solutions (1.0 mg of polymer per mL of THF) were filtered through a 0.45 μm syringe filter prior to injection. SEC was performed with a pump supplied by Viscotek (GPCmax VE 2001), employing ViscoGEL columns. Signals were detected by means of a triple detection array (TDA 305) and calibrated against polystyrene standards (M_w/M_n < 1.15). The flow rate was set to 1.0 mL min^{-1}. The microstructure of the polyisoprenes was examined by means of ^1H, ^{13}C, and two-dimensional $^1H-^{13}C$ HSQC NMR experiments on the Bruker AVII+400 spectrometer at ambient temperature, using $CDCl_3$ as solvent.

General Procedure for the Synthesis of $(C_5Me_4CH_2CH_2NMe_2)Ln(C_3H_5)_2$ (1). *Route A.* In a glovebox, $LiCp^{NMe2}$ was suspended in 4 mL of toluene and added dropwise to a stirred suspension of $LnCl_3(THF)_x$ in 4 mL of toluene. The mixture was stirred for 4 h, and C_3H_5MgCl in THF (1.7 M) was added. After complete addition the reaction mixture was stirred for another 16 h at ambient temperature. After evaporation of the solvent, the crude mixture was redissolved in toluene and LiCl and $MgCl_2$ were removed via centrifugation and filtration. The clear solution was reduced to 3 mL, layered with *n*-hexane, and stored at −35 °C to yield crystalline complexes **1**, which were further purified by repeated recrystallization from saturated *n*-hexane solutions at −35 °C.

Alternatively, the following route was successfully tested for the yttrium and holmium complexes.

Route B. In a glovebox, $LiCp^{NMe2}$ was added to a stirred suspension of $LnCl_3(THF)_x$ in 4 mL of THF chilled to −35 °C. After 0.5 h at ambient temperature the solution became clear and C_3H_5MgCl in THF (1.7 M) was added. The reaction mixture was stirred another 1 h at ambient temperature, and 0.5 mL of dioxane was added. After 1 h, the precipitated $MgCl_2$–dioxane adduct was removed via centrifugation and filtration. The solvent was evaporated and the crude product extracted with *n*-hexane. For crystallization of complexes **1** the clear solution was reduced to 3 mL and stored at −35 °C.

*Synthesis of $(C_5Me_4CH_2CH_2NMe_2)Y(C_3H_5)_2$ (**1a**).* Following synthesis route A described above, $LiCp^{NMe2}$ (199 mg, 1.00 mmol), $YCl_3(THF)_{3.5}$ (448 mg, 1.00 mmol), and C_3H_5MgCl (1.18 mL, 2.00 mmol, 1.7 M in THF) yielded **1a** (319 mg, 0.88 mmol, 88%) as slightly yellow crystals. Following synthesis route B described above, $LiCp^{NMe2}$ (66 mg, 0.33 mmol), $YCl_3(THF)_{3.5}$ (148 mg, 0.33 mmol), and C_3H_5MgCl (0.39 mL, 0.66 mmol, 1.7 M in THF) yielded **1a** (102 mg, 0.28 mmol, 85%) as slightly yellow crystals. ^1H NMR (400 MHz, C_6D_6, 25 °C): σ 6.31 (dquin, 2 H, $^3J_{HH}$ = 12.36 Hz, $^2J_{YH}$ = 1.36 Hz, CH_2CHCH_2), 3.04 (d(br), 8 H, CH_2CHCH_2), 2.32–2.24 (m, 4 H, NCH_2CH_2Cp), 2.10 (s, 6 H, CH_3Cp), 2.00 (s, 6 H, CH_3Cp), 1.80 (s, 6 H, CH_3N). ^{13}C NMR (101 MHz, C_6D_6, 25 °C): σ 147.9 (CH_2CHCH_2), 120.0, 117.9, 113.8 ($C_5(CH_3)_4$), 68.8 (CH_2CHCH_2), 64.7 (NCH_2CH_2), 46.9 (CH_3N), 22.8 (CH_2CH_2Cp), 11.8, 11.4 ($C_5(CH_3)_4$). IR (cm^{-1}): 3068 m, 3000 m, 2970 m, 2952 m, 2904 br, 2864 br, 2833 br, 2802 m, 2723 m, 1545 s, 1461 s, 1438 br, 1376 w, 1367 w, 1244 m, 1230 s, 1029 m, 1008 m, 909 m, 765 s, 752 m, 715 m, 680 s, 576 w. Anal. Calcd for $C_{19}H_{32}NY$ (363.37): C, 62.80; H, 8.88; N, 3.85. Found: C, 62.18; H, 8.73; N, 3.91.

*Synthesis of $(C_5Me_4CH_2CH_2NMe_2)Ho(C_3H_5)_2$ (**1b**).* Following synthesis route A described above, $LiCp^{NMe2}$ (199 mg, 1.00 mmol), $HoCl_3(THF)_3$ (509 mg, 1.00 mmol), and C_3H_5MgCl (1.18 mL, 2.00 mmol, 1.7 M in THF) yielded **1b** (360 mg, 0.82 mmol, 82%) as orange crystals. Following synthesis route B described above, $LiCp^{NMe2}$ (66 mg, 0.33 mmol), $HoCl_3(THF)_3$ (168 mg, 0.33 mmol), and C_3H_5MgCl (0.39 mL, 0.66 mmol, 1.7 M in THF) yielded **1b** (120 mg, 0.27 mmol, 83%) as orange crystals. IR (cm^{-1}): 3068 m, 3006 m, 2974 m, 2952 m, 2909 br, 2852 br, 2800 m, 2723 m, 1546 s, 1461 s, 1440 s, 1376 w, 1367 w, 1244 m, 1227 s, 1028 m, 1007 m, 909 m, 766 s, 718 m, 685 s, 571 w. Anal. Calcd for $C_{19}H_{32}NHo$ (439.39): C, 51.94; H, 7.34; N, 3.19. Found: C, 51.42; H, 6.84; N, 3.15.

*Synthesis of $(C_5Me_4CH_2CH_2NMe_2)Lu(C_3H_5)_2$ (**1c**).* Following synthesis route A described above, $LiCp^{NMe2}$ (199 mg, 1.00 mmol), $LuCl_3(THF)_3$ (497 mg, 1.00 mmol), and C_3H_5MgCl (1.18 mL, 2.00 mmol, 1.7 M in THF) yielded **1c** (369 mg, 0.87 mmol, 87%) as slightly yellow crystals. ^1H NMR (400 MHz, C_6D_6, 25 °C): σ 6.37 (quin, 2 H, $^3J_{HH}$ = 12.36 Hz, CH_2CHCH_2), 3.07 (d, 8H, $^3J_{HH}$ = 12.36 Hz, CH_2CHCH_2), 2.31–2.22 (m, 4 H, NCH_2CH_2Cp), 2.09 (s, 6 H, CH_3Cp), 2.01 (s, 6 H, CH_3Cp), 1.79 (s, 6 H, CH_3N). ^{13}C NMR (101

DOI: 10.1021/om500725g
Organometallics 2015, 34, 32–41

MHz, C_6D_6, 25 °C): σ 149.1 (CH_2CHCH_2), 125.7, 116.6, 112.9 ($C_5(CH_3)_4$), 68.3 (CH_2CHCH_2), 64.9 (NCH_2CH_2), 47.4 (CH_3N), 22.5 (CH_2CH_2Cp), 11.7, 11.3 ($Cp(CH_3)_4$). IR (cm^{-1}): 3068 m, 3001 m, 2970 m, 2951 m, 2908 br, 2853 br, 2802 m, 2723 m, 1545 s, 1461 s, 1440 s, 1376 w, 1367 w, 1244 m, 1229 s, 1029 m, 1007 m, 909 m, 765 s, 753 m, 715 m, 680 s, 576 w. Anal. Calcd for $C_{19}H_{32}NLu$ (449.43): C, 50.78; H, 7.18; N, 3.12. Found: C, 50.18; H, 7.10; N, 3.08.

*Synthesis of [(C$_5$Me$_4$CH$_2$CH$_2$NMe$_2$)Nd(C$_3$H$_5$)(μ-Cl)]$_2$ (**2**).* Following synthesis route A described above, $LiCp^{NMe2}$ (199 mg, 1.00 mmol), $NdCl_3(thf)_{1.75}$ (370 mg, 1.00 mmol), and C_3H_5MgCl (1.18 mL, 2.00 mmol, 1.7 M in THF) yielded **3** (281 mg, 0.34 mmol, 68%) as green crystals. IR (cm^{-1}): 3066 w, 2953 m, 2938 m, 2901 s, 2865 s, 2835 m, 2823 m, 2802 m, 2723 w, 1544 s, 1462 s, 1431 m, 1376 w, 1245 m, 1036 w, 1014 m, 912 m, 779 s, 766 m, 737 m, 681 s. Anal. Calcd for $C_{32}H_{54}Cl_2N_2Nd_2$·(toluene) (918.31): C, 51.01; H, 6.81; N, 3.05. Found: C, 51.14; H, 6.86; N, 2.98.

General Procedure for the Synthesis of [{(C$_5$Me$_4$CH$_2$CH$_2$NMe$_2$AlEt$_3$)$_2$(C$_5$Me$_4$CH$_2$CH$_2$NMe$_2$)Ln$_3$(μ$_2$-Cl)$_3$(μ$_3$-Cl)$_2$}(μ$_2$-Cl)}]$_2$ (3). Et_2AlCl was diluted in 0.5 mL of C_6D_6 and added to a solution of complex **1** in 0.5 mL of C_6D_6. The mixture was charged with pentane via the vapor diffusion method at ambient temperature until small crystals appeared. For crystal growth the solution was then stored at −35 °C for several days.

*Synthesis of [{(Cp^{NMe2AlEt3})$_2$(Cp^{NMe2})Y$_3$Cl$_5$}(μ-Cl)]$_2$ (**3a**).* Following the procedure described above, complex **1a** (25 mg, 0.069 mmol) and Et_2AlCl (16.6 mg, 0.138 mmol) yielded **3a** (19 mg, 0.007 mmol, 64%) as colorless crystals. IR (cm^{-1}): 3058 vw(sh), 2972 s, 2922 s, 2894 s, 2855 s, 2791 m, 2728 w, 2633 w, 2279 w, 1467 s, 1452 s, 1408 m, 1378 w, 1328 w, 1272 w, 1241 w, 1228 w, 1189 w, 1137 w, 1098 w, 1064 w, 1027 m, 1009 m, 988 m, 950 m, 913 w, 856 w, 803 w, 765 w, 668 m, 647 s, 634 s. Anal. Calcd for for $C_{102}H_{192}Al_4Cl_{12}N_6Y_6$ (2569.45): C, 47.68; H, 7.53; N, 3.27. Calcd for **3a**·(benzene)$_2$: C, 50.23; H, 7.54; N, 3.08. Found: C, 51.16; H, 7.83; N, 3.35. Multiple attempts to obtain a more satisfactory microanalysis failed.

*Synthesis of [{(Cp^{NMe2AlEt3})$_2$(Cp^{NMe2})Ho$_3$Cl$_5$}(μ-Cl)]$_2$ (**3b**).* Following the procedure described above, complex **1b** (25 mg, 0.057 mmol) and Et_2AlCl (13.7 mg, 0.114 mmol) yielded **3b** (24 mg, 0.008 mmol, 83%) as pink crystals. IR (cm^{-1}): 3063 vw(sh), 2973 s, 2922 s, 2893 s, 2855 s, 2791 m, 2728 w, 2634 w, 2279 w, 1467 s, 1452 s, 1408 m, 1378 w, 1328 w, 1272 w, 1241 w, 1228 w, 1189 w, 1137 w, 1098 w, 1064 w, 1027 m, 1009 m, 988 m, 950 m, 913 w, 856 w, 856 w, 804 w, 766 w, 667 m, 647 s, 633 s. Anal. Calcd for $C_{102}H_{192}Al_4Cl_{12}Ho_6N_6$ (3025.60): C, 40.49; H, 6.40; N, 2.78. Calcd for **3b**·2(benzene): C, 43.03; H, 6.46; N, 2.64. Found: C, 43.26; H, 6.14; N, 2.71.

Polymerization of Isoprene. A detailed polymerization procedure (Table 2, run 1) is described as a typical example. [Ph_3C][B(C_6F_5)$_4$] (**A**; 18 mg, 0.02 mmol, 1 equiv) was added to a solution of **1a** (7.27 mg, 0.02 mmol) in toluene (8 mL), and the mixture was aged at ambient temperature for 30 min. After the addition of isoprene (1.36 g, 20 mmol), the polymerization was carried out at 40 °C for 2 h. The reaction was terminated by pouring the polymerization mixture into 200 mL of methanol containing 0.1% (w/w) 2,6-di-*tert*-butyl-4-methylphenol as a stabilizer and stirred for 12 h. The polymer was washed with methanol and dried under vacuum at ambient temperature to constant weight. In case of the ternary catalyst system (example Table 2, run 3), the precatalyst was mixed with the trialkylaluminum compound for 30 min prior to activation with the cocatalyst. The polymerization was following the procedure described above.

Crystallographic Details. Single crystals suitable for X-ray diffraction measurements were selected in a glovebox, covered in Parabar 10312 (previously known as Paratone-N), and mounted on a glass fiber. The crystal data for the complexes were collected on a STOE IPDS II diffractometer using graphite-monochromated Mo K_α radiation (λ = 0.71073 Å) at 173(2) K performing φ scans. Raw data were collected, integrated, and reduced using the program package X-Area.[74] Corrections for absorption effects were applied using Platon/Mulabs.[75] Structure solutions and refinements were performed using the programs SHELXS[76] and SHELXL.[77] The structures in this article are represented using the program ORTEP-III.[78] For further experimental details on refinement and crystallographic data see Table S1 (Supporting Information).

■ ASSOCIATED CONTENT

Ⓢ Supporting Information

CIF files giving full crystallographic data for complexes **1**, **2**, and **3b**, ^1H, ^{13}C, and 2D ^1H–^{13}C HSQC NMR spectra of compounds **1a** (Figures S1–S3), **1c** (Figures S4–S6), and **4** (Figures S7 and S8), ^1H NMR reaction spectra of **1a** with $AlMe_3$ (Figure S9), ORTEP representations of **1b** (Figure S10), **1c** (Figure S11), **3a** (Figure S12), and **3b** (Figure S13), crystallographic data for complexes **1**–**3** (Table S1), ^1H and ^{13}C NMR data for polyisoprene from run 11 (Table S2), and ^{13}C NMR spectra from polyisoprenes obtained from precatalyst **1a** under various conditions (Figure S14). This material is available free of charge via the Internet at http://pubs.acs.org. Crystallographic data have also been deposited at the Cambridge Crystallographic Data Centre under CCDC reference numbers 974988 (**1a**), 974989 (**1b**), 974990 (**2**), 974991 (**1c**), and 994213 (**3b**), which can be obtained free of charge via www.ccdc.cam.ac.uk/data_request/cif.

■ AUTHOR INFORMATION

Corresponding Author

*E-mail for R.A.: reiner.anwander@uni-tuebingen.de.

Notes

The authors declare no competing financial interest.

■ ACKNOWLEDGMENTS

We are grateful to the German Science Foundation for support (Grant No. AN 238/14-2).

■ REFERENCES

(1) Brintzinger, H. H.; Fischer, D.; Mülhaupt, R.; Rieger, B.; Waymouth, R. M. *Angew. Chem., Int. Ed.* **1995**, *34*, 1143.
(2) Nakayama, Y.; Yasuda, H. *J. Organomet. Chem.* **2004**, *689*, 4489.
(3) Gromada, J.; Carpentier, J.-F.; Mortreux, A. *Coord. Chem. Rev.* **2004**, *248*, 397.
(4) Shapiro, P. J.; Bunel, E.; Schaefer, W. P.; Bercaw, J. E. *Organometallics* **1990**, *9*, 867.
(5) Stevens, J. C.; Timmers, F. J.; Rosen, G. W.; Knight, G. W.; Lai, S. Y. Eur. Pat. Appl. EP 0 416 815 A2, 1991.
(6) Canich, J. A. Eur. Pat. Appl. EP 0 420 436 A1, 1991.
(7) Okuda, J. *Dalton Trans.* **2003**, 2367.
(8) Kaita, S.; Doi, Y.; Kaneko, K.; Horiuchi, A. C.; Wakatsuki, Y. *Macromolecules* **2004**, *37*, 5860.
(9) Kaita, S.; Hou, Z.; Nishiura, M.; Doi, Y.; Kurazumi, J.; Horiuchi, A. C.; Wakatsuki, Y. *Macromol. Rapid Commun.* **2003**, *24*, 179.
(10) Kaita, S.; Hou, Z.; Wakatsuki, Y. *Macromolecules* **1999**, *32*, 9078.
(11) Kaita, S.; Yamanaka, M.; Horiuchi, A. C.; Wakatsuki, Y. *Macromolecules* **2006**, *39*, 1359.
(12) Zhang, L.; Luo, Y.; Hou, Z. *J. Am. Chem. Soc.* **2005**, *127*, 14562.
(13) Kirillov, E.; Lehmann, C. W.; Razavi, A.; Carpentier, J.-F. *J. Am. Chem. Soc.* **2004**, *126*, 12240.
(14) Rodrigues, A.-S.; Kirillov, E.; Vuillemin, B.; Razavi, A.; Carpentier, J.-F. *Polymer* **2008**, *49*, 2039.
(15) Arndt, S.; Okuda, J. *Chem. Rev.* **2002**, *102*, 1953.
(16) Zimmermann, M.; Anwander, R. *Chem. Rev.* **2010**, *110*, 6194.
(17) Jian, Z.; Tang, S.; Cui, D. *Chem. Eur. J.* **2010**, *16*, 14007.
(18) Jian, Z.; Cui, D.; Hou, Z. *Chem. Eur. J.* **2012**, *18*, 2674.
(19) Panda, T. K.; Hrib, C. G.; Jones, P. G.; Jenter, J.; Roesky, P. W.; Tamm, M. *Eur. J. Inorg. Chem.* **2008**, *2008*, 4270.
(20) Jian, Z.; Tang, S.; Cui, D. *Macromolecules* **2011**, *44*, 7675.
(21) Beetstra, D. J.; Meetsma, A.; Hessen, B.; Teuben, J. H. *Organometallics* **2003**, *22*, 4372.

DOI: 10.1021/om500725g
Organometallics 2015, 34, 32–41

(22) Jian, Z.; Petrov, A. R.; Hangaly, N. K.; Li, S.; Rong, W.; Mou, Z.; Rufanov, K. A.; Harms, K.; Sundermeyer, J.; Cui, D. *Organometallics* **2012**, *31*, 4267.
(23) Otero, A.; Fernández-Baeza, J.; Antiñolo, A.; Lara-Sánchez, A.; Martínez-Caballero, E.; Tejeda, J.; Sánchez-Barba, L. F.; Alonso-Moreno, C.; López-Solera, I. *Organometallics* **2008**, *27*, 976.
(24) Jian, Z.; Cui, D.; Hou, Z.; Li, X. *Chem. Commun.* **2010**, *46*, 3022.
(25) Wang, Y.; Lei, Y.; Chi, S.; Luo, Y. *Dalton Trans.* **2013**, *42*, 1862.
(26) Jian, Z.; Zhao, W.; Liu, X.; Chen, X.; Tang, T.; Cui, D. *Dalton Trans.* **2010**, *39*, 6871.
(27) Royo, B.; Peris, E. *Eur. J. Inorg. Chem.* **2012**, *2012*, 1309.
(28) Pan, Y.; Rong, W.; Jian, Z.; Cui, D. *Macromolecules* **2012**, *45*, 1248.
(29) Wang, B.; Cui, D.; Lv, K. *Macromolecules* **2008**, *41*, 1983.
(30) Wang, B.; Wang, D.; Cui, D.; Gao, W.; Tang, T.; Chen, X.; Jing, X. *Organometallics* **2007**, *26*, 3167.
(31) Wang, B.; Tang, T.; Li, Y.; Cui, D. *Dalton Trans.* **2009**, 8963.
(32) Rufanov, K. A.; Petrov, A. R.; Kotov, V. V.; Laquai, F.; Sundermeyer, J. *Eur. J. Inorg. Chem.* **2005**, *2005*, 3805.
(33) Li, X.; Nishiura, M.; Hu, L.; Mori, K.; Hou, Z. *J. Am. Chem. Soc.* **2009**, *131*, 13870.
(34) Taube, R.; Maiwald, S.; Sieler, J. *J. Organomet. Chem.* **2001**, *621*, 327.
(35) Enders, M.; Rudolph, R.; Pritzkow, H. *Chem. Ber.* **1996**, *129*, 459.
(36) Jutzi, P.; Dahlhaus, J.; Bangel, M. *J. Organomet. Chem.* **1993**, *460*, C13.
(37) Zimmermann, M.; Volbeda, J.; Törnroos, K. W.; Anwander, R. *C. R. Chim.* **2010**, *13*, 651.
(38) Zimmermann, M.; Törnroos, K. W.; Sitzmann, H.; Anwander, R. *Chem. Eur. J.* **2008**, *14*, 7266.
(39) Zimmermann, M.; Törnroos, K. W.; Anwander, R. *Angew. Chem., Int. Ed.* **2008**, *47*, 775.
(40) Zimmermann, M.; Frøystein, N. Å.; Fischbach, A.; Sirsch, P.; Dietrich, H. M.; Törnroos, K. W.; Herdtweck, E.; Anwander, R. *Chem. Eur. J.* **2007**, *13*, 8784.
(41) Litlabø, R.; Enders, M.; Törnroos, K. W.; Anwander, R. *Organometallics* **2010**, *29*, 2588.
(42) Evans, W. J.; Kozimor, S. A.; Brady, J. C.; Davis, B. L.; Nyce, G. W.; Seibel, C. A.; Ziller, J. W.; Doedens, R. J. *Organometallics* **2005**, *24*, 2269.
(43) Yu, N.; Nishiura, M.; Li, X.; Xi, Z.; Hou, Z. *Chem. Asian J.* **2008**, *3*, 1406.
(44) Maiwald, S.; Taube, R.; Hemling, H.; Schumann, H. *J. Organomet. Chem.* **1998**, *552*, 195.
(45) Fischbach, A.; Anwander, R. *Adv. Polym. Sci.* **2006**, *204*, 155.
(46) Friebe, L.; Nuyken, O.; Obrecht, W. *Adv. Polym. Sci.* **2006**, *204*, 1.
(47) Fischbach, A.; Klimpel, M. G.; Widenmeyer, M.; Herdtweck, E.; Scherer, W.; Anwander, R. *Angew. Chem., Int. Ed.* **2004**, *43*, 2234.
(48) Meermann, C.; Törnroos, K. W.; Nerdal, W.; Anwander, R. *Angew. Chem., Int. Ed.* **2007**, *46*, 6508.
(49) Fischbach, A.; Perdih, F.; Herdtweck, E.; Anwander, R. *Organometallics* **2006**, *25*, 1626.
(50) Fischbach, A.; Meermann, C.; Eickerling, G.; Scherer, W.; Anwander, R. *Macromolecules* **2006**, *39*, 6811.
(51) Sieler, J.; Simon, A.; Peters, K.; Taube, R.; Geitner, M. *J. Organomet. Chem.* **1989**, *362*, 297.
(52) Anwander, R. *Angew. Chem., Int. Ed.* **1998**, *37*, 599.
(53) Barnea, E.; Averbuj, C.; Kapon, M.; Botoshansky, M.; Eisen, M. S. *Eur. J. Inorg. Chem.* **2007**, *2007*, 4535.
(54) Bonnet, F.; Visseaux, M.; Barbier-Baudry, D.; Hafid, A.; Vigier, E.; Kubicki, M. M. *Inorg. Chem.* **2004**, *43*, 3682.
(55) Evans, W. J.; Champagnea, T. M.; Davisa, B. L.; Allena, N. T.; Nycea, G. W.; Johnstona, M. A.; Lina, Y.-C.; Khvostova, A.; Zillera, J. W. *J. Coord. Chem.* **2006**, *59*, 1069.
(56) Paolucci, G.; Vignola, M.; Zanella, A.; Bertolasi, V.; Polo, E.; Sostero, S. *Eur. J. Inorg. Chem.* **2006**, *2006*, 4104.
(57) Jende, L. N.; Maichle-Mössmer, C.; Anwander, R. *Chem. Eur. J.* **2013**, *19*, 16321.
(58) Zhang, L.; Nishiura, M.; Yuki, M.; Luo, Y.; Hou, Z. *Angew. Chem., Int. Ed.* **2008**, *47*, 2642.
(59) Wang, L.; Liu, D.; Cui, D. *Organometallics* **2012**, *31*, 6014.
(60) Du, G.; Wei, Y.; Ai, L.; Chen, Y.; Xu, Q.; Liu, X.; Zhang, S.; Hou, Z.; Li, X. *Organometallics* **2011**, *30*, 160.
(61) Ajellal, N.; Furlan, L.; Thomas, C. M.; Casagrande, O. L.; Carpentier, J.-F. *Macromol. Rapid Commun.* **2006**, *27*, 338.
(62) Inoue, S. *J. Macromol. Sci., Part A: Chem.* **1988**, *25*, 571.
(63) Inoue, S. *J. Polym. Sci., Part A: Polym. Chem.* **2000**, *38*, 2861.
(64) Tanaka, Y.; Sato, H.; Ogura, A.; Nagoya, I. *J. Polym. Sci., Part A: Polym. Chem. Ed.* **1976**, *14*, 73.
(65) Yao, C.; Liu, D.; Li, P.; Wu, C.; Li, S.; Liu, B.; Cui, D. *Organometallics* **2014**, *33*, 684.
(66) Makhiyanov, N. *Polym. Sci. Ser. A* **2014**, *56*, 241.
(67) Makhiyanov, N.; Akhmetov, I. G.; Vagizov, A. M. *Polym. Sci. Ser. A* **2012**, *54*, 942.
(68) Qiu, Z. W.; Chen, X.; Sun, B.; Zhou, Z.; Wang, F. *J. Macromol. Sci. Part A: Chem.* **1988**, *25*, 127.
(69) Xie, D.; Sun, Q. *Chin. J. Polym. Sci.* **1987**, *5*, 114.
(70) Jende, L. N.; Maichle-Mössmer, C.; Schädle, C.; Anwander, R. *J. Organomet. Chem.* **2013**, *744*, 74.
(71) Lichtenberg, C.; Robert, D.; Spaniol, T. P.; Okuda, J. *Organometallics* **2010**, *29*, 5714.
(72) Abrams, M. B.; Yoder, J. C.; Loeber, C.; Day, M. W.; Bercaw, J. E. *Organometallics* **1999**, *18*, 1389.
(73) Evans, W. J.; Anwander, R.; Ziller, J. W. *Organometallics* **1995**, *14*, 1107.
(74) *X-Area*, V. 155; Stoe & Cie GmbH: Darmstadt, Germany, 2009.
(75) Spek, A. *Acta Crystallogr., Sect. D* **2009**, *65*, 148.
(76) Sheldrick, G. M. *SHELXS-97 Program for crystal structure solution*; University of Göttingen, Göttingen, Germany, 1997.
(77) Scheldrick, G. M. *SHELXL-97 Program for crystal structure refinement*; University of Göttingen, Göttingen, Germany, 1997.
(78) Farrugia, L. J. *J. Appl. Crystallogr.* **1997**, *30*, 565.

DOI: 10.1021/om500725g
Organometallics 2015, 34, 32−41

Paper II: Supporting Information

This Supporting Information is reprinted with permission from the Supporting Information of:

"Rare-Earth-Metal Allyl Complexes Supported by the [2-(*N*,*N*-Dimethylamino)ethyl]tetramethylcyclopentadienyl Ligand: Structural Characterization, Reactivity, and Isoprene Polymerization"

by
Lars N. Jende, Christoph O. Hollfelder, Cäcilia Maichle-Mössmer, and Reiner Anwander

published in:
Organometallics, **2015**, *34*, 32–41
doi: 10.1021/om500725g

Copyright (2015) American Chemical Society.

Supporting Information

Rare-Earth Metal Bis(allyl) Complexes Supported by the [2-(*N*,*N*-Dimethylamino)ethyl]tetramethylcyclopentadienyl Ligand: Structural Characterization, Reactivity, and Isoprene Polymerization

Lars N. Jende, Christoph O. Hollfelder, Cäcilia Maichle-Mössmer, and Reiner Anwander*

Figure S1. ^{1}H NMR spectrum (C_6D_6, 25 °C) of complex **1a**

Figure S2. ^{13}C NMR spectrum (C_6D_6, 25 °C) of complex **1a**

Figure S3. 2D ^{1}H-^{13}C HSQC NMR spectrum (C_6D_6, 25 °C) of complex **1a**

Figure S4. ^{1}H NMR spectrum (C_6D_6, 25 °C) of complex **1c**

Figure S5. ^{13}C NMR spectrum (C_6D_6, 25 °C) of complex **1c**

Figure S6. 2D ^{1}H-^{13}C HSQC NMR spectrum (C_6D_6, 25 °C) of complex **1c**

Figure S7. ^{1}H NMR spectrum (C_6D_6, 25 °C) of complex **4**

Figure S8. ^{13}C NMR spectrum (C_6D_6, 25 °C) of complex **4**

Figure S9. ^{1}H NMR reaction spectra of $[Cp^{NMe2}Y(C_3H_5)_2]$ (**1a**) with $AlMe_3$

Figure S10. Molecular structure of $[Cp^{NMe2}Ho(C_3H_5)_2]$ (**1b**)

Figure S11. Molecular structure of $[Cp^{NMe2}Lu(C_3H_5)_2]$ (**1c**)

Figure S12. Molecular structure of $[\{(Cp^{NMe2AlEt3})_2(Cp^{NMe2})Y_3Cl_5\}(\mu\text{-}Cl)]_2$ (**3a**)

Figure S13. Molecular structure of $[\{(Cp^{NMe2AlEt3})_2(Cp^{NMe2})Ho_3Cl_5\}(\mu\text{-}Cl)]_2$ (**3b**)

Table S1. Crystallographic data for complexes **1**, **2**, and **3**

Table S2. ^{1}H and ^{13}C NMR data of polyisoprene obtained from **2**/**B**/$AlMe_3$

Figure S14. ^{13}C NMR spectra of polyisoprenes obtained with pre-catalyst **1a**

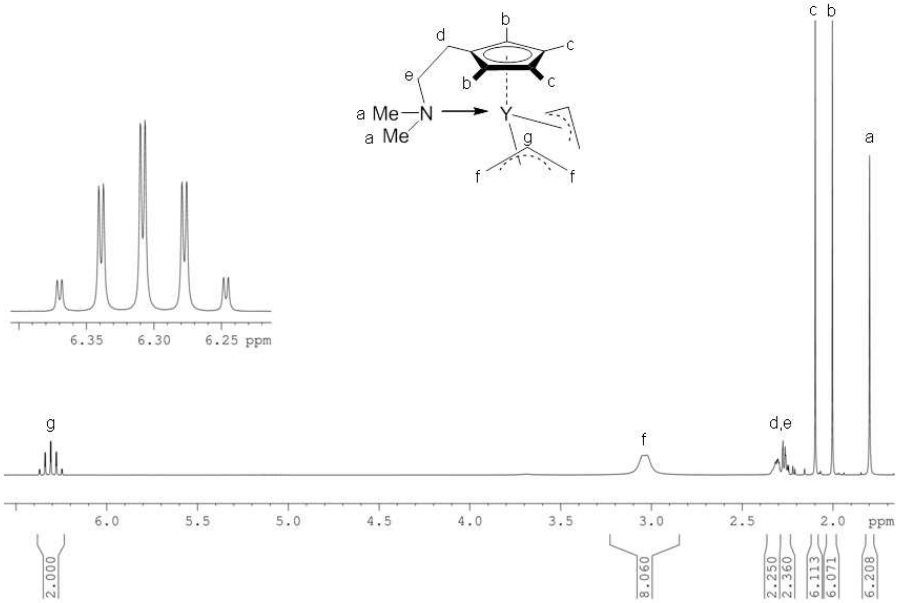

Figure S1. ^{1}H NMR spectrum (C_6D_6, 25 °C) of complex **1a**.

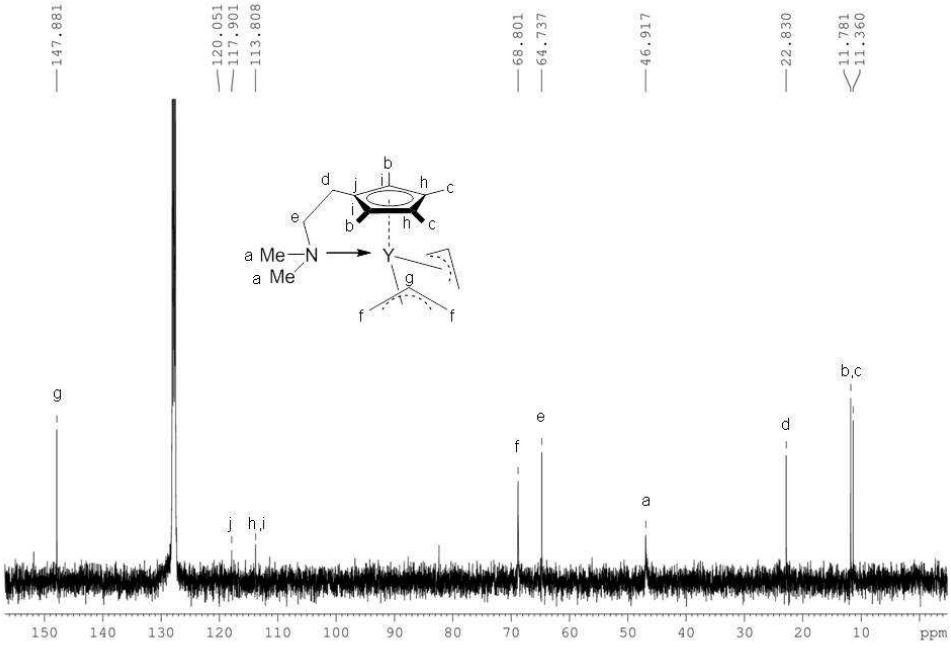

Figure S2. ^{13}C NMR spectrum (C_6D_6, 25 °C) of complex **1a**.

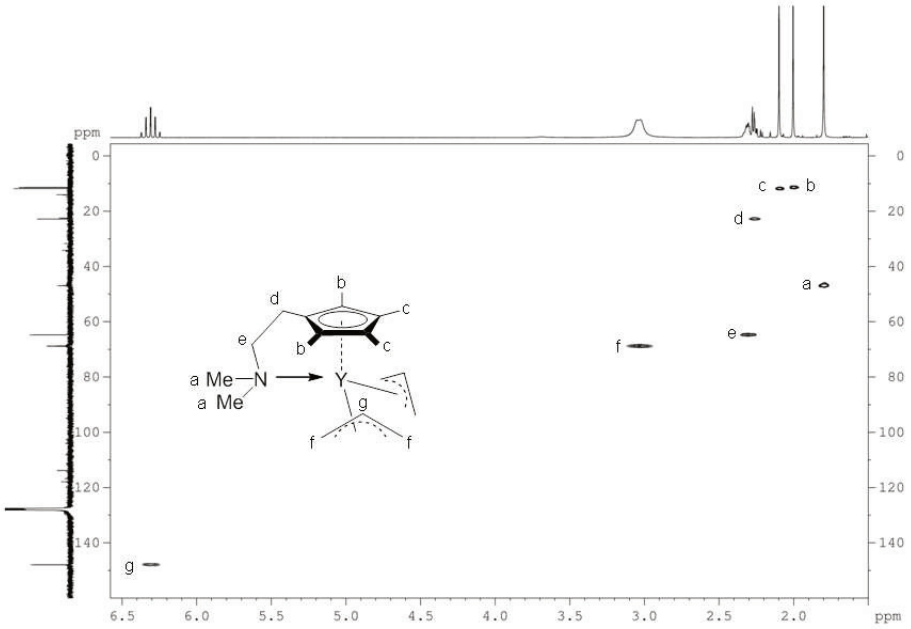

Figure S3. 2D ^{1}H-^{13}C HSQC NMR spectrum (C_6D_6, 25 °C) of complex **1a**.

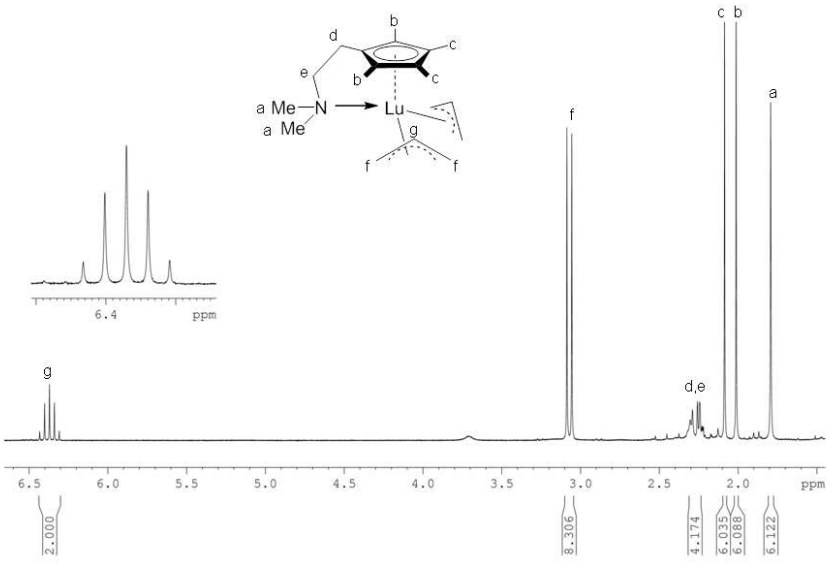

Figure S4. ^{1}H NMR spectrum (C_6D_6, 25 °C) of complex **1c**.

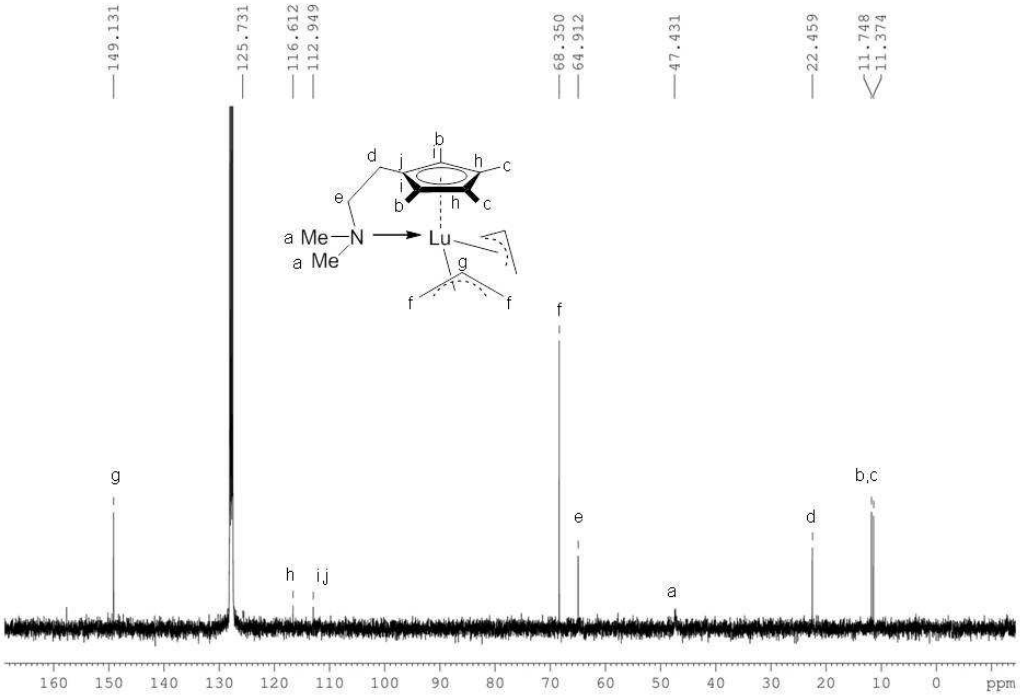

Figure S5. ^{13}C NMR spectrum (C_6D_6, 25 °C) of complex **1c**.

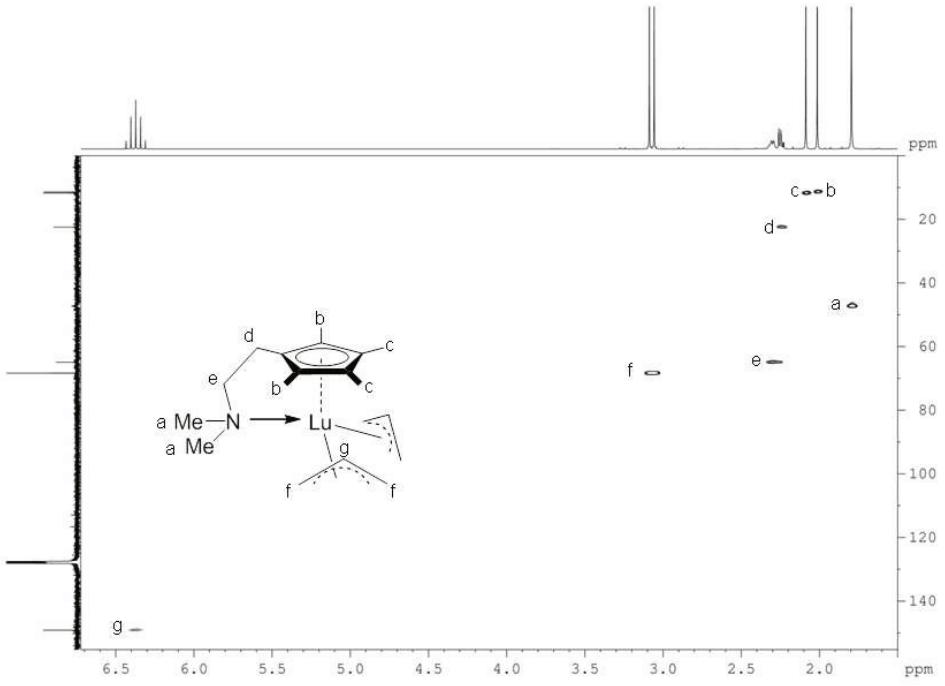

Figure S6. 2D ^{1}H-^{13}C HSQC NMR spectrum (C_6D_6, 25 °C) of complex **1c**.

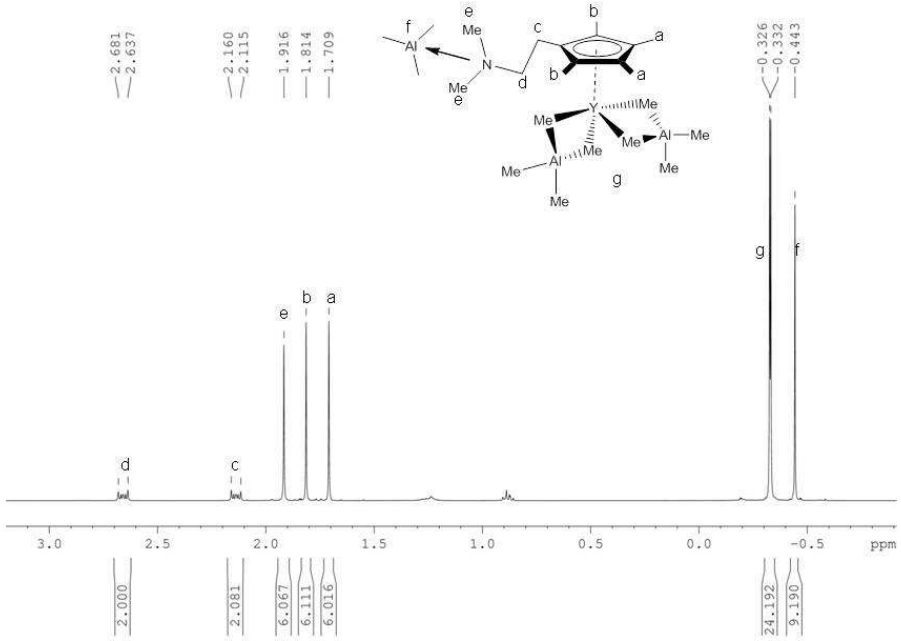

Figure S7. ^{1}H NMR spectrum (C_6D_6, 25 °C) of complex **4**.

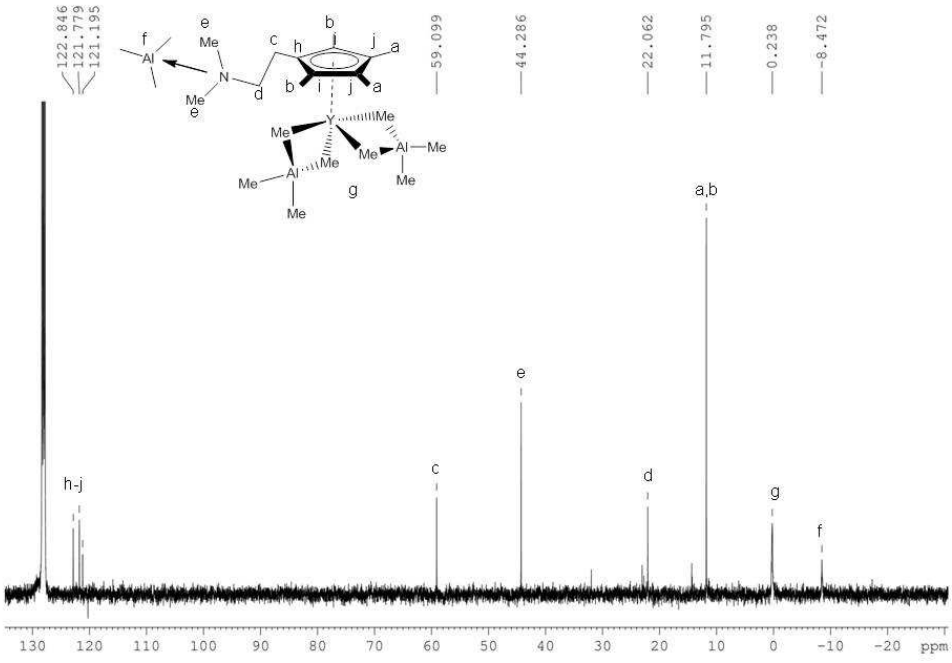

Figure S8. ^{13}C NMR spectrum (C_6D_6, 25 °C) of complex **4**.

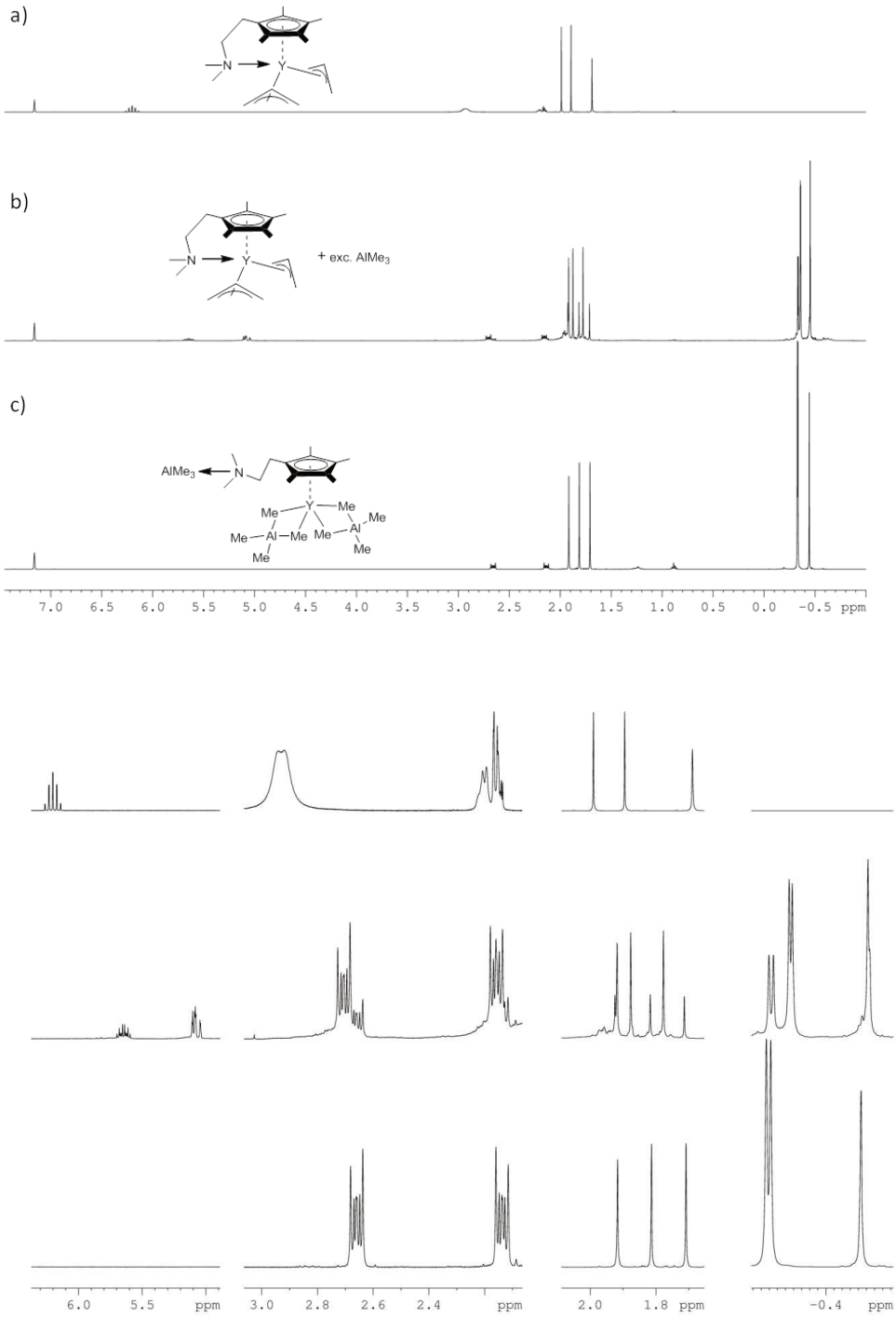

Figure S9. Top) ^{1}H NMR spectra (400 MHz, 25 °C, C_6D_6) of a) pure [$Cp^{NMe2}Y(\eta^3\text{-}C_3H_5)_2$] (**1a**); b) reaction product of [$Cp^{NMe2}Y(\eta^3\text{-}C_3H_5)_2$] with 10 eq. $AlMe_3$ after evaporation of volatiles; c) [$Cp^{NMe2AlMe3}Y(AlMe_4)_2$] (**4**). Bottom) selected regions.

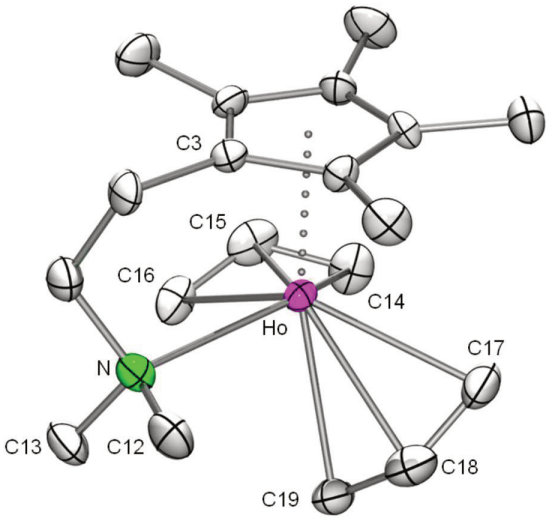

Figure S10. Molecular structure of $[Cp^{NMe2}Ho(C_3H_5)_2]$ (**1b**); atomic displacement parameters set at the 50% level; hydrogen atoms omitted for clarity.

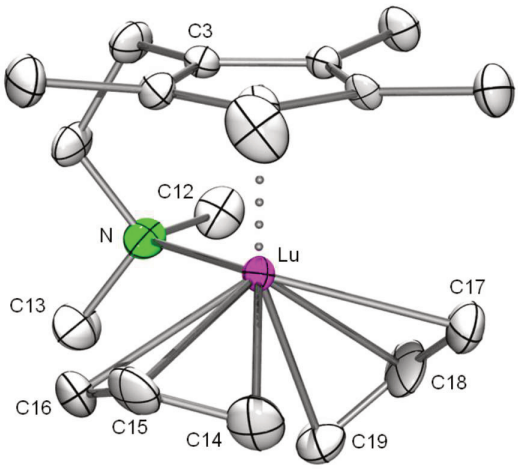

Figure S11. Molecular structure of $[Cp^{NMe2}Lu(C_3H_5)_2]$ (**1c**); atomic displacement parameters set at the 50% level; hydrogen atoms omitted for clarity.

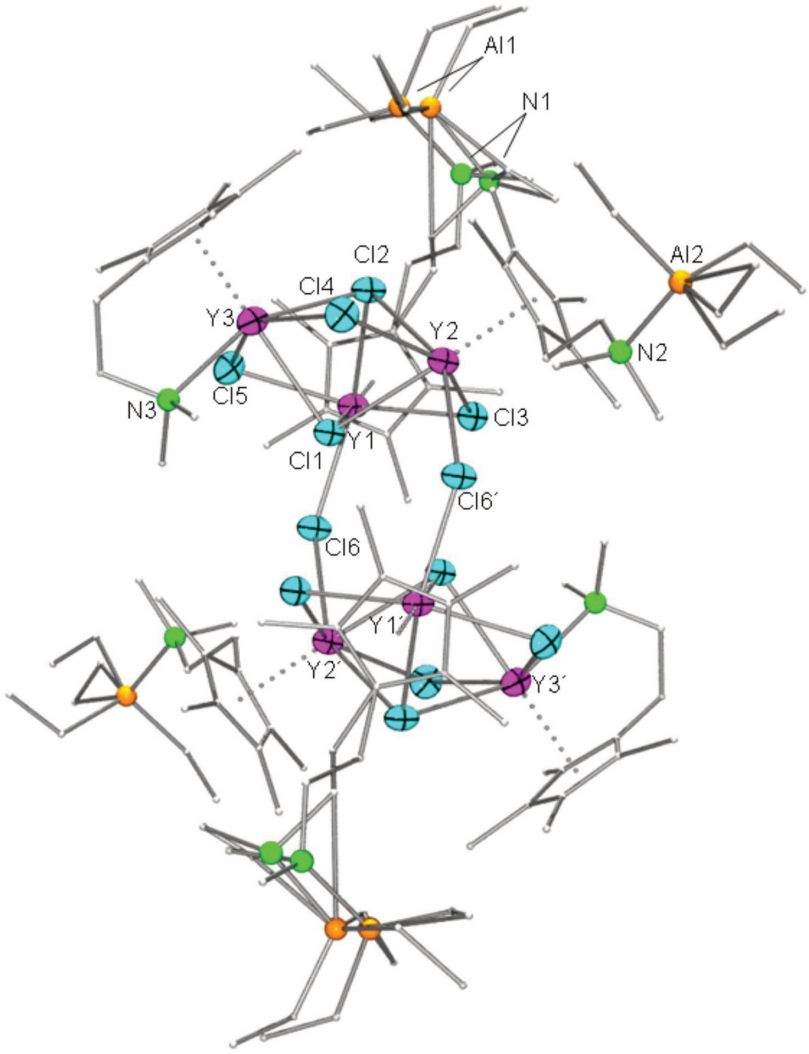

Figure S12. Molecular structure of $[\{(Cp^{NMe2AlEt3})_2(Cp^{NMe2})Y_3Cl_5\}(\mu\text{-}Cl)]_2$ (**3a**); atomic displacement parameters set at the 50% level; aluminum, carbon, and nitrogen atoms are shown as ball-stick representation; hydrogen atoms have for clarity. Disorders of the cyclopentadienyl sidearm and of the ethyl groups at the aluminum centers are shown.

Cell parameters (*P*-1): a = 13.9232, b = 17.0282, c = 18.0040 [Å]; α = 65.191, β = 67.445, γ = 89.805 [°].

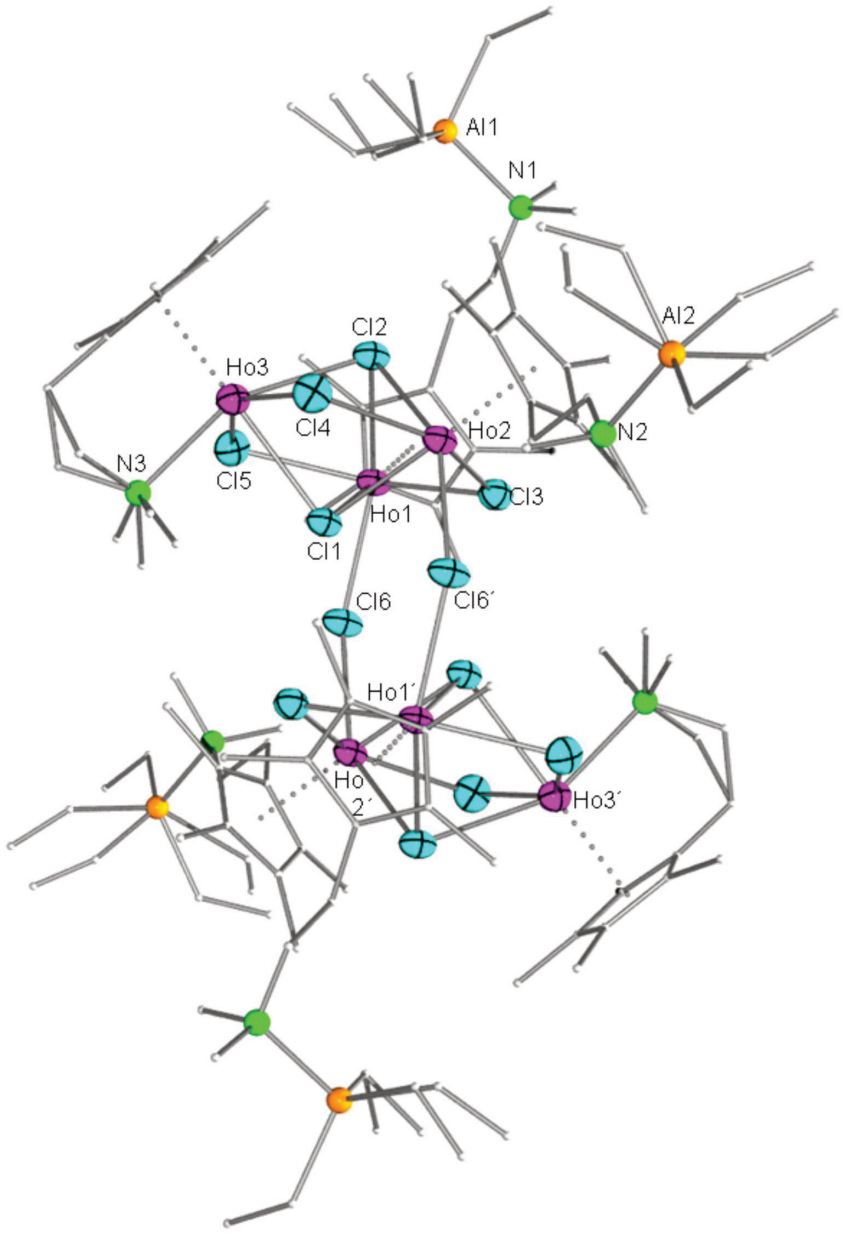

Figure S13. Molecular structure of $[\{(Cp^{NMe2AlEt3})_2(Cp^{NMe2})Ho_3Cl_5\}(\mu\text{-}Cl)\}]_2$ (**3b**); atomic displacement parameters set at the 50% level; aluminum, carbon, and nitrogen atoms are shown as ball-stick representation; hydrogen atoms omitted for clarity. Disorders of the cyclopentadienyl sidearm at N3 and of the ethyl groups at the aluminum centers are shown.

Table S1. Crystallographic data for complexes **1**, **2**, and **3**

	1a (Ln = Y)	**1b** (Ln = Ho)	**1c** (Ln = Lu)	**2** (Ln = Nd)	**3b** (Ln = Ho)·$(C_6H_6)_4$
Formular	$C_{19}H_{32}NY$	$C_{19}H_{32}NHo$	$C_{19}H_{32}NLu$	$C_{39}H_{62}Cl_2N_2Nd_2$	$C_{126}H_{216}Al_4Cl_{12}Ho_6N_6$
Fw	363.37	439.39	449.43	918.29	3337.94
temp (K)	173(2)	173(2)	173(2)	173(2)	173(2)
cryst syst	monoclinic	monoclinic	monoclinic	triclinic	triclinic
space group	$P2_1$	$P2_1$	$P2_1$	P-1	P-1
a (Å)	8.4644(4)	8.4569(8)	8.4482(9)	8.7736(9)	14.0630(11)
b (Å)	13.9975(5)	13.9798(13)	13.9076(10)	10.4931(15)	17.0674(12)
c (Å)	8.5546(4)	8.5604(8)	8.5517(9)	12.2435(15)	17.9374(14)
α (deg)	90.00	90.00	90.00	67.958(11)	66.845(6)
β (deg)	114.260(3)	114.331(7)	114.482(8)	81.853(9)	68.304(6)
γ (deg)	90.00	90.00	90.00	74.973(10)	88.529(6)
vol (Å^3)	924.05(7)	922.17(15)	914.44(15)	1007.8(2)	3641.8(5)
Z	2	2	2	1	1
ρ_{calcd} (mg/mm^3)	1.306	1.582	1.632	1.513	1.522
μ (mm^{-1})	3.151	4.285	5.393	2.707	3.508
R_1(all) [a]	0.0416	0.0304	0.0198	0.0430	0.0498
wR_2(all) [b]	0.0928	0.0677	0.0399	0.0919	0.1027
GOF (on F^2) [c]	1.154	1.052	1.051	1.223	1.100

[a] $R1 = \Sigma(||F_0|-|F_c||)/\Sigma|F_0|$; [b] $wR2 = \{\Sigma[w(F_0^2-F_c^2)^2/\Sigma[w(F_0^2)^2]\}^{1/2}$; [c] GOF = $\{\Sigma[w(F_0^2-F_c^2)^2]/(n-p)\}^{1/2}$.

Table S2. NMR data of *trans*-1,4- (**T**) and 3,4- (**V**) units of polyisoprene obtained from **2**/**B**/$AlMe_3$.

Position	^{13}C	^{1}H	Position	^{13}C	^{1}H
T_5	16.0	1.61	T_5^{I}	16.2	n.d.
T_4	26.7	2.08	T_4^{I}	32.1	2.04
T_1	39.7	2.00	T_1^{I}	37.4	1.89
T_3	124.2	5.13	T_3^{I}	123.0	5.09
T_2	134.9	–	T_2^{I}	135.3	–
V_5	18.6	1.63	T_5^{II}	n.d.	n.d.
V_4	31.3	1.43	T_4^{II}	n.d.	n.d.
V_3	47.2	2.03	T_1^{II}	39.8	n.d.
V_1	111.2	4.71	T_3^{II}	124.0	n.d.
V_2	147.6	–	T_2^{II}	135.1	–

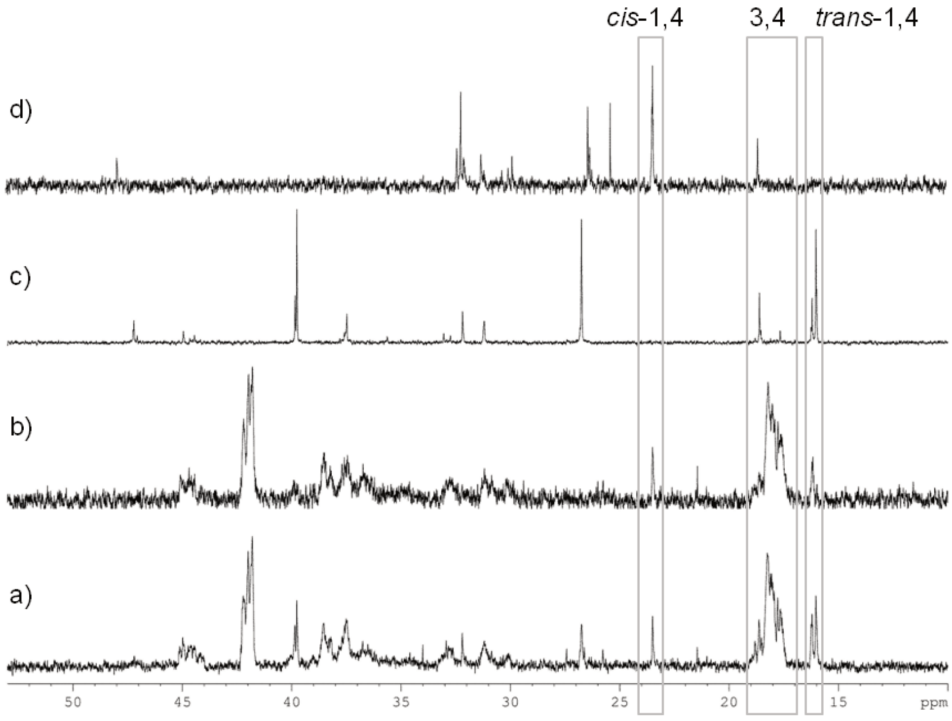

Figure S14. ^{13}C NMR ($CDCl_3$, 25 °C) spectra of polyisoprenes obtained from pre-catalyst **1a** activated with co-catalyst **A** (a), **B** (b), **B** with 10 equiv $AlMe_3$ (c) and **B** with 10 equiv $Al\mathit{i}Bu_3$ (d).

Paper III: C–H Bond Activation and Isoprene Polymerization by Lutetium Alkylaluminate / gallate Complexes Bearing a Peripheral Boryl and a Bulky Hydrotris(pyrazolyl) Borate Ligand

This aricle is reprinted with permission (License Number 4705980258412) from:

"C–H Bond Activation and Isoprene Polymerization by Lutetium Alkylaluminate / gallate Complexes Bearing a Peripheral Boryl and a Bulky Hydrotris(pyrazolyl)borate Ligand"

by
Martin Bonath, Christoph O. Hollfelder, Dorothea Schädle, Cäcilia Maichle-Mössmer, Peter Sirsch, and Reiner Anwander

published in:
Eur. J. Inorg. Chem. **2017**, *2017*, 4683–4692
doi: 10.1002/ejic.201700730

Copyright (2017) by John Wiley and Sons.

ChemPubSoc Europe

DOI: 10.1002/ejic.201700730

EurJIC European Journal of Inorganic Chemistry

Full Paper

Polymerization Precatalysts | *Very Important Paper* | CLUSTER ISSUE

VIP

C–H Bond Activation and Isoprene Polymerization by Lutetium Alkylaluminate/gallate Complexes Bearing a Peripheral Boryl and a Bulky Hydrotris(pyrazolyl)borate Ligand

Martin Bonath,[a][‡] Christoph O. Hollfelder,[a][‡] Dorothea Schädle,[a] Cäcilia Maichle-Mössmer,[a] Peter Sirsch,*[a] and Reiner Anwander*[a]

Abstract: The bimetallic lutetium alkylaluminate complex [(Tp^{tBu,Me})Lu(Me)(AlMe$_3${B(NDippCH)$_2$})] {Tp^{tBu,Me} = hydrotris(3-Me-5-*t*Bu-pyrazolyl)borate} formed readily upon addition of 0.5 equivalents of the organoaluminum boryl compound [Me$_2$Al{B(NDippCH)$_2$}]$_2$ (Dipp = C$_6$H$_3$*i*Pr$_2$-2,6) to [(Tp^{tBu,Me})LuMe$_2$] in *n*-hexane solution. Thermally induced cyclometalative C–H bond activation of this compound led to the formation of [(Tp$^{(tBu-H)}_2$/*t*Bu,Me)Lu(AlMe$_2${B(NDippCH)$_2$})] {Tp$^{(tBu-H)}_2$/*t*Bu,Me = hydro(3-Me-5-*t*Bu-pyrazolyl)bis[μ-(3-Me-5-Me$_2$CCH$_2$-pyrazolyl)]-borate} in quantitative yields. The latter complex bears an unusual κ^5 coordination mode of the activated tris(pyrazolyl)-borate ligand. Additionally, one Lu–CH$_2$(R) moiety is coordinated by a "neutral" [Me$_2$Al{B(NDippCH)$_2$}] unit, which can be separated off by addition of THF or trimethylaluminum. The gallium analogue of complex [(Tp^{tBu,Me})Lu(Me)(AlMe$_3$-{B(NDippCH)$_2$})] could not be isolated from the respective reaction of monomeric [Me$_2$Ga{B(NDippCH)$_2$}] with [(Tp^{tBu,Me})-LuMe$_2$], but the C–H bond activated gallate complex [(Tp$^{(tBu-H)}_2$/*t*Bu,Me)Lu(GaMe$_2${B(NDippCH)$_2$})] was obtained instead following a prolonged mild thermal treatment. The performance of the new lutetium complexes as precatalysts in the polymerization of isoprene was assessed and possible activation and deactivation scenarios were studied by NMR spectroscopy.

Introduction

Bis(hydrocarbyl) rare-earth-metal complexes supported by a monoanionic ancillary ligand (**L**) of the type [**L**LnR$_2$(Do)] (R = CH$_2$SiMe$_3$, *o*-CH$_2$PhNMe$_2$, η^3-C$_3$H$_5$; Do = neutral donor ligand) have been studied extensively for their exceptional performance in olefin polymerization reactions.[1] Given the importance of organoaluminum cocatalysts in rare-earth-metal-based 1,3-diene polymerization, we set out to develop a bis(hydrocarbylaluminate) postmetallocene library to better understand any potential Ln–Al bimetallic cooperativity as well as ancillary ligand effects.[2] Initially, we and others introduced half-sandwich bis(tetramethylaluminate) rare-earth-metal complexes of the general type [Cp$^R_5$Ln(AlMe$_4$)$_2$] [R$_5$ = HMe$_4$,[3] Me$_5$,[4] H$_2$*t*Bu$_3$,[5] Me$_4$SiMe$_3$,[5,6] H$_3$(SiMe$_3$)$_2$,[5] Me$_4$(quinolyl),[7] Me$_4$(*N*,*N*-dimethylanilyl),[8] Me$_4$(C$_2$H$_4$NMe$_2$)[8]] as donor-solvent free derivatives and established them as versatile precatalysts for the synthesis of highly stereoregular polyisoprene, when pretreated with borane/borate cocatalysts (Figure 1). Varying the substitution pattern of the cyclopentadienyl (Cp) ligand allowed for a comprehensive assessment of the electronic and steric implications of the ancillary ligand for the catalytic performance.[3,4b,5,7–9] In the course of these studies, the bulky carbanion-like boryl ligand {B(NDippCH)$_2$} (Dipp = C$_6$H$_3$*i*Pr$_2$-2,6)[10] was utilized to implement a heterosubstituted aluminato actor ligand which significantly affected the polymerization as well.[11] The microstructure of the polymers resulting from those heteroaluminate precatalysts, [Cp*Ln(AlMe$_3${B(NDippCH)$_2$})$_2$] (Ln = Lu, Y; Cp* = C$_5$Me$_5$), are of special interest as the corresponding active species add the monomers in a predominantly vinylic fashion.

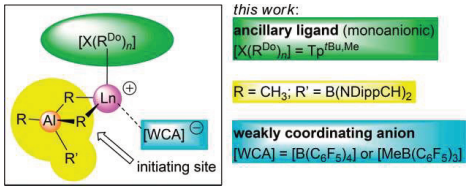

Figure 1. Active species of polymerization reactions previously proposed for the rare-earth-metal (Ln)-based bis(hydrocarbylaluminate) postmetallocene/half-sandwich library. [X(R^{Do})$_n$] = ancillary ligand like cyclopentadienyl, amido, or alkoxy featuring intraligand donor functionalities.

Over the past few years, a variety of rare-earth-metal tetramethylaluminate complexes bearing N-coordinating monoanionic ancillary ligands has been added to this postmetallocene library, including imino-amido-pyridinate,[12] benzamidinate,[13] triazenide,[14] diketiminate,[15] and formamidinate de-

[a] *Institut für Anorganische Chemie, Universität Tübingen, Auf der Morgenstelle 18, 72076 Tübingen Germany*
E-mail: reiner.anwander@uni-tuebingen.de
http://uni-tuebingen.de/syncat-anwander
http://www.mnf.uni-tuebingen.de/fachbereiche/chemie/institute/anorganische-chemie/institut/ag-sirsch.html
[‡] These authors contributed equally to this publication.
Supporting information and ORCID(s) from the author(s) for this article are available on the WWW under https://doi.org/10.1002/ejic.201700730.

© 2017 Wiley-VCH Verlag GmbH & Co. KGaA, Weinheim

ChemPubSoc Europe

EurJIC European Journal of Inorganic Chemistry
Full Paper

rivatives,[16] considerably enhancing the opportunities for further manipulations of the electronic and steric situation at the rare-earth-metal center. Accordingly, the performance in isoprene polymerization of such systems is significantly altered as well.[13a,13c,14–16] Occasional shortcomings observed for such highly reactive bimetallic complexes are Ln-to-Al *N*-coordinating ancillary ligand transfer[14] and C–H bond activation of the ancillary ligand,[8,16,17] the latter displaying a recurrent phenomenon in the field of organometallic chemistry.[18] Interestingly, Jende et al. demonstrated that complexes resulting from ancillary ligand activation can still be active precatalysts.[8]

Previously, our group reported on the synthesis of [(Tp^{tBu,Me})Ln(Me)(AlMe$_4$)] compounds (Ln = Y,[19] Ho,[20] Lu[19]) as yet another class of donor-solvent free Lewis-acid stabilized compounds of the general type [**L**LnR$_2$] (**L** = ancillary ligand, R = hydrocarbyl). We anticipated that these complexes would be suitable precatalysts for isoprene polymerization, as well. For further comprehensive studies of the effect of heteroaluminato actor ligands we targeted the synthesis and characterization of lutetium-Tp^{tBu,Me} complexes bearing an alkylaluminato ligand with a peripheral boryl ligand.

Results and Discussion

Synthesis and Degradation of Heteroaluminate Complex [(Tp^{tBu,Me})Lu(Me)(AlMe$_3${B(NDippCH)$_2$})] (1)

Addition of 0.5 equivalents of [Me$_2$Al{B(NDippCH)$_2$}]$_2$[21] to [(Tp^{tBu,Me})LuMe$_2$][20] formed a new rare-earth-metal alkyl complex, [(Tp^{tBu,Me})Lu(Me)(AlMe$_3${B(NDippCH)$_2$})] (**1**), in almost quantitative yield (Scheme 1). Similar to previously reported [(Tp^{tBu,Me})Lu(Me)(AlMe$_4$)] (**I^{Lu}**), the ^{1}H NMR spectrum of **1** recorded in [D$_6$]benzene revealed a highly fluxional behavior of the metal-bonded methyl groups.

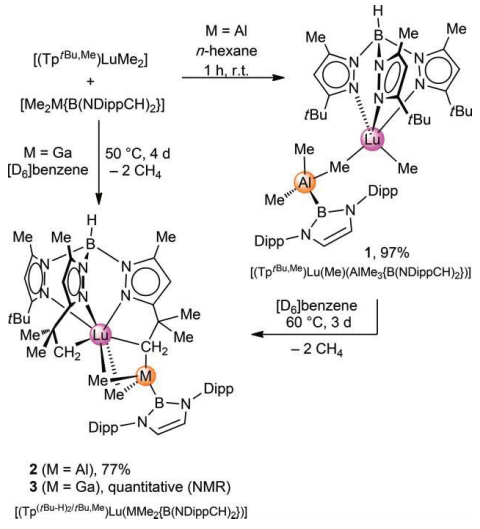

Scheme 1. Reaction of [(Tp^{tBu,Me})LuMe$_2$] with 1/2 [Me$_2$M{B(NDippCH)$_2$}]$_2$ (M = Al, Ga) and thermally induced C–H bond activation.

At ambient temperature two broad singlets were detected at δ = –0.14 ppm [6 H, Lu(C*H*$_3$)$_2$] and –1.20 ppm [6 H, Al(C*H*$_3$)$_2$], indicating that under these conditions the [Me$_2$Al{B(NDippCH)$_2$}] unit rapidly exchanges between the two Lu-bonded methyl groups, while exchange between Al- and Lu-bonded methyl groups is markedly slowed down. This suggests that the sterically demanding {B(NDippCH)$_2$} moiety keeps the Al-bonded methyl groups outside the inner coordination sphere of the Lu center thus impeding a fast methyl exchange process. A ^{1}H-^{1}H EXSY NMR spectroscopic experiment revealed that indeed slow exchange of the Al- and Lu-bonded methyl groups occurs at ambient temperature (Figure S5). Variable-temperature (VT) ^{1}H NMR spectroscopic studies in [D$_8$]toluene were performed for obtaining deeper insights into the dynamic behavior of complex **1** (Figure 2 and S3, Supporting Information). At the coalescence temperature of 70 °C the resonances of the metal alkyl groups merge to a broad singlet at δ = –0.77 ppm besides minor signals of a particular decomposition product (vide infra). Upon cooling to –10 °C the signal of the Lu–C*H*$_3$ moieties separates into two broad singlets at δ = 0.14 ppm (3 H) and –0.55 ppm (3 H). At –30 °C all of the CH and CH$_3$ pyrazolyl proton signals have decoalesced in a 2:1 ratio, indicating different environments for the pyrazolyl moieties.

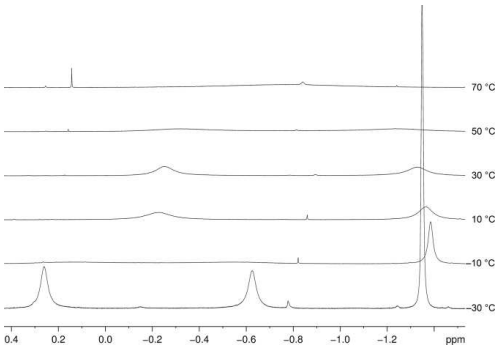

Figure 2. Variable-temperature ^{1}H NMR spectra (500 MHz) of **1**, in the region of metal-bonded *CH*, in [D$_8$]toluene.

In good agreement with the respective homoaluminate derivatives [(Tp^{tBu,Me})Ln(Me)(AlMe$_4$)] [Ln = Y (**I^{Y}**),[19] Ho (**I^{Ho}**)[20]] complex **1** adopts a distorted trigonal bipyramidal coordination geometry (Figure 3). The Lu–C bond lengths of **1** [Lu1–C25 = 2.321(1) Å, Lu1–C26 2.613(3) Å] are similar to those in **I^{Y}** [2.382(3) Å, 2.715(3) Å] and **I^{Ho}** [2.376(3) Å, 2.696(3) Å] considering the differences in the ionic radii.[22] In analogy to **I^{Y}** and **I^{Ho}** the [μ_2-MeAlMe$_2${B(NDippCH)$_2$}$_2$] unit coordinates in an η^1 fashion where the bridging methyl group almost linearly connects the two metal atoms ($\measuredangle$ Lu1C26Al1 = 164.6°). Relating to the Lu–methyl–Al axis the {B(NDippCH)$_2$} moiety captures a diagonal position relative to the Tp^{tBu,Me} ligand to minimize steric strain. Consequently, the Al-bonded methyl groups and the two pyrazolyl rings are located opposite each other.

 © 2017 Wiley-VCH Verlag GmbH & Co. KGaA, Weinheim

ChemPubSoc Europe

EurJIC European Journal of Inorganic Chemistry
Full Paper

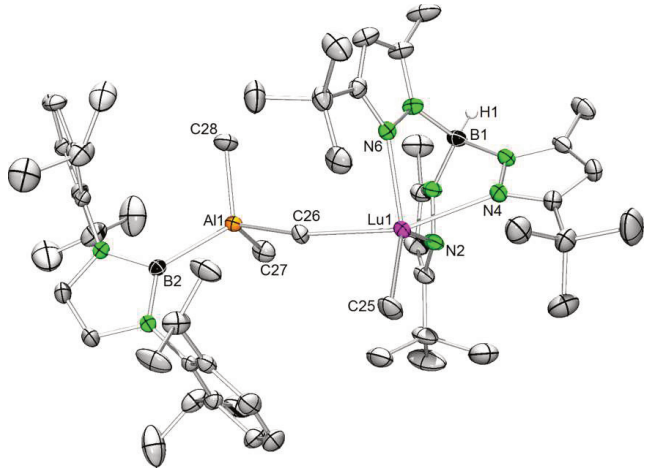

Figure 3. Solid-state structure of **1**; atomic displacement ellipsoids are set at the 50 % probability level. Cocrystallized *n*-hexane, the disorder in the Dipp moieties and one *tert*-butyl group of the $Tp^{tBu,Me}$ ligand and hydrogen atoms except for B–H are omitted for clarity. Selected bond lengths (Å) and angles (°): Lu1–C25 2.321(1), Lu1–C26 2.613(3), Lu1–N2 2.286(2), Lu1–N4 2.369(2), Lu1–N6 2.307(2), Al1–C26 2.092(3), Al1–C27 1.993(3), Al1–C28 2.002(3), Al1–B2 2.171(3), C25–Lu1–C26 96.5(1), Lu1–C26–Al1 164.5(2), N4–Lu1–C26 153.62(9).

Complex **1** dissolves readily in benzene but decomposes slowly at ambient temperature. While decomposition of $\mathbf{I^{Lu}}$ results in a variety of undefined products,[19] decomposition of **1** yielded exclusively [($Tp^{(tBu-H)}_2$/*t*Bu,Me)Lu($AlMe_2${B(NDippCH)$_2$})] (**2**) with concomitant formation of two equivalents of methane {Scheme 1; $Tp^{(tBu-H)}_2$/*t*Bu,Me = hydro(3-Me-5-*t*Bu-pyrazolyl)bis-[μ-(3-Me-5-Me_2C-CH_2-pyrazolyl)]borate}. The reaction is driven to completeness at 60 °C after three days according to ^{1}H NMR spectroscopy.

The solid-state structure of **2** revealed a doubly metalated $Tp^{tBu,Me}$ ligand resulting from σ-bond metathesis between the C–H bonds of two *t*Bu groups and the Lu–CH_3 bonds (Figure 4).

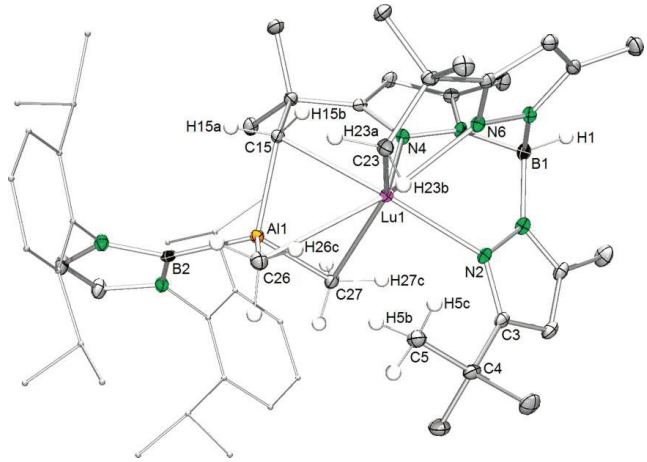

Figure 4. Solid-state structure of **2**; atomic displacement ellipsoids are set at the 50 % probability level. The carbon atoms of the Dipp moieties are shown with reduced radii. Cocrystallized *n*-hexane, the disorder in one Dipp moiety and hydrogen atoms except for B–H, C5–H, methyl and methylene groups are omitted for clarity. Selected bond lengths (Å) and angles (°): Lu1–C15 2.666(3), Lu1–C23 2.391(3), Lu1–C26 2.961(3), Lu1–C27 2.858(3), Lu1···H5b 2.57(3), Lu1···H5c 2.78(3), Lu1···H15b 2.36(3), Lu1···H23a 2.92(4), Lu1···H23b 2.79(3), Lu1···H26c 2.59(3), Lu1···H27c 2.58(3), Lu1–N2 2.409(3), Lu1–N4 2.322(3), Lu1–N6 2.300(2), Al1–C15 2.085(3), Al1–C26 2.024(4), Al1–C27 2.020(3), Al1–B2 2.142(4), C15–Lu1–C23 97.7(1), Lu1–C15–Al1 74.6(1), Lu1–C26–Al1 68.7(1), Lu1–C27–Al1 71.1(1); selected bond lengths (Å) and angles (°) of isostructural complex **3**: Lu1–C15 2.769(3), Lu1–C23 2.386(3), Lu1–C26 2.911(4), Lu1–C27 2.813(4), Ga1–C15 2.091(3), Ga1–C26 2.072(3), Ga1–C27 2.055(4), Ga1–B2 2.099(4), C15–Lu1–C23 97.0(1), Lu1–C15–Ga1 71.7(1), Lu1–C26–Ga1 68.8(1), Lu1–C27–Ga1 71.2(1).

 © 2017 Wiley-VCH Verlag GmbH & Co. KGaA, Weinheim

ChemPubSoc Europe

EurJIC European Journal of Inorganic Chemistry
Full Paper

As a consequence, the rare-earth-metal center is coordinated by the Tp^{tBu,Me} ligand in a κ^5 fashion via three nitrogen atoms and two methylene groups. Metalation of the Tp^{tBu,Me} ligand at one *tert*-butyl group was reported previously by the group of Takats for the decomposition of lanthanide dialkyl complex [(Tp^{tBu,Me})Y(CH_2SiMe_3)$_2$], to yield a mixture of products[23] while a similar structural motif was reported by our group for a side product resulting from the salt metathesis reaction of [La($AlMe_4$)$_3$] and K(Tp^{tBu,Me}).[24] The Lu–C(methylene) bond lengths in **2** differ considerably involving a longer Lu–C15 [2.666(3) Å] and a shorter Lu–C23 bond of 2.391(3) Å. While the closer methylene group displays a metal interaction with the lutetium center only, the other methylene moiety additionally connects to the [Me_2Al{B(NDippCH)$_2$}] unit.

In contrast to **1**, there are two methyl groups (C26 and C27) in **2** bridging between the Al atom and the rare-earth-metal center. As a consequence, the Al–Me distances in **2** are somewhat shorter than for the singly bridging methyl group in **1**, whereas the Lu–Me distances in **2** are clearly larger. In the X-ray structure analysis of **2**, a number of H atoms were located in close proximity to the Lu center, including two H atoms of the uncoordinated *tert*-butyl substituent at C3 (Figure 4). As H atom positions are only approximate in X-ray diffraction studies, a DFT geometry optimization of **2** (model system **2a**) was carried out in order to obtain accurate positions and to identify potential agostic interactions in **2**. The geometry obtained for **2a** was in excellent agreement with the solid-state structure of **2** (for details, see the Supporting information). Six H atoms were confirmed to display short contacts to the Lu center, ranging between 2.37 and 2.81 Å (Figure 5; for further details, see the Supporting Information). However, no significant elongation of the respective C–H bonds was observed in the case of the methyl groups, and only very small differences in C–H bond lengths for the two methylene groups (for further details, see the Supporting Information). It is interesting to note, that on C15, C26 and C27 only a single H atom is directed at the Lu atom, instead of two, as commonly observed for bridging alkyl groups.[25] In order to quantify the extent of interaction, if any, between the aforementioned C–H bonds and the Lu center, the natural bond orbital (NBO) approach was employed.[26] The calculated set of natural localized molecular orbitals (NLMOs) revealed that between 1.9 and 2.7 % of the C–H bonding electron pairs are delocalized onto the Lu atom (for details, see the Supporting Information).[27]

While this electronic effect almost appears negligible, a total of six such interactions might represent a small, but significant extra contribution to the stabilization of this complex. Based on our findings, strong agostic interactions, however, can be safely ruled out for **2**.

Finally, we investigated whether the coordination mode of the aluminate ligand would change, when the sterics of the bulky Tp^{tBu,Me} ligand was altered. Optimized model systems, in which the *tert*-butyl moiety at C3 was replaced by a methyl group (model system **2b**) and by a hydrogen atom (model system **2c**), displayed, indeed, a stepwise transition from η^3- to η^2-bridging of the aluminato ligand (for details, see the Supporting information). The distance between the Lu atom and the methyl group on C27 increased from 2.955 in **2a** to 3.381 (**2b**) and 3.678 Å (**2c**), signaling that this methyl group was moving out of the bridging position. At the same time, the interaction between Lu and the bridging methyl group on C26 increased in strength; the Lu–C26 distance shortened notably from 2.808 (**2a**) to 2.571 (**2b**) and 2.477 Å (**2c**). By fixing the angle Lu1–Al1–B2 in **2c** at the value observed in **2a** (174°) and re-optimizing the geometry (model system **2d**), we obtained a good estimate of the energy difference between the two coordination modes: Therefore, the η^2-coordination is about 12 kJ/mol lower in energy, which is outside the typical error range in DFT calculations.

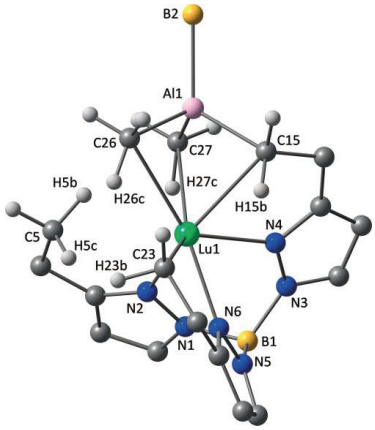

Figure 5. Coordination environment of the Lu center in the DFT-optimized model system of **2**; all further atoms are omitted for clarity. All hydrogen atoms with Lu···H distances shorter than 3 Å are labelled; the distances to Lu1 are as follows (Å): H15b 2.367, H26c 2.481, H27c 2.566, H5b 2.719, H5c 2.778, H23b 2.811.

These findings suggest that in **2**, the observed η^3-coordination is only adopted, since a more favorable coordination by two bridging C atoms is prevented by the bulky Tp^{tBu,Me} ligand. The latter seems to be more favorable, as it brings two carbon atoms in closer proximity to the Lu atom compared to the η^3 mode. Once the steric restraint is removed, as in **2b** and **2c**, the coordination mode changes accordingly to η^2.

The ^{1}H NMR spectrum of **2** recorded in [D_6]benzene revealed a very rigid coordination environment at the rare-earth-metal center, as clearly indicated by three sets of signals for the pyrazolyl moieties. Also, two sharp singlets at 0.36 (3 H) and –1.13 ppm (3 H) could be assigned to the Al-Me groups and the resonances attributed to the {B(NDippCH)$_2$} unit split in two sets of signals, indicating a rotational barrier around the Al–B bond. According to ^{1}H,^{1}H-COSY and ^{1}H,^{13}C-HMBC NMR spectroscopic experiments, the protons of the bridging methylene moiety Lu–CH_2(pyrazolyl)–Al resonate as doublets at δ = 1.89 and 1.08 ppm with geminal coupling constants of ^2J(H,H) = 16.9 and 17.2 Hz, respectively, while the remaining two doublets of the non-bridging methylene group are located at δ = 1.07 and 0.75 ppm [^2J(H,H) = 13.6 and 13.7 Hz]. Hence, the doublets at δ = 1.08 and 1.07 ppm are mutually overlapped and addition-

 © 2017 Wiley-VCH Verlag GmbH & Co. KGaA, Weinheim

ChemPubSoc Europe

EurJIC European Journal of Inorganic Chemistry
Full Paper

ally interfered by a singlet at δ = 1.11 ppm (Figures S10 and S11). However, for those protons four well resolved doublets are found in the ^{1}H NMR spectrum recorded in [D$_8$]toluene at 1.80 [^2J(H,H) = 17.0 Hz], 0.98 [^2J(H,H) = 17.1 Hz], 0.96 [^2J(H,H) = 13.6 Hz] and 0.62 ppm [^2J(H,H) = 13.7 Hz], unequivocally corroborating the asymmetric environment for the methylene protons (Figure S7). The differences of the chemical shifts is a consequence of the different binding situations at the methylene groups. The signal of the CH_2(pyrazolyl) moiety coordinating exclusively to the rare-earth-metal center is shifted to lower field. In contrast, coordination of the [Me$_2$Al{B(NDippCH)$_2$}] unit would decrease electron density at the respective methylene group and shift the proton signals to higher fields.

The high mobility of the [Me$_2$Al{B(NDippCH)$_2$}] unit in methyl complex **1** vs. its apparent immobility in methylene complex **2** points at a likely mechanistic scenario of the process of C–H bond activation. The four-center-transposition required for σ-bond metathesis seems to involve the terminal Lu–CH_3 moiety, which is forced into close proximity with a *t*Bu group by the bulky heteroaluminato entity. Tallying with this, precursor [(Tp^{tBu,Me})LuMe$_2$] featuring two terminal methyl ligands was ascribed a remarkable thermal stability.[28] Following this first C–H bond activation and formation of the first methylene moiety, the [Me$_2$Al{B(NDippCH)$_2$}] unit switches positions from methyl to methylene and stays locked in this position (adopting a η^3-heteroaluminato coordination). Subsequently, the now available "second" terminal Lu–CH_3 moiety can engage in σ-bond metathesis and formation of the second methylene group.

A Gallate Variant of Complex [(Tp$^{(tBu–H)}_2$/*t*Bu,Me)Lu-(AlMe$_2${B(NDippCH)$_2$})] (2) and Reactivity of 2 with THF and AlMe$_3$

Treating [(Tp^{tBu,Me})LuMe$_2$] with one equivalent of [Me$_2$Ga{B(NDippCH)$_2$}][29] in [D$_6$]benzene at ambient temperature did not result in any reaction. However, the gallium analogue of compound **2**, [(Tp$^{(tBu–H)}_2$/*t*Bu,Me)Lu(GaMe$_2${B-(NDippCH)$_2$})] (**3**), formed quantitatively within four days at 50 °C according to ^{1}H NMR spectroscopy (Scheme 1) and crystallized isostructurally to **2** (Figure S15). Moreover, complex **3** displays the same rigid coordination behavior in solution as complex **2** (Figure S13). This reactivity is in accordance with the aforementioned mechanistic scenario, that increased steric pressure exerted by even a weakly coordinating [Me$_2$Ga{B(NDippCH)$_2$}] unit enforces C–H bond activation and that the methylene moiety engages in a stronger interaction with the [Me$_2$Ga{B(NDippCH)$_2$}] unit than a terminal methyl group does.

The reaction of complex **2** with an excess of THF and AlMe$_3$, respectively, was monitored by ^{1}H NMR spectroscopy in [D$_6$]benzene. Thus, in the presence of THF separation of the [Me$_2$Al{B(NDippCH)$_2$}] unit occurred via formation of THF adduct [(THF)Me$_2$Al{B(NDippCH)$_2$}] (about 92 %) and a new lutetium compound, presumably [(Tp$^{(tBu–H)}_2$/*t*Bu,Me)Lu(THF)$_x$] (Scheme 2), indicated by a new set of signals assigned to two different pyrazolyl moieties in a 2:1 ratio. The increased symmetry of the new complex is further evidenced by two doublets assigned to the methylene protons at 0.82 [2 H, ^2J(H,H) = 12.5 Hz] and 0.64 ppm [2 H, ^2J(H,H) = 12.4 Hz] (Figure S17). However, crystallization at –40 °C seemed to favor the back reaction, since chilled solutions of **2** in *n*-pentane/THF generated only crystals of **2**.

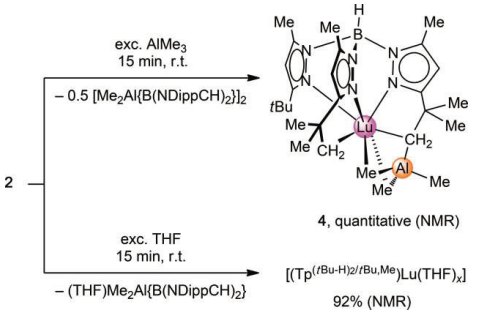

Scheme 2. Reaction of [(Tp$^{(tBu–H)}_2$/*t*Bu,Me)Lu(AlMe$_2${B(NDippCH)$_2$})] (**2**) with an excess of AlMe$_3$ and THF, respectively, in [D$_6$]benzene.

The AlMe$_3$-reaction led to the exchange of [Me$_2$Al-{B(NDippCH)$_2$}]$_2$ through AlMe$_3$ and formation of the new complex [(Tp$^{(tBu–H)}_2$/*t*Bu,Me)Lu(AlMe$_3$)] (**4**) (Scheme 2), which was identified by X-ray diffraction analysis (Figure 6).

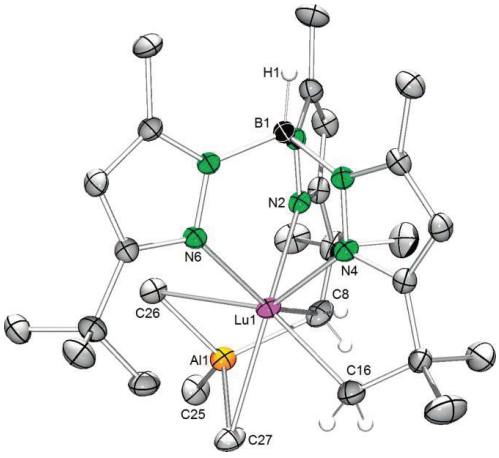

Figure 6. Solid-state structure of **4**; atomic displacement ellipsoids are set at the 50 % probability level. The second molecule of the asymmetric unit and the hydrogen atoms except for B–H and methylene groups are omitted for clarity. Selected bond lengths (Å) and angles (°): Lu1–C8 2.823(6), Lu1–C16 2.418(5), Lu1–C26 2.824(6), Lu1–C27 2.870(6), Lu1–N2 2.487(3), Lu1–N4 2.197(3), Lu1–N6 2.320(3), Al1–C8 2.203(6), Al1–C25 1.85(1), Al1–C26 2.096(7), Al1–C27 2.057(6), C8–Lu1–C16 96.0(2), Lu1–C8–Al1 64.4(2), Lu1–C26–Al1 65.4(2), Lu1–C27–Al1 64.8(2).

Compound **4** adopts a similar crystal structure as complex **2**. However, due to less steric hindrance at the [AlMe$_3$CH$_2$] unit,

 © 2017 Wiley-VCH Verlag GmbH & Co. KGaA, Weinheim

ChemPubSoc Europe

EurJIC European Journal of Inorganic Chemistry

Full Paper

the Lu1···Al1 distance [2.729(3) Å] is shorter than in **2** [2.917(1) Å] and the Lu1–CH_2 bond to the bridging methylene group is elongated [2.823(6) vs. 2.673(3) Å]. As a consequence the [$AlMe_3CH_2$] unit engages in a η^3 coordination mode and the aluminum carbon bonds to the coordinating methyl/methylene groups are elongated [2.203(6), 2.096(7), 2.057(6) Å] compared to compound **2**.

Polymerization of Isoprene

The performance of complexes **1** and **2** was assessed in the polymerization of isoprene. While none of the complexes served as a single-component catalyst, in situ activation with borate and borane cocatalysts, respectively, led to the fabrication of polyisoprene within one hour (Table 1, Figure 7).

Applying **1** in combination with the borate cocatalysts [Ph_3C][$B(C_6F_5)_4$] (**A**) or [$PhNMe_2H$][$B(C_6F_5)_4$] (**B**) polyisoprenes with predominant *cis*-1,4 units in low to moderate yields were obtained (runs 1–4), while for the borane cocatalyst [$B(C_6F_5)_3$] (**C**) an unselective microstructure was found (run 5). The binary systems **1**/**A** and **1**/**C** gave multimodal molecular weight distributions (MWDs) with a main mode at 67 and 33 kg/mol, respectively, which revealed polydispersity indices (PDIs) of 1.91 and 1.80, representing 85 and 78 mol-% of the polymer, respectively. For cocatalyst **B** a monomodal MWD with a PDI as high as 2.98 was obtained (run 4). These findings and ^{1}H NMR spectroscopic studies of the active species (Figures S19, S20, and S21) led us to conclude that the catalyst has altered (degraded) during the catalytic process. Such "degradation" products display active catalysts in combination with cocatalysts **A** and **C**, initiating new polymerizations responsible for the MWD side modes in these products. However, in combination with cocatalyst **B**, the "degradation" products seem to be inactive, in the first place. This means that the number of active centers changes during the polymerization causing the augmented polydispersity of the polymer (vide infra).

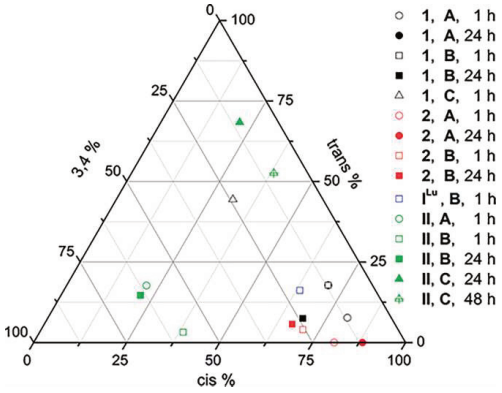

Figure 7. Ternary plot of the microstructures of the polyisoprenes obtained from precatalysts **1**, **2**, $\mathbf{I^{Lu}}$ and **II** upon activation with **A** (●), **B** (■) and **C** (▲) (see Table 1).

If the thermolytic product **2** is applied as a precatalyst in combination with cocatalysts **A**–**C**, in in situ activation reactions, polyisoprenes were obtained only for the borate cocatalysts **A** and **B** (runs 6–9). With these binary systems higher *cis*-1,4 selectivities were observed [up to 88 % (**2**/**A**), Table 1, run 7]. Multimodal MWDs were found with **2**/**A** and **2**/**B**, as well, while in case of cocatalyst **A** only 24 % of the obtained blend was THF soluble and could therefore be analyzed (run 7). With cocatalyst **B**, which produced a less active initiator compared

Table 1. Selected examples for isoprene homopolymerization applying precatalysts **1** and **2**.

Entry[a]	Pre-catalyst	Co-catalyst[b]	Time (h)	Yield (%)	*cis*-1,4[c]	*trans*-1,4[c]	3,4[c]	M_n[d] (× 10^4 g/mol)	M_w/M_n[d]	T_g[e] (°C)
1	**1**	**A**	1	14	80.6	7.7	11.8	6.7[f]	1.91[f]	–56.9
2	**1**	**A**	24	90	70.3	17.8	11.9	14.0	2.63	–56.1
3	**1**	**B**	1	47	72.5	2.6	24.9	11.9	3.72	–47.5
4	**1**	**B**	24	89	68.7	7.5	23.9	14.0	2.98	–48.2
5	**1**	**C**	1	31	31.4	44.4	24.2	3.3[f]	1.80[f]	–38.6
6	**2**	**A**	1	32	80.8	0.0	19.2	26.4	1.77	–52.8
7	**2**	**A**	24	> 99	88.4	0.0	11.6	5.6[g]	2.41[g]	–54.6
8	**2**	**B**	1	2	70.4	4.0	25.6	36.1[f]	1.81[f]	–46.0
9	**2**	**B**	24	90	66.7	5.7	27.6	27.9[f]	2.60[f]	–45.9
10	$\mathbf{I^{Lu}}$	**A**	1	0	–	–	–	–	–	–
11	$\mathbf{I^{Lu}}$	**B**	1	90	63.5	16.2	20.3	15.3	2.40	–51.5
12[h]	**II**	**A**	1	> 99	21.5	17.7	60.8	4.7	1.44	n.d.
13[h]	**II**	**B**	1	5.5	38.6	3.2	58.2	n.d.[i]	n.d.[i]	n.d.
14[h]	**II**	**B**	24	> 99	21.4	14.7	63.9	6.0	1.23	n.d.
15[h]	**II**	**C**	1	traces	n.d.[j]	n.d.[j]	n.d.[j]	n.d.[j]	n.d.[j]	n.d.
16[h]	**II**	**C**	24	34.1	21.2	68.4	10.4	3.0	1.97	n.d.
17[h]	**II**	**C**	48	65.9	38.3	52.6	9.1	3.2	2.07	n.d.

[a] Conditions: 0.02 mmol precatalyst, 8 mL of toluene, 20 mmol isoprene, ambient temperature. [b] Aged with cocatalyst at ambient temperature for 5 min: **A** = [Ph_3C][$B(C_6F_5)_4$], **B** = [$PhNMe_2H$][$B(C_6F_5)_4$], **C** = [$B(C_6F_5)_3$]. [c] Determined by ^{1}H and ^{13}C NMR spectroscopy in $CDCl_3$. [d] Determined by means of size-exclusion chromatography (SEC) against polystyrene standards. [e] Determined on a Perkin–Elmer DSC 8000; heat rate: 20 K/min, cooling rate: 60 K/min. [f] MWD contains more than one mode. The data of the main mode is given here; it represents 85 mol-% (run 1), 78 mol-% (run 5), 98 mol-% (run 8), and > 99 mol-% (run 9) of the polymer. [g] The polymers are not fully soluble in THF. The data of the soluble part is given here; it represents 24 mol-% of the actual polymer mixture. [h] Taken from ref.[11] [i] Not determined due to low polymer solubility in THF. [j] Not determined due to low yield.

 © 2017 Wiley-VCH Verlag GmbH & Co. KGaA, Weinheim

ChemPubSoc Europe

EurJIC European Journal of Inorganic Chemistry
Full Paper

to **1**/**B**, the formed polyisoprene is completely soluble, but bimodal MWDs were observed in GPC analysis. For **2**/**B** the content of the smaller mode at M_n of about 1200 kg/mol was at 2 mol-% of the polymer after 1 h and <0.1 mol-% after 24 h (Table 1, runs 8 and 9), which implies that the production of the polymer with high M_n ceased already in the beginning of the polymerization reaction. Thereafter, the main part of the polymer was produced with a higher PDI but a shorter average chain length. The corresponding active species resulting from the binary system **2**/**B** was stable in solution over several days and was investigated by ^{1}H NMR spectroscopy (Figure S23). These findings can be interpreted by a continuous, slow initiation process, taking place over a long period upon monomer addition. As the active species is formed quantitatively within five minutes in the prereaction, according to NMR spectroscopic data, this is probably due to a low affinity of this active species to coordinate the first monomer.

Comparing the performance of **1** with its [$AlMe_4$] analogue [($Tp^{tBu,Me}$)Lu(Me)($AlMe_4$)] (**I^{Lu}**), (Table 1, runs 10 and 11) revealed that **I^{Lu}** is only active, when activated by a Brønsted acid, that is, cocatalyst **B** under the given conditions. Binary system **I^{Lu}**/**B** produced polymers with higher *trans* contents compared to the boryl-implemented system **1**/**B**, which is in analogy the polymers fabricated by similar Cp*-supported systems.[5,9] Furthermore, complex [Cp*Lu($AlMe_3${B(NDippCH)$_2$})$_2$] (**II**) has been investigated previously by us (Table 1, runs 12–17).[11] Based on a ^{1}H NMR spectroscopic study, the active species of the binary system **II**/**A** was described as a weakly coordinated (via Lu···F) cation/anion pair with the lutetium center surrounded by a Cp* and a heteroaluminato ligand, the latter of which forming two Lu–CH_3-linkages and a Lu···arene contact involving the peripheral boryl moiety. This catalytic system produced a polymer that contains mainly monomer units, added in vinylic 3,4-fashion, as a consequence of the crowded coordination sphere at the lutetium center. The low vinyl content of the polyisoprenes detected in the present study applying **1** suggests a sterically less saturated active lutetium species (vide infra). Interestingly, for both binary systems **1**/**C** and **II**/**C** a large shift toward *trans*-selectivity was observed.

Investigation of the catalytic species resulting from the binary system **1**/**B** by ^{1}H NMR spectroscopy did indicate a different activation process compared to the binary system **II**/**A**.[11,30] Although a comprehensive/accurate peak assignment of the active species was hampered by signal overlapping (Figure S19, Supporting Information), some approximations were possible. The sharpening of the [Me_2Al{B(NDippCH)$_2$}] proton signal that occurred, is characteristic of donor-coordinated monomer species of the [(Do)Me_2Al{B(NDippCH)$_2$}] structural motif. This indicated the formation of [(NMe_2Ph)Me_2Al{B(NDippCH)$_2$}], which implied the concomitant formation of [($Tp^{tBu,Me}$)LuMe][B(C_6F_5)$_4$] (**5a**) (Scheme 3). Species **5a** could react further to [($Tp^{(tBu-H)/tBu}_2$,Me)Lu][B(C_6F_5)$_4$] (**5b**) [$Tp^{(tBu-H)/tBu}_2$,Me = hydrobis-(3-Me-5-*t*Bu-pyrazolyl){μ-(3-Me-5-Me_2CCH_2-pyrazolyl)}borate], which would explain the ongoing methane formation monitored by ^{1}H NMR spectroscopy. If the formation of the C–H bond activated complex **5b** would occur after initiation, this would have terminated the growing polymer chain and therewith caused the high polydispersity. Complex **5b** shows a similar structural motif as the active species [($Tp^{(tBu-H)/tBu}_2$,Me)-Lu(Me_2Al{B(NDippCH)$_2$})][B(C_6F_5)$_4$] (**6**) targeted for the system **2**/**B** (Scheme 3).

Monitoring the activation of **2** with cocatalyst **B** (only benzene soluble part) by ^{1}H NMR spectroscopy (Figure S23) showed neither the abovementioned sharpening of the [Me_2Al-{B(NDippCH)$_2$}] signal of the main product nor the occurrence of free $PhNMe_2$. Moreover, the signal pattern observed for the

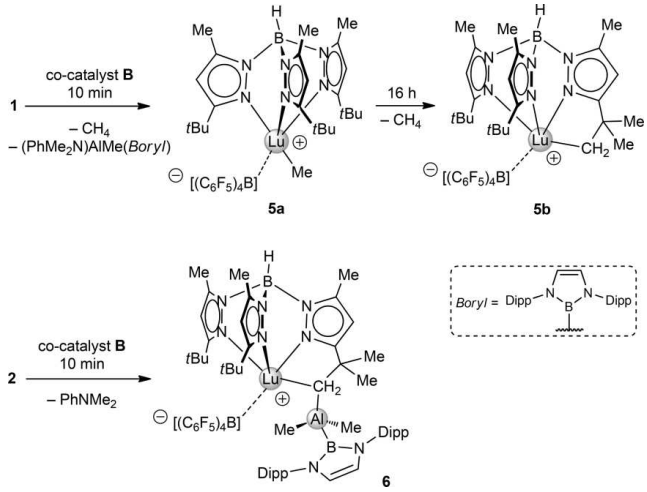

Scheme 3. Proposed activation scenario of [($Tp^{tBu,Me}$)Lu(Me)($AlMe_3${B(NDippCH)$_2$})] (**1**) and [($Tp^{(tBu-H)}_2$/*t*Bu,Me)Lu($AlMe_2${B(NDippCH)$_2$})] (**2**) with cocatalyst [$PhNMe_2$H][B(C_6F_5)$_4$] (**B**).

 © 2017 Wiley-VCH Verlag GmbH & Co. KGaA, Weinheim

ChemPubSoc Europe

EurJIC European Journal of Inorganic Chemistry
Full Paper

tris(pyrazolyl)borato ligand was in agreement with the formation of complex **6**, requiring the re-protonation of one [μ-CH_2(R)] moiety. Hence, **6** differs from **5b** through the [μ-CH_2(R)] moiety which is linked to a [Me_2Al{B(NDippCH)$_2$}] unit. Preservation of the Lu–CH_2(R)–Al linkage further proved the high stability of this moiety and also underpinned the mechanistic C–H bond activation scenario considered vide supra. In contrast to the arene-stabilized active species obtained from **II**/**A**, the steric encumbrance of the Tp system in **5b** or **6** disfavors a similar π-interaction with the peripheral boryl, as suggested by NMR spectroscopy. Since, both in **5b** and **6**, the Lu–CH_2(R)–Al linkage features supposedly the initiating site chain propagation will accomplish Lu centers of almost identical environment (off-migration of the bulky boryl moiety). This explains, why the polymerization results applying **1**/**B** and **2**/**B** differed after one hour (Table 1, runs 3 and 8), but after 24 h, a rather identical polymer was observed (Table 1, runs 4 and 9).

The ^{19}F NMR spectroscopic analysis (Figures S22 and S24) according to Horton et al.[31] indicated weak interactions between the [B(C_6F_5)$_4$] anion and the respective cationic entity in both catalyst mixtures (**1**/**B** and **2**/**B**).[32]

Conclusions

The terminal lutetium methyl complex [(Tp^{tBu,Me})LuMe_2] adds selectively one equivalent of the bulky organoaluminum boryl moiety [Me_2Al{B(NDippCH)$_2$}] (Dipp = C_6H_3iPr$_2$-2,6) to afford [(Tp^{tBu,Me})Lu(Me)(AlMe_3{B(NDippCH)$_2$})] featuring a Lu–CH_3–Al linkage (η^1-heteroaluminato coordination). This nicely reflects the enhanced steric demand of the Tp^{tBu,Me} vs. the C_5Me_5 ancillary ligand, since it has been shown previously that [(C_5Me_5)LuMe_2]$_3$ does form a twofold addition compound.[11] [(Tp^{tBu,Me})Lu(Me)(AlMe_3{B(NDippCH)$_2$})] was found to undergo a thermally induced intramolecular cyclometalative C–H bond activation (Tp^{tBu,Me} ligand degradation) giving complex [(Tp$^{(tBu-H)}_2$/*t*Bu,Me)Lu(AlMe_2{B(NDippCH)$_2$})] by releasing two equivalents of methane. The increased steric unsaturation implied by the twofold cyclometalation effects a η^3-heteroaluminato coordination of the organoaluminum boryl fragment. In contrast to the highly fluxional η^1-heteroaluminato coordination, the latter η^3-mode stays locked at ambient temperature as shown by VT NMR spectroscopy. Nevertheless, the [Me_2Al{B(NDippCH)$_2$}] unit can be fully separated off/displaced by addition of THF or trimethylaluminum. The gallium analogue of complex [(Tp^{tBu,Me})Lu(Me)(AlMe_3{B(NDippCH)$_2$})] was found not isolable but the C–H bond activated gallate complex [(Tp$^{(tBu-H)}_2$/*t*Bu,Me)Lu(GaMe_2{B(NDippCH)$_2$})] could be obtained quantitatively following prolonged mild thermal treatment. Such distinct aluminate/gallate reactivity is in line with our previous findings of a weaker gallate bonding.[28] Applying [(Tp^{tBu,Me})Lu(Me)(AlMe_3{B(NDippCH)$_2$})] and cyclometalated [(Tp$^{(tBu-H)}_2$/*t*Bu,Me)Lu(AlMe_2{B(NDippCH)$_2$})] in the presence of fluorinated borate cocatalysts in isoprene polymerization resulted in moderately *cis*-selective monomer addition. The resulting polymers are mainly bimodal and of augmented polydispersity due to active species degradation, which could be corroborated by ^{1}H NMR spectroscopy. A most likely active (and degraded) species is featured by [(Tp$^{(tBu-H)/tBu}_2$,Me)Lu(Me_2Al{B(NDippCH)$_2$})][B(C_6F_5)$_4$] comprising three distinct boron sites.

Experimental Section

General Considerations: Syntheses and manipulations of all organometallic compounds were carried out under dry argon by using standard *Schlenk*, high-vacuum, and glovebox techniques (MBraun MB 200B; <1 ppm O_2, <1 ppm $H_2$0). *n*-Pentane, *n*-hexane, toluene, and THF were purified by using *Grubbs* columns (MBraun SPS-800, solvent purification system) and stored in a glovebox. [D_6]benzene and [D_8]toluene were obtained from Aldrich, dried with sodium for 24 h, and filtered prior to use. [D]Chloroform and $AlMe_3$ were purchased from Aldrich and used as received. Isoprene was obtained from Aldrich, dried with trioctylaluminum, and vacuum transferred prior to use. [Ph_3C][B(C_6F_5)$_4$] (**A**) [PhNMe_2H][B(C_6F_5)$_4$] (**B**), and B(C_6F_5)$_3$ (**C**) were purchased from Boulder Scientific Company and used without any further purification. [(Tp^{tBu,Me})LuMe_2],[20] [(Tp^{tBu,Me})Lu(Me)AlMe_4],[19] [Me_2Al{B(NDippCH)$_2$}]$_2$[21] (Dipp = C_6H_3iPr$_2$-2,6) and [Me_2Ga{B(NDippCH)$_2$}][29] were synthesized according to literature procedures. NMR spectra of air- and moisture-sensitive compounds were recorded by using *J. Young* valve NMR tubes at 26 °C with a *Bruker* DMX-400 Avance (^{1}H: 400.13 Hz; ^{13}C: 100.61 MHz). ^{1}H and ^{13}C shifts are referenced to internal solvent resonances and reported in parts per million (ppm) relative to TMS. IR spectra were recorded with a NICOLET 6700 FTIR spectrometer using a DRIFT chamber with dry KBr/sample mixtures and KBr windows. For the latter the collected data were converted using the Kubelka–Munk refinement. Elemental analyses were performed with an *Elementar Vario MICRO cube*. Single crystals suitable for X-ray structure analyses were selected in a glovebox, coated with Paratone-N (Hampton Research). X-ray data were collected with a Bruker APEX II DUO diffractometer by using QUAZAR optics and Mo-K_α radiation (λ = 0.71073 Å) with ω and φ scans. Raw data were processed by using APEX2[33] and SAINT[34] software; structure solution and final model refinement were performed by using SHELXTL and SHELXLE.[35] Corrections for absorption effects were applied by using SADABS.[36] All plots were generated utilizing the programs ORTEP-3[37] and POV-Ray.[38] The molar masses (M_W and M_n) of the polymers were determined by size-exclusion chromatography (SEC). Sample solutions (1.0 mg of polymer per mL THF) were filtered through a 0.45 μm syringe filter prior to injection. SEC was performed with a pump supplied by Viscotek (GPCmax VE 2001), employing ViscoGEL columns. Signals were detected by means of a triple detection array (TDA 305) and calibrated against polystyrene standards (M_W/M_n < 1.15). The flowrate was set to 1.0 mL min^{-1}. The microstructures of the polyisoprenes were examined by means of ^{1}H and ^{13}C NMR spectroscopic experiments with AV400 spectrometers at ambient temperature, using [D]chloroform as a solvent. Glass transition temperatures of the polyisoprenes (T_g) were recorded with a Perkin–Elmer DSC 8000 calibrated with indium and cyclohexane standards, scanning from –100 °C up to +100 °C with heating rates of 20 K/min and cooling rates of 60 K/min in N_2 atmosphere.

[(Tp^{tBu,Me})Lu(Me)(AlMe_3{B(NDippCH)$_2$})] (1): A solution of [Me_2Al{B(NDippCH)$_2$}]$_2$ (106 mg, 0.12 mmol) in *n*-hexane (5 mL) was stirred into a suspension of [(Tp^{tBu,Me})LuMe_2] (150 mg, 0.24 mmol) in *n*-hexane (4 mL). The white suspension turned into an almost clear solution within 30 minutes. The reaction mixture was stirred for 1 h at ambient temperature and then cooled to –40 °C for 16 h. Clear, colorless crystals formed. The supernatant was decanted, and

 © 2017 Wiley-VCH Verlag GmbH & Co. KGaA, Weinheim

ChemPubSoc Europe

EurJIC European Journal of Inorganic Chemistry

Full Paper

the product was concentrated to dryness in vacuo to yield **1** as a white powder (253 mg, 0.24 mmol, 97 %). Single crystals suitable for X-ray crystallography were grown from a saturated *n*-hexane solution at –40 °C. ^{1}H NMR ([D$_6$]benzene, 400 MHz, 26 °C): δ = 7.29 (s, 6 H, H_{Ar}), 6.47 (s, 2 H, NC*H*), 5.59 (s, 3 H, 4-pz-*H*), 4.40 (br. s, 1 H, B*H*), 3.65 [sept, ^3J(H,H) = 6.8 Hz, 4 H, C*H*(CH$_3$)$_2$], 1.91 (s, 9 H, pz-C*H*$_3$), 1.47 [d, ^3J(H,H) = 6.8 Hz, 12 H, CH(C*H*$_3$)$_2$], 1.33 [d, ^3J(H,H) = 6.8 Hz, 12 H, CH(C*H*$_3$)$_2$, overlapping with peak 1.32], 1.32 [s, 27 H, pz-C(C*H*$_3$)$_3$], –0.14 [br. s, 6 H, Lu(C*H*$_3$)$_2$], –1.20 [br. s, 6 H, Al(C*H*$_3$)$_2$] ppm. ^{13}C{^{1}H} NMR ([D$_6$]benzene, 101 MHz, 26 °C): δ = 166.0 (3-pz-*C*), 148.3 (5-pz-*C*), 146.5 (Ar, C_{ortho}), 144.0 (Ar, C_{ipso}), 126.4 (Ar, C_{para}), 123.0 (Ar, C_{meta}), 120.7 (NCH), 105.0 (4-pz-*C*), 32.3 [*C*(CH$_3$)$_3$], 31.4 [C(*C*H$_3$)$_3$], 28.6 [CH(*C*H$_3$)$_2$], 25.7 [CH(*C*H$_3$)$_2$], 24.2 [CH(*C*H$_3$)$_2$], 12.9 (pz-*C*H$_3$), –4.5 [Lu(*C*H$_3$)$_2$ or Al(*C*H$_3$)$_2$] ppm; for the carbon atoms of the Lu(CH$_3$)$_2$ or Al(CH$_3$)$_2$ groups, respectively, only one very broad signal could be detected. ^{11}B{^{1}H} NMR ([D$_6$]benzene, 80 MHz, 26 °C): δ = 39.3 (*B*Al), –8.8 (*B*H) ppm. DRIFT (KBr): $\tilde{\nu}$ = 2562 (m, B–H) cm^{-1}. $C_{54}H_{88}AlB_2LuN_8$ (1072.92 g mol^{-1}): calcd. C 60.45, H 8.27, N 10.44; found C 60.67, H 8.11, N 10.40.

[(Tp$^{(tBu–H)}$$_2$/*t*Bu,Me)Lu(AlMe$_2${B(NDippCH)$_2$})] (2): A solution of **1** (261 mg, 0.24 mmol) in benzene (4 mL) was stirred in a pressure tube for 72 h at 60 °C. The solvent was removed in vacuo and the resulting yellow, sticky residue triturated with *n*-pentane (1.5 mL). The resulting white precipitate was washed with *n*-pentane (2 × 1 mL) and concentrated to dryness in vacuo to yield a white powder (194 mg, 0.19 mmol, 77 %). Single crystals suitable for X-ray crystallography were grown from a saturated *n*-hexane solution at –40 °C. ^{1}H NMR ([D$_6$]benzene, 400 MHz, 26 °C): δ = 7.19 (m, 4 H, H_{Ar}), 7.12 (m, 2 H, H_{Ar}), 6.48 (s, 2 H, NC*H*), 5.55 [d, ^4J(H,H) = 0.5 Hz, 1 H, 4-pz-*H*], 5.53 [d, ^4J(H,H) = 0.6 Hz, 1 H, 4-pz-*H*], 5.49 [d, ^4J(H,H) = 0.5 Hz, 1 H, 4-pz-*H*], 4.57 (br. s, 1 H, B*H*), 3.59 [sept, ^3J(H,H) = 6.8 Hz, 2 H, C*H*(CH$_3$)$_2$], 3.48 [sept, ^3J(H,H) = 6.8 Hz, 2 H, C*H*(CH$_3$)$_2$], 2.11 (s, 3 H, pz-C*H*$_3$), 2.07 (s, 3 H, pz-C*H*$_3$), 1.89 (s, 3 H, pz-C*H*$_3$), 1.89 [d, ^2J(H,H) = 16.9 Hz, 1 H, C(CH$_3$)$_2$C*H*$_2$], 1.54 [s, 3 H, C(C*H*$_3$)$_2$CH$_2$], 1.45 [d, ^3J(H,H) = 6.9 Hz, 6 H, CH(C*H*$_3$)$_2$], 1.40 [s, 3 H, C(C*H*$_3$)$_2$CH$_2$], 1.37 [d, ^3J(H,H) = 6.9 Hz, 6 H, CH(C*H*$_3$)$_2$], 1.31 [s, 3 H, C(C*H*$_3$)$_2$CH$_2$], 1.28 [d, ^3J(H,H) = 6.8 Hz, 6 H, CH(C*H*$_3$)$_2$], 1.21 [d, ^3J(H,H) = 6.8 Hz, 6 H, CH(C*H*$_3$)$_2$], 1.17 [s, 9 H, pz-C(C*H*$_3$)$_3$], 1.11 [s, 3 H, C(C*H*$_3$)$_2$CH$_2$], 1.08 [d, ^2J(H,H) = 17.2 Hz, 1 H, C(CH$_3$)$_2$C*H*$_2$], 1.07 [d, ^2J(H,H) = 13.6 Hz, 1 H, C(CH$_3$)$_2$C*H*$_2$], 0.75 [d, ^2J(H,H) = 13.7 Hz, 1 H, C(CH$_3$)$_2$C*H*$_2$], 0.36 (s, 3 H, AlC*H*$_3$), –1.13 (s, 3 H, AlC*H*$_3$) ppm. ^{13}C{^{1}H} NMR ([D$_6$]benzene, 101 MHz, 26 °C): δ = 173.1 (3-pz-*C*), 167.4 (3-pz-*C*), 164.5 (3-pz-*C*), 146.8 (5-pz-*C*), 146.4 (Ar, C_{ortho}), 146.4 (Ar, C_{ortho}), 145.4 (5-pz-*C*), 144.6 (5-pz-*C*), 142.5 (Ar, C_{ipso}), 127.2 (Ar, C_{para}), 123.4 (Ar, C_{meta}), 123.3 (Ar, C_{meta}), 121.8 (NCH), 103.5 (4-pz-*C*), 101.9 (4-pz-*C*), 101.1 (4-pz-*C*), 68.4 [C(CH$_3$)$_2$CH$_2$], 40.0 [*C*(CH$_3$)$_2$CH$_2$], 38.6 [C(CH$_3$)$_2$CH$_2$], 37.6 [*C*(CH$_3$)$_2$CH$_2$], 35.9 [C(CH$_3$)$_2$CH$_2$], 35.6 [C(CH$_3$)$_2$CH$_2$], 35.5 [C(CH$_3$)$_2$CH$_2$], 32.3 [*C*(CH$_3$)$_3$], 31.0 [C(CH$_3$)$_3$], 30.2 [C(CH$_3$)$_2$CH$_2$], 28.9 [CH(CH$_3$)$_2$], 28.5 [CH(CH$_3$)$_2$], 27.0 [CH(CH$_3$)$_2$], 26.8 [CH(CH$_3$)$_2$], 23.6 [CH(CH$_3$)$_2$], 22.8 [CH(CH$_3$)$_2$], 13.5 (pz-*C*H$_3$), 12.6 (pz-CH$_3$), 11.8 (pz-*C*H$_3$), –3.5 (AlCH$_3$), –7.5 (AlCH$_3$) ppm. ^{11}B{^{1}H} NMR ([D$_6$]benzene, 80 MHz, 26 °C): δ = 34.8 (*B*Al), –8.8 (*B*H) ppm. DRIFT (KBr): $\tilde{\nu}$ = 2509 (m, B–H) cm^{-1}. $C_{52}H_{80}AlB_2LuN_8$ (1040.84 g mol^{-1}): calcd. C 60.01, H 7.75, N 10.77; found C 60.32, H 7.48, N 10.45.

[(Tp$^{(tBu–H)}$$_2$/*t*Bu,Me)Lu(GaMe$_2${B(NDippCH)$_2$})] (3): In a *J. Young* valved NMR tube, [(Tp^{tBu,Me})LuMe$_2$] (16.8 mg, 0.027 mmol) in 0.5 mL [D$_6$]benzene was treated with Me$_2$Ga{B(NDippCH)$_2$} (13.0 mg, 0.027 mmol) and heated up to 50 °C for 96 h. The reaction was monitored by ^{1}H NMR spectroscopy. Complete conversion was indicated by the evolution of methane and quantitative formation of **3**. Single crystals suitable for X-ray crystallography were grown from a saturated *n*-pentane solution at –40 °C. ^{1}H NMR ([D$_6$]benzene, 400 MHz, 26 °C): δ = 7.18 (m, 4 H, H_{Ar}), 7.12 (m, 2 H, H_{Ar}), 6.47 (s, 2 H, NC*H*), 5.56 (s, 1 H, 4-pz-*H*), 5.53 (s, 1 H, 4-pz-*H*), 5.50 (s, 1 H, 4-pz-*H*), 4.58 (br. s, 1 H, B*H*), 3.58 [sept, ^3J(H,H) = 6.9 Hz, 2 H, C*H*(CH$_3$)$_2$], 3.46 [sept, ^3J(H,H) = 6.9 Hz, 2 H, C*H*(CH$_3$)$_2$], 2.12 (s, 3 H, pz-C*H*$_3$), 2.08 [d, ^2J(H,H) = 16.8 Hz, 1 H, C(CH$_3$)$_2$C*H*$_2$], 2.08 (s, 3 H, pz-C*H*$_3$), 1.89 (s, 3 H, pz-C*H*$_3$), 1.54 [s, 3 H, C(C*H*$_3$)$_2$CH$_2$], 1.44 [d, ^3J(H,H) = 6.9 Hz, 6 H, CH(C*H*$_3$)$_2$], 1.40 [s, 3 H, C(C*H*$_3$)$_2$CH$_2$], 1.37 [d, ^3J(H,H) = 6.9 Hz, 6 H, CH(C*H*$_3$)$_2$], 1.28 [s, 3 H, C(C*H*$_3$)$_2$CH$_2$], 1.27 [d, ^3J(H,H) = 6.8 Hz, 6 H, CH(C*H*$_3$)$_2$], 1.20 [d, ^3J(H,H) = 6.8 Hz, 6 H, CH(C*H*$_3$)$_2$], 1.16 [s, 9 H, pz-C(C*H*$_3$)$_3$], 1.12 [s, 3 H, C(C*H*$_3$)$_2$CH$_2$], 1.10 [d, ^2J(H,H) = 13.6 Hz, 1 H, C(CH$_3$)$_2$C*H*$_2$], 1.01 [d, ^2J(H,H) = 16.6 Hz, 1 H, C(CH$_3$)$_2$C*H*$_2$], 0.74 [d, ^2J(H,H) = 13.6 Hz, 1 H, C(CH$_3$)$_2$C*H*$_2$], 0.44 (s, 3 H, GaC*H*$_3$), –1.08 (s, 3 H, GaC*H*$_3$) ppm. ^{11}B{^{1}H} NMR ([D$_6$]benzene, 80 MHz, 26 °C): δ = 30.2 (*B*Ga), –9.6 (*B*H) ppm.

Homopolymerization of Isoprene: A detailed polymerization procedure is described as a typical example (Table 1, run 1). [Ph$_3$C][B(C$_6$F$_5$)$_4$] (**A**) (18 mg, 0.02 mmol, 1 equiv.) was added to a solution of **1** (21.5 mg, 0.02 mmol) in toluene (8 mL) and the mixture was aged at ambient temperature for 5 min. After the addition of isoprene (1.36 g, 20 mmol), the polymerization was carried out at 25 °C for 1 h. The reaction was terminated by pouring the polymerization mixture into 25 mL of methanol containing 0.1 % (w/w) 2,6-di-*tert*-butyl-4-methylphenol as a stabilizer and stirred for 1 h. The polymer was washed with methanol and dried under vacuum at ambient temperature to constant weight.

Computational Details: DFT calculations were carried out with the Gaussian 09 program suite[39] using the BP86 density functional,[40] along with the implemented cc-pVTZ basis set for the p block elements and the cc-pVDZ basis set for all H atoms.[41] For the Lu center, a Stuttgart/Dresden effective core potential for 28 core electrons (MWB28) was employed,[42] in combination with the optimized valence basis set as implemented in Gaussian 09. All geometry optimizations were performed without imposing any symmetry constraints, and the structures obtained were confirmed as true minima by calculating analytical frequencies. NBO analyses were carried out by using the NBO 6.0 software.[43] Plots were generated with the software Chemcraft.[44]

Acknowledgments

The authors are grateful to the German Science Foundation (Grant: An238/14-2) and Bridgestone Japan for support, as well as for the computational resources provided by the bwForCluster JUSTUS, funded by the State of Baden-Württemberg, Germany, through the bwHPC project, and by the Deutsche Forschungsgemeinschaft (DFG). We thank Cornelius Knappe for assistance with the DFT calculations.

Keywords: Aluminum · C–H activation · Borates · Gallium · Lutetium

[1] For recent review articles, see: a) M. Nishiura, Z. Hou, *Nat. Chem.* **2010**, *2*, 257–268; b) Z. Zhang, D. Cui, B. Wang, B. Liu, Y. Yang, *Struct. Bonding (Berlin)* **2010**, *137*, 49–108; c) M. Nishiura, F. Guo, Z. Hou, *Acc. Chem. Res.* **2015**, *48*, 2209–2220; d) R. P. Kelly, P. W. Roesky, *Struct. Bonding (Berlin)* **2015**, *172*, 85–118; e) A. A. Trifonov, D. M. Lyobov, *Coord. Chem. Rev.* **2017**, *340*, 10–61; f) F. Yang, X. Li, *J. Polym. Sci., Part A* **2017**, *55*, 000–000.

[2] a) A. Fischbach, R. Anwander, *Adv. Polym. Sci.* **2006**, *204*, 155–281; b) M. Zimmermann, R. Anwander, *Chem. Rev.* **2010**, *110*, 6194–6259.

[3] M. Zimmermann, J. Volbeda, K. W. Törnroos, R. Anwander, *C. R. Chim.* **2010**, *13*, 651–660.

 © 2017 Wiley-VCH Verlag GmbH & Co. KGaA, Weinheim

ChemPubSoc Europe

EurJIC European Journal of Inorganic Chemistry
Full Paper

[4] a) R. Anwander, M. G. Klimpel, H. M. Dietrich, D. J. Shorokhov, W. Scherer, *Chem. Commun.* **2003**, 1008–1009; b) H. M. Dietrich, C. Zapilko, E. Herdtweck, R. Anwander, *Organometallics* **2005**, *24*, 5767–5771.
[5] M. Zimmermann, K. W. Törnroos, H. Sitzmann, R. Anwander, *Chem. Eur. J.* **2008**, *14*, 7266–7277.
[6] D. Robert, T. P. Spaniol, J. Okuda, *Eur. J. Inorg. Chem.* **2008**, 2801–2809.
[7] R. Litlabø, M. Enders, K. W. Törnroos, R. Anwander, *Organometallics* **2010**, *29*, 2588–2595.
[8] L. N. Jende, C. Maichle-Mössmer, R. Anwander, *Chem. Eur. J.* **2013**, *19*, 16321–16333.
[9] M. Zimmermann, K. W. Törnroos, R. Anwander, *Angew. Chem. Int. Ed.* **2008**, *47*, 775–778; *Angew. Chem.* **2008**, *120*, 787–790.
[10] a) Y. Segawa, M. Yamashita, K. Nozaki, *Science* **2006**, *314*, 113–115; b) Y. Segawa, Y. Suzuki, M. Yamashita, K. Nozaki, *J. Am. Chem. Soc.* **2008**, *130*, 16069–16079.
[11] N. Dettenrieder, C. O. Hollfelder, L. N. Jende, C. Maichle-Mössmer, R. Anwander, *Organometallics* **2014**, *33*, 1528–1531.
[12] M. Zimmermann, K. W. Törnroos, R. Anwander, *Angew. Chem. Int. Ed.* **2007**, *46*, 3126–3130; *Angew. Chem.* **2007**, *119*, 3187–3191.
[13] a) L. Zhang, M. Nishiura, M. Yuki, Y. Luo, Z. Hou, *Angew. Chem. Int. Ed.* **2008**, *47*, 2642–2645; *Angew. Chem.* **2008**, *120*, 2682–2685; b) J. Hong, L. Zhang, X. Yu, M. Li, Z. Zhang, P. Zheng, M. Nishiura, Z. Hou, X. Zhou, *Chem. Eur. J.* **2011**, *17*, 2130–2137; c) Y. Luo, Y. Lei, S. Fan, Y. Wang, J. Chen, *Dalton Trans.* **2013**, *42*, 4040–4051.
[14] a) R. Litlabø, H. S. Lee, M. Niemeyer, K. W. Törnroos, R. Anwander, *Dalton Trans.* **2010**, *39*, 6815–6825; b) H. Kaneko, H. Martin Dietrich, C. Schädle, C. Maichle-Mössmer, H. Tsurugi, K. W. Törnroos, K. Mashima, R. Anwander, *Organometallics* **2013**, *32*, 1199–1208.
[15] S. Sun, H. Ouyang, Y. Luo, Y. Zhang, Q. Shen, Y. Yao, *Dalton Trans.* **2013**, *42*, 16355–16364.
[16] S. Hamidi, L. N. Jende, H. Martin Dietrich, C. Maichle-Mössmer, K. W. Törnroos, G. B. Deacon, P. C. Junk, R. Anwander, *Organometallics* **2013**, *32*, 1209–1223.
[17] M. Zimmermann, F. Estler, E. Herdtweck, K. W. Törnroos, R. Anwander, *Organometallics* **2007**, *26*, 6029–6041.
[18] a) M. I. Bruce, *Angew. Chem. Int. Ed. Engl.* **1977**, *16*, 73–86; *Angew. Chem.* **1977**, *89*, 75–89; b) K. R. D. Johnson, P. G. Hayes, *Chem. Soc. Rev.* **2013**, *42*, 1947–1960.
[19] M. Zimmermann, J. Takats, G. Kiel, K. W. Törnroos, R. Anwander, *Chem. Commun.* **2008**, 612–614.
[20] D. Schädle, C. Maichle-Mössmer, C. Schädle, R. Anwander, *Chem. Eur. J.* **2015**, *21*, 662–670.
[21] N. Dettenrieder, H. M. Dietrich, C. Schädle, C. Maichle-Mössmer, K. W. Törnroos, R. Anwander, *Angew. Chem. Int. Ed.* **2012**, *51*, 4461–4465; *Angew. Chem.* **2012**, *124*, 4537–4541.
[22] R. Shannon, *Acta Crystallogr., Sect. A: Found. Crystallogr.* **1976**, *32*, 751–767.
[23] J. Cheng, K. Saliu, M. J. Ferguson, R. McDonald, J. Takats, *J. Organomet. Chem.* **2010**, *695*, 2696–2702.
[24] R. Litlabø, PhD Thesis, University of Bergen, **2010**.
[25] W. T. Klooster, R. S. Lu, R. Anwander, W. J. Evans, T. F. Koetzle, R. Bau, *Angew. Chem. Int. Ed.* **1998**, *37*, 1268–1270; *Angew. Chem.* **1998**, *110*, 1326–1329.
[26] E. D. Glendening, C. R. Landis, F. Weinhold, *Wiley Interdiscip. Rev.: Comput. Mol. Sci.* **2012**, *2*, 1–42.
[27] For comparison, in a typical Lu hydride bond, more than 20 % of the bonding electrons of the respective NBO are assigned to the Lu center (for details, see the Supporting Information).
[28] M. Zimmermann, R. Litlabø, K. W. Törnroos, R. Anwander, *Organometallics* **2009**, *28*, 6646–6649.
[29] N. Dettenrieder, C. Schädle, C. Maichle-Mössmer, P. Sirsch, R. Anwander, *J. Am. Chem. Soc.* **2014**, *136*, 886–889.
[30] Neither arene coordination as found for complex **II**, nor free $[Me_2Al\{B(NDippCH)_2\}]_2$ was observed (Figures S20 and S21; c. f., ref.[11]).
[31] a) A. D. Horton, *Organometallics* **1996**, *15*, 2675–2677; b) A. D. Horton, J. de With, A. J. van der Linden, H. van de Weg, *Organometallics* **1996**, *15*, 2672–2674.
[32] The chemical shifts of the resonances of *meta*- and *para*-fluorine atoms differ by 3.73 (**1**/**B**) and 3.70 (**2**/**B**) ppm, respectively, while tight ion pairs show differences in the range of 5.4 ppm and completely free anions in the range of 2.5 ppm, according to ref.[31]
[33] APEX v. **2008**.5–0, Madison, 2008.
[34] Bruker Saint v. 756A, Madison, **2009**.
[35] a) G. M. Sheldrick, *Acta Crystallogr., Sect. A* **2008**, *64*, 112–122; b) C. B. Hubschle, G. M. Sheldrick, B. Dittrich, *J. Appl. Crystallogr.* **2011**, *44*, 1281–1284.
[36] SADABS v. **2008**/1 (SADABS v. 2008/1), University of Göttingen, Göttingen, 2008.
[37] L. J. Farrugia, *J. Appl. Crystallogr.* **1997**, *30*, 565.
[38] POV-Ray v. 3.6, Williamstown, Victoria, Australia, **2004** (http://www.povray.org).
[39] M. J. Frisch, G. W. Trucks, H. B. Schlegel, G. E. Scuseria, M. A. Robb, J. R. Cheeseman, G. Scalmani, V. Barone, B. Mennucci, G. A. Petersson, H. Nakatsuji, M. Caricato, X. Li, H. P. Hratchian, A. F. Izmaylov, J. Bloino, G. Zheng, J. L. Sonnenberg, M. Hada, M. Ehara, K. Toyota, R. Fukuda, J. Hasegawa, M. Ishida, T. Nakajima, Y. Honda, O. Kitao, H. Nakai, T. Vreven, J. A. Montgomery Jr., J. E. Peralta, F. Ogliaro, M. Bearpark, J. J. Heyd, E. Brothers, K. N. Kudin, V. N. Staroverov, R. Kobayashi, J. Normand, K. Raghavachari, A. Rendell, J. C. Burant, S. S. Iyengar, J. Tomasi, M. Cossi, N. Rega, J. M. Millam, M. Klene, J. E. Knox, J. B. Cross, V. Bakken, C. Adamo, J. Jaramillo, R. Gomperts, R. E. Stratmann, O. Yazyev, A. J. Austin, R. Cammi, C. Pomelli, J. W. Ochterski, R. L. Martin, K. Morokuma, V. G. Zakrzewski, G. A. Voth, P. Salvador, J. J. Dannenberg, S. Dapprich, A. D. Daniels, Ö. Farkas, J. B. Foresman, J. V. Ortiz, J. Cioslowski, D. J. Fox, *Gaussian 09, Revision D.01*, Gaussian, Inc., Wallingford CT, **2013**.
[40] a) A. D. Becke, *Phys. Rev. A* **1988**, *38*, 3098–3100; b) J. P. Perdew, *Phys. Rev. B* **1986**, *33*, 8822–8824.
[41] a) T. H. Dunning Jr., *J. Chem. Phys.* **1989**, *90*, 1007–1023; b) R. A. Kendall, T. H. Dunning Jr., R. J. Harrison, *J. Chem. Phys.* **1992**, *96*, 6796–6806; c) D. E. Woon, T. H. Dunning Jr., *J. Chem. Phys.* **1993**, *98*, 1358–1371.
[42] a) X. Cao, M. Dolg, *J. Chem. Phys.* **2001**, *115*, 7348–7355; b) X. Cao, M. Dolg, *THEOCHEM* **2002**, *581*, 139–147.
[43] E. D. Glendening, J. K. Badenhoop, A. E. Reed, J. E. Carpenter, J. A. Bohmann, C. M. Morales, C. R. Landis, F. Weinhold, NBO 6.0, University of Wisconsin, Madison, WI, USA, **2013**.
[44] G. A. Zhurko, CHEMCRAFT (http://www.chemcraftprog.com).

Received: June 20, 2017

 © 2017 Wiley-VCH Verlag GmbH & Co. KGaA, Weinheim

Paper III: Supporting Information

This Supporting Information is reprinted with permission (License Number 4705980258412) from the Supporting Information of:

"C–H Bond Activation and Isoprene Polymerization by Lutetium Alkylaluminate / gallate Complexes Bearing a Peripheral Boryl and a Bulky Hydrotris(pyrazolyl)borate Ligand"

by
Martin Bonath, Christoph O. Hollfelder, Dorothea Schädle, Cäcilia Maichle-Mössmer, Peter Sirsch, and Reiner Anwander

published in:
Eur. J. Inorg. Chem. **2017**, *2017*, 4683–4692
doi: 10.1002/ejic.201700730

Copyright (2017) by John Wiley and Sons.

Eur. J. Inorg. Chem. **2017** · ISSN 1099–0682

https://doi.org/10.1002/ejic.201700730

SUPPORTING INFORMATION

Title: C–H Bond Activation and Isoprene Polymerization by Lutetium Alkylaluminate/gallate Complexes Bearing a Peripheral Boryl and a Bulky Hydrotris(pyrazolyl)borate Ligand

Author(s): Martin Bonath, Christoph O. Hollfelder, Dorothea Schädle, Cäcilia Maichle-Mössmer, Peter Sirsch,* Reiner Anwander*

Table of Contents

Figure S1. ^{1}H NMR spectrum of **1** in [D_6]benzene S3
Figure S2. ^{13}C{^{1}H} NMR spectrum of **1** in [D_6]benzene S3
Figure S3. VT ^{1}H NMR spectrum of **1** in [D_8]toluene S4
Figure S4. ^{1}H-^{13}C HSQC NMR spectrum of **1** in [D_6]benzene S5
Figure S5. ^{1}H-^{1}H EXSY NMR spectrum of **1** in [D_6]benzene S5
Figure S6. ^{11}B NMR spectrum of **1** in [D_6]benzene S6
Figure S7. ^{1}H NMR spectrum of **2** in [D_6]benzene S6
Figure S8. ^{1}H NMR spectrum of **2** in [D_8]toluene S7
Figure S9. ^{13}C{^{1}H} NMR spectrum of **2** in [D_6]benzene S7
Figure S10. ^{1}H-^{13}C HSQC NMR spectrum of **2** in [D_6]benzene S8
Figure S11. ^{1}H-^{13}C HMBC NMR spectrum of **2** in [D_6]benzene S8
Figure S12. ^{1}H-^{1}H COSY NMR spectrum of **2** in [D_6]benzene S9
Figure S13. ^{11}B NMR spectrum of **2** in [D_6]benzene S9
Figure S14. ^{1}H NMR spectrum of **3** in [D_6]benzene S10
Figure S15. ^{11}B NMR spectrum of **3** in [D_6]benzene S10
Figure S16. Solid-state structure of **3** S11
Reactivity of **2** toward excess $AlMe_3$ - [($Tp^{(tBu-H)2/tBu,Me}$)Lu($AlMe_3$)] (**4**) S11
Figure S17. ^{1}H NMR spectrum monitoring reaction of **2** toward $AlMe_3$ S12
Figure S18. Solid-state structure of **4** S12
Reactivity of **2** toward THF S13
Figure S19. ^{1}H NMR spectrum monitoring reaction of **2** toward THF S13
Investigations into the active species of the system **1**/**B** S14
Figure S20. ^{1}H NMR spectrum of system **1**/**B** after 10 min in [D_6]benzene S14
Figure S21. ^{1}H NMR spectrum of system **1**/**B** after 16 h in [D_6]benzene S15
Figure S22. Comparing ^{1}H NMR spectra of system **1**/**B** after 10 min and 16 h S16
Figure S23. ^{19}F{^{1}H} NMR spectrum of system **1**/**B** after 10 min in [D_6]benzene S16
Investigations into the active species of the system **2**/**B** S17
Figure S24. ^{1}H NMR spectrum of system **2**/**B** after 10 min in [D_6]benzene S17
Figure S25. ^{19}F{^{1}H} NMR spectrum of system **1**/**B** after 10 min in [D_6]benzene S18
Table S1. Crystallographic data S19
DFT Calculations S20
Figure S26. Optimized geometry for the DFT-optimized model system **2a** S20
Table S2. Selected geometrical parameters for **2a** S20
Table S3. Lu occupancy for selected C−H NLMOs S21
Figure S27. Optimized geometry for the DFT-optimized model system **2b** S24
Table S4. Selected geometrical parameters for **2b** S24
Figure S28. Optimized geometry for the DFT-optimized model system **2c** S27
Table S5. Selected geometrical parameters for **2c** S27
Figure S29. Optimized geometry for the DFT-optimized model system **2d** S30
Figure S30. Optimized geometry, salient geometrical parameters, and Lu−H NBO composition for the DFT-optimized model system [($C_5Me_4SiMe_3$)$_2$LuH(THF)] S32

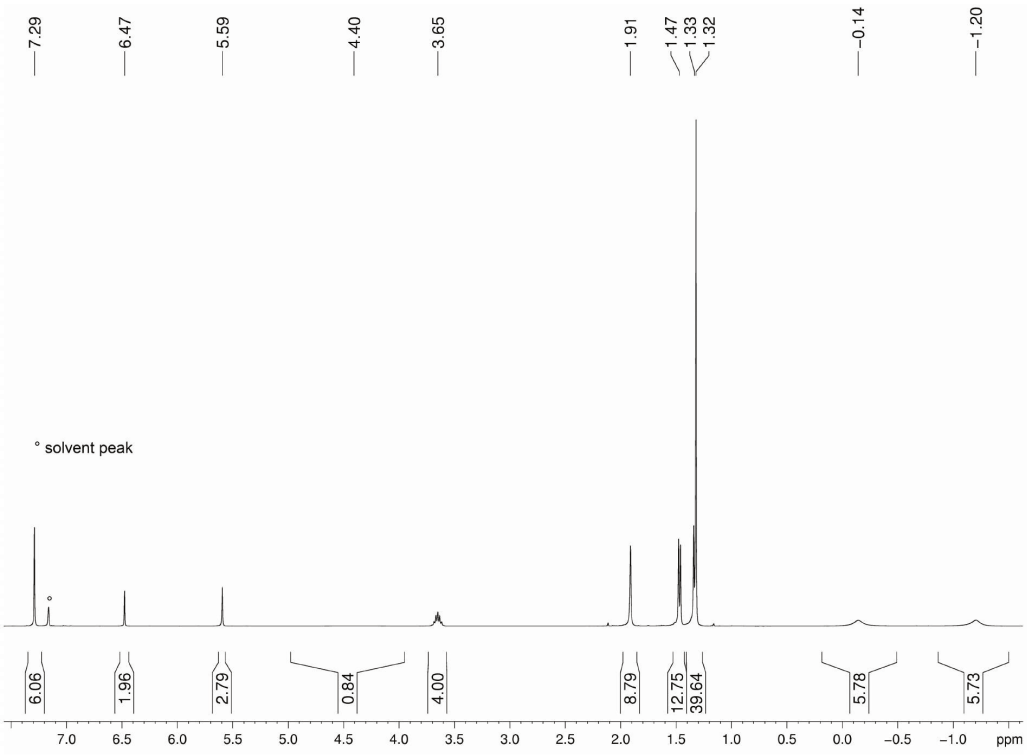

Figure S1. ^{1}H NMR spectrum (400 MHz) of **1** in [D_6]benzene at 26 °C.

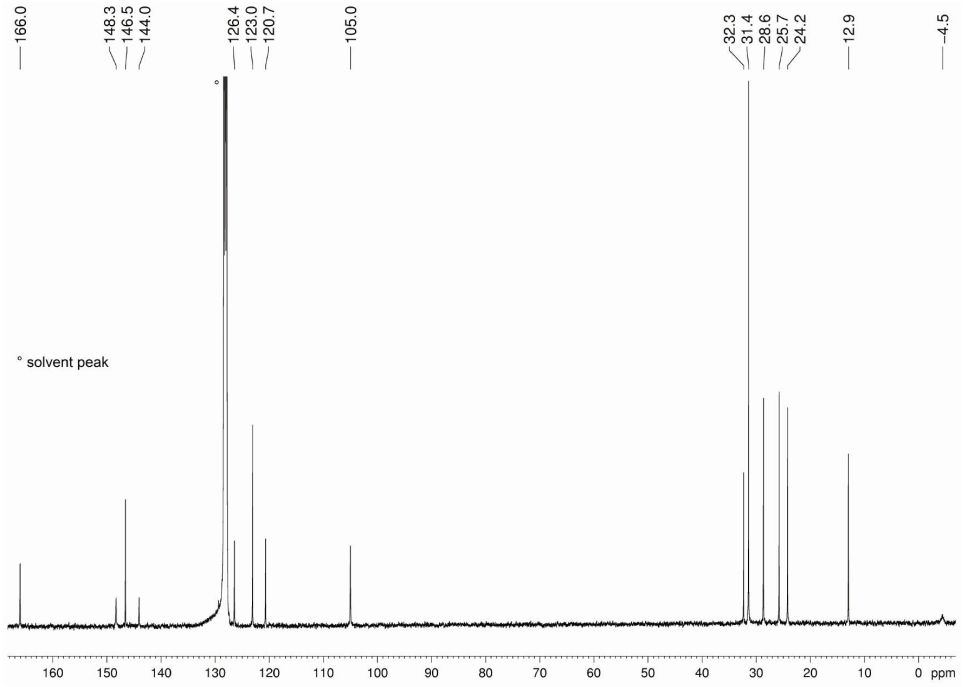

Figure S2. ^{13}C{^{1}H} NMR spectrum (101 MHz) of **1** in [D_6]benzene at 26 °C.

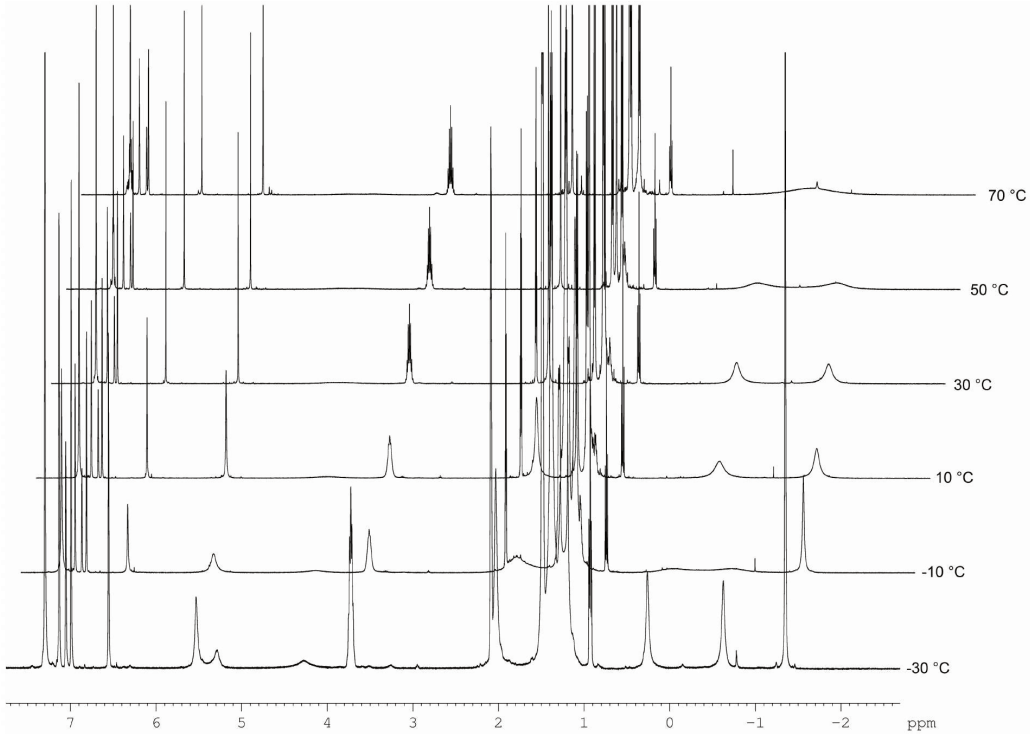

Figure S3. Variable-temperature ^{1}H NMR spectra (500 MHz) of **1** in [D_8]toluene.

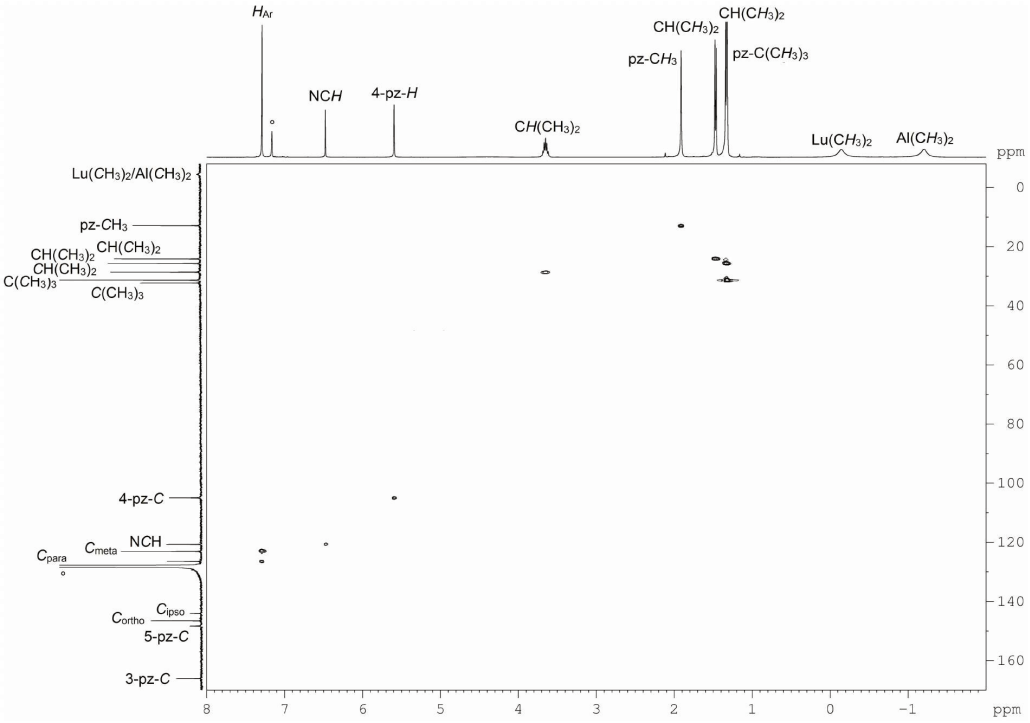

Figure S4. ^{1}H-^{13}C HSQC NMR spectrum (400 MHz, 101 MHz) of **1** in [D$_6$]benzene at 26 °C.

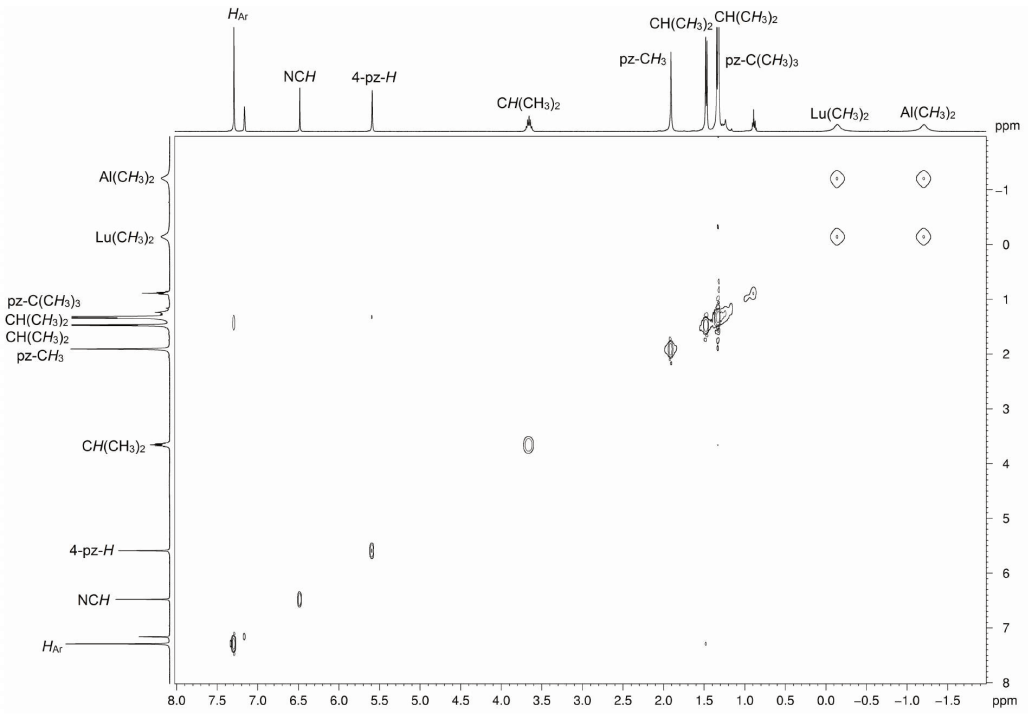

Figure S5. ^{1}H-^{1}H EXSY NMR spectrum (400 MHz) of **1** in [D$_6$]benzene at 26 °C.

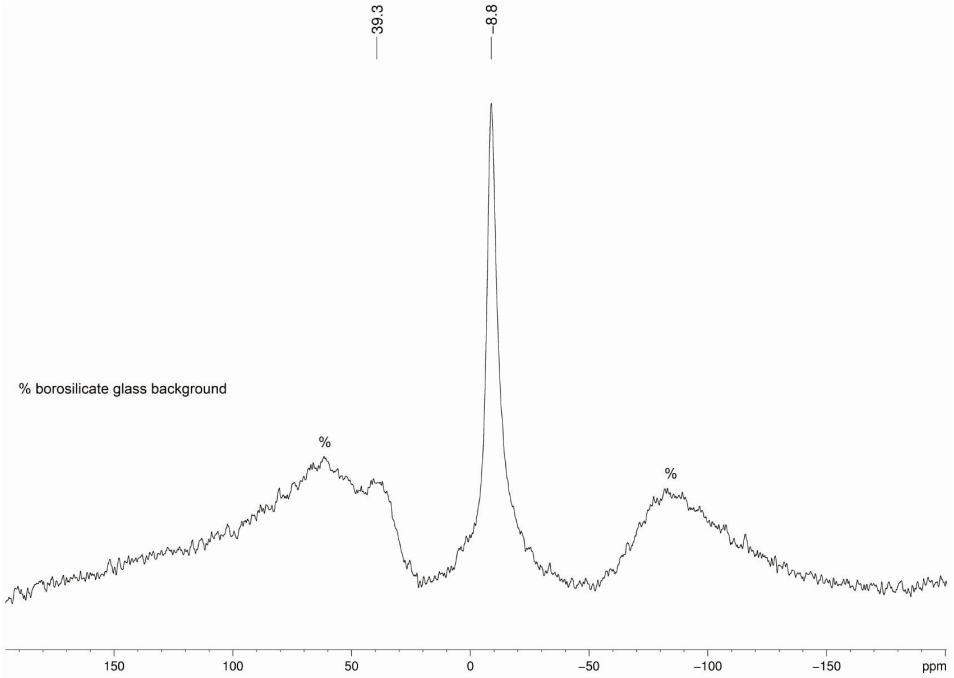

Figure S6. $^{11}B\{^{1}H\}$ NMR spectrum (80 MHz) of **1** in [D_6]benzene at 26 °C.

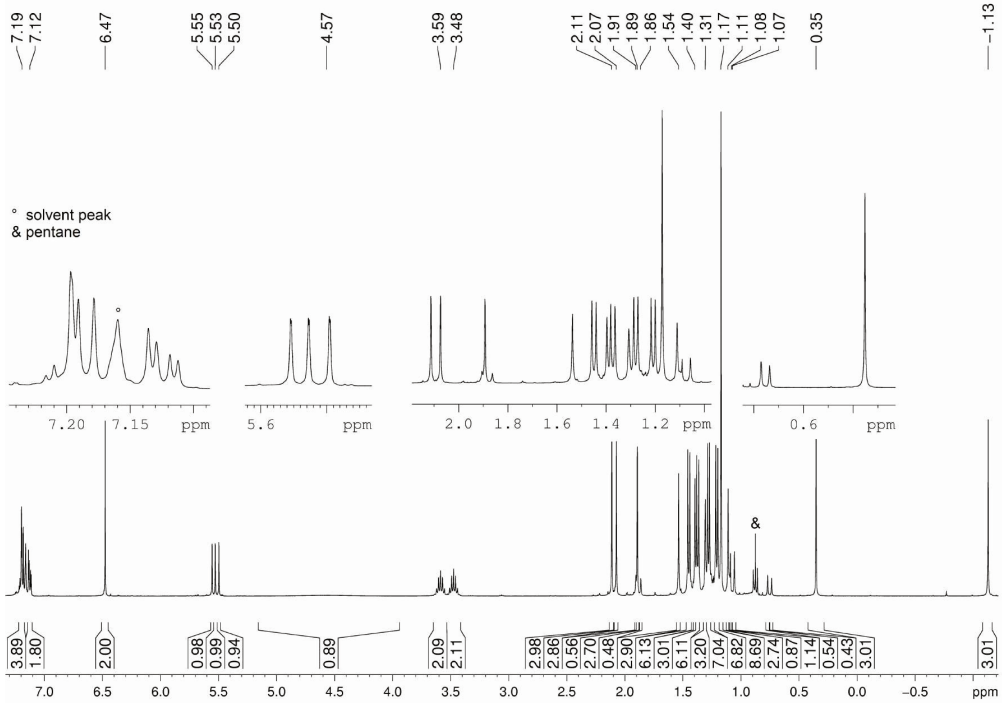

Figure S7. ^{1}H NMR spectrum (400 MHz) of **2** in [D_6]benzene at 26 °C.

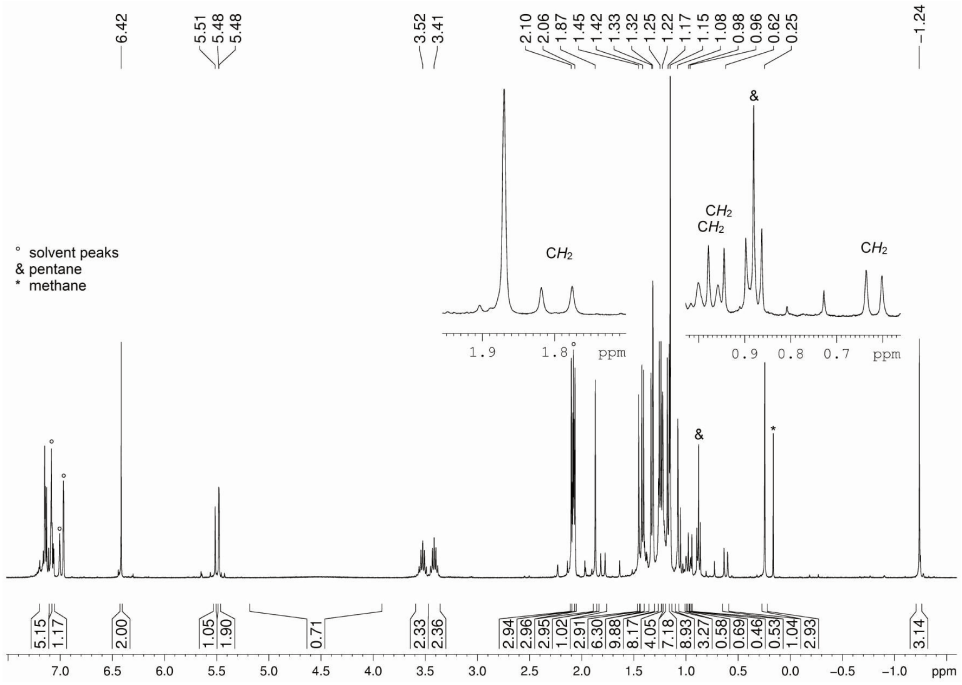

Figure S8. ^{1}H NMR spectrum (400 MHz) of **2** in [D_8]toluene at 26 °C. Recorded after heating **1** to 60 °C for 4 d in a sealed *J. Young* valved NMR tube.

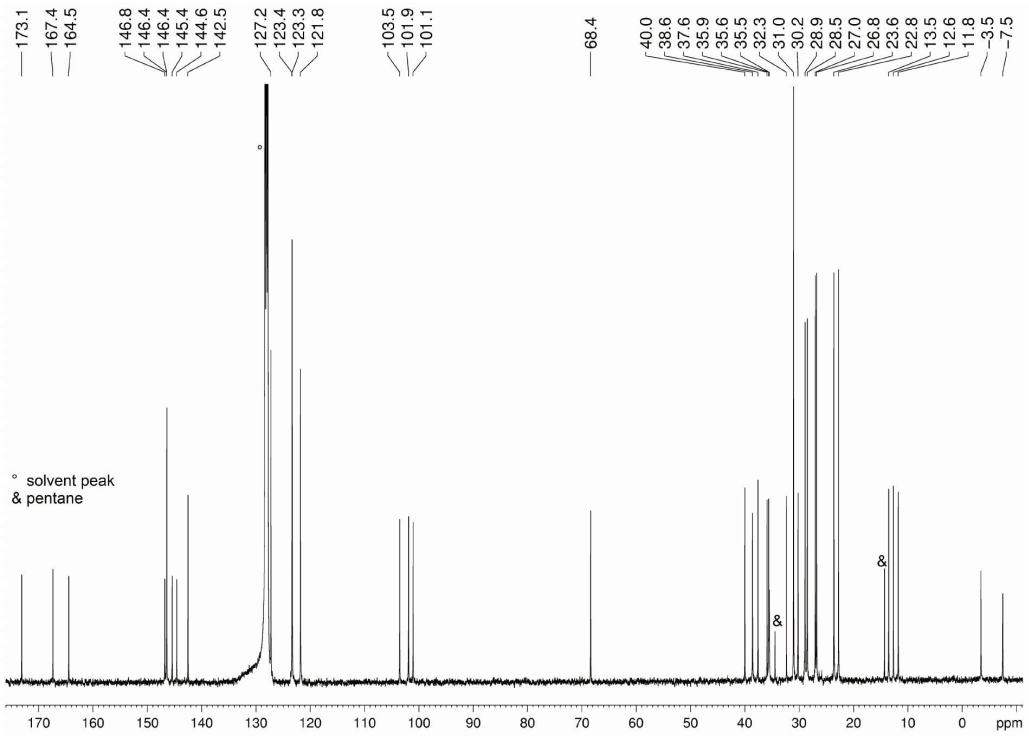

Figure S9. ^{13}C{^{1}H} NMR spectrum (101 MHz) of **2** in [D_6]benzene at 26 °C.

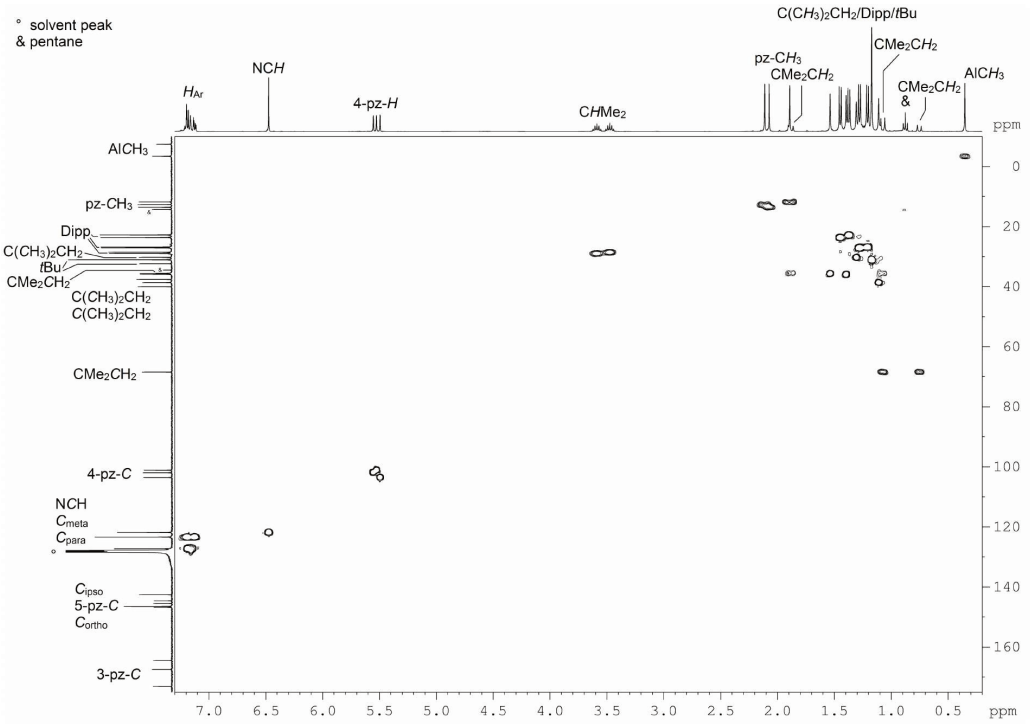

Figure S10. ^{1}H-^{13}C HSQC NMR spectrum (400 MHz, 101 MHz) of **2** in [D$_6$]benzene at 26 °C.

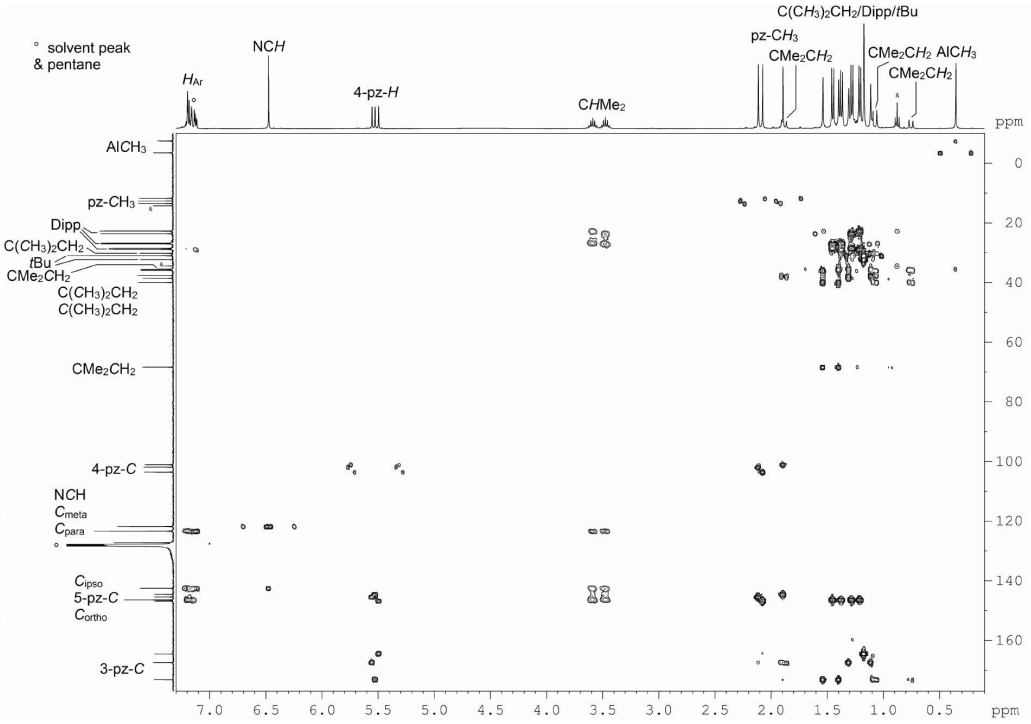

Figure S11. ^{1}H-^{13}C HMBC NMR spectrum (400 MHz, 101 MHz) of **2** in [D$_6$]benzene at 26 °C.

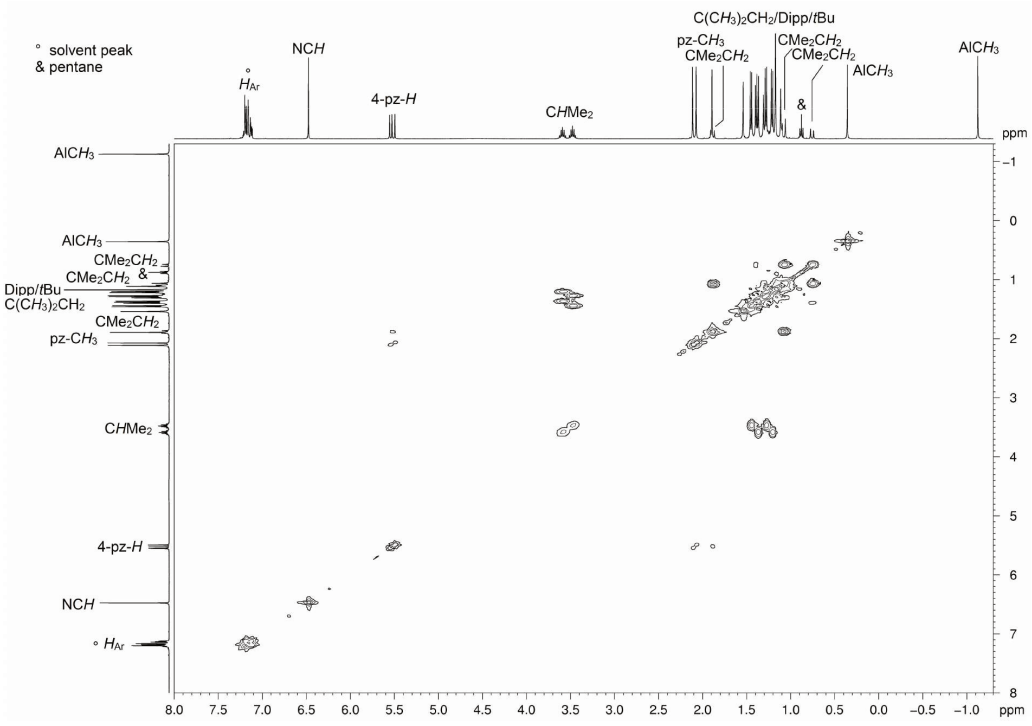

Figure S12. ^{1}H-^{1}H COSY NMR spectrum (400 MHz) of **2** in [D$_6$]benzene at 26 °C.

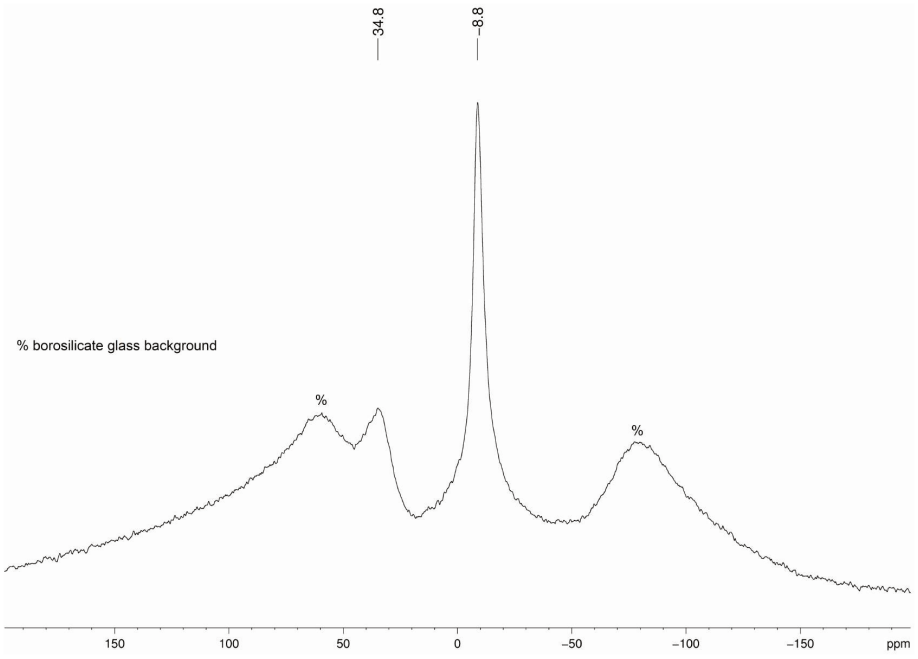

Figure S13. ^{11}B{^{1}H} NMR spectrum (80 MHz) of **2** in [D$_6$]benzene at 26 °C.

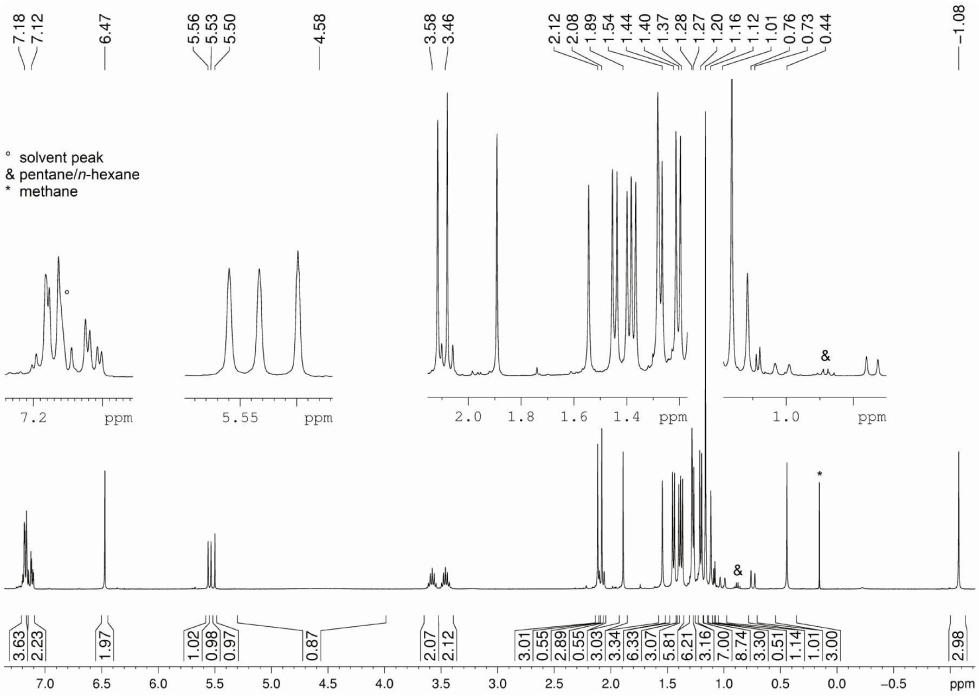

Figure S14. ^{1}H NMR spectrum (400 MHz) in [D_6]benzene at 26 °C of the reaction of [($Tp^{tBu,Me}$)$LuMe_2$] with [Me_2Ga{$B(NDippCH)_2$}] after heating for 96 h to 50 °C in a sealed *J.-Young* valved NMR tube.

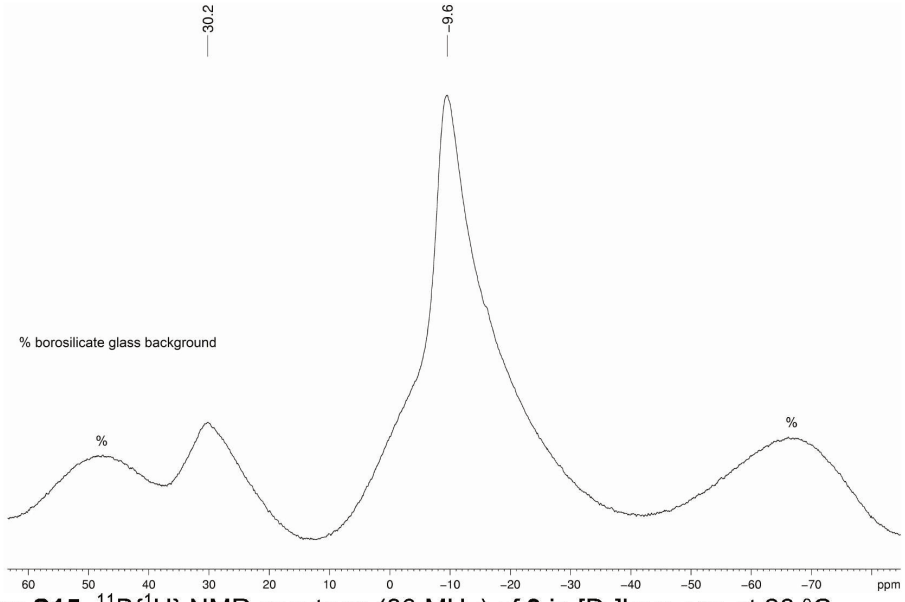

Figure S15. ^{11}B{^{1}H} NMR spectrum (80 MHz) of **3** in [D_6]benzene at 26 °C.

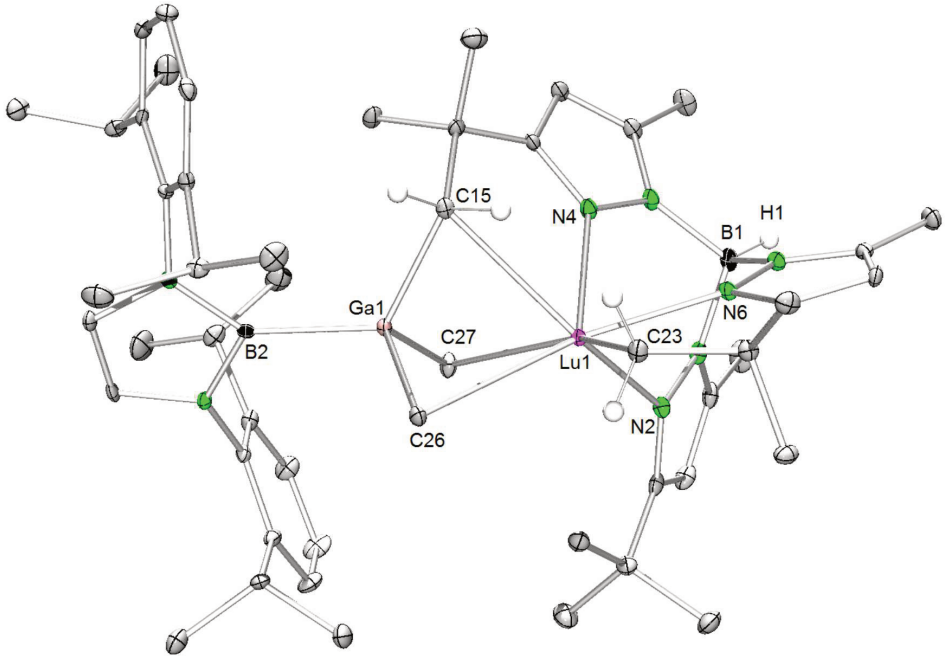

Figure S16. Solid-state structure of [(Tp$^{(t\text{Bu-H})2/t\text{Bu,Me}}$)Lu(GaMe$_2${B(NDippCH)$_2$})] (**3**); thermal ellipsoids are set at the 50% probability level. Hydrogen atoms except for B–H and methylene groups are omitted for clarity. Selected bond lengths [Å] and angles [°]: Lu1–C23 2.386(3), Lu1–C15 2.769(3), Lu1–C26 2.911(4), Lu1–C27 2.813(4), Lu1–N2 2.397(3), Lu1–N4 2.335(3), Lu1–N6 2.306(3), Ga1–C15 2.091(3), Ga1–C27 2.055(4), Ga1–C26 2.072(3), Ga1–B2 2.099(4), Lu1–N2 2.397(3), Lu1–N4 2.335(3), Lu1–N6 2.306(3), C15-Lu1-C23 97.0(1), Lu1-C15-Ga1 71.7(1), Lu1-C26-Ga1 68.8(1), Lu1-C27-Ga1 71.2(1).

Reactivity of 2 toward excess AlMe$_3$ - [(Tp$^{(t\text{Bu-H})2/t\text{Bu,Me}}$)Lu(AlMe$_3$)] (4)

A [D$_6$]benzene solution of **2** (23.2 mg, 0.022 mmol) was treated with an excess of AlMe$_3$ at ambient temperature. The ^{1}H NMR spectrum indicates instant separation of unsolvated [Me$_2$Al{B(NDippCH)$_2$}$_2$]$_2$ and formation of the new complex **4**. Single crystals suitable for X-ray crystallography could be obtained from the reaction mixture after drying *in vacuo*, redissolving in *n*-pentane and storing at –40 °C.

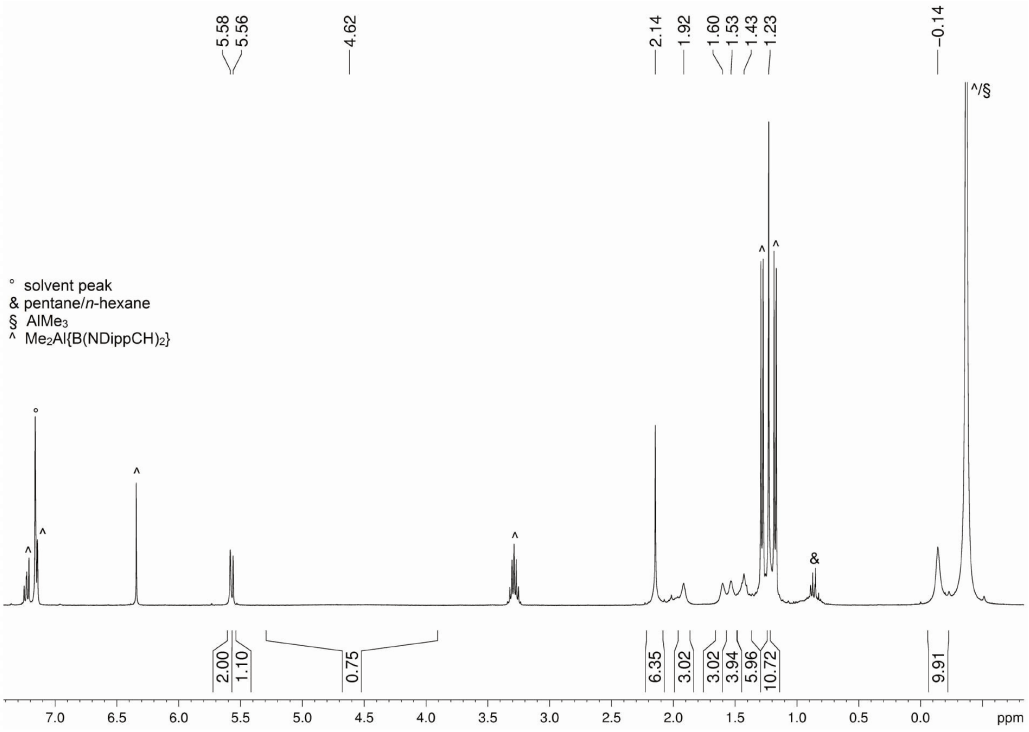

Figure S17. ^{1}H NMR spectrum (400 MHz) in [D_6]benzene of the reaction of **2** with an excess of $AlMe_3$ after 15 min in a sealed *J.-Young* valved NMR tube at 26 °C.

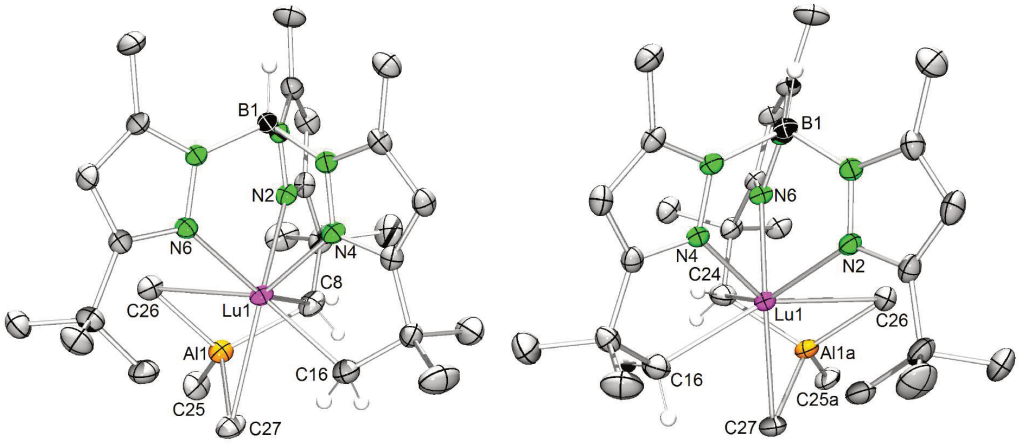

Figure S18. Solid-state structure of **4** showing the two molecules in the asymmetric unit; thermal ellipsoids are set at the 50% probability level. The hydrogen atoms except for B–H and methylene groups are omitted for clarity. Selected bond lengths [Å] and angles [°]: Lu1–C16 2.418(5), Lu1–C8 2.823(6), Lu1–C24 3.070(6), Lu1–C26 2.824(6), Lu1–C27 2.870(6), Al1–C8 2.203(6), Al1–C25 1.85(1), Al1–C26 2.096(7), Al1–C27 2.057(6), Lu1–N2 2.487(3), Lu1–N4 2.197(3), Lu1–N6 2.320(3), Al1–C8 2.203(6), Al1–C25 1.85(1), Al1–C26 2.096(7), Al1–C27 2.057(6), Al1a–C24 2.074(6), Al1a–C25a 1.95(1), Al1a–C26 2.146(6), Al1a–C27 2.013(7), C8-Lu1-C16 96.0(2), C24-Lu1-C16 89.2(2), Lu1-C8-Al1 64.4(2), Lu1-C26-Al1 65.4(2), Lu1-C27-Al1 64.8(2), Lu1-C24-Al1a 66.0(2), Lu1-C26-Al1a 70.5(2), Lu1-C27-Al1a 71.1(2).

Reactivity of 2 toward THF

A [D_6]benzene solution of **2** (9.7 mg, 0.009 mmol) was treated with an excess of THF at ambient temperature. The ^{1}H NMR spectrum indicated separation of the [$Me_2Al\{B(NDippCH)_2\}_2$] unit in about 92% by forming the THF adduct [$(THF)Me_2Al\{B(NDippCH)_2\}_2$] and a new compound, tentatively assigned as [$(Tp^{(t\text{Bu-H})2/t\text{Bu,Me}})Lu(THF)_x$].

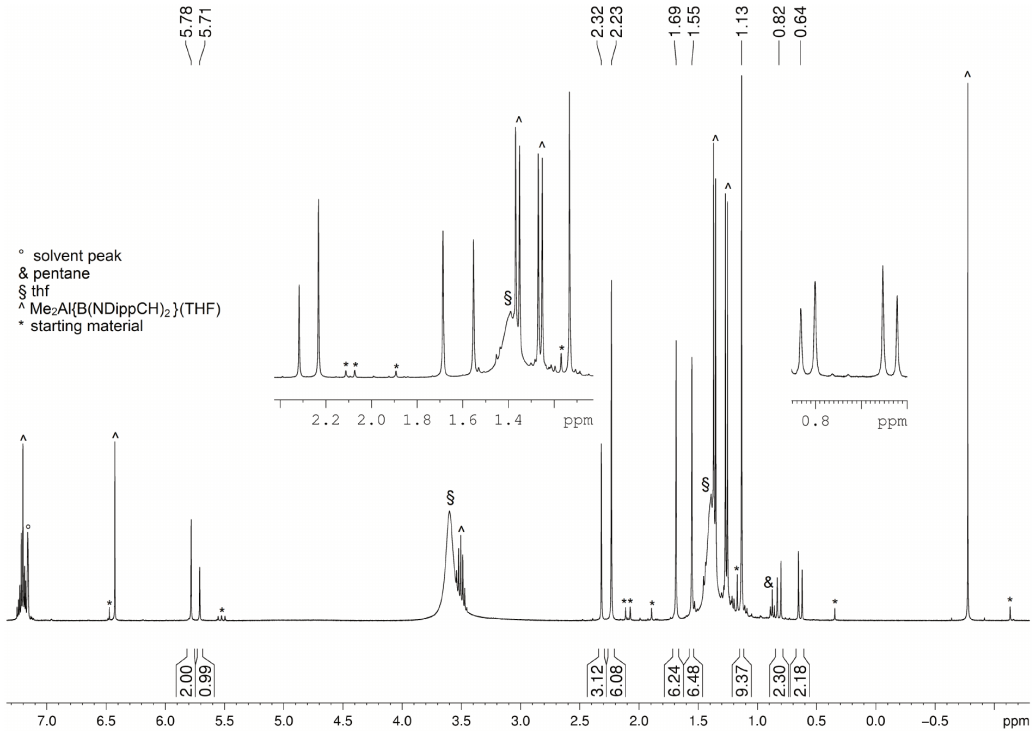

Figure S19. ^{1}H NMR spectrum (400 MHz) in [D_6]benzene of the reaction of **2** with an excess of THF after 1 h in a sealed *J.-Young* valved NMR tube at 26 °C.

Investigations into the active species of the system 1/B

A solution of **1** (21.5 mg, 0.02 mmol) in 0.5 mL [D_6]benzene was treated with [$PhNMe_2H$][$B(C_6F_5)_4$] (**B**) (18 mg, 0.02 mmol) in a *J.-Young* valved NMR tube. After 10 min a first ^{1}H NMR spectrum was recorded (Figure S19) showing complete consumption of the starting materials, the formation of methane, and separation of the [$Me_2Al\{B(NDippCH)_2\}_2$] unit forming [$(PhNMe_2)Me_2Al\{B(NDippCH)_2\}_2$]. Besides, signals matching the assumed ion pair [$Tp^{tBu,Me}LuMe$][$B(C_6F_5)_4$] (**5a**) were found at 5.62, 1.95, 1.11 and 0.25 ppm in a 3:9:27:3 ratio accompanied by minor side products. After 16 h a second ^{1}H NMR spectrum was recorded (Figure S20) of the same sample in a sealed *J.-Young* valved NMR tube. While the signals for [$(PhNMe_2)Me_2Al\{B(NDippCH)_2\}_2$] and the side product were still present signals attributed to **5a** had vanished and the methane peak showed increased intensity. However, new signals appeared and can be assigned to the CH-actived product [$(Tp^{(tBu-H)/tBu2,Me})Lu$][$B(C_6F_5)_4$] (**5b**) revealing two different pyrazolyl moieties in a 2:1 ratio.

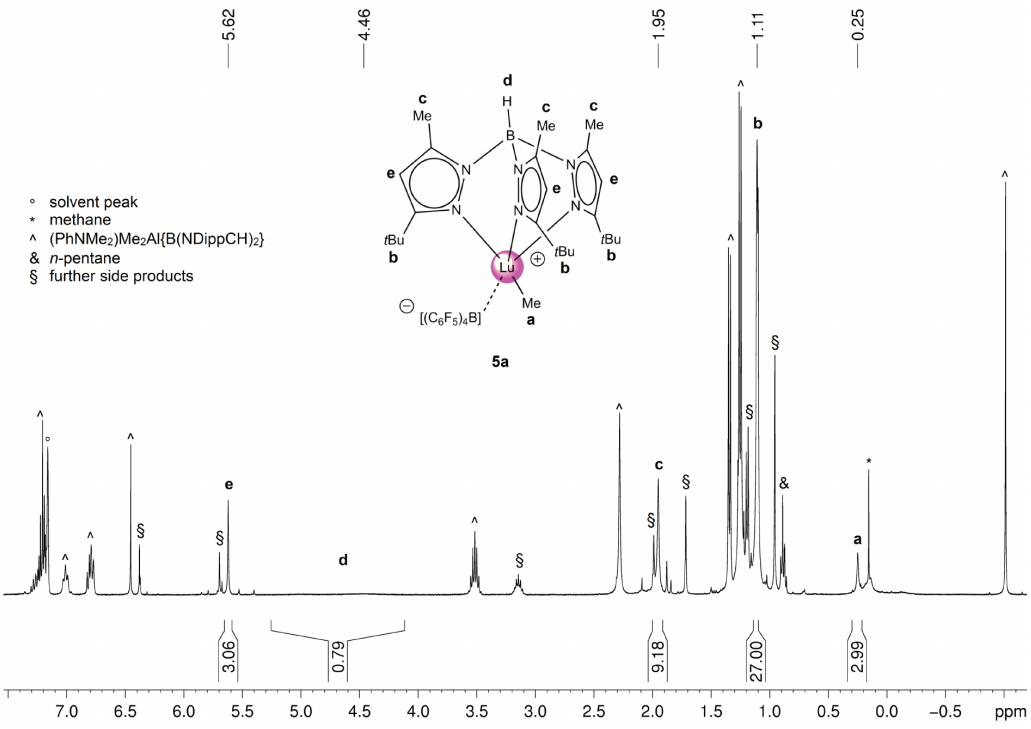

Figure S20. ^{1}H NMR spectrum (400 MHz) in [D_6]benzene of the reaction of **1** with co-catalyst **B** after 10 min in a sealed *J.-Young* valved NMR tube at 26 °C.

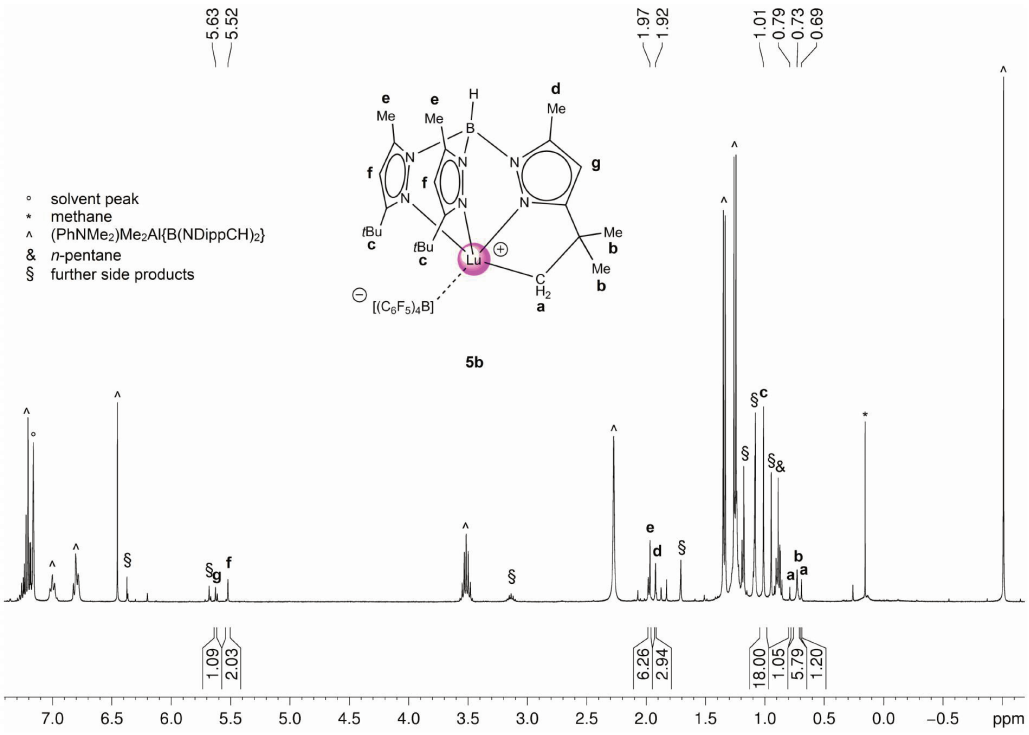

Figure S21. ^{1}H NMR spectrum (400 MHz) in [D_6]benzene of the reaction of **1** with co-catalyst **B** after 16 h in a sealed *J.-Young* valved NMR tube at 26 °C.

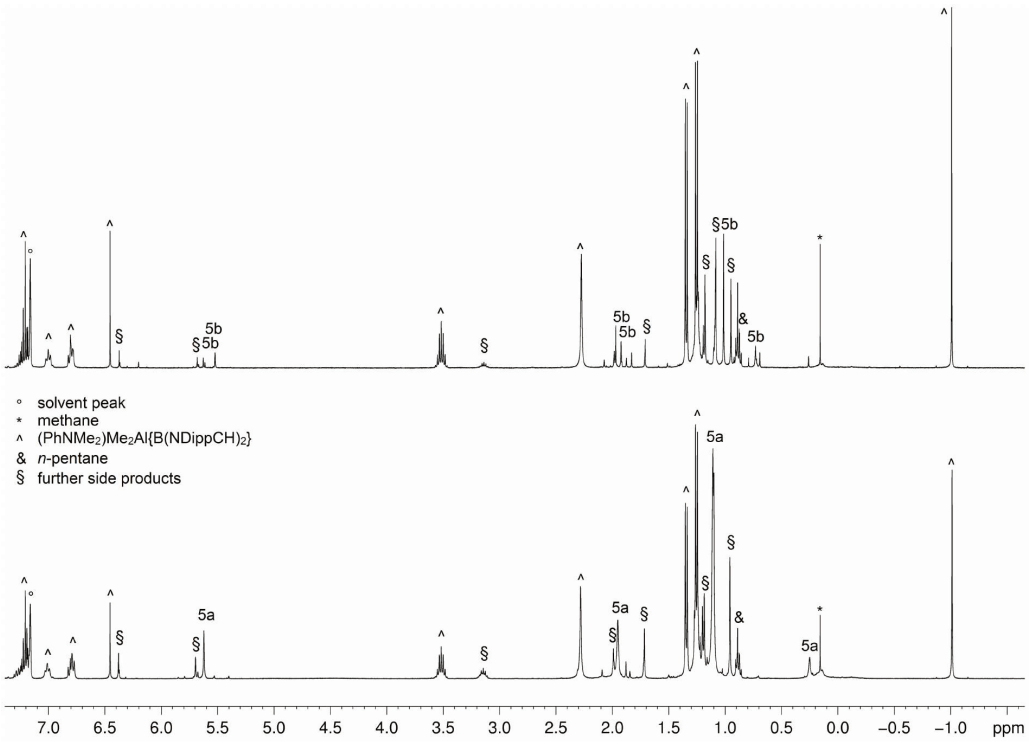

Figure S22. Comparing ^{1}H NMR spectra (400 MHz) in [D_6]benzene of the reaction of **1** with co-catalyst **B** after 10 min and 16 h at 26 °C.

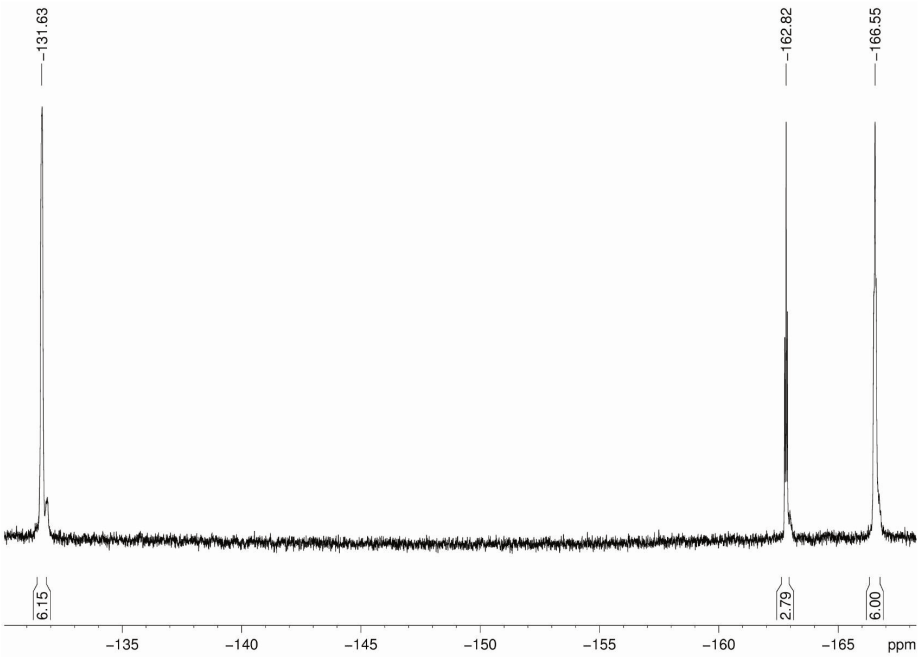

Figure S23. ^{19}F{^{1}H} NMR spectrum (400 MHz) in [D_6]benzene of the reaction of **1** with co-catalyst **B** after 10 min in a sealed *J.-Young* valved NMR tube at 26 °C.

Investigations into the active species of the system 2/B

In a *J.-Young* valved NMR tube, **2** (20.9 mg, 0.02 mmol) in 0.5 mL [D_6]benzene was treated with [$PhNMe_2H$][$B(C_6F_5)_4$] (**B**) (18 mg, 0.02 mmol) and aged for 5 min. The ^{1}H NMR spectrum showed almost complete conversion, release of methane and formation of a species assignable to [($Tp^{(tBu\text{-}H)/tBu2,Me}$)$LuMe_2Al$(boryl)][$B(C_6F_5)_4$] (**6**). The formation of a yellow oil phase was observed in the course of the reaction, which implied the non-equimolar integrals of main and side-product ($PhNMe_2$) in the ^{1}H NMR spectrum to be due to different solubility of product and side product in [D_6]benzene. ^{1}H NMR (400 MHz, [D_6]benzene, 26 °C): δ = 7.24 (m, 2 H, $H_{Ar(m)}$ of $PhNMe_2$), 7.20 (m, 2 H, $H_{Ar(p)}$ of $C_6H_3(CH(CH_3)_2)_2$), 7.14 (d, 4 H, ^3J(HH) = 7.3 Hz, $H_{Ar(m)}$ of $C_6H_3(CH(CH_3)_2)_2$), 6.80 (t, 1 H, ^3J(HH) = 7.3 Hz, $H_{Ar(p)}$ of $PhNMe_2$), 6.64 (d, 2 H, ^3J(HH) = 8.2 Hz, $H_{Ar(o)}$ of $PhN(CH_3)_2$), 6.37 (s, 2 H, NC*H*) 5.43 (s, 1 H, 4-pz-*H*), 5.41 (s, 2 H, 4-pz-*H*), 4.3 (bs, 1 H, B*H*), 3.20 (sep, 4 H, ^3J = 6.8 Hz, $CH(CH_3)_2$), 2.51 (s, 6 H, $PhNMe_2$) 2.01 (s, 3 H, pz-CH_3), 1.90 (s, 6 H, pz-CH_3), 1.27 (d, 12 H, ^3J(HH) = 6.8 Hz, $CH(CH_3)_2$), 1.17 (d, 12 H, ^3J(HH) = 6.8 Hz, $CH(CH_3)_2$) 1.03 (s, 18 H, pz-$C(CH_3)_3$), 0.94 (s, 8 H, pz-$C(CH_3)_2CH_2$)), 0.00 (bs, 6 H, $Al(CH_3)_2$) ppm. ^{19}F{^{1}H} NMR (376.5 MHz, [D_6]benzene, 26 °C): δ = –131.7 (d, 8 F, ^3J(FF) = 9.5 Hz $F_{Ar(o)}$), –162.8 (t, 4 F, ^3J(FF) = 20.8 Hz, $F_{Ar(p)}$), –166.5 (m, 8 F, $F_{Ar(m)}$) ppm.

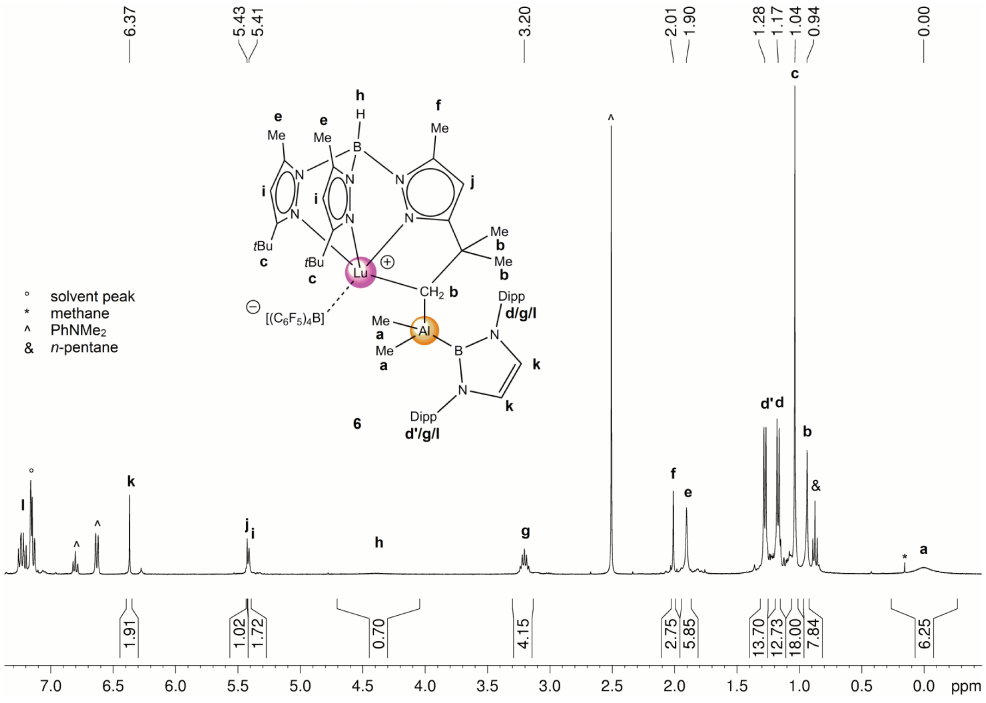

Figure S24. ^{1}H NMR spectrum (400 MHz) in [D_6]benzene of the reaction of **2** with co-catalyst **B** after 10 min in a sealed *J.-Young* valved NMR tube at 26 °C.

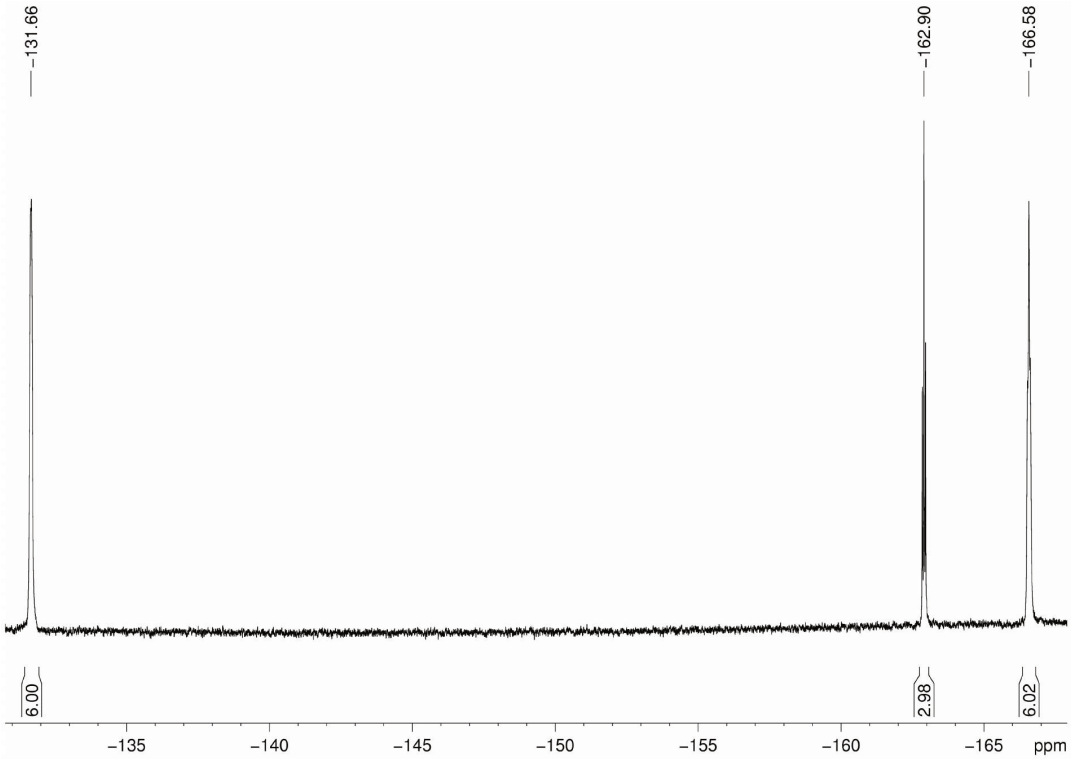

Figure S25. $^{19}F\{^{1}H\}$ NMR spectrum (400 MHz) in $[D_6]$benzene of the reaction of **2** with co-catalyst **B** after 10 min in a sealed *J.-Young* valved NMR tube at 26 °C.

Crystallographic Data

Table S1. Crystallographic data information of complexes **1**, **2**, **3** and **4**

	1	**2**	**3**	**4**
Formula	$C_{57}H_{95}AlB_2LuN_8$	$C_{58}H_{94}AlB_2LuN_8$	$C_{52}H_{80}B_2GaLuN_8$	$C_{27}H_{47}AlBLuN_6$
Fw	1115.97	1126.98	1083.55	668.46
temp (K)	180(2)	121(2)	100(2)	100(2)
cryst syst	Triclinic	Orthorhombic	Monoclinic	Triclinic
space group	$P\bar{1}$	$P2_12_12_1$	$P2_1/n$	$P\bar{1}$
a (Å)	13.0103(4)	16.116(1)	11.182(1)	12.207(6)
b (Å)	13.9770(4)	18.866(1)	39.772(4)	12.210(8)
c (Å)	18.1287(5)	19.800(1)	11.648(1)	12.954(6)
α (deg)	92.076(2)	90	90	71.94(2)
β (deg)	102.072(2)	90	96.389(2)	75.156(5)
γ (deg)	101.852(1)	90	90	60.47(1)
V ($Å^3$)	3144.2(2)	6020.0(8)	5148.0(9)	1585(2)
Z	2	4	4	2
ρ_{calcd} (mg/mm^3)	1.179	1.243	1.398	1.401
μ (mm^{-1})	1.623	1.696	2.472	3.167
R1[a] ($I > 2.0\sigma(I)$)	0.0328	0.0234	0.0361	0.0344
wR2[b] (all data)	0.0743	0.0498	0.0672	0.0903
solvent	*n*-hexane	*n*-hexane	*n*-pentane	*n*-pentane

[a] $R1 = \Sigma(||F0|-|Fc||)/\Sigma|F0|$. [b] $wR2 = \{\Sigma[w(F0^2-Fc^2)^2/\Sigma[w(F0^2)^2]\}^{1/2}$.

DFT Calculations

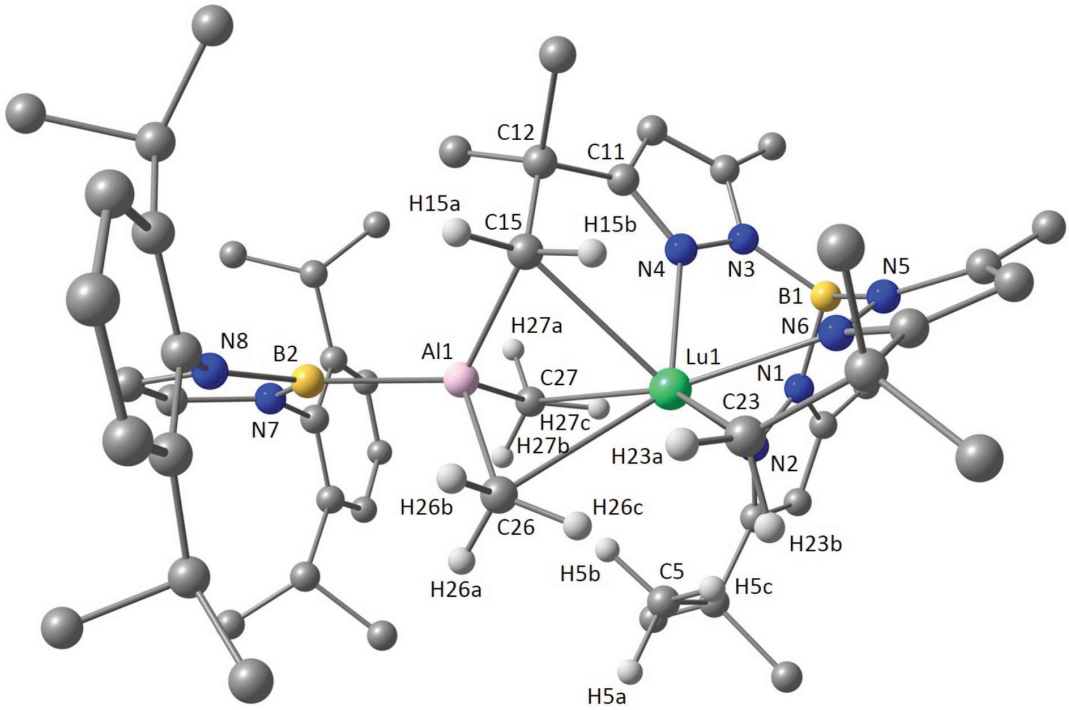

Figure S26. Optimized geometry for the DFT-optimized model system **2a**.

Table S2. Selected geometrical parameters for **2a** (distances in Å, angles in deg); deviations with respect to the X-ray parameters of **2** are given in square brackets

Lu1−C15	2.716 [+1.8 %]	C26−H26a	1.106	B1−N1	1.561 [+0.7 %]
Lu1−C23	2.395 [+0.2 %]	C26−H26b	1.105	B1−N3	1.555 [+0.1 %]
Lu1−C26	2.808 [-5.2 %]	C26−H26c	1.106	B1−N5	1.548 [+0.1 %]
Lu1−C27	2.955 [+3.4 %]	Lu1···H26c	2.481	N1−N2	1.383 [+0.1 %]
Lu1−N4	2.330 [+0.3 %]	C27−H27a	1.105	N3−N4	1.373 [-0.1 %]
Lu1−N6	2.315 [+0.7 %]	C27−H27b	1.106	N5−N6	1.367 [+0.3 %]
Lu1···Al1	2.918 [+0.1 %]	C27−H27c	1.108	B2−Al1−C15	117.5 [+4.2 %]
C15−H15a	1.111	Lu1···H27c	2.566	B2−Al1−C26	108.3 [-6.2 %]
C15−H15b	1.121	Al1−C15	2.114 [+1.4 %]	B2−Al1−C27	114.1 [+3.6 %]
Lu1···H15b	2.367	Al1−C26	2.059 [+1.7 %]	C26−Al1−C27	108.2 [-0.2 %]
C23−H23a	1.107	Al1−C27	2.050 [+1.5 %]	C15−Al1−C26	99.6 [-0.3 %]
C23−H23b	1.118	Al1−B2	2.165 [+1.1 %]	C15−Al1−C27	107.9 [-0.5 %]
Lu1···H23a	3.064	B2−N7	1.468 [+1.4 %]	C26−Lu1−C27	70.5 [+2.8 %]
Lu1···H23b	2.811	B2−N8	1.470 [+1.6 %]	C11−C12−C15	110.4 [0 %]

Table S3. Lu occupancy for selected C−H NLMOs

NLMO	Percent from parent NBO	Percent Lu
C5−H5a	99.2	0.1
C5−H5b	97.2	1.9
C5−H5c	97.6	1.6
C15−H15a	98.2	0.2
C15−H15b	96.1	2.7
C23−H23a	98.1	0.9
C23−H23b	97.0	1.9
C26−H26a	99.0	0.2
C26−H26b	98.9	0.3
C26−H26c	97.0	2.3
C27−H27a	99.0	0.2
C27−H27b	99.1	0.2
C27−H27c	97.5	1.8

Cartesian Coordinates for **2a**:

6	-5.016861000	3.594118000	-2.659690000
6	-2.550129000	3.182182000	-3.054669000
6	1.878609000	3.872720000	-2.980544000
6	-3.054591000	4.869645000	-0.545514000
6	-3.726250000	2.979222000	-2.085092000
6	3.634951000	2.516720000	-4.181499000
6	-2.828902000	5.421288000	0.712713000
6	-3.434938000	3.527840000	-0.692770000
6	-5.609147000	-1.314085000	-3.365139000
6	-3.329234000	-2.011457000	-4.168207000
6	2.663425000	2.541971000	-2.978402000
6	4.474573000	3.309591000	-1.264777000
6	-2.987767000	4.634803000	1.851937000
6	-4.154448000	-1.603643000	-2.937653000
6	1.681347000	1.374669000	-3.102480000
6	-3.575020000	2.737445000	0.472790000
6	3.467612000	2.430005000	-1.698159000
6	-3.365588000	3.287876000	1.759520000
6	-5.362631000	1.081267000	0.276029000
6	4.963467000	2.777594000	-0.077963000
6	6.055287000	3.310849000	0.792935000
6	-0.042696000	1.716849000	0.213052000
6	-5.527710000	-0.241824000	0.015618000
6	-4.121256000	-2.629379000	-1.808035000
6	-5.010203000	2.676136000	3.574812000
6	-0.617535000	-0.746890000	-1.947813000
6	-4.077238000	-3.997816000	-2.110282000
6	-3.584388000	2.467152000	3.024736000
6	-4.201121000	-2.247379000	-0.444283000
6	-2.547433000	2.758100000	4.121081000
6	-4.128161000	-4.964016000	-1.108036000
6	-4.282297000	-3.218791000	0.582318000
6	2.215900000	-2.411965000	-1.877775000
6	-4.236413000	-4.574200000	0.223601000
6	-0.119482000	-1.530638000	1.103238000
6	-1.005427000	-0.618127000	3.303401000
6	-5.972902000	-2.915644000	2.432711000

6	-4.482505000	-2.831888000	2.043438000
6	1.438129000	-0.519990000	2.800762000
6	3.268005000	0.500382000	3.584863000
6	4.368057000	-2.495262000	-0.655548000
6	4.150880000	-3.900702000	-2.713847000
6	3.412047000	-3.321330000	-1.486498000
6	4.326807000	1.133025000	4.429014000
6	0.174762000	-1.328540000	2.612776000
6	5.991207000	-1.585531000	0.594253000
6	2.052526000	-0.053831000	3.979770000
6	7.252207000	-1.266498000	1.331000000
6	5.688002000	-2.693780000	-0.199441000
6	-3.644468000	-3.681440000	3.011626000
6	2.907511000	-4.498405000	-0.617870000
6	0.406331000	-2.697647000	3.305822000
5	-3.211527000	0.148744000	0.099953000
5	4.581915000	0.577990000	1.288290000
13	-1.060665000	-0.040218000	-0.065494000
71	1.787366000	-0.483770000	-0.522875000
7	-3.993405000	1.367709000	0.339147000
7	3.335166000	1.414362000	-0.813453000
7	-4.271582000	-0.849808000	-0.103489000
7	4.271384000	1.633751000	0.181037000
7	2.230608000	-0.240399000	1.751533000
7	3.361719000	0.373075000	2.230523000
7	3.912920000	-1.328967000	-0.167612000
7	4.896807000	-0.772509000	0.600762000
1	-4.913205000	4.684955000	-2.790039000
1	-2.348469000	4.251787000	-3.233826000
1	-5.248321000	3.155893000	-3.644945000
1	-2.775409000	2.719793000	-4.030171000
1	-2.938908000	5.495156000	-1.434927000
1	1.298781000	3.972470000	-3.913421000
1	2.559832000	4.735358000	-2.910082000
1	-5.876332000	3.413574000	-1.995229000
1	3.071699000	2.602235000	-5.126076000
1	-2.530918000	6.468647000	0.807197000
1	4.350158000	3.352892000	-4.134830000
1	-5.629444000	-0.562262000	-4.172090000
1	-1.628053000	2.724549000	-2.663060000
1	-3.284463000	-1.171359000	-4.880516000
1	1.179863000	3.920382000	-2.130312000
1	4.816995000	4.218186000	-1.750901000
1	-3.889348000	1.894563000	-1.983882000
1	-6.090195000	-2.232485000	-3.743550000
1	-3.784450000	-2.862471000	-4.702512000
1	4.211252000	1.577748000	-4.205151000
1	1.110209000	1.434368000	-4.042376000
1	-6.210544000	-0.929705000	-2.528244000
1	-2.297600000	-2.284340000	-3.899279000
1	-3.728413000	-0.667230000	-2.539672000
1	6.399231000	4.276114000	0.394268000
1	-2.815857000	5.077816000	2.835536000
1	-0.520133000	2.473297000	-0.437062000
1	-6.116571000	1.851313000	0.412870000
1	0.935477000	1.400089000	-2.289081000
1	-1.145586000	-0.044980000	-2.619189000
1	-5.169141000	3.732307000	3.853047000
1	2.211192000	0.403980000	-3.121306000
1	-5.773583000	2.399775000	2.831587000
1	-4.006781000	-4.314339000	-3.152997000
1	-6.449362000	-0.805366000	-0.096673000
1	-0.254973000	2.028264000	1.252317000
1	5.715417000	3.468678000	1.828716000
1	1.046200000	1.891062000	0.107186000
1	6.919766000	2.628534000	0.831806000
1	-2.675946000	3.766615000	4.549181000
1	0.329625000	-0.985475000	-2.466698000
1	-1.167986000	-1.704668000	-1.979755000

1	-5.172038000	2.058350000	4.474288000
1	-3.491421000	1.406036000	2.739927000
1	-1.517173000	2.682322000	3.739165000
1	2.482456000	-1.913039000	-2.841856000
1	-4.089590000	-6.025017000	-1.367681000
1	-2.660979000	2.038174000	4.947996000
1	-1.177048000	0.379637000	2.871601000
1	5.525363000	0.954000000	1.935297000
1	-6.594235000	-2.259567000	1.804951000
1	1.351109000	-3.052125000	-2.136038000
1	4.535613000	2.168425000	4.114120000
1	4.557885000	-3.091827000	-3.342742000
1	0.679723000	-2.193972000	0.682103000
1	7.708367000	-0.328162000	0.974213000
1	-1.929046000	-1.206389000	3.184685000
1	-4.167330000	-1.780333000	2.149097000
1	-0.984791000	-2.222361000	1.025829000
1	-0.817968000	-0.492645000	4.382557000
1	-4.290907000	-5.337976000	1.002868000
1	3.448368000	-4.489379000	-3.326676000
1	-6.344266000	-3.948675000	2.319698000
1	-6.114903000	-2.614599000	3.484363000
1	3.995887000	1.155644000	5.477152000
1	5.277523000	0.577413000	4.381449000
1	7.076921000	-1.155801000	2.413707000
1	4.987448000	-4.563074000	-2.424872000
1	1.677139000	-0.118250000	4.996777000
1	7.981065000	-2.076366000	1.184761000
1	6.347207000	-3.531084000	-0.409322000
1	-2.584420000	-3.705373000	2.715126000
1	2.356878000	-4.128900000	0.262639000
1	2.223490000	-5.132403000	-1.206488000
1	-4.003087000	-4.723303000	3.058743000
1	-0.488414000	-3.331994000	3.199425000
1	-3.708235000	-3.269752000	4.032336000
1	1.258350000	-3.226833000	2.849268000
1	0.616513000	-2.578236000	4.382134000
1	3.741836000	-5.126524000	-0.262234000

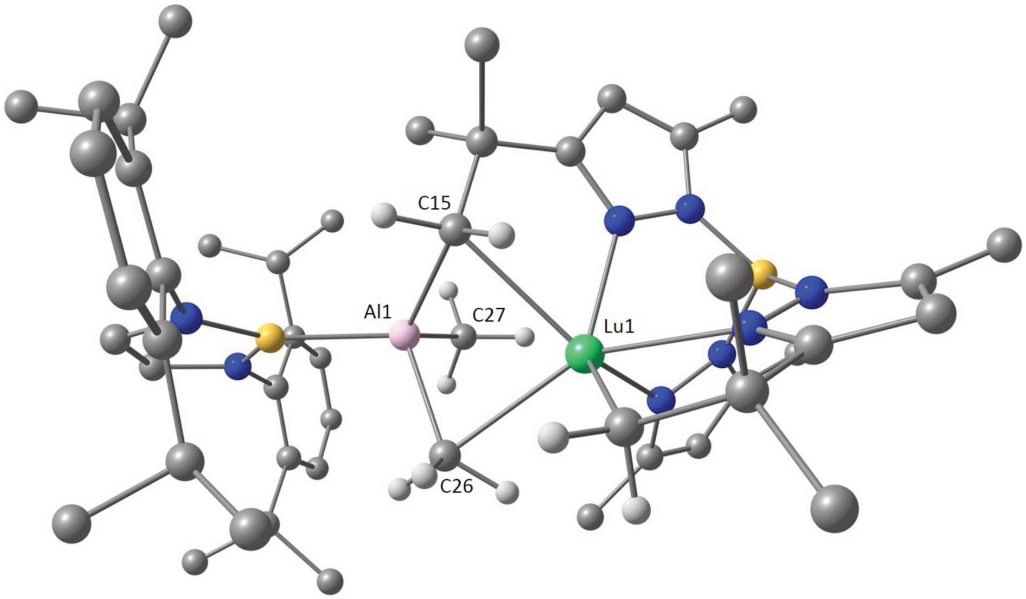

Figure S27. Optimized geometry for the DFT-optimized model system **2b**.

Table S4. Selected geometrical parameters for **2b** (distances in Å)

Lu1–C15	2.627	Al1–C15	2.142
Lu1–C23	2.371	Al1–C26	2.121
Lu1–C26	2.571	Al1–C27	2.019
Lu1···C27	3.381	Lu1···Al1	2.943

Cartesian Coordinates for **2b**:

6	-5.276942000	2.616198000	-3.487126000
6	-2.785715000	2.892393000	-3.806162000
6	-3.709239000	4.600037000	-1.492126000
6	-3.891754000	2.457630000	-2.829828000
6	-3.685531000	5.314521000	-0.297354000
6	-3.828057000	3.202327000	-1.500716000
6	-4.363181000	-2.708661000	-3.271797000
6	-1.879874000	-3.141281000	-3.377738000
6	3.912157000	3.913345000	-1.285960000
6	-3.781749000	4.637723000	0.916942000
6	-3.024568000	-2.594909000	-2.512252000
6	-3.922928000	2.529995000	-0.259785000
6	2.945549000	2.959337000	-1.631311000
6	-3.905747000	3.242494000	0.963951000
6	-5.375437000	0.558034000	-0.352041000
6	4.676501000	3.336421000	-0.274057000
6	5.839775000	3.925941000	0.457336000
6	-0.277034000	2.149699000	0.475736000
6	-5.290394000	-0.796604000	-0.286404000
6	-3.131803000	-3.263108000	-1.146008000
6	-5.543919000	2.525312000	2.743502000
6	-0.246090000	0.117166000	-2.030925000
6	-2.818571000	-4.622160000	-1.003325000
6	-4.065628000	2.532512000	2.303392000

6	-3.612318000	-2.562516000	-0.011527000
6	-3.182873000	3.122549000	3.414029000
6	-2.994766000	-5.282169000	0.210855000
6	-3.820616000	-3.226489000	1.223083000
6	2.309066000	-2.028161000	-2.084855000
6	-3.499529000	-4.589417000	1.307613000
6	0.090168000	-1.211793000	1.025347000
6	-0.655104000	-0.272523000	3.272129000
6	-5.924458000	-2.854481000	2.573810000
6	-4.424610000	-2.521224000	2.433490000
6	1.764508000	-0.285372000	2.678943000
6	3.644651000	0.714066000	3.369397000
6	4.587642000	-1.963840000	-1.118433000
6	4.251516000	-3.304130000	-3.207088000
6	3.614053000	-2.840500000	-1.877963000
6	4.757467000	1.323653000	4.159465000
6	0.460281000	-1.038228000	2.528986000
6	6.255587000	-0.961015000	-0.004727000
6	2.464514000	0.129600000	3.828947000
6	7.557796000	-0.559738000	0.609797000
6	5.962821000	-2.058240000	-0.818215000
6	-3.701936000	-2.855017000	3.749514000
6	3.314350000	-4.089737000	-1.014955000
6	0.636789000	-2.429114000	3.190456000
5	-3.099604000	0.029904000	-0.097899000
5	4.732675000	1.019476000	0.959547000
13	-0.958322000	0.321250000	-0.043355000
71	1.878148000	-0.213924000	-0.620097000
7	-4.090827000	1.101868000	-0.240281000
7	3.104916000	1.849299000	-0.873979000
7	-3.948998000	-1.168399000	-0.128669000
7	4.180217000	2.092110000	-0.037498000
7	2.482741000	0.040160000	1.590980000
7	3.639992000	0.646243000	2.007930000
7	4.092490000	-0.864640000	-0.525386000
7	5.102428000	-0.252957000	0.160931000
1	-5.482459000	3.675687000	-3.717691000
1	-2.923445000	3.933755000	-4.142712000
1	-5.324681000	2.047149000	-4.430694000
1	-2.796881000	2.253296000	-4.704546000
1	-3.636927000	5.137917000	-2.440807000
1	-6.079592000	2.250917000	-2.828014000
1	-3.591826000	6.403418000	-0.311436000
1	-4.296452000	-2.202260000	-4.249573000
1	-1.787988000	2.818180000	-3.344925000
1	-1.759500000	-2.517152000	-4.278014000
1	4.040656000	4.902765000	-1.715187000
1	-3.747292000	1.386698000	-2.611771000
1	-4.616165000	-3.767627000	-3.452665000
1	-2.079767000	-4.169917000	-3.722806000
1	-5.188266000	-2.249397000	-2.706239000
1	-0.921084000	-3.146901000	-2.835131000
1	-2.834633000	-1.522785000	-2.338719000
1	6.024071000	4.944239000	0.085980000
1	-3.762671000	5.206283000	1.849485000
1	-0.704575000	2.898459000	-0.216497000
1	-6.255999000	1.182979000	-0.470757000
1	-1.066180000	0.729973000	-2.447613000
1	-5.910916000	3.555817000	2.890875000
1	-6.184504000	2.038006000	1.992504000
1	-2.436302000	-5.177580000	-1.862122000
1	-6.085903000	-1.533242000	-0.347409000
1	-0.610783000	2.440406000	1.487015000
1	5.654677000	3.985365000	1.541858000
1	0.818631000	2.301821000	0.472017000
1	6.759453000	3.336422000	0.313424000
1	-3.515012000	4.131215000	3.712727000
1	0.641717000	0.568556000	-2.533888000
1	-0.356458000	-0.884924000	-2.476983000

1	-5.661450000	1.982569000	3.696628000
1	-3.757503000	1.484338000	2.151916000
1	-2.129157000	3.192345000	3.100872000
1	2.434412000	-1.415978000	-3.013040000
1	-2.742301000	-6.341813000	0.299969000
1	-3.233510000	2.486212000	4.312803000
1	-0.746638000	0.757120000	2.896831000
1	5.698592000	1.464597000	1.524006000
1	-6.491893000	-2.575253000	1.673718000
1	1.485165000	-2.726264000	-2.329077000
1	4.912587000	2.382855000	3.896752000
1	4.511394000	-2.439307000	-3.839296000
1	0.834132000	-1.917757000	0.569489000
1	7.884949000	0.434510000	0.262813000
1	-1.623664000	-0.779060000	3.136640000
1	-4.335712000	-1.435842000	2.260093000
1	-0.802159000	-1.870354000	0.996114000
1	-0.446552000	-0.222469000	4.353478000
1	-3.648504000	-5.118241000	2.252209000
1	3.534941000	-3.930478000	-3.763477000
1	-6.066763000	-3.935742000	2.743173000
1	-6.360334000	-2.315464000	3.431687000
1	4.520049000	1.269950000	5.231493000
1	5.713338000	0.800852000	3.993074000
1	7.496758000	-0.520029000	1.709913000
1	5.169479000	-3.898804000	-3.046190000
1	2.167014000	0.020855000	4.867616000
1	8.335297000	-1.287688000	0.337712000
1	6.665808000	-2.820822000	-1.140340000
1	-2.615771000	-2.695284000	3.672230000
1	2.839849000	-3.804010000	-0.061844000
1	2.622888000	-4.759438000	-1.553293000
1	-3.866851000	-3.902928000	4.050912000
1	-0.295701000	-3.010678000	3.103358000
1	-4.084691000	-2.218208000	4.564041000
1	1.440635000	-2.998279000	2.695932000
1	0.891184000	-2.340245000	4.260092000
1	4.233488000	-4.654571000	-0.785290000
6	1.870386000	3.087823000	-2.663389000
1	1.953629000	4.060444000	-3.168761000
1	1.945061000	2.303146000	-3.435001000
1	0.867945000	3.027252000	-2.209496000

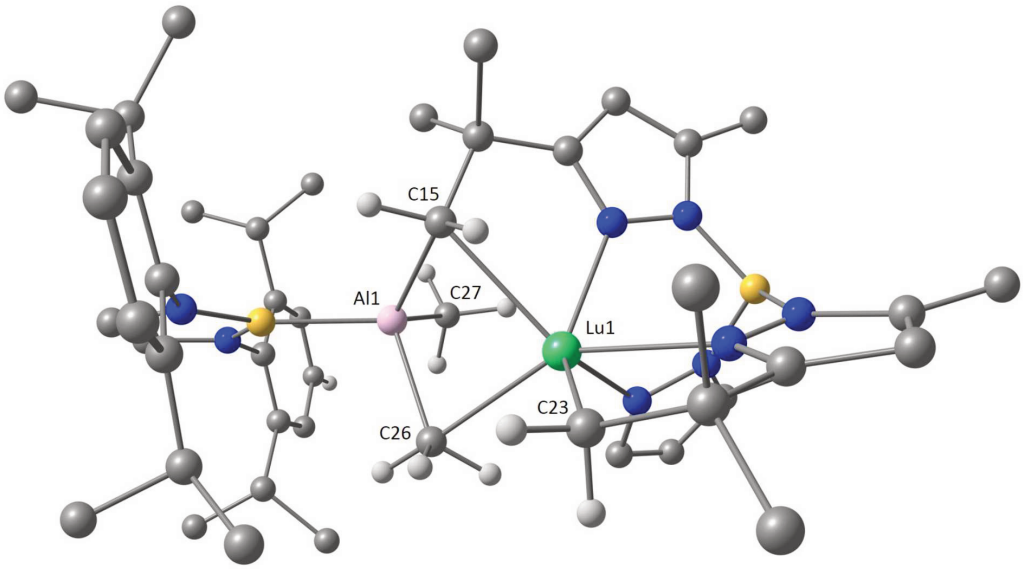

Figure S28. Optimized geometry for the DFT-optimized model system **2c**.

Table S5. Selected geometrical parameters for **2c** (distances in Å)

Lu1–C15	2.603	Al1–C15	2.166
Lu1–C23	2.373	Al1–C26	2.135
Lu1–C26	2.477	Al1–C27	2.011
Lu1···C27	3.678	Lu1···Al1	2.985

Cartesian Coordinates for **2c**:

6	-5.161503000	2.066689000	-3.782313000
6	-2.698362000	2.628352000	-3.909968000
6	-4.013334000	4.348230000	-1.809509000
6	-3.832789000	2.122628000	-3.003082000
6	-4.190970000	5.131250000	-0.671498000
6	-3.981548000	2.948692000	-1.730689000
6	-4.012152000	-3.033847000	-3.171517000
6	-1.507454000	-3.296010000	-3.266144000
6	3.496107000	3.837796000	-1.974323000
6	-4.337081000	4.521535000	0.572320000
6	-2.685020000	-2.785379000	-2.423817000
6	-4.129763000	2.344732000	-0.459813000
6	2.601279000	2.767999000	-2.055667000
6	-4.310376000	3.126503000	0.706229000
6	-5.374788000	0.238160000	-0.454485000
6	4.391964000	3.488947000	-0.962348000
6	5.556875000	4.268611000	-0.443042000
6	-0.500702000	2.378818000	0.330258000
6	-5.158896000	-1.097277000	-0.323374000
6	-2.745505000	-3.382524000	-1.021758000
6	-6.002645000	2.490927000	2.469975000
6	-0.123470000	0.108760000	-1.972215000
6	-2.297173000	-4.690473000	-0.792330000
6	-4.511648000	2.492258000	2.077493000
6	-3.317562000	-2.670078000	0.062088000
6	-3.670715000	3.163117000	3.176057000

6	-2.428743000	-5.292425000	0.457848000
6	-3.480016000	-3.277499000	1.331353000
6	2.394198000	-2.290669000	-1.709317000
6	-3.023901000	-4.592788000	1.503419000
6	0.134155000	-0.905062000	1.243387000
6	-0.543113000	0.333988000	3.361167000
6	-5.612387000	-3.084515000	2.673958000
6	-4.172120000	-2.564939000	2.488817000
6	1.851386000	0.306516000	2.664361000
6	3.705993000	1.479538000	3.106295000
6	4.698995000	-1.892147000	-0.879130000
6	4.384683000	-3.634232000	-2.651892000
6	3.762259000	-2.958441000	-1.409455000
6	4.806444000	2.269590000	3.737759000
6	0.568626000	-0.496811000	2.685954000
6	6.332137000	-0.603358000	-0.041850000
6	2.556041000	0.955721000	3.697117000
6	7.622405000	-0.021460000	0.438559000
6	6.086537000	-1.847800000	-0.626853000
6	-3.401300000	-2.684905000	3.813726000
6	3.581406000	-4.027861000	-0.305261000
6	0.827150000	-1.767342000	3.536459000
5	-3.061117000	-0.050889000	-0.156214000
5	4.709377000	1.413534000	0.639754000
13	-0.958802000	0.455924000	-0.038452000
71	1.886407000	-0.269254000	-0.574487000
7	-4.150896000	0.910138000	-0.358037000
7	2.917340000	1.812397000	-1.161204000
7	-3.789308000	-1.326745000	-0.140295000
7	4.027732000	2.265784000	-0.485604000
7	2.542286000	0.434799000	1.519202000
7	3.681998000	1.150166000	1.783761000
7	4.152018000	-0.731791000	-0.480243000
7	5.140934000	0.055092000	0.038350000
1	-5.470226000	3.076332000	-4.103854000
1	-2.928167000	3.617478000	-4.340457000
1	-5.056421000	1.439701000	-4.683721000
1	-2.545515000	1.933160000	-4.752049000
1	-3.901581000	4.834168000	-2.782063000
1	-5.969872000	1.644237000	-3.165452000
1	-4.213511000	6.220892000	-0.753803000
1	-3.978500000	-2.581089000	-4.176878000
1	-1.749759000	2.716000000	-3.356660000
1	-1.430146000	-2.709154000	-4.195839000
1	3.499131000	4.750655000	-2.561571000
1	-3.585776000	1.092903000	-2.695948000
1	-4.190205000	-4.116492000	-3.290595000
1	-1.640795000	-4.350571000	-3.561621000
1	-4.867836000	-2.600984000	-2.631743000
1	-0.548465000	-3.214830000	-2.730137000
1	-2.571340000	-1.694620000	-2.307813000
1	5.632173000	5.219771000	-0.989015000
1	-4.476084000	5.142959000	1.460374000
1	-0.804714000	3.000518000	-0.532367000
1	-6.309686000	0.767720000	-0.614793000
1	-1.009664000	0.501294000	-2.496183000
1	-6.387411000	3.522426000	2.548965000
1	-6.614853000	1.956211000	1.727344000
1	-1.843093000	-5.253935000	-1.609861000
1	-5.877921000	-1.910773000	-0.352010000
1	-1.041971000	2.785842000	1.202131000
1	5.450846000	4.496670000	0.629742000
1	0.572414000	2.575415000	0.503891000
1	6.505470000	3.722671000	-0.570367000
1	-4.005447000	4.194628000	3.377983000
1	0.702787000	0.695827000	-2.442066000
1	-0.010267000	-0.931990000	-2.333654000
1	-6.145570000	1.999827000	3.447347000
1	-4.183672000	1.442831000	2.000300000

1	-2.605081000	3.202040000	2.900943000
1	2.446260000	-1.858878000	-2.739511000
1	-2.072517000	-6.313884000	0.613657000
1	-3.762269000	2.599932000	4.119540000
1	-0.717300000	1.277201000	2.823023000
1	5.659002000	2.012793000	1.075168000
1	-6.210317000	-2.959253000	1.758592000
1	1.620451000	-3.079818000	-1.779429000
1	4.904677000	3.268918000	3.283081000
1	4.550244000	-2.898473000	-3.455807000
1	0.835450000	-1.711959000	0.895838000
1	7.857782000	0.928157000	-0.069593000
1	-1.486466000	-0.235135000	3.381196000
1	-4.231291000	-1.495393000	2.228877000
1	-0.775742000	-1.528188000	1.360811000
1	-0.275974000	0.579161000	4.402107000
1	-3.138512000	-5.077221000	2.476376000
1	3.701527000	-4.410094000	-3.034878000
1	-5.610612000	-4.157137000	2.933237000
1	-6.117881000	-2.538970000	3.488413000
1	4.596683000	2.401703000	4.808716000
1	5.781747000	1.765942000	3.638839000
1	7.600553000	0.182112000	1.522035000
1	5.353266000	-4.116018000	-2.424799000
1	2.279294000	1.041336000	4.743616000
1	8.442663000	-0.726188000	0.241254000
1	6.827668000	-2.614393000	-0.833256000
1	-2.357391000	-2.352227000	3.706895000
1	3.124065000	-3.586177000	0.595418000
1	2.917653000	-4.830905000	-0.667094000
1	-3.386770000	-3.722544000	4.187484000
1	-0.083143000	-2.387110000	3.585211000
1	-3.880061000	-2.064801000	4.589564000
1	1.631490000	-2.377799000	3.094543000
1	1.123643000	-1.508588000	4.566825000
1	4.544992000	-4.479580000	-0.015423000
1	1.739792000	2.644525000	-2.707451000

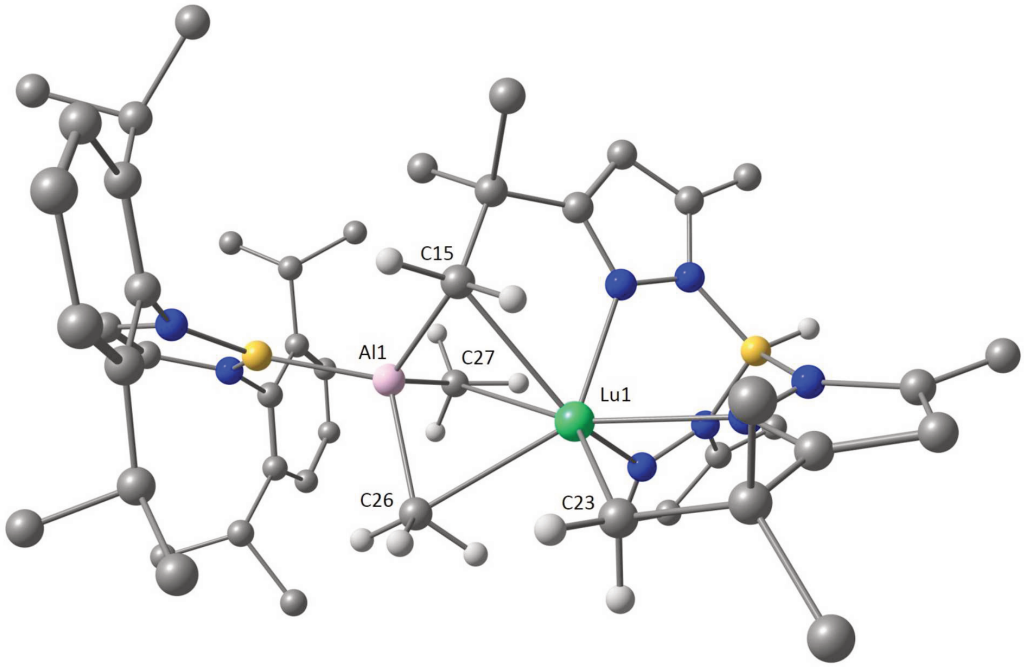

Figure S29. Optimized geometry for the DFT-optimized model system **2d** (partial optimization of **2c** with a fixed Lu-Al-B-angle of 174.0°).

Cartesian Coordinates for **2d**:

6	-4.996626000	2.527710000	-3.576405000
6	-2.515391000	2.603754000	-4.055498000
6	-3.119018000	4.583670000	-1.886265000
6	-3.585605000	2.348211000	-2.981707000
6	-2.993228000	5.415781000	-0.776476000
6	-3.404879000	3.218411000	-1.742918000
6	-4.782258000	-2.472692000	-3.047572000
6	-2.403710000	-3.290879000	-3.259515000
6	3.931927000	3.722554000	-1.671803000
6	-3.152259000	4.891276000	0.503748000
6	-3.403363000	-2.550585000	-2.359271000
6	-3.559360000	2.700005000	-0.435066000
6	3.008509000	2.708037000	-1.938829000
6	-3.439032000	3.533432000	0.702410000
6	-5.249437000	0.946171000	-0.192535000
6	4.656688000	3.276291000	-0.565058000
6	5.773067000	3.965596000	0.150940000
6	-0.076248000	1.886456000	0.018534000
6	-5.339026000	-0.400467000	-0.035524000
6	-3.541897000	-3.157585000	-0.966979000
6	-5.066287000	3.345825000	2.623101000
6	-0.200575000	-0.301125000	-2.266683000
6	-3.404686000	-4.541521000	-0.792252000
6	-3.651440000	3.002689000	2.115455000
6	-3.886182000	-2.368173000	0.160112000
6	-2.594087000	3.506818000	3.111588000
6	-3.622252000	-5.141428000	0.446064000
6	-4.124994000	-2.967098000	1.422742000
6	2.448077000	-2.209728000	-2.023903000
6	-3.985945000	-4.358504000	1.537077000
6	0.114050000	-1.337264000	0.933400000

6	-0.778008000	-0.202410000	3.031981000
6	-6.079567000	-2.305371000	2.889110000
6	-4.563507000	-2.162269000	2.642936000
6	1.671762000	-0.190748000	2.582310000
6	3.474050000	0.942004000	3.280085000
6	4.675617000	-2.046600000	-0.952428000
6	4.467778000	-3.508320000	-2.972087000
6	3.754800000	-2.983689000	-1.705143000
6	4.521300000	1.658436000	4.069827000
6	0.398946000	-0.999741000	2.431042000
6	6.274675000	-0.944722000	0.170174000
6	2.297070000	0.342300000	3.728031000
6	7.539657000	-0.480547000	0.817093000
6	6.036575000	-2.097298000	-0.581786000
6	-3.802227000	-2.550907000	3.922566000
6	3.434138000	-4.187753000	-0.787500000
6	0.573507000	-2.312653000	3.236432000
5	-3.052602000	0.121587000	-0.146998000
5	4.683942000	1.078896000	0.910081000
13	-0.904883000	0.051003000	-0.324199000
71	1.918652000	-0.310203000	-0.692724000
7	-3.899248000	1.312548000	-0.260198000
7	3.150162000	1.696278000	-1.063520000
7	-4.050272000	-0.947015000	0.004541000
7	4.171705000	2.052236000	-0.212561000
7	2.431888000	0.081020000	1.509895000
7	3.540945000	0.770824000	1.928331000
7	4.136485000	-0.921443000	-0.455593000
7	5.104306000	-0.247808000	0.235081000
1	-5.153010000	3.570483000	-3.902329000
1	-2.620368000	3.603157000	-4.510081000
1	-5.133973000	1.872182000	-4.452734000
1	-2.609902000	1.864907000	-4.868233000
1	-2.995475000	5.004212000	-2.887254000
1	-5.776679000	2.279787000	-2.840077000
1	-2.769299000	6.477216000	-0.910143000
1	-4.690096000	-2.014054000	-4.046525000
1	-1.498739000	2.527574000	-3.638247000
1	-2.239514000	-2.718630000	-4.186883000
1	4.063242000	4.660794000	-2.201634000
1	-3.493058000	1.298169000	-2.658693000
1	-5.207928000	-3.483092000	-3.173567000
1	-2.775017000	-4.286464000	-3.556384000
1	-5.492498000	-1.871093000	-2.460082000
1	-1.428858000	-3.426231000	-2.764575000
1	-3.039189000	-1.517431000	-2.232920000
1	5.955384000	4.944592000	-0.314734000
1	-3.051715000	5.550846000	1.369176000
1	-0.389271000	2.574884000	-0.787685000
1	-6.046841000	1.680086000	-0.267669000
1	-1.026776000	0.254007000	-2.750536000
1	-5.205832000	4.439294000	2.676861000
1	-5.843577000	2.936460000	1.959762000
1	-3.133048000	-5.165208000	-1.646038000
1	-6.227999000	-1.019474000	0.038454000
1	-0.539975000	2.271113000	0.944486000
1	5.537697000	4.130254000	1.214637000
1	1.005034000	2.057444000	0.164346000
1	6.708926000	3.385534000	0.107626000
1	-2.690844000	4.589683000	3.298385000
1	0.691260000	0.179391000	-2.737830000
1	-0.231408000	-1.324413000	-2.671227000
1	-5.226771000	2.932170000	3.633053000
1	-3.570066000	1.904520000	2.064640000
1	-1.571191000	3.317774000	2.749149000
1	2.607398000	-1.657840000	-2.983885000
1	-3.512934000	-6.223098000	0.557985000
1	-2.715133000	2.996828000	4.081481000
1	-0.885911000	0.777708000	2.544478000

1	5.612209000	1.589275000	1.482795000
1	-6.669680000	-1.985012000	2.017808000
1	1.647774000	-2.937476000	-2.258814000
1	4.651777000	2.697464000	3.725720000
1	4.739508000	-2.675309000	-3.640972000
1	0.919259000	-2.029933000	0.576245000
1	7.871078000	0.492371000	0.417630000
1	-1.720100000	-0.756472000	2.900042000
1	-4.354629000	-1.100716000	2.430535000
1	-0.739953000	-2.045804000	0.933641000
1	-0.630034000	-0.030599000	4.110921000
1	-4.164586000	-4.836485000	2.503260000
1	3.793956000	-4.183466000	-3.524903000
1	-6.339300000	-3.355666000	3.106299000
1	-6.389216000	-1.693520000	3.753009000
1	4.230639000	1.684452000	5.129663000
1	5.502489000	1.161936000	3.994940000
1	7.423578000	-0.366005000	1.907436000
1	5.390375000	-4.068525000	-2.732795000
1	1.952656000	0.300698000	4.757129000
1	8.338952000	-1.212841000	0.634685000
1	6.764862000	-2.866866000	-0.820547000
1	-2.711961000	-2.528869000	3.774529000
1	2.911599000	-3.857923000	0.125517000
1	2.778226000	-4.898145000	-1.318135000
1	-4.074523000	-3.562488000	4.267058000
1	-0.340254000	-2.925301000	3.162993000
1	-4.051192000	-1.851579000	4.737751000
1	1.414031000	-2.906236000	2.841608000
1	0.769385000	-2.111802000	4.303237000
1	4.349526000	-4.723402000	-0.484168000
1	2.241585000	2.660588000	-2.709199000

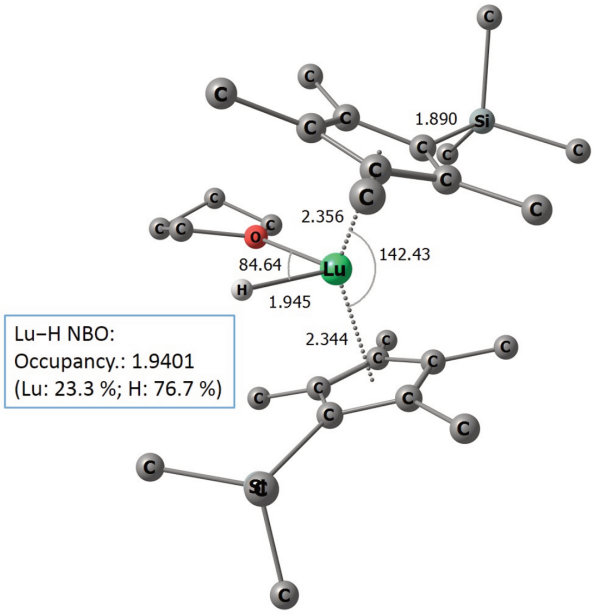

Figure S30. Optimized geometry, salient geometrical parameters, and Lu–H NBO composition for the DFT-optimized model system $[(C_5Me_4SiMe_3)_2LuH(THF)]$ (starting coordinates were taken from the X-ray structure determination, published in the following reference: Y. Takenaka, Z. Hou, *Organometallics* **2009**, *28*, 5196).

Cartesian Coordinates for the DFT-optimized model system $[(C_5Me_4SiMe_3)_2LuH(THF)]$ from Figure S30:

6	1.589470000	-3.215978000	0.592630000
6	4.020655000	-2.481533000	-1.553944000
6	-1.818673000	-3.120909000	-0.498476000
6	0.251058000	-2.231790000	-2.773786000
6	1.578419000	-1.781397000	1.046681000
6	-1.629647000	-1.718289000	-1.015640000
6	0.046939000	-2.140984000	3.137068000
6	-0.671821000	-1.335018000	-1.999113000
6	5.455427000	-0.566210000	0.298528000
6	-3.946538000	-1.771610000	1.818477000
6	0.913763000	-1.328814000	2.218019000
6	-5.460664000	-1.276025000	-0.808565000
6	2.377963000	-0.693096000	0.516394000
6	3.795163000	0.505507000	-2.057408000
6	-2.477805000	-0.585789000	-0.729715000
6	-0.919371000	0.032131000	-2.347867000
6	-0.255853000	0.734217000	-3.501732000
6	1.301393000	0.028160000	2.459483000
6	2.201104000	0.414270000	1.434112000
6	-2.030759000	0.486584000	-1.581888000
6	0.936846000	0.820700000	3.682014000
6	2.965072000	1.711629000	1.430954000
6	-4.596010000	1.069493000	0.970957000
6	-2.690222000	1.831254000	-1.732773000
6	0.794718000	3.173306000	-1.036751000
6	-0.496037000	3.315291000	0.978679000
6	0.865662000	4.598062000	-0.498079000
6	-0.424589000	4.692073000	0.329800000
1	4.159419000	-3.310502000	-0.842867000
1	2.468514000	-3.749336000	1.000279000
1	-1.051623000	-3.800111000	-0.898101000
1	0.700029000	-3.757155000	0.948372000
1	4.923770000	-2.432602000	-2.187428000
1	1.628884000	-3.317190000	-0.500140000
1	0.442439000	-3.183590000	-2.257771000
1	3.170532000	-2.729000000	-2.208033000
1	-2.799774000	-3.525751000	-0.804480000
1	-1.776187000	-3.185608000	0.600515000
1	-0.187004000	-2.482742000	-3.758933000
1	1.225592000	-1.757205000	-2.972407000
1	-0.419027000	-2.996431000	2.623498000
1	0.632200000	-2.551649000	3.981429000
1	-3.867137000	-2.836112000	1.549744000
1	5.545517000	-1.328485000	1.090217000
1	-5.234381000	-2.287133000	-1.186267000
1	6.326745000	-0.669424000	-0.371246000
1	-4.862252000	-1.649494000	2.422832000
1	-6.415542000	-1.327328000	-0.257542000
1	-0.763077000	-1.528863000	3.564486000
1	-3.084898000	-1.500035000	2.448940000
1	4.661600000	0.369831000	-2.727408000
1	-0.495167000	0.230205000	-4.456551000
1	5.516102000	0.422921000	0.778881000
1	2.883162000	0.411783000	-2.670664000
1	-5.609406000	-0.621459000	-1.683615000
1	0.845258000	0.750141000	-3.425780000
1	3.841785000	1.537030000	-1.670561000
1	1.518117000	0.483572000	4.561256000
1	-1.368094000	0.488012000	1.637989000
1	-0.595206000	1.776513000	-3.601143000
1	-0.132040000	0.719327000	3.926258000
1	3.807339000	1.677086000	2.146518000
1	3.394784000	1.943081000	0.444890000
1	-5.467961000	0.926867000	1.632895000
1	-3.684337000	1.737896000	-2.206532000

1	-3.787539000	1.521751000	1.567903000
1	-4.893948000	1.771331000	0.177070000
1	1.148913000	1.894230000	3.554315000
1	-2.099651000	2.504684000	-2.373854000
1	1.776859000	2.708254000	-1.208740000
1	2.338853000	2.568571000	1.730358000
1	-2.846525000	2.337825000	-0.767584000
1	0.200334000	3.116758000	-1.963760000
1	0.104713000	3.260146000	1.902735000
1	-1.507825000	2.948589000	1.195765000
1	1.750198000	4.725367000	0.147663000
1	0.919091000	5.340599000	-1.307812000
1	-1.294380000	4.855659000	-0.327613000
1	-0.400513000	5.497025000	1.078792000
8	0.102007000	2.400322000	-0.006041000
14	3.839402000	-0.807807000	-0.676577000
14	-4.059695000	-0.627582000	0.307962000
71	-0.127791000	0.054980000	0.203716000

Paper IV: 1,3-Diene Polymerization Mediated by Homoleptic Tetramethylaluminates of the Rare-Earth Metals

© (2018) by the authors, This article is reprinted without modifications under the terms and conditions of the Creative Commons Attribution (CC BY 4.0, http://creativecommons.org/licences/4.0/) and has been published as:

"1,3-Diene Polymerization Mediated by Homoleptic Tetramethylaluminates of the Rare-Earth Metals"

by
Christoph O. Hollfelder, Lars N. Jende, Dominic Diether, Theresa Zelger, Rita Stauder, Cäcilia Maichle-Mössmer and Reiner Anwander

in
Catalysts, **2018**, *8*, 61, ISSN: 2073-4344
doi:10.3390/catal8020061.

It is available free of charge at https://www.mdpi.com/2073-4344/8/2/61.

catalysts

MDPI

Article

1,3-Diene Polymerization Mediated by Homoleptic Tetramethylaluminates of the Rare-Earth Metals

Christoph O. Hollfelder, Lars N. Jende, Dominic Diether, Theresa Zelger, Rita Stauder, Cäcilia Maichle-Mössmer and Reiner Anwander *

Institut für Anorganische Chemie, Eberhard-Karls-Universität Tübingen, 72076 Tübingen, Germany; christoph.hollfelder@anorg.uni-tuebingen.de (C.O.H.); lars.jende@univ-rennes1.fr (L.N.J.); dominic.diether@anorg.uni-tuebingen.de (D.D.); theresa.zelger@student.uni-tuebingen.de (T.Z.); rita.stauder@student.uni-tuebingen.de (R.S.); caecilia.maichle-moessmer@uni-tuebingen.de (C.M.-M.)
* Correspondence: reiner.anwander@uni-tuebingen.de; Tel.: +49-7071-29-72069

Received: 30 December 2017; Accepted: 23 January 2018; Published: 3 February 2018

Abstract: During the past two decades homoleptic tetramethylaluminates of the trivalent rare-earth metals, $Ln(AlMe_4)_3$, have emerged as useful components for efficient catalyst design in the field of 1,3-diene polymerization. Previous work had focused on isoprene polymerization applying $Ln(AlMe_4)_3$ precatalysts with Ln = La, Ce, Pr, Nd, Gd and Y, in the presence of Et_2AlCl as an activator. Polymerizations employing $Ln(AlMe_4)_3$ with Ln = La, Y and Nd along with borate/borane co-catalysts $[Ph_3C][B(C_6F_5)_4]$, $[PhNMe_2H][B(C_6F_5)_4]$ and $[B(C_6F_5)_3]$ were mainly investigated for reasons of comparison with ancillary ligand-supported systems (cf. half-sandwich complexes). The present study investigates into a total of eleven rare-earth elements, namely Ln = La, Ce, Pr, Nd, Gd, Tb, Dy, Ho, Y, Er and Lu. A full overview on the polymerization behavior of $Ln(AlMe_4)_3$ in the presence of perfluorinated borate/borane cocatalysts and R_2AlCl-type activators (R = Me, Et) is provided, probing the monomers isoprene and 1,3-butadiene (and preliminary ethylene). Virtually complete *cis*-1,4-selectivities are obtained for several catalyst/cocatalyst combinations (e.g., $Gd(AlMe_4)_3/Me_2AlCl$, >99.9%). Insights into the 'black box' of active species are obtained by indirect observations via screening of pre-reaction time and cocatalyst concentration. The microstructure of the polydienes is investigated by combined $^1H/^{13}C$ NMR and ATR-IR spectroscopies. Furthermore, the reaction of $[LuMe_6(Li(thf)_x)_3]$ with $AlMe_3$ has been applied as a new strategy for the efficient synthesis of $Lu(AlMe_4)_3$. The solid-state structures of $Gd(AlMe_4)_3$ and $Tb(AlMe_4)_3$ are reported.

Keywords: lanthanide; rare-earth elements; synthetic rubber; 1,3-diene polymerization; alkyl; aluminum; tetramethylaluminate

1. Introduction

Since its discovery and development in the 1950s and 1960s, Ziegler-Natta polymerization catalysis has undergone various empirical optimizations regarding the composition of the catalyst mixtures applied [1–3]. While the actual active (bimetallic) catalysts/sites have remained elusive and are subject of ongoing research, the properties of the industrially fabricated polymer products have been tailored by choice of component concentrations and additives [1,4–6].

'Ziegler Mischkatalysatoren' gain their exceptional reactivity through the cooperativity of a transition metal component and an organoaluminum(magnesium) activator [1–5]. Industrial 1,3-diene polymerization processes also take advantage of Ziegler-type catalysts and ternary mixtures like carboxylate-based $Nd(O_2CR)_3/Et_3Al_2Cl_3/iBu_2AlH$ (1:1:8) or $Nd(O_2CR)_3/Et_3Al_2Cl_3/AliBu_3$ (1:1:30) [6] proved superior to ternary 'no-less-complex' d-transition metal-based catalyst systems in terms of activity and stereospecificity issues [6–9]. On the other hand, thermally stable homoleptic

tetramethylaluminates of the rare-earth metals, $Ln(AlMe_4)_3$, feature a preset heterobimetallic arrangement, per se simplifying the assessment of structure reactivity relationships (ternary versus binary catalyst system) [4,10–13]. Especially, when applying dialkylaluminum chlorides as cocatalysts/activators, complexes $Ln(AlMe_4)_3$ display one of the closest possible modelling approaches to in situ generated Ziegler-type systems [14,15]. Previous studies on the use of homoleptic $Ln(AlMe_4)_3$ as precatalysts for isoprene polymerization have been reported on several occasions, some of them even out of the main spotlight of the respective article, so that they are easily missed [11–13,16–18]. Accordingly, Et_2AlCl has been applied as an activator for $Ln(AlMe_4)_3$ (Ln = La, Ce, Pr, Nd, Gd and Y) [11–13,16,17]. Moreover, investigations using borate and borane cocatalysts $[Ph_3C][B(C_6F_5)_4]$ (**A**), $[PhNMe_2H][B(C_6F_5)_4]$ (**B**) and $[B(C_6F_5)_3]$ (**C**) have been performed for reasons of comparison [13,18]. Herein, we present a full account of the polymerization performance of complexes $Ln(AlMe_4)_3$ giving consideration to eleven different rare-earth metals (La, Ce, Pr, Nd, Gd, Tb, Dy, Ho, Y, Er and Lu), as well as borate (**A**, **B**)/borane cocatalysts (**C**) and R_2AlCl activators (R = Me (**D**), Et (**E**)). The redox-active rare-earth elements Sm, Eu and Yb, favoring the formation of divalent alkylaluminate species [19], are not included in the present study. The active species involved in 1,3-diene polymerization reactions are investigated indirectly by screening of the polymerizations at various conditions applying $Nd(AlMe_4)_3$.

Furthermore, a new protocol for efficiently synthesizing homoleptic methylaluminates of the smaller lanthanides, e.g., $Lu(AlMe_4)_3$, is introduced and active catalyst systems derived from $Nd(AlMe_4)_3$ are initially probed for the polymerization of ethylene.

2. Results and Discussion

2.1. Catalyst Systems

2.1.1. Precatalyst Synthesis and Structural Characterization

Homoleptic tris(tetramethylaluminate)s of the rare-earth elements are routinely accessible in a two-step synthesis starting from the tetrahydrofuran (thf) adducts of the commercially available chlorides. Salt metathesis with lithium dimethylamide in THF gives ate complexes $[Ln(NMe_2)_3(LiCl)_3]$ ($\mathbf{1^{Ln}}$) which are treated subsequently with an excess of $AlMe_3$ in *n*-hexane to afford $Ln(AlMe_4)_3$ ($\mathbf{2^{Ln}}$; Ln = La [11,12], Ce [12,20], Pr [12], Nd [12,21], Gd [11], Tb (this work), Dy [22], Ho [12], Y [12,21], Er [20] and Lu [12] (this work)) envisaged along with dimeric $[Me_2Al(\mu\text{-}NMe_2)]_2$ (Scheme 1, route **I**) [4,11–13,20–23].

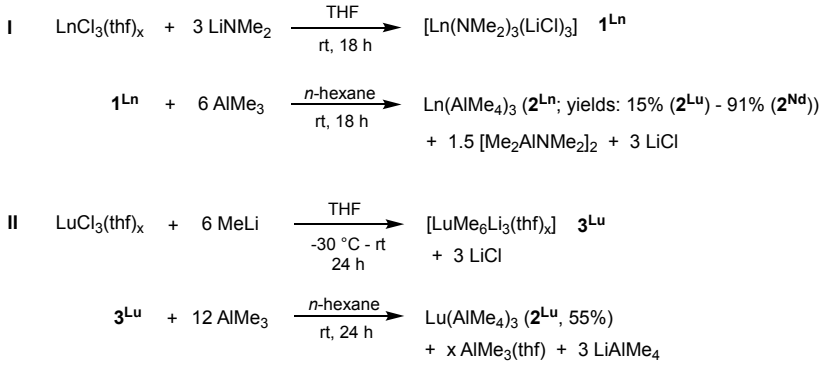

Scheme 1. Synthesis of homoleptic rare-earth metal(III) tetramethylaluminates (Ln = La ($\mathbf{2^{La}}$), Ce ($\mathbf{2^{Ce}}$), Pr ($\mathbf{2^{Pr}}$), Nd ($\mathbf{2^{Nd}}$), Gd ($\mathbf{2^{Gd}}$), Tb ($\mathbf{2^{Tb}}$), Dy ($\mathbf{2^{Dy}}$), Ho ($\mathbf{2^{H\circ}}$), Y ($\mathbf{2^{Y}}$), Er ($\mathbf{2^{Er}}$) and Lu ($\mathbf{2^{Lu}}$)).

Catalysts **2018**, *8*, 61

The major drawback of amide elimination protocol **I** is that the $AlMe_3$-mediated $[NMe_2] \rightarrow [AlMe_4]$ exchange in *n*-hexane provides decent yields only for the larger rare-earth metal ions [12]. In case of the smallest rare-earth metal, lutetium, purification requires subsequent sublimation allowing isolation of the desired $Lu(AlMe_4)_3$ only in ca. 15% yield [24]. Therefore, a new synthesis approach was developed, based on the trianionic hexamethylate ate complexes $[LnMe_6\{Li(Do)_x\}_3]$ (Do = tetramethylethylenediamine (tmeda), dimethoxyethane (dme), thf, diethyl ether) reported by Schumann et al. [25–27]. Treatment of $[LuMe_6\{Li(thf)_x\}_3]$ with excess of $AlMe_3$ produced the homoleptic methylaluminate complex $Lu(AlMe_4)_3$ ($\mathbf{2^{Lu}}$) in moderate crystalline yields (Scheme 1, route **II**). The side-products $LiAlMe_4$ and donor-coordinated $AlMe_3$ can easily be removed via filtration and evaporation, respectively. The absence of ate complex formation is due to the high steric saturation of the metal center by the tetramethylaluminate moieties, which show additional agostic or coordinative interactions only for the larger rare-earth metal ions [12].

The solid-state structures of complexes $\mathbf{2^{Ln}}$ employed in this study were known to all rare-earth elements except gadolinium and terbium. Putative $\mathbf{2^{Sc}}$, $\mathbf{2^{Pm}}$, and $\mathbf{2^{Eu}}$ (and hence their crystal structures) are not accessible due to reasons of stereoelectronic mismatch (Sc), radioactivity issues (Pm), and redox instability (Eu), respectively. Since complex $\mathbf{2^{Gd}}$ gave a catalyst system of exceptional performance, its crystal structure was determined (Figure 1a, Table S4.1, Supplementary Materials). To complete the series of accessible crystal structures we include also the data of $\mathbf{2^{Tb}}$ (Figure S4.1, Table S4.1, Supplementary Materials).

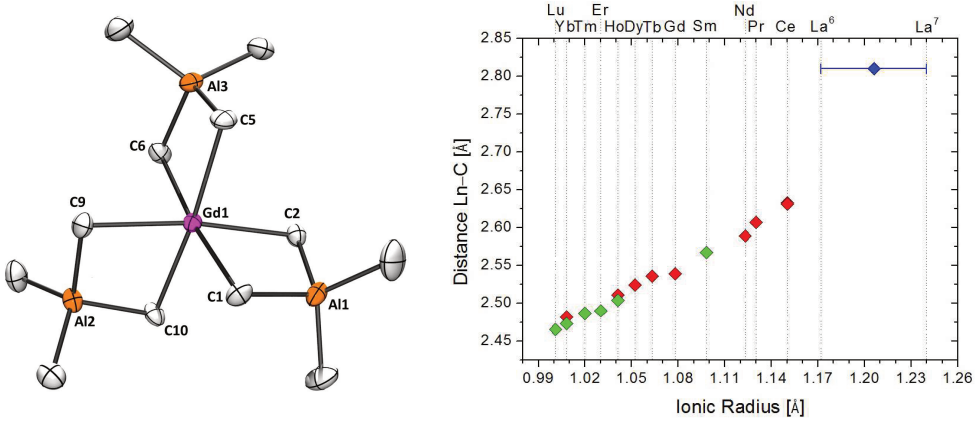

(**a**) (**b**)

Figure 1. (**a**) ORTEP view of one of two individuals in the unit cell of $\mathbf{2^{Gd}}$. Atoms are represented by atomic displacement ellipsoids at the 50% level. Hydrogen atoms are omitted for clarity. Selected distances (Å) and angles (deg): Gd1—C1 2.543(4), Gd1—C2 2.542(4), Gd1—C5 2.550(4), Gd1—C6 2.529(4), Gd1—C9 2.529(4), Gd1—C10 2.552(4), average Gd1—CX (X = 1, 2, 5, 6, 9, 10) 2.539, Al1—C1, 2.082(4), Al1—C2, 2.086(4); C1—Gd1—C2 83.92(12), C1—Gd1—C5 92.43(13), C1—Gd1—C6 174.78(13), C1—Al1—C2 109.30(16). $\mathbf{2^{Tb}}$ crystallizes isostructurally, see Section S4, Supplementary Materials. (**b**) Overview chart on average distances of Ln—C vs. the ionic radii of the rare-earth metal trivalent cations according to Shannon and Prewitt [28,29] with a coordination number (CN) of 6. In case of $\mathbf{2^{La}}$, featuring η^3-coordination of one of the tetramethylaluminate moieties [12], the span of CN = 6 to CN = 7 is given. Crystal structures in space group $P2_1/c$ are represented by red symbols, those in $C2/c$ by green symbols and that of $\mathbf{2^{La}}$, not following the general motifs due to the coordination of one additional methyl group and crystallizing in $P2_1/n$, by a blue symbol. Data are taken from references [12,19–22] and this work.

Figure 1b gives an overview on the Ln—C distances of all known $\mathbf{2}^{\mathbf{Ln}}$, thus displaying the first comprehensive structural data compilation on rare-earth metal alkyl complexes of the same type. While the smaller lanthanides show a tendency towards crystallization as blocks in space group $C2/c$ (green symbols) the larger representatives crystallize as needles in space group $P2_1/c$ (red symbols, two individuals per unit cell). The largest rare-earth metal center lanthanum adopts a different molecular structure (7- instead of 6-coordinate La(III) centers; space group $P2_1/n$ [12], marked in blue). The structures of $\mathbf{2}^{\mathbf{Gd}}$ and $\mathbf{2}^{\mathbf{Tb}}$ added to the series in this study (see Section S4, Supplementary Materials) are part of the first group and show the expected Ln—C distances to fit the linear increase with the ionic radii (Figure 1b). For Ln = Ho and Yb both crystal habits/modifications exist and were achieved by applying different crystallization parameters [19,20]. In case of Ln = Ce, two modifications in space group $P2_1/c$ are known [19,20].

2.1.2. Activation by Cationizing Cocatalysts

In order to activate the precatalysts for diene polymerization, the five most common cationizing agents were applied. Organoperfluoroborates and –borane $[Ph_3C][B(C_6F_5)_4]$ (**A**), $[PhNMe_2H][B(C_6F_5)_4]$ (**B**) and $B(C_6F_5)_3$ (**C**), respectively, cationize neutral homoleptic complexes $\mathbf{2}^{\mathbf{Ln}}$ following ligand abstraction (**A**, **C**) and protonolysis (**B**) pathways (Scheme 2, upper part) [30–32]. Similar species were suggested to form in the silylamide-based catalyst system $Nd[N(SiMe_3)_2]_3$/**B**/Al*i*Bu_3 (1:1:10) employed for 1,3-butadiene polymerization in heptane at 70 °C (*cis*:*trans* = 86.5:11) [33].

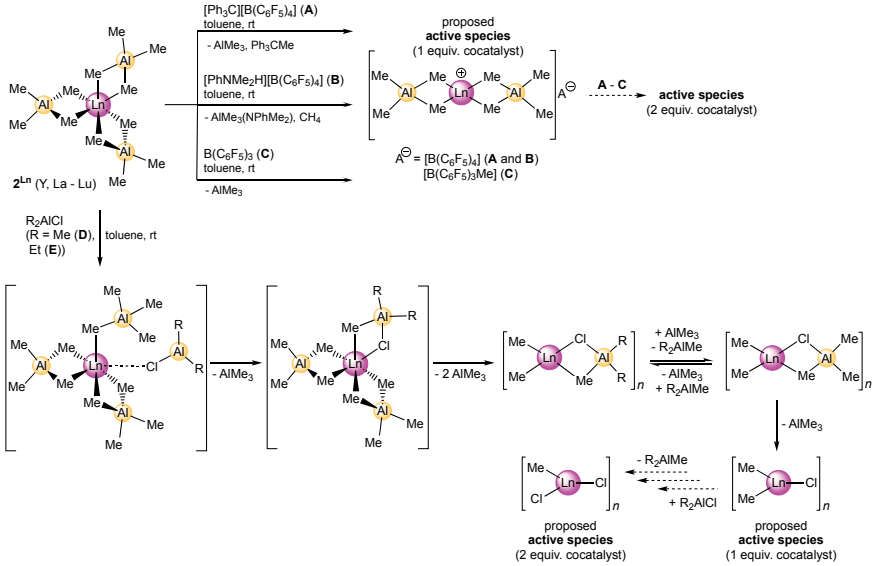

Scheme 2. Scenario of the activation of homoleptic rare-earth metal(III) tetramethylaluminates $\mathbf{2}^{\mathbf{Ln}}$ by cocatalysts **A**–**E** (**A** = $[Ph_3C][B(C_6F_5)_4]$, **B** = $[PhNMe_2H][B(C_6F_5)_4]$, **C** = $B(C_6F_5)_3$, **D** = Me_2AlCl, **E** = Et_2AlCl), lower part adapted from ref. [10]. Activation side-product $AlMe_3(NPhMe_2)$, obtaind via activation of $\mathbf{2}^{\mathbf{Ln}}$ with **B** is according to previous findings [31,32].

In contrast to cocatalysts **A**–**C**, R_2AlCl-based activators (**D**, R = Me; **E**, R = Et) are supposed to cationize the precatalysts by formation of large, multimetallic systems. It is presumed, that R_2AlCl replaces $AlMe_3$ in the aluminate precursors and that larger clusters form by chlorido bridging, as it has been observed for lanthanide half-sandwich complexes carrying tetramethylaluminate moieties and for lanthanidocene model systems for Ziegler-Natta catalysis [4,32,34–36], as well as for lanthanide

mixed silylamide/chloride complexes [13]. With release of R_2AlMe multimetallic species are formed (Scheme 2) [4,13,35]. As the precursor carries three $[AlMe_4]^-$ moieties, the exchange of $AlMe_3$ vs. R_2AlCl can happen multiple times. Temporary re-coordination of R_2AlMe and therefore exchange of a methyl moiety in the final active species for R cannot be ruled out. This causes the presence of several distinct (cationic) clusters. As these are all assumed active species in diene polymerization with different polymerization rates, high PDI values have to be expected for the polymer products. Equilibria between clusters of different sizes could even provide enhanced complexity to these systems. It has to be mentioned, that coordination of comparably bulky substrates like monomer molecules is for all these reasons likely to have a strong impact on the structure/agglomeration of these systems. Therefore, the active initiating and propagating species might differ markedly. Interestingly, elemental analysis of the catalysts obtained from $\mathbf{2^{Nd}}$ or $\mathbf{2^{Y}}$ and **E** showed very low aluminium contents (<6%) [13], which indicates that the ratio n(Al)/n(Ln) in the active species is far smaller than 1, implying the active species being close to $[LnMe_xCl_y]_n$ (x + y = 3), shown in the lower part of Scheme 2.

2.2. Isoprene Polymerization Catalysis

2.2.1. Polymers Obtained at Standard Conditions

Previous isoprene polymerization reactions applying homoleptic complexes $\mathbf{2^{Ln}}$ were routinely run for 24 h revealing full conversion. In order to better assess the polymerization rate, in this study, a period of only 1 h was chosen as standard reaction time. Prior to monomer addition, the precatalyst and 1 or 2 equiv. of the respective cocatalyst were allowed to react for 30 min to ensure complete activation. For further details on the polymerization procedures, see Section 3.3.

Activation by a Single Equivalent of Borate/Borane. Overviewing the polymer data obtained with precatalysts $\mathbf{2^{Ln}}$ activated by borates/borane **A**–**C** (Figure 2a–c,f–h and Figure 3a–c; Tables S1.1.1–1.1.3, Supplementary Materials) shows high yields with both 1 and 2 equiv. of the respective cocatalyst after 1 h.

The microstructures revealed an overall increasing *cis*-content from Ce to Lu (from 44% to 77% (**A**), 44% to 78% (**B**) and, less steadily from 55% to 74% (**C**)), a decreasing *trans*-content (from 52% to 17% (**A**), 53% to 17% (**B**) and less steadily from 60% (La) to 28% (**C**)), a maximum of the 3,4-content for $\mathbf{2^{Dy}}$/**A** and $\mathbf{2^{Ho}}$/**B**, as well as a constantly levelling 3,4-content at <5% in case of cocatalyst **C** (Figure 2a–c). These findings might seem counterintuitive, as larger ions should provide more steric space for monomer coordination and the growing polymer chain and therefore favor *cis*-selectivity. As a clear identification of the active species was not successful so far, due to the paramagnetic character of most of the lanthanide ions and the low tendency of the active species toward crystallization, active species elucidation remains challenging. A reasonable interpretation of this polymerization behavior seems to be that solvent [4,5,13,37], pre-reaction side products (e.g., Ph_3CMe (**A**) and $PhNMe_2$ (**B**): Ln(III)—arene coordination) [38–40], or even anion coordination (e.g., via Ln(III)—F interactions) [41] come into play. Furthermore, dimerization might take place or a η^2-to-η^3 coordination switch of the remaining tetramethylaluminate moiety, which tendency seems more pronounced for the larger lanthanides as found for the neutral precatalysts [4,10,12]. Interestingly, the chain length/molecular weight averages of the obtained polymers were quite different throughout the series, revealing no clearly observable trend, although, a maximum in M_n seems likely for $\mathbf{2^{Dy}}$/**A** and $\mathbf{2^{Ho}}$/**B** (Figure 3a–c). Maximum PDIs were obtained for the smallest Ln(III) centers. In case of cocatalyst **C**, an increasing degree of polymerization and PDI was found with decreasing Ln ion size.

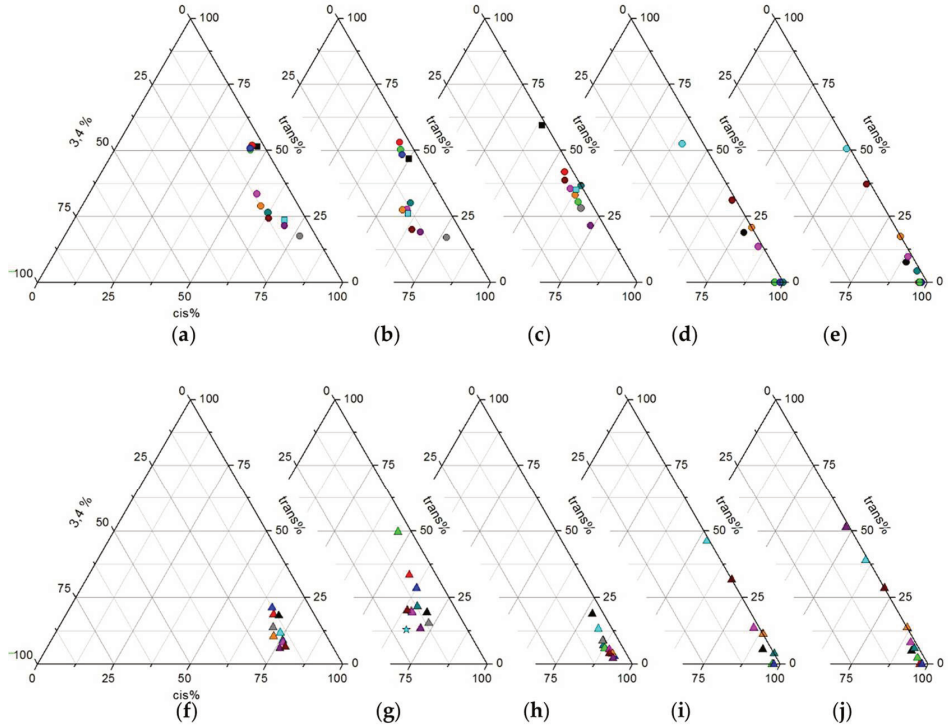

Figure 2. Ternary diagrams representing the microstructure of the polyisoprenes obtained from $Ln(AlMe_4)_3$ ($\mathbf{2^{Ln}}$). Panels (**a**–**j**) give details on the selectivity obtained by the application of a certain cocatalyst (**A**–**E** (**a**–**e**) and 2 equiv. of **A**–**E** (**f**–**j**); **A** = $[Ph_3C][B(C_6F_5)_4]$, **B** = $[PhNMe_2H][B(C_6F_5)_4]$, **C** = $B(C_6F_5)_3$, **D** = Me_2AlCl, **E** = Et_2AlCl). Results for the addition of 1 equiv. of cocatalyst per $\mathbf{2^{Ln}}$ after 1 h are shown by circles, 2 equiv. by triangles. If such results were not available, microstructures of reaction times of 24 h are shown marked with squares and stars, respectively. Complexes $\mathbf{2^{Ln}}$ are color-coded regarding the Ln as follows: black (La), red (Ce), green (Pr), blue (Nd), teal (Gd), pink (Tb), orange (Dy), brown (Ho), cyan (Y), violet (Er) and grey (Lu). For a more traditional compilation of the polymer data in table form, sorted by precatalyst, see Tables S1.2.1—S1.2.11, Supplementary Materials.

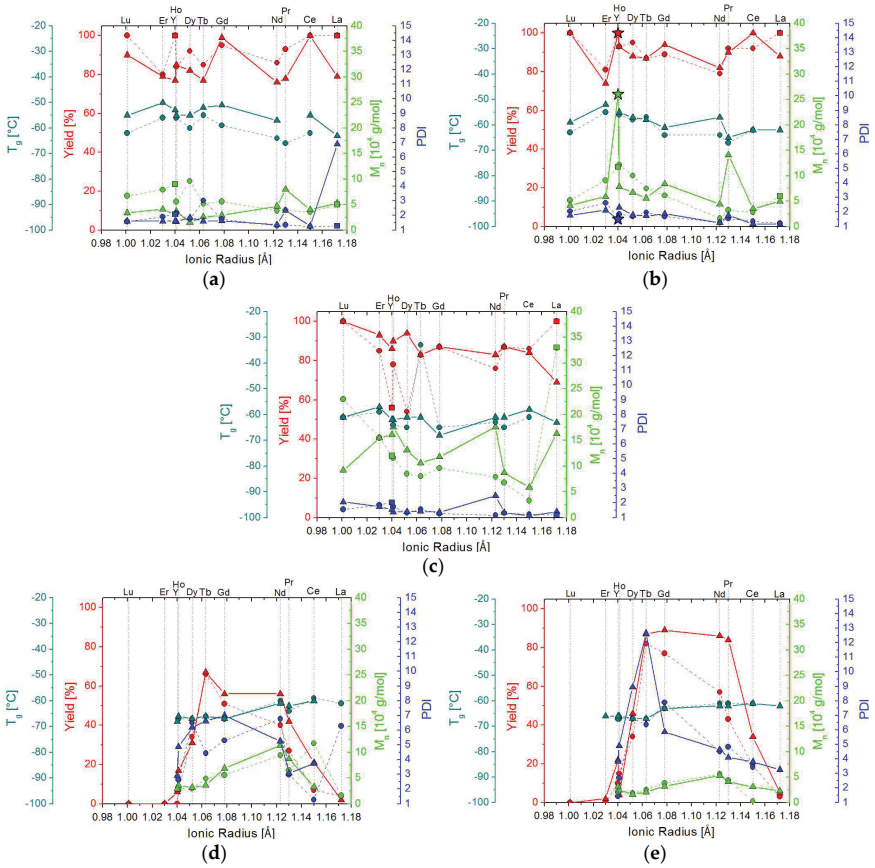

Figure 3. Overview charts representing the chain properties, yield and glass transition temperature of the polyisoprenes obtained from the homoleptic rare-earth metal tetramethylaluminates $\mathbf{2}^{\mathbf{Ln}}$. Panels (**a**–**e**) give details on the data obtained from the application of a certain cocatalyst (**A**–**E**; **A** = $[Ph_3C][B(C_6F_5)_4]$, **B** = $[PhNMe_2H][B(C_6F_5)_4]$, **C** = $B(C_6F_5)_3$, **D** = Me_2AlCl, **E** = Et_2AlCl). Results for the addition of 1 equiv. of cocatalyst per aluminate precatalyst after 1 h are shown by circles (dashed lines), 2 equiv. by triangles (solid lines). If such results were not available, data of reaction times of 24 h are shown marked with squares and stars, respectively. The lanthanide precatalysts $Ln(AlMe_4)_3$ ($\mathbf{2}^{\mathbf{Ln}}$) are shown in the order of increasing ionic radii (*x*-axis) [28,29]; the corresponding data are shown referring to four different y-axes: red (yield), green (M_n), blue (PDI) and teal (T_g). In all panels lines are meant to assist the reader to follow the certain curves within the plot and not to indicate linear behavior of the curves in between the points of measurement. For a more traditional compilation of the polymer data in table form, sorted by precatalyst, see Tables S1.2.1—S1.2.11, Supplementary Materials.

With respect to the uniformity of the polymerizing species (La–Lu), the ratio of the number of polymer chains and the number of lanthanide centers showed maxima with the larger Ln for **A** and **B** (e.g., 3.37 for $\mathbf{2}^{\mathbf{Nd}}$) and minima, where M_n is at its maximum (Ln = Dy (**A**) and Ln = Ho (**B**)), while it decreased for cocatalyst **C** (with exceptions for Ln = La and Lu, Table S3.1, Supplementary Materials). Therefore, the total number of active centers was lowest for Ln = Dy (**A**) and Ln = Ho (**B**) and decreased from Ce to Er for cocatalyst **C**. This can be rationalized on the basis of coordination equilibria at least for the chain propagating species involving increasing coordination restrictions when moving from Ce to Er. For **A** and **B** then, substrate coordination capability is least pronounced, most likely caused by

strong Ln^{3+}—$[B(C_6F_5)_4]^-$ interactions and competitive interactions with pre-reaction side products such as dimethylaniline. In total, these effects and peculiarities had only little influence on the glass transition temperatures, due to the vinylic content staying rather low in all cases. Besides these general trends in microstructure, several precatalyst/cocatalyst combinations stuck out. Here, especially for $\mathbf{2^{Gd}}$/**A**, a much higher *cis*-content was found, than the trends discussed (*vide infra*) would imply.

Activation by a Single Equivalent of Dialkylaluminum Chloride. Unsurprisingly, the entirely different nature of cocatalysts R_2AlCl (R = Me (**D**), Et (**E**)) and associated distinct activation pathways, led to a different set of results and interpretations (Figure 2d,e and Figure 3d,e, and Tables S1.1.4 and S1.1.5, Supplementary Materials). Most striking were the much higher *cis*-contents, achievable especially for the larger Ln ($\mathbf{2^{Nd}}$/**D**, 98.9%; $\mathbf{2^{Gd}}$/**D**, >99.9%). The *cis*-content then dropped from Ln = Ho on, giving way to an upcoming *trans*-content. As the transition state leading to *trans*-1,4-addition requires less space at the Ln(III) center than its *cis*-adding analogue, this result is in good agreement with the literature (for the evaluation of the microstructure data obtained, see Section 3.7) [42,43]. The obtained polymers showed constantly low contents of vinylic addition and therefore almost unaffected glass transition temperatures. Such binary catalyst systems $\mathbf{2^{Ln}}$/**D** and $\mathbf{2^{Ln}}$/**E** revealed a trend towards decreasing M_n for smaller Ln with (almost) no yield at all for the smallest lutetium. Interestingly, the PDI and with it the (non)uniformity of the intended multimetallic active species, revealed a maximum for Ln = Dy. These data can be interpreted by the presence of an active species, that produces 'high-*cis*'-polyisoprene for the large rare-earth metals only. Due to coordination/space restraints at smaller lanthanide ions, *cis*-selectivity decreases on the expense of increasing *trans*-contents until monomer coordination is infeasible. The high *cis*-contents reached up to regions, where the other possible microstructures could not be observed anymore at all. While in the past, this had only been found for systems applying cocatalyst **E** in *n*-hexane [11], for Ln = Gd such a high *cis*-content is also found in toluene (system $\mathbf{2^{Gd}}$/**D**, Table S1.2.5, run 7, Supplementary Materials). Since the polydiene microstructure is routinely determined by combined $^1H/^{13}C$ NMR spectroscopies and the highest *cis*-contents have been routinely observed for the rare-earth elements neodymium and gadolinium, we would like to stress a degree of uncertainty related to selectivities larger than 98%. Polymerization reactions are usually terminated by alcoholysis (=deactivation) of the catalyst system (see experimental part), resulting in inclusion of the quenching products into the polymer, which in case of, e.g., Nd(III) or Gd(III) is reflected in paramagnetic line broadening of the NMR spectra (Figure 4).

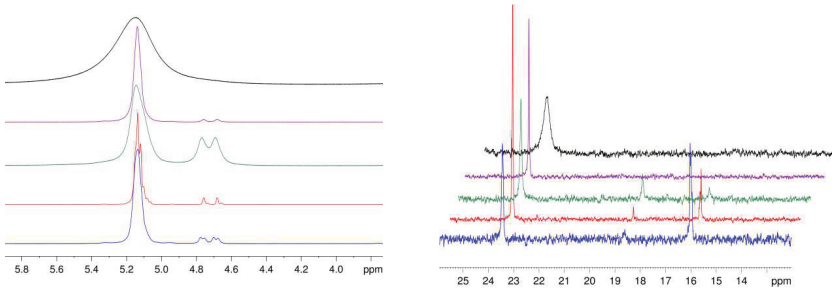

(**a**) (**b**)

Figure 4. Comparison of ^1H NMR (**a**) and ^{13}C NMR spectra (**b**) of selected polyisoprene samples (sorted by microstructure: decreasing *trans*-content bottom to top) produced by the systems $Nd(AlMe_4)_3$ ($\mathbf{2^{Nd}}$)/$[PhNMe_2H][B(C_6F_5)_4]$ (**B**) (blue; *cis*/*trans*/vinylic = 47/48/5%), $La(AlMe_4)_3$ ($\mathbf{2^{La}}$)/2 $B(C_6F_5)_3$ (**C**) (red; 78/19/4%), $Dy(AlMe_4)_3$ ($\mathbf{2^{Dy}}$)/2 $[Ph_3C][B(C_6F_5)_4]$ (**A**) (green; 72/10/18%), $Nd(AlMe_4)_3$ ($\mathbf{2^{Nd}}$)/Me_2AlCl (**D**) (violet, 99/0/1%) and $Gd(AlMe_4)_3$ ($\mathbf{2^{Gd}}$)/Me_2AlCl (**D**) (black; >99/0/0%). Inclusion of the quenching products into the polymer cannot be fully avoided. In case of polymers produced by paramagnetic catalyst systems this causes a broadening of the signals that increases the error of microstructure determination.

Moreover, the suitability of ATR-IR spectroscopy was probed as a pre-screening method for examining the microstructure of the polyisoprenes. For several polymer samples, both NMR and ATR-IR spectroscopic data have been compiled, in order to determine any significant deviation (Figure 5; Figures S2.1.1–S2.4.1 and Tables S2.1.1–S2.4.1, Supplementary Materials). Most satisfyingly, both methods are in good agreement taking into account the errors of the measurements.

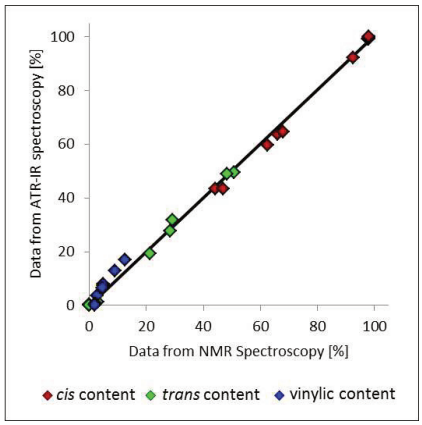

Figure 5. (See also Figure S2.2.1, Supplementary Materials). Comparison of the microstructure results obtained by NMR and ATR-IR spectroscopy, applying $Nd(AlMe_4)_3$ ($\mathbf{2}^{\mathbf{Nd}}$) and cocatalysts **A**–**E** (**A** = $[Ph_3C][B(C_6F_5)_4]$, **B** = $[PhNMe_2H][B(C_6F_5)_4]$, **C** = $B(C_6F_5)_3$, **D** = Me_2AlCl, **E** = Et_2AlCl) in both 1 and 2 equiv. For detailed polymerization data see Tables S1.2.4 and S2.2.1 (Supplementary Materials).

Activation by Two Equivalents of Borate/Borane. Addition of a second equiv. of the respective cocatalyst theoretically produces two cationic charges per lanthanide metal center and is therefore assumed to change the polymerization capabilities of the active sites significantly [44,45]. Surprisingly, for cocatalysts **A** or **B** and with the exception of Ln = La, the polydispersities were found in the same range as in case of single cationization, although some polyisoprenes revealed smaller values as anticipated (Figure 3a,b, Tables S1.1.1 and S1.1.2, Supplementary Materials). Taking into account similar polymer yields, this implies that the uniformity of the active center is not much affected. In contrast, the number average molecular weights differed markedly. Although there was still no clear trend observable across the series La-Lu, polymerization initiation was visibly influenced by the second equiv. of cocatalyst as the n(chains)/n(Ln centers) ratios have changed to a large extent (Table S3.1, Supplementary Materials). Interestingly, throughout the whole Ln series, the *cis*-contents were found in the same area as observed for the catalysts derived from smaller Ln using 1 equiv. of cocatalyst. Twofold cationization is proposed to displace another tetramethylaluminate moiety, thus increasing steric unsaturation (and electron deficiency) at the rare-earth metal center. This can explain the comparatively higher *cis*-selectivities for the larger Ln, but cannot account for the concomitantly observed increased 3,4-contents (also affecting the glass transition temperatures). A preferred coordination of solvent or pre-reaction side products at such highly electron-deficient Ln(III) centers seems a plausible explanation for the latter [13,46]. When 2 equiv. of **A** were applied on the largest Ln(III), Ln = La and Pr (where Ce is an exception due to its potential to undergo redox behavior) a radical side reaction was observed that caused crosslinking of the resulting polymers and swelling on the application of solvents.

For 2 equiv. of cocatalyst **C**, even higher *cis*-contents than in case of **A** and **B** could be realized (Figure 2h, Table S1.1.3, Supplementary Materials). As with this neutral borane no pre-reaction side products are formed, competition for coordination sites with the monomer seems less pronounced, which might also explain the relatively low PDI. In contrast to the polymers formed with only 1 equiv.

of cocatalyst **C**, there is no clear trend visible for the chain length. Instead, several more or less favored combinations of ion size with its environment and monomer are suggested.

Activation by Two Equivalents of Dialkylaluminum Chloride. Addition of 2 equiv. of the cocatalysts R_2AlCl (see Section 2.2.2, for a more detailed study on the influence of the cocatalyst concentration) resulted in even more complicated systems in terms of PDI values than observed for 1:1 binary mixtures. Still, extremely high *cis*-contents and acceptable yields could be achieved for the larger Ln, down to Tb, where yields and *cis*-contents once again dropped and *trans*-1,4-addition became significant. Here, neodymium displayed the highest *cis*-contents with both cocatalysts **D** and **E** (maximum 98%). The application of R_2AlCl is limited though, as it only provides reasonable yields with the medium-sized lanthanides.

Overall Maxima. Overviewing all results (Tables S1.3.1–S1.3.7, Supplementary Materials) revealed that there are high-yielding precatalyst/cocatalyst combinations for each lanthanide and cocatalyst (cf. Figure 2). The highest *cis*-contents were found for cocatalysts R_2AlCl (**D** and **E**), especially with Ln = Ce, Pr, Nd, Gd, showing virtually complete *cis*-selectivity, while the highest induced by the borate/borane cocatalysts was found for $\mathbf{2^{Nd}}$/2**C** (92.7%). The most *trans*-selective combinations accomplished medium selectivity (<60%) for Ln = La and the borate/borane cocatalysts (**A**–**C**) [18]. The vinylic contents did not succeed 20% ($\mathbf{2^{Y}}$/2**B**) [16]. Interestingly, the uniformity of the active systems was highest for Ln = Ce showing even a PDI <1.2 with 2 equiv. of **B** and a surprisingly low PDI (<1.3) with 1 equiv. of **D** as well (Table S1.2.2, Supplementary Materials), in comparison with the generally high PDIs for R_2AlCl-cocatalyzed polymerizations.

2.2.2. Screening Studies

Screening of the Pre-Reaction Time. The pre-reaction time of 0.5 h has originally been chosen to ensure complete catalyst formation before monomer addition. Due to the paramagnetic character of most of the lanthanides, an exact determination of the active species by NMR spectroscopy during the process of formation remains challenging. For the few diamagnetic systems, the small total number of signals and the high mobility of the $[AlMe_4]^-$ moieties further hampered a detailed elucidation [4,10,12]. Therefore, the active species was investigated indirectly by empirically screening various pre-reaction times applying $Nd(AlMe_4)_3$ ($\mathbf{2^{Nd}}$) and cocatalyst **E**, which, in this study, served as a representative example for the R_2AlCl cocatalyst systems. It was revealed that the microstructure remained surprisingly constant (*cis*/*trans*/vinylic = 98/0/2%, Figure S1.4.1 and Table S1.4.1, Supplementary Materials). Interestingly, polymer yields were higher for shorter pre-reaction times than for the standardized 30 min, if a minimum of 10 min was allowed. At the same time, the number average molecular weight remained rather constant, which implies a higher number of initiating Nd centers under these conditions (Figure 6a). At 22 min of pre-reaction time almost every Nd center (extrapolated) produced a polymer chain (for details on the calculation of ratios n(chains)/n(Ln centers), see Section S3 in the Supplementary Materials). In addition, the ratio n(chains)/n(Ln centers) decreased below 80% at the originally applied 0.5 h. Considering the occurrence of multimetallic active species (cluster), the elucidation of the nature of such seemingly high initiation rates remain subject to future research.

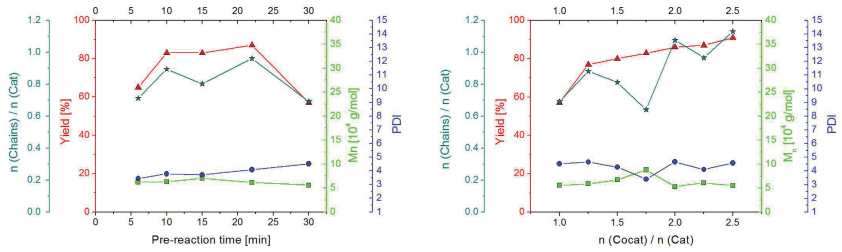

Figure 6. Overview on isoprene polymerization data obtained, when investigating the influence of pre-reaction time (panel **a**) and cocatalyst concentration (**b**), applying the catalytic system $Nd(AlMe_4)_3$ ($\mathbf{2^{Nd}}$)/Et_2AlCl (**E**) with a pre-reaction time of 30 min as an example. The corresponding data are shown referring to four different *y*-axes: red (yield), green (M_n), blue (PDI) and teal (extrapolated ratio n(polymer chains)/n(Nd centers)). For details on the calculation of ratios n(chains)/n(Ln centers), see Section S3 of the Supplementary Materials. During these screenings, the microstructure remained constantly around *cis*/*trans*/3,4 = 98/0/2% (see Figure S1.4.1, Supplementary Materials). In both panels, lines are meant to assist the reader to follow the respective curves within the plot and not to indicate linear behavior of the curves in between the points of measurement.

We hypothesize that monomer coordination breaks up the multimetallic entities (compare Section 2.3.2). This theory would not interfere with the PDI values, which increase with longer pre-reaction times as a result of the formation of a variety of cationic multimetallic species. More precisely, initially formed larger units might dissociate into chain propagating species in multiple steps, releasing propagating systems stepwise and therefore subsequently. Table S3.1 (Supplementary Materials) gives an overview on the ratio n(chains)/n(Ln centers) found in this study at standard conditions (1 and 2 equiv. of cocatalyst and 0.5 h pre-reaction time, screening of precatalysts $\mathbf{2^{Ln}}$ and cocatalysts **A**–**E**). Apparently, values above 1, implying chain transfer at monocationic species, are more often obtained with cocatalysts **A**–**C**, while low values (<<1) accumulated with cocatalysts **D** and **E**. Therefore, we assume that disaggregation did not occur to full extent for all precatalysts, as the steric situations created by those vary due to the different ion sizes.

Screening of the Cocatalyst Concentration. Since multimetallic cationic species have been proposed to form upon cocatalyst addition [11], gradual variation of the cocatalyst concentration should provide further insight into the active species (Figure 6b, Table S1.4.2, Supplementary Materials). Accordingly, increasing amounts of cocatalyst resulted in an overall increase in yield and the extrapolated molar ratio of polymer chains per Nd center, while the microstructures and chain lengths remained once more rather unaffected. The ratio n(chains)/n(Ln centers) even reached beyond 1, implying minimal amounts of chain transfer. This can be explained by free $AlMe_3$, which has a low capability of serving as a chain transfer agent [47]. This would also cause the occurrence of dormant species as described by Brintzinger et al. [48]. As the capability of AlR_3 species to serve as a chain transfer agent increases with the length of R that of 'Et_2AlMe' (formed in the pre-reaction applying cocatalyst **E**) should be higher than that of $AlMe_3$ [49,50]. The slightly increasing yield with increasing cocatalyst concentration implies a slightly increasing number of catalytically active centers, in view of the almost constant molecular weight. Interpretations ascribing these findings to chain transfer behavior alone seem rather unlikely, as it would then be implausible to obtain constant number average molecular weights. Still, chain transfer plays undoubtedly a (small) role with these systems (*vide supra*). As well, it seems unlikely, that these results could be caused by a multimetallic species containing several active centers. In such a sterically crowded event, it would occur counterintuitive, that the same active species provides higher ratios n(chains)/n(Nd centers) for isoprene than for the sterically less demanding 1,3-butadiene (*vide infra*).

Isoprene Polymerization in *n*-Hexane. Polymerizations in *n*-hexane, applying $\mathbf{2}^{\mathbf{Nd}}/\mathbf{E}$ (Table S1.4.3., Supplementary Materials) showed that while microstructure, molecular weight and yield are only affected slightly, the impact on the polydispersity is significant at ambient temperature. Such high PDI values can be explained by the re-dissolution of the precipitated multimetallic catalyst species upon monomer addition, which is slower in *n*-hexane than toluene [4,11,13]. The availability of the active species should be limited in a system, where the precipitate is less soluble. Increasing the solubility by application of higher temperatures (e.g., 40 °C) resulted in quantitative yields after 24 h and a lower PDI than in toluene [13]. Addition of only a small amount of toluene (Table S1.4.3, run 2) afforded the microstructure and chain length obtained in pure toluene. Interestingly, the latter system seemed to yield more lanthanide centers growing a polymer chain, which resulted in a lower PDI and higher yield.

Longer Reaction Times with Less-Active Catalysts. Precatalyst/cocatalyst combinations that have only resulted in traces of polymer after a reaction time of 1 h, were probed in 24 h terms as well (Table S1.4.4, Supplementary Materials). The binary system $\mathbf{2}^{\mathbf{La}}/\mathbf{D}$ resulted in microstructure and chain properties in the anticipated range but uniquely in this study, 1,2-addition was found for one polyisoprene sample (0.8%). Furthermore, the notably high *trans*-contents observed for the smaller Ln (Er, Lu) are to mention, following the trends described in Section 2.2.1 to the maximal extent of 81% of 1,4-*trans* linkages ($\mathbf{2}^{\mathbf{Lu}}/2\mathbf{E}$).

2.3. 1,3-Butadiene Polymerization Catalysis

2.3.1. Polymers Obtained at Standard Conditions

The polymerization of 1,3-butadiene was investigated for praseodymium, neodymium and yttrium. Overall, a similar set of results was obtained as in case of isoprene polymerization although vinylic addition was even less pronounced (Figure 7a and Tables S1.6.1–S1.6.3). While the microstructure of polybutadienes obtained with $\mathbf{2}^{\mathbf{Pr}}$ activated by borate/borane cocatalysts (**A**–**C**) showed predominant *trans*-1,4 selectivity, the high *cis*-1,4 selectivities in the presence of cocatalysts R_2AlCl (**D** and **E**) were detected for 1,3-butadiene as well. As in the isoprene case, the smaller-sized **D** produced the highest *cis*-selectivities, accomplishing 99.7% for Ln = Nd (Figure 7a, Table S1.6.2, Supplementary Materials). In all cases the yields remained rather low, probably due to shear-induced gelation of the solutions of growing polymer chains and low initiation rates. These are also the reasons for the rather high molecular weights and the variations in PDI (see Figure 7b and Tables S1.6.1–S1.6.3). For geometric reasons, 3000 equiv. of monomer per Ln center were not reached in all experiments (the actual amounts were determined by flowmeter and are given in the respective tables in Sections S1.6 and S1.7, Supplementary Materials).

2.3.2. Screening Studies

Both panels of Figure 8 show that the catalytic situation is more complicated when applying 1,3-butadiene, instead of isoprene (compare Section 2.2.2). Once again, neodymium tetramethylaluminate $\mathbf{2}^{\mathbf{Nd}}$ was chosen as an exemplary precatalyst. The number of polymer chains produced per Nd center is significantly lower than in the isoprene case, especially at pre-reaction times longer than 15 min. This initiation deficit implies that the suggested disaggregation of the multimetallic cationic species is less pronounced (if it happens at all in the 1,3-butadiene case).

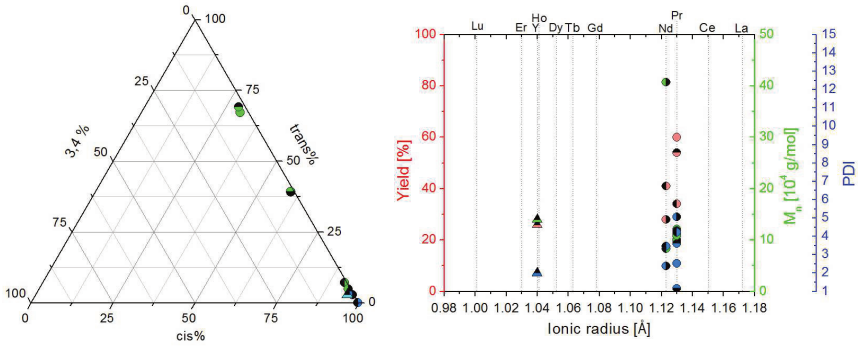

(**a**) (**b**)

Figure 7. Overview on 1,3-butadiene polymerization data. In both panels, the black parts of the marks represent the cocatalyst applied: none: **A**, top: **B**, bottom: **C**, right: **D** and left **E** (**A** = $[Ph_3C][B(C_6F_5)_4]$, **B** = $[PhNMe_2H][B(C_6F_5)_4]$, **C** = $B(C_6F_5)_3$, **D** = Me_2AlCl, **E** = Et_2AlCl). Results for the addition of 1 equiv. of cocatalyst per aluminate precatalyst are shown by circles, 2 equiv. by triangles. (**a**) ternary diagram representing the microstructure of the polybutadienes obtained from homoleptic lanthanide tetramethylaluminates. Precatalysts $\mathbf{2^{Ln}}$ (Ln = Pr, Nd, Y) are color-coded as follows: green (Pr), blue (Nd), cyan (Y). (**b**) overview chart representing the chain properties and yield of the polybutadienes. Rare-earth metal precatalysts $\mathbf{2^{Ln}}$ are shown in the order of increasing ionic radius (*x*-axis); the corresponding data are shown referring to three different *y*-axes: red (yield), green (M_n), blue (PDI).

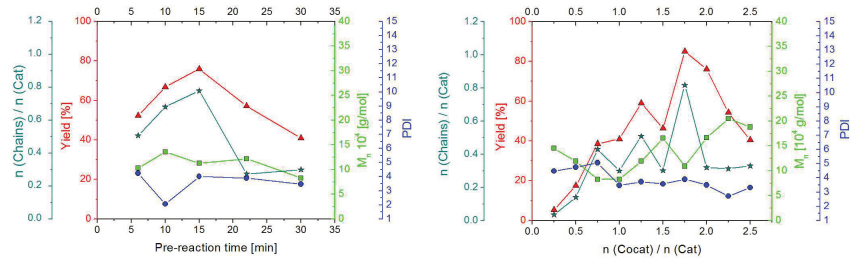

(**a**) (**b**)

Figure 8. Overview on 1,3-butadiene polymerization data obtained, when investigating the influence of pre-reaction time panel (**a**) and cocatalyst concentration (**b**), applying the catalytic system $Nd(AlMe_4)_3$ ($\mathbf{2^{Nd}}$)/Et_2AlCl (**E**) with a pre-reaction time of 30 min as an example. The corresponding data are shown referring to four different *y*-axes: red (yield), green (M_n), blue (PDI) and teal (extrapolated ratio n(polymer chains)/n(Nd centers)). For details on the calculation of ratios n(chains)/n(Ln centers), see Section S3 of the Supplementary Materials. During these screenings, the polybutadiene microstructure showed a small increase 96.7–98.8% with shorter pre-reaction times and remained constant with higher cocatalyst concentrations until 2.5 equiv. were reached, where it increased to *cis*/*trans*/vinylic = 99.5/0.4/0.1% (Figure S1.7.1 and Tables S1.7.1 and S1.7.2, Supplementary Materials). In both panels lines are meant to assist the reader to follow the certain curves within the plot and not to indicate linear behavior of the curves in between the points of measurement.

Screening of the Pre-Reaction Time. Variation of the pre-reaction time resulted in maximum monomer conversion after 15 min, while M_n remained rather constant. The latter can be explained by an increased number of active centers (or enhanced chain transfer, which once more seems unlikely, see Section 2.2.2). With an enduring activation reaction, such an increase would not be

too surprising, but interestingly, after 15 min, the number of active centers seem to decrease as indicated by a significant drop of the ratio of chains per Ln center. Assuming the growth of one polymer chain per Ln(III) center, about two of three Ln centers seem not to grow a polymer chain. The following two scenarios seem likely: either it is indeed higher aggregates that propagate polymer chains or a disaggregation/re-aggregation occurs, which causes chain termination at a very early state and terminates the catalytic capabilities of certain Ln centers. While the approximate 1:2 molar ratio of polymer chains per Ln center favors the first option, the fact that PDI, degree of polymerization and even the microstructure was not affected might speak in favor of the second scenario. The highest *cis*-contents were observed at the shortest pre-reaction time (98.8% after 6 min), staying at a very high level of 96.7% even after a pre-reaction time of 30 min.

Screening of the Cocatalyst Concentration. As 30 min was the originally chosen pre-reaction time, it was also applied in the cocatalyst concentration screening (Figure 8b, Table S1.7.2, see Supplementary Materials). Not unexpectedly, using 0.25 equiv. of cocatalyst per Nd center gave low polymer yield, featuring long polymer chains as only a small number of active Nd centers propagated chain growth. Up to 0.75 equiv. of cocatalyst, the curves followed the expected paths, revealing increasing yield, decreasing molecular weight, since involving a higher number of active Nd centers. Noteworthy, a comparatively high PDI was observed for a ratio $\mathbf{E}/\mathbf{2}^{\mathbf{Nd}} < 1$. The polymerization performance appeared completely altered at higher cocatalyst concentrations. The number of active centers as well as the PDI dropped at 1 equiv. of cocatalyst. Hence, less but more uniform active centers were produced. Furthermore, the new species seemed less active as monomer uptake, that had remained constant so far, dropped as well (34.1 → 22.4 mmol), at rather constant yield (Table S1.7.2, Supplementary Materials). Despite of two exceptional catalyst/cocatalyst ratios (1.25 and 1.75), the active species present with 1 equiv. of cocatalyst seemed to stay intact up to the highest tested ratio of 2.5, as PDI and ratio n(chains)/n(Ln center) remained rather constant. As expected, cocatalyst concentrations larger than 2 equiv. resulted in lower yields due to loss of active Nd–alkyl moieties (=catalyst poisoning) [11]. Interestingly, the molar ratio of chains per Nd center seemed not affected. It is not yet clear why the catalyst species generated by 1.25 and 1.75 equiv. of cocatalyst **E** afforded a seemingly increased number of active centers and higher yield at rather unaffected polymer chain properties (M_n, PDI).

Further Studies on 1,3-Butadiene Polymerization. As a prove of principle, a 1,3-butadiene polymerization with $\mathbf{2}^{\mathbf{Nd}}/\mathbf{E}$ was run for 2 h (Table S1.7.3, Supplementary Materials). Increased yield, M_n as well as monomer uptake suggested that the reaction continues with a slight loss of polymerization rate, due to enhanced viscosity.

1,3-Butadiene polymerization with $\mathbf{2}^{\mathbf{Nd}}/\mathbf{E}$ in *n*-hexane (Table S1.7.4, Supplementary Materials) differed markedly from the same experiment performed with isoprene (Section 2.2.2). The polydispersity of the polybutadienes seemed unaffected by the solvent change. However, the number average molecular weights were much higher in *n*-hexane than in toluene at rather constant yield, suggesting that less Nd centers grow a polymer chain. The increased monomer uptake of the solution is ascribed to the different solubility of 1,3-butadiene in the applied solvents. Still, the availability of the monomer is therefore high, which causes the high M_n produced by the fewer active sites.

2.4. Ethylene Polymerization

Preliminary ethylene polymerizations have been performed with $\mathbf{2}^{\mathbf{Nd}}/\mathbf{E}$ and $\mathbf{2}^{\mathbf{Nd}}/2\mathbf{E}$ (Table S1.8.1, Supplementary Materials), affording 12% and 87% yield of polyethylene, respectively, with similar average molecular weights. The higher PDI of 4.0 in case of 2 equiv. of cocatalyst (compared to 3.4 with 1 equiv.) is reflected in the melting points of the two samples which differ by 8 K (**E**: 138 °C, **2E**: 130 °C). An extension of this study is subject to further research.

3. Materials and Methods

3.1. General Remarks

All operations were performed with rigorous exclusion of air and water, using standard Schlenk, high-vacuum and argon glovebox techniques (MBraun MB 200B; <1 ppm O_2, <1 ppm H_2O). When autoclaves did not fit into the antechambers of the applied gloveboxes (Parr type, used for ethylene polymerization), air and moisture were excluded from autoclaves as well by evacuation at reaction temperature for 24 h prior to the polymerizations and insertion of educts applying shuttles filled in a glovebox. Otherwise (Büchi type, used for 1,3-butadiene polymerization) the applied miniclaves were filled and sealed inside a glovebox. *n*-Hexane, toluene and THF (Sigma-Aldrich, St. Louis, MO, USA) were purified by using Grubbs columns (MBraun SPS-800, solvent purification system, Garching, Germany) and stored in a glovebox. C_6D_6 and toluene-d_8 were obtained from Sigma-Aldrich, dried over NaK alloy for 24 h and filtered. Anhydrous $LnCl_3$ were purchased from ABRC chemicals (Karlsruhe, Germany) and were activated by Soxhlet extraction with THF. $CDCl_3$ and $AlMe_3$ were purchased from Sigma-Aldrich and used as received. Trioctylaluminum and methyllithium were obtained from Sigma-Aldrich as solutions in hexanes and were used after solvent evaporation. $LiNMe_2$ was synthesized from $HNMe_2$ and *n*-BuLi (both Sigma-Aldrich) and employed as white powder. Isoprene was obtained from Sigma-Aldrich, dried over trioctylaluminum and vacuum transferred prior to use. $[Ph_3C][B(C_6F_5)_4]$ (**A**), $[PhNMe_2H][B(C_6F_5)_4]$ (**B**) and $B(C_6F_5)_3$ (**C**) were purchased from Boulder Scientific Company (Longmont, CO, USA) and used without any further purification. 1,3-Butadiene and ethylene, as well as nitrogen and helium (atmosphere gasses for DSC), were purchased from Westphalen Gas (Münster, Germany) and purified and dried over Grubbs columns prior to use. Their amounts were determined using a Bronkhorst EL Flow Select Flow Controller (Ruurlo, The Netherlands). Homoleptic methylaluminate complexes $\mathbf{2^{Ln}}$ were prepared according to literature methods [4,11–13,20–23]. The NMR spectra of air- and moisture-sensitive compounds were recorded at 25 °C on a Bruker DMX-400 Avance (^{1}H: 400.13 MHz; ^{13}C: 100.61 MHz; ^{27}Al: 130.33 MHz) (Billerica, MA, USA). ^{1}H, ^{13}C and ^{27}Al shifts are referenced to internal solvent resonances and reported in parts per million (ppm) relative to TMS. Elemental analyses were performed on an Elementar Vario MICRO cube (Hanau, Germany). The molar weights (M_W and M_n) of the polymers were determined by size-exclusion chromatography (SEC). Sample solutions (1.0 mg polymer per mL THF) were filtered through a 0.45 µm syringe filter (Macherey-Nagel, Düren, Germany) prior to injection. SEC was performed with a pump supplied by Viscotek (GPCmax VE 2001, Malvern, UK), employing ViscoGEL columns. Signals were detected by means of a triple detection array (TDA 305) and calibrated against polystyrene standards (M_W/M_n < 1.15; Malvern, UK, and PSS Polymer Standards Service GmbH, Mainz, Germany). The flowrate was set to 1.0 mL min^{-1}. High temperature GPC was performed by Malvern Instruments Ltd. The microstructures of the polydienes were examined by means of ^{1}H and ^{13}C NMR spectroscopic experiments on the AV400 spectrometer at ambient temperature, using $CDCl_3$ as a solvent and by ATR-IR spectroscopy on a Thermo Fisher Scientific NICOLET 6700 FTIR spectrometer using a diamond ATR setup (Waltham, MA, USA). Glass transition temperatures of the polymers (T_g) were obtained applying a Perkin-Elmer DSC 8000 calibrated with indium and cyclohexane standards, scanning from −100 °C up to +100 °C with heating rates of 20 K/min and cooling rates of 60 K/min in N_2 atmosphere (polyisoprene) and He atmosphere (polybutadiene). Crystals of $\mathbf{2^{Gd}}$ and $\mathbf{2^{Tb}}$ suitable for X-ray crystallography were grown by standard techniques from solutions using *n*-hexane at −35 °C. Single crystals were selected, coated with Parabar 10312 (previously known as Paratone N, Hampton Research, Aliso Viejo, CA, USA) and fixed on a microloop. Data were collected on a Bruker APEX DUO instrument (Billerica, MA, USA) equipped with an IµS microfocus sealed tube and QUAZAR optics for MoK_α radiation (λ = 0.71073 Å). The data collection strategy was determined using COSMO (Version 1.61, Bruker AXS Inc., Madison, WI, USA) employing ω- and φ scans. Raw data were processed using APEX 3 (Version 2016.5-0, Bruker AXS Inc., Madison, WI, USA) and SAINT (Version 8.37A, Bruker AXS Inc.,

Madison, WI, USA), corrections for absorption effects were applied using SADABS (Bruker AXS Inc., Madison, WI, USA, [51]). The structures were solved by direct methods and refined against all data by full-matrix least-squares methods on F^2 using SHELXTL [52,53] and SHELXLE [54]. Further details of the refinement and crystallographic data are listed in Table S4.1 (Supplementary Materials) and in the below mentioned CIF files. CCDCs 1817852 and 1817853 contain the supplementary crystallographic data for this paper. These data can be obtained free of charge from The Cambridge Crystallographic Data Centre via www.ccdc.cam.ac.uk/data_request/cif.

3.2. Synthesis of $Tb(AlMe_4)_3$ ($\mathbf{2^{Tb}}$)

Homoleptic $\mathbf{2^{Tb}}$ was synthesized according to the literature from $TbCl_3(thf)_{1.66}$ [4,11–13,20–23]. The chloride precursor was obtained via Soxhlet extraction of anhydrous $TbCl_3$ (5.00 g, 18.8 mmol) in THF at 100 °C for 7d, yielding 49% of the thf adduct. To a slurry of $TbCl_3(thf)_{1.66}$ (3.514 g, 9.128 mmol) in THF (40 mL) was added $LiNMe_2$ (1.397 g, 27.384 mmol) and the mixture was stirred for 1 d. Thereafter the solvent was removed under vacuum and 40 mL of *n*-hexane as well as $AlMe_3$ (5.915 g, 82.152 mmol) were added subsequently. After stirring for another day at ambient temperature, solid side products (e.g., LiCl) were removed by centrifugation and filtration and the solvent and by-product $(Me_2AlNMe_2)_2$ were removed under vacuum. Homoleptic $\mathbf{2^{Tb}}$ was recrystallized three times from *n*-hexane (-35 °C, total crystallized yield 1.38 g, 3.29 mmol, 36%). ^{27}Al NMR (130 MHz, C_6D_6, 26 °C): $\delta = -203.3$ ppm. Elemental analysis calcd (%) for $C_{12}H_{36}Al_3Tb$ (420.28): C 34.29, H 8.63; found: C 33.88, H 9.11.

3.3. New Protocol for the Synthesis of $Lu(AlMe_4)_3$ ($\mathbf{2^{Lu}}$)

In a 100 mL Schlenk flask, $LuCl_3(thf)_3$ (4.97 g, 10.0 mmol) was dissolved in THF (30 mL) and methyllithium (1.32 g, 60.0 mmol) was added under vigorous stirring. After 24 h, the solvent was removed under vacuum, the residue redissolved in toluene (10 mL) and the LiCl was removed via centrifugation and filtration. The toluene solution was evaporated in vacuo and the crude $[LuMe_3(MeLi)_3(thf)_x]$ was suspended in *n*-hexane (15 mL). Trimethylaluminum (8.64 g, 120.0 mmol) was added, the reaction mixture was stirred for 24 h and $LiAlMe_4$ was separated via filtration. Homoleptic $\mathbf{2^{Lu}}$ crystallized from a saturated *n*-hexane solution at −35 °C (2.55 g, 5.84 mmol, 58%). ^{1}H NMR (400 MHz, C_6D_6, 26 °C): $\delta = -0.19$ (s, 36 H, $AlCH_3$) ppm. $^{13}C\{^1H\}$ NMR (100 MHz, C_6D_6, 26 °C): $\delta = 3.7$ ppm; elemental analysis calcd (%) for $C_{12}H_{36}Al_3Lu$ (436.33): C 33.03, H 8.32; found: C 33.08, H 8.61.

3.4. Polymerization of Isoprene

A detailed polymerization procedure is described as a typical example (Table S1.2.4, run 1). $[Ph_3C][B(C_6F_5)_4]$ (**A**) (18.2 mg, 0.02 mmol) was added to a solution of $\mathbf{2^{Nd}}$ (8.1 mg, 0.02 mmol) in toluene (8 mL) and the mixture was aged at ambient temperature for 30 min. After the addition of isoprene (1.36 g, 20 mmol), the polymerization was carried out at 25 °C for 1 h. The reaction was terminated by pouring the polymerization mixture into 25 mL of methanol containing 0.1% (*w*/*w*) 2,6-di-tert-butyl-4-methylphenol as a stabilizer and stirred for 1 h. The polymer was washed with methanol and dried under vacuum at ambient temperature to constant weight.

Liquid cocatalysts (**D** and **E**) were added as 1 mL of a solution of a concentration of 1 equiv./mL. The amount of additional solvent applied was then reduced by 1 mL compared to the procedure given above in order to ensure highest possible similarity regarding the rheological properties of the polymerization mixture.

3.5. Polymerization of 1,3-Butadiene

A detailed polymerization procedure is described as a typical example (Table S1.6.3, run 1). $[Ph_3C][B(C_6F_5)_4]$ (**A**) (18.2 mg, 0.02 mmol) was added to a solution of $\mathbf{2^{Pr}}$ (8.05 mg, 0.02 mmol)

in toluene (28 mL) and the mixture was aged at ambient temperature for 30 min. The mixture was poured into an evacuated 50-mL Büchi miniclave and 1440 mL (60 mmol) of 1,3-butadiene were added at 90 mLn/min under constant stirring at 100 rpm. The polymerization was carried out at 25 °C for 1 h. After release of the remaining monomer pressure, if any, the reaction was terminated by pouring the polymerization mixture into 200 mL of methanol containing 0.1% (*w*/*w*) 2,6-di-tert-butyl-4-methylphenol as a stabilizer and stirred for 1 h. The polymer was washed with methanol and dried under vacuum at ambient temperature to constant weight.

Liquid cocatalysts (**D** and **E**) were added as 1 mL of a solution of a concentration of 1 equiv./mL. The amount of additional solvent applied was then reduced by 1 mL compared to the procedure given above in order to ensure highest possible similarity regarding the rheologic properties of the polymerization mixture.

3.6. Polymerization of Ethylene

A detailed polymerization procedure is described as a typical example (Table S1.8.1, run 1). Et_2AlCl (**E**) (3 mL of a solution of 0.02 mol/L in toluene, 1 equiv.) was added to a solution of $\mathbf{2^{Nd}}$ (24.3 mg, 0.06 mmol) in toluene (25 mL) and the mixture was aged at ambient temperature for 30 min. The mixture was poured into an evacuated 300-mL Parr autoclave, 100 mL toluene and 2100 mLn (60 mmol) of ethylene were added at a maximum flow rate of 450 mLn/min under constant stirring at 50 rpm. The polymerization was carried out at 60 °C for 1 h. After release of the remaining monomer pressure, if any, the reaction was terminated by pouring the polymerization mixture into 200 mL of methanol and stirred for 1 h. The polymer was washed with methanol and dried under vacuum at ambient temperature to constant weight.

3.7. Application of NMR Spectroscopic Techniques for Microstructure Determination

The microstructures of the polydiene samples produced in this study were evaluated by NMR spectroscopy Previously, the microstructure has been estimated measuring peak heights in the ^{13}C NMR spectra only [11,13]. Especially the vinylic content has been underestimated by this method as the variety in tacticity causes wide multiplets and therefore underrepresented peak heights. Furthermore, the nuclear Overhauser effect affects the vinylic and 1,4-polyisoprene signals significantly differently. The ratio of 1,4-/1,2 or 3,4-linkages is obtained from the ^1H NMR spectrum by integration of the respective multiplets in the vinylic region of the spectrum (approx. 4.5 to 4.9 ppm for the vinylic linkages and 4.9 to 5.5 ppm for the 1,4-linkages in case of polyisoprene and 4.5 to 5.15 ppm and 5.15 to 6.0 ppm, respectively, in case of polybutadiene). The *cis*/*trans* ratio of the 1,4-linked part of the polymer is obtained from its ^{13}C NMR spectrum, by integration of the respective methyl (methylene in case of 1,3-butadiene) peaks at 23.5 and 16 ppm in case of isoprene and 27.4 and 32 ppm, respectively, in case of 1,3-butadiene. In order to compare integration results in a proton decoupled ^{13}C NMR spectrum, the respective carbon atoms are assumed to be affected by relatively similar nuclear Overhauser effects, as they are decorated with the same number of hydrogen atoms and are located in similar chemical environments [55–58]. For meaningful evaluations, ^{13}C NMR spectra should show a low signal to noise ratio, requiring time-consuming data collection. Another drawback of this method is the fact that paramagnetic Ln ions, that have not been removed in the washing process, cause signal broadening via interaction with the polymer, which results in a loss of accuracy. Therefore, by far less time-consuming ATR-IR techniques have been probed in this study as a pre-screening method.

3.8. Application of ATR-Infrared Spectroscopic Techniques for Microstructure Detection

For pre-screening of the microstructure of the obtained polyisoprenes, ATR-IR spectroscopy was applied as a comparative method. NMR spectroscopic data were used for calibration. Hence, the obtained polymer data are considered to be less accurate than NMR-spectroscopy based data sets. But as ATR-IR spectroscopy is by far less costly and time-consuming, its suitability for pre-screening purposes was investigated. To ensure the lowest possible errors of the measurements, the comparative

algorithm provided by the equipment manufacturer (Thermo Fisher Scientific, Waltham, MA, USA) was calibrated with a large data set of different polyisoprenes mirroring all possible microstructure compositions. In order to determine any deviation, both NMR and ATR-IR spectroscopic data were obtained and compared. Overviewing the findings (Figures S2.1.1–S2.4.1 and Tables S2.1.1–S2.4.1, Supplementary Materials) and considering the errors of the measurements, both methods are in good agreement. The highest individual absolute deviation found in the four series was 7.25%, on average 2.07%. Therefore, ATR-IR spectroscopy can very well serve as a pre-screening method for the microstructures of polyisoprenes. Furthermore, an optimized calibration of the algorithms might provide even more accurate results of wider applicability.

In order to provide an idea of the limits of the applicability of this method, surface manipulation of the polymers was performed by applying UV-light irradiation (Table S1.5.1, Supplementary Materials). Thereafter, the microstructure of the polymer samples was once more investigated by both techniques and compared. For NMR spectroscopy, no significant difference of the data before and after the manipulation was observed. But due to the low penetration depth of the IR-radiation into the polymer samples, in case of the ATR-IR data, such surface manipulation effects on the microstructure are emphasized (Table S2.5.1, Supplementary Materials). The observed shift toward vinylic linkage is supposed to be an artefact and due to an overlap of vibrations in the IR spectrum. UV-induced crosslinking is probably the origin of these new signals.

4. Conclusions

Homoleptic lanthanide and yttrium tris(tetramethylaluminate)s $Ln(AlMe_4)_3$ (Ln = La, Ce, Pr, Nd, Gd, Tb, Dy, Ho, Y, Er, and Lu) exhibit exceptional performance in 1,3-diene polymerization. Importantly, the reaction of $[LnMe_6(Li(do)_x)_3]$ with trimethylaluminum provides a more efficient precatalyst synthesis for the smaller rare-earth metal centers as shown for lutetium.

Due to the different nature of the borate/borane or R_2AlCl cocatalysts, distinct activation mechanisms occur, all providing individual trends and high-yielding precatalyst/cocatalyst combinations. The highest *cis*-1,4-contents were found when employing R_2AlCl cocatalysts and tetramethylaluminate complexes with Ln = Ce, Pr, Nd, and Gd, showing virtually complete *cis*-1,4-selectivity (>99.9% for Ln = Gd with cocatalyst Me_2AlCl). The highest *cis*-selectivity induced by the borate/borane cocatalysts was found for the combination of $Nd(AlMe_4)_3$ with 2 equiv. of $[B(C_6F_5)_3]$ (92.7%) although the general trend for these systems points to higher *cis*-selectivities with the smallest lanthanides. The most *trans*-selective combinations reach medium selectivity (<60%) for Ln = La and borate/borane cocatalysts. Interestingly, the uniformity of the active systems was best with Ln = Ce showing even a PDI < 1.2 with 2 equiv. of cocatalyst $[PhNMe_2H][B(C_6F_5)_4]$ and a surprisingly low PDI with Me_2AlCl, in comparison with the generally high PDI for the R_2AlCl-cocatalyzed polymers. Deeper insights into the polymerization performance of the binary system $Nd(AlMe_4)_3/Et_2AlCl$ could be gained by screening the pre-reaction time and the cocatalyst concentration. Here, different behaviors for the polymerization of 1,3-butadiene and isoprene were found. While the multimetallic cationic species, proposed in the literature seem to disaggregate upon monomer coordination for the bulkier isoprene, larger agglomerates are suggested to polymerize 1,3-butadiene. Interesting side reactions at high cocatalyst loadings as well as a comparatively high number of polymer chains per catalyst center, including further elucidation of the active species, will be subject to further research. Finally, ATR-IR spectroscopy displays an effective pre-screening method for the microstructures of polyisoprenes.

Supplementary Materials: The following are available online at www.mdpi.com/2073-4344/8/2/61/s1, Supplementary Materials (pdf) containing polymerization and crystal data. CIF files containing crystal data for complexes $\mathbf{2}^{\mathbf{Gd}}$ and $\mathbf{2}^{\mathbf{Tb}}$. The latter data have been deposited as well at CCDC (1817852 and 1817853).

Acknowledgments: We are grateful to the German Science Foundation (An238/14-2) and Bridgestone Japan for generous support, as well as Bassem Sabagh, Amy Ross (Malvern Instruments Ltd., Malvern, UK), and Bernd Schäfer (Malvern Instruments Ltd., Herrenberg, Germany) for performing the high temperature GPC measurements.

Author Contributions: C.O.H. and L.N.J. conceived and designed the experiments; D.D. contributed to the design of the ethylene polymerization experiments; C.O.H., L.N.J., D.D., T.Z. and R.S. performed the experiments; C.O.H., L.N.J., D.D., T.Z. and R.S. analyzed the data; C.M.-M. performed the X-ray structure analyses; C.O.H. wrote the paper; R.A. contributed reagents/materials/analysis tools, supervised all contributions and contributed to writing the paper.

Conflicts of Interest: The authors declare no conflict of interest.

References

1. Boor, J.J. *Ziegler-Natta Catalysts and Polymerizations*; Academic Press: New York, NY, USA; San Francisco, CA, USA; London, UK, 1979.
2. Mülhaupt, R. Catalytic Polymerization and Post Polymerization Catalysis Fifty Years After the Discovery of Ziegler's Catalysts. *Macromol. Chem. Phys.* **2003**, *204*, 289–327. [CrossRef]
3. Eisch, J.J. Fifty Years of Ziegler–Natta Polymerization: From Serendipity to Science. A Personal Account. *Organometallics* **2012**, *31*, 4917–4932. [CrossRef]
4. Fischbach, A.; Anwander, R. Rare-Earth Metals and Aluminum getting Close in Ziegler Type Organometallics. *Adv. Polym. Sci.* **2006**, *204*, 155–281.
5. Friebe, L.; Nuyken, O.; Obrecht, W. Neodymium-Based Ziegler/Natta Catalysts and their Application in Diene Polymerization. *Adv. Polym. Sci.* **2006**, *204*, 1–154.
6. Porri, L.; Ricci, G.; Giarrusso, A.; Shubin, N.; Lu, Z. Recent Developments in Lanthanide Catalysts for 1,3-Diene Polymerization. In *ACS Symposium Series 749—Olefin Polymerization: Emerging Frontiers*; Arjunan, P., McGrath, J.C., Hanlon, T., Eds.; Oxford University Press: New York, NY, USA, 2000; pp. 15–30.
7. Osakada, K.; Takeuchi, D. Coordination Polymerization of Dienes, Allenes, and Methylenecycloalkanes. In *Polymer Synthesis*; Springer: Berlin/Heidelberg, UK, 2004; pp. 137–194.
8. Shen, Z.; Ouyang, J. *Handbook on the Physics and Chemistry of Rare Earths*; Gschneidner, K.A., Jr., Fleming, L., Eds.; Elsevier Science Publishers: Amsterdam, The Netherlands, 1987; Chapter 61.
9. Taube, R.; Sylvester, G. *Applied Homogeneous Catalysis with Organometallic Compounds*; Cornils, B., Herrmann, W.A., Eds.; Wiley-VCH: Weinheim, Germany, 2002; pp. 280–318.
10. Zimmermann, M.; Anwander, R. Homoleptic Rare-Earth Metal Complexes Containing Ln−C σ-Bonds. *Chem. Rev.* **2010**, *110*, 6194–6259. [CrossRef] [PubMed]
11. Fischbach, A.; Klimpel, M.G.; Widenmeyer, M.; Herdtweck, E.; Scherer, W.; Anwander, R. Stereospecific Polymerization of Isoprene with Molecular and MCM-48-Grafted Lanthanide(III) Tetraalkylaluminates. *Angew. Chem. Int. Ed.* **2004**, *43*, 2234–2239. [CrossRef] [PubMed]
12. Zimmermann, M.; Frøystein, N.Å.; Fischbach, A.; Sirsch, P.; Dietrich, H.M.; Törnroos, K.W.; Herdtweck, E.; Anwander, R. Homoleptic Rare-Earth Metal(III) Tetramethylaluminates: Structural Chemistry, Reactivity, and Performance in Isoprene Polymerization. *Chem. Eur. J.* **2007**, *13*, 8784–8800. [CrossRef] [PubMed]
13. Meermann, C.; Törnroos, K.W.; Nerdal, W.; Anwander, R. Rare-Earth Metal Mixed Chloro/Methyl Compounds: Heterogeneous–Homogeneous Borderline Catalysts in 1,3-Diene Polymerization. *Angew. Chem. Int. Ed.* **2007**, *46*, 6508–6513. [CrossRef] [PubMed]
14. Fischbach, A.; Perdih, F.; Herdtweck, E.; Anwander, R. Structure−Reactivity Relationships in Rare-Earth Metal Carboxylate-Based Binary Ziegler-Type Catalysts. *Organometallics* **2006**, *25*, 1626–1642. [CrossRef]
15. Fischbach, A.; Perdih, F.; Sirsch, P.; Scherer, W.; Anwander, R. Rare-Earth Ziegler−Natta Catalysts: Carboxylate−Alkyl Interchange. *Organometallics* **2002**, *21*, 4569–4571. [CrossRef]
16. Arndt, S.; Beckerle, K.; Zeimentz, P.M.; Spaniol, T.P.; Okuda, J. Cationic Yttrium Methyl Complexes as Functional Models for Polymerization Catalysts of 1,3-Dienes. *Angew. Chem. Int. Ed.* **2005**, *44*, 7473–7477. [CrossRef] [PubMed]
17. Robert, D.; Spaniol, T.P.; Okuda, J. Neutral and Monocationic Half-Sandwich Methyl Rare-Earth Metal Complexes: Synthesis, Structure, and 1,3-Butadiene Polymerization Catalysis. *Eur. J. Inorg. Chem.* **2008**, 2801–2809. [CrossRef]
18. Litlabø, R.; Lee, H.S.; Niemeyer, M.; Törnroos, K.W.; Anwander, R. Rare-Earth metal bis(tetramethylaluminate) complexes supported by a sterically crowded triazenido ligand. *Dalton Trans.* **2010**, *39*, 6815–6825. [CrossRef] [PubMed]

19. Occhipinti, G.; Meermann, C.; Dietrich, H.M.; Litlabø, R.; Auras, F.; Törnroos, K.W.; Maichle-Mössmer, C.; Jensen, V.R.; Anwander, R. Synthesis and Stability of Homoleptic Metal(III) Tetramethylaluminates. *J. Am. Chem. Soc.* **2011**, *133*, 6323–6337. [CrossRef] [PubMed]
20. Nieland, A.; Mix, A.; Neumann, B.; Stammler, H.G.; Mitzel, N.W. Lanthanoid Tetramethylaluminates and Their Paramagnetic NMR Parameters. *Eur. J. Inorg. Chem.* **2014**, 51–57. [CrossRef]
21. Evans, W.J.; Anwander, R.; Ziller, J.W. Inclusion of Al_2Me_6 in the Crystalline Lattice of the Organometallic Complexes $LnAl_3Me_{12}$. *Organometallics* **1995**, *14*, 1107–1109. [CrossRef]
22. König, S.N.; Chilton, N.F.; Maichle-Mössmer, C.; Pineda, E.M.; Pugh, T.; Anwander, R.; Layfield, R.A. Fast magnetic relaxation in an octahedral dysprosium tetramethyl-aluminate complex. *Dalton Trans.* **2014**, *43*, 3035–3038. [CrossRef] [PubMed]
23. Klooster, W.T.; Lu, R.S.; Anwander, R.; Evans, W.J.; Koetzle, T.F.; Bau, R. Neutron Diffraction Study of $[Nd(AlMe_4)_3]$ $0.5\,Al_2Me_6$ at 100 K: The First Detailed Look at a Bridging Methyl Group with a Trigonal-Bipyramidal Carbon Atom. *Angew. Chem. Int. Ed.* **1998**, *37*, 1268–1270. [CrossRef]
24. Dietrich, H.M.; Raudaschl-Sieber, G.; Anwander, R. Trimethylyttrium and Trimethyllutetium. *Angew. Chem. Int. Ed.* **2005**, *44*, 5303–5306. [CrossRef] [PubMed]
25. Schumann, H.; Mueller, J.; Bruncks, N.; Lauke, H.; Pickardt, J.; Schwarz, H.; Eckart, K. Organometallic compounds of the lanthanides. Part 17. Tris[(tetramethylethylenediamine)lithium] hexamethyl derivatives of the rare earths. *Organometallics* **1984**, *3*, 69–74. [CrossRef]
26. Schumann, H.; Müller, J. Tris[(*N*,*N*,*N*′,*N*′-tetramethylethylenediamine)lithium]hexamethylerbate(III) and -lutetate(III). *Angew. Chem. Int. Ed.* **1978**, *17*, 276. [CrossRef]
27. Schumann, H.; Pickardt, J.; Bruncks, N. Crystal and Molecular Structure of$[Li(tmen)]_3[Er(CH_3)_6]$. *Angew. Chem. Int. Ed.* **1981**, *20*, 120–121. [CrossRef]
28. Shannon, R.D.; Prewitt, C.T. Effective Ionic Radii in Oxides and Fluorides. *Acta Cryst.* **1969**, *B25*, 925–946. [CrossRef]
29. Shannon, R.D. Revised Effective Ionic Radii and Systematic Studies of Interatomic Distances in Halides and Chalcogenides. *Acta Cryst.* **1976**, *A32*, 751–767. [CrossRef]
30. Chen, E.Y.-X.; Marks, T.J. Cocatalysts for Metal-Catalyzed Olefin Polymerization: Activators, Activation Processes, and Structure−Activity Relationships. *Chem. Rev.* **2000**, *100*, 1391–1434. [CrossRef] [PubMed]
31. Bonath, M.; Hollfelder, C.O.; Schädle, D.; Maichle-Mössmer, C.; Sirsch, P.; Anwander, R. C-H Bond Activation and Isoprene Polymerization by Lutetium Alkylaluminate/gallate Complexes Bearing a Peripheral Boryl and a Bulky Hydridotris(pyrazolyl)borato Ligand. *Eur. J. Inorg. Chem.* **2017**, 4683–4692. [CrossRef]
32. Diether, D.; Tyulyunov, K.; Maichle-Mössmer, C.; Anwander, R. Fluorenyl Half-Sandwich Bis(tetramethylaluminate) Complexes of the Rare-Earth Metals: Synthesis, Structure, and Isoprene Polymerization. *Organometallics* **2017**, *36*, 4649–4659. [CrossRef]
33. Monteil, V.; Spitz, R.; Boisson, C. Polymerization of butadiene and copolymerization of butadiene with styrene using neodymium amide catalysts. *Polym. Int.* **2004**, *53*, 576–581. [CrossRef]
34. Dietrich, H.M.; Schuster, O.; Törnroos, K.W.; Anwander, R. Heterobimetallic Half-Lanthanidocene Clusters: Novel Mixed Tetramethylaluminato/Chloro Coordination. *Angew. Chem. Int. Ed.* **2006**, *45*, 4858–4863. [CrossRef] [PubMed]
35. Evans, W.J.; Champagne, T.M.; Giarikos, D.G.; Ziller, J.W. Lanthanide Metallocene Reactivity with Dialkyl Aluminum Chlorides: Modeling Reactions Used to Generate Isoprene Polymerization Catalysts. *Organometallics* **2005**, *24*, 570–579. [CrossRef]
36. Evans, W.J.; Champagne, T.M.; Ziller, J.W. An Ethyl Aluminum Oxide (EAO) Complex with μ-η^1:η^2-Ethyl Coordination Derived from a Samarocene Carboxylate and Triethylaluminum. *Organometallics* **2005**, *24*, 4882–4885. [CrossRef]
37. Hayes, P.G.; Piers, W.E.; Parvez, M. Cationic Organoscandium β-Diketiminato Chemistry: Arene Exchange Kinetics in Solvent Separated Ion Pairs. *J. Am. Chem. Soc.* **2003**, *125*, 5622–5623. [CrossRef] [PubMed]
38. Yu, N.; Nishiura, M.; Li, X.; Xi, Z.; Hou, Z. Cationic Scandium Allyl Complexes Bearing Mono(cyclopentadienyl) Ligands: Synthesis, Novel Structural Variety, and Olefin Polymerization Catalysis. *Chem. Asian J.* **2008**, *3*, 1406–1414. [CrossRef] [PubMed]
39. Tardif, O.; Kaita, S. Generation of cationic indenyl silylamide gadolinium and scandium complexes $[(Ind)Ln\{N(SiMe_3)_2\}]^+[B(C_6F_5)_4]^-$ and their reactivity for 1,3-butadiene polymerization. *Dalton Trans.* **2008**, 2531–2533. [CrossRef] [PubMed]

40. Lei, Y.; Su, Q.; Chen, J.; Luo, Y. Synthesis, characterization of cationic half-sandwich scandium mono(silylamide) complexes and their unexpected reactivity toward C–Cl σ bond activation of chlorobenzene. *J. Organomet. Chem.* **2014**, *769*, 119–123. [CrossRef]
41. Zimmermann, M.; Törnroos, K.W.; Anwander, R. Cationic Rare-Earth-Metal Half-Sandwich Complexes for the Living *trans*-1,4-Isoprene Polymerization. *Angew. Chem. Int. Ed.* **2008**, *47*, 775–778. [CrossRef] [PubMed]
42. Tobisch, S.; Bögel, H.; Taube, R. Mechanistic Studies of the 1,4-Cis Polymerization of Butadiene According to the π-Allyl Insertion Mechanism. 1. Density Functional Study of the C−C Bond Formation Reaction in Cationic (η^3-Allyl)(η^2-/η^4-butadiene)nickel(II) Complexes $[Ni(C_3H_5)(C_4H6)]^+$ and $[Ni(C_3H_5)(C_4H_6)(C_2H_4)]^+$. *Organometallics* **1996**, *15*, 3563–3571.
43. Taube, R.; Windisch, H.; Maiwald, S. The catalysis of the stereospecific butadiene polymerization by Allyl Nickel and Allyl Lanthanide complexes—A mechanistic comparison. *Macromol. Symp.* **1995**, *89*, 393–409. [CrossRef]
44. Ward, B.D.; Bellemin-Laponnaz, S.; Gade, L.H. C_3 Chirality in Polymerization Catalysis: A Highly Active Dicationic Scandium(III) Catalyst for the Isoselective Polymerization of 1-Hexene. *Angew. Chem. Int. Ed.* **2005**, *44*, 1668–1671. [CrossRef] [PubMed]
45. Arndt, S.; Spaniol, T.P.; Okuda, J. Homogeneous Ethylene-Polymerization Catalysts Based on Alkyl Cations of the Rare-Earth Metals: Are Dicationic Mono(alkyl) Complexes the Active Species? *Angew. Chem. Int. Ed.* **2003**, *42*, 5075–5079. [CrossRef] [PubMed]
46. Dettenrieder, N.; Hollfelder, C.O.; Jende, L.N.; Maichle-Mössmer, C.; Anwander, R. Half-Sandwich Rare-Earth-Metal Alkylaluminate Complexes Bearing Peripheral Boryl Ligands. *Organometallics* **2014**, *33*, 1528–1531. [CrossRef]
47. Valente, A.; Mortreux, A.; Visseaux, M.; Zinck, P. Coordinative Chain Transfer Polymerization. *Chem. Rev.* **2013**, *113*, 3836–3857. [CrossRef] [PubMed]
48. Brintzinger, H.H.; Fischer, D.; Mülhaupt, R.; Rieger, B.; Waymouth, R.M. Stereospecific Olefin Polymerization with Chiral Metallocene Catalysts. *Angew. Chem. Int. Ed.* **1995**, *34*, 1143–1170. [CrossRef]
49. Rocha, T.C.J.; Coutinho, F.M.B.; Soares, B.G. Effect of alkylaluminum structure on Ziegler-Natta catalyst systems based on neodymium for producing high-cis polybutadiene. *Polym. Bull.* **2009**, *62*, 1–10. [CrossRef]
50. Hagihara, H.; Shiono, T.; Ikeda, T. Stereospecificity of propene polymerization with achiral titanocene-based catalysts. *Macromol. Chem. Phys.* **1998**, *199*, 2439–2444. [CrossRef]
51. Krause, L.; Herbst-Irmer, R.; Sheldrick, G.M.; Stalke, D. Comparison of silver and molybdenum microfocus X-ray sources for single-crystal structure determination. *J. Appl. Cryst.* **2015**, *48*, 3–10. [CrossRef] [PubMed]
52. Sheldrick, G.M. *SHELXT*—Integrated space-group and crystal-structure determination. *Acta Cryst.* **2015**, *A71*, 3–8. [CrossRef] [PubMed]
53. Sheldrick, G.M. Crystal structure refinement with *Shelxl*. *Acta Cryst.* **2015**, *C71*, 3–8.
54. Hubschle, C.B.; Sheldrick, G.M.; Dittrich, B. ShelXle: A Qt graphical user interface for SHELXL. *J. Appl. Crystallogr.* **2011**, *44*, 1281–1284. [CrossRef] [PubMed]
55. Elgert, K.-F.; Quack, G.; Stützel, B. Zur Struktur des Polybutadiens, 3. Das ^{13}C-NMR-Spektrum des *cis*-1,4-1,2-polybutadiens. *Makromol. Chem.* **1975**, *176*, 759–765. [CrossRef]
56. Elgert, K.-F.; Quack, G.; Stützel, B. Zur Struktur des Polybutadiens, 2. Das ^{13}C-NMR-Spektrum des 1,2-polybutadiens. *Makromol. Chem.* **1974**, *175*, 1955–1960. [CrossRef]
57. Elgert, K.-F.; Stützel, B.; Frenzel, P.; Cantow, H.-J.; Streck, R. Zur Struktur des Polybutadiens, 1. Das ^{13}C-NMR-Spektrum der 1,4-Polybutadiene. *Makromol. Chem.* **1973**, *170*, 257–260. [CrossRef]
58. Santee, E.R.; Chang, R.; Morton, M. 300 MHz proton NMR of polybutadiene: Measurement of *cis-trans* isomeric content. *J. Polym. Sci. Polym. Lett. Ed.* **1973**, *11*, 449–452. [CrossRef]

© 2018 by the authors. Licensee MDPI, Basel, Switzerland. This article is an open access article distributed under the terms and conditions of the Creative Commons Attribution (CC BY) license (http://creativecommons.org/licenses/by/4.0/).

Paper IV:Supplementary Materials

© (2018) by the authors, This Supplementary Materials are reprinted without modifications under the terms and conditions of the Creative Commons Attribution (CC BY 4.0, http://creativecommons.org/licences/4.0/) and have been published as the Supplementary Materials of:

"1,3-Diene Polymerization Mediated by Homoleptic Tetramethylaluminates of the Rare-Earth Metals"

by
Christoph O. Hollfelder, Lars N. Jende, Dominic Diether, Theresa Zelger, Rita Stauder, Cäcilia Maichle-Mössmer and Reiner Anwander

in
Catalysts, **2018**, *8*, 61, ISSN: 2073-4344
doi:10.3390/catal8020061.

It is available free of charge at https://www.mdpi.com/2073-4344/8/2/61.

Catalysts **2018**, *8*, x FOR PEER REVIEW

Suppplementary Materials: 1,3-Diene Polymerization Mediated by Homoleptic Tetramethylaluminates of the Rare-Earth Metals

Christoph O. Hollfelder [1], Lars N. Jende [1], Dominic Diether [1], Theresa Zelger [1], Rita Stauder [1], Cäcilia Maichle-Mössmer [1] and Reiner Anwander [1,*]

S1. Polymerization Data

S1.1 Isoprene polymerization at standard conditions

If not mentioned otherwise in the respective table, the polymers shown in this section have been synthesized according to the procedure given in Section 3.4 of the main article (Materials and Methods) or are taken from the literature for comparison.

Table S1.1.1. Comparison of the polyisoprenes obtained applying cocatalyst **A**[a]

entry[b]	precatalyst	cocatalyst[c]	yield [%]	*cis*-content [%][d]	*trans*-content [%][d]	vinylic content [%][d]	M_n [10^4 g/mol][e]	*PDI*[e]	T_g [°C][g]	ref.
1[h]	La(AlMe$_4$)$_3$ (**2^{La}**)	**A**	>99	46.3	51.4	2.3	5.0	1.29	n.d.	[1]
2	Ce(AlMe$_4$)$_3$ (**2^{Ce}**)	**A**	>99	44.4	51.8	3.8	3.5	1.25	-62	-[s]
3	Pr(AlMe$_4$)$_3$ (**2^{Pr}**)	**A**	93	44.7	50.2	5.1	3.9	1.35	-66	-[s]
4	Nd(AlMe$_4$)$_3$ (**2Nd**)	**A**	86	44.3	50.9	4.9	3.8	1.29	-64	-[s]
5	Gd(AlMe$_4$)$_3$ (**2^{Gd}**)	**A**	95	62.4	26.4	11.3	5.6	1.76	-59	-[s]
6	Tb(AlMe$_4$)$_3$ (**2^{Tb}**)	**A**	85	55.1	33.5	11.4	5.2	3.02	-55	-[s]
7	Dy(AlMe$_4$)$_3$ (**2^{Dy}**)	**A**	92	58.7	29.0	12.3	9.6	1.74	-60	-[s]
8	Ho(AlMe$_4$)$_3$ (**2^{Ho}**)	**A**	84	63.7	24.2	12.1	5.6	2.15	-56	-[s]
9[h]	Y(AlMe$_4$)$_3$ (**2^{Y}**)	**A**	>99	69.1	23.6	7.3	9.0	2.09	n.d.	[1]
10	Er(AlMe$_4$)$_3$ (**2Er**)	**A**	80	70.3	21.5	8.3	7.9	1.91	-56	-[s]
11	Lu(AlMe$_4$)$_3$ (**2^{Lu}**)	**A**	>99	77.1	17.6	5.3	6.7	1.58	-62	-[s]
12	La(AlMe$_4$)$_3$ (**2^{La}**)	2**A**	79	69.9	18.2	11.9	5.3[f]	6.90[f]	-63	-[s]
13	Ce(AlMe$_4$)$_3$ (**2^{Ce}**)	2**A**	>99	68.1	18.7	13.3	4.0	1.28	-55	-[s]
14	Pr(AlMe$_4$)$_3$ (**2^{Pr}**)	2**A**	78	n.d.[u]	n.d.[u]	n.d.[u]	8.0[f]	2.35[f]	n.d.	-[s]
15	Nd(AlMe$_4$)$_3$ (**2Nd**)	2**A**	76	66.2	21.2	12.6	4.7	1.38	-57	-[s]
16	Gd(AlMe$_4$)$_3$ (**2^{Gd}**)	2**A**	99	75.8	9.0	15.2	2.9	1.63	-51	-[s]
17	Tb(AlMe$_4$)$_3$ (**2^{Tb}**)	2**A**	77	76.3	8.2	15.5	2.6	1.62	-52	-[s]
18	Dy(AlMe$_4$)$_3$ (**2^{Dy}**)	2**A**	82	72.1	10.4	17.5	1.5	1.87	-55	-[s]
19	Ho(AlMe$_4$)$_3$ (**2^{Ho}**)	2**A**	85	77.9	6.5	15.6	3.7	1.57	-55	-[s]
20	Y(AlMe$_4$)$_3$ (**2^{Y}**)	2**A**	77	73.7	11.7	14.5	3.1	1.62	-53	-[s]
21	Er(AlMe$_4$)$_3$ (**2Er**)	2**A**	79	76.5	5.9	17.7	4.1	1.62	-50	-[s]
22	Lu(AlMe$_4$)$_3$ (**2^{Lu}**)	2**A**	90	70.3	13.8	15.9	3.4	1.62	-55	-[s]

[a] For data sorted by precatalyst, see Section S1.2. [b] Conditions: 0.02 mmol of the resp. Ln precatalyst, 0.02 or 0.04 mmol co-catalyst, in toluene, [Ln]:[isoprene] 1:1000 (n/n), reaction time 1 h, pre-reaction time 0.5 h. [c] **A** = [Ph$_3$C][B(C$_6$F$_5$)$_4$]. [d] Determined by ^{1}H and ^{13}C NMR spectroscopy in CDCl$_3$. [e] Determined by means of size-exclusion chromatography (SEC) against polystyrene standards. [g] Determined by differential scanning calorimetry; heating rate: 20 K/min, cooling rate: 60 K/min. [h] Reaction time 24 h. [f] These data represent only 28.5 mol% (**2^{La}**) and 75 mol% (**2^{Pr}**) of the polymer, the rest showed swelling behavior in THF implying crosslinking. [s] This study. [u] Insoluble in CDCl$_3$.

Table S1.1.2. Comparison of the polyisoprenes obtained applying cocatalyst **B**[a]

entry[b]	precatalyst	cocatalyst[c]	yield [%]	*cis*-content [%][d]	*trans*-content [%][d]	vinylic content [%][d]	M_n [10^4 g/mol][e]	*PDI*[e]	T_g [°C][g]	ref.
1[h]	$La(AlMe_4)_3$ (**2^{La}**)	**B**	>99	49.8	46.8	3.4	6.0	1.23	n.d.	[1]
2	$Ce(AlMe_4)_3$ (**2^{Ce}**)	**B**	92	43.7	53.0	3.3	2.8	1.35	-62	-[s]
3	$Pr(AlMe_4)_3$ (**2^{Pr}**)	**B**	92	45.5	50.2	4.3	3.2	1.55	-67	-[s]
4	$Nd(AlMe_4)_3$ (**2Nd**)	**B**	79	46.8	48.4	4.8	1.6	1.27	-64	-[s]
5	$Gd(AlMe_4)_3$ (**2^{Gd}**)	**B**	89	58.8	30.0	11.2	6.1	1.70	-64	-[s]
6	$Tb(AlMe_4)_3$ (**2^{Tb}**)	**B**	87	58.9	27.6	13.4	7.5	1.97	-57	-[s]
7	$Dy(AlMe_4)_3$ (**2^{Dy}**)	**B**	95	57.5	27.4	15.1	10.0	1.70	-58	-[s]
8	$Ho(AlMe_4)_3$ (**2^{Ho}**)	**B**	93	64.3	20.0	15.7	12.1	1.85	-56	-[s]
9[h]	$Y(AlMe_4)_3$ (**2^{Y}**)	**B**	>99	60.0	26.0	14.0	11.7	1.60	n.d.	[2]
10	$Er(AlMe_4)_3$ (**2Er**)	**B**	81	67.6	19.0	13.5	9.1	2.63	-55	-[s]
11	$Lu(AlMe_4)_3$ (**2^{Lu}**)	**B**	>99	77.2	16.9	5.9	5.2	2.06	-63	-[s]
12	$La(AlMe_4)_3$ (**2^{La}**)	2**B**	88	70.5	19.4	10.1	5.0	1.15	-62	-[s]
13	$Ce(AlMe_4)_3$ (**2^{Ce}**)	2**B**	>99	57.7	33.5	8.8	3.5	1.18	-62	-[s]
14	$Pr(AlMe_4)_3$ (**2^{Pr}**)	2**B**	90	45.9	49.7	4.4	14.1	1.78	-65	-[s]
15	$Nd(AlMe_4)_3$ (**2Nd**)	2**B**	82	62.6	28.5	8.9	4.4	1.26	-57	-[s]
16	$Gd(AlMe_4)_3$ (**2^{Gd}**)	2**B**	94	66.3	21.6	12.0	8.4	1.88	-61	-[s]
17	$Tb(AlMe_4)_3$ (**2^{Tb}**)	2**B**	87	65.6	19.4	15.0	5.6	1.74	-58	-[s]
18	$Dy(AlMe_4)_3$ (**2^{Dy}**)	2**B**	88	65.2	19.9	14.9	6.7	1.79	-57	-[s]
19	$Ho(AlMe_4)_3$ (**2^{Ho}**)	2**B**	93	63.7	20.1	16.2	7.8	2.31	-55	-[s]
20[h]	$Y(AlMe_4)_3$ (**2^{Y}**)	2**B**	>99	67.0	13.0	20.0	26.0	1.50	n.d.	[2]
21	$Er(AlMe_4)_3$ (**2Er**)	2**B**	74	71.4	13.4	15.2	5.9	2.13	-52	-[s]
22	$Lu(AlMe_4)_3$ (**2^{Lu}**)	2**B**	>99	73.1	15.4	11.5	4.2	1.78	-59	-[s]

[a] For data sorted by precatalyst, see Section S1.2 .[b] Conditions: 0.02 mmol of the resp. Ln precatalyst, 0.02 or 0.04 mmol cocatalyst, in toluene, [Ln]:[isoprene] 1:1000 (n/n), reaction time 1 h, pre-reaction time 0.5 h. [c] **B** = $[PhNMe_2H][B(C_6F_5)_4]$. [d] Determined by ^1H and ^{13}C NMR spectroscopy in $CDCl_3$. [e] Determined by means of size-exclusion chromatography (SEC) against polystyrene standards.[g] Determined by differential scanning calorimetry; heating rate: 20 K/min, cooling rate: 60 K/min. [h] Reaction time 24 h. [s] This study.

Table S1.1.3. Comparison of the polyisoprenes obtained applying cocatalyst C[a]

entry[b]	precatalyst	cocatalyst[c]	yield [%]	*cis*-content [%][d]	*trans*-content [%][d]	vinylic content [%][d]	M_n [10^4 g/mol][e]	*PDI*[e]	T_g [°C][g]	ref.
1[h]	La(AlMe$_4$)$_3$ (**2^{La}**)	**C**	>99	39.1	59.5	1.4	33.0	1.18	n.d.	[1]
2	Ce(AlMe$_4$)$_3$ (**2^{Ce}**)	**C**	86	55.4	41.8	2.7	3.3	1.22	-61	-[s]
3	Pr(AlMe$_4$)$_3$ (**2^{Pr}**)	**C**	87	65.6	30.4	4.0	6.8	1.32	-65	-[s]
4	Nd(AlMe$_4$)$_3$ (**2Nd**)	**C**	76	68.0	29.2	2.7	7.9	1.16	-63	-[s]
5	Gd(AlMe$_4$)$_3$ (**2^{Gd}**)	**C**	87	63.4	36.6	0.0	9.6	1.28	-65	-[s]
6	Tb(AlMe$_4$)$_3$ (**2^{Tb}**)	**C**	83	60.4	35.5	4.1	8.0	1.57	-66	-[s]
7	Dy(AlMe$_4$)$_3$ (**2^{Dy}**)	**C**	54	63.3	33.0	3.7	8.5	1.33	-65	-[s]
8	Ho(AlMe$_4$)$_3$ (**2^{Ho}**)	**C**	78	57.0	38.8	4.3	11.6	1.73	-64	-[s]
9[h]	Y(AlMe$_4$)$_3$ (**2^{Y}**)	**C**	56	62.5	35.1	2.4	12.0	2.03	n.d.	[1]
10	Er(AlMe$_4$)$_3$ (**2Er**)	**C**	85	74.2	21.4	4.5	15.5	1.86	-59	-[s]
11	Lu(AlMe$_4$)$_3$ (**2^{Lu}**)	**C**	>99	67.6	28.1	4.3	23.0	1.55	-61	-[s]
12	La(AlMe$_4$)$_3$ (**2^{La}**)	**2C**	69	77.6	18.8	3.7	16.3	1.40	-63	-[s]
13	Ce(AlMe$_4$)$_3$ (**2^{Ce}**)	**2C**	84	86.0	8.8	5.2	5.9	1.13	-58	-[s]
14	Pr(AlMe$_4$)$_3$ (**2^{Pr}**)	**2C**	87	87.9	6.0	6.1	8.7	1.35	-61	-[s]
15	Nd(AlMe$_4$)$_3$ (**2Nd**)	**2C**	83	92.7	2.9	4.5	17.6	2.48	-61	-[s]
16	Gd(AlMe$_4$)$_3$ (**2^{Gd}**)	**2C**	87	87.0	7.0	6.0	11.8	1.36	-68	-[s]
17	Tb(AlMe$_4$)$_3$ (**2^{Tb}**)	**2C**	83	89.7	5.5	4.8	10.6	1.43	-61	-[s]
18	Dy(AlMe$_4$)$_3$ (**2^{Dy}**)	**2C**	94	91.5	3.9	4.6	13.1	1.40	-61	-[s]
19	Ho(AlMe$_4$)$_3$ (**2^{Ho}**)	**2C**	90	90.4	4.1	5.5	17.6	1.39	-62	-[s]
20	Y(AlMe$_4$)$_3$ (**2^{Y}**)	**2C**	86	82.2	13.3	4.4	16.1	1.55	-62	-[s]
21	Er(AlMe$_4$)$_3$ (**2Er**)	**2C**	93	92.6	2.1	5.2	15.5	1.75	-57	-[s]
22	Lu(AlMe$_4$)$_3$ (**2^{Lu}**)	**2C**	>99	85.9	8.7	5.4	9.2	2.07	-61	-[s]

[a] For data sorted by precatalyst, see Section S1.2. [b] Conditions: 0.02 mmol of the resp. Ln precatalyst, 0.02 or 0.04 mmol cocatalyst, in toluene, [Ln]:[isoprene] 1:1000 (n/n), reaction time 1 h, pre-reaction time 0.5 h. [c] **C** = B(C$_6$F$_5$)$_3$. [d] Determined by ^{1}H and ^{13}C NMR spectroscopy in CDCl$_3$. [e] Determined by means of size-exclusion chromatography (SEC) against polystyrene standards. [g] Determined by differential scanning calorimetry; heating rate: 20 K/min, cooling rate: 60 K/min. [h] Reaction time 24 h. [s] This study.

Table S1.1.4. Comparison of the polyisoprenes obtained applying cocatalyst D[a]

entry[b]	precatalyst	cocatalyst[c]	yield [%]	*cis*-content [%][d]	*trans*-content [%][d]	vinylic content [%][d]	M_n [10^4 g/mol][e]	*PDI*[e]	T_g [°C][g]	ref.
1[z]	La(AlMe$_4$)$_3$ (**2^{La}**)	**D**	4	-[f]	-[f]	-[f]	1.6	6.28	-61	-[s]
2	Ce(AlMe$_4$)$_3$ (**2^{Ce}**)	**D**	7	97.1	0.0	2.9	11.7	1.28	-59	-[s]
3	Pr(AlMe$_4$)$_3$ (**2^{Pr}**)	**D**	27	97.2	0.0	2.8	6.5	2.98	-64	-[s]
4	Nd(AlMe$_4$)$_3$ (**2Nd**)	**D**	40	98.9	0.0	1.1	9.4	6.77	-60	-[s]
5	Gd(AlMe$_4$)$_3$ (**2^{Gd}**)	**D**	51	>99.9	0.0	0.0	5.6	5.30	-67	-[s]
6	Tb(AlMe$_4$)$_3$ (**2^{Tb}**)	**D**	66	85.0	13.5	1.5	4.9	4.44	-66	-[s]
7	Dy(AlMe$_4$)$_3$ (**2^{Dy}**)	**D**	34	79.3	20.7	0.0	3.0	6.52	-67	-[s]
8	Ho(AlMe$_4$)$_3$ (**2^{Ho}**)	**D**	7	67.6	31.1	1.3	2.9	2.64	-67	-[s]
9	Y(AlMe$_4$)$_3$ (**2^{Y}**)	**D**	traces	40.6	52.5	6.9	-[f]	-[f]	-[f]	-[s]
10	Er(AlMe$_4$)$_3$ (**2Er**)	**D**	traces	-[f]	-[f]	-[f]	-[f]	-[f]	-[f]	-[s]
11	Lu(AlMe$_4$)$_3$ (**2^{Lu}**)	**D**	none	-[f]	-[f]	-[f]	-[f]	-[f]	-[f]	-[s]
12	La(AlMe$_4$)$_3$ (**2^{La}**)	**2D**	2	91.5	5.6	2.9	-[f]	-[f]	-[f]	-[s]
13	Ce(AlMe$_4$)$_3$ (**2^{Ce}**)	**2D**	21	97.4	0.0	2.6	3.3	3.73	-60	-[s]
14	Pr(AlMe$_4$)$_3$ (**2^{Pr}**)	**2D**	42	97.4	0.0	2.6	8.7	3.09	-62	-[s]
15	Nd(AlMe$_4$)$_3$ (**2Nd**)	**2D**	56	97.9	0.0	2.1	11.3	5.26	-61	-[s]
16	Gd(AlMe$_4$)$_3$ (**2^{Gd}**)	**2D**	56	96.0	4.0	0.0	6.9	7.00	-67	-[s]
17	Tb(AlMe$_4$)$_3$ (**2^{Tb}**)	**2D**	67	84.6	13.6	1.9	3.6	6.63	-66	-[s]
18	Dy(AlMe$_4$)$_3$ (**2^{Dy}**)	**2D**	31	88.7	11.3	0.0	3.2	6.19	-67	-[s]
19	Ho(AlMe$_4$)$_3$ (**2^{Ho}**)	**2D**	17	68.3	31.7	0.0	3.6	4.87	-66	-[s]
20	Y(AlMe$_4$)$_3$ (**2^{Y}**)	**2D**	6	52.9	46.2	0.9	2.9	2.92	-68	-[s]
21[z]	Er(AlMe$_4$)$_3$ (**2Er**)	**2D**	traces	-[f]	-[f]	-[f]	-[f]	-[f]	-[f]	-[s]
22	Lu(AlMe$_4$)$_3$ (**2^{Lu}**)	**2D**	none	-[f]	-[f]	-[f]	-[f]	-[f]	-[f]	-[s]

[a] For data sorted by precatalyst, see Section S1.2.[b] Conditions: 0.02 mmol of the resp. Ln precatalyst, 0.02 or 0.04 mmol cocatalyst, in toluene, [Ln]:[isoprene] 1:1000 (n/n), reaction time 1 h, pre-reaction time 0.5 h. [c] **D** = Me_2AlCl. [d] Determined by ^1H and ^{13}C NMR spectroscopy in $CDCl_3$. [e] Determined by means of size-exclusion chromatography (SEC) against polystyrene standards. [f] No further evaluation possible due to low yield. [g] Determined by differential scanning calorimetry; heating rate: 20 K/min, cooling rate: 60 K/min. [s] This study. [z] For data obtained for a reaction time of 24 h with this active system, see Table S1.4.4.

Table S1.1.5. Comparison of the polyisoprenes obtained applying cocatalyst **E**[a]

entry[b]	precatalyst	cocatalyst[c]	yield [%]	*cis*-content [%][d]	*trans*-content [%][d]	vinylic content [%][d]	M_n [10^4 g/mol][e]	*PDI*[e]	T_g [°C][g]	ref.
1[z]	La(AlMe$_4$)$_3$ (**2^{La}**)	**E**	3	89.3	7.6	3.1	–[f]	–[f]	–[f]	–[s]
2	Ce(AlMe$_4$)$_3$ (**2^{Ce}**)	**E**	19	97.2	0.0	2.8	0.2	3.44	-61	–[s]
3	Pr(AlMe$_4$)$_3$ (**2^{Pr}**)	**E**	43	97.6	0.0	2.4	4.4	4.84	-61	–[s]
4	Nd(AlMe$_4$)$_3$ (**2Nd**)	**E**	57	98.2	0.0	1.8	5.6	4.52	-61	–[s]
5	Gd(AlMe$_4$)$_3$ (**2^{Gd}**)	**E**	77	94.6	4.2	1.2	3.8	7.89	-63	–[s]
6	Tb(AlMe$_4$)$_3$ (**2^{Tb}**)	**E**	82	88.8	9.7	1.5	2.5	6.36	-67	–[s]
7	Dy(AlMe$_4$)$_3$ (**2^{Dy}**)	**E**	34	82.6	17.4	0.0	1.9	6.80	-67	–[s]
8	Ho(AlMe$_4$)$_3$ (**2^{Ho}**)	**E**	15	61.5	37.1	1.4	2.2	2.70	-67	–[s]
9	Y(AlMe$_4$)$_3$ (**2^{Y}**)	**E**	10	48.4	50.6	1.0	2.1	1.43	-67	–[s]
10[z]	Er(AlMe$_4$)$_3$ (**2Er**)	**E**	traces	–[f]	–[f]	–[f]	–[f]	–[f]	–[f]	–[s]
11	Lu(AlMe$_4$)$_3$ (**2^{Lu}**)	**E**	none	–[f]	–[f]	–[f]	–[f]	–[f]	–[f]	–[s]
12[z]	La(AlMe$_4$)$_3$ (**2^{La}**)	**2E**	5	92.1	5.0	2.9	2.3	3.27	-62	–[s]
13	Ce(AlMe$_4$)$_3$ (**2^{Ce}**)	**2E**	34	97.3	0.0	2.7	3.1	3.81	-61	–[s]
14	Pr(AlMe$_4$)$_3$ (**2^{Pr}**)	**2E**	84	95.4	2.3	2.3	4.1	4.10	-62	–[s]
15	Nd(AlMe$_4$)$_3$ (**2Nd**)	**2E**	86	98.0	0.0	2.0	5.3	4.66	-62	–[s]
16	Gd(AlMe$_4$)$_3$ (**2^{Gd}**)	**2E**	89	92.6	5.9	1.5	3.2	5.87	-63	–[s]
17	Tb(AlMe$_4$)$_3$ (**2^{Tb}**)	**2E**	87	90.2	8.1	1.7	2.1	12.66	-67	–[s]
18	Dy(AlMe$_4$)$_3$ (**2^{Dy}**)	**2E**	46	86.3	13.7	0.0	1.6	8.95	-67	–[s]
19	Ho(AlMe$_4$)$_3$ (**2^{Ho}**)	**2E**	4	71.5	28.5	0.0	2.5	4.90	-66	–[s]
20	Y(AlMe$_4$)$_3$ (**2^{Y}**)	**2E**	22	60.1	39.0	0.9	3.2	3.84	-66	–[s]
21[z]	Er(AlMe$_4$)$_3$ (**2Er**)	**2E**	2	47.4	51.3	1.3	–[f]	–[f]	-66	–[s]
22[z]	Lu(AlMe$_4$)$_3$ (**2^{Lu}**)	**2E**	traces	–[f]	–[f]	–[f]	–[f]	–[f]	–[f]	–[s]

[a] For data sorted by precatalyst, see Section S1.2. [b] Conditions: 0.02 mmol of the resp. Ln precatalyst, 0.02 or 0.04 mmol cocatalyst, in toluene, [Ln]:[isoprene] 1:1000 (n/n), reaction time 1 h, pre-reaction time 0.5 h. [c] **E** = Et_2AlCl. [d] Determined by ^1H and ^{13}C NMR spectroscopy in $CDCl_3$. [e] Determined by means of size-exclusion chromatography (SEC) against polystyrene standards. [f] No further evaluation possible due to low yield. [g] Determined by differential scanning calorimetry; heating rate: 20 K/min, cooling rate: 60 K/min. [h] Reaction time 24 h. [s] This study. [z] For data obtained for a reaction time of 24 h with this active system, see Table S1.4.4.

S1.2 Isoprene polymerization at standard conditions sorted by rare-earth metal

If not mentioned otherwise in the respective table, the polymers shown in this section have been synthesized according to the procedure given in Section 3.4 of the main article (Materials and Methods) or are taken from the literature for comparison.

Table S1.2.1. Comparison of the polyisoprenes obtained applying precatalyst **2**[La]

entry[b]	cocatalyst[c]	yield [%]	*cis*-content [%][d]	*trans*-content [%][d]	vinylic content [%][d]	M_n [10^4 g/mol][e]	*PDI*[e]	T_g [°C][g]	ref.
1[h]	**A**	>99	46.3	51.4	2.3	5.0	1.29	n.d.	[1]
2	2**A**	79	69.9	18.2	11.9	5.3	6.90	-63	-[s]
3[h]	**B**	>99	49.8	46.8	3.4	6.0	1.23	n.d.	[1]
4	2**B**	88	70.5	19.4	10.1	5.0	1.15	-62	-[s]
5[h]	**C**	>99	39.1	59.5	1.4	33.0	1.18	n.d.	[1]
6	2**C**	69	77.6	18.8	3.7	16.3	1.40	-63	-[s]
7	**D**	4	-[f]	-[f]	-[f]	1.6	6.28	-61	-[s]
8	2**D**	2	91.5	5.6	2.9	-[f]	-[f]	-[f]	-[s]
9	**E**	3	89.3	7.6	3.1	-[f]	-[f]	-[f]	-[s]
10	2**E**	5	92.1	5.0	2.9	2.3	3.27	-62	-[s]

[b] Conditions: 0.02 mmol of **2**[La], 0.02 or 0.04 mmol cocatalyst, in toluene, [Ln]:[isoprene] 1:1000 (n/n), reaction time 1 h, pre-reaction time 0.5 h. [c] **A** = $[Ph_3C][B(C_6F_5)_4]$, **B** = $[PhNMe_2H][B(C_6F_5)_4]$, **C** = $B(C_6F_5)_3$, **D** = Me_2AlCl, **E** = Et_2AlCl. [d] Determined by ^1H and ^{13}C NMR spectroscopy in $CDCl_3$. [e] Determined by means of size-exclusion chromatography (SEC) against polystyrene standards. [g] Determined by differential scanning calorimetry; heating rate: 20 K/min, cooling rate: 60 K/min. [f] No further evaluation possible due to low yield. [h] Reaction time 24 h. [s] This study.

Table S1.2.2. Comparison of the polyisoprenes obtained applying precatalyst **2**[Ce]

entry[b]	cocatalyst[c]	yield [%]	*cis*-content [%][d]	*trans*-content [%][d]	vinylic content [%][d]	M_n [10^4 g/mol][e]	*PDI*[e]	T_g [°C][g]	ref.
1	**A**	> 99	44.4	51.8	3.8	3.5	1.25	-62	-[s]
2	2**A**	> 99	68.1	18.7	13.3	4.0	1.28	-55	-[s]
3	**B**	92	43.7	53.0	3.3	2.8	1.35	-62	-[s]
4	2**B**	> 99	57.7	33.5	8.8	3.5	1.18	-62	-[s]
5	**C**	86	55.4	41.8	2.7	3.3	1.22	-61	-[s]
6	2**C**	84	86.0	8.8	5.2	5.9	1.13	-58	-[s]
7	**D**	7	97.1	0.0	2.9	11.7	1.28	-59	-[s]
8	2**D**	21	97.4	0.0	2.6	3.3	3.73	-60	-[s]
9	**E**	19	97.2	0.0	2.8	0.2	3.44	-61	-[s]
10	2**E**	34	97.3	0.0	2.7	3.1	3.81	-61	-[s]

[b] Conditions: 0.02 mmol of **2**[Ce], 0.02 or 0.04 mmol cocatalyst, in toluene, [Ln]:[isoprene] 1:1000 (n/n), reaction time 1 h, pre-reaction time 0.5 h. [c] **A** = $[Ph_3C][B(C_6F_5)_4]$, **B** = $[PhNMe_2H][B(C_6F_5)_4]$, **C** = $B(C_6F_5)_3$, **D** = Me_2AlCl, **E** = Et_2AlCl. [d] Determined by ^1H and ^{13}C NMR spectroscopy in $CDCl_3$. [e] Determined by means of size-exclusion chromatography (SEC) against polystyrene standards. [g] Determined by differential scanning calorimetry; heating rate: 20 K/min, cooling rate: 60 K/min. [s] This study.

Table S1.2.3. Comparison of the polyisoprenes obtained applying pre-catalyst **2^{Pr}**

entry[b]	cocatalyst[c]	yield [%]	*cis*-content [%][d]	*trans*-content [%][d]	vinylic content [%][d]	M_n [10^4 g/mol][e]	*PDI*[e]	T_g [°C][g]	ref.
1	**A**	93	44.7	50.2	5.1	3.9	1.35	-66	-[s]
2	2**A**	78	n.d.[u]	n.d.[u]	n.d.[u]	8.0	2.35	n.d.	-[s]
3	**B**	92	45.5	50.2	4.3	3.2	1.55	-67	-[s]
4	2**B**	90	45.9	49.7	4.4	14.1	1.78	-65	-[s]
5	**C**	87	65.6	30.4	4.0	6.8	1.32	-65	-[s]
6	2**C**	87	87.9	6.0	6.1	8.7	1.35	-61	-[s]
7	**D**	27	97.2	0.0	2.8	6.5	2.98	-64	-[s]
8	2**D**	42	97.4	0.0	2.6	8.7	3.09	-62	-[s]
9	**E**	43	97.6	0.0	2.4	4.4	4.84	-61	-[s]
10	2**E**	84	95.4	2.3	2.3	4.1	4.10	-62	-[s]

[b] Conditions: 0.02 mmol of **2^{Pr}**, 0.02 or 0.04 mmol cocatalyst, in toluene, [Ln]:[isoprene] 1:1000 (n/n), reaction time 1 h, pre-reaction time 0.5 h. [c] **A** = $[Ph_3C][B(C_6F_5)_4]$, **B** = $[PhNMe_2H][B(C_6F_5)_4]$, **C** = $B(C_6F_5)_3$, **D** = Me_2AlCl, **E** = Et_2AlCl. [d] Determined by ^1H and ^{13}C NMR spectroscopy in $CDCl_3$. [e] Determined by means of size-exclusion chromatography (SEC) against polystyrene standards. [f] No further evaluation possible due to low yield. [g] Determined by differential scanning calorimetry; heating rate: 20 K/min, cooling rate: 60 K/min. [s] This study. [u] Insoluble in $CDCl_3$.

Table S1.2.4. Comparison of the polyisoprenes obtained applying precatalyst **2Nd**

entry[b]	cocatalyst[c]	yield [%]	*cis*-content [%][d]	*trans*-content [%][d]	vinylic content [%][d]	M_n [10^4 g/mol][e]	*PDI*[e]	T_g [°C][g]	ref.
1	**A**	86	44.3	50.9	4.9	3.8	1.29	-64	-[s]
2	2**A**	76	66.2	21.2	12.6	4.7	1.38	-57	-[s]
3	**B**	79	46.8	48.4	4.8	1.6	1.27	-64	-[s]
4	2**B**	82	62.6	28.5	8.9	4.4	1.26	-57	-[s]
5	**C**	76	68.0	29.2	2.7	7.9	1.16	-63	-[s]
6	2**C**	83	92.7	2.9	4.5	17.6	2.48	-61	-[s]
7	**D**	40	98.9	0.0	1.1	9.4	6.77	-60	-[s]
8	2**D**	56	97.9	0.0	2.1	11.3	5.26	-61	-[s]
9	**E**	57	98.2	0.0	1.8	5.6	4.52	-61	-[s]
10	2**E**	86	98.0	0.0	2.0	5.3	4.66	-62	-[s]

[b] Conditions: 0.02 mmol of **2Nd**, 0.02 or 0.04 mmol cocatalyst, in toluene, [Ln]:[isoprene] 1:1000 (n/n), reaction time 1 h, pre-reaction time 0.5 h. [c] **A** = $[Ph_3C][B(C_6F_5)_4]$, **B** = $[PhNMe_2H][B(C_6F_5)_4]$, **C** = $B(C_6F_5)_3$, **D** = Me_2AlCl, **E** = Et_2AlCl. [d] Determined by ^1H and ^{13}C NMR spectroscopy in $CDCl_3$.

[e] Determined by means of size-exclusion chromatography (SEC) against polystyrene standards. [g] Determined by differential scanning calorimetry; heating rate: 20 K/min, cooling rate: 60 K/min. [s] This study.

Table S1.2.5. Comparison of the polyisoprenes obtained applying precatalyst **2**^{Gd}

entry[b]	cocatalyst[c]	yield [%]	*cis*-content [%][d]	*trans*-content [%][d]	vinylic content [%][d]	M_n [10^4 g/mol][e]	*PDI*[e]	T_g [°C][g]	ref.
1	**A**	95	62.4	26.4	11.3	5.6	1.76	-59	-[s]
2	2**A**	99	75.8	9.0	15.2	2.9	1.63	-51	-[s]
3	**B**	89	58.8	30.0	11.2	6.1	1.70	-64	-[s]
4	2**B**	94	66.3	21.6	12.0	8.4	1.88	-61	-[s]
5	**C**	87	63.4	36.6	0.0	9.6	1.28	-65	-[s]
6	2**C**	87	87.0	7.0	6.0	11.8	1.36	-66	-[s]
7	**D**	51	>99.9	0.0	0.0	5.6	5.30	-67	-[s]
8	2**D**	56	96.0	4.0	0.0	6.9	7.00	-67	-[s]
9	**E**	77	94.6	4.2	1.2	3.8	7.89	-63	-[s]
10	2**E**	89	92.6	5.9	1.5	3.2	5.87	-63	-[s]

[b] Conditions: 0.02 mmol of **2**^{Gd}, 0.02 or 0.04 mmol cocatalyst, in toluene, [Ln]:[isoprene] 1:1000 (n/n), reaction time 1 h, pre-reaction time 0.5 h. [c] **A** = $[Ph_3C][B(C_6F_5)_4]$, **B** = $[PhNMe_2H][B(C_6F_5)_4]$, **C** = $B(C_6F_5)_3$, **D** = Me_2AlCl, **E** = Et_2AlCl. [d] Determined by ^1H and ^{13}C NMR spectroscopy in $CDCl_3$.

[e] Determined by means of size-exclusion chromatography (SEC) against polystyrene standards. [g] Determined by differential scanning calorimetry; heating rate: 20 K/min, cooling rate: 60 K/min. [s] This study.

Table S1.2.6. Comparison of the polyisoprenes obtained applying precatalyst **2**^{Tb}

entry[b]	cocatalyst[c]	yield [%]	*cis*-content [%][d]	*trans*-content [%][d]	vinylic content [%][d]	M_n [10^4 g/mol][e]	*PDI*[e]	T_g [°C][g]	ref.
1	**A**	85	55.1	33.5	11.4	5.2	3.02	-55	-[s]
2	2**A**	77	76.3	8.2	15.5	2.6	1.62	-52	-[s]
3	**B**	87	58.9	27.6	13.4	7.5	1.97	-57	-[s]
4	2**B**	87	65.6	19.4	15.0	5.6	1.74	-58	-[s]
5	**C**	83	60.4	35.5	4.1	8.0	1.57	-66	-[s]
6	2**C**	83	89.7	5.5	4.8	10.6	1.43	-61	-[s]
7	**D**	66	85.0	13.5	1.5	4.9	4.44	-66	-[s]
8	2**D**	67	84.6	13.6	1.9	3.6	6.63	-66	-[s]
9	**E**	82	88.8	9.7	1.5	2.5	6.36	-67	-[s]
10	2**E**	87	90.2	8.1	1.7	2.1	12.66	-67	-[s]

[b] Conditions: 0.02 mmol of **2**^{Tb}, 0.02 or 0.04 mmol cocatalyst, in toluene, [Ln]:[isoprene] 1:1000 (n/n), reaction time 1 h, pre-reaction time 0.5 h. [c] **A** = $[Ph_3C][B(C_6F_5)_4]$, **B** = $[PhNMe_2H][B(C_6F_5)_4]$, **C** = $B(C_6F_5)_3$, **D** = Me_2AlCl, **E** = Et_2AlCl. [d] Determined by ^1H and ^{13}C NMR spectroscopy in $CDCl_3$.

[e] Determined by means of size-exclusion chromatography (SEC) against polystyrene standards. [g] Determined by differential scanning calorimetry; heating rate: 20 K/min, cooling rate: 60 K/min. [s] This study.

Table S1.2.7. Comparison of the polyisoprenes obtained applying precatalyst **2^{Dy}**

entry[b]	cocatalyst[c]	yield [%]	*cis*-content [%][d]	*trans*-content [%][d]	vinylic content [%][d]	M_n [10^4 g/mol][e]	*PDI*[e]	T_g [°C][g]	ref.
1	**A**	92	58.7	29.0	12.3	9.6	1.74	-60	-[s]
2	2**A**	82	72.1	10.4	17.5	1.5	1.87	-55	-[s]
3	**B**	95	57.5	27.4	15.1	10.0	1.70	-58	-[s]
4	2**B**	88	65.2	19.9	14.9	6.7	1.79	-57	-[s]
5	**C**	54	63.3	33.0	3.7	8.5	1.33	-65	-[s]
6	2**C**	94	91.5	3.9	4.6	13.1	1.40	-61	-[s]
7	**D**	34	79.3	20.7	0.0	3.0	6.52	-67	-[s]
8	2**D**	31	88.7	11.3	0.0	3.2	6.19	-67	-[s]
9	**E**	34	82.6	17.4	0.0	1.9	6.80	-67	-[s]
10	2**E**	46	86.3	13.7	0.0	1.6	8.95	-67	-[s]

[b] Conditions: 0.02 mmol of **2^{Dy}**, 0.02 or 0.04 mmol cocatalyst, in toluene, [Ln]:[isoprene] 1:1000 (n/n), reaction time 1 h, pre-reaction time 0.5 h.
[c] **A** = $[Ph_3C][B(C_6F_5)_4]$, **B** = $[PhNMe_2H][B(C_6F_5)_4]$, **C** = $B(C_6F_5)_3$, **D** = Me_2AlCl, **E** = Et_2AlCl. [d] Determined by ^1H and ^{13}C NMR spectroscopy in $CDCl_3$.
[e] Determined by means of size-exclusion chromatography (SEC) against polystyrene standards. [g] Determined by differential scanning calorimetry; heating rate: 20 K/min, cooling rate: 60 K/min. [s] This study.

Table S1.2.8 Comparison of the polyisoprenes obtained applying precatalyst **2^{Ho}**

entry[b]	cocatalyst[c]	yield [%]	*cis*-content [%][d]	*trans*-content [%][d]	vinylic content [%][d]	M_n [10^4 g/mol][e]	*PDI*[e]	T_g [°C][g]	ref.
1	**A**	84	63.7	24.2	12.1	5.6	2.15	-56	-[s]
2	2**A**	85	77.9	6.5	15.6	3.7	1.57	-55	-[s]
3	**B**	93	64.3	20.0	15.7	12.1	1.85	-56	-[s]
4	2**B**	93	63.7	20.1	16.2	7.8	2.31	-55	-[s]
5	**C**	78	57.0	38.8	4.3	11.6	1.73	-64	-[s]
6	2**C**	90	90.4	4.1	5.5	17.6	1.39	-62	-[s]
7	**D**	7	67.6	31.1	1.3	2.9	2.64	-67	-[s]
8	2**D**	17	68.3	31.7	0.0	3.6	4.87	-66	-[s]
9	**E**	15	61.5	37.1	1.4	2.2	2.7	-67	-[s]
10	2**E**	4	71.5	28.5	0.0	2.5	4.9	-66	-[s]

[b] Conditions: 0.02 mmol of **2^{Ho}**, 0.02 or 0.04 mmol cocatalyst, in toluene, [Ln]:[isoprene] 1:1000 (n/n), reaction time 1 h, pre-reaction time 0.5 h.
[c] **A** = $[Ph_3C][B(C_6F_5)_4]$, **B** = $[PhNMe_2H][B(C_6F_5)_4]$, **C** = $B(C_6F_5)_3$, **D** = Me_2AlCl, **E** = Et_2AlCl. [d] Determined by ^1H and ^{13}C NMR spectroscopy in $CDCl_3$.
[e] Determined by means of size-exclusion chromatography (SEC) against polystyrene standards. [g] Determined by differential scanning calorimetry; heating rate: 20 K/min, cooling rate: 60 K/min. [s] This study.

Table S1.2.9. Comparison of the polyisoprenes obtained applying pre-catalyst **2**^{Y}[a]

entry[b]	cocatalyst[c]	yield [%]	*cis*-content [%][d]	*trans*-content [%][d]	vinylic content [%][d]	M_n [10^4 g/mol][e]	*PDI*[e]	T_g [°C][g]	ref.
1[h]	**A**	>99	69.1	23.6	7.3	9.0	2.09	n.d.	[1]
2	2**A**	77	73.7	11.7	14.5	3.1	1.62	-53	-[s]
3[h]	**B**	>99	60.0	26.0	14.0	11.7	1.60	n.d.	[2]
4[h]	2**B**	> 99	67.0	13.0	20.0	26.0	1.50	n.d.	[2]
5[h]	**C**	56	62.5	35.1	2.4	12.0	2.03	n.d.	[1]
6	2**C**	86	82.2	13.3	4.4	16.1	1.55	-62	-[s]
7	**D**	traces	40.6	52.5	6.9	-[f]	-[f]	-[f]	-[s]
8	2**D**	6	52.9	46.2	0.9	2.9	2.92	-68	-[s]
9	**E**	10	48.4	50.6	1.0	2.1	1.43	-67	-[s]
10	2**E**	22	60.1	39.0	0.9	3.2	3.84	-66	-[s]

[a] For data produced by systems of **2**^{Y}/**B** and **2**^{Y}/2**B** in the presence of Al*i*Bu$_3$, see ref. [2]. [b] Conditions 0.02 mmol of **2**^{Y}, 0.02 or 0.04 mmol cocatalyst, in toluene, [Ln]:[isoprene] 1:1000 (n/n), reaction time 1 h, pre-reaction time 0.5 h. [c] **A** = [Ph_3C][$B(C_6F_5)_4$], **B** = [$PhNMe_2H$][$B(C_6F_5)_4$], **C** = $B(C_6F_5)_3$, **D** = Me_2AlCl, **E** = Et_2AlCl. [d] Determined by ^1H and ^{13}C NMR spectroscopy in $CDCl_3$. [e] Determined by means of size-exclusion chromatography (SEC) against polystyrene standards. [f] No further evaluation possible due to low yield. [g] Determined by differential scanning calorimetry; heating rate: 20 K/min, cooling rate: 60 K/min. [s] This study.

Table S1.2.10. Comparison of the polyisoprenes obtained applying precatalyst **2**^{Er}

entry[b]	cocatalyst[c]	yield [%]	*cis*-content [%][d]	*trans*-content [%][d]	vinylic content [%][d]	M_n [10^4 g/mol][e]	*PDI*[e]	T_g [°C][g]	ref.
1	**A**	80	70.3	21.5	8.3	7.9	1.91	-56	-[s]
2	2**A**	79	76.5	5.9	17.7	4.1	1.62	-50	-[s]
3	**B**	81	67.6	19.0	13.5	9.1	2.63	-55	-[s]
4	2**B**	74	71.4	13.4	15.2	5.9	2.13	-52	-[s]
5	**C**	85	74.2	21.4	4.5	15.5	1.86	-59	-[s]
6	2**C**	93	92.6	2.1	5.2	15.5	1.75	-57	-[s]
7	**D**	traces	-[f]	-[f]	-[f]	-[f]	-[f]	-[f]	-[s]
8	2**D**	traces	-[f]	-[f]	-[f]	-[f]	-[f]	-[f]	-[s]
9	**E**	traces	-[f]	-[f]	-[f]	-[f]	-[f]	-[f]	-[s]
10	2**E**	2	47.4	51.3	1.3	-[f]	-[f]	-[f]	-[s]

[b] Conditions 0.02 mmol of **2**^{Er}, 0.02 or 0.04 mmol cocatalyst, in toluene, [Ln]:[isoprene] 1:1000 (n/n), reaction time 1 h, pre-reaction time 0.5 h.
[c] **A** = [Ph_3C][$B(C_6F_5)_4$], **B** = [$PhNMe_2H$][$B(C_6F_5)_4$], **C** = $B(C_6F_5)_3$, **D** = Me_2AlCl, **E** = Et_2AlCl. [d] Determined by ^1H and ^{13}C NMR spectroscopy in $CDCl_3$.
[e] Determined by means of size-exclusion chromatography (SEC) against polystyrene standards. [f] No further evaluation possible due to low yield. [g] Determined by differential scanning calorimetry; heating rate: 20 K/min, cooling rate: 60 K/min. [s] This study.

Table S1.2.11. Comparison of the polyisoprenes obtained applying precatalyst **2^{Lu}**

entry[b]	cocatalyst[c]	yield [%]	*cis*-content [%][d]	*trans*-content [%][d]	vinylic content [%][d]	M_n [10^4 g/mol][e]	*PDI*[e]	T_g [°C][g]	ref.
1	**A**	>99	77.1	17.6	5.3	6.7	1.58	-62	-[s]
2	2**A**	90	70.3	13.8	15.9	3.4	1.62	-55	-[s]
3	**B**	>99	77.2	16.9	5.9	5.2	2.06	-63	-[s]
4	2**B**	>99	73.1	15.4	11.5	4.2	1.78	-59	-[s]
5	**C**	>99	67.6	28.1	4.3	23	1.55	-61	-[s]
6	2**C**	>99	85.9	8.7	5.4	9.2	2.07	-61	-[s]
7	**D**	none	-[f]	-[f]	-[f]	-[f]	-[f]	-[f]	-[s]
8	2**D**	none	-[f]	-[f]	-[f]	-[f]	-[f]	-[f]	-[s]
9	**E**	none	-[f]	-[f]	-[f]	-[f]	-[f]	-[f]	-[s]
10	2**E**	traces	-[f]	-[f]	-[f]	-[f]	-[f]	-[f]	-[s]

[b] Conditions: 0.02 mmol of **2^{Lu}**, 0.02 or 0.04 mmol cocatalyst, in toluene, [Ln]:[isoprene] 1:1000 (n/n), reaction time 1 h, pre-reaction time 0.5 h.
[c] **A** = $[Ph_3C][B(C_6F_5)_4]$, **B** = $[PhNMe_2H][B(C_6F_5)_4]$, **C** = $B(C_6F_5)_3$, **D** = Me_2AlCl, **E** = Et_2AlCl. [d] Determined by ^1H and ^{13}C NMR spectroscopy in $CDCl_3$.
[e] Determined by means of size-exclusion chromatography (SEC) against polystyrene standards. [f] No further evaluation possible due to low yield. [g] Determined by differential scanning calorimetry; heating rate: 20 K/min, cooling rate: 60 K/min. [s] This study.

S1.3 Isoprene polymerization at standard conditions by results

If not mentioned otherwise in the respective table, the polymers shown in this section have been synthesized according to the procedure given in Section 3.4 of the main article (Materials and Methods) or are taken from the literature for comparison.

Table S1.3.1. Comparison of the yields obtained for the polyisoprenes[a]

		cocatalyst[c]									
entry[b]	precatalyst	**A**	**2A**	**B**	**2B**	**C**	**2C**	**D**	**2D**	**E**	**2E**
1	$La(AlMe_4)_3$ (**2^{La}**)	>99[h]	79	>99[h]	88	>99[h]	69	4	2	3	5
2	$Ce(AlMe_4)_3$ (**2^{Ce}**)	>99	>99	92	100	86	84	7	21	19	34
3	$Pr(AlMe_4)_3$ (**2^{Pr}**)	93	78	92	90	87	87	27	42	43	84
4	$Nd(AlMe_4)_3$(**2Nd**)	86	76	79	82	76	83	40	56	57	86
5	$Gd(AlMe_4)_3$ (**2^{Gd}**)	95	99	89	94	87	87	51	56	77	89
6	$Tb(AlMe_4)_3$ (**2^{Tb}**)	85	77	87	87	83	83	66	67	82	87
7	$Dy(AlMe_4)_3$ (**2^{Dy}**)	92	82	95	88	54	94	34	31	34	46
8	$Ho(AlMe_4)_3$ (**2^{Ho}**)	84	85	93	93	78	90	7	17	15	4
9	$Y(AlMe_4)_3$ (**2^{Y}**)	>99[h]	77	>99[h]	>99[h]	56[h]	86	tr[t]	6	10	22
10	$Er(AlMe_4)_3$ (**2Er**)	80	79	81	74	85	93	tr[t]	tr[t]	tr[t]	2
11	$Lu(AlMe_4)_3$ (**2^{Lu}**)	>99	90	>99	>99	>99	>99	0	0	0	tr[t]

[a] For detailed information on polymerization data and origin of the values (literature or this study), see sections S1.1 and S1.2. The values in this table are given in [%]. [b] Conditions: 0.02 mmol of the resp. Ln precatalyst, 0.02 or 0.04 mmol cocatalyst, in toluene, [Ln]:[isoprene] 1:1000 (n/n), reaction time 1 h, pre-reaction time 0.5 h. [c] **A** = $[Ph_3C][B(C_6F_5)_4]$, **B** = $[PhNMe_2H][B(C_6F_5)_4]$, **C** = $B(C_6F_5)_3$, **D** = Me_2AlCl, **E** = Et_2AlCl. [h] Reaction time 24 h. [s] This study. [t] tr. = traces.

Table S1.3.2. Comparison of the *cis*-1,4-contents obtained for the polyisoprenes[ad]

		cocatalyst[c]									
entry[b]	precatalyst	**A**	**2A**	**B**	**2B**	**C**	**2C**	**D**	**2D**	**E**	**2E**
1	$La(AlMe_4)_3$ (**2^{La}**)	46.3[h]	69.9	49.8[h]	70.5	39.1[h]	77.6	-[f]	91.5	89.3	92.1
2	$Ce(AlMe_4)_3$ (**2^{Ce}**)	44.4	68.1	43.7	57.7	55.4	86.0	97.1	97.4	97.2	97.3
3	$Pr(AlMe_4)_3$ (**2^{Pr}**)	44.7	0.0	45.5	45.9	65.6	87.9	97.2	97.4	97.6	95.4
4	$Nd(AlMe_4)_3$ (**2Nd**)	44.3	66.2	46.8	62.6	68.0	92.7	98.9	97.9	98.2	98.0
5	$Gd(AlMe_4)_3$ (**2^{Gd}**)	62.4	75.8	58.8	66.3	63.4	87.0	100.0	96.0	94.6	92.6
6	$Tb(AlMe_4)_3$ (**2^{Tb}**)	55.1	76.3	58.9	65.6	60.4	89.7	85.0	84.6	88.8	90.2
7	$Dy(AlMe_4)_3$ (**2^{Dy}**)	58.7	72.1	57.5	65.2	63.3	91.5	79.3	88.7	82.6	86.3
8	$Ho(AlMe_4)_3$ (**2^{Ho}**)	63.7	77.9	64.3	63.7	57.0	90.4	67.6	68.3	61.5	71.5
9	$Y(AlMe_4)_3$ (**2^{Y}**)	69.1[h]	73.7	60.0[h]	67.0[h]	62.5[h]	82.2	40.6	52.9	48.4	60.1
10	$Er(AlMe_4)_3$ (**2Er**)	70.3	76.5	67.6	71.4	74.2	92.6	-[f]	-[f]	-[f]	47.4
11	$Lu(AlMe_4)_3$ (**2^{Lu}**)	77.1	70.3	77.2	73.1	67.6	85.9	-[f]	-[f]	-[f]	-[f]

[a] For detailed information on polymerization data and origin of the values (literature or this study), see sections S1.1 and S1.2. The values in this table are given in [%]. Selectivities of >99.9 % are represented by 100. [b] Conditions: 0.02 mmol of the resp. Ln precatalyst, 0.02 or 0.04 mmol cocatalyst, in toluene, [Ln]:[isoprene] 1:1000 (n/n), reaction time 1 h, pre-reaction time 0.5 h. [c] **A** = $[Ph_3C][B(C_6F_5)_4]$, **B** = $[PhNMe_2H][B(C_6F_5)_4]$, **C** = $B(C_6F_5)_3$, **D** = Me_2AlCl, **E** = Et_2AlCl. [d] Determined by ^1H and ^{13}C NMR spectroscopy in $CDCl_3$. [f] No further evaluation possible due to low yield. [h] Reaction time 24 h.

Table S1.3.3. Comparison of the *trans*-1,4-contents obtained for the polyisoprenes[ad]

		cocatalyst[c]									
entry[b]	precatalyst	**A**	2A	**B**	2**B**	**C**	2**C**	**D**	2**D**	**E**	2**E**
1	La(AlMe$_4$)$_3$ (**2^{La}**)	51.4[h]	18.2	46.8[h]	19.4	59.5[h]	18.8	-[f]	5.6	7.6	5.0
2	Ce(AlMe$_4$)$_3$ (**2^{Ce}**)	51.8	18.7	53.0	33.5	41.8	8.8	0.0	0.0	0.0	0.0
3	Pr(AlMe$_4$)$_3$ (**2^{Pr}**)	50.2	0.0	50.2	49.7	30.4	6.0	0.0	0.0	0.0	2.3
4	Nd(AlMe$_4$)$_3$ (**2Nd**)	50.9	21.2	48.4	28.5	29.2	2.9	0.0	0.0	0.0	0.0
5	Gd(AlMe$_4$)$_3$ (**2^{Gd}**)	26.4	9.0	30.0	21.6	36.6	7.0	0.0	4.0	4.2	5.9
6	Tb(AlMe$_4$)$_3$ (**2^{Tb}**)	33.5	8.2	27.6	19.4	35.5	5.5	13.5	13.6	9.7	8.1
7	Dy(AlMe$_4$)$_3$ (**2^{Dy}**)	29.0	10.4	27.4	19.9	33.0	3.9	20.7	11.3	17.4	13.7
8	Ho(AlMe$_4$)$_3$ (**2^{Ho}**)	24.2	6.5	20.0	20.1	38.8	4.1	31.1	31.7	37.1	28.5
9	Y(AlMe$_4$)$_3$ (**2^{Y}**)	23.6[h]	11.7	26.0[h]	13.0[h]	35.1[h]	13.3	52.5	46.2	50.6	39.0
10	Er(AlMe$_4$)$_3$ (**2Er**)	21.5	5.9	19.0	13.4	21.4	2.1	-[f]	-[f]	-[f]	51.3
11	Lu(AlMe$_4$)$_3$ (**2^{Lu}**)	17.6	13.8	16.9	15.4	28.1	8.7	-[f]	-[f]	-[f]	-[f]

[a] For detailed information on polymerization data and origin of the values (literature or this study), see sections S1.1 and S1.2. The values in this table are given in [%]. Selectivities of >99.9 % are represented by 100.0. [b] Conditions: 0.02 mmol of the resp. Ln precatalyst, 0.02 or 0.04 mmol cocatalyst, in toluene, [Ln]:[isoprene] 1:1000 (n/n), reaction time 1 h, pre-reaction time 0.5 h. [c] **A** = [Ph$_3$C][B(C$_6$F$_5$)$_4$], **B** = [PhNMe$_2$H][B(C$_6$F$_5$)$_4$], **C** = B(C$_6$F$_5$)$_3$, **D** = Me$_2$AlCl, **E** = Et$_2$AlCl. [d] Determined by ^{1}H and ^{13}C NMR spectroscopy in CDCl$_3$. [f] No further evaluation possible due to low yield. [h] Reaction time 24 h.

Table S1.3.4. Comparison of the vinylic 3,4-contents obtained for the polyisoprenes[ad]

		cocatalyst[c]									
entry[b]	precatalyst	**A**	2A	**B**	2**B**	**C**	2**C**	**D**	2**D**	**E**	2**E**
1	La(AlMe$_4$)$_3$ (**2^{La}**)	2.3[h]	11.9	3.4[h]	10.1	1.4[h]	3.7	-[f]	2.9	3.1	2.9
2	Ce(AlMe$_4$)$_3$ (**2^{Ce}**)	3.8	13.3	3.3	8.8	2.7	5.2	2.9	2.6	2.8	2.7
3	Pr(AlMe$_4$)$_3$ (**2^{Pr}**)	5.1	0.0	4.3	4.4	4.0	6.1	2.8	2.6	2.4	2.3
4	Nd(AlMe$_4$)$_3$ (**2Nd**)	4.9	12.6	4.8	8.9	2.7	4.5	1.1	2.1	1.8	2.0
5	Gd(AlMe$_4$)$_3$ (**2^{Gd}**)	11.3	15.2	11.2	12.0	0.0	6.0	0.0	0.0	1.2	1.5
6	Tb(AlMe$_4$)$_3$ (**2^{Tb}**)	11.4	15.5	13.4	15.0	4.1	4.8	1.5	1.9	1.5	1.7
7	Dy(AlMe$_4$)$_3$ (**2^{Dy}**)	12.3	17.5	15.1	14.9	3.7	4.6	0.0	0.0	0.0	0.0
8	Ho(AlMe$_4$)$_3$ (**2^{Ho}**)	12.1	15.6	15.7	16.2	4.3	5.5	1.3	0.0	1.4	0.0
9	Y(AlMe$_4$)$_3$ (**2^{Y}**)	7.3[h]	14.5	14.0[h]	20.0[h]	2.4[h]	4.4	6.9	0.9	1.0	0.9
10	Er(AlMe$_4$)$_3$ (**2Er**)	8.3	17.7	13.5	15.2	4.5	5.2	-[f]	-[f]	-[f]	1.3
11	Lu(AlMe$_4$)$_3$ (**2^{Lu}**)	5.3	15.9	5.9	11.5	4.3	5.4	-[f]	-[f]	-[f]	-[f]

[a] For detailed information on polymerization data and origin of the values (literature or this study), see sections S1.1 and S1.2. The values in this table are given in [%]. Selectivities of >99.9 % are represented by 100.0. [b] Conditions: 0.02 mmol of the resp. Ln precatalyst, 0.02 or 0.04 mmol cocatalyst, in toluene, [Ln]:[isoprene] 1:1000 (n/n), reaction time 1 h, pre-reaction time 0.5 h. [c] **A** = [Ph$_3$C][B(C$_6$F$_5$)$_4$], **B** = [PhNMe$_2$H][B(C$_6$F$_5$)$_4$], **C** = B(C$_6$F$_5$)$_3$, **D** = Me$_2$AlCl, **E** = Et$_2$AlCl. [d] Determined by ^{1}H and ^{13}C NMR spectroscopy in CDCl$_3$. [f] No further evaluation possible due to low yield. [h] Reaction time 24 h.

Table S1.3.5. Comparison of the number average molar weights obtained for the polyisoprenes[ae]

		cocatalyst[c]									
entry[b]	precatalyst	**A**	2**A**	**B**	2**B**	**C**	2**C**	**D**	2**D**	**E**	2**E**
1	La(AlMe$_4$)$_3$ (**2^{La}**)	5.0[h]	5.3	6.0[h]	5.0	33.0[h]	16.3	1.6	-[f]	-[f]	2.3
2	Ce(AlMe$_4$)$_3$ (**2^{Ce}**)	3.5	4.0	2.8	3.5	3.3	5.9	11.7	3.3	0.2	3.1
3	Pr(AlMe$_4$)$_3$ (**2^{Pr}**)	3.9	8.0	3.2	14.1	6.8	8.7	6.5	8.7	4.4	4.1
4	Nd(AlMe$_4$)$_3$ (**2Nd**)	3.8	4.7	1.6	4.4	7.9	17.6	9.4	11.3	5.6	5.3
5	Gd(AlMe$_4$)$_3$ (**2^{Gd}**)	5.6	2.9	6.1	8.4	9.6	11.8	5.6	6.9	3.8	3.2
6	Tb(AlMe$_4$)$_3$ (**2^{Tb}**)	5.2	2.6	7.5	5.6	8.0	10.6	4.9	3.6	2.5	2.1
7	Dy(AlMe$_4$)$_3$ (**2^{Dy}**)	9.6	1.5	10.0	6.7	8.5	13.1	3.0	3.2	1.9	1.6
8	Ho(AlMe$_4$)$_3$ (**2^{Ho}**)	5.6	3.7	12.1	7.8	11.6	17.6	2.9	3.6	2.2	2.5
9	Y(AlMe$_4$)$_3$ (**2^{Y}**)	9.0[h]	3.1	11.7[h]	26.0[h]	12.0[h]	16.1	-[f]	2.9	2.1	3.2
10	Er(AlMe$_4$)$_3$ (**2Er**)	7.9	4.1	9.1	5.9	15.5	15.5	-[f]	-[f]	-[f]	-[f]
11	Lu(AlMe$_4$)$_3$ (**2^{Lu}**)	6.7	3.4	5.2	4.2	23.0	9.2	-[f]	-[f]	-[f]	-[f]

[a] For detailed information on polymerization data and origin of the values (literature or this study), see sections S1.1 and S1.2. The values in this table are given in [10^4 g/mol]. [b] Conditions: 0.02 mmol of the resp. Ln precatalyst, 0.02 or 0.04 mmol co-catalyst, in toluene, [Ln]:[isoprene] 1:1000 (n/n), reaction time 1 h, pre-reaction time 0.5 h. [c] **A** = [Ph$_3$C][B(C$_6$F$_5$)$_4$], **B** = [PhNMe$_2$H][B(C$_6$F$_5$)$_4$], **C** = B(C$_6$F$_5$)$_3$, **D** = Me$_2$AlCl, **E** = Et$_2$AlCl.[e] Determined by means of size-exclusion chromatography (SEC) against polystyrene standards. [f] No further evaluation possible due to low yield. [h] Reaction time 24 h.

Table S1.3.6. Comparison of the polydispersity indices obtained for the polyisoprenes[ae]

		cocatalyst[c]									
entry[b]	precatalyst	**A**	2**A**	**B**	2**B**	**C**	2**C**	**D**	2**D**	**E**	2**E**
1	La(AlMe$_4$)$_3$ (**2^{La}**)	1.29[h]	6.90	1.23[h]	1.15	1.18[h]	1.40	6.28	-[f]	-[f]	3.27
2	Ce(AlMe$_4$)$_3$ (**2^{Ce}**)	1.25	1.28	1.35	1.18	1.22	1.13	1.28	3.73	3.44	3.81
3	Pr(AlMe$_4$)$_3$ (**2^{Pr}**)	1.35	2.35	1.55	1.78	1.32	1.35	2.98	3.09	4.84	4.10
4	Nd(AlMe$_4$)$_3$ (**2Nd**)	1.29	1.38	1.27	1.26	1.16	2.48	6.77	5.26	4.52	4.66
5	Gd(AlMe$_4$)$_3$ (**2^{Gd}**)	1.76	1.63	1.70	1.88	1.28	1.36	5.30	7.00	7.89	5.87
6	Tb(AlMe$_4$)$_3$ (**2^{Tb}**)	3.02	1.62	1.97	1.74	1.57	1.43	4.44	6.63	6.36	12.66
7	Dy(AlMe$_4$)$_3$ (**2^{Dy}**)	1.74	1.87	1.70	1.79	1.33	1.40	6.52	6.19	6.80	8.95
8	Ho(AlMe$_4$)$_3$ (**2^{Ho}**)	2.15	1.57	1.85	2.31	1.73	1.39	2.64	4.87	2.70	4.90
9	Y(AlMe$_4$)$_3$ (**2^{Y}**)	2.09[h]	1.62	1.60[h]	1.50[h]	2.03[h]	1.55	-[f]	2.92	1.43	3.84
10	Er(AlMe$_4$)$_3$ (**2Er**)	1.91	1.62	2.63	2.13	1.86	1.75	-[f]	-[f]	-[f]	-[f]
11	Lu(AlMe$_4$)$_3$ (**2^{Lu}**)	1.58	1.62	2.06	1.78	1.55	2.07	-[f]	-[f]	-[f]	-[f]

[a] For detailed information on polymerization data and origin of the values (literature or this study), see sections S1.1 and S1.2. [b] Conditions: 0.02 mmol of the resp. Ln precatalyst, 0.02 or 0.04 mmol co-catalyst, in toluene, [Ln]:[isoprene] 1:1000 (n/n), reaction time 1 h, pre-reaction time 0.5 h. [c] **A** = [Ph$_3$C][B(C$_6$F$_5$)$_4$], **B** = [PhNMe$_2$H][B(C$_6$F$_5$)$_4$], **C** = B(C$_6$F$_5$)$_3$, **D** = Me$_2$AlCl, **E** = Et$_2$AlCl. [e] Determined by means of size-exclusion chromatography (SEC) against polystyrene standards. [f] No further evaluation possible due to low yield. [h] Reaction time 24 h.

Table S1.3.7. Comparison of the glass transition temperatures obtained for the polyisoprenes[ag]

		cocatalyst[c]									
entry[b]	precatalyst	**A**	2**A**	**B**	2**B**	**C**	2**C**	**D**	2**D**	**E**	2**E**
1	$La(AlMe_4)_3$ (**2^{La}**)	n.d.[h]	-63	n.d.[h]	-62	n.d.[h]	-63	-61	-[f]	-[f]	-62
2	$Ce(AlMe_4)_3$ (**2^{Ce}**)	-62	-55	-62	-62	-61	-58	-59	-60	-61	-61
3	$Pr(AlMe_4)_3$ (**2^{Pr}**)	-66	n.d.	-67	-65	-65	-61	-64	-62	-61	-62
4	$Nd(AlMe_4)_3$ (**2Nd**)	-64	-57	-64	-57	-63	-61	-60	-61	-61	-62
5	$Gd(AlMe_4)_3$ (**2^{Gd}**)	-59	-51	-64	-61	-65	-66	-67	-67	-63	-63
6	$Tb(AlMe_4)_3$ (**2^{Tb}**)	-55	-52	-57	-58	-66	-61	-66	-66	-67	-67
7	$Dy(AlMe_4)_3$ (**2^{Dy}**)	-60	-55	-58	-57	-65	-61	-67	-67	-67	-67
8	$Ho(AlMe_4)_3$ (**2^{Ho}**)	-56	-55	-56	-55	-64	-62	-67	-66	-67	-66
9	$Y(AlMe_4)_3$ (**2^{Y}**)	n.d.[h]	-53	n.d.[h]	n.d.[h]	n.d.[h]	-62	-[f]	-68	-67	-66
10	$Er(AlMe_4)_3$ (**2Er**)	-56	-50	-55	-52	-59	-57	-[f]	-[f]	-[f]	-[f]
11	$Lu(AlMe_4)_3$ (**2^{Lu}**)	-62	-55	-63	-59	-61	-61	-[f]	-[f]	-[f]	-[f]

[a] For detailed information on polymerization data and origin of the values (literature or this study), see sections S1.1 and S1.2. The values in this table are given in [°C]. [b] Conditions: 0.02 mmol of the resp. Ln precatalyst, 0.02 or 0.04 mmol co-catalyst, in toluene, [Ln]:[isoprene] 1:1000 (n/n), reaction time 1 h, pre-reaction time 0.5 h. [c] **A** = $[Ph_3C][B(C_6F_5)_4]$, **B** = $[PhNMe_2H][B(C_6F_5)_4]$, **C** = $B(C_6F_5)_3$, **D** = Me_2AlCl, **E** = Et_2AlCl. [f] No further evaluation possible due to low yield. [g] Determined by differential scanning calorimetry; heating rate: 20 K/min, cooling rate: 60 K/min. [h] Reaction time 24 h.

S1.4 Isoprene polymerization screenings

In order to gain more insight into the polymerization-active species, the standard conditions given in Section 3.4 of the main article (Materials and Methods) have been augmented as presented in the respective tables. Besides the obtained data, our group has reported on isoprene polymerization in *n*-hexane applying combinations of $Ln(AlMe_4)_3$/**E** (Ln = La [4,5], Pr [6], Gd [4,5]) resulting in high yields after 24 h and nearly quantitative *cis*-selectivity. Moderate yields and selectivity were obtained for Ln = Y [4,5] and low yields (<7%) but high *cis*-contents after 24 h reaction time for $Sm(AlMe_4)_3$ [4,5]. Polymerization attempts with $Nd(AlMe_4)_3$ applying Me_3SiCl as a chlorine source did not reveal any polyisoprene formation, nor is $Nd(AlMe_4)_3$ active as a single component catalyst. Furthermore, polymerizations with some of the low yielding systems at standard conditions have been repeated with a reaction time of 24 h (results can be found in Table S1.4.4).

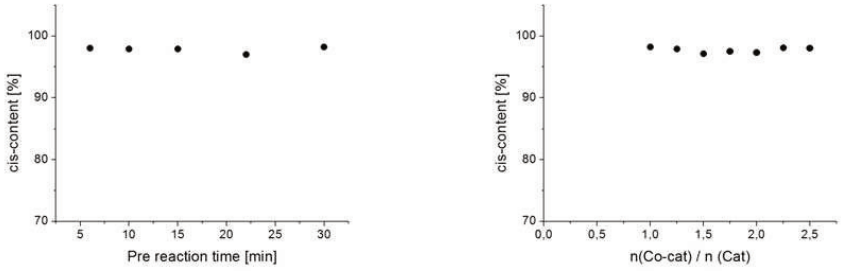

(**a**) (**b**)

Figure S1.4.1. Overview on the *cis*-contents obtained by screening the pre-reaction time (**a**) and cocatalyst concentration (**b**) of the isoprene polymerization applying $Nd(AlMe_4)_3$ ($\mathbf{2^{Nd}}$)/Et_2AlCl (**E**).

Table S1.4.1. Influence of pre-reaction time on isoprene polymerization by $\mathbf{2^{Nd}}$/**E**[a]

entry[b]	pre-reaction time [min]	yield [%]	*cis*-content [%][d]	*trans*-content [%][d]	vinylic content [%][d]	M_n [10^4 g/mol][e]	*PDI*[e]	ref.
1	30	57	98.2	0	1.8	5.6	4.52	-[s]
2	22	87	97.0	0.8	2.2	6.2	4.11	-[s]
3	15	83	97.9[i]	0	2.1[i]	7.0	3.71	-[s]
4	10	83	97.9[i]	0	2.1[i]	6.3	3.86	-[s]
5	6	65	98.0	0	2.0	6.2	3.45	[3]

[a] For data produced at standard conditions, see Table S1.2.4 as well. [b] Conditions: 0.02 mmol $\mathbf{2^{Nd}}$, 0.02 mmol cocatalyst, 8 mL toluene, [Ln]:[isoprene] 1:1000 (n/n), reaction time 1 h. [c] **E** = Et_2AlCl. [d] Determined by ^1H and ^{13}C NMR spectroscopy in $CDCl_3$. [e] Determined by means of size-exclusion chromatography (SEC) against polystyrene standards. [i] For entries 3 and 4 identical microstructures were obtained. [s] This study.

Table S1.4.2. Influence of cocatalyst concentration on isoprene polymerization by **2**Nd/**E**[a]

entry[b]	cocatalyst[c]	yield [%]	*cis*-content [%][d]	*trans*-content [%][d]	vinylic content [%][d]	M_n [10^4 g/mol][e]	*PDI*[e]	ref.
1	**E**	57	98.2	0.0	1.8	5.6	4.52	-[s]
2	1.25 **E**	77	97.9	0.0	2.1	5.9	4.65	-[s]
3	1.5 **E**	80	97.1	0.9	2.0	6.7	4.28	-[s]
4	1.75 **E**	83	97.5	0.4	2.1	8.8	3.40	-[s]
5	2 **E**	86	97.3	0.9	1.8	5.3	4.66	-[s]
6	2.25 **E**	87	98.1	0.0	1.9	6.1	4.11	-[s]
7	2.5 **E**	91	98.0	0.0	2.0	5.5	4.58	-[s]

[a] For data produced standard conditions, see Table S1.6.2. [b] Conditions: 0.02 mmol **2**Nd, 8 mL toluene, reaction time 1 h, pre-reaction time 0.5 h. [c] **E** = Et_2AlCl. [d] Determined by ^1H and ^{13}C NMR spectroscopy in $CDCl_3$. [e] Determined by means of size-exclusion chromatography (SEC) against polystyrene standards. [s] This study.

Table S1.4.3. Influence of solvent on isoprene polymerization applying **2**Nd/**E**[a]

entry[b]	solvent	yield [%]	*cis*-content [%][d]	*trans*-content [%][d]	vinylic content [%][d]	M_n [10^4 g/mol][e]	*PDI*[e]	ref.
1	toluene	57	98.2	0.0	1.8	5.6	4.52	-[s]
2	toluene:*n*-hexane (1:7)	73	98.0	0.0	2.0	5.9	3.61	-[s]
3	*n*-hexane	52	94.6	3.2	2.2	7.2	7.07	-[s]

[a] For data produced standard conditions, see Table S1.1.5. [b] Conditions: 0.02 mmol **2**Nd, 0.02 mmol cocatalyst, 25 mL solvent, pre-reaction time: 0.5 h, reaction time 1 h. [c] **E** = Et_2AlCl. [d] Determined by ^1H and ^{13}C NMR spectroscopy in $CDCl_3$. [e] Determined by means of size-exclusion chromatography (SEC) against polystyrene standards. [s] this study.

Table S1.4.4. 24 h-Reaction time for selected low-yielding systems in Tables S1.1.1 – S1.3.7 [a]

entry[b]	precatalyst	cocatalyst[c]	yield [%]	*cis*-content [%][d]	*trans*-content [%][d]	vinylic content [%][d]	M_n [10^4 g/mol][e]	*PDI*[e]	ref.
1	$La(AlMe_4)_3$ (**2**^{La})	**D**	38	77.6	18.8	2.8/0.8[q]	3.3	3.62	-[s]
2	$La(AlMe_4)_3$ (**2**^{La})	**E**	43	87.0	10.0	2.9	2.7	2.71	-[s]
3	$La(AlMe_4)_3$ (**2**^{La})	2**E**	83	87.2	10.1	2.8	5.1	2.73	-[s]
4	$Er(AlMe_4)_3$ (**2**^{Er})	2**D**	37	34.6	64.0	1.4	3.4	2.65	-[s]
5	$Er(AlMe_4)_3$ (**2**^{Er})	**E**	14	35.8	63.0	1.1	1.4	2.11	-[s]
6	$Er(AlMe_4)_3$ (**2**^{Er})	2**E**	54	24.3	74.1	1.5	2.2	1.91	-[s]
7	$Lu(AlMe_4)_3$ (**2**^{Lu})	2**E**	4	14.1	81.8	4.1	6.0	2.46	-[s]

[a] For data produced at standard conditions, see Tables S1.2.1, S1.2.10 and S1.2.11. [b] Conditions: 0.02 mmol of the resp. precatalyst, 0.02 or 0.04 mmol cocatalyst, 8 mL toluene, reaction time 24 h, pre-reaction time 0.5 h. [c] **D** = Me_2AlCl, **E** = Et_2AlCl. [d] Determined by ^1H and ^{13}C NMR spectroscopy in $CDCl_3$. [e] Determined by means of size-exclusion chromatography (SEC) against polystyrene standards. [q] 3,4-Content / 1,2-content. [s] This study.

S1.5 Polyisoprene data on UV-light irradiated samples

Polymer data reported in this section were obtained from samples produced according to the standard conditions given in Sections 3.4 and 3.5 of the main article (Materials and Methods) and thereafter irradiated applying UV-light of 254 nm for 48 h under air. Data obtained before radiation are presented for comparison.

Table S1.5.1. Polymer data of polyisoprenes applying $\mathbf{2}^{\mathbf{Nd}}$ after exposure to UV-light of 254 nm [a]

entry[b]	cocatalyst[c]	*cis*-content [%][d]	*trans*-content [%][d]	vinylic content [%][d]	M_n [10^4 g/mol][e]	*PDI*[e]	ref.
1	**A**	43.9	51.9	4.3	3.3	1.25	-[s]
2	**B**	39.9	55.8	4.3	5.6	1.14	-[s]
3	**C**	57.0	40.7	2.3	6.7	1.13	-[s]
4	**D**	97.9	0.0	2.1	8.9	6.66	-[s]
5	**E**	98.0	0.0	2.0	4.2	5.50	-[s]

[a] For data of the original polymers, see Table S1.2.4, for ATR-IR data of the polymers, see Table S2.5.1. [b] 48 h Exposure to UV-light of 254 nm.[c] **A** = $[Ph_3C][B(C_6F_5)_4]$, **B** = $[PhNMe_2H][B(C_6F_5)_4]$, **C** = $B(C_6F_5)_3$, **D** = Me_2AlCl, **E** = Et_2AlCl. [d] Determined by ^1H and ^{13}C NMR spectroscopy in $CDCl_3$. [e] Determined by means of size-exclusion chromatography (SEC) against polystyrene standards. [s] This study.

S1.6 Polymerization of 1,3-butadiene at standard conditions by precatalyst

If not mentioned otherwise in the respective table, the polybutadienes shown in this section have been synthesized according to the procedure given in Section 3.5 of the main article (Materials and Methods) or taken from the literature for comparison.

Table S1.6.1. Polybutadiene applying $Y(AlMe_4)_3$ ($\mathbf{2}^{\mathbf{Y}}$)[a]

entry[b]	cocatalyst[c]	pre-reaction time [h]	reaction time [h]	yield [%]	*cis*-content [%][d]	*trans*-content [%][d]	vinylic content [%][d]	M_n [10^4 g/mol][e]	*PDI*[e]	ref.
1	**B**	0.5	0.5	<5	-[f]	-[f]	-[f]	-[f]	-[f]	[2]
2	**B**	4	0.5	73	n.d.	n.d.	n.d.	18.6	4.4	[2]
3	**2B**	0.5	0.5	26	95	3	2	14.0	2.0	[2]
4	**2B**	4	0.5	93	n.d.	n.d.	n.d.	31.2	2.6	[2]

[a] For data produced by systems of $\mathbf{2}^{\mathbf{Y}}$/**B** and $\mathbf{2}^{\mathbf{Y}}$/**2B** in the presence of $AliBu_3$, see [2]. [b] Conditions: 0.02 mmol $\mathbf{2}^{\mathbf{Y}}$, 0.02 or 0.04 mmol resp. co-catalyst, 8 mL toluene, [**9**]:[1,3-butadiene] 1:1000 (n/n). [c] **B** = $[PhNMe_2H][B(C_6F_5)_4]$. [d] Determined by ^1H and ^{13}C NMR spectroscopy in $CDCl_3$. [e] Determined by means of size-exclusion chromatography (SEC) against polystyrene standards. [f] No further evaluation possible due to low yield.

Table S1.6.2. Polybutadiene applying $Nd(AlMe_4)_3$ ($\mathbf{2^{Nd}}$)[a]

entry[b]	cocatalyst[c]	BD [mmol]	yield [%]	*cis*-content [%][d]	*trans*-content [%][d]	vinylic content [%][d]	M_n [10^4 g/mol][e]	*PDI*[e]	ref.
1	**D**	53.5	28	99.7	0.0	0.3	40.7	2.39	-[s]
2	**E**	22.4	41	96.7	2.9	0.4	8.3	3.47	-[s]

[a] For data produced by optimization screenings, see Section S1.7; Polymerization attempts with $Nd(AlMe_4)_3$ applying Me_3SiCl as a chlorine source did not reveal any polyisoprene formation, nor is $Nd(AlMe_4)_3$ active as a single component catalyst.. [b] Conditions: 0.02 mmol $\mathbf{2^{Nd}}$, 0.02 mmol cocatalyst, 25 mL toluene, 100 rpm, 1 bar of BD pressure, reaction time 1 h, pre-reaction time 0.5 h. [c] **D** = Me_2AlCl, **E** = Et_2AlCl. [d] Determined by ^1H and ^{13}C NMR spectroscopy in $CDCl_3$. [e] Determined by means of size-exclusion chromatography (SEC) against polystyrene standards. [s] This study.

Table S1.6.3 Polybutadiene applying $Pr(AlMe_4)_3$($\mathbf{2^{Pr}}$)

entry[a]	cocatalyst[b]	yield [%]	*cis*-content [%][c]	*trans*-content [%][c]	vinylic content [%][c]	M_n [10^4 g/mol][d]	*PDI*[d]	ref.
1	**A**	60	30.2	67.2	1.8	10.8	2.52	-[s]
2	**B**	54	28.8	69.2	2.0	11.8	3.60	-[s]
3	**C**	54	59.7	39.2	1.0	12.1	1.15	-[s]
4	**D**	22	92.2	7.1	0.7	10.0	5.07	-[s]
5	**E**	34	94.3	5.0	0.7	9.8	4.22	-[s]

[a] Conditions: 0.02 mmol $\mathbf{2^{Pr}}$, 0.02 mmol cocatalyst, 25 mL toluene, [**3**]:[1,3-butadiene] 1:3000 (n/n), 100 rpm, reaction time 1 h, pre-reaction time 0.5 h. [b] **A** = $[Ph_3C][B(C_6F_5)_4]$, **B** = $[PhNMe_2H][B(C_6F_5)_4]$, **C** = $B(C_6F_5)_3$, **D** = Me_2AlCl, **E** = Et_2AlCl. [c] Determined by ^1H and ^{13}C NMR spectroscopy in $CDCl_3$. [d] Determined by means of size-exclusion chromatography (SEC) against polystyrene standards. [s] This study.

Okuda *et al.* used $La(AlMe_4)_3$ ($\mathbf{2^{La}}$) and $Gd(AlMe_4)_3$ ($\mathbf{2^{Gd}}$) along with co-catalyst **A** in the presence of Al*i*Bu$_3$ for 1,3-butadiene polymerization[7].

S1.7 1,3-Butadiene polymerization screenings

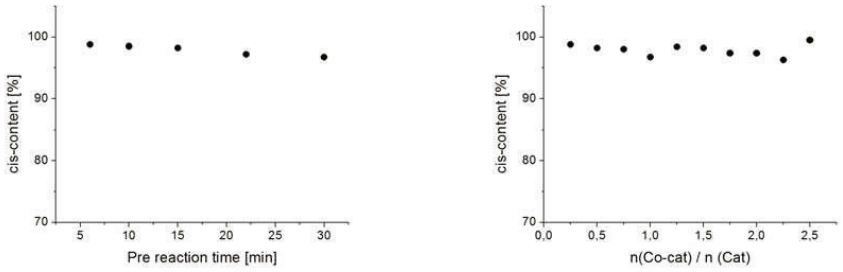

(**a**) (**b**)

Figure S1.7.1. Overview on the *cis*-contents obtained by screening the pre-reaction time (**a**) and co-catalyst concentration (**b**) of the 1,3-butadiene polymerization applying $Nd(AlMe_4)_3$ (**2**Nd)/Et_2AlCl (**E**).

Table S1.7.1. Influence of pre-reaction time on 1,3-butadiene polymerization applying **2**Nd/**E**[a]

entry[b]	pre-reaction time [min]	BD [mmol]	yield [%]	*cis*-content [%][d]	*trans*-content [%][d]	vinylic content [%][d]	M_n [10^4 g/mol][e]	*PDI*[e]	ref.
1	30	22.4	41	96.7	2.9	0.4	8.3	3.47	-[s]
2	22	21.6	57	97.2	2.7	0.1	12.2	3.90	-[s]
3	15	42.9	76	98.2	1.6	0.2	11.3	4.02	-[s]
4	10	51.3	67	98.5	1.3	0.2	13.6	2.51	-[s]
5	6	36.9	52	98.8	0.9	0.3	10.3	4.24	-[s]

[a] For data produced at standard conditions, see Table S1.6.2. [b] Conditions: 0.02 mmol **2**Nd, 0.02 mmol cocatalyst, 25 mL toluene, 100 rpm, 1 bar of BD pressure, reaction time 1h. [c] **E** = Et_2AlCl. [d] Determined by ^1H and ^{13}C NMR spectroscopy in $CDCl_3$. [e] Determined by means of size-exclusion chromatography (SEC) against polystyrene standards. [s] This study.

Table S1.7.2. Influence of cocatalyst concentration on 1,3-butadiene polymerization applying **2**Nd/**E**[a]

entry[b]	cocatalyst[c]	BD [mmol]	yield [%]	*cis*-content [%][d]	*trans*-content [%][d]	vinylic content [%][d]	M_n [10^4 g/mol][e]	*PDI*[e]	ref.
1	0.25 **E**	35.6	5	98.8	1.0	0.2	14.5	4.62	-[s]
2	0.5 **E**	35.4	18	98.2	1.5	0.3	11.9	4.76	-[s]
3	0.75 **E**	34.1	39	98.0	1.9	0.1	8.3	5.12	-[s]
4	**E**	22.4	41	96.7	2.9	0.4	8.3	3.47	-[s]
5	1.25 **E**	38.0	59	98.4	1.5	0.1	11.9	3.72	-[s]
6	1.5 **E**	39.9	46	98.2	1.6	0.2	16.5	3.57	-[s]
7	1.75 **E**	38.8	85	97.4[i]	2.5[i]	0.1[i]	10.9	3.92	-[s]
8	2 **E**	25.9	76	97.4[i]	2.5[i]	0.1[i]	16.6	3.50	-[s]
9	2.25 **E**	43.7	3	96.3	3.6	0.1	20.5	2.72	-[s]
10	2.5 **E**	56.6	41	99.5	0.4	0.1	18.8	3.31	-[s]

[a] For data produced at standard conditions, see Table S1.6.2. [b] Conditions: 0.02 mmol **2**Nd, 25 mL toluene, 100 rpm, 1 bar of BD pressure, reaction time 1 h, pre-reaction time 0.5 h. [c] **E** = Et_2AlCl. [d] Determined by ^1H and ^{13}C NMR spectroscopy in $CDCl_3$. [e] Determined by means of size-exclusion chromatography (SEC) against polystyrene standards. [i] These polymerizations resulted in identical micorstructures. [s] This study.

Table S1.7.3. Influence of reaction time on 1,3-butadiene polymerization applying **2**Nd/**E**[a]

entry[b]	reaction time [h]	BD [mmol]	yield [%]	*cis*-content [%][d]	*trans*-content [%][d]	vinylic content [%][d]	M_n [10^4 g/mol][e]	*PDI*[e]	ref.
1	1	22.4	41	96.7	2.9	0.4	8.3	3.47	-[s]
2	2	30.9	78	97.6	2.2	0.2	11.3	3.85	-[s]

[a] For data produced at standard conditions, see Table S1.6.2. [b] Conditions: 0.02 mmol **2**Nd, 0.02 mmol co-catalyst, 25 mL toluene, 100 rpm, 1 bar of BD pressure, pre-reaction time 0.5 h. [c] **E** = Et_2AlCl. [d] Determined by ^1H and ^{13}C NMR spectroscopy in $CDCl_3$. [e] Determined by means of size-exclusion chromatography (SEC) against polystyrene standards. [s] This study.

Table S1.7.4. Influence of solvent on 1,3-butadiene polymerization applying **2**Nd/**E**[a]

entry[b]	solvent	BD [mmol]	yield [%]	*cis*-content [%][d]	*trans*-content [%][d]	vinylic content [%][d]	M_n [10^4 g/mol][e]	*PDI*[e]	ref.
1	toluene	22.4	41	96.7	2.9	0.4	8.3	3.47	-[s]
2	*n*-hexane	60.0	49	99.3	0.0	0.7	25.5	3.66	-[s]

[a] For data produced at standard conditions, see Table S1.6.2 [b] Conditions: 0.02 mmol **2**Nd, 0.02 mmol cocatalyst, 25 mL solvent, pre-reaction time: 0.5 h, reaction time 1 h, 100 rpm. [c] **E** = Et_2AlCl. [d] Determined by ^1H and ^{13}C NMR spectroscopy in $CDCl_3$. [e] Determined by means of size-exclusion chromatography (SEC) against polystyrene standards. [s] This study.

S1.8 Polymerization of ethylene

Table S1.8.1. Results of ethylene polymerization applying **2Nd/E** and **2Nd/2E**

entry[b]	precatalyst	cocatalyst[c]	yield [%]	M_n [10^4 g/mol][e]	*PDI*[e]	T_m[g] [°C]	ref.
1	Nd(AlMe$_4$)$_3$ (**2Nd**)	**E**	8	16.3	3.4	138	-[s]
2	Nd(AlMe$_4$)$_3$ (**2Nd**)	**2E**	58	13.2	4.0	130	-[s]

[b] Conditions: 0.06 mmol **2Nd**, 0.06 or 0.12 mmol cocatalyst, 125 mL toluene, 60 mmol of ethylene, pre-reaction time: 0.5 h, 60 °C, 50 rpm, reaction time 1 h. [c] **E** = Et$_2$AlCl. [e] Determined by means of high temperature size-exclusion chromatography (SEC) against polystyrene standards. [g] Determined by differential scanning calorimetry; heating rate: 20 K/min, cooling rate: 60 K/min. [s] This study.

S2. Comparison of Microstructure Data Obtained from ATR-IR and NMR Spectroscopic Analyses

The data obtained from the prescreening of the microstructure by ATR-IR spectroscopy is plotted versus the microstructure data calculated from the NMR spectra according to section 3.5 in the main article.

*S2.1 Polyisoprene applying precatalyst Ce(AlMe$_4$)$_3$ (**2^{Ce}**)*

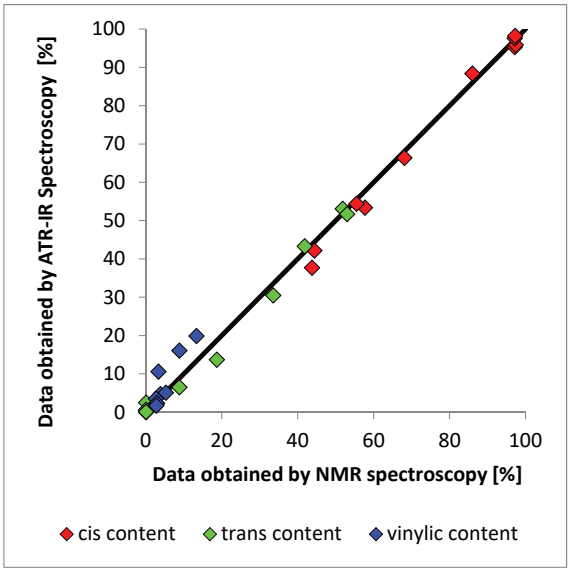

Figure S2.1.1. Comparison of the microstructure results obtained by NMR and ATR-IR spectroscopy, applying **2^{Ce}** and cocatalysts **A**-**E** (**A** = [Ph$_3$C][B(C$_6$F$_5$)$_4$], **B** = [PhNMe$_2$H][B(C$_6$F$_5$)$_4$], **C** = B(C$_6$F$_5$)$_3$, **D** = Me$_2$AlCl, **E** = Et$_2$AlCl) in both one and two equivalents. For detailed polymerization data see Tables S1.2.2 and S2.1.1.

Table S2.1.1. Comparison of the microstructure results by NMR and ATR-IR spectroscopy, data from isoprene polymerization applying **2**^{Ce} [a]

		NMR			ATR-IR			
entry[b]	**cocatalyst**[c]	***cis*-content [%]**[d]	***trans*-content [%]**[d]	**vinylic content [%]**[d]	***cis*-content [%]**[e]	***trans*-content [%]**[e]	**vinylic content [%]**[e]	**ref.**
1	**A**	42.2	53.1	4.7	44.4	51.8	3.8	-[s]
2	2**A**	66.4	13.7	19.9	68.1	18.7	13.3	-[s]
3	**B**	37.7	51.7	10.6	43.7	53.0	3.3	-[s]
4	2**B**	53.4	30.5	16.1	57.7	33.5	8.8	-[s]
5	**C**	54.4	43.3	2.3	55.4	41.8	2.7	-[s]
6	2**C**	88.4	6.5	5.1	86.0	8.8	5.2	-[s]
7	**D**	95.3	2.5	2.2	97.1	0.0	2.9	-[s]
8	2**D**	95.9	0.6	3.5	97.4	0.0	2.6	-[s]
9	**E**	97.6	0.0	2.4	97.2	0.0	2.8	-[s]
10	2**E**	98.2	0.1	1.7	97.3	0.0	2.7	-[s]

[a] For detailed data on the respective chain properties, see Table S1.2.2. [b] Conditions: 0.02 mmol **2**^{Ce}, 0.02 or 0.04 mmol resp. co-catalyst, 8 mL solvent, pre-reaction time: 0.5 h, reaction time 1 h. [c] **A** = $[Ph_3C][B(C_6F_5)_4]$, **B** = $[PhNMe_2H][B(C_6F_5)_4]$, **C** = $B(C_6F_5)_3$, **D** = Me_2AlCl, **E** = Et_2AlCl. [d] Determined by ^1H and ^{13}C NMR spectroscopy in $CDCl_3$. [e] Determined by ATR-IR spectroscopy. [s] This study.

*S2.2 Polyisoprene applying precatalyst Nd(AlMe$_4$)$_3$ (**2**Nd)*

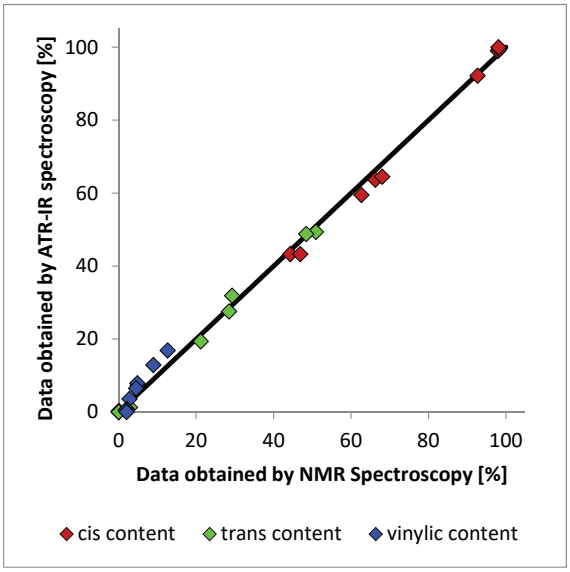

Figure S2.2.1. Comparison of the microstructure results obtained by NMR and ATR-IR spectroscopy, applying Nd(AlMe$_4$)$_3$ (**2**Nd) and cocatalysts **A**-**E** (**A** = $[Ph_3C][B(C_6F_5)_4]$, **B** = $[PhNMe_2H][B(C_6F_5)_4]$, **C** = $B(C_6F_5)_3$, **D** = Me_2AlCl, **E** = Et_2AlCl) in both one and two equivalents. For detailed polymerization data see Tables S1.2.4 and S2.2.1.

Table S2.2.1. Comparison of the microstructure results by NMR and ATR-IR spectroscopy, data from isoprene polymerization applying **2**Nd [a]

		NMR			ATR-IR			
entry[b]	co-catalyst[c]	*cis*-content [%][d]	*trans*-content [%][d]	vinylic content [%][d]	*cis*-content [%][e]	*trans*-content [%][e]	vinylic content [%][e]	ref.
1	**A**	44.3	50.9	4.9	43.3	49.4	7.3	-[s]
2	2**A**	66.2	21.2	12.6	63.7	19.4	16.9	-[s]
3	**B**	46.8	48.4	4.8	43.3	48.8	7.9	-[s]
4	2**B**	62.6	28.5	8.9	59.5	27.6	12.9	-[s]
5	**C**	68.0	29.2	2.7	64.5	31.9	3.6	-[s]
6	2**C**	92.7	2.9	4.5	92.2	1.3	6.5	-[s]
7	**D**	98.0	0.0	2.0	99.2	0.0	0.8	-[s]
8	2**D**	97.9	0.0	2.1	99.0	0.3	0.7	-[s]
9	**E**	98.2	0.0	1.8	99.5	0.0	0.5	-[s]
10	2**E**	98.0	0.0	2.0	99.9	0.0	0.0	-[s]

[a] For detailed data on the respective chain properties, see Table S1.2.4. [b] Conditions: 0.02 mmol **2**Nd, 0.02 or 0.04 mmol resp. co-catalyst, 8 mL solvent, pre-reaction time: 0.5 h, reaction time 1 h. [c] **A** = $[Ph_3C][B(C_6F_5)_4]$, **B** = $[PhNMe_2H][B(C_6F_5)_4]$, **C** = $B(C_6F_5)_3$, **D** = Me_2AlCl, **E** = Et_2AlCl. [d] Determined by ^1H and ^{13}C NMR spectroscopy in $CDCl_3$. [e] Determined by ATR-IR spectroscopy. [s] This study.

*S2.3 Polyisoprene applying precatalyst Tb(AlMe$_4$)$_3$ (**2**^{Tb})*

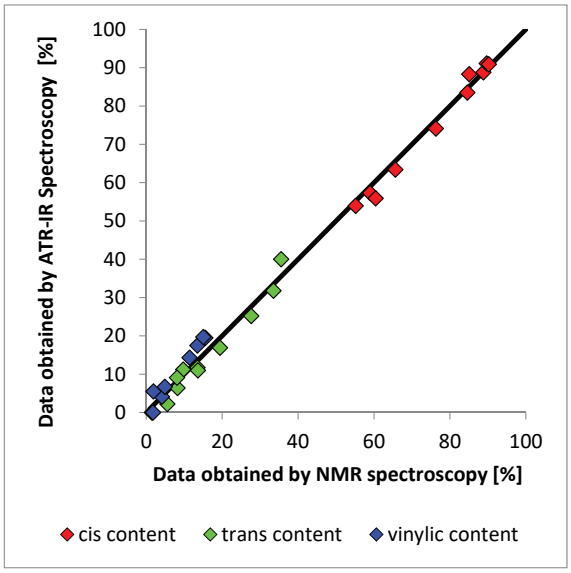

Figure S2.3.1. Comparison of the microstructure results obtained by NMR and ATR-IR spectroscopy, applying Tb(AlMe$_4$)$_3$ (**2**^{Tb}) and cocatalysts **A**-**E** (**A** = $[Ph_3C][B(C_6F_5)_4]$, **B** = $[PhNMe_2H][B(C_6F_5)_4]$, **C** = $B(C_6F_5)_3$, **D** = Me_2AlCl, **E** = Et_2AlCl) in both one and two equivalents. For detailed polymerization data see Tables S1.2.6 and S2.3.1.

Table S2.3.1. Comparison of the microstructure results by NMR and ATR-IR spectroscopy, data from isoprene polymerization applying **2^{Tb}** [a]

		NMR			ATR-IR			
entry[b]	**cocatalyst**[c]	***cis*-content [%]**[d]	***trans*-content [%]**[d]	**vinylic content [%]**[d]	***cis*-content [%]**[e]	***trans*-content [%]**[e]	**vinylic content [%]**[e]	**ref.**
1	**A**	55.1	33.5	11.4	53.9	31.8	14.3	-[s]
2	**2A**	58.9	27.6	13.4	57.3	25.2	17.5	-[s]
3	**B**	60.4	35.5	4.1	55.9	40.0	4.1	-[s]
4	**2B**	85.0	13.5	1.5	88.3	11.7	0.0	-[s]
5	**C**	88.8	9.7	1.5	88.8	11.2	0.0	-[s]
6	**2C**	76.3	8.2	15.5	74.1	6.4	19.5	-[s]
7	**D**	65.6	19.4	15.0	63.4	16.9	19.7	-[s]
8	**2D**	89.7	5.5	4.8	91.1	2.2	6.7	-[s]
9	**E**	84.6	13.6	1.9	83.5	11.0	5.5	-[s]
10	**2E**	90.2	8.1	1.7	90.9	9.1	0.0	-[s]

[a] For detailed data on the respective chain properties, see Table S1.2.6. [b] Conditions: 0.02 mmol **2^{Tb}**, 0.02 or 0.04 mmol resp. co-catalyst, 8 mL solvent, pre-reaction time: 0.5 h, reaction time 1 h. [c] **A** = $[Ph_3C][B(C_6F_5)_4]$, **B** = $[PhNMe_2H][B(C_6F_5)_4]$, **C** = $B(C_6F_5)_3$, **D** = Me_2AlCl, **E** = Et_2AlCl. [d] Determined by ^1H and ^{13}C NMR spectroscopy in $CDCl_3$. [e] Determined by ATR-IR spectroscopy. [s] This study.

*S2.4 Polyisoprene applying precatalyst Er(AlMe$_4$)$_3$ (**2Er**)*

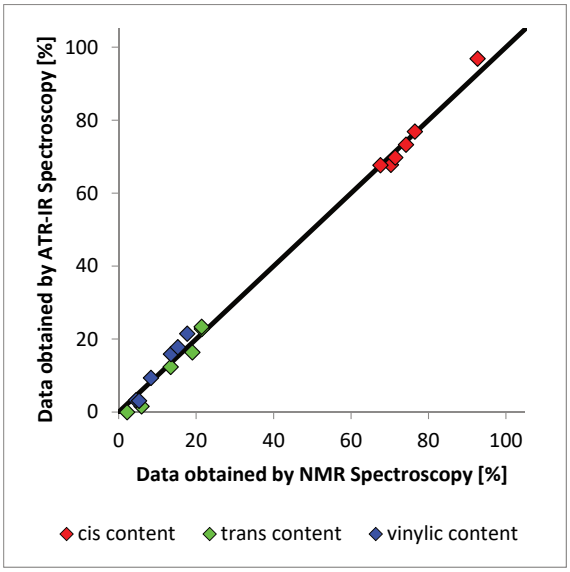

Figure S2.4.1. Comparison of the microstructure results obtained by NMR and ATR-IR spectroscopy, applying Er(AlMe$_4$)$_3$ (**2Er**) and cocatalysts **A**-**E** (**A** = $[Ph_3C][B(C_6F_5)_4]$, **B** = $[PhNMe_2H][B(C_6F_5)_4]$, **C** = $B(C_6F_5)_3$, **D** = Me_2AlCl, **E** = Et_2AlCl) in both one and two equivalents. For detailed polymerization data see Tables S1.2.10 and S2.4.1.

Table S2.4.1. Comparison of the microstructure results by NMR and ATR-IR spectroscopies, data from isoprene polymerization applying **2**^{Er} [a]

		NMR			ATR-IR			
entry[b]	cocatalyst[c]	*cis*-content [%][d]	*trans*-content [%][d]	vinylic content [%][d]	*cis*-content [%][e]	*trans*-content [%][e]	vinylic content [%][e]	ref.
1	**A**	67.8	22.8	9.4	70.3	21.5	8.3	-[s]
2	2**A**	76.9	1.6	21.5	76.5	5.9	17.7	-[s]
3	**B**	67.7	16.4	15.9	67.6	19.0	13.5	-[s]
4	2**B**	69.8	12.4	17.8	71.4	13.4	15.2	-[s]
5	**C**	73.3	23.4	3.3	74.2	21.4	4.5	-[s]
6	2**C**	96.9	0.0	3.1	92.6	2.1	5.2	-[s]

[a] For detailed data on the respective chain properties, see Table S1.2.10. [b] Conditions: 0.02 mmol **2**^{Er}, 0.02 or 0.04 mmol resp. cocatalyst, 8 mL solvent, pre-reaction time: 0.5 h, reaction time 1 h. [c] **A** = $[Ph_3C][B(C_6F_5)_4]$, **B** = $[PhNMe_2H][B(C_6F_5)_4]$, **C** = $B(C_6F_5)_3$, **D** = Me_2AlCl, **E** = Et_2AlCl. [d] Determined by ^1H and ^{13}C NMR spectroscopy in $CDCl_3$. [e] Determined by ATR-IR spectroscopy. [s] This study.

S2.5 Polyisoprene irradiated by UV-light at 254 nm

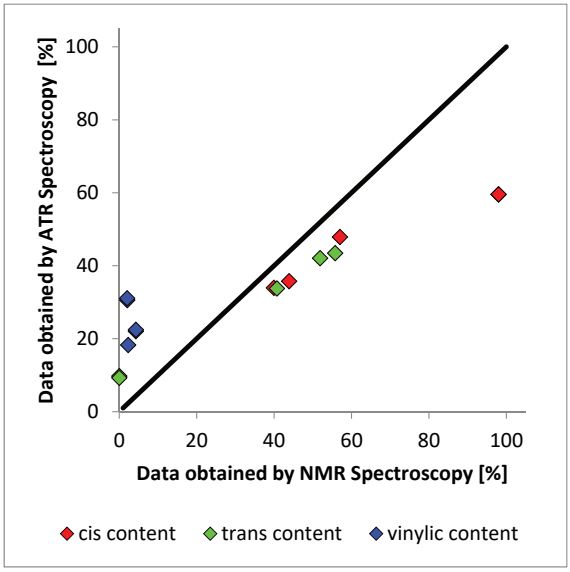

Figure S2.5.1. Comparison of the microstructure results obtained by NMR and ATR-IR spectroscopy, applying $Nd(AlMe_4)_3$ (**2**Nd) and cocatalysts **A**-**E** (**A** = $[Ph_3C][B(C_6F_5)_4]$, **B** = $[PhNMe_2H][B(C_6F_5)_4]$, **C** = $B(C_6F_5)_3$, **D** = Me_2AlCl, **E** = Et_2AlCl) in one equivalent and 48 h of UV radiation at 254 nm. For detailed polymerization data see Tables S1.2.4, S1.5.1 and S2.5.1.

Table S2.5.1 Comparison of the microstructure results by NMR and ATR-IR spectroscopy, data from UV-irradiated samples of isoprene polymerization applying **2Nd** [a]

		NMR			ATR-IR			
entry[b]	**cocatalyst**[c]	***cis*-content [%]**[d]	***trans*-content [%]**[d]	**vinylic content [%]**[d]	***cis*-content [%]**[e]	***trans*-content [%]**[e]	**vinylic content [%]**[e]	**ref.**
1	**A**	43.9	51.9	4.3	35.8	42.1	22.1	-[s]
2	**B**	39.9	55.8	4.3	34.0	43.5	22.5	-[s]
3	**C**	57.0	40.7	2.3	47.9	33.8	18.3	-[s]
4	**D**	97.9	0.0	2.1	59.6	9.8	30.6	-[s]
5	**E**	98.0	0.0	2.0	59.6	9.3	31.1	-[s]

[a] For detailed data on the respective chain properties, see Tables S1.2.4 and S1.5.1. [b] Conditions: samples obtained from isoprene polymerization were exposed to UV-light of 254 nm for 48 h. [c] **A** = $[Ph_3C][B(C_6F_5)_4]$, **B** = $[PhNMe_2H][B(C_6F_5)_4]$, **C** = $B(C_6F_5)_3$, **D** = Me_2AlCl, **E** = Et_2AlCl. [d] Determined by ^1H and ^{13}C NMR spectroscopy in $CDCl_3$. [e] Determined by ATR-IR spectroscopy. [s] This study.

Values reported for the 3,4 contents in Table and Figure S2.5.1 are given, as obtained from the algorithm. As a shift towards vinylic linkage by UV radiation does not seem likely, it is assumed, that UV-induced crosslinking creates oscillations in the IR spectrum that are misinterpreted by the algorithm.

S3. Extrapolation of the Ratio n(Chains) / n(Ln Centers)

In order to obtain the ratio of polymer chains per lanthanide center, the assumption is made, that if the polymerization would not be stopped after 1 h of reaction time, it would continue in the same fashion until all monomer is consumed.
The extrapolated number average molecular mass is then given by

$$M_{n,ext}(c_M = 0) = \frac{M_n(1\,h)}{Yield(1\,h)}, \quad (1)$$

where c_M is the concentration of the monomer. Due to the assumtion discussed above, errors occur, as the system, investigated in this study, is intended to set free a chain transfer agent $AlMe_3$, that could cause the initiation of new chains at all times. As the chain transfer capability of $AlMe_3$ is known to be low, and chain termination plays only a minor role in catalyzed polymerization, these errors are assumed to be low enough to be neglected.

The respective degree of polymerization is given by equation (2).

$$P_{n,ext} = \frac{M_{n,ext}}{M_M}, \quad (2)$$

where M_M is the molecular mass of the monomer.
For 100% monomer consumption, equation (3) applies.

$$P_n = \frac{n_M}{n_{act\ Ln}} = \frac{n_M}{n(chains)}, \quad (3)$$

where n_M is the amount of monomer fed [mol] and therefore constant during the whole reaction. $n_{act\ Ln}$ is the amount of active lanthanide centers [mol], and n(chains) the amount of polymer chains formed during the reaction [mol].
$P_{n,\,exp}$, the expected degree of polymerization if all Ln centers grow polymer chains is given by

$$P_{n,exp} = \frac{n_M}{n_{Ln}} = \frac{n_M}{n(chains)_{exp}}, \quad (4)$$

where n_{Ln} is the total amount of Ln centers. Therefore,

$$\frac{P_{n,exp}}{P_{n,ext}} = \frac{n(chains)}{n_{Ln}} = \frac{n_{act\ Ln}}{n_{Ln}} \quad (5)$$

Applying this extrapolation to the isoprene polymerizations discussed in Sections S1.1 - S1.3 led to the matrix shown as Table S3.1.

Table S3.1 Comparison of the ratios of the amounts of polymer chains and lanthanide centers obtained for the polyisoprenes[a]

		precatalyst [Ln(AlMe$_4$)$_3$] (**2**^{Ln})										
entry[b]	**cocatalyst**[c]	**2**^{La}	**2**^{Ce}	**2**^{Pr}	**2**Nd	**2**^{Gd}	**2**^{Tb}	**2**^{Dy}	**2**^{Ho}	**2**^{Y}	**2**^{Er}	**2**^{Lu}
1	**A**	1.36[h]	1.94	1.62	1.54	1.15	1.11	0.65	1.02	0.76[h]	0.69	1.01
2	**2A**	1.01	1.70	0.66	1.09	2.32	2.01	3.72	1.56	0.18	1.31	1.80
3	**B**	1.13[h]	2.23	1.96	3.37	0.99	0.79	0.65	0.52	0.58[h]	0.61	1.31
4	**2B**	1.20	1.94	0.43	1.25	0.76	1.06	0.89	0.81	0.17[h]	0.85	1.62
5	**C**	0.16[h]	1.78	0.87	0.65	0.62	0.71	0.43	0.46	0.32[h]	0.37	0.30
6	**2C**	0.29	0.97	0.68	0.32	0.50	0.53	0.49	0.35	0.36	0.41	–[f]
7	**D**	0.17	0.04	0.28	0.29	0.62	0.92	0.77	0.16	–[f]	–[f]	–[f]
8	**2D**	–[f]	0.44	0.33	0.34	0.55	1.27	0.66	0.32	0.14	–[f]	–[f]
9	**E**	–[f]	6.53	0.66	0.69	1.38	2.23	1.22	0.46	0.32	–[f]	–[f]
10	**2E**	0.15	0.75	1.39	1.11	1.89	2.82	1.96	0.11	0.47	–[f]	–[f]

[a] For detailed information on polymerization data and origin of the values (literature or this study), see sections S1.1 and S1.2. For information on the color code, *vide infra*. [b] Conditions: 0.02 mmol of the resp. Ln precatalyst, 0.02 or 0.04 mmol cocatalyst, in toluene, [Ln]:[isoprene] 1:1000 (n/n), reaction time 1 h, pre-reaction time 0.5 h. [c] **A** = [Ph$_3$C][B(C$_6$F$_5$)$_4$], **B** = [PhNMe$_2$H][B(C$_6$F$_5$)$_4$], **C** = B(C$_6$F$_5$)$_3$, **D** = Me$_2$AlCl, **E** = Et$_2$AlCl. [f] No further evaluation possible due to low yield. [h] Reaction time 24 h.

Table S3.1 shows the values implying multinary active species or low initiation rates (as n(chains) / n(n Ln centers) < 1) in green color. Those, which grow more than one chain per metal center or imply chain transfer or termination are given in blue and red; red highlights those active systems, that grow more than two chains per Ln center.

S4. Crystal Structure Data

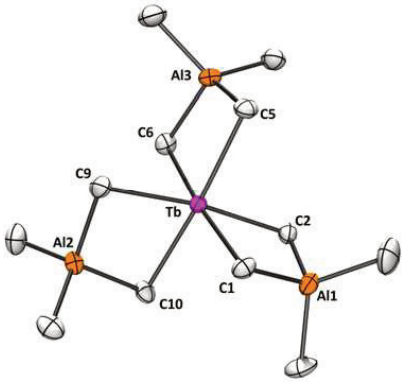

Figure S4.1. ORTEP view of one of two individuals in the unit cell of **2**^{Tb}. Atoms are represented by atomic displacement ellipsoids at the 50% level. Hydrogen atoms are omitted for clarity. Selected distances (Å) and angles (deg): Tb1—C1 2.537(4), Tb1—C2 2.520(4), Tb1—C5 2.536(4), Tb1—C6 2.519(4), Tb1—C9 2.522(4), Tb1—C10 2.544(4), average Tb1—CX (X = 1, 2, 5, 6, 9, 10) 2.536, Al1—C1, 2.089(4), Al1—C2, 2.083(4); C1—Tb1—C2 84.27(12), C1—Tb1—C5 92.14(13), C1—Tb1—C6 175.02(13), C1—Al1—C2 108.81(15).

Table S4.1. Crystal data and structure refinement for $\mathbf{2^{Gd}}$ and $\mathbf{2^{Tb}}$

	$\mathbf{2^{Gd}}$	$\mathbf{2^{Tb}}$
CCDC Deposition	1817853	1817852
Empirical formula	$C_{12}H_{36}Al_3Gd$	$C_{12}H_{36}Al_3Tb$
Mw [g mol^{-1}]	418.60	420.27
T[K]	100(2)	100(2)
Wavelength	0.71073 Å	0.71073 Å
Crystal system	monoclinic	monoclinic
Space group	$P2_1/c$	$P2_1/c$
a [Å]	7.3841(4)	7.3790(18)
b [Å]	17.7049(10)	17.703(5)
c [Å]	32.1650(18)	32.277(8)
α [°]	90	90
β [°]	92.4360(10)	92.552(4)
γ [°]	90	90
Volume [Å^3]	4201.3(4)	4205.7 (19)
Z	8	8
density (calculated) [mg mm-^{3}]	1.324	1.327
Absorption coefficient μ [mm^{-1}]	3.265	3.417
Theta range	2.222 to 27.103°	1.313 to 28.281°
Reflections collected	60729	65817
Independent reflections	9286 [$R_{(int)}$ = 0.0762]	10430 [$R_{(int)}$ = 0.061]
Data / restraints / parameters	9286 / 0 / 445	10430 / 0 / 445
R_1(obs)[a]	0.0388	0.0306
wR_2(all)[b]	0.0689	0.0670

[a] Final R indices [I>2σ(I)]; [b] R indices (all data).

References

Litlabø R, Lee H.S.; Niemeyer M.; Törnroos, K.W.; Anwander R. Rare-earth metal bis(tetramethylaluminate) complexes supported by a sterically crowded triazenido ligand. *Dalton Trans.* **2010**, *39*, 6815-6825.

Arndt, S.; Beckerle, K.; Zeimentz, P.M.; Spaniol, T.P.; Okuda, J. Cationic Yttrium Methyl Complexes as Functional Models for Polymerization Catalysts of 1,3-Dienes. *Angew. Chem. Int. Ed.* **2005**, *44*, 7473-7477.

Schädle, D., *Personal Communication,* Eberhard Karls Universität Tübingen, 2013.

Fischbach, A.; Klimpel, M.G.; Widenmeyer, M.; Herdtweck, E.; Scherer, W.; Anwander R. Stereospecific Polymerization of Isoprene with Molecular and MCM-48-Grafted Lanthanide(III) Tetraalkylaluminates. *Angew. Chem. Int. Ed.* **2004**, *43*, 2234-2239.

Fischbach, A.; Anwander, R. Rare-Earth Metals and Aluminum getting Close in Ziegler Type Organometallics. *Adv. Polym. Sci.* **2006**, *204*, 155-281.

Zimmermann, M.; Frøystein, N.A.; Fischbach, A.; Sirsch, P.; Dietrich, H.M.; Törnroos, K.W.; Herdtweck, E.; Anwander, R. Homoleptic Rare-Earth Metal(III) Tetramethylaluminates: Structural Chemistry, Reactivity, and Performance in Isoprene Polymerization. *Chem. Eur. J.* **2007**, *13*, 8784-8800.

Robert, D.; Spaniol, T.P.; Okuda, J. Neutral and Monocationic Half-Sandwich Methyl Rare-Earth Metal Complexes: Synthesis, Structure, and 1,3-Butadiene Polymerization Catalysis. *Eur. J. Inorg. Chem.* **2008**, 2801-2809.

Paper V: 1,3-Diene Polymerization Promoted by Half-Sandwich Rare-Earth Metal Dimethyl Complexes: Active Species Clustering and Cationization / Deactivation Processes

This aricle is reprinted with permission (License Number 4705971115575) from:

"1,3-Diene Polymerization Promoted by Half-Sandwich Rare-Earth Metal Dimethyl Complexes: Active Species Clustering and Cationization / Deactivation Processes"

by
Christoph O. Hollfelder, Lars N. Jende, Hans-Martin Dietrich, Klaus Eichele, Cäcilia Maichle-Mössmer, and Reiner Anwander

published in:
Chem. Eur. J. **2019**, *25*, 7298-7302.
doi: 10.1002/chem.201901269

Copyright (2019) by John Wiley and Sons.

ChemPubSoc Europe

DOI: 10.1002/chem.201901269

CHEMISTRY A European Journal Communication

Rare Earth Metals

1,3-Diene Polymerization Promoted by Half-Sandwich Rare-Earth-Metal Dimethyl Complexes: Active Species Clustering and Cationization/Deactivation Processes

Christoph O. Hollfelder, Lars N. Jende, Hans-Martin Dietrich, Klaus Eichele, Cäcilia Maichle-Mössmer, and Reiner Anwander*[a]

Abstract: When activated with fluorinated borate cocatalysts the trimetallic complexes $[Cp^*LnMe_2]_3$ (Ln = Y, Lu; $Cp^* = C_5Me_5$) promote efficiently the formation of high-*cis* polybutadiene. Respective polyisoprenes instead bear much less pronounced microstructures, but reveal cross-linked products at lower polymerization temperatures. Varying the amount of cocatalyst, the emerging active species were examined by NMR spectroscopic techniques (incl. ^{1}H DOSY). The occurrence of donor-solvent and thermally induced degradation products of the highly reactive precatalyst $[Cp^*YMe_2]_3$ and derived catalyst species was revealed by the elucidation of methylidene clusters $[Cp^*_3Y_3Me_4(CH_2)(thf)_2]$ and $[Cp^*_6Y_6Me_4(CH_2)_4]$, as well as $[(Cp^*Y)_2Me_2(N(Me)_2(C_6H_4)]_n[B(C_6F_5)_4]_n$, implying a multimetallic active species.

Numerous cyclopentadienyl-derived half-sandwich and sandwich Group IV tri/dimethyl complexes have been applied as catalysts in the anionic coordinative polymerization of 1,3-dienes.[1,2] Moreover, dominant pathways of catalyst degradation have been assessed and corroborated by structural analyses of the proposed degradation products.[3,4] The extremely efficient and commerically applied rare-earth metal(Ln)-based coordinative 1,3-diene polymerization depends on highly reactive alkyl species generated in situ.[5] Any likely (rapid) decomposition/degradation of the involved Ziegler-type Ln^{III} active species seems to be plausible, but has remained elusive.[6] Moreover, the intitial clustering of the active species generated in Ziegler-type ternary catalyst mixture has been pointed out, but isolation of the respective species was apparently not targeted.[7] Further investigation into Ln^{III}-promoted 1,3-diene polymerization by using cyclopentadienyl-supported monometallic precatalysts accessible to more comprehensive characterization seemed to be rewarding.[8,9] For example, earlier 1,3-diene polymerization catalysis applying half-sandwich lanthanide dialkyls as precatalysts, by Hou and co-workers[10,11] gave polyisoprenes with predominantly vinylic linkages[10] and copolymers of dicyclopentadiene with *n*-hexene.[11] Insights into the nature of the corresponding catalytically active species were obtained by X-ray diffraction (XRD) studies of the donor-stabilized active species model compound $[Cp'Sc(CH_2SiMe_3)(thf)_2]^+$ ($Cp' = C_5Me_4SiMe_3$).[10] In the case of $[Cp'Sc(o\text{-}CH_2\text{-}C_6H_4\text{-}NMe_2)\{((\mu\text{-}F)_2C_6F_3)B(C_6F_5)_3\}]$, even the active species itself could be analyzed by XRD.[11] Also, allyl–lanthanide half-sandwich compounds with[12] and without[13] N-donor side-arm have shown remarkably high activity in the alkylaluminum-free polymerization of isoprene.

Although half-sandwich dimethyl complexes $[Cp^*ScMe_2]_x$ and $[Cp^*YMe_2]_3$ have been known since 1991[14] and 1994,[15] respectively, it was not until 2006 that the trimeric methyl-bridged solid-state structure of the yttrium derivative $[Cp^*YMe_2]_3$ (**1^Y**)[16] and the dimeric nature of $[Cp'ScMe_2]_2$ were unveiled.[17] Noteworthy, recent theoretical approaches predicted the generation of high *cis*-1,4 polyisoprene at monometallic cationic "aluminum-free" $[Cp^*Y(C_6H_{11})]^+$ ($C_6H_{11} = CH_3^-$/isoprene).[18] Herein, we report the performance of these "simplest" donor- and aluminum-free half-sandwich hydrocarbyl complexes in 1,3-diene polymerization and potential degradation pathways of the active species.

When treated with borate cocatalysts $[Ph_3C][B(C_6F_5)_4]$ (**A**) or $[PhNMe_2H][B(C_6F_5)_4]$ (**B**), yttrium complex **1^Y** showed a remarkable tendency toward *cis*-1,4-polymerization in case of 1,3-butadiene (Table 1, runs 1 and 2). This selectivity was less pronounced with complex **1^{Lu}** featuring the smaller lutetium metal center (Table 1, runs 4 and 5).[19] The latter effect is enhanced through the bulkier monomer isoprene, which preferentially engages in the less space-demanding vinylic addition (Table 1, runs 13 and 14). Polyisoprenes with smaller *cis*-1,4-contents (compared to the corresponding polybutadiene) were also observed for **1^Y** concerning trityl cocatalyst **A** (Table 1, run 6). This finding contradicts the formation of high *cis*-1,4 polyisoprene as proposed by DFT calculations.[18] The mixtures **1^Y**(**1^{Lu}**)/**B**/isoprene led to a dominant vinylic 3,4-addition (Table 1, runs 7 and 14), which we ascribe to the coordination of the protonolysis side product $PhNMe_2$ (vide infra). In contrast, activation reactions utilizing the commonly applied borane cocatalyst $B(C_6F_5)_3$ (**C**) did not yield any polymer. For both monomers the combination **1^Y**/**B** yielded narrow molecu-

[a] C. O. Hollfelder, Dr. L. N. Jende, Dr. H.-M. Dietrich, Dr. K. Eichele, Dr. C. Maichle-Mössmer, Prof. Dr. R. Anwander
Institut für Anorganische Chemie
Eberhard-Karls-Universität Tübingen, Auf der Morgenstelle 18
72076 Tübingen (Germany)
E-mail: reiner.anwander@uni-tuebingen.de

Supporting information and the ORCID identification number(s) for the author(s) of this article can be found under: https://doi.org/10.1002/chem.201901269.

© 2019 Wiley-VCH Verlag GmbH & Co. KGaA, Weinheim

These are not the final page numbers! ↗↗

ChemPubSoc Europe

CHEMISTRY A European Journal Communication

Table 1. Selected examples of butadiene and isoprene homopolymerization applying $[Cp^*LnMe_2]_3$ as precatalysts.

Run[a]	Precatalyst	Co-catalyst[b]	Initial T	Yield [%]	*cis*-1,4[c]	*trans*-1,4[c]	3,4[c]	M_n[d] (x 10^4)	M_w/M_n[d]	T_g[e]
				1,3-Butadiene						
1	$[Cp^*YMe_2]_3$ ($\mathbf{1^Y}$)	**A**	25	21	91.4	4.2	4.4	76.4	1.58	−97.1
2	$[Cp^*YMe_2]_3$ ($\mathbf{1^Y}$)	**B**	25	48	95.2	2.2	2.6	49.6	1.20	−97.4
3	$[Cp^*YMe_2]_3$ ($\mathbf{1^Y}$)	**B**	0	67	94.8	3.1	2.1	123.0	1.21	−98.4
4	$[Cp^*LuMe_2]_3$ ($\mathbf{1^{Lu}}$)	**A**	25	>99	85.3	8.0	6.7	39.7	1.84	−94.0
5	$[Cp^*LuMe_2]_3$ ($\mathbf{1^{Lu}}$)	**B**	25	95	84.9	8.2	6.9	33.0	1.77	−93.0
				Isoprene						
6	$[Cp^*YMe_2]_3$ ($\mathbf{1^Y}$)	**A**	25	>99	50.8	17.5	31.7	8.4	2.33	−47.3
7	$[Cp^*YMe_2]_3$ ($\mathbf{1^Y}$)	**B**	25	90	35.8	10.8	53.4	14.1	1.16	−27.1
8[f]	$[Cp^*YMe_2]_3$ ($\mathbf{1^Y}$)	**B**	40	>99	32.7	10.8	56.5	12.7	1.09	−21.0
9[g]	$[Cp^*YMe_2]_3$ ($\mathbf{1^Y}$)	**A**	−10	96	92.2	0.0	7.8	–[h]	–[h]	−56.2
10[i]	$[Cp^*YMe_2]_3$ ($\mathbf{1^Y}$)	**B**	25	92	3.9	85.5	10.6	15.2	1.37	−61.8
11[k]	$[Cp^*YMe_2]_3$ ($\mathbf{1^Y}$)	**B**	25	88	31.4	12.7	55.9	1.6	1.37	−23.3
12[m]	$[Cp^*YMe_2]_3$ ($\mathbf{1^Y}$)	**B**	25	44	8.7	2.7	88.6	20.2	1.97	−3.5[n]
13	$[Cp^*LuMe_2]_3$ ($\mathbf{1^{Lu}}$)	**A**	25	>99	21.5	20.5	58.0	26.8	2.00	−15.5
14	$[Cp^*LuMe_2]_3$ ($\mathbf{1^{Lu}}$)	**B**	25	>99	21.4	21.5	57.1	29.2	1.38	−16.8
15	$[(Cp^*Y)_3Me_4(CH_2)(thf)_2]$ (**3**)	**A**	25	48	44.4	14.3	41.3	18.5[p]	2.75[p]	−30.6
16	$[(Cp^*Y)_3Me_4(CH_2)(thf)_2]$ (**3**)	**B**	25	7	76.5	0.0	23.5	55.1	1.97	−47.9

[a] Conditions: 0.007 mmol precatalyst (0.020 mmol of Ln centers), 0.020 mmol of cocatalyst, 30 min pre-reaction time, 1 h reaction time; for 1,3-butadiene polymerization: 25 mL toluene, 60 mmol 1,3-butadiene, stirring at 300 rpm; for isoprene polymerization: 8 mL toluene, 20 mmol isoprene. [b] Cocatalyst: **A** = $[Ph_3C][B(C_6F_5)_4]$, **B** = $[PhNMe_2H][B(C_6F_5)_4]$. [c] Determined by ^1H and ^{13}C NMR spectroscopy in $CDCl_3$. [d] Determined by means of size-exclusion chromatography (SEC) against polystyrene standards. [e] Determined by DSC, heating rate: 20 K min^{-1}; cooling rate: 60 K min^{-1}. [f] Reaction time 1 min. [g] Pre-reaction at polymerization temperature. [h] No SEC data available due to crosslinking. Flory–Rehner data: $N_{Gel} = 1.2 \times 10^2$, see the Supporting Information for details of the determination of N_{Gel} (distance between cross-linkages in numbers of monomer units).[24] [i] $AlMe_3$ (10 equiv). [k] Al*i*Bu$_3$ (30 equiv). [m] [Dipp-N=C]$_2$ (1 equiv) was added prior to the activation and the mixture was stirred for 30 min. [n] Determined by DSC; heating rate: 10 K min^{-1}, cooling rate: 100 K min^{-1}. [p] Bimodal MWD: M_n 13.9, polydispersity index (PDI = M_w/M_n) 1.42, contains approximately 75 mol% of the polymer.

lar weight distributions (MWDs), and in case of 1,3-butadiene, the highest achieved *cis*-content of 95.2%. Another striking difference of the monomer's polymerization behavior are the rather low conversions obtained for $\mathbf{1^Y}$/**A**(**B**)/1,3-butadiene after one hour (Table 1, runs 1 and 2), whereas system $\mathbf{1^Y}$/**B**/isoprene gave full conversion after one minute at slightly increased polymerization temperature (Table 1, run 8).

To drive the reaction in a more controlled fashion, and thereby obtain a more selective microstructure, experiments were performed at lower temperatures. For butadiene polymerization, $\mathbf{1^Y}$/**A** gave only traces of polymer at 0 °C, whereas $\mathbf{1^Y}$/**B** instead showed an increased monomer conversion accompanied by a decreased total amount of polymer chains, but no significant shift in selectivity (Table 1, run 3). In contrast, polymerizing isoprene at lower temperatures affected the microstructure by eliminating the *trans*-1,4-content completely, especially in the case of cocatalyst **A** (cf., Tables 1, run 9 and S8, run S16, in the Supporting Information).

Surprisingly, applying system $\mathbf{1^Y}$/**A** at lower temperatures also featured polymer crosslinking (ca. one link per 100 monomer units, see Section 3.2 in the Supporting Information and Table 1, run 9 and S8 in the Supporting Information).[20] This implies the presence of a second reaction pathway, because catalyzed 1,3-diene polymerizations are known to give linear polymer chains exclusively. Assuming any hampered pre-reaction between $\mathbf{1^Y}$ and **A**, polyisoprene with a high 3,4-content was further treated with $\mathbf{1^Y}$/**A** and isoprene monomer. Next to linear polyisoprene, a crosslinked polymer was observed, which is not present, if only **A** is added to the polymer, before further monomer addition (see Section 3.2.2 in the Supporting Information, for details). Therefore, it can be concluded that both $\mathbf{1^Y}$ and **A** or their pre-reaction product is involved in the crosslinking mechanism.

The molecular weight averages far above 54 kg mol^{-1} (polybutadiene) and 68 kg mol^{-1} (polyisoprene; Table 1 and Section 3 in the Supporting Information) suggest a multimetallic nature of the active species. As a proof of principle, $\mathbf{1^Y}$ was treated with a ninefold excess of $AlMe_3$ prior to the activation with **B**. Comparing the obtained polyisoprenes (Table 1, run 10) with previous results accomplished by precatalyst $[Cp^*Y(AlMe_4)_2]$,[21] the clear tendency for 1,4-*trans*-polymerization, induced by the presence of $AlMe_3$, was confirmed.[22] However, the resulting polymers differ as expected from the earlier studies on $[Cp^*Ln(AlMe_4)_2]$.[21] Furthermore, ternerization with a ninefold excess of the frequently applied chain transfer agent Al*i*Bu$_3$[12,23,24] resulted in polymers showing the expected low molecular weight and an unaffected microstructure (Tables 1, run 11 and S10, run S29) as known for chain-transfer polymerizations.[24] As a further indication of the multimetallic nature of the active species applying $\mathbf{1^Y}$/**B**, the obtained polymer of the system $\mathbf{1^Y}$/**B**/10$AlMe_3$ was compared to the stoichiometrically identical system $[Cp^*Y(AlMe_4)_2]$/**B**/8$AlMe_3$ (Tables 1, run 10 and S10, run S34). Most significantly, in the latter case derived from a monoyttrium complex, a polymer without the high amount of 1,4-*trans* linkages as found for $\mathbf{1^Y}$/**B**/10$AlMe_3$ was obtained. But still the presence of $AlMe_3$ shifted the microstructure toward 1,4-*trans* compared to $[Cp^*Y(AlMe_4)_2]$/**B**.[21]

Examination of the activation processes of complex $\mathbf{1^Y}$ by means of standard NMR spectroscopic methods revealed that, for both **A** and **B**, use of one equivalent of cocatalyst per tri-

© 2019 Wiley-VCH Verlag GmbH & Co. KGaA, Weinheim

ChemPubSoc Europe

CHEMISTRY
A European Journal
Communication

metallic precatalyst complex $\mathbf{1}^{Y}$ (Table S7, runs S1 and S5) led to another symmetric species of composition "$Cp^*_3Y_3Me_{4\text{-}5}$" (**I**, Figures S7 and S17, in the Supporting Information; the apparent methyl group deficiency might result from degradation). Investigation of **I** by ^{1}H DOSY NMR spectroscopy[25] (Section 4.2, in the Supporting Information) revealed a high molecular mass of approximately 2 kg mol^{-1} (Table S15), suggesting the existence of a larger, possibly hexametallic cluster (see below). Another indication for a multimetallic complex is the fact that **I** is inactive in 1,3-diene polymerization, but the addition of another one sixth equivalent of the respective cocatalyst per Y center activated this species. Thus with 1.5 equivalents cocatalyst per trimetallic complex $\mathbf{1}^{Y}$, catalysis is fully activated, although the obtained polymer still differed from that obtained with three equivalents per trimetallic complex $\mathbf{1}^{Y}$. Most interestingly, the obtained ratio of polymer chains per Y center is approximately 0.8 in case of cocatalyst **A**, and approximately 0.4 when **B** was applied. In the absence of any chain transfer, it seems that for **A** every single cocatalyst ion pair added after the formation of "$Cp^*_3Y_3Me_{4\text{-}5}$" (**I**) activates four to six Y centers for polymerization. This implies several active centers per multimetallic ion and/or probably degradation/transformation of **I** into smaller units than hexamers. ^{1}H DOSY NMR data confirmed the latter assumption, because for the respective species smaller hydrodynamic radii/molecular masses were obtained (Section 4.2 in the Supporting Information).

The respective NMR spectra (Figures S10 and S11 in the Supporting Information) show the presence of one dominant species with a Cp* signal at 1.76 ppm ("$Cp^*_3Y_3Me_{4\text{-}5}$", **I**) for the addition of one equiv of **A** per trimetallic complex $\mathbf{1}^{Y}$. This peak decreased upon addition of further cocatalyst, whereas at three equivalents per trimetallic complex $\mathbf{1}^{Y}$, a species with a Cp* proton signal at 1.45 ppm was dominant. Interestingly, this emerging species lacks a methyl peak, assignable by ^{1}H DOSY NMR spectroscopy. The corresponding activation with cocatalyst **B** (Figure S19 in the Supporting Information) gave the same inactive species (Cp* signal at 1.76 ppm) and the formation of non-coordinated $PhNMe_2$ from the onset. Adding more than one equivalent per trimetallic complex $\mathbf{1}^{Y}$, several potentially active species seem to form, the species with a Cp* peak at 1.45 ppm being dominant in the case of one full equivalent of **B** even after 30 minutes. Also, the side-product cannot be considered innocent anymore and coordination as an N-donor ligand is likely. This causes the formation of different products and intermediates for the ongoing degradation (c.f., degradation product **2**, see below) compared to the system $\mathbf{1}^{Y}$/**A**.[26]

Targeting potential catalyst degradation products, a dominant degradation compound (**2**) could be crystallized from the reaction mixture $\mathbf{1}^{Y}$/**B** (Scheme 1). Compound **2** is considered to be one of the final products as the NMR peaks assigned to this species appear and grow after 25 minutes, and vanish later after approximately five hours due to crystallization (Figure S21 and Chart S1b in the Supporting Information). In the solid state, compound **2** consists of the dicationic fragment $(Cp^*YMe)_2$, in which the yttrium centers are additionally bridged by a $C_6H_4NMe_2$ anionic moiety, the C–H-bond activation product of side product $PhNMe_2$. The resulting monocationic dimeric species are bridged by BAr^F_4 anions to form a linear polymeric structure (Figures 1 and S2, Table S2 in the Supporting Information), involving the fluorine atoms F3 and F9. The intermolecular interaction is further enhanced by a π-π-interaction between the parallel-displaced aryl ring of $C_6H_4NMe_2$ and one of the Ar^F rings (bound to B1 via C34) exhibiting an interplanar distance of 3.32 Å[27] and an interplanar angle of 15.7°. The Y2–Ct and Y–Me distances in **2** are very similar to those in $\mathbf{1}^{Y}$ but the additional Y–N_{donor} contact affects the Y1–Ct distance significantly.

A likely scenario for the formation of **2** might involve the initial formation of a cationic dimeric intermediate $[(Cp^*Y)_2(\mu\text{-}Me)_3(PhNMe_2)]$ with a molecule of $PhNMe_2$ coordinating to one

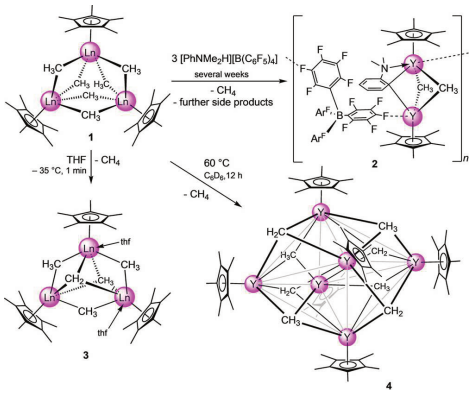

Scheme 1. Degradation products of $\mathbf{1}^{Y}$ observed upon (a) activation with cocatalyst **B** giving **2**; (b) in the presence of donor molecules forming **3**; and (c) at 60 °C giving **4**.

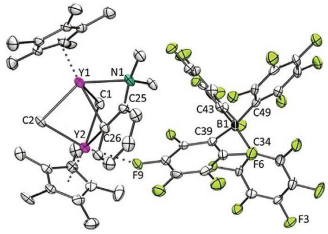

Figure 1. ORTEP view of the repetition unit of the polymeric crystal structure of **2**: $\{[(Cp^*Y)_2Me_2(NMe_2(C_6H_4))][B(C_6F_5)_4]\}_n$. Atomic displacement parameters are set at the 50% probability level. Hydrogen atoms and five molecules of toluene per unit cell are omitted for clarity. Selected bond lengths and angles for **2** can be found in the Supporting Information (Table S2), as well as Figure S2, highlighting the intended π–π interaction between the Ar^F ring bound to B1 via C34 and the $C_6H_4NMe_2$-aryl ring and the polymeric character of this structure.

© 2019 Wiley-VCH Verlag GmbH & Co. KGaA, Weinheim

These are not the final page numbers! ↗↗

ChemPubSoc Europe

CHEMISTRY
A European Journal
Communication

of the yttrium centers. Next, a methyl moiety could either abstract a proton from the *ortho* position of the aniline forming methane as a byproduct or follow a pathway that involves a methylene species such as $[(Cp^*Y)_2(\mu\text{-}Me)_2(\mu\text{-}CH_2)(PhNMe_2)]$, which would subsequently deprotonate the aniline to form **2** (Scheme S1 in the Supporting Information).

Probing the stability of complex $\mathbf{1^Y}$ in the presence of donor molecules or at elevated temperatures, it was exposed to thf at −35 °C and heated to 60 °C in C_6D_6 solution (mimicking heat of reaction during catalyst activation or polymerization). In both cases, methane formation displayed the prominent reaction pathway and led to the isolation of distinct mixed methylene/methyl half-sandwich complexes $[(Cp^*_3Y_3Me_4(CH_2)(thf)_2]$ (**3**, $^2J_{YH,CH2} = 4.6$ Hz) and $[Cp^*_6Y_6Me_4(CH_2)_4]$ (**4**).[28]

Complex **3** was formed also when treating a mixture of $\mathbf{1^Y}$/1/3**B** (inactive) with THF at ambient temperature (Figures 2, top and S3 in the Supporting Information). While the Y_3 cluster resembles other known methyl/methylene complexes,[29] the hexametallic species **4** features a new structural motif (Figure 2/bottom and S4 in the Supporting Information). The Y–C(CH_2) and Y–C(CH_3) distances in **3** range from 2.283(4)–2.477(3) and 2.548(4)–2.778(4) Å, respectively. Complex **4** features a distorted octahedral arrangement of the yttrium centers with the eight faces randomly capped by methyl and methylene groups (Y–C, 2.461(10)–2.613(10) Å).

Furthermore, single crystals of **3** were tested in the polymerization of isoprene resulting in low (+**B**) to moderate (+**A**) yields of polymer, with a focus on *cis* stereoregularity in the case of cocatalyst **B** (Table 1, runs 15 and 16).[30] For the reaction of **3** with **A** several species were indicated and the ^{1}H DOSY NMR spectroscopic studies suggested nucleation alternation (Charts S27 and S28, as well as Table S15 in the Supporting Information). Preliminary investigations of the catalytic performance of $\mathbf{1^Y}$ in the presence of donor molecules indicated a pronounced influence but is subject to further research. For example, addition of diimine [Dipp-N=C]$_2$ (Dipp = diisopropylphenyl) to the pre-formed catalyst gave a polyisoprene with a high vinylic content (Table 1, run 12).

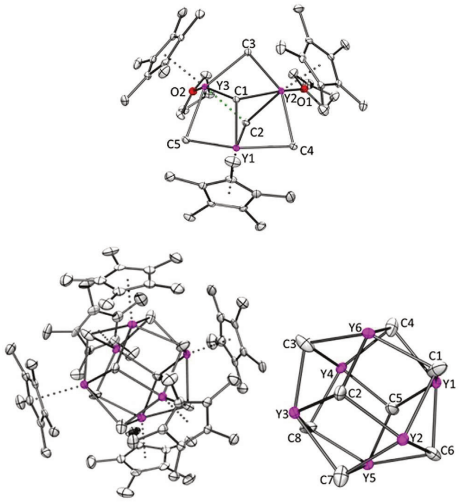

Figure 2. ORTEP views of the crystal structures of methylene complexes **3** (top) and **4** (bottom left) and the distorted octahedral core of **4** (bottom right). Atomic displacement parameters are set at the 50% probability level. Hydrogen atoms and one molecule of C_6D_6 (**4**) are omitted for clarity. Selected bond lengths and angles can be found in the Supporting Information (Tables S4 and S5).

For further understanding of the polymerization and targeting the catalytic limits, the following experiments were performed: polymerization of isoprene in *n*-hexane (Table S9 in the Supporting Information) resulted in lower yields than in toluene, if any, due to the low solubility of $\mathbf{1^Y}$ and $\mathbf{1^{Lu}}$ in this solvent. Furthermore, $\mathbf{1^Y}$ has been tested in the polymerization of styrene, in which only traces of syndiotactic polystyrene could be obtained after one hour at ambient temperature. Full conversion was observed after a reaction time of 14 hours, and 29% were found after one hour at 40 °C (Table S13 in the Supporting Information). Copolymerization reactions with ethylene yielded 4% within one hour, whereas a homo-polymerization of ethylene resulted in 89% conversion. Further results on copolymerization reactions, for example, of styrene, 1-hexene, and isoprene can be found in Table S13 in the Supporting Information.

In conclusion, cationization of trimetallic $[Cp^*LnMe_2]_3$ (Ln = Y, Lu) gave highly active catalysts for 1,3-diene polymerization. We hypothesize that the observed intricate polymerization behavior is caused by the presence of multimetallic species, supposedly also the active species of respective commercial catalysts. Although for 1,3-butadiene high *cis*-contents up to 95% were achieved, the bulkier isoprene is prone to vinylic linkages. Insights into the active polymerization species were provided by NMR spectroscopy, particularly, ^{1}H DOSY measurements and the solid-state structures of degradation products of the active species.

Acknowledgement

We thank the German Science Foundation (Grant AN 238/14-2) for generous support, Prof. Dr. Garreth Morris, University of Manchester, for providing tools for ^{1}H DOSY NMR evaluation, Dr. Stefanie Wunder (Fraunhofer IPA, Stuttgart) and Dr. Ralf Stehle (Technical University of Munich) for taking part in the scientific discussion, and Dr. Daniel Werner for assistance in XRD analysis.

Conflict of interest

The authors declare no conflict of interest.

Keywords: active species · catalyst degradation · diene polymerization · DOSY NMR spectroscopy · rare earth metals

© 2019 Wiley-VCH Verlag GmbH & Co. KGaA, Weinheim

ChemPubSoc Europe

CHEMISTRY
A European Journal
Communication

[1] a) S. Thiele, D. R. Wilson, *J. Macromol. Sci. Part C* **2003**, *43*, 581 – 628; b) G. Ricci, A. Sommazzi, F. Masi, M. Ricci, A. Boglia, G. Leone, *Coord. Chem. Rev.* **2010**, *254*, 661 – 676.
[2] G. Erker, G. Kehr, R. Fröhlich, *J. Organomet. Chem.* **2004**, *689*, 4305 – 4318.
[3] a) E. Y.-X. Chen, T. J. Marks, *Chem. Rev.* **2000**, *100*, 1391 – 1434; b) D. W. Stephan, *Organometallics* **2005**, *24*, 2548 – 2560.
[4] For examples, see: a) F. Guérin, D. W. Stephan, *Angew. Chem. Int. Ed.* **1999**, *38*, 3698 – 3701; *Angew. Chem.* **1999**, *111*, 3910 – 3913; b) J. E. Kickham, F. Guérin, J. C. Stewart, D. W. Stephan, *Angew. Chem. Int. Ed.* **2000**, *39*, 3263 – 3266; *Angew. Chem.* **2000**, *112*, 3406 – 3409; c) J. E. Kickham, F. Guérin, D. W. Stephan, *J. Am. Chem. Soc.* **2002**, *124*, 11486 – 11494.
[5] a) L. Friebe, O. Nuyken, W. Obrecht, *Adv. Polym. Sci.* **2006**, *204*, 1 – 154; b) A. Fischbach, R. Anwander, *Adv. Polym. Sci.* **2006**, *204*, 155 – 281; c) Z. Zhang, D. Cui, B. Wang, B. Liu, Y. Yang in *Molecular Catalysis of Rare-Earth Elements* (Ed.: P. W. Roesky), Springer, Berlin, **2010**, pp. 49 – 108; d) M. Nishiura, F. Guo, Z. Hou, *Acc. Chem. Res.* **2015**, *48*, 2209 – 2220; e) R. P. Kelly, P. W. Roesky, *Struct. Bonding* **2017**, *172*, 85 – 117; f) J. Jothieswaran, S. Fadlallah, F. Bonnet, M. Visseaux, *Catalysts* **2017**, *7*, 378; g) A. A. Trifonov, D. M. Lyubov, *Coord. Chem. Rev.* **2017**, *340*, 10 – 61; h) J. Huang, Z. Liu, D. Cui, X. Liu, *ChemCatChem* **2018**, *10*, 42 – 61.
[6] a) A. Fischbach, M. G. Klimpel, M. Widenmeyer, E. Herdtweck, W. Scherer, R. Anwander, *Angew. Chem. Int. Ed.* **2004**, *43*, 2234 – 2239; *Angew. Chem.* **2004**, *116*, 2284 – 2289; b) G. Occhipinti, C. Meermann, H. M. Dietrich, R. Litlabø, F. Auras, K. W. Törnroos, C. Maichle-Mössmer, V. R. Jensen, R. Anwander, *J. Am. Chem. Soc.* **2011**, *133*, 6323 – 6337; c) C. O. Hollfelder, L. N. Jende, D. Diether, T. Zelger, R. Stauder, C. Maichle-Mössmer, R. Anwander, *Catalysts* **2018**, *8*, 61.
[7] a) A. Fischbach, C. Meermann, G. Eickerling, W. Scherer, R. Anwander, *Macromolecules* **2006**, *39*, 6811 – 6816; b) C. Meermann, K. W. Törnroos, W. Nerdal, R. Anwander, *Angew. Chem. Int. Ed.* **2007**, *46*, 6508 – 6513; *Angew. Chem.* **2007**, *119*, 6628 – 6633.
[8] F. Bonnet, M. Visseaux, A. Pereira, D. Barbier-Baudry, *Macromolecules* **2005**, *38*, 3162 – 3169 and references therein.
[9] M. Zimmermann, K. W. Törnroos, R. Anwander, *Angew. Chem. Int. Ed.* **2008**, *47*, 775 – 778; *Angew. Chem.* **2008**, *120*, 787 – 790.
[10] X. Li, M. Nishiura, L. Hu, K. Mori, Z. Hou, *J. Am. Chem. Soc.* **2009**, *131*, 13870 – 13882.
[11] X. Li, M. Nishiura, K. Mori, T. Mashiko, Z. Hou, *Chem. Commun.* **2007**, 4137 – 4139.
[12] a) Z. Jian, D. Cui, Z. Hou, X. Li, *Chem. Commun.* **2010**, *46*, 3022 – 3024; b) Z. Jian, S. Tang, D. Cui, *Chem. Eur. J.* **2010**, *16*, 14007 – 14015; c) Z. Jian, S. Tang, D. Cui, *Macromolecules* **2011**, *44*, 7675 – 7681; d) L. N. Jende, C. O. Hollfelder, C. Maichle-Mössmer, R. Anwander, *Organometallics* **2015**, *34*, 32 – 41.
[13] N. Yu, M. Nishiura, X. Li, Z. Xi, Z. Hou, *Chem. Asian J.* **2008**, *3*, 1406 – 1414.
[14] W. E. Piers, E. E. Bunel, J. E. Bercaw, *J. Organomet. Chem.* **1991**, *407*, 51 – 60.
[15] C. J. Schaverien, *Organometallics* **1994**, *13*, 69 – 82.
[16] H. M. Dietrich, H. Grove, K. W. Törnroos, R. Anwander, *J. Am. Chem. Soc.* **2006**, *128*, 1458 – 1459.
[17] D. Robert, T. P. Spaniol, J. Okuda, *Eur. J. Inorg. Chem.* **2008**, 2801 – 2809.
[18] X. Kang, Y. Luo, G. Zhou, X. Wang, X. Yu, Z. Hou, J. Qu, *Macromolecules* **2014**, *47*, 4596 – 4606.
[19] For the solid-sate structure of $\mathbf{1^{Lu}}$, see the Supporting Information (Figure S1 and Table S1).
[20] Evaluated in analogy to: a) A. Fernández-Barbero, A. Fernández-Nieves, I. Grillo, E. López-Cabarcos, *Phys. Rev. E* **2002**, *66*, 051803; b) J. J. Crassous, A. Wittemann, M. Siebenbürger, M. Schrinner, M. Drechsler, M. Ballauff, *Coll. Polym. Sci.* **2008**, *286*, 805 – 812.
[21] a) M. Zimmermann, K. W. Törnroos, H. Sitzmann, R. Anwander, *Chem. Eur. J.* **2008**, *14*, 7266 – 7277; b) N. Dettenrieder, C. O. Hollfelder, L. N. Jende, C. Maichle-Mössmer, R. Anwander, *Organometallics* **2014**, *33*, 1528 – 1531.
[22] Increasing the amount of $AlMe_3$ to 30 equivalents led to a further increase of the *trans*-1,4-content (Table S10/run S28). **Extreme care has to be taken when handling larger amounts of $AlMe_3$!!!**
[23] S. Arndt, K. Beckerle, P. M. Zeimentz, T. P. Spaniol, J. Okuda, *Angew. Chem. Int. Ed.* **2005**, *44*, 7473 – 7477; *Angew. Chem.* **2005**, *117*, 7640 – 7644.
[24] A. Valente, A. Mortreux, M. Visseaux, P. Zinck, *Chem. Rev.* **2013**, *113*, 3836 – 3857.
[25] a) W. S. Price, *Concepts Magn. Reson.* **1997**, *9*, 299 – 336; b) W. S. Price, *Concepts Magn. Reson.* **1998**, *10*, 197 – 237; c) R. Evans, Z. Deng, A. K. Rogerson, A. S. McLachlan, J. J. Richards, M. Nilsson, G. A. Morris, *Angew. Chem. Int. Ed.* **2013**, *52*, 3199 – 3202; *Angew. Chem.* **2013**, *125*, 3281 – 3284.
[26] Both active systems, $\mathbf{1^Y/A}$ and $\mathbf{1^Y/B}$, were also followed by NMR spectroscopy in their respective degradation processes over time (Figures S16 and S21 and Charts S1a and S1b).
[27] Stacking dimers of free C_6H_6 and C_6F_6 are separated by an interplanar distance of 3.4 Å: B. W. Gung, J. C. Amicangelo, *J. Org. Chem.* **2006**, *71*, 9261 – 9270.
[28] W. X. Zhang, Z. Wang, M. Nishiura, X. Zhenfeng, Z. Hou, *J. Am. Chem. Soc.* **2011**, *133*, 5712 – 5715.
[29] a) M. Zimmermann, D. Rauschmaier, K. Eichele, K. W. Törnroos, R. Anwander, *Chem. Commun.* **2010**, *46*, 5346 – 5348; b) J. Hong, L. Zhang, X. Yu, Z. Zhang, P. Zheng, M. Nishiura, Z. Hou, X. Zhou, *Chem. Eur. J.* **2011**, *17*, 2130 – 2137; c) D. Schädle, M. Meermann-Zimmermann, C. Maichle-Mössmer, C. Schädle, K. W. Törnroos, R. Anwander, *J. Chem. Soc. Dalton Trans.* **2015**, *44*, 18101 – 18110; d) J. Hong, Z. Li, Z. Chen, L. Weng, X. Zhou, L. Zhang, *J. Chem. Soc. Dalton Trans.* **2016**, *45*, 6641 – 6649.
[30] Isoprene polymerization in the prensence of CH_2 moieties was shown previously: L. N. Jende, C. Maichle-Mössmer, R. Anwander, *Chem. Eur. J.* **2013**, *19*, 16321 – 16333.

Manuscript received: March 18, 2019
Accepted manuscript online: April 4, 2019
Version of record online: ■■ ▮▮, 0000

© 2019 Wiley-VCH Verlag GmbH & Co. KGaA, Weinheim

ChemPubSoc Europe

CHEMISTRY
A European Journal
Communication

COMMUNICATION

Rare Earth Metals

*C. O. Hollfelder, L. N. Jende, H.-M. Dietrich, K. Eichele, C. Maichle-Mössmer, R. Anwander**

■■ – ■■

1,3-Diene Polymerization Promoted by Half-Sandwich Rare-Earth-Metal Dimethyl Complexes: Active Species Clustering and Cationization/ Deactivation Processes

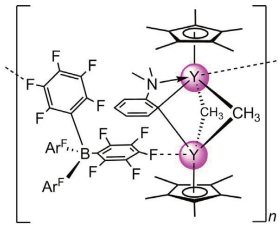

Catalyst degradation: Cationized $[(C_5Me_5)LnMe_2]_3$ (Ln = Y, Lu) display highly efficient catalysts for 1,3-diene polymerization, but the high reactivity implies distinct catalyst degradation pathways caused by activation side products (see figure) and heat of reaction (e.g., methylidene formation).

© 2019 Wiley-VCH Verlag GmbH & Co. KGaA, Weinheim

Paper V: Supporting Information

This Supporting Information is reprinted with permission (License Number 4705971115575) from the Supporting Information of:

"1,3-Diene Polymerization Promoted by Half-Sandwich Rare-Earth Metal Dimethyl Complexes: Active Species Clustering and Cationization / Deactivation Processes"

by
Christoph O. Hollfelder, Lars N. Jende, Hans-Martin Dietrich, Klaus Eichele, Cäcilia Maichle-Mössmer, and Reiner Anwander

published in:
Chem. Eur. J. **2019**, *25*, 7298-7302. doi: 10.1002/chem.201901269

Copyright (2019) by John Wiley and Sons.

CHEMISTRY
A European Journal

Supporting Information

1,3-Diene Polymerization Promoted by Half-Sandwich Rare-Earth-Metal Dimethyl Complexes: Active Species Clustering and Cationization/Deactivation Processes

Christoph O. Hollfelder, Lars N. Jende, Hans-Martin Dietrich, Klaus Eichele, Cäcilia Maichle-Mössmer, and Reiner Anwander*[a]

chem_201901269_sm_miscellaneous_information.pdf

WILEY-VCH

SUPPORTING INFORMATION

0. Table of Contents

0. Table of contents S2
1. Experimental Section S2
2. Crystal Structures S6
3. Polymer Data S12
4. Active Species Determination – NMR Spectra S19
5. Proposed Degradation Mechanisms S53
6. References S54

1. Experimental Procedures

1.1 General remarks

All operations were performed with rigorous exclusion of air and water, using standard Schlenk, high-vacuum, and argon glovebox techniques (MBraun MB 200B; < 1 ppm O_2, < 1 ppm H_2O). *n*-Hexane, toluene, and THF were purified by using Grubbs-type columns (MBraun SPS-800, solvent purification system) and stored in a glovebox. C_6D_6 and toluene-d_8 were obtained from Aldrich, dried over NaK alloy for 24 h, and filtered. Heptane, *n*-propanol, $CDCl_3$ and $AlMe_3$ were purchased from Aldrich and used as received. Isoprene was obtained from Aldrich, dried over trioctylaluminum (Aldrich), and vacuum transferred prior to use. $[Ph_3C][B(C_6F_5)_4]$ (**A**), $[PhNMe_2H][B(C_6F_5)_4]$ (**B**), and $B(C_6F_5)_3$ (**C**) were purchased from Boulder Scientific Company and used without any further purification. The NMR spectra of air and moisture sensitive compounds were recorded by using J. Young valve NMR tubes at 26 °C on a Bruker AVII+ 400 Avance (^{1}H: 400.11 MHz; ^{13}C: 100.61 MHz; ^{11}B: 80.25 MHz; ^{19}F: 376.43 MHz). ^{1}H DOSY NMR spectroscopic experiments were performed on a Bruker AVII+500 (^{1}H: 500.13 MHz; ^{13}C: 125.76 MHz).^{1}H and ^{13}C shifts are referenced using internal solvent resonances and reported in parts per million (ppm) relative to TMS. IR spectra were recorded on a NICOLET 6700 FTIR spectrometer using a DRIFT chamber with dry KBr/sample mixtures and KBr windows. For the latter the collected data were converted using the Kubelka-Munk refinement. Elemental analyses were performed on an Elementar Vario MICRO cube. The molar mass averages (M_w and M_n) of the polymers were determined by size-exclusion chromatography (SEC). Sample solutions (1.0 mg polymer per mL THF) were filtered through a 0.45 µm syringe filter prior to injection. SEC was performed with a pump supplied by Viscotek (GPCmax VE 2001), employing ViscoGEL columns. Signals were detected by means of a triple detection array (TDA 305) and calibrated against polystyrene standards (M_W/M_n < 1.15). The flowrate was set to 1.0 mL min^{-1}. The microstructures of the polydienes were examined by means of ^{1}H and ^{13}C NMR experiments on the AVII+ 400 Avance spectrometer at ambient temperature, using $CDCl_3$ as a solvent. Glass transition temperatures of the polymers (T_g) were obtained applying a Perkin-Elmer DSC 8000 calibrated with Indium and cyclohexane standards, scanning from –100 °C up to +100 °C with heating rates of 20 K/min and cooling rates of 60 K/min in N_2 atmosphere for polyisoprenes and in He atmosphere for polybutadienes using separate calibrations. Homoleptic aluminate complexes $[Y(AlMe_4)_3]$ and $[Lu(AlMe_4)_3]$, the half-sandwich complexes $[Cp^*Y(AlMe_4)_2]$ and the trimeric methyl complex $[Cp^*YMe_2]_3$ (**1^Y**) were prepared according to literature methods.[1-7] $[Cp^*Lu(AlMe_4)_2]$ was prepared following a new synthesis route, vide infra (Section 1.2).

1.2 Synthesis of $[(C_5Me_5)Lu(AlMe_4)_2]$

Complex $[Lu(AlMe_4)_3]$ (131 mg, 0.30 mmol) was dissolved in deuterated benzene (2 mL), 1,2,3,4,5-pentamethycyclopentadiene (45 mg, 0.33 mmol) was added and the reaction mixture was stirred overnight at 60 °C. After evaporation of the solvent, complex $[Cp^*Lu(AlMe_4)_2]$ was crystallized from *n*-hexane at –35 °C (136 mg, 0.28 mmol, 94 %). ^{1}H NMR (400 MHz, C_6D_6, 25 °C): δ = 1.76 (s, 15 H, CpCH_3), –0.17 (s, 24 H, AlCH_3). ^{13}C NMR (100 MHz, C_6D_6, 25 °C): δ = 120.7 ($C_5(CH_3)_5$), 11.6 (Cp(CH_3)$_5$), 1.1 (Al(CH_3)$_4$). Elemental analysis calculated (%) for $C_{18}H_{39}Al_2Lu$ (484.43): C 44.63, H 8.11; found: C 44.32, H 8.47.

1.3 Synthesis of $[(C_5Me_5)Lu(\mu\text{-}Me)_2]_3$ (**1^{Lu}**)

Following the procedure published previously,[6,7] $[Cp^*Lu(AlMe_4)_2]$ (484 mg, 1.00 mmol) was dissolved in *n*-hexane (5 mL) and diethyl ether (148 mg, 2.00 mmol) was added under vigorous stirring. The white precipitate was separated via centrifugation and washed three times with *n*-hexane. Drying in vacuo yielded **1^{Lu}** (315 mg, 93 %) as a white powder. Single crystals were obtained by recrystallization from a hot (60 °C) benzene solution at ambient temperature. ^{1}H NMR (400 MHz, C_6D_6, 25 °C): δ = 2.00 (s, 45 H, CH_3Cp), 0.05 (s, 18 H, LuCH_3). ^{13}C NMR (100 MHz, C_6D_6, 25 °C): δ = 117.4 ($C_5(CH_3)_4$), 36.1 (CH_3), 11.5 (Cp(CH_3)$_5$). IR (cm^{-1}): 3016 m, 2989 m, 2974 m,

2921 s, 2821 m, 2735 w, 1477 m, 1462 m, 1439 m, 1384 w, 1301 w, 1256 w, 1223 m, 1201 m, 1185 s, 1142 w, 1064 w, 1047 w, 1015 w, 964 m. 858 m, 808 w, 703 s, 665 m, 573 m; elemental analysis calcd (%) for $C_{36}H_{63}Lu_3$ (1020.78): C 42.36, H 6.22; found: C 42.81, H 6.57.

1.4 Synthesis of the degradation product $[(Cp^*Y)_2Me_2(N(Me)_2(C_6H_4)]_n[B(C_6F_5)_4]_n$ (2)

In a *J. Young* NMR tube, 5.0 mg (0.007 mmol, 0.020 mmol of yttrium centers) of complex **1^Y** and 16.0 mg (1 equiv. per yttrium center, 0.02 mmol) of $[PhNMe_2H][B(C_6F_5)_4]$ (**B**) were dissolved in 400 µL of toluene-d_8. After 24 h, the dimeric degradation product **2** crystallized in lightly teal colored blocks, suitable for X-ray crystallography.

1.5 Synthesis of $(Cp^*Y)_3Me_4(CH_2)(thf)_2$ (3)

Route A: Complex **1^Y** (40 mg, 0.053 mmol) was dissolved in 10 mL of THF. Instant gas formation was observed. The clear solution was layered with toluene and stored at -35 °C. Single crystals suitable for X-ray diffraction analysis could be obtained after two days.

Route B: The synthesis described in Route A was performed in a *J. Young* NMR tube applying 5 mg (0.007 mmol) of **1^Y** and 400 µL of precooled (-35 °C) THF. After allowing the solution to warm to ambient temperature, single crystals suitable for X-ray diffraction could be obtained after one day. ^{1}H NMR (400 MHz, C_6D_6, 25 °C): δ = 3.58 (br, 4 H, THF), 1.92 (s, 45 H,CH_3Cp), 1.73 (br, 4 H, THF), –0.31 (q, 2 H, µ$_3$-CH_2), –0.53 (vbr, 3 H, µ$_3$-CH_3). –0.89 (br, 9 H, µ$_2$-CH_3). ^{13}C NMR (100 MHz, C_6D_6, 25 °C): δ = 120.0 (µ$_3$-CH_3), 113.0 (C_5Me_5), 95.6 (µ$_3$-CH_2), 64.5 (THF), 24.7 (µ$_2$-CH_3), 22.5 (THF), 9.3 (Cp(CH_3)$_5$). IR (cm^{-1}): 2958 s, 2896 s, 2855 s, 2754 m, 2722 m, 2241 m, 2184 w, 2160 w, 2138 w, 2125 w, 2105 w, 2088 w, 1492 w, 1440 m, 1374 m, 1249 w, 1176 m, 1110 m, 1059 w, 1006 s, 994 s, 961 w, 824 s, 748 s, 590 m, 548 m, 512 m; elemental analysis calcd (%) for $C_{43}H_{75}O_2Y_3$ (890.77): C 57.98, H 8.49; calcd (%) for **3**–$(THF)_2$, $C_{35}H_{59}Y_3$ (746.56): C 56.31, H 7.97; found: C 56.37, H 7.74.

1.6 Synthesis of the thermolytic product $[Cp^*_6Y_6Me_4(CH_2)_4]$ (4)

In a *J. Young* NMR tube, 40 mg (0.053 mmol) of complex **1^Y** were dissolved in 1 mL of C_6D_6 and heated to 60 °C overnight. The tube was allowed to cool to ambient temperature with the surrounding oil bath. During the cooling, crystals suitable for X-ray crystallography formed, that were immediately transferred to the X-ray diffractometer.

1.7 Homopolymerization of butadiene

A detailed polymerization procedure is described as a typical example (Table 1/run 1). $[Ph_3C][B(C_6F_5)_4]$ (**A**) (18 mg, 0.02 mmol, 3 equivs per trimer) was added to a solution of **1^Y** (5.0 mg, 0.007 mmol, 0.020 mmol of yttrium centers) in toluene (28 mL) and the mixture was aged at ambient temperature for 30 min. The mixture was poured into a 50 ml Büchi miniclave and 1440 mLn (20 mmol) of 1,3-butadiene were added at 90 mLn / min under stirring at 100 rpm. The polymerization was carried out at 25 °C for 1 h. After release of the remaining monomer pressure, if any, the reaction was terminated by pouring the polymerization mixture into 200 mL of methanol containing 0.1 % (w/w) 2,6-di-*tert*-butyl-4-methylphenol as a stabilizer and stirred for 1 h at ambient temperature. The polymer was washed with methanol and dried under vacuum at ambient temperature to constant weight.

1.8 Homopolymerization of isoprene

A detailed polymerization procedure is described as a typical example (Table 1/run 6). $[Ph_3C][B(C_6F_5)_4]$ (**A**) (18 mg, 0.02 mmol, 3 equiv per trimer) was added to a solution of **1^Y** (5.0 mg, 0.007 mmol, 0.020 mmol of yttrium centers) in toluene (8 mL) and the mixture was aged at ambient temperature for 30 min. After the addition of isoprene (1.36 g, 20 mmol), the polymerization was carried out at 25 °C for 1 h. The reaction was terminated by pouring the polymerization mixture into 25 mL of methanol containing 0.1% (w/w) 2,6-di-*tert*-butyl-4-methylphenol as a stabilizer and stirred for 1 h at ambient temperature. The polymer was washed with methanol and dried under vacuum at ambient temperature to constant weight.

1.9 Homopolymerization of styrene

A detailed polymerization procedure is described as a typical example (Table S13/run S62). $[PhNMe_2H][B(C_6F_5)_4]$ (**B**) (16 mg, 0.02 mmol, 3 equiv per trimer) was added to a solution of **1^Y** (5.0 mg, 0.007 mmol, 0.020 mmol of yttrium centers) in toluene (8 mL) and the mixture was aged at ambient temperature for 30 min. After the addition of styrene (2.08 g, 20 mmol), the polymerization was

carried out at 25 °C for 14 h. The reaction was terminated by pouring the polymerization mixture into 25 mL of methanol/water (v/v: 1/1) containing 0.1% (w/w) 2,6-di-*tert*-butyl-4-methylphenol as a stabilizer and stirred for 1 h at ambient temperature. The polymer was washed with methanol and dried under vacuum at ambient temperature to constant weight.

1.10 Copolymerization of liquid monomers

The polymerization reactions were carried out in analogy to the homopolymerization reactions with the only difference, that a 1/1 (n/n) mixture of 10 mmol of each of the monomers was added.

1.11 Copolymerization of ethylene and styrene

A 300 mL Parr Autoclave was evacuated and filled with 100 mL of toluene. 1000 mLn of ethylene (40 mmol) were added and the solution was stirred for 1 h. Styrene (6.240 g, 60 mmol) was dissolved in 20 mL of toluene und added to the autoclave applying an overpressure of the monomer gas and therefore adding another 250 mLn of ethylene (10 mmol) at 150 mLn / min. $[PhNMe_2H][B(C_6F_5)_4]$ (**B**) (16 mg, 0.02 mmol, 3 equiv per trimer) was added to a solution of $\mathbf{1}^{Y}$ (5 mg, 0.007 mmol, 0.020 mmol of yttrium centers) in toluene (25 mL) and the mixture was aged at ambient temperature for 30 min. The solution was then poured into the autoclave applying an overpressure of the monomer gas and therefore adding another 250 mLn of ethylene (10 mmol) at 150 mLn / min under stirring at 50 rpm. The polymerization was carried out at 25 °C for 1 h. After release of the monomer pressure, the reaction was terminated by pouring the polymerization mixture into 200 mL of methanol/water (v/v: 1/1) containing 0.1% (w/w) 2,6-di-*tert*-butyl-4-methylphenol as a stabilizer and stirred for 1 h at ambient temperature. The polymer was washed with methanol and dried under vacuum at ambient temperature to constant weight.

1.12 Polymerization and copolymerization involving 4-vinyl cyclo-1-hexene

Attempts to copolymerize 4-vinyl cyclo-1-hexene, the auto-Diels-Alder product of 1,3-butadiene, with isoprene or 1,3-butadiene did not yield any polymer within 24 h of reaction time. Reports describing the slight catalyst poisoning effect of this reactant[8] are therefore considered being confirmed. After 41 h homopolyisoprene was found as product revealing no effect of the comonomer on the microstructure of the polyisoprene.

1.13 Swelling experiments of crosslinked polymers

In order to determine data quantifying the crosslinkage of some of the obtained polymers, swelling experiments were performed. The theoretical background of these experiments can be found in Section 3.2.1. Ca. 40 mg (ca. 30 µl) of the respective polymer was exactly weighted, the volume determined, and placed into ca. 600 µl of a 69.5/30.5 (w/w) mixture of *n*-propanol and *n*-heptane. The materials were allowed to swell at ϑ-temperature for 6 h. Then, after removal of the solvent, the swollen samples were weighted again and their volume was once more determined.

1.14 NMR-spectroscopic investigations of the catalytically active species

Both $\mathbf{1}^{Y}$ (5.0 mg, 0.007 mmol, 0.020 mmol of yttrium centers) and the respective cocatalyst (6 mg, 3.7 µmol per equivalent of **A** and 5.3 mg, 3.7 µmol per equivalent of **B**) were weighted into a *J. Young* NMR tube and dissolved in 400 µl of the respective solvent (*e.g.*, toluene-d_8). The sample was taken to the spectrometer and measured immediately or after the intended prereaction time.

1.15 ^{1}H DOSY-NMR-spectroscopic investigations of the catalytically active species

^{1}H DOSY-NMR-spectroscopic analysis of the catalytically active species was performed by preparing the respective catalyst-cocatalyst-system in toluene-d_8 in analogy to the experiments described in section 1.14. In order to ensure that the whole sample fitted into the gradient coil, the applied amount of solvent was reduced to 200 µl. After the addition of the solvent, t_1, the decay of the magnetization of the complex was measured to adjust δ, the duration of the gradient pulses for the DOSY experiments. The actual DOSY experiment was performed with a gradient strength of 4.99 G mm^{-1} (determined by a standard measurement of 1% H_2O in D_2O mixture, $D = 1.91 \cdot 10^{-9}$ m^{2}s^{-1}) and a separation between the pulses 0.1 s (Δ). To achieve a sufficient signal / noise ratio, 16 scans were averaged.

SUPPORTING INFORMATION

1.16 Crosslinking experiments with polyisoprene

A sample of polyisoprene (256 mg) (*cis*% / *trans*% / 3,4% = 32.1 / 13.3 / 54.6) was precleaned from any possibly remaining methanol (see Section 1.8, quenching process) by dissolving it in $CHCl_3$ and evaporating the solvent. The sample was transferred into a glovebox with Ar atmosphere and dissolved in 16 mL of toluene. The solution was spread in 7 vials (2 mL of the solution each) and the respective 7 sample solutions were treated with different amounts of $[Ph_3C][B(C_6F_5)_4]$ (**A**), $[Cp^*YMe_2]_3$ (**1**$^{\mathbf{Y}}$), and isoprene monomer after a pre-reaction time of 5 min. A detailed overview on the applied amounts can be found in Section 3.2.2, details on the products can be found in Table S13.

1.17 Crystallography

Crystals of **1**$^{\mathbf{Lu}}$, **2**, **3**, and **4** suitable for X-ray crystallography were grown by standard techniques from solutions described in the respective synthesis protocol (see sections 1.3 – 1.6). Single crystals were selected, coated with Parabar 10312 (previously known as Paratone N) and fixed on a microloop. Data were collected on a Bruker APEX DUO instrument equipped with an IμS microfocus sealed tube and QUAZAR optics for MoK_α radiation (λ = 0.71073 Å). The data collection strategy was determined using COSMO[9] employing ω- and ϕ scans. Raw data were processed using APEX[10] and SAINT,[11] corrections for absorption effects were applied using SADABS.[12] The structures were solved by direct methods and refined against all data by full-matrix least-squares methods on F^2 using SHELXTL[13] and SHELXLE.[14] All graphics were produced employing ORTEP-3 and POV-Ray.[15] Further details of the refinement and crystallographic data are listed in Table S6.

WILEY-VCH

SUPPORTING INFORMATION

2. Crystal Structures

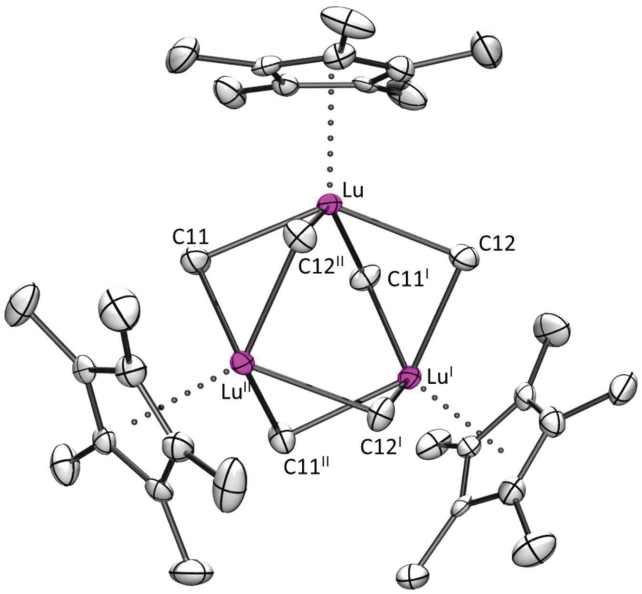

Figure S1. ORTEP view of the molecular structure of $[Cp^*LuMe_2]_3$ ($\mathbf{1}^{Lu}$). Atomic displacement parameters are set at the 50% probability level. Hydrogen atoms are omitted for clarity.

Table S1. Selected bond lengths (Å) and angles (°) for $\mathbf{1}^{Lu}$

Lu–C(Cp)	2.581(16)-2.662(17)	Lu---Ct[1]	2.338		
Lu–C11	2.49(2)	Lu–C12	2.53 (3)		
Lu–C11^{I}	2.45(2)	Lu–C12^{II}	2.51(2)		
C11-Lu-C12	135.5(5)	C11-Lu-C12^{II}	80.0(3)	C12-Lu-C12^{II}	78.6(12)
C11-Lu-C11^{I}	87.8(11)	C12-Lu-C11^{I}	80.4(3)	C11^{I}-Lu-C12^{II}	135.8(6)

Symmetry operations: I = -y, x-y, z; II= -x+y, -x, z

[1] Ct represents the centroid of the Cp* ligand at the Y atom.

SUPPORTING INFORMATION

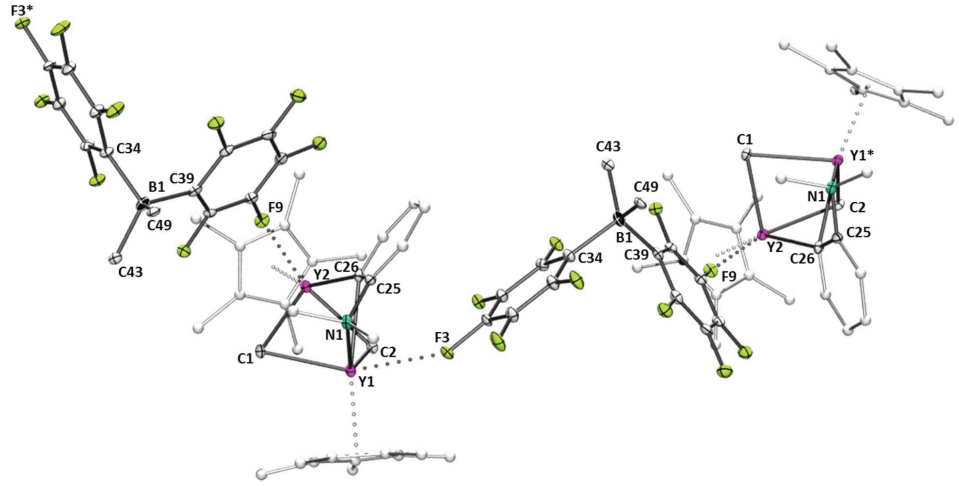

Figure S2. ORTEP view of two asymmetric units of the molecular structure of the degradation structure of system 1^{Y}/**B** (**2**). Atomic displacement parameters are set at the 50% probability level. Hydrogen atoms and Ar^{F} rings at carbon atoms C43 and C49 as well as twelve toluene molecules (six per asymmetric unit) are omitted for clarity. Cp* ligands and parts of the dimethylaniniline ligand are shown in ball and stick model to allow focus on the intermolecular polymeric connection of the yttrium and fluorine atoms (Y1---F3 and Y2---F9). As the structure is polymeric, the chain continues at the atoms labeled with an asterisk (*) bonding the respective Y1 or F3 of the proximate asymmetric unit.

Table S2. Selected bond lengths (Å) and angles (°) for **2**

Y1–C(Cp1)	2.578(6)-2.666(7)	Y2–C(Cp2)	2.616(6)-2.681(6)	B1-C34	1.675(10)
Y1---Ct_1[2]	2.355	Y2---Ct_2[3]	2.319	B1–C39	1.661(10)
Y1–C1	2.578(6)	Y2–C1	2.474(6)	B1–C43	1.649(11)
Y1–C2	2.540(6)	Y2–C2	2.519(6)	B1–C49	1.643(10)
Y1–C26	2.579(7)	Y2–C26	2.463(6)	C34-B1-C39	101.3(5)
Y1---F3	2.673(4)	Y2---F9	2.569(3)	C34-B1-C43	113.6(6)
Y1-N1	2.513(5)			C34-B1-C49	111.5(5)
C1-Y1-C2	86.63(18)	C1-Y2-C2	89.3(2)	C39-B1-C43	113.9(6)
C1-Y1-C26	84.0(2)	C1-Y2-C26	88.6(2)	C39-B1-C49	114.2(6)
C2-Y1-C26	76.77(19)	C2-Y2-C26	79.3(2)	C43-B1-C49	102.8(6)
C1-Y1-F3	157.24(17)	C1-Y2-F9	89.46(17)	C34---$Ar^{NMe}{}_{2\ cent}$	3.194
C2-Y1-F3	82.97(16)	C2-Y2-F9	154.44(17)	Interplanar Angle Ar^{F}(C34) -Ar^{NMe}	15.7[3]
C26-Y1-F3	74.00(16)	C26-Y2-F9	75.14(16)		
C1-Y1-N1	93.94(18)	C26-Y1-N1	56.58(18)		
C2-Y1-N1	132.94(19)	F3-Y1-N1	78.75(14)		

[2] Ct_x represents the centroid of the Cp* ligand at Yx.
[3] The determination of this angle is described in the next section.

SUPPORTING INFORMATION

Determination of the interplanar angle in the crystal structure of 2

The cif-file of the crystal structure of **2** gives the coordinates of the atoms of the respective aromatic rings in a.u. For the calculation of the equations of the two planes, three non-neighboring carbon atoms were chosen (given in Table S4) for each plane.

Table S3. Selected carbon atom coordinate sets for determining the interplanar angle

Carbon	x	y	z
C35 (ArF)	0.2911	0.7024	1.2386
C33 (ArF)	0.3913	0.7314	1.1777
C31 (ArF)	0.3143	0.6517	1.1388
C26 ($ArNMe_2$)	0.2274	0.6807	0.9696
C30 ($ArNMe_2$)	0.1549	0.7143	1.0614
C28 ($ArNMe_2$)	0.2534	0.7759	1.0245

These values lead to the equations of the planes:

$$E_{ArF}: \vec{x} = \begin{pmatrix} 0.2911 \\ 0.7024 \\ 1.2386 \end{pmatrix} + S_{ArF} \begin{pmatrix} 0.1002 \\ 0.0290 \\ -0.0609 \end{pmatrix} + T_{ArF} \begin{pmatrix} 0.0232 \\ -0.0507 \\ 0.0998 \end{pmatrix}$$

$$E_{ArNMe_2}: \vec{x} = \begin{pmatrix} 0.2274 \\ 0.6807 \\ 0.9696 \end{pmatrix} + S_{ArNMe_2} \begin{pmatrix} -0.0725 \\ 0.0336 \\ -0.0918 \end{pmatrix} + T_{ArNMe_2} \begin{pmatrix} 0.0260 \\ 0.0952 \\ 0.0549 \end{pmatrix}$$

For both these planes, the normal vectors are calculated as

$$\overrightarrow{n_{ArF}} = \begin{pmatrix} 0.1002 \\ 0.0290 \\ -0.0609 \end{pmatrix} \times \begin{pmatrix} 0.0232 \\ -0.0507 \\ 0.0998 \end{pmatrix} = \begin{pmatrix} -0.0060 \\ 0.0086 \\ -0.0058 \end{pmatrix} \text{ and } \overrightarrow{n_{ArNMe_2}} = \begin{pmatrix} -0.0725 \\ 0.0336 \\ -0.0918 \end{pmatrix} \times \begin{pmatrix} 0.0260 \\ 0.0952 \\ 0.0549 \end{pmatrix} = \begin{pmatrix} -0.0069 \\ 0.0064 \\ -0.078 \end{pmatrix}$$

The angle between the planes is the angle between their normal vectors, which is obtained by

$$cos\alpha = \frac{|\overrightarrow{n_{ArF}} \bullet \overrightarrow{n_{ArNMe_2}}|}{|\overrightarrow{n_{ArF}}| \bullet |\overrightarrow{n_{ArNMe_2}}|}$$

$$\underline{\alpha = 15.7°}$$

SUPPORTING INFORMATION

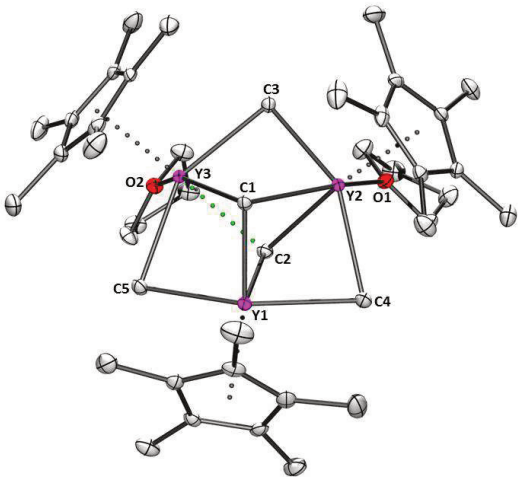

Figure S3. ORTEP view of the molecular structure of $[(Cp^*Y)_3Me_4(CH_2)(thf)_2]$ (**3**). Atomic displacement parameters are set at the 50% probability level. Hydrogen atoms are omitted for clarity. C1 marks the methylene, C2 marks the capping methyl carbon / moiety. The asymmetry of the methyl cap is highlighted by the green bond.

Table S4. Selected bond lengths (Å) and angles (°) for **3**

Y1–C(Cp1)	2.703(3)-2.711(3)	Y2–C(Cp2)	2.678(3)-2.710(3)	Y3–C(Cp3)	2.697(3)-2.719(3)
Y1---Ct_1[4]	2.422	Y2---Ct_2[2]	2.413	Y3---Ct_3[2]	2.423
Y1–C1	2.283(4)	Y2–C1	2.477(3)	Y3–C1	2.446(3)
Y1–C2	2.597(4)	Y2–C2	2.744(4)	Y3–C2	2.777(4)
Y1–C4	2.591(4)	Y2–C3	2.550(4)	Y3–C3	2.575(4)
Y1–C5	2.548(4)	Y2–C4	2.562(4)	Y3–C5	2.561(4)
		Y2–O1	2.629(2)	Y3–O2	2.567(2)
C4-Y1-C5	144.11(12)	C3-Y2-C4	146.60(12)	C3-Y3-C5	147.65(11)
Ct1-Y1-C1	122.93	Ct2-Y2-C1	109.18	Ct3-Y3-C1	108.11
Ct1-Y1-C2	151.90	Ct2-Y2-C2	172.43	Ct3-Y3-C2	171.85
C1-Y1-C2	85.15(13)	C1-Y2-C2	78.51(12)	C1-Y3-C2	78.35(12)

[4] Ct_x represents the centroid of the Cp* ligand at Yx.

SUPPORTING INFORMATION

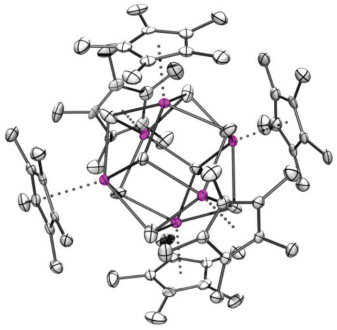

Figure S4a. ORTEP view of the thermolytic product $[Cp^*_6Y_6Me_4(CH_2)_4]$ (**4**) of $\mathbf{1}^Y$ at 60 °C. Atomic displacement parameters are set at the 50% probability level. Hydrogen atoms as well as one C_6D_6 molecule are omitted for clarity.

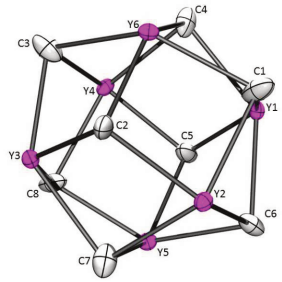

Figure S4b. ORTEP view of the core bonding situation in $[Cp^*_6Y_6Me_4(CH_2)_4]$ (**4**). Atomic displacement parameters are set at the 50% probability level. The distorted octahedral arrangement of the Y atoms is clearly visible. Each face is capped by a Me or CH_2 moiety, which are located randomly across the complex and can therefore not be individually localized. This also excludes any localization of the respective H atoms.

Table S5. Selected lengths (Å) and angles (°) for **4**

Y1---Ct_1[5]	2.394	Y2---Ct_2[5]	2.394	Y3---Ct_3[5]	2.393
Y1–C(Cp1)	2.670(8)-2.687(9)	Y2-C(Cp2)	2.672(8)-2.687(9)	Y3–C(Cp3)	2.657(8)-2.700(8)
Y4---Ct_4[5]	2.385	Y5---Ct_5[5]	2.399	Y6---Ct_6[5]	2.391
Y4–C(Cp4)	2.647(9)-2.698(9)	Y5–C(Cp5)	2.666(9)-2.699(8)	Y6–C(Cp6)	2.661(9)-2.694(9)
Y1–C1	2.520(10)	Y2–C1	2.536(9)	Y3–C2	2.524(9)
Y1–C4	2.490(9)	Y2–C2	2.541(9)	Y3–C3	2.479(10)
Y1–C5	2.536(10)	Y2–C6	2.515(9)	Y3–C7	2.610(10)
Y1–C6	2.590(9)	Y2–C7	2.522(9)	Y3–C8	2.461(10)
Y4–C3	2.597(10)	Y5–C5	2.613(10)	Y6–C1	2.510(10)
Y4–C4	2.545(9)	Y5–C6	2.524(9)	Y6–C2	2.470(10)
Y4–C5	2.487(10)	Y5–C7	2.514(10)	Y6–C3	2.540(10)
Y4–C8	2.526(9)	Y5–C8	2.511(10)	Y6–C4	2.573(10)
Y1-C1-Y2	94.3(3)	Y2-C2-Y3	98.0(3)	Y3-C3-Y4	91.3(4)
Y1-C1-Y6	94.2(4)	Y2-C2-Y6	93.1(3)	Y3-C3-Y6	92.1(3)
Y2-C1-Y6	92.3(3)	Y3-C2-Y6	92.8(8)	Y4-C3-Y6	95.5(3)
Y1-C4-Y4	91.5(3)	Y1-C5-Y4	91.8(3)	Y1-C6-Y2	93.1(3)
Y1-C4-Y6	93.3(3)	Y1-C5-Y5	94.9(4)	Y1-C6-Y5	95.8(3)
Y4-C4-Y6	96.0(3)	Y4-C5-Y5	92.9(3)	Y2-C6-Y5	91.4(3)
Y2-C7-Y3	96.2(3)	Y3-C8-Y4	93.5(3)		
Y2-C7-Y5	91.5(3)	Y3-C8-Y5	96.0(4)		
Y3-C7-Y5	92.3(3)	Y4-C8-Y5	94.5(3)		

[5] Ct_x represents the centroid of the Cp* ligand at Yx

SUPPORTING INFORMATION

Table S6. Crystal data and structure refinement for **1**^{Lu}, **2**, **3**, and **4**

	1^{Lu}	**2**	**3**	**4**
CCDC Deposition	1898848	1898851	1898850	1898849
Empirical formula	$C_{36}H_{63}Lu_3$	$C_{89}H_{86}BF_{20}NY_2$	$C_{43}H_{75}O_2Y_3$	$C_{74}H_{110}D_6Y_6$
Mw [g mol^{-1}]	1020.77	1738.21	890.76	1545.16
T[K]	173(2)	100(2)	100(2)	100(2)
Wavelength	0.71073 Å	0.71073 Å	0.71073 Å	0.71073 Å
Crystal system	hexagonal	monoclinic	orthorhombic	monoclinic
Space group	P 6_3	P 2_1/n	$P2_12_12_1$	P 2_1/c
a [Å]	12.1276(4)	17.7474(10)	12.8500(14)	17.865(4)
b [Å]	12.1276(4)	22.7380(12)	14.4065(16)	14.024(3)
c [Å]	14.6663(5)	19.9936(10)	22.935(2)	27.858(6)
α [°]	90	90	90	90
β [°]	90	94.8810(10)	90	91.647(3)
γ [°]	120	90	90	90
Volume [Å^3]	1868.10(14)	8039.0(7)	4245.8(8)	6977(3)
Z	2	4	4	4
Density (calculated) [mg mm^{-3}]	1.815	1.436	1.394	1.471
Absorption coefficient μ [mm^{-1}]	7.885	1.529	4.099	4.972
Theta range	1.94 to 30.54°	1.459 to 27.16°	1.669 to 30.98°	1.46 to 25.147°
Reflections collected	18215	46447	58942	46875
Independent reflections	3448 [$R_{(int)}$ = 0.0357]	15053 [$R_{(int)}$ = 0.0830]	13434 [$R_{(int)}$ = 0.0646]	12396 [$R_{(int)}$ = 0.1188]
Data / restraints / parameters	3448 / 745 / 239	15053 / 255 / 1106	13434 / 0 / 493	12396 / 1404 / 754
R_1(obs)[a]	0.0236	0.0739	0.0354	0.0731
wR_2(all)[b]	0.0497	0.1885	0.0606	0.1597

[a] Final R indices [I > 2σ (I)]; [b] R indices (all data).

SUPPORTING INFORMATION

3. Polymer Data

3.1 Additional observations made and conclusions drawn from the polymerization reactions

- In case of $\mathbf{1}^{Y}$/**A**, the formation of the active species is presumed to be less precise at ambient temperature than with $\mathbf{1}^{Y}$/**B** as broader MWDs are obtained in isoprene polymerization (Table 1).
- $\mathbf{1}^{Y}$/**A** initiates almost one chain per metal center with isoprene, which does neither apply for the butadiene polymerization with $\mathbf{1}^{Y}$/**A**, nor for any polymerization applying $\mathbf{1}^{Y}$/**B** (Table 1).
- lutetium precatalyst $\mathbf{1}^{Lu}$ seems better suited for butadiene polymerization than $\mathbf{1}^{Y}$ as the yields are almost quantitative and the molecular weight averages are much smaller. Statistically only one out of eight lutetium centers grows a polymer chain with cocatalyst **B**, compared to one out of fourteen with $\mathbf{1}^{Y}$/**B**. In case of the bulkier isoprene, this ratio points in the opposite direction instead, although, it is much more cocatalyst dependent for $\mathbf{1}^{Y}$. Ratios of chains per Ln center for the polymerization of isoprene: $\mathbf{1}^{Y}$/**A**: 1:1.3, $\mathbf{1}^{Y}$/**B**: 1:2.3, $\mathbf{1}^{Lu}$/**A** = $\mathbf{1}^{Lu}$/**B**: 1:4 (Table 1).
- applying system $\mathbf{1}^{Y}$/**B** at lower temperatures in isoprene polymerization (Table S8/runs S18-S20 Supporting Information) did not yield any polymer. Considering run S20 in Table S8, where both initiation and chain propagation reactions have successfully been performed under such thermal conditions, it seems likely that the prereaction of $\mathbf{1}^{Y}$ with **B** is hampered at temperatures below 20 °C. Prereaction of $\mathbf{1}^{Y}$ with **B** at ambient temperature followed by polymerization reaction at -20 °C yielded polymer (Table S8/run S21).
- considering the polyisoprene data (Table S7/runs S3 and S7), the respective active species are apparently not affected by a twofold amount of cocatalyst per Ln center, while a significant gain in PDI is observed with the full equivalent of **B** and a slight shift in the microstructure is found for the addition of a full equivalent of **A** per metal center.
- isoprene polymerization reactions were also performed at reaction times, when the composition of the mixture had significantly altered (Table S11/runs S42 (**A**) and S49 – S51 (**B**)). Crosslinking dominates the polymer formed by degraded $\mathbf{1}^{Y}$/**A** while with cocatalyst **B**, the degradation products are inactive in polymerization catalysis. The addition of 2 equivalents of cocatalyst per Y atom resulted in further augmented active species. While for both cocatalysts shifts of the microstructure toward *cis*-1,4-addition were observed, the high cocatalyst concentrations provoke side reactions. For cocatalyst **A** (Table S7/run S4), another crosslinked polymer was obtained. In case of cocatalyst **B** (Table S7/run S8), the amount of active Y centers is much lower, compared to the equimolar addition of cocatalyst (per Y atom).

- polymerization of isoprene in *n*-hexane (Table S9) results in lower yields than in toluene, if any, due to the low solubility of $\mathbf{1}^{Y}$ and $\mathbf{1}^{Lu}$ in this solvent.

- $\mathbf{1}^{Y}$ has been tested in the polymerization of styrene, where only traces of syndiotactic polystyrene could be obtained after 1 h at ambient temperature. Full conversion was observed after a reaction time of 14 h, and 29% are found after 1 h at 40 °C (Table S13).

- copolymerization reactions with ethylene yielded 4 % within 1 h, while a homopolymerization of ethylene resulted in 89 % conversion. Further copolymerizations, e.g. of styrene, 1-hexene and isoprene can be found in Table S13.

SUPPORTING INFORMATION

Additional polymer tables

Table S7. Selected examples of isoprene homopolymerization, applying $[Cp^*LnMe_2]_3$ as precatalysts and studying cocatalyst concentration

run[a]	precatalyst	cocatalyst[b]	yield (%)	*cis*-1,4[c]	*trans*-1,4[c]	3,4[c]	M_n[d] (x 10^4)	M_w/M_n[d]	T_g[e]
6	$[Cp^*YMe_2]_3$ (**1^Y**)	**A**	>99	50.8	17.5	31.7	8.4	2.33	-47.3
S1	$[Cp^*YMe_2]_3$ (**1^Y**)	**1/3A**	none	-[f]	-[f]	-[f]	-[f]	-[f]	-[f]
S2	$[Cp^*YMe_2]_3$ (**1^Y**)	**1/2A**	96	40.5	14.7	44.8	8.3	2.63	-22.9
S3	$[Cp^*YMe_2]_3$ (**1^Y**)	**2/3A**	94	40.9	15.0	44.1	9.8	2.51	-25.0
S4	$[Cp^*YMe_2]_3$ (**1^Y**)	**2A**	94	66.2	29.3	4.5	-[x]	-[x]	-30.9
7	$[Cp^*YMe_2]_3$ (**1^Y**)	**B**	90	35.8	10.8	53.4	14.1	1.16	-27.1
S5	$[Cp^*YMe_2]_3$ (**1^Y**)	**1/3B**	none	-[f]	-[f]	-[f]	-[f]	-[f]	-[f]
S6	$[Cp^*YMe_2]_3$ (**1^Y**)	**1/2B**	95	39.5	10.2	50.3	19.0	1.87	-23.0
S7	$[Cp^*YMe_2]_3$ (**1^Y**)	**2/3B**	97	35.6	13.4	51.0	15.5	2.11	-23.0
S8	$[Cp^*YMe_2]_3$ (**1^Y**)	**2B**	67	49.6	0.0	50.4	30.5	1.80	-26.7
13	$[Cp^*LuMe_2]_3$ (**1^{Lu}**)	**A**	>99	21.5	20.5	58.0	26.8	2.00	-15.5
S9	$[Cp^*LuMe_2]_3$ (**1^{Lu}**)	**1/3A**	traces[f]	-[f]	-[f]	-[f]	-[f]	-[f]	-[f]
S10	$[Cp^*LuMe_2]_3$ (**1^{Lu}**)	**1/2A**	49	24.4	17.6	57.9	10.5	1.59	-3.1
S11	$[Cp^*LuMe_2]_3$ (**1^{Lu}**)	**2/3A**	>99	23.4	11.4	65.2	17.1	1.62	-17.2
14	$[Cp^*LuMe_2]_3$ (**1^{Lu}**)	**B**	>99	21.4	21.5	57.1	29.2	1.38	-16.8
S12	$[Cp^*LuMe_2]_3$ (**1^{Lu}**)	**1/3B**	traces[f]	-[f]	-[f]	-[f]	-[f]	-[f]	-[f]
S13	$[Cp^*LuMe_2]_3$ (**1^{Lu}**)	**1/2B**	29	22.9	8.7	68.4	5.6	2.80	-6.4
S14	$[Cp^*LuMe_2]_3$ (**1^{Lu}**)	**2/3B**	95	23.6	19.8	56.5	12.5	1.65	-15.2

[a]Conditions: 0.007 mmol precatalyst (0.020 mmol of Ln centers), 8 mL toluene, 20 mmol isoprene, 25 °C. [b]Cocatalyst: **A** = $[Ph_3C][B(C_6F_5)_4]$, **B** = $[PhNMe_2H][B(C_6F_5)_4]$, equivalents given per Ln center; [c]Determined by ^1H and ^{13}C NMR spectroscopy in $CDCl_3$. [d]Determined by means of size-exclusion chromatography (SEC) against polystyrene standards. [e]Determined by a Perkin Elmer DSC 8000; heating rate: 20 K/min, cooling rate: 60 K/min [f]Not determined. [x]No SEC data available due to crosslinking. DLS Data: run S4: R_H= 20 nm, Flory-Rehner Data: N_{Gel} = 0.6 x 10^2, vide infra (Section 3.2.1) for details on the determination of N_{Gel} (distance between crosslinkages in numbers of monomer units).

SUPPORTING INFORMATION

Table S8. Selected examples of isoprene homopolymerization, applying $[Cp^*LnMe_2]_3$ as precatalysts and investigating the polymerization temperature as well as outlooking to a future study on donor addition

run[a]	precatalyst	cocatalyst[b]	Temp. (°C)	yield (%)	*cis*-1,4[c]	*trans*-1,4[c]	3,4[c]	M_n[d] (x 10^4)	M_w/M_n[d]	T_g[e]	N_{Gel}[l] (x 10^2)
6	$[Cp^*YMe_2]_3$ (**1^Y**)	**A**	25	>99	50.8	17.5	31.7	8.4	2.33	-47.3	-[k]
S15[m]	$[Cp^*YMe_2]_3$ (**1^Y**)	**A**	0	>99	76.8	15.9	7.3	-[x]	-[x]	-56.6	2.1
9[m]	$[Cp^*YMe_2]_3$ (**1^Y**)	**A**	-10	96	92.2	0.0	7.8	-[x]	-[x]	-56,2	1.2
S16[m]	$[Cp^*YMe_2]_3$ (**1^Y**)	**A**	-20	40	90.8	0.0	9.2	-[x]	-[x]	-57.9	3.4
S17[n]	$[Cp^*YMe_2]_3$ (**1^Y**)	**A**	-20	30	77.8	0.0	22.2	-[x]	-[x]	-57.4	1.0
7	$[Cp^*YMe_2]_3$ (**1^Y**)	**B**	25	90	35.8	10.8	53.4	14.1	1.16	-27.1	-[k]
S18[m]	$[Cp^*YMe_2]_3$ (**1^Y**)	**B**	0	none[f]	-[f]	-[f]	-[f]	-[f]	-[f]	-[f]	-[f]
S19[m]	$[Cp^*YMe_2]_3$ (**1^Y**)	**B**	-10	none[f]	-[f]	-[f]	-[f]	-[f]	-[f]	-[f]	-[f]
S20[m]	$[Cp^*YMe_2]_3$ (**1^Y**)	**B**	-20	none[f]	-[f]	-[f]	-[f]	-[f]	-[f]	-[f]	-[f]
S21[n]	$[Cp^*YMe_2]_3$ (**1^Y**)	**B**	-20	39	29.2	5.7	65.1	6.8[h]	1.05[h]	-15,8	-[k]
S22	$[Cp^*LuMe_2]_3$ (**1^{Lu}**)	**A**	40	>99	18.9	15.9	65.2	31.1	1.36	-12.6	-[k]
S23	$[Cp^*LuMe_2]_3$ (**1^{Lu}**)	**B**	40	>99	17.9	26.9	55.2	16.1	1.29	-8.9	-[k]

[a]Conditions: 0.007 mmol precatalyst (0.020 mmol of Ln centers), 8 mL toluene, 20 mmol isoprene, 1h. [b]Cocatalyst: **A** = $[Ph_3C][B(C_6F_5)_4]$, **B** = $[PhNMe_2H][B(C_6F_5)_4]$, equivalents given per Ln center. [c]Determined by ^1H and ^{13}C NMR spectroscopy in $CDCl_3$. [d]Determined by means of size-exclusion chromatography (SEC) against polystyrene standards. [e]Determined by DSC: heaing rate: 20 K/min, cooling rate: 60 K/min. [h]Multimodal MWD. [l] Vide infra (Section 3.2.1) for details on the determination of N_{Gel} (distance between crosslinkages in numbers of monomer units).[k]No swelling detectable. [l]Determined by DSC: heating rate: 10 K/min, cooling rate: 100 K/min. [m]Prereaction at polymerization temperature. [n]Prereaction at ambient temperature, polymerization at given temperature. [x] No SEC data available due to crosslinking.

Table S9. Isoprene polymerization applying $[Cp^*LnMe_2]_3$ as precatalysts in *n*-hexane

run[a]	precatalyst	cocatalyst[b]	yield (%)	*cis*-1,4[c]	*trans*-1,4[c]	3,4[c]	M_n[d] (x 10^4)	M_w/M_n[d]	T_g[e]
S24	$[Cp^*YMe_2]_3$ (**1^Y**)	**A**	51	48.0	5.1	46.9	18.6	2.20	-30.1
S25	$[Cp^*YMe_2]_3$ (**1^Y**)	**B**	traces[f]	9.3	52.3	38.4	-[f]	-[f]	-[f]
S26	$[Cp^*LuMe_2]_3$ (**1^{Lu}**)	**A**	none[f]	-[f]	-[f]	-[f]	-[f]	-[f]	-[f]
S27	$[Cp^*LuMe_2]_3$ (**1^{Lu}**)	**B**	none[f]	-[f]	-[f]	-[f]	-[f]	-[f]	-[f]

[a]Conditions: 0.007 mmol precatalyst (0.020 mmol of Ln centers), [Ln]/[cocat] = 1:1, 8 mL *n*-hexane, 20 mmol isoprene, 25 °C. [b]Cocatalyst: **A** = $[Ph_3C][B(C_6F_5)_4]$, **B** = $[PhNMe_2H][B(C_6F_5)_4]$, equivalents given per Ln center; [c]Determined by ^1H and ^{13}C NMR spectroscopy in $CDCl_3$. [d]Determined by means of size-exclusion chromatography (SEC) against polystyrene standards. [e]Determined by DSC. [f]No such evaluation possible, due to low yield.

SUPPORTING INFORMATION

Table S10. Isoprene Polymerization applying [Cp*YMe$_2$]$_3$ as a precatalyst, along with cocatalyst [PhNMe$_2$H][B(C$_6$F$_5$)$_4$] (**B**) and aluminium alkyls

run[a]	precatalyst[b]	activator /equivs	t (h)	yield (%)	*cis*-1,4[c]	*trans*-1,4[c]	3,4[c]	M_w/M_n[d]	M_n[d] (x 10^4)	T_g[e]
10	[Cp*YMe$_2$]$_3$ (**1^Y**)	AlMe$_3$/10	1	92	3.9	85.5	10.6	1.37	15.2	-61.8
S28	[Cp*YMe$_2$]$_3$ (**1^Y**)	AlMe$_3$/30[l]	1	34	1.7	89.0	9.3	1.23	11.5	-59.1
S29	[Cp*YMe$_2$]$_3$ (**1^Y**)	Al*i*Bu$_3$/10	1	86	31.6	13.5	55.0	1.25	4.0	-25.9
11	[Cp*YMe$_2$]$_3$ (**1^Y**)	Al*i*Bu$_3$/30	1	88	31.4	12.7	55.9	1.37	1.6	-23.3
S30	[Cp*YMe$_2$]$_3$ (**1^Y**)	Al*i*Bu$_2$H/10	1	none[f]	-[f]	-[f]	-[f]	-[f]	-[f]	-[f]
S31	[Cp*YMe$_2$]$_3$ (**1^Y**)	Al*i*Bu$_2$H/30	1	none[f]	-[f]	-[f]	-[f]	-[f]	-[f]	-[f]
S32	[Cp*YMe$_2$]$_3$ (**1^Y**)	Al*i*Bu$_2$H/10	24	88	27.7	22.2	50.1	1.62	0.4	-33.3
S33	[Cp*YMe$_2$]$_3$ (**1^Y**)	Al*i*Bu$_2$H/30	24	26	29.7	19.5	50.8	1.90[g]	0.6[g]	-32.7
S34	[Cp*Y(AlMe$_4$)$_2$]	AlMe$_3$/8	1	86	50.2	40.5	9.3	1.27	17.4	-64.1
S35[h]	[Cp*Y(AlMe$_4$)$_2$]	none/0	24	>99	43.5	28.7	27.8	1.59	6.0	n.d.

[a]Conditions: 0.02 mmol of Y centers in pre-catalysts, [Y]/[cocat] = 1:1, 8 mL toluene, 20 mmol isoprene, 25 °C. [b]Cocatalyst: **B** = [PhNMe$_2$H][B(C$_6$F$_5$)$_4$], equivalents given per Ln center; [c]Determined by ^{1}H and ^{13}C NMR spectroscopy in CDCl$_3$. [d]Determined by means of size-exclusion chromatography (SEC) against polystyrene standards. [e]Determined by DSC. [f]No such evaluation possible, due to low yield. [g]Multimodal MWD. [h]Reaction at 40 °C, taken from ref. 16. [l]Caution, reaction mixture detonated upon quenching due to high AlMe$_3$ concentration.

Table S11. Isoprene polymerization, applying [Cp*YMe$_2$]$_3$ as a precatalyst and varying the pre-reaction time (t_{Pre}) and cocatalyst concentration

run[a]	precatalyst	cocatalyst[b]	t_{Pre}	yield (%)	*cis*-1,4[c]	*trans*-1,4[c]	3,4[c]	M_n[d] (x 10^4)	M_w/M_n[d]	T_g[e]	N_{Ge}[h] (x 10^2)
S36	[Cp*YMe$_2$]$_3$ (**1^Y**)	**A**	0 min	none[f]	-[f]	-[f]	-[f]	-[f]	-[f]	-[f]	-[f]
S37	[Cp*YMe$_2$]$_3$ (**1^Y**)	**A**	1 min	98	71.2	0.0	28.8	11.2	3.72	-39.7	-[i]
S38	[Cp*YMe$_2$]$_3$ (**1^Y**)	**A**	5 min	87	59.4	6.8	33.7	13.3	2.53	-34.8	-[i]
S39	[Cp*YMe$_2$]$_3$ (**1^Y**)	**A**	10 min	88	41.9	13.5	44.6	15.0	1.84	-23.8	-[i]
S40	[Cp*YMe$_2$]$_3$ (**1^Y**)	**A**	20 min	91	49.2	8.6	42.2	24.6	2.08	-28.4	-[i]
S41	[Cp*YMe$_2$]$_3$ (**1^Y**)	**A**	45 min	96	46.9	8.9	44.2	-[x]	-[x]	-32.4	n.d.
S42	[Cp*YMe$_2$]$_3$ (**1^Y**)	**A**	5 h	92	33.9	15.3	50.8	2.1[y]	1.53[y]	-24.0	7.4
S43	[Cp*YMe$_2$]$_3$ (**1^Y**)	**B**	0 min	traces[f]	-[f]	-[f]	-[f]	-[f]	-[f]	-[f]	-[f]
S44	[Cp*YMe$_2$]$_3$ (**1^Y**)	**B**	1 min	79	40.0	11.6	48.4	7.2	1.80	-27.9	-[i]
S45	[Cp*YMe$_2$]$_3$ (**1^Y**)	**B**	5 min	89	31.3	16.3	52.4	9.3	1.28	-27.9	-[i]
S46	[Cp*YMe$_2$]$_3$ (**1^Y**)	**B**	10 min	89	34.9	12.2	52.9	9.5	1.25	-25.9	-[i]
S47	[Cp*YMe$_2$]$_3$ (**1^Y**)	**B**	20 min	89	33.3	14.0	52.7	10.3	1.18	-27.2	-[i]
S48	[Cp*YMe$_2$]$_3$ (**1^Y**)	**B**	45 min	86	30.5	15.9	53.6	11.4	1.12	-27.3	-[i]
S49	[Cp*YMe$_2$]$_3$ (**1^Y**)	**B**	3 h	95	32.0	12.8	55.1	12.5	1.11	-22.0	-[i]
S50	[Cp*YMe$_2$]$_3$ (**1^Y**)	**B**	6 h	90	34.0	10.5	55.5	18.6	1.13	-20.0	-[i]
S51	[Cp*YMe$_2$]$_3$ (**1^Y**)	**B**	12 h	>99	33.9	15.3	50.8	42.6	1.33	-17.0	-[i]
S52	[Cp*YMe$_2$]$_3$ (**1^Y**)	**0.33 B**[k]	30 min	30	33.8	6.1	60.1	3.9	1.78	-14.0	-[i]

[a]Conditions: 0.007 mmol precatalyst (0.020 mmol of Y centers), [Y]/[cocat] = 1:1, 8 mL toluene, 20 mmol isoprene, 25 °C. [b]Cocatalyst: **A** = [Ph$_3$C][B(C$_6$F$_5$)$_4$]; **B** = [PhNMe$_2$H][B(C$_6$F$_5$)$_4$], equivalents given per Ln center. [c]Determined by ^{1}H and ^{13}C NMR spectroscopy in CDCl$_3$. [d]Determined by means of size-exclusion chromatography (SEC) against polystyrene standards. [e]Determined by DSC. [f]No such evaluation possible, due to low yield. [h]Determined as reported in Section 3.2.1. [i]No swelling detectable. [k][Y]/[cocat] < 3 / 1; after the addition of one equiv. of cocatalyst **B**, 1 mg of further cocatalyst was added; a [polymer chains] / [Y-atoms] ratio of 14 % can be estimated,[4] according to the obtained data. [x]Did not dissolve in THF due to crosslinking. [y]Only 10 wt% of the polymer were soluble in THF due to crosslinking.

SUPPORTING INFORMATION

Table S12. Isoprene polymerization applying $[Cp^*YMe_2]_3$ as a precatalyst and studying crosslinking experiments

run[a]	precatalyst	cocatalyst[b]	IP (equiv)	t_{Pre}	yield (%)	*cis*-1,4[c]	*trans*-1,4[c]	3,4[c]	M_n[d] (x 10^4)	M_w/M_n[d]	T_g[e]	N_{Gel}[h] (x 10^2)
S53	---	**---**	0	---	only ed.[f]	-[f]	-[f]	-[f]	-[f]	-[f]	-[f]	-[i]
S54	---	**A**	0	---	only ed.[f]	-[f]	-[f]	-[f]	-[f]	-[f]	-[f]	-[i]
S55	---	**A**	100	5 min	only ed.[f]	-[f]	-[f]	-[f]	-[f]	-[f]	-[f]	-[i]
S56	---	**0.1 A**	0	---	only ed.[f]	-[f]	-[f]	-[f]	-[f]	-[f]	-[f]	-[i]
S57	---	**0.1 A**	100	5 min	only ed.[f]	-[f]	-[f]	-[f]	-[f]	-[f]	-[f]	-[i]
S58	---	**A**	10	5 min	only ed.[f]	-[f]	-[f]	-[f]	-[f]	-[f]	-[f]	-[i]
S59	$[Cp^*YMe_2]_3$ (**1^Y**)	**0.1 A**	10	5+30 min	74	57.6	8.1	34.3	-[x]	-[x]	-13	7.3

[a]Conditions: 2 ml of a solution of PIP with (*cis*% / *trans*% / 3,4% = 32.1 / 13.3 / 54.6), 8 mL toluene. [b]Cocatalyst: **A** = $[Ph_3C][B(C_6F_5)_4]$, equivalents given per vinyl unit of the starting polymer. [c]Determined by ^1H and ^{13}C NMR spectroscopy in $CDCl_3$. [d]Determined by means of size-exclusion chromatography (SEC) against polystyrene standards. [e]Determined by DSC. [f]Only starting polymer detected,[h] Determined as reported in Section 3.2.1. [i]No swelling detectable. [x]Did not dissolve in THF due to crosslinking.

Table S13. Selected examples of polymerization and copolymerization reactions applying $[Cp^*YMe_2]_3$ as a precatalyst and cocatalyst $[PhNMe_2H][B(C_6F_5)_4]$ (**B**)

run[a]	precatalyst[b]	monomer	*T* (h)	*T* (°C)	yield (%)	*cis*-1,4[c]	*trans*-1,4[c]	3,4[c]	M_n[d] (x 10^4)	M_w/M_n[d]	T_g[e]
S60	$[Cp^*YMe_2]_3$ (**1^Y**)	St	1	25	0.5	-[g]	-[g]	-[g]	-[g]	-[g]	-[g]
S61	$[Cp^*YMe_2]_3$ (**1^Y**)	St	1	40	29	-[h]	-[h]	-[h]	-[h]	-[h]	n.d.
S62	$[Cp^*YMe_2]_3$ (**1^Y**)	St	14	25	>99	-[h]	-[h]	-[h]	-[i]	-[i]	108.2[k]
S63	$[Cp^*YMe_2]_3$ (**1^Y**)	Et	24	60	89	-[h]	-[h]	-[h]	--[i]	-[i]	139.1[k]
S64	$[Cp^*YMe_2]_3$ (**1^Y**)	Et co St	1	60	4	-[h]	-[h]	-[h]	-[i]	-[i]	136.6[k]
S65	$[Cp^*YMe_2]_3$ (**1^Y**)	St co Hex	41	25	28	-[h]	-[h]	-[h]	-[i]	-[i]	79.9+98.9[k]
S66	$[Cp^*YMe_2]_3$ (**1^Y**)	IP co St	1	25	>99	31.6[l]	16.3[l]	52.1[l]	4.1[m]	1.83	-24.3
S67	$[Cp^*YMe_2]_3$ (**1^Y**)	IP co Hex	41	25	35	32.7[l]	14.0[l]	53.3[l]	5.8[m]	1.36	-24.6

[a]Conditions: 0.007 mmol precatalyst (0.020 mmol of Y centers), [Y]/[cocat] = 1:1, amounts of toluene are given in sections 0 - 0, 20 mmol styrene in runs S60-62 and ethylene in run S63, 10 mmol of each comonomer in runs S65-S67, 60 mmol each in case of run S64. [b]Cocatalyst: **B** = $[PhNMe_2H][B(C_6F_5)_4]$, equivalents given per Ln center. [c]St = styrene, Et = ethylene, Hex = 1-hexene, IP = isoprene. [d]Determined by ^1H and ^{13}C NMR spectroscopy in $CDCl_3$. [e]Determined by means of size-exclusion chromatography (SEC) against polystyrene standards. [f]Determined by DSC. [g]No evaluation possible, due to low yield. [h]No such evaluation possible due to sort of polymer. [i]No such evaluation possible, due to insolubility of the product polymer in THF. [k]Melting point (T_m). [l]Referring to the PIP parts of the polymer. [m]Comonomer contents: run S66: 47.8% (St), run S67: 4.8 % (Hex).

SUPPORTING INFORMATION

3.2 Crosslinking

3.2.1 Flory-Rehner-Evaluation of crosslinked polymers

In order to quantify the crosslinkage of the polymers obtained from polymerizations at low temperatures applying cocatalyst **A** (Table 1, run 9, Table S7 run S4, Table S8, Table S11 run S41, Table S12, run S59), swelling experiments were performed (see section 1.13). The data were evaluated as follows:[17,18]
According to the Flory-Rehner-Equation[19]

$$\Pi = \frac{k_B T}{a^3}\left\{-\phi - \ln(1-\phi) - \chi\phi^2 + \frac{\phi_0}{N_{Gel}}\left[0.5\left(\frac{\phi}{\phi_0}\right) - \sqrt[3]{\frac{\phi}{\phi_0}}\right]\right\} \quad (1)$$

where Π is the osmotic pressure, k_B is the Boltzmann constant, T is the temperature, a is the segment length of a monomer unit, ϕ is the volume fraction of the swollen polymer, ϕ_0 is the volume fraction before swelling, χ is the Flory solvency parameter and N_{Gel} is the average degree of polymerization of the polymer chain between two cross links. As the swelling is assumed to be isotropic in all dimensions,

$$\frac{\phi}{\phi_0} = \frac{V_0}{V} \quad (2)$$

where V is the volume of the swollen polymer and V_0 is the Volume of the polymer before swelling. Furthermore, as the polymer is not dissolved before swelling

$$\phi_0 = 100\% = 1 \quad (3)$$

and as the setup is kept at ϑ-temperature, so

$$\frac{\vartheta}{T} = 1 \text{ and } \Pi = 0 \quad (4a+b)$$

applies. This simplifies the Flory-Rehner-Equation to

$$0 = \left\{-\frac{V_0}{V} - \ln\left(1-\frac{V_0}{V}\right) - \chi\left(\frac{V_0}{V}\right)^2 + \frac{1}{N_{Gel}}\left[0.5\left(\frac{V_0}{V}\right) - \sqrt[3]{\frac{V_0}{V}}\right]\right\} \quad (5)$$

or

$$N_{Gel} = \frac{0.5\left(\frac{V_0}{V}\right) - \sqrt[3]{\frac{V_0}{V}}}{\frac{V_0}{V} + \ln\left(1-\frac{V_0}{V}\right) + \chi\left(\frac{V_0}{V}\right)^2} \quad (6)$$

According to the Flory-Krigbaum-Equation[20,21]

$$\chi = 0.5 - A\left(1 - \frac{\vartheta}{T}\right) \quad (7)$$

where $A = (2\Delta S + k_B)/2k_B$, but due to the condition given in eq. 4a,

$$\chi = 0.5 \quad (8)$$

in the given case. As both V and V_0 are determined in the experiment, N_{Gel} can now be calculated from eq. 6 applying eq. 8.
N_{Gel} can serve to roughly quantify the crosslinkage of polyisoprenes, as ϑ depends on the microstructure of the polymer and therefore χ might deviate slightly from the ideal value of 0.5 for microstructures different from the 96/0/4 (*cis*/*trans*/3,4) utilized for ϑ-determination according to Barton.[22]
Results of these experiments are given in the respective polymer properties tables (Table 1 in the main article and Tables S8, S11, S12).

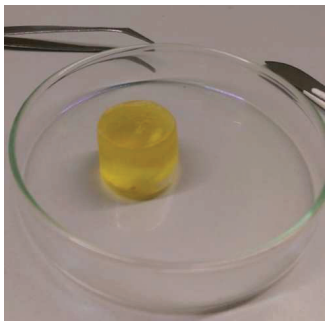

Figure S5. Example of a crosslinked polymer sample.
For details on the polymer, see run S16, Table S8.

SUPPORTING INFORMATION

3.2.2 Studies on the initiation of the crosslinking process

In order to investigate the crosslinking mechanism occurring upon application of cocatalyst **A**, the following experiments have been performed.

A sample of polyisoprene (*cis*% / *trans*% / 3,4% = 32.1 / 13.3 / 54.6), precleaned from any possibly remaining methanol (see Section 1.8, quenching process) by dissolving it in $CHCl_3$ and evaporating the solvent, was dissolved in toluene and the concentration of vinylic groups in the solution was calculated. The solution was spread in 7 vials and the respective 7 sample solutions were treated differently as follows, details on the products can be found in Table S12:

0. The control sample was left as it was, the solvent was evaporated off after 1 h and the obtained polymer showed no parameters different from the starting polymer, as expected.
1. This sample was treated with one equiv. of cocatalyst **A** per vinylic unit in the educt polymer. After adding methanol and evaporating off the solvents, no significant difference compared to the educt polymer could be detected (after 1 h reaction time).
2. In addition to the equivalent of **A** in Sample 1, here 100 equiv. of isoprene monomer per vinylic unit were added after a prereaction time of 5 min. Adding methanol to quench any ongoing polymerization, no significant difference, compared to the educt polymer could be detected after 1 h of reaction time, while the solution showed the typical smell of unreacted isoprene.
3. In analogy to Sample 1, the polymer solution was only treated with cocatalyst **A**. Here, a cocatalyst concentration of only 10 mol% of the vinylic units was chosen, to allow possible reactions of potentially activated groups with non-activated vinyl moieties. After 1 h the solution was treated with methanol and the solvents were evaporated off. Once again, no significant difference compared to the starting polymer could be detected.
4. In addition to the 10 mol% of **A** in Sample 3, here 100 equiv. of isoprene monomer per vinylic unit were added after a prereaction time of 5 min. Adding methanol to quench any ongoing polymerization, no significant difference compared to the educt polymer could be detected after 1 h of reaction time, while the solution showed the typical smell of unreacted isoprene.
5. In addition to the equivalent of **A** in sample 1, here 10 equiv. of isoprene monomer per vinylic unit were added after a prereaction time of 5 min. Adding methanol to quench any ongoing polymerization, no significant difference compared to the educt polymer could be detected after 1 h of reaction time, while the solution showed the typical smell of unreacted isoprene.
6. In addition to the equivalent of **A** and 0.1 equiv. of isoprene of sample 5, here 0.05 equiv. (per vinylic units) of $\mathbf{1}^{\mathbf{Y}}$ have been added after a pre-reaction time of 5 min. Adding methanol to quench any ongoing polymerization, crosslinking was detected. Details on the crosslinked polymer are given in Table S12.

From these results, we conclude that both $\mathbf{1}^{\mathbf{Y}}$ and **A** are necessary to form the species that is responsible for the crosslinking mechanism.

SUPPORTING INFORMATION

4. Active Species Determination – NMR Spectra

4.1 Standard NMR Spectroscopic Approaches

NMR spectroscopic investigations of the active species were performed according to Section 1.14.

*4.1.1 $[Cp^*YMe_2]_3$ (**1**^{Y}) without activation*

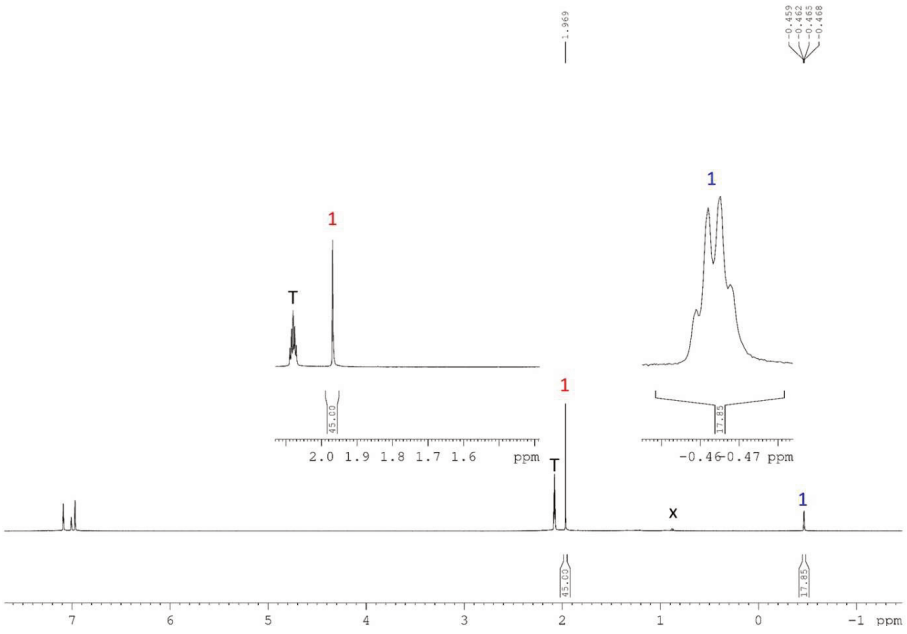

Figure S6. ^{1}H NMR spectrum (400.11 MHz, 26 °C, toluene-d_8) of the $[Cp^*YMe_2]_3$ (**1**^{Y}). Peaks that were evaluated for molecular mass by ^{1}H DOSY-NMR spectroscopy are labeled with red figures (see Section 4.2), those which can be associated to these respective species but not evaluated for molecular mass are indicated with blue figures. Peaks labeled with T are caused by the solvent (toluene-d_8), x represents reactant impurities.

*4.1.2 System **1**^{Y}/**A**: [Cp*YMe$_2$]$_3$ reacted with [Ph$_3$C][B(C$_6$F$_5$)$_4$]*

The accuracy of the integrals in this system suffers from the formation of an insoluble, liquid compound, possibly an ionic liquid that forms a second phase. Droplets of this second phase cause signal underlying broad signals that impede the interpretation of the integrals.

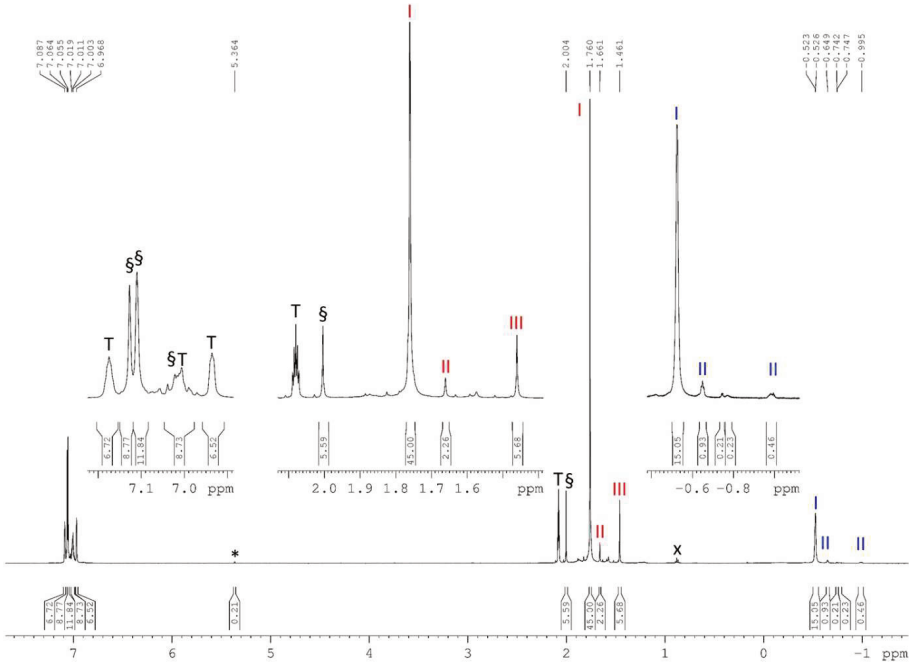

Figure S7. ^{1}H NMR spectrum (400.11 MHz, 26 °C, toluene-d$_8$) of a mixture of 1/3 equiv. [Ph$_3$C][B(C$_6$F$_5$)$_4$] (**A**) per Y atom in [Cp*YMe$_2$]$_3$ (**1**^{Y}). Peaks that were evaluated for molecular mass by ^{1}H DOSY-NMR spectroscopy are labeled with red figures (see Section 4.2), those which can be associated to these respective species but not evaluated for molecular mass are indicated with blue figures. Peaks labeled with T are caused by the solvent (toluene-d$_8$), those with § are produced by the activation side product Ph$_3$CMe, x represents reactant impurities and * indicates the aliphatic peak of the minimal amounts of Ph$_3$CH found in the spectra. The aromatic peaks of this byproduct of an activation side reaction are underlying those of Ph$_3$CMe. For comparison with the other spectra given in this section, the integral of the Cp* peak of the main species (1.76 ppm) has been calibrated to 45 H (3 Cp*). An overview figure on the subsequent addition of cocatalyst **A** to **1**^{Y} can be found in Figure S11.

SUPPORTING INFORMATION

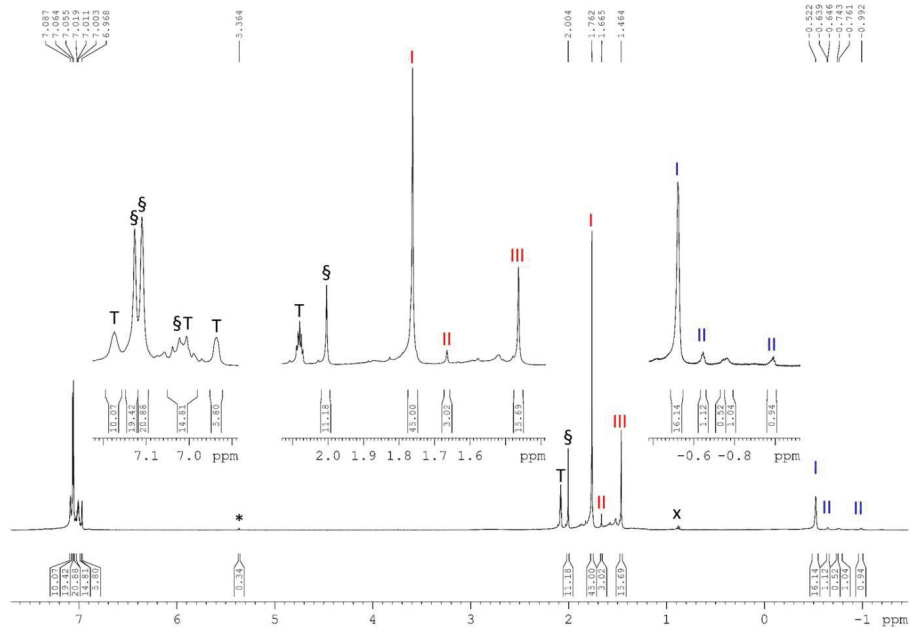

Figure S8. ^{1}H NMR spectrum (400.11 MHz, 26 °C, toluene-d_8) of a mixture of a half equiv. $[Ph_3C][B(C_6F_5)_4]$ (**A**) per Y atom in $[Cp^*YMe_2]_3$ (**1^{Y}**). Peaks that were evaluated for molecular mass by ^{1}H DOSY-NMR spectroscopy are labeled with red figures (see Section 4.2), those which can be associated to these respective species but not evaluated for molecular mass are indicated with blue figures. Peaks labeled with T are caused by the solvent (toluene-d_8), those with § are produced by the activation side product Ph_3CMe, x represents reactant impurities and * indicates the aliphatic peak of the minimal amounts of Ph_3CH found in the spectra. The aromatic peaks of this byproduct of an activation side reaction are underlying those of Ph_3CMe. For comparison with the other spectra given in this section, the integral of the Cp* peak of the main species (1.76 ppm) has been calibrated to 45 H (3 Cp*). An overview figure on the subsequent addition of cocatalyst **A** to **1^{Y}** can be found in Figure S11.

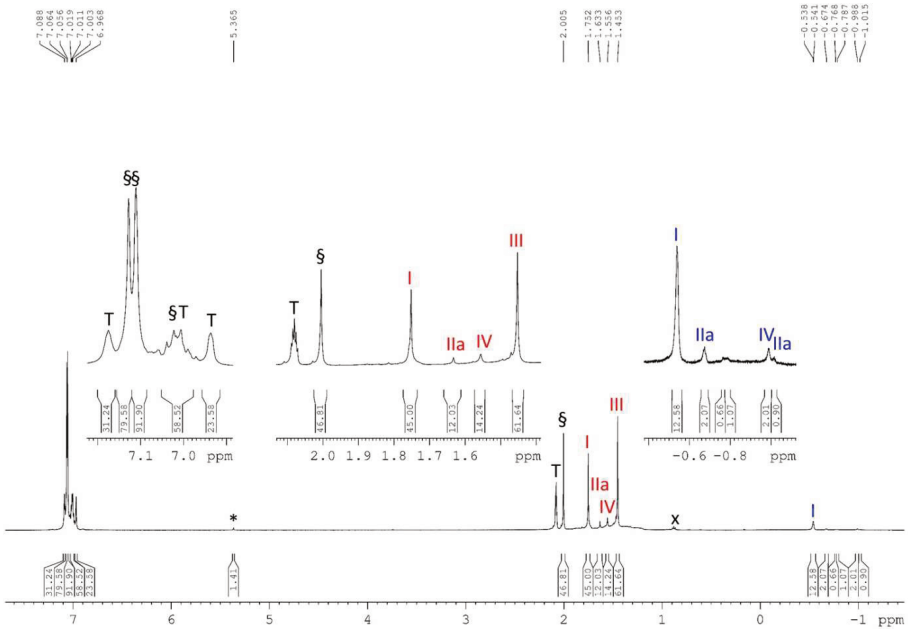

Figure S9. ^{1}H NMR spectrum (400.11 MHz, 26 °C, toluene-d_8) of a mixture of two third equiv. $[Ph_3C][B(C_6F_5)_4]$ (**A**) per Y atom in $[Cp^*YMe_2]_3$ (**1^Y**). Peaks that were evaluated for molecular mass by ^{1}H DOSY-NMR spectroscopy are labeled with red figures (see Section 4.2), those which can be associated to these respective species but not evaluated for molecular mass are indicated with blue figures. Peaks labeled with T are caused by the solvent (toluene-d_8), those with § are produced by the activation side product Ph_3CMe, x represents reactant impurities and * indicates the aliphatic peak of the minimal amounts of Ph_3CH found in the spectra. The aromatic peaks of this byproduct of an activation side reaction are underlying those of Ph_3CMe. For comparison with the other spectra given in this section, the integral of the Cp*- peak of species **I** (1.75 ppm) has been calibrated to 45 H (3 Cp*). An overview figure on the subsequent addition of cocatalyst **A** to **1^Y** can be found in Figure S11.

SUPPORTING INFORMATION

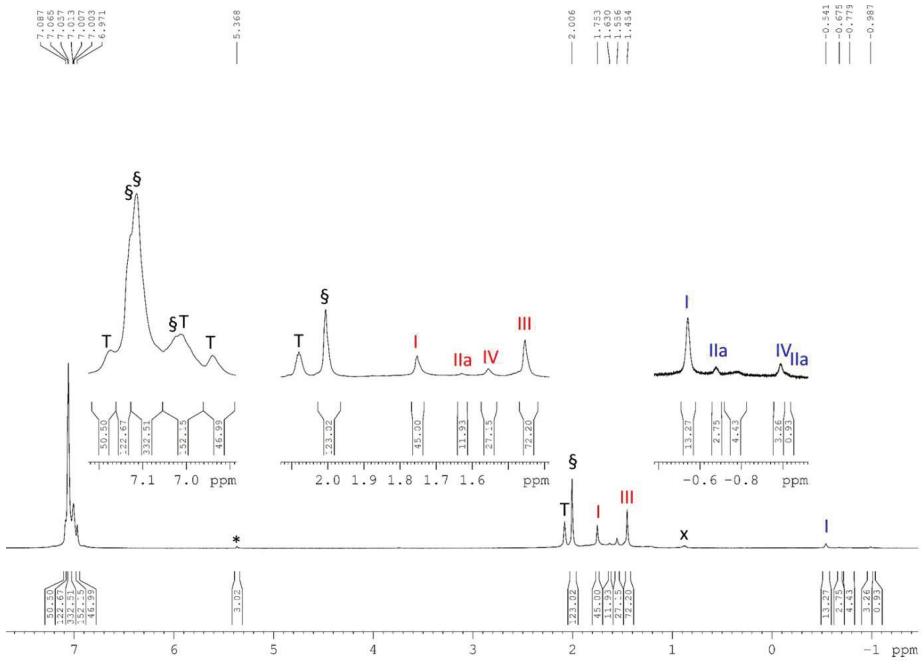

Figure S10. ^{1}H NMR spectrum (400.11 MHz, 26 °C, toluene-d_8) of a mixture of one equiv. $[Ph_3C][B(C_6F_5)_4]$ (**A**) per Y atom in $[Cp^*YMe_2]_3$ (**1^Y**). Peaks that were evaluated for molecular mass by ^{1}H DOSY-NMR spectroscopy are labeled with red figures (see Section 4.2), those which can be associated to these respective species but not evaluated for molecular mass are indicated with blue figures. Peaks labeled with T are caused by the solvent (toluene-d_8), those with § are produced by the activation side product Ph_3CMe, x represents reactant impurities and * indicates the aliphatic peak of the minimal amounts of Ph_3CH found in the spectra. The aromatic peaks of this byproduct of an activation side reaction are underlying those of Ph_3CMe. For comparison with the other spectra given in this section, the integral of the Cp* peak of species **I** (1.75 ppm) has been calibrated to 45 H (3 Cp*). An overview figure on the subsequent addition of cocatalyst **A** to **1^Y** can be found in Figure S11.

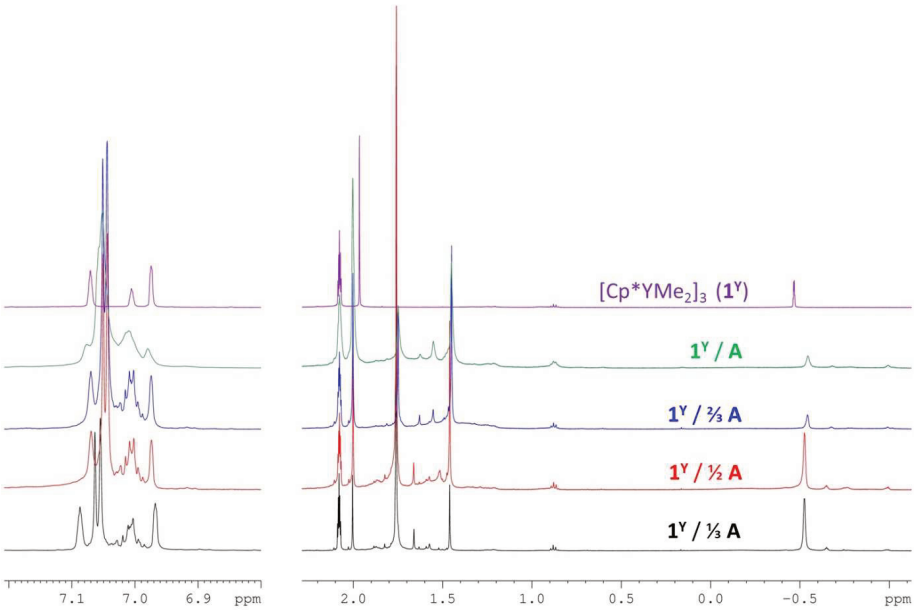

Figure S11. Overview of ^{1}H NMR spectra (400.11 MHz, 26 °C, toluene-d_8) of mixtures of indicated amounts of equiv. $[Ph_3C][B(C_6F_5)_4]$ (**A**) per Y atom in $[Cp^*YMe_2]_3$ (**1^Y**). See Figures S7 – S10 for details on the spectra.

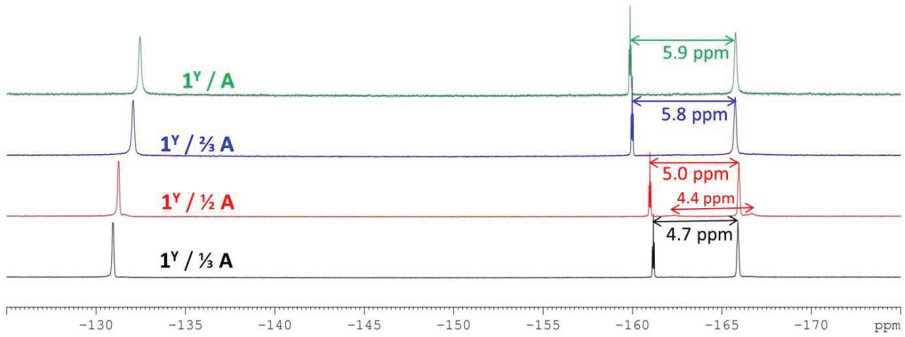

Figure S12. Overview on ^{19}F NMR spectra (376.43 MHz, 26 °C, toluene-d_8) of a mixtures of indicated amounts of equiv. $[Ph_3C][B(C_6F_5)_4]$ (**A**) per Y atom in $[Cp^*YMe_2]_3$ (**1^Y**). The distances between meta and para fluorine signals are indicated to allow interpretation according to the Horton scale, where 2.7 ppm means weak and 5.4 ppm means strong coordination of the $[B(C_6F_5)_4]$ anion.[23,24]

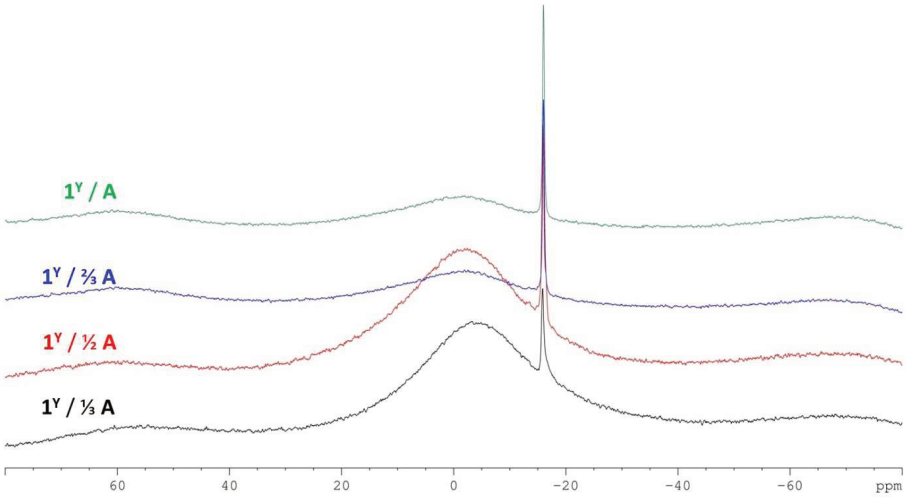

Figure S13. Overview on ^{11}B NMR spectra (80.25 MHz, 26 °C, toluene-d_8) of a mixtures of indicated amounts of equiv. $[Ph_3C][B(C_6F_5)_4]$ (**A**) per Y atom in $[Cp^*YMe_2]_3$ (**1^Y**). The background signals caused by the boron-containing NMR probes has been suppressed. The broad peak at ca. -5 ppm originates from the boron silicate NMR tubes.

SUPPORTING INFORMATION

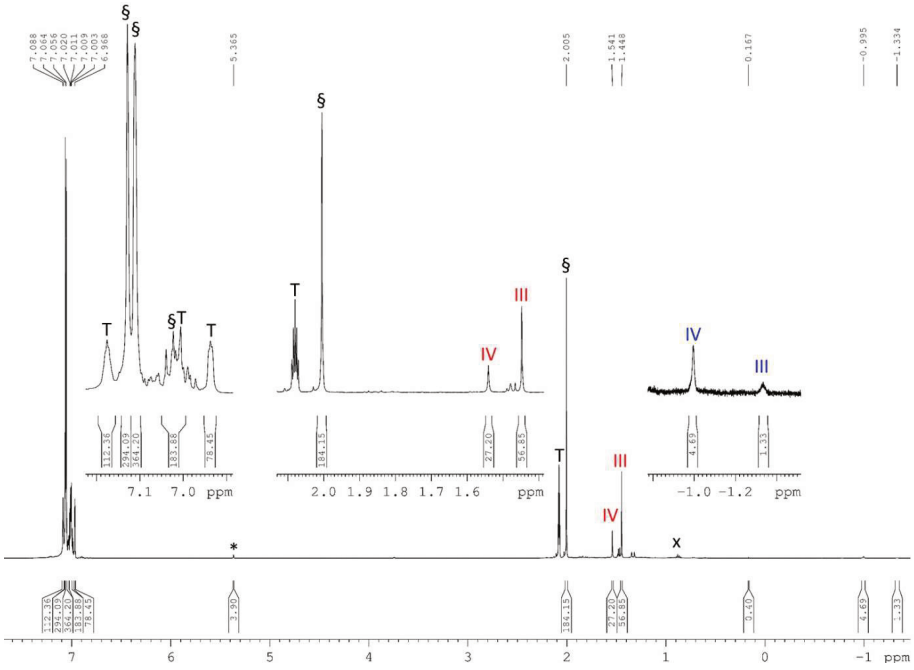

Figure S14. ^{1}H NMR spectrum (400.11 MHz, 26 °C, toluene-d_8) of the supernatant of a mixture of one equiv. $[Ph_3C][B(C_6F_5)_4]$ (**A**) per Y atom in $[Cp^*YMe_2]_3$ (**1^Y**). Peaks that were evaluated for molecular mass by ^{1}H DOSY-NMR spectroscopy are labeled with red figures (Section 4.2), those which can be associated to these respective species but not evaluated for molecular mass are indicated with blue figures. Peaks labeled with T are caused by the solvent (toluene-d_8), those with § are produced by the activation side product Ph_3CMe, x represents reactant impurities and * indicates the aliphatic peak of the minimal amounts of Ph_3CH found in the spectra. The aromatic peaks of this byproduct of an activation side reaction are underlying those of Ph_3CMe. For comparison with the other spectra given in this section, the integral of the Cp* peak of species **IV** (1.54 ppm) has been calibrated to 27.2 H (in analogy to species **IV** in the non-decanted spectrum (Figure S10)). A comparison of the decanted and the non-decanted spectrum of this mixture can be found in Figure S15.

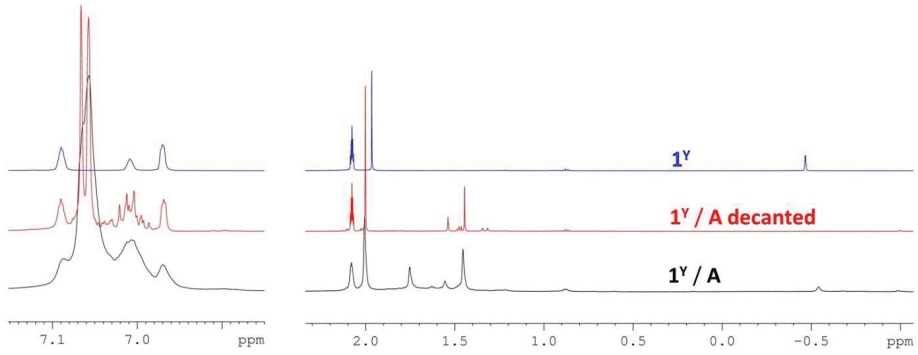

Figure S15. Comparison of the ^{1}H NMR spectra (400.11 MHz, 26 °C, toluene-d_8) of a decanted and a non-decanted mixture of one equiv. $[Ph_3C][B(C_6F_5)_4]$ (**A**) per Y atom in $[Cp^*YMe_2]_3$ (**1^Y**). For details on the respective NMR spectroscopic data see Figures S10 and S14

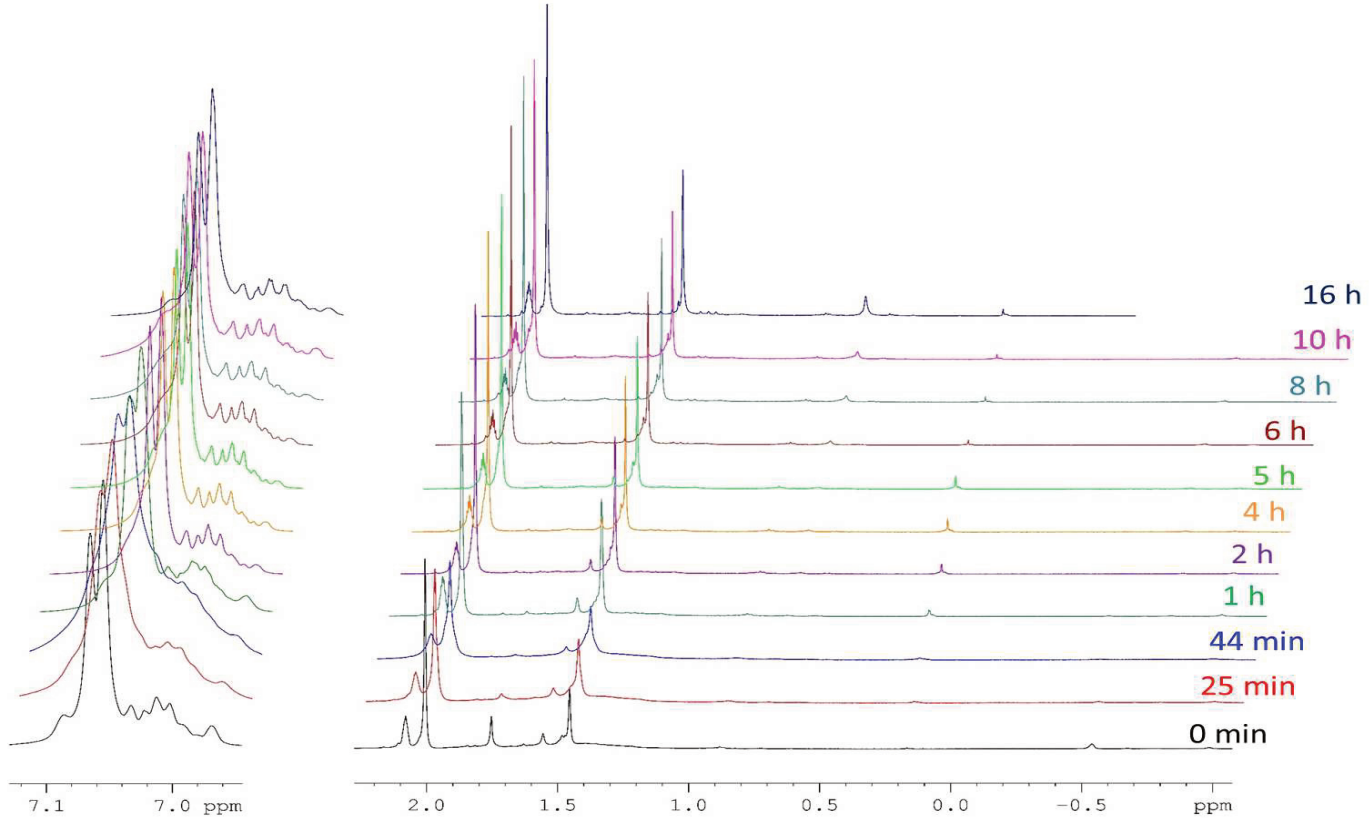

Figure S16. Overview on the ^{1}H NMR spectra (400.11 MHz, 26 °C, toluene-d_8) of a mixture of one equiv. $[Ph_3C][B(C_6F_5)_4]$ (**A**) per Y atom in $[Cp^*YMe_2]_3$ (**1**) versus reaction time after the addition of the solvent.

SUPPORTING INFORMATION

*4.1.3 System **1^{Y}/B**: [Cp*YMe$_2$]$_3$ reacted with [PhNMe$_2$H][B(C$_6$F$_5$)$_4$]*

This system reacts with the instant formation of a yellow amorphous solid and methane after addition of the solvent for all tested concentrations of the cocatalyst. For concentrations above one third equivalent per Y atom, this solid is redissolved over time and the reaction leads to the coordination polymer that crystallizes from the reaction mixture in bright teal color (see Section 1.4). Here, detailed spectra for one third and one full equivalent are given as well as comparative figures, to indicate the formation of **2** over time and the identical products of the initial reaction. Due to the amorphous solid formed, broad peaks are present throughout the spectra for this system. Moreover, only in case of **B, I** is present in the spectra next to precatalyst **1^{Y}** in a 2 (**I**): 1 (**1^{Y}**) molar ratio, while in case of **A**, **1^{Y}** was already consumed totally at this stage of cocatalyst addition.

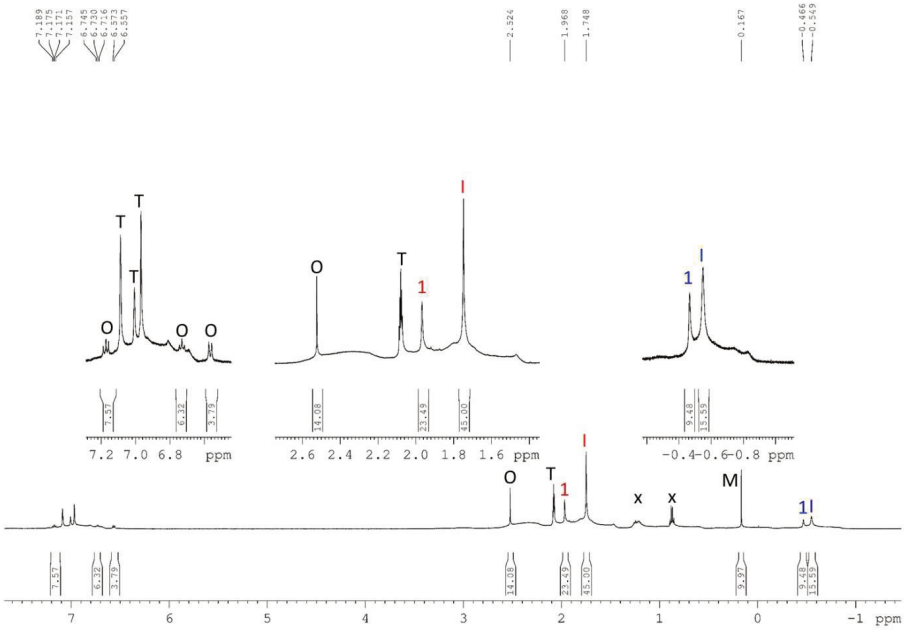

Figure S17. ^{1}H NMR spectrum (400.11 MHz, 26 °C, toluene-d$_8$) of a mixture of one third equiv. [PhNMe$_2$H][B(C$_6$F$_5$)$_4$] (**B**) per Y atom in [Cp*YMe$_2$]$_3$ (**1^{Y}**). Peaks that were evaluated for molecular mass by ^{1}H DOSY-NMR spectroscopy are labeled with red figures (see Section 4.2), those which can be associated to these respective species but not evaluated for molecular mass are indicated with blue figures. Peaks labeled with T are caused by the solvent (toluene-d$_8$), those with O are produced by the activation side product PhNMe$_2$, M marks the methane peak and x represents reactant impurities. For comparison with the other spectra given in this section, the integral of the Cp* peak of species **I** (1.75 ppm) has been calibrated to 45 H (3 Cp*). An overview figure on the subsequent addition of cocatalyst **B** to **1^{Y}** can be found in Figure S19.

SUPPORTING INFORMATION

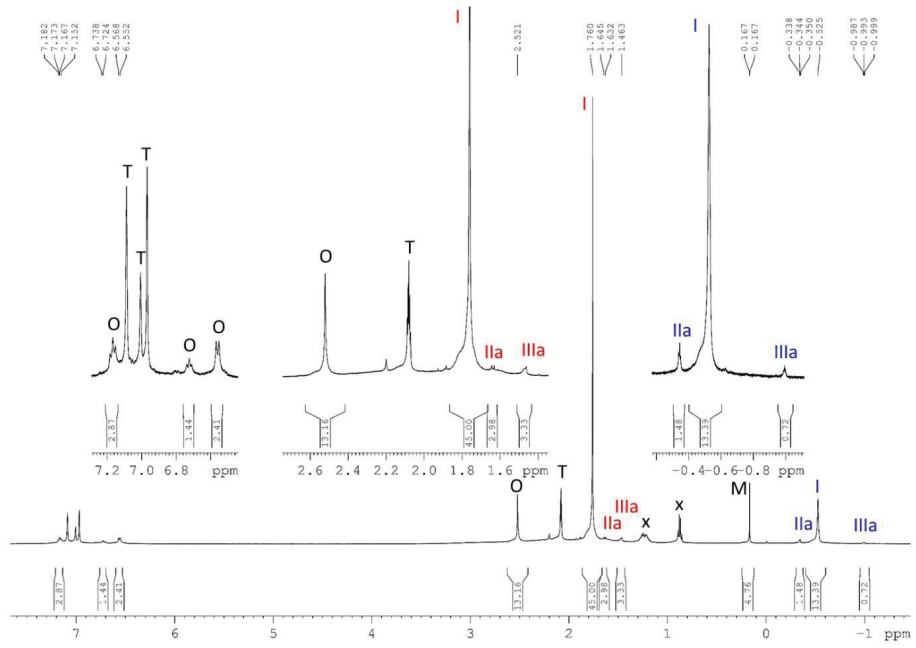

Figure S18. ^{1}H NMR-spectrum (400.11 MHz, 26 °C, toluene-d_8) of a mixture of one equiv. $[PhNMe_2H][B(C_6F_5)_4]$ (**B**) per Y atom in $[Cp^*YMe_2]_3$ ($\mathbf{1^Y}$). Peaks that were evaluated for molecular mass by ^{1}H DOSY-NMR spectroscopy are labeled with red figures (see Section 4.2), those which can be associated to these respective species but not evaluated for molecular mass are indicated with blue figures. (Note: ^{1}H DOSY NMR was performed for a sample that had been reacted for approx. 1 h, so that species **IIa** and **IIIa** were present in higher concentrations than depicted in this spectrum, taken ca. 5 min after the addition of the solvent.) Peaks labeled with T are caused by the solvent (toluene-d_8), those with O are produced by the activation side product $PhNMe_2$. M marks the methane peak and x represents reactant impurities. For comparison with the other spectra given in this section, the integral of the Cp* peak of species **I** (1.76 ppm) has been calibrated to 45 H (3 Cp*). An overview figure on the subsequent addition of cocatalyst **B** to $\mathbf{1^Y}$ can be found in Figure S19.

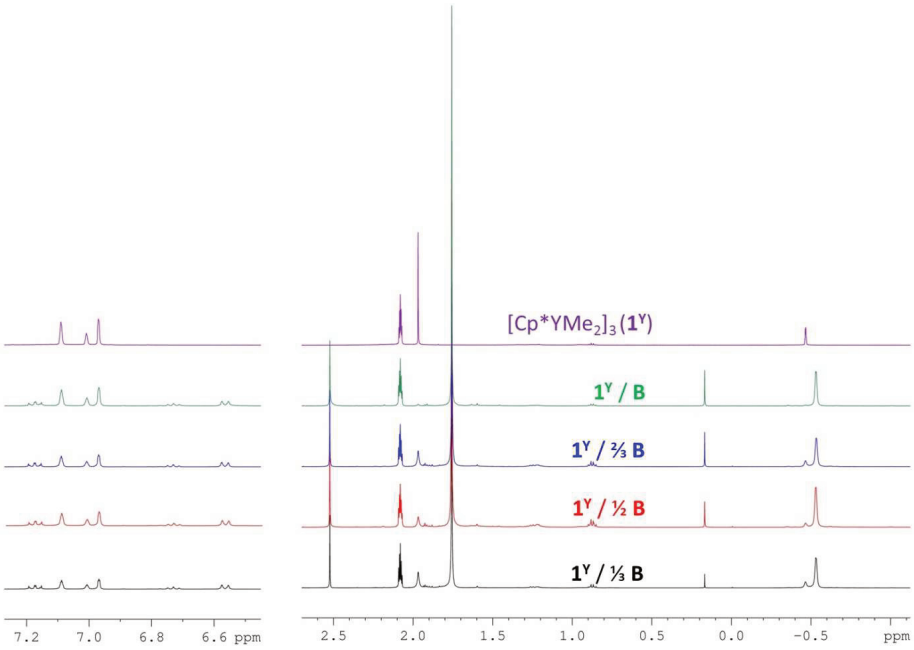

Figure S19. Overview on ^{1}H NMR spectra (400.11 MHz, 26 °C, toluene-d_8) of a mixtures of indicated concentrations of [$PhNMe_2H$][$B(C_6F_5)_4$] (**B**) per Y atom in [$Cp^*YMe_2]_3$ (**1^Y**), directly after the addition of the solvent. See Figures S17 and S18 for details on mixtures with one third and one full equivalent of **B** per Y atom, respectively.

SUPPORTING INFORMATION

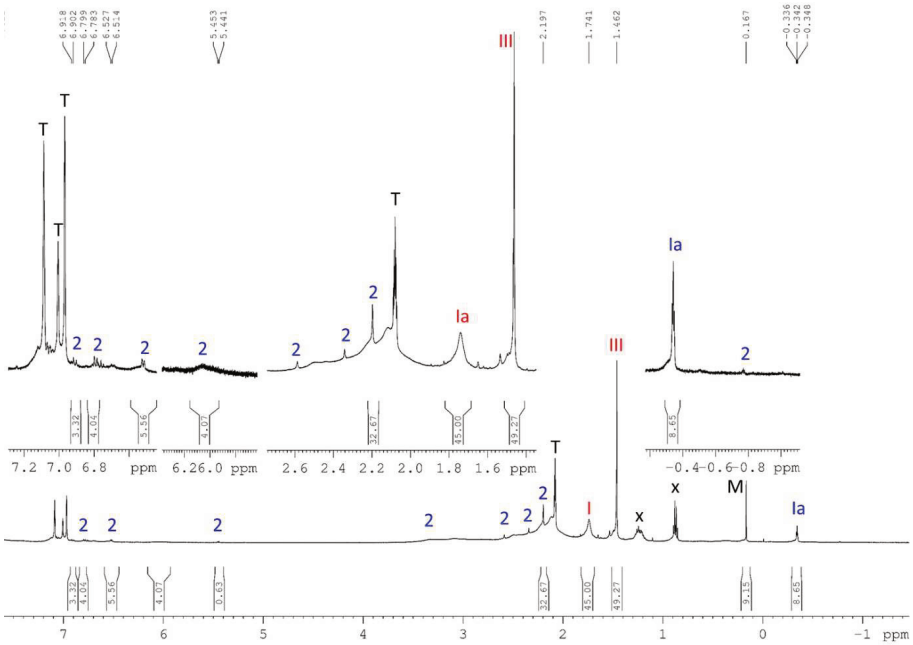

Figure S20. ^{1}H NMR spectrum (400.11 MHz, 26 °C, toluene-d_8) of a mixture of one equiv. [$PhNMe_2H$][$B(C_6F_5)_4$] (**B**) per Y atom in [Cp*YMe_2]$_3$ (**1^{Y}**), 6 h after the addition of the solvent. Peaks that were evaluated for molecular mass by ^{1}H DOSY-NMR spectroscopy are labeled with red figures (see Section 4.2), those which can be associated to these respective species but not evaluated for molecular mass are indicated with blue figures. Peaks labeled with T are caused by the solvent (toluene-d_8), those with O are produced by the activation side product $PhNMe_2$, M marks the methane peak and x represents reactant impurities and peaks labeled with **2** are assigned to the coordination polymer **2**, that forms from the reaction mixture over time. For comparison with the other spectra given in this section, the integral of the Cp* peak of species **I** (1.74 ppm) has been calibrated to 45 H (3 Cp*). An overview figure on the reaction of one equiv. of cocatalyst **B** per Y atom with **1^{Y}** can be found in Figure S21.

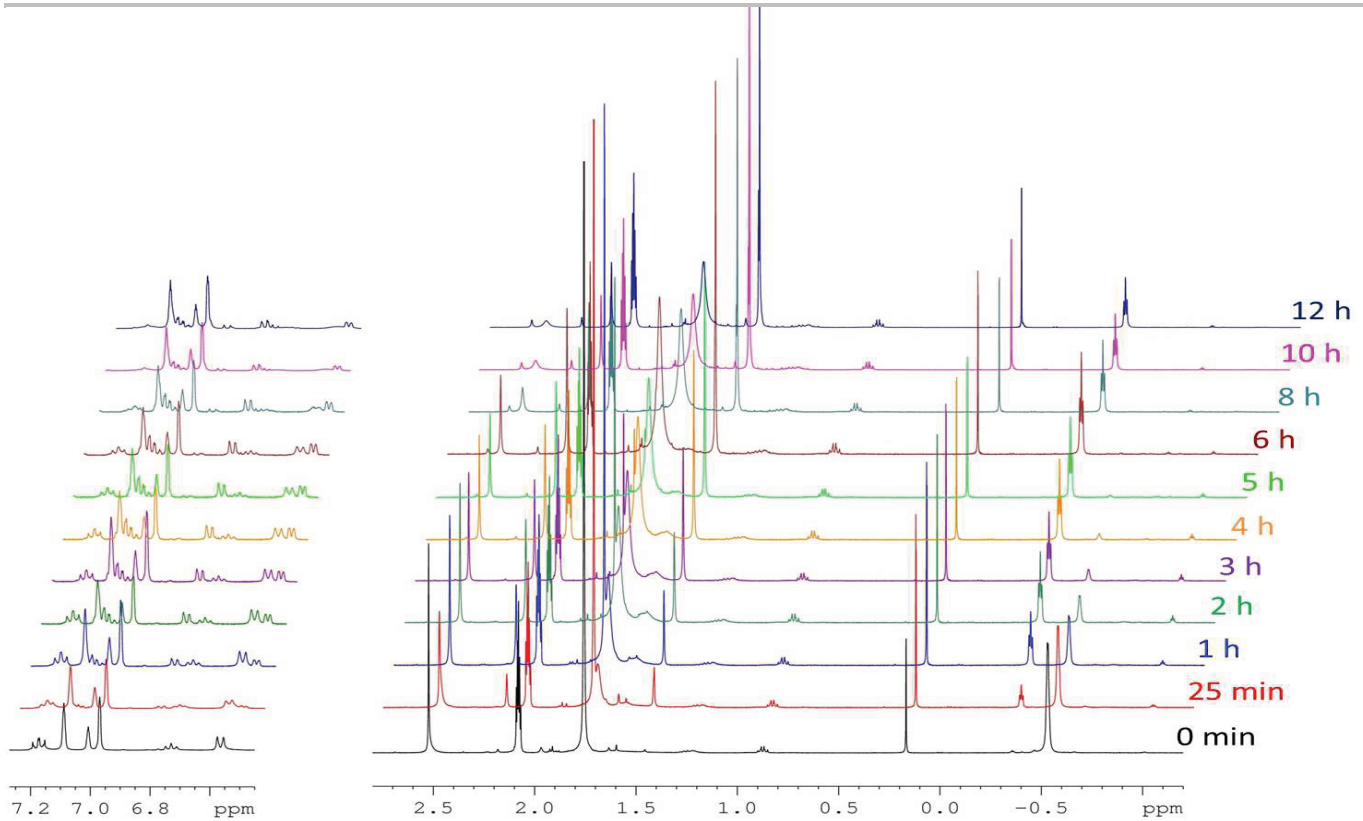

Figure S21. Overview on the ^{1}H NMR spectra (400.11 MHz, 26 °C, toluene-d_8) of a mixture of one equiv. $[PhNMe_2H][B(C_6F_5)_4]$ (**B**) per Y atom in $[Cp^*YMe_2]_3$ (**1^Y**), versus reaction time after the addition of the solvent.

SUPPORTING INFORMATION

4.1.4 Comparison of the concentration of the Cp species occurring in activation experiments with both cocatalysts over time*

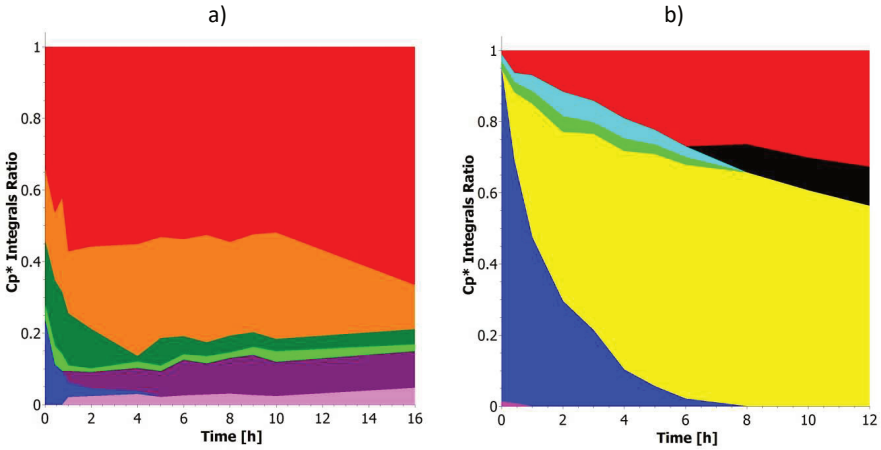

Charts S1a and b. Molar compositions of the distinguishable Cp* species in the activation reactions of $\mathbf{1^Y}$ applying cocatalyst **A** (Chart S1a) and **B** (Chart S1b) (3 equiv. per trimer = 1 equiv. per Y atom) obtained from the integrals in the respective ^{1}H NMR spectra (see Figures S16 and S22 for details). Species showing the same chemical shifts in both reactions are pictured in the same color in both charts. Some of the species indicated in these charts were not evaluated by ^{1}H-DOSY NMR spectroscopy due to low signal to noise ratio. Legend [ppm]: 1.97 light magenta ($\mathbf{1^Y}$), 1.83 magenta, 1.76 blue (**I**), 1.74 yellow (**Ia**), 1.68 purple (**II**), 1.63 bright green (**IIa**), 1.60 cyan, 1.55 dark green (**IV**), 1.47 black, 1.46 orange (**III**), 1.45 red (**III**). Polymerization data on catalysis with varying prereaction times can be found in Table S13. Signals with a reasonably high signal to noise ratio were investigated by ^{1}H DOSY NMR spectroscopy. Results can be found in Section 4.2.

*4.1.5 [(Cp*Y)$_3$Me$_4$(CH$_2$)(thf)$_2$] (**3**) without activation*

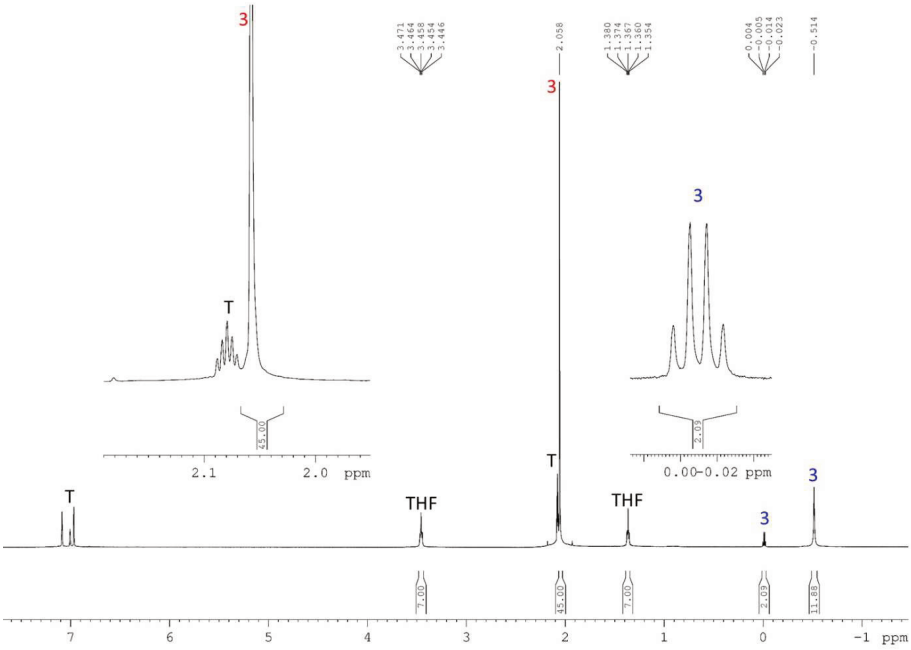

Figure S22. ^{1}H NMR-spectrum (400.11 MHz, 26 °C, toluene-d$_8$) of [(Cp*Y)$_3$Me$_4$(CH$_2$)(thf)$_2$] (**3**). Peaks that were evaluated for molecular mass by ^{1}H DOSY-NMR spectroscopy are labeled with red figures (see Section 4.2), those which can be associated to these respective species but not evaluated for molecular mass are indicated with blue figures. Peaks labeled with T are caused by the solvent (toluene-d$_8$), x represents reactant impurities and THF the peaks of the coordinated THF.

*4.1.6 System **3** / **A**: [(Cp*Y)$_3$Me$_4$(CH$_2$)(thf)$_2$] reacted with [Ph$_3$C][B(C$_6$F5)$_4$]*

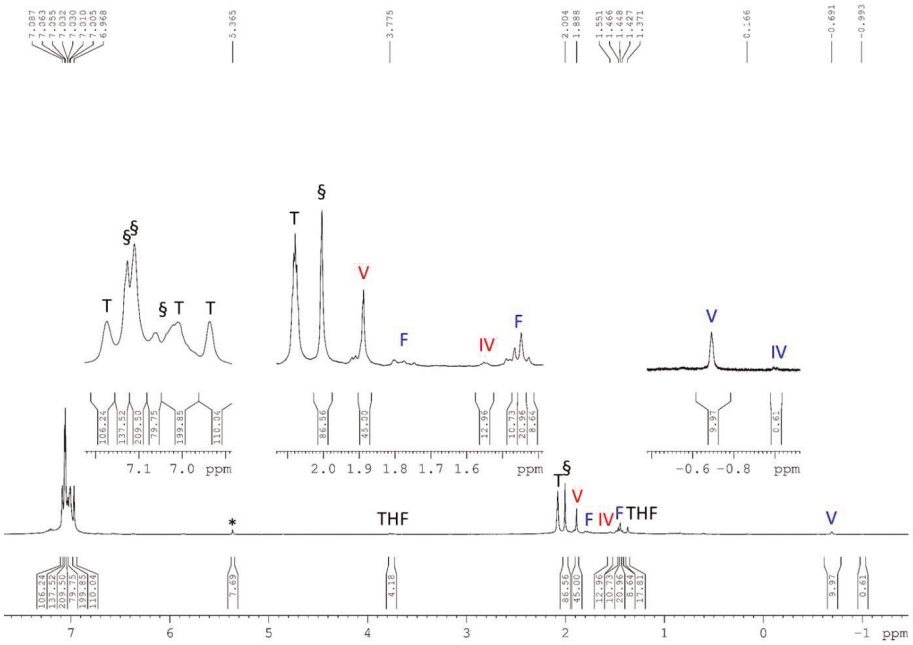

Figure S23. ^{1}H NMR spectrum (400.11 MHz, 26 °C, toluene-d$_8$) of a mixture of one equiv. [Ph$_3$C][B(C$_6$F$_5$)$_4$] (**A**) per Y atom in [(Cp*Y)$_3$Me$_4$(CH$_2$)(thf)$_2$] (**3**). Peaks that were evaluated for molecular mass by ^{1}H DOSY-NMR spectroscopy are labeled with red figures (see Section 4.2), those which can be associated to these respective species but not evaluated for molecular mass are indicated with blue figures. Peaks labeled with T are caused by the solvent (toluene-d$_8$), those with § are produced by the activation side product Ph$_3$CMe, x represents reactant impurities and * indicates the aliphatic peak of the minimal amounts of Ph$_3$CH found in the spectra. The aromatic peaks of this byproduct of an activation side reaction are underlying those of Ph$_3$CMe. F represents several species that are present but could not be investigated by ^{1}H DOSY NMR spectroscopy due the overlaying of multiple species and low signal to noise ratio of the respective individual contributions to the peaks. For comparison with the other spectra given in this section, the integral of the Cp* peak of species **V** (1.88 ppm) has been calibrated to 45 H. Comparison of the spectrum of this mixture with that of **3** without activation can be found in Figure S24.

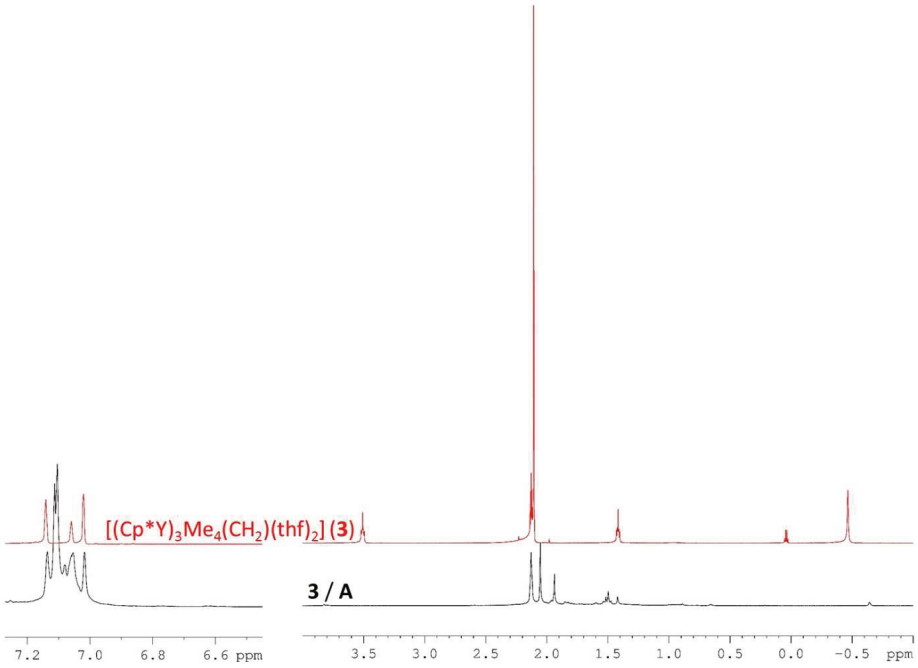

Figure S24. Comparison of ^{1}H NMR spectra (400.11 MHz, 26 °C, toluene-d_8) of a mixture of one equiv. $[Ph_3C][B(C_6F_5)_4]$ (**A**) per Y atom in $[(Cp^*Y)_3Me_4(CH_2)(thf)_2]$ (**3**) with that of **3** without activation.

4.2 DOSY NMR Spectroscopic Approaches

^{1}H diffusion-ordered NMR spectroscopy (^{1}H DOSY measurements) has not only been performed in order to allow the assignment of the peaks in the NMR spectra to the respective peak set of a certain species. It has also been applied, in order to provide insight into the molecular weight of the species, where the signal/noise ratio was high enough to allow such interpretations.

4.2.1 Determination of the Diffusion Coefficients

The measurements were performed as given in section 1.16 and evaluated by linear fitting the resulting Stjeskal-Tanner Plots.[25-27] (In several cases, where signals were overlapping, the plots were fitted to the natural logarithm of eq. 9). Fitting the obtained raw data of the gradient dependent intensity (I(G)) according to equation 9 gave large errors especially in case of signals of relatively low maximum (starting) intensity (I_0) and therefore low signal to noise ratios.

$$I(G) = \sum_{i=1}^{n} I_{0,i} \exp\left(-D_i(\gamma\delta G)^2\left(\Delta - \frac{\delta}{3}\right)\right) \quad (9)$$

Where n is the amount of overlapping peaks at the investigated chemical shift and therefore the amount of contributions to I_0, D_i is the respective diffusion coefficient, G is the applied magnetic gradient strength, δ is the duration of the gradient pulses, Δ is the separation between the gradient pulses and γ is the gyromagnetic ratio of the observed nucleus (^{1}H). Values for these systematic constants are given in Table S14.
In section 4.2.2 both the raw data and fitted Stejskal-Tanner plots are shown using the substitution shown in equation 10.

$$Q = -(\gamma\delta G)^2\left(\Delta - \frac{\delta}{3}\right) \quad (10)$$

For n > 1, no linearization is possible. Here the data sets are fitted to the natural logarithm of eq. 9. As ln(x) is undefined for x < 0, the $\ln(I(G)/I_0)$ is plotted as function of –Q in these cases to enable fitting. Approaches of simply fitting two linear curves to the data sets are theoretically as accurate, but are not possible in the given case, as the measured parts do not contain the linear ranges of the curves.
The fit-data is given both in the captions of the respective plot and an overview table (Table S15) in section 4.2.4.

Table S14. Systematic constants of the ^{1}H DOSY measurements

Precat.	Cocat.[a]	Equiv. Cocat.[a]	Δ [s]	δ [s]	γ [Hz / G]
1	none	0	0.1	0.0015	4257.7
1	**A**	1/3	0.1	0.0023	4257.7
1	**A**	1/2	0.1	0.0023	4257.7
1	**A**	2/3	0.1	0.0023	4257.7
1	**A**	1	0.1	0.0023	4257.7
1	**A**	1D	0.1	0.0018	4257.7
1	**B**	1/3	0.1	0.0013	4257.7
1	**B**	1	0.1	0.0013	4257.7
1	**B**	1T	0.1	0.0013	4257.7
3	none	0	0.1	0.0015	4257.7
3	**A**	1	0.1	0.0015	4257.7

[a] **A** = $[Ph_3C][B(C_6F_5)_4]$; **B** = $[PhNMe_2H][B(C_6F_5)_4]$, Equivalents given per Y atom. D indicates decantation, T indicates a prolonged pre-reaction time of 6 h.

4.2.2 DOSY-NMR-Spectroscopic Data and Evaluations

In the following subsection, only the peak showing the largest integral of a certain species has been evaluated in terms of diffusion coefficient determination and in subsection 4.2.3 in terms of molecular weight. This is reasoned by the fact that smaller peaks vanish into the noise of the spectrum at higher gradients. Therefore, the resulting error of the measurement and fit are expected to be higher, so averaging such a result with another one with a lower error would not be beneficial for the accuracy of the data. The given errors are only those by the fit. The actual errors might be higher due to the reasons mentioned in subsections 4.1, 4.2.1 and 4.2.3.

4.2.2.1 $[Cp^*YMe_2]_3$ (1) trimer without activation:

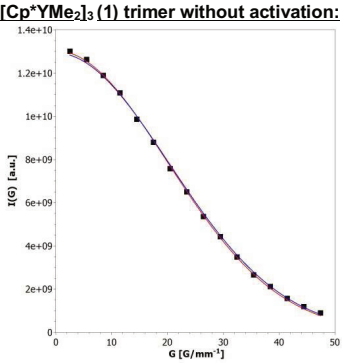

Chart S2a. Plot of the magnetization decay raw data of the Cp* species in the NMR spectrum of the $[Cp^*YMe_2]_3$ ($\mathbf{1^Y}$) trimer at a chemical shift of 1.97 ppm. The function shown in blue represents the ideal raw data curve for the diffusion coefficient found by fitting the Stejskal-Tanner plot (Chart S2b), the red curve is the best possible fit for the raw data.

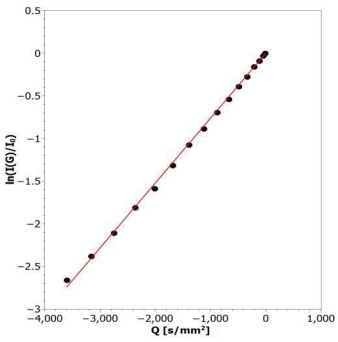

Chart S2b. Stejskal-Tanner plot of the magnetization decay data for the Cp* signal in the NMR spectrum of the $[Cp^*YMe_2]_3$ ($\mathbf{1^Y}$) trimer at a chemical shift of 1.97 ppm.
The solid red line indicates a linear fit, resulting in a diffusion coefficient (slope of the fit) of $D = 7.61 \cdot 10^{-10} \pm 4.7 \cdot 10^{-12}$ m^{2}s^{-1}. (For a definition of Q, please see eq. 10).

4.2.2.2 One third equivalent of cocatalyst A per Y atom in $[Cp^*YMe_2]_3$ (1):

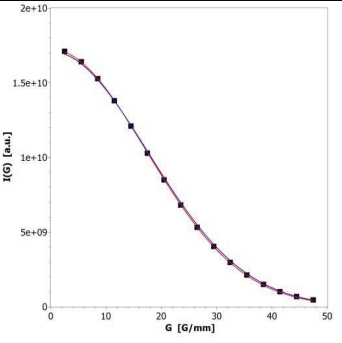

Chart S3a. Plot of the magnetization decay raw data of the Cp* species **I** in the NMR spectrum of a mixture of one third equiv. $[Ph_3C][B(C_6F_5)_4]$ (**A**) per Y atom in $[Cp^*YMe_2]_3$ ($\mathbf{1^Y}$) at a chemical shift of 1.76 ppm. The function shown in blue represents the ideal raw data curve for the diffusion coefficient found by fitting the Stejskal-Tanner plot (Chart S3b), the red curve is the best possible fit for the raw data.

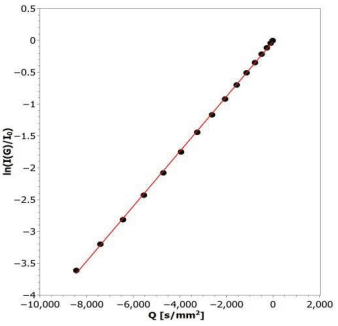

Chart S3b. Stejskal-Tanner plot of the magnetization decay data for the Cp* signal of **I** in the NMR spectrum of a mixture of one third equiv. $[Ph_3C][B(C_6F_5)_4]$ (**A**) per Y atom in $[Cp^*YMe_2]_3$ ($\mathbf{1^Y}$) at a chemical shift of 1.76 ppm.
The solid red line indicates a linear fit, resulting in a diffusion coefficient (slope of the fit) of $D = 4.32 \cdot 10^{-10} \pm 2.2 \cdot 10^{-12}$ m^{2}s^{-1} (For a definition of Q, please see eq. 10).

SUPPORTING INFORMATION

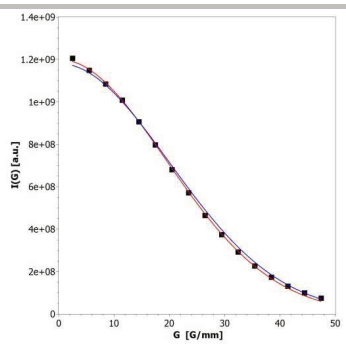

Chart S4a. Plot of the magnetization decay raw data of the Cp* species **II** in the NMR spectrum of a mixture of one third equiv. $[Ph_3C][B(C_6F_5)_4]$ (**A**) per Y atom in $[Cp^*YMe_2]_3$ (**1**^{Y}) at a chemical shift of 1.69 ppm. The function shown in blue represents the ideal raw data curve for the diffusion coefficient found by fitting the Stejskal-Tanner plot (Chart S4b), the red curve is the best possible fit for the raw data.

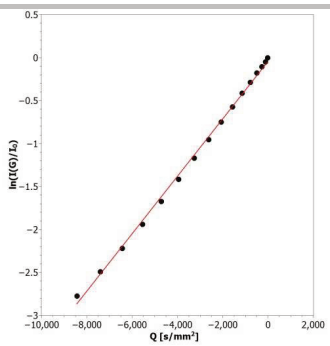

Chart S4b. Stejskal-Tanner plot of the magnetization decay data for the Cp* signal of **II** in the NMR spectrum of a mixture of one third equiv. $[Ph_3C][B(C_6F_5)_4]$ (**A**) per Y atom in $[Cp^*YMe_2]_3$ (**1**^{Y}) at a chemical shift of 1.69 ppm. The solid red line indicates a linear fit, resulting in a diffusion coefficient (slope of the fit) of
$D = 3.34 \cdot 10^{-10} \pm 4.1 \cdot 10^{-12}\ m^2s^{-1}$
(For a definition of Q, please see eq. 10).

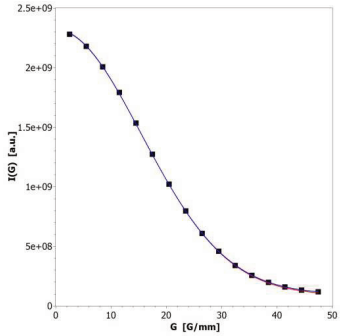

Chart S5a. Plot of the magnetization decay raw data of the Cp* species **III** in the NMR spectrum of a mixture of one third equiv. $[Ph_3C][B(C_6F_5)_4]$ (**A**) per Y atom in $[Cp^*YMe_2]_3$ (**1**) at a chemical shift of 1.46 ppm. The function shown in blue represents the ideal raw data curve for the diffusion coefficient found by fitting the Stejskal-Tanner plot (Chart S5b), the red curve is the best possible fit for the raw data.

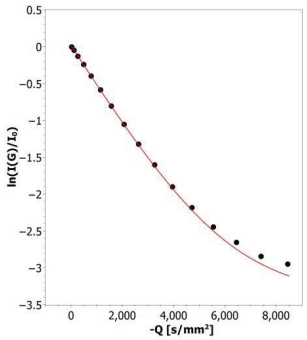

Chart S5b. Stejskal-Tanner plot of the magnetization decay data for the Cp* signal of **III** in the NMR spectrum of a mixture of one third equiv. $[Ph_3C][B(C_6F_5)_4]$ (**A**) per Y atom in $[Cp^*YMe_2]_3$ (**1**) at at a chemical shift of 1.46 ppm. The solid red lines indicate two linear fits, as two overlaying signals were detected. These fits result in diffusion coefficients of:
$D_1 = 5.59 \cdot 10^{-10} \pm 2.4 \cdot 10^{-11}\ m^2s^{-1}$ and $D_2 = 1.96 \cdot 10^{-12} \pm 5.0 \cdot 10^{-11}\ m^2s^{-1}$
(For a definition of Q, please see eq. 10).

SUPPORTING INFORMATION

4.2.2.3 One half equivalent of cocatalyst A per Y atom in $[Cp^*YMe_2]_3$ (1):

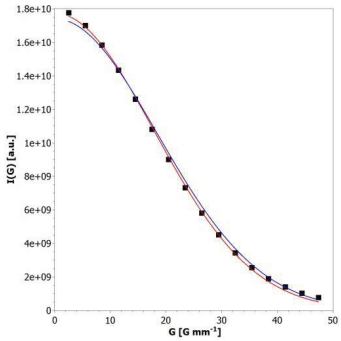

Chart S6a. Plot of the magnetization decay raw data of the Cp* species **I** in the NMR spectrum of a mixture of a half equiv. $[Ph_3C][B(C_6F_5)_4]$ (**A**) per Y atom in $[Cp^*YMe_2]_3$ (**1^Y**) at a chemical shift of 1.76 ppm. The function shown in blue represents the ideal raw data curve for the diffusion coefficient found by fitting the Stejskal-Tanner plot (Chart S6b), the red curve is the best possible fit for the raw data.

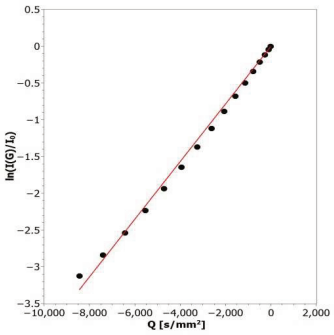

Chart S6b. Stejskal-Tanner plot of the magnetization decay data for the Cp* signal **I** in the NMR spectrum of a mixture of a half equiv. $[Ph_3C][B(C_6F_5)_4]$ (**A**) per Y atom in $[Cp^*YMe_2]_3$ (**1^Y**) at a chemical shift of 1.76 ppm.
The solid red line indicates a linear fit, resulting in a diffusion coefficient (slope of the fit) of $D = 3.92 \cdot 10^{-10} \pm 4.9 \cdot 10^{-12}\ m^2s^{-1}$
(For a definition of Q, please see eq. 10).

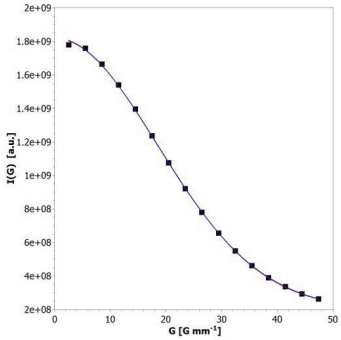

Chart S7a. Plot of the magnetization decay raw data of the Cp* species **II** in the NMR spectrum of a mixture of a half equiv. $[Ph_3C][B(C_6F_5)_4]$ (**A**) per Y atom in $[Cp^*YMe_2]_3$ (**1^Y**) at a chemical shift of 1.66 ppm. The function shown in blue represents the ideal raw data curve for the diffusion coefficient found by fitting the Stejskal-Tanner plot (Chart S7b), the red curve is the best possible fit for the raw data.

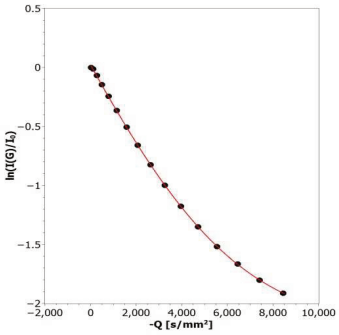

Chart S7b. Stejskal-Tanner plot of the magnetization decay data for the Cp* signal **II** in the NMR spectrum of a mixture of a half equiv. $[Ph_3C][B(C_6F_5)_4]$ (**A**) per Y atom in $[Cp^*YMe_2]_3$ (**1^Y**) at a chemical shift of 1.66 ppm. The solid red lines indicate two linear fits, as two overlaying signals were detected. These fits result in diffusion coefficients of:
$D_1 = 4.47 \cdot 10^{-10} \pm 4.7 \cdot 10^{-11}\ m^2s^{-1}$ and $D_2 = 6.55 \cdot 10^{-11} \pm 3.9 \cdot 10^{-11}\ m^2s^{-1}$
(For a definition of Q, please see eq. 10).

SUPPORTING INFORMATION

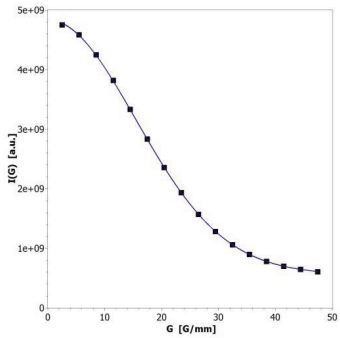

Chart S8a. Plot of the magnetization decay raw data of the Cp* species **III** in the NMR spectrum of a mixture of a half equiv. $[Ph_3C][B(C_6F_5)_4]$ (**A**) per Y atom in $[Cp^*YMe_2]_3$ (**1^Y**) at a chemical shift of 1.46 ppm. The function shown in blue represents the ideal raw data curve for the diffusion coefficient found by fitting the Stejskal-Tanner plot (Chart S8b), the red curve is the best possible fit for the raw data.

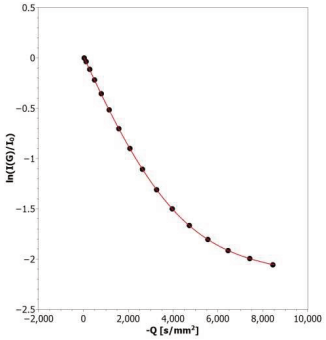

Chart S8b. Stejskal-Tanner plot of the magnetization decay data for the Cp* signal **III** in the NMR spectrum of a mixture of a half equiv. $[Ph_3C][B(C_6F_5)_4]$ (**A**) per Y atom in $[Cp^*YMe_2]_3$ (**1^Y**) at a chemical shift of 1.46 ppm. The solid red lines indicate two linear fits, as two overlaying signals were detected. These fits result in diffusion coefficients of:
$D_1 = 6.67 \cdot 10^{-10} \pm 4.1 \cdot 10^{-11}$ m^{2}s^{-1} and $D_2 = 8.08 \cdot 10^{-11} \pm 1.7 \cdot 10^{-11}$ m^{2}s^{-1}
(For a definition of Q, please see eq. 10).

4.2.2.4 Two thirds of equivalents of cocatalyst A per Y atom in $[Cp^*YMe_2]_3$ (1):

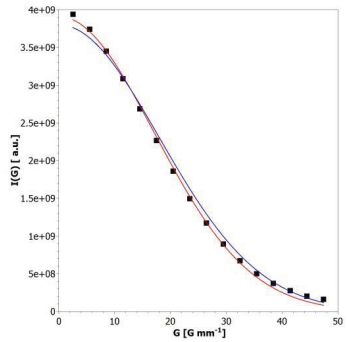

Chart S9a. Plot of the magnetization decay raw data of the Cp* species **I** in the NMR spectrum of a mixture of two third equiv. $[Ph_3C][B(C_6F_5)_4]$ (**A**) per Y atom in $[Cp^*YMe_2]_3$ (**1^Y**) at a chemical shift of 1.75 ppm. The function shown in blue represents the ideal raw data curve for the diffusion coefficient found by fitting the Stejskal-Tanner plot (Chart S9b), the red curve is the best possible fit for the raw data.

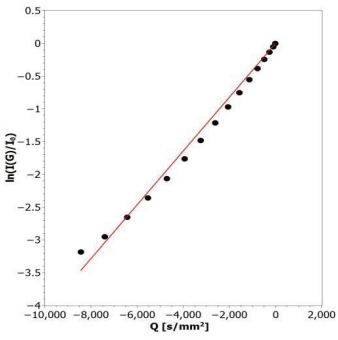

Chart S9b. Stejskal-Tanner plot of the magnetization decay data for the Cp* signal **I** in the NMR spectrum of a mixture of two third equiv. $[Ph_3C][B(C_6F_5)_4]$ (**A**) per Y atom in $[Cp^*YMe_2]_3$ (**1^Y**) at a chemical shift of 1.75 ppm.
The solid red line indicates a linear fit, resulting in a diffusion coefficient (slope of the fit) of $D = 4.11 \cdot 10^{-10} \pm 7.5 \cdot 10^{-12}$ m^{2}s^{-1}
(For a definition of Q, please see eq. 10).

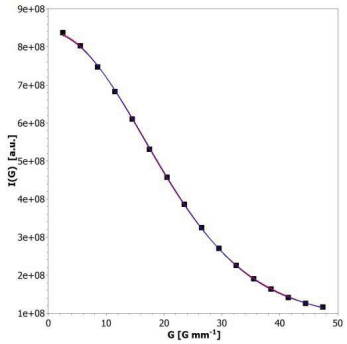

Chart S10a. Plot of the magnetization decay raw data of the Cp* species **IIa** in the NMR spectrum of a mixture of two third equiv. $[Ph_3C][B(C_6F_5)_4]$ (**A**) per Y atom in $[Cp^*YMe_2]_3$ (**1^Y**) at a chemical shift of 1.63 ppm. The function shown in blue represents the ideal raw data curve for the diffusion coefficient found by fitting the Stejskal-Tanner plot (Chart S10b), the red curve is the best possible fit for the raw data.

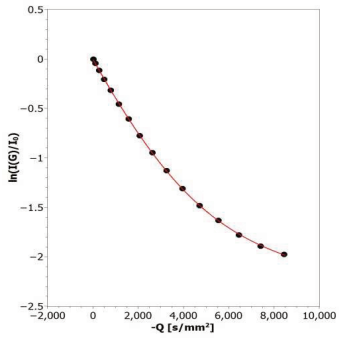

Chart S10b. Stejskal-Tanner plot of the magnetization decay data for the Cp* signal **IIa** in the NMR spectrum of a mixture of two third equiv. $[Ph_3C][B(C_6F_5)_4]$ (**A**) per Y atom in $[Cp^*YMe_2]_3$ (**1^Y**) at a chemical shift of 1.63 ppm. The solid red lines indicate two linear fits, as two overlaying signals were detected. These fits result in diffusion coefficients of:
$D_1 = 4.85 \cdot 10^{-10} \pm 9.9 \cdot 10^{-12}\ m^2s^{-1}$ and $D_2 = 3.81 \cdot 10^{-10} \pm 8.1 \cdot 10^{-12}\ m^2s^{-1}$
(For a definition of Q, please see eq. 10)

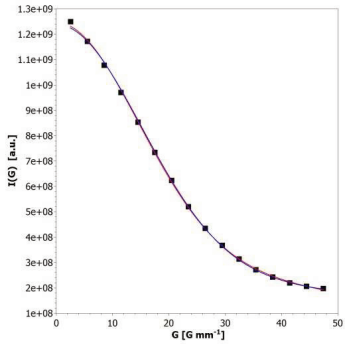

Chart S11a. Plot of the magnetization decay raw data of the Cp* species **IV** in the NMR spectrum of a mixture of two third equiv. $[Ph_3C][B(C_6F_5)_4]$ (**A**) per Y atom in $[Cp^*YMe_2]_3$ (**1^Y**) at a chemical shift of 1.55 ppm. The function shown in blue represents the ideal raw data curve for the diffusion coefficient found by fitting the Stejskal-Tanner plot (Chart 11b), the red curve is the best possible fit for the raw data.

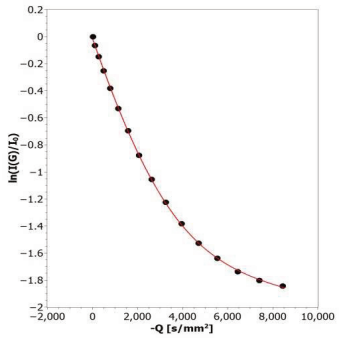

Chart S11b. Stejskal-Tanner plot of the magnetization decay data for the Cp* signal **IV** in the NMR spectrum of a mixture of two third equiv. $[Ph_3C][B(C_6F_5)_4]$ (**A**) per Y atom in $[Cp^*YMe_2]_3$ (**1^Y**) at a chemical shift of 1.55 ppm.
The solid red lines indicate two linear fits, as two overlaying signals were detected. These fits result in diffusion of:
$D_1 = 5.89 \cdot 10^{-10} \pm 1.4 \cdot 10^{-11}\ m^2s^{-1}$ and $D_2 = 2.78 \cdot 10^{-10} \pm 7.4 \cdot 10^{-12}\ m^2s^{-1}$
(For a definition of Q, please see eq. 10).

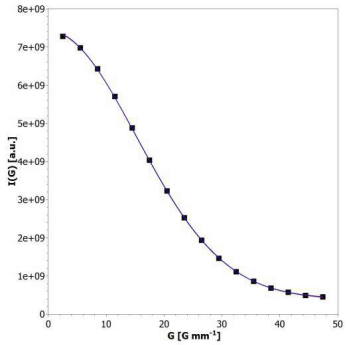

Chart S12a. Plot of the magnetization decay raw data of the Cp* species **III** in the NMR spectrum of a mixture of two third equiv. $[Ph_3C][B(C_6F_5)_4]$ (**A**) per Y atom in $[Cp^*YMe_2]_3$ (**1^Y**) at a chemical shift of 1.45 ppm. The function shown in blue represents the ideal raw data curve for the diffusion coefficient found by fitting the Stejskal-Tanner plot (Chart 12b), the red curve is the best possible fit for the raw data.

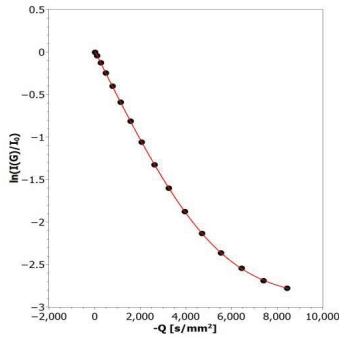

Chart S12b. Stejskal-Tanner plot of the magnetization decay data for the Cp* signal **III** in the NMR spectrum of a mixture of two third equiv. $[Ph_3C][B(C_6F_5)_4]$ (**A**) per Y atom in $[Cp^*YMe_2]_3$ (**1^Y**) at 1.45 ppm. The solid red lines indicate two linear fits, as two overlaying signals were detected. These fits result in diffusion coefficients of:
$D_1 = 5.79 \cdot 10^{-10} \pm 3.0 \cdot 10^{-12}\ m^2s^{-1}$ and $D_2 = 2.25 \cdot 10^{-12} \pm 4.6 \cdot 10^{-12}\ m^2s^{-1}$
(For a definition of Q, please see eq. 10).

SUPPORTING INFORMATION

4.2.2.5 One equivalent of cocatalyst A per Y atom in $[Cp^*YMe_2]_3$ (1):

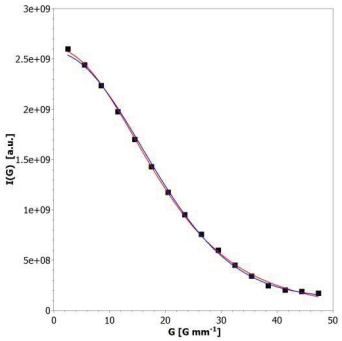

Chart S13a. Plot of the magnetization decay raw data of the Cp* species **I** in the NMR spectrum of a mixture of one equiv. $[Ph_3C][B(C_6F_5)_4]$ (**A**) per Y atom in $[Cp^*YMe_2]_3$ (**1^Y**) at a chemical shift of 1.75 ppm. The function shown in blue represents the ideal raw data curve for the diffusion coefficient found by fitting the Stejskal-Tanner plot (Chart S13b), the red curve is the best possible fit for the raw data.

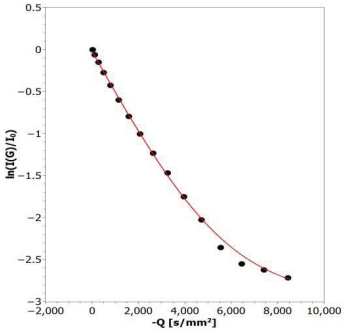

Chart S13b. Stejskal-Tanner plot of the magnetization decay data for the Cp* signal **I** in the NMR spectrum of a mixture of onr equiv. $[Ph_3C][B(C_6F_5)_4]$ (**A**) per Y atom in $[Cp^*YMe_2]_3$ (**1^Y**) at a chemical shift of 1.75 ppm.
The solid red lines indicate two linear fits, as two overlaying signals were detected. These fits result in diffusion coefficients of:
$D_1 = 5.29 \cdot 10^{-10} \pm 2.2 \cdot 10^{-11}$ m^2s^{-1} and $D_2 = 1.37 \cdot 10^{-11} \pm 4.1 \cdot 10^{-11}$ m^2s^{-1}
(For a definition of Q, please see eq. 10)

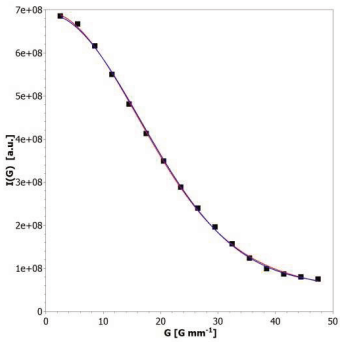

Chart S14a. Plot of the magnetization decay raw data of the Cp* species **IIa** in the NMR spectrum of a mixture of one equiv. $[Ph_3C][B(C_6F_5)_4]$ (**A**) per Y atom in $[Cp^*YMe_2]_3$ (**1^Y**) at a chemical shift of 1.62 ppm. The function shown in blue represents the ideal raw data curve for the diffusion coefficient found by fitting the Stejskal-Tanner plot (Chart S14b), the red curve is the best possible fit for the raw data.

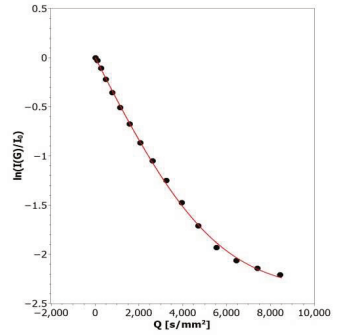

Chart S14b. Stejskal-Tanner plot of the magnetization decay data for the Cp* signal **IIa** in the NMR spectrum of a mixture of one equiv. $[Ph_3C][B(C_6F_5)_4]$ (**A**) per Y atom in $[Cp^*YMe_2]_3$ (**1^Y**) at a chemical shift of 1.62 ppm. The solid red lines indicate two linear fits, as two overlaying signals were detected. These fits result in diffusion coefficients of:
$D_1 = 4.92 \cdot 10^{-10} \pm 2.8 \cdot 10^{-11}$ m^2s^{-1} and $D_2 = 1.26 \cdot 10^{-12} \pm 3.7 \cdot 10^{-11}$ m^2s^{-1}
(For a definition of Q, please see eq. 10)

SUPPORTING INFORMATION

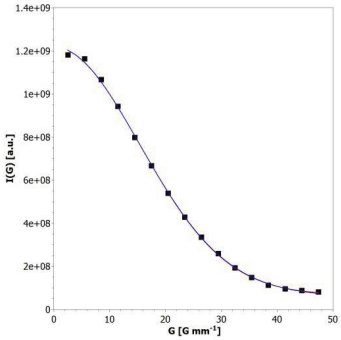

Chart S15a. Plot of the magnetization decay raw data of the Cp* species **IV** in the NMR spectrum of a mixture of one equiv. $[Ph_3C][B(C_6F_5)_4]$ (**A**) per Y atom in $[Cp^*YMe_2]_3$ (**1^Y**) at a chemical shift of 1.55 ppm. The function shown in blue represents the ideal raw data curve for the diffusion coefficient found by fitting the Stejskal-Tanner plot (Chart S15b), the red curve is the best possible fit for the raw data.

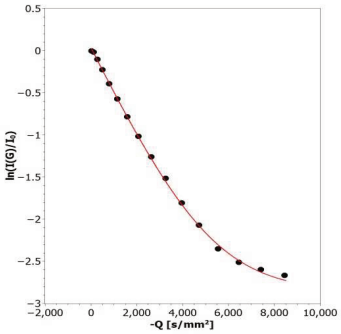

Chart S15b. Stejskal-Tanner plot of the magnetization decay data for the Cp* signal **IV** in the NMR spectrum of a mixture of one equiv. $[Ph_3C][B(C_6F_5)_4]$ (**A**) per Y atom in $[Cp^*YMe_2]_3$ (**1^Y**) at a chemical shift of 1.55 ppm.
The solid red lines indicate two linear fits, as two overlaying signals were detected. These fits result in diffusion coefficients of:
$D_1 = 5.69 \cdot 10^{-10} \pm 2.6 \cdot 10^{-10}$ m^2s^{-1} and $D_2 = 1.21 \cdot 10^{-13} \pm 3.9 \cdot 10^{-10}$ m^2s^{-1}
(For a definition of Q, please see eq. 10).

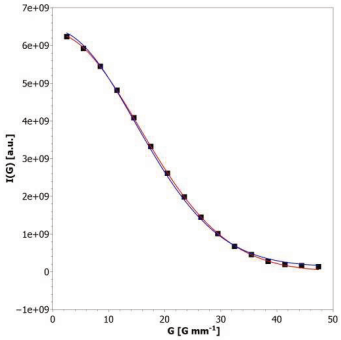

Chart S16a. Plot of the magnetization decay raw data of the Cp* species **III** in the NMR spectrum of a mixture of one equiv. $[Ph_3C][B(C_6F_5)_4]$ (**A**) per Y atom in $[Cp^*YMe_2]_3$ (**1^Y**) at a chemical shift of 1.45 ppm. The function shown in blue represents the ideal raw data curve for the diffusion coefficient found by fitting the Stejskal-Tanner plot (Chart S16b), the red curve is the best possible fit for the raw data.

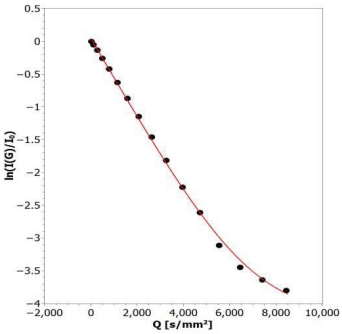

Chart S16b. Stejskal-Tanner plot of the magnetization decay data for the Cp* signal **III** in the NMR spectrum of a mixture of one equiv. $[Ph_3C][B(C_6F_5)_4]$ (**A**) per Y atom in $[Cp^*YMe_2]_3$ (**1^Y**) at 1.45 ppm. The solid red lines indicate two linear fits, as two overlaying signals were detected. These fits result in diffusion coefficients of:
$D_1 = 6.13 \cdot 10^{-10} \pm 7.9 \cdot 10^{-12}$ m^2s^{-1} and $D_2 = 7.28 \cdot 10^{-12} \pm 3.3 \cdot 10^{-10}$ m^2s^{-1}
(For a definition of Q, please see eq. 10).

4.2.2.6 One equivalent of cocatalyst A per Y atom in $[Cp^*YMe_2]_3$ (1), supernatant[6]:

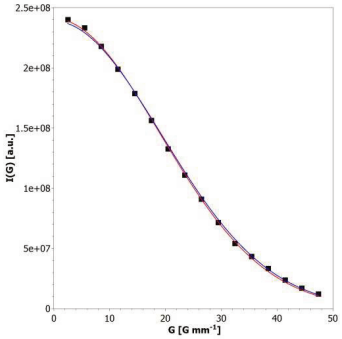

Chart S17a. Plot of the magnetization decay raw data of the Cp* species **IV** in the NMR spectrum of the decantate of a mixture of one equiv. $[Ph_3C][B(C_6F_5)_4]$ (**A**) per Y atom in $[Cp^*YMe_2]_3$ (**1^Y**) at a chemical shift of 1.54 ppm. The blue function represents the ideal raw data curve for the diffusion coefficient found by fitting the Stejskal-Tanner plot (Chart S17b), the red curve is the best possible fit for the raw data.

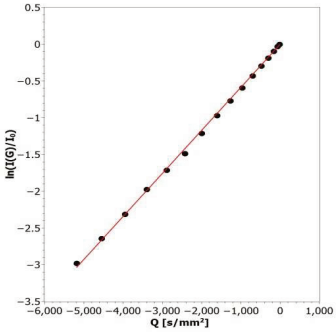

Chart S17b. Stejskal-Tanner plot of the magnetization decay data for the Cp* signal **IV** in the NMR spectrum of the supernatant of a mixture of one equiv. $[Ph_3C][B(C_6F_5)_4]$ (**A**) per Y atom in $[Cp^*YMe_2]_3$ (**1^Y**) at a chemical shift of 1.54 ppm.
The solid red line indicates a linear fit, resulting in a diffusion coefficient (slope of the fit) of $D = 5.86 \cdot 10^{-10} \pm 3.1 \cdot 10^{-12}$ m^2s^{-1} (For a definition of Q, please see eq. 10).

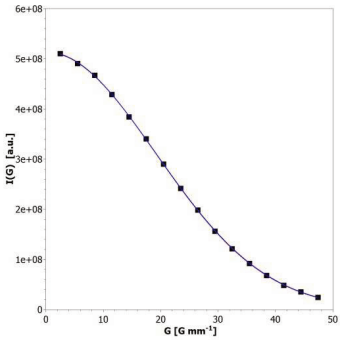

Chart S18a. Plot of the magnetization decay raw data of the Cp* species **III** in the NMR spectrum of the decantate of a mixture of one equiv. $[Ph_3C][B(C_6F_5)_4]$ (**A**) per Y atom in $[Cp^*YMe_2]_3$ (**1^Y**) at a chemical shift of 1.45 ppm. The blue function represents the ideal raw data curve for the diffusion coefficient found by fitting the Stejskal-Tanner plot (Chart S18b), the red curve is the best possible fit for the raw data.

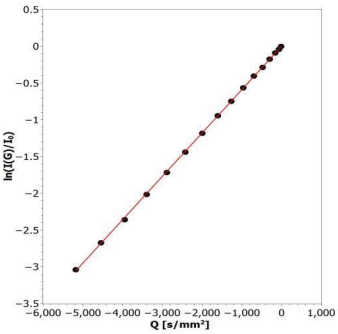

Chart S18b. Stejskal-Tanner plot of the magnetization decay data for the Cp* signal **III** in the NMR spectrum of the decantate of a mixture of one equiv. $[Ph_3C][B(C_6F_5)_4]$ (**A**) per Y atom in $[Cp^*YMe_2]_3$ (**1^Y**) at a chemical shift of 1.45 ppm. The solid red line indicates a linear fit, resulting in a diffusion coefficient (slope of the fit) of $D = 5.90 \cdot 10^{-10} \pm 1.0 \cdot 10^{-12}$ m^2s^{-1} (For a definition of Q, please see eq. 10).

[6] Main parts of the formed insoluble liquid were removed by decantation.

4.2.2.7 One third equivalent of cocatalyst B per Y atom in $[Cp^*YMe_2]_3$ (1)[7]:

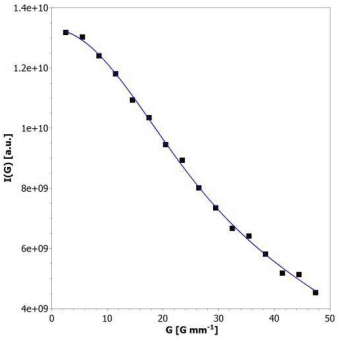

Chart S19a. Plot of the magnetization decay raw data of the Cp* species **1** (reactant) in the NMR spectrum of a mixture of one third equiv. $[PhNMe_2H][B(C_6F_5)_4]$ (**B**) per Y atom in $[Cp^*YMe_2]_3$ (**1^Y**) at a chemical shift of 1.96 ppm. The function shown in blue represents the ideal raw data curve for the diffusion coefficient found by fitting the Stejskal-Tanner plot (Chart S19b), the red curve is the best possible fit for the raw data.

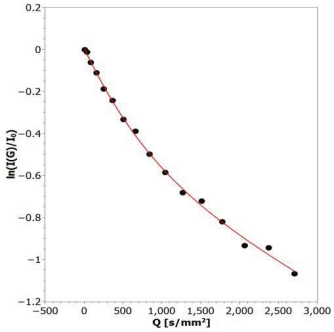

Chart S19b. Stejskal-Tanner plot of the magnetization decay data for the Cp* signal **1** (reactant) in the NMR spectrum of a mixture of one third equiv. $[PhNMe_2H][B(C_6F_5)_4]$ (**B**) per Y atom in $[Cp^*YMe_2]_3$ (**1^Y**) at a chemical shift of 1.96 ppm. The solid red lines indicate two linear fits, as two overlaying signals were detected. These fits result in diffusion coefficients of:
$D_1 = 2.11 \cdot 10^{-10} \pm 4.5 \cdot 10^{-11}$ m^2s^{-1} and $D_2 = 1.64 \cdot 10^{-9} \pm 3.4 \cdot 10^{-10}$ m^2s^{-1}
(For a definition of Q, please see eq. 10)

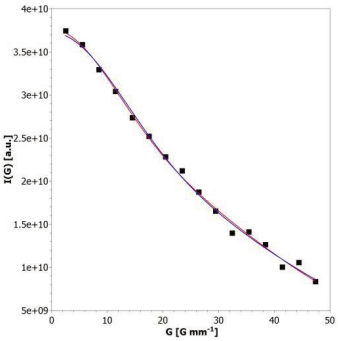

Chart S20a. Plot of the magnetization decay raw data of the Cp* species **Ia** in the NMR spectrum of a mixture of one third equiv. $[PhNMe_2H][B(C_6F_5)_4]$ (**B**) per Y atom in $[Cp^*YMe_2]_3$ (**1^Y**) at a chemical shift of 1.74 ppm. The function shown in blue represents the ideal raw data curve for the diffusion coefficient found by fitting the Stejskal-Tanner plot (Chart S20b), the red curve is the best possible fit for the raw data.

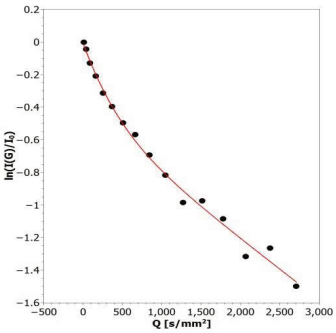

Chart S20b. Stejskal-Tanner plot of the magnetization decay data for the Cp* signal **Ia** in the NMR spectrum of a mixture of one third equiv. $[PhNMe_2H][B(C_6F_5)_4]$ (**B**) per Y atom in $[Cp^*YMe_2]_3$ (**1^Y**) at a chemical shift of 1.74 ppm.
The solid red lines indicate two linear fits, as two overlaying signals were detected. These fits result in diffusion coefficients of:
$D_1 = 3.74 \cdot 10^{-10} \pm 4.8 \cdot 10^{-11}$ m^2s^{-1} and $D_2 = 2.90 \cdot 10^{-9} \pm 9.0 \cdot 10^{-10}$ m^2s^{-1}
(For a definition of Q, please see eq. 10).

[7] At least two more Cp* signals of additional species were visible in the spectrum, with a very low signal to noise ratio.

SUPPORTING INFORMATION

4.2.2.8 One equivalent of cocatalyst B per Y atom in[Cp*YMe$_2$]$_3$ (1), directly after cocatalyst addition:

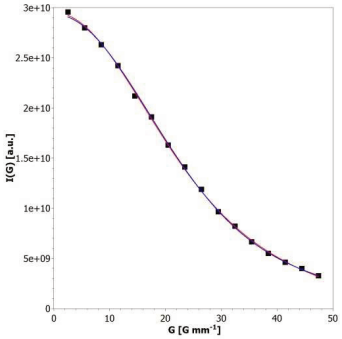

Chart S21a. Plot of the magnetization decay raw data of the Cp* species **I** in the NMR spectrum of a mixture of one equiv. [PhNMe$_2$H][B(C$_6$F$_5$)$_4$] (**B**) per Y atom in [Cp*YMe$_2$]$_3$ (**1^Y**) at a chemical shift of 1.76 ppm. The function shown in blue represents the ideal raw data curve for the diffusion coefficient found by fitting the Stejskal-Tanner plot (Chart S21b), the red curve is the best possible fit for the raw data.

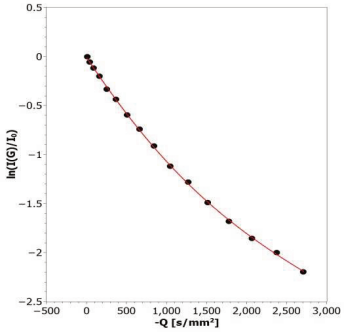

Chart S21b. Stejskal-Tanner plot of the magnetization decay data for the Cp* signal **I** in the NMR spectrum of a mixture of one equiv. [PhNMe$_2$H][B(C$_6$F$_5$)$_4$] (**B**) per Y atom in [Cp*YMe$_2$]$_3$ (**1^Y**) at a chemical shift of 1.76 ppm. The solid red lines indicate two linear fits, as two overlaying signals were detected. These fits result in diffusion coefficients of:
$D_1 = 3.87 \cdot 10^{-10} \pm 6.4 \cdot 10^{-11}$ m^{2}s^{-1} and $D_2 = 1.57 \cdot 10^{-9} \pm 1.1 \cdot 10^{-10}$ m^{2}s^{-1}
(For a definition of Q, please see eq. 10)

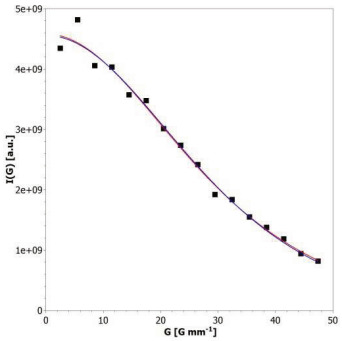

Chart S22a. Plot of the magnetization decay raw data of the Cp* species **IIa** in the NMR spectrum of a mixture of one equiv. [PhNMe$_2$H][B(C$_6$F$_5$)$_4$] (**B**) per Y atom in [Cp*YMe$_2$]$_3$ (**1^Y**) at a chemical shift of 1.63 ppm. The function shown in blue represents the ideal raw data curve for the diffusion coefficient found by fitting the Stejskal-Tanner plot (Chart S22b), the red curve is the best possible fit for the raw data.

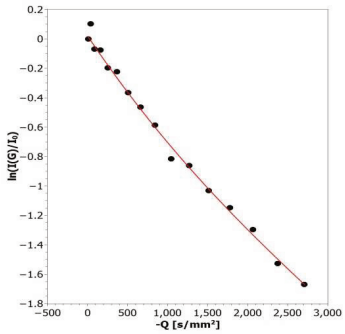

Chart S22b. Stejskal-Tanner plot of the magnetization decay data for the Cp* signal **IIa** in the NMR spectrum of a mixture of one equiv. [PhNMe$_2$H][B(C$_6$F$_5$)$_4$] (**B**) per Y atom in [Cp*YMe$_2$]$_3$ (**1^Y**) at a chemical shift of 1.63 ppm.
The solid red lines indicate two linear fits, as two overlaying signals were detected. These fits result in diffusion coefficients of:
$D_1 = 5.05 \cdot 10^{-10} \pm 1.2 \cdot 10^{-10}$ m^{2}s^{-1} and $D_2 = 1.83 \cdot 10^{-9} \pm 1.1 \cdot 10^{-9}$ m^{2}s^{-1}
(For a definition of Q, please see eq. 10).

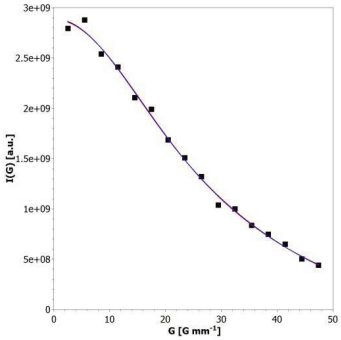

Chart S23a. Plot of the magnetization decay raw data of the Cp* species **IIIa** in the NMR spectrum of a mixture of one equiv. $[PhNMe_2H][B(C_6F_5)_4]$ (**B**) per Y atom in $[Cp^*YMe_2]_3$ ($\mathbf{1^Y}$) at a chemical shift of 1.47 ppm. The function shown in blue represents the ideal raw data curve for the diffusion coefficient found by fitting the Stejskal-Tanner plot (Chart S23b), the red curve is the best possible fit for the raw data.

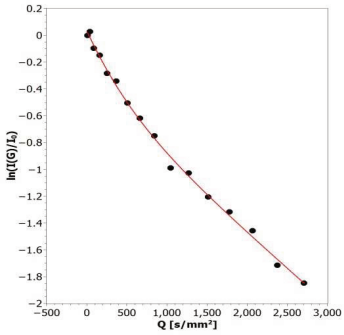

Chart S23b. Stejskal-Tanner plot of the magnetization decay data for the Cp* signal **IIIa** in the NMR spectrum of a mixture of one equiv. $[PhNMe_2H][B(C_6F_5)_4]$ (**B**) per Y atom in $[Cp^*YMe_2]_3$ ($\mathbf{1^Y}$) at a chemical shift of 1.47 ppm.
The solid red lines indicate two linear fits, as two overlaying signals were detected. These fits result in diffusion coefficients (slope of the fit) of:
$D_1 = 5.27 \cdot 10^{-10} \pm 5.3 \cdot 10^{-11}$ m^2s^{-1} and $D_2 = 2.53 \cdot 10^{-9} \pm 7.0 \cdot 10^{-11}$ m^2s^{-1}
(For a definition of Q, please see eq. 10).

4.2.2.9 Three equivalents of cocatalyst B per $[Cp^*YMe_2]_3$ (1) trimer, 6 h after cocatalyst addition:

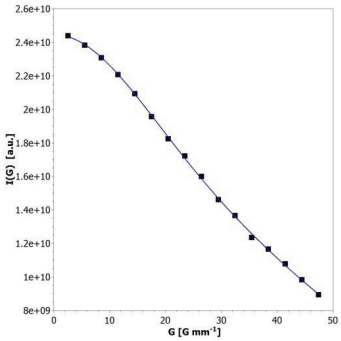

Chart S24a. Plot of the magnetization decay raw data of the Cp* species **Ia** in the NMR spectrum of a mixture of one equiv. $[PhNMe_2H][B(C_6F_5)_4]$ (**B**) per Y atom in $[Cp^*YMe_2]_3$ ($\mathbf{1^Y}$), 6 h after cocatalyst addition, at a chemical shift of 1.74 ppm. The function shown in blue represents the ideal raw data curve for the diffusion coefficient found by fitting the Stejskal-Tanner plot (Chart S24b), the red curve is the best possible fit for the raw data.

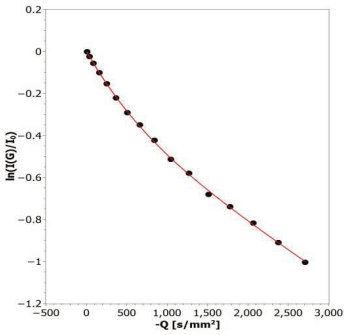

Chart S24b. Stejskal-Tanner plot of the magnetization decay data for the Cp* signal **Ia** in the NMR spectrum of a mixture of one equiv. $[PhNMe_2H][B(C_6F_5)_4]$ (**B**) per Y atom in $[Cp^*YMe_2]_3$ ($\mathbf{1^Y}$), 6 h after cocatalyst addition, at at a chemical shift of 1.74 ppm. The solid red lines indicate two linear fits, as two overlaying signals were detected. These fits result in diffusion coefficients (slope of the fit) of:
$D_1 = 2.60 \cdot 10^{-10} \pm 1.4 \cdot 10^{-11}$ m^2s^{-1} and $D_2 = 1.85 \cdot 10^{-9} \pm 2.2 \cdot 10^{-10}$ m^2s^{-1}
(For a definition of Q, please see eq. 10)

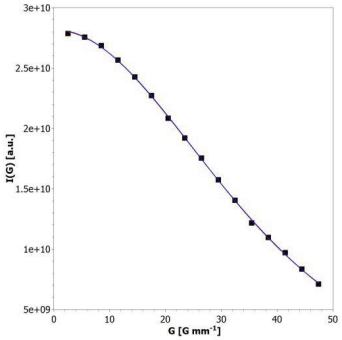

Chart S25a. Plot of the magnetization decay raw data of the Cp* species **III** in the NMR spectrum of a mixture of one equiv. $[PhNMe_2H][B(C_6F_5)_4]$ (**B**) per Y atom in $[Cp^*YMe_2]_3$ (**1Y**), 6 h after cocatalyst addition, at a chemical shift of 1.46 ppm. The function shown in blue represents the ideal raw data curve for the diffusion coefficient found by fitting the Stejskal-Tanner plot (Chart S25b), the red curve is the best possible fit for the raw data.

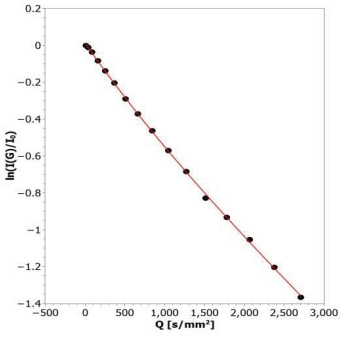

Chart S25b. Stejskal-Tanner plot of the magnetization decay data for the Cp* signal **III** in the NMR spectrum of a mixture of one equiv. $[PhNMe_2H][B(C_6F_5)_4]$ (**B**) per Y atom in $[Cp^*YMe_2]_3$ (**1Y**), 6 h after cocatalyst addition, at a chemical shift of 1.46 ppm.The solid red lines indicate two linear fits, as two overlaying signals were detected. These fits result in diffusion coefficients (slope of the fit) of:
$D_1 = 3.78 \cdot 10^{-10} \pm 1.4 \cdot 10^{-11}\ m^2s^{-1}$ and $D_2 = 9.97 \cdot 10^{-10} \pm 4. \cdot 10^{-11}\ m^2s^{-1}$
(For a definition of Q, please see eq. 10).

4.2.2.10 $[(Cp^*Y)_3Me_4(CH_2)(thf)_2]$(3) without activation:

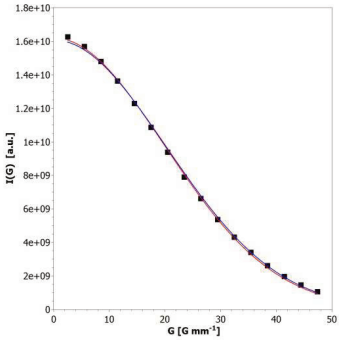

Chart S26a. Plot of the magnetization decay raw data of the Cp* species in the NMR spectrum of $[(Cp^*Y)_3Me_4(CH_2)(thf)_2]$(**3**) at a chemical shift of 1.39 ppm. The function shown in blue represents the ideal raw data curve for the diffusion coefficient found by fitting the Stejskal-Tanner plot (Chart S26b), the red curve is the best possible fit for the raw data.

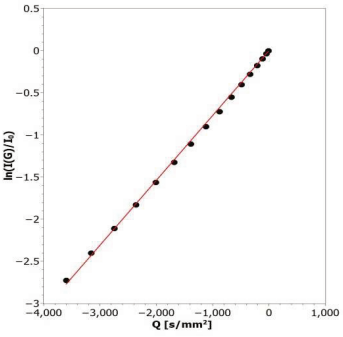

Chart S26b. Stejskal-Tanner plot of the magnetization decay data for the Cp* signal in the NMR spectrum of $[(Cp^*Y)_3Me_4(CH_2)(thf)_2]$(**3**) at a chemical shift of 1.39 ppm. The solid red line indicates a linear fit, resulting in a diffusion coefficient (slope of the fit) of
$D = 7.70 \cdot 10^{-10} \pm 4.1 \cdot 10^{-12}\ m^2s^{-1}$ (For a definition of Q, please see eq. 10).

4.2.2.11 One equivalent of cocatalyst A per Y atom in $[(Cp^*Y)_3Me_4(CH_2)(thf)_2]$(3):

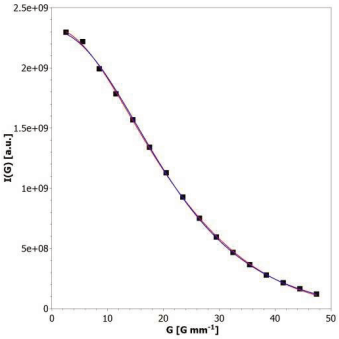

Chart S27a. Plot of the magnetization decay raw data of the Cp* species **V** in the NMR spectrum of a mixture of one equiv. $[Ph_3C][B(C_6F_5)_4]$ (**A**) per Y atom in $[(Cp^*Y)_3Me_4(CH_2)(thf)_2]$(**3**) at a chemical shift of 1.89 ppm. The function shown in blue represents the ideal raw data curve for the diffusion coefficient found by fitting the Stejskal-Tanner plot (Chart S28b), the red curve is the best possible fit for the raw data.

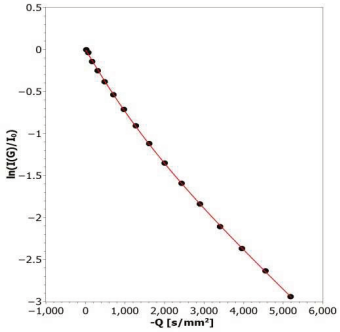

Chart S27b. Stejskal-Tanner plot of the magnetization decay data for the Cp* signal **V** in the NMR spectrum of a mixture of one equiv. $[Ph_3C][B(C_6F_5)_4]$ (**A**) per Y atom in $[(Cp^*Y)_3Me_4(CH_2)(thf)_2]$(**3**) at a chemical shift of 1.89 ppm. The solid red lines indicate two linear fits, as two overlaying signals were detected. These fits result in diffusion coefficients (slope of the fit) of:
$D_1 = 1.24 \cdot 10^{-9} \pm 8.0 \cdot 10^{-11}$ m^2s^{-1} and $D_2 = 4.51 \cdot 10^{-10} \pm 1.3 \cdot 10^{-11}$ m^2s^{-1}
(For a definition of Q, please see eq. 10).

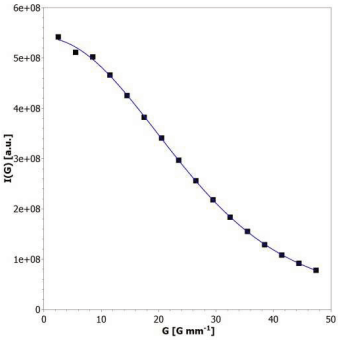

Chart S28a. Plot of the magnetization decay raw data of the Cp* species **IV** in the NMR spectrum a mixture of one equiv. $[Ph_3C][B(C_6F_5)_4]$ (**A**) per Y atom in $[(Cp^*Y)_3Me_4(CH_2)(thf)_2]$(**3**) at a chemical shift of 1.55 ppm. The function shown in blue represents the ideal raw data curve for the diffusion coefficient found by fitting the Stejskal-Tanner plot (Chart S28b), the red curve is the best possible fit for the raw data.

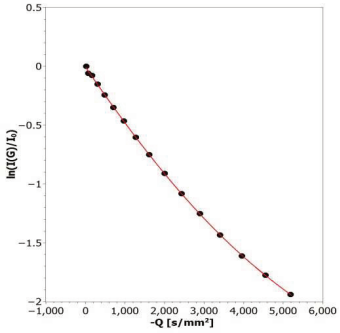

Chart S28b. Stejskal-Tanner plot of the magnetization decay data for the Cp* signal **IV** in the NMR spectrum of a mixture of one equiv. $[Ph_3C][B(C_6F_5)_4]$ (**A**) Y atom in per $[(Cp^*Y)_3Me_4(CH_2)(thf)_2]$(**3**) at a chemical shift of 1.55 ppm. The solid red lines indicate two linear fits, as two overlaying signals were detected. These fits result in diffusion coefficients (slope of the fit) of:
$D_1 = 5.83 \cdot 10^{-10} \pm 3.4 \cdot 10^{-11}$ m^2s^{-1} and $D_2 = 1.15 \cdot 10^{-10} \pm 4.5 \cdot 10^{-11}$ m^2s^{-1}
(For a definition of Q, please see eq. 10).

4.2.3 Determination of the Molecular Masses

As the solvent cannot be treated as continuum due to the relative size of toluene-d_8 to the investigated complexes and the complexes themselves cannot be estimated to be anisotropic some adjustments to the Stokes-Einstein Equation[28] (Eq. 11) have to be made to minimize the errors.[29]

$$D = \frac{k_B T}{6\pi\eta_S r_H f} \tag{11}$$

where D is the diffusion coefficient, k_B is the Boltzmann constant, T is the temperature, η_S is the viscosity of the solvent (continuum fluent), f is the friction factor (f = 1 for hard spheres) and r_H is the hydrodynamic radius.
These adjustments were published by Morris et al.[29] and are shown in equation 12.

$$D = \frac{k_B T \left(\frac{3}{2}\sqrt[3]{\frac{M_S}{M}} + \left(1 + \sqrt[3]{\frac{M_S}{M}}\right)^{-1}\right)}{6\pi\eta_S \sqrt[3]{\frac{3M}{4\pi N_A \rho_{eff}}}} \tag{12}$$

Where M_S is the molecular weight of the solvent, M is the molecular weight of the dissolved molecule, N_A is the Avogadro constant and ρ_{eff} is the constant effective density of a single molecule.
The fact that Morris et al. only investigated molecules of smaller M than the complexes targeted in this study and only atoms smaller than chlorine were present in their study, could cause further errors. However, these are expected to be much smaller than by application of the non-amplified Stokes-Einstein Equation.
The respective results are shown in Table S15.

In case of cocatalyst **A**, the formation of a second liquid phase, possibly an ionic liquid, is a source of large margins. In the DOSY data this is represented by the presence of a second, large molecular weight species that can be interpreted as moving droplets of that toluene insoluble liquid. The DOSY measurements furthermore confirm the statement, that the species present after the addition of one equivalent of the cocatalyst is not much altered by the addition of another half equivalent of cocatalyst **A**.
In case of cocatalyst **B**, the formation of the coordination polymer **2** is visible in the ^{1}H DOSY NMR spectroscopic data. Besides species **I** with one full equivalent of cocatalyst **B** per Y atom in $\mathbf{1}^{\mathbf{Y}}$ after 6 h given in Table S15, but further peaks that do only possess contributions with M > 20 kg / mol can be found in the respective spectra (Figure S20).

4.2.4 Summary of the data obtained by DOSY-NMR spectroscopy

Table S15. Summary of the data obtained by evaluation of the Stejskal-Tanner plots

Precat.	Cocat.[a]	Equiv. Cocat.[a]	Species	Peak Pos. [ppm]	D_1 [m^2s^{-1}]	s_{D1}[d] [m^2s^{-1}]	D_2 [m^2s^{-1}]	s_{D2}[d] [m^2s^{-1}]	M_1 [g mol^{-1}]	s^-_{M1}[d] [g mol^{-1}]	s^+_{M1}[d] [g mol^{-1}]	M_2 [g mol^{-1}]	s^-_{M2}[d] [g mol^{-1}]	s^+_{M2}[d] [g mol^{-1}]
1^Y	none	0	**1**	1.97	7,61E-10	4,7E-12	---	---	558	7	7	---	---	---
1^Y	**A**	1/3	**I**	1.76	4,32E-10	2,2E-12	---	---	1978	24	24	---	---	---
1^Y	**A**	1/3	**II**	1.69	3,34E-10	4,1E-12	---	---	3661	108	113	---	---	---
1^Y	**A**	1/3	**III**	1.46	5,59E-10	2,4E-11	(2,0E-12)[e]	(5,0E-11)[e]	1093	99	115	(> 20E3[b])[e]	(> 20E3[b])[e]	(> 20E3[b])[e]
1^Y	**A**	1/2	**I**	1.76	3,92E-10	4,9E-12	---	---	2486	72	75	---	---	---
1^Y	**A**	1/2	**II**	1.66	4,47E-10	4,7E-11	6,55E-11	3,9E-11	1821	379	551	> 20E3[b]	> 20E3[b]	> 20E3[b]
1^Y	**A**	1/2	**III**	1.46	6,67E-10	4,1E-11	8,08E-11	1,7E-11	740	89	109	> 20E3[b]	> 20E3[b]	> 20E3[b]
1^Y	**A**	2/3	**I**	1.75	4,11E-10	7,5E-12	---	---	2228	93	100	---	---	---
1^Y	**A**	2/3	**IIa**	1.63	4,85E-10	9,9E-12	3,81E-11	8,1E-12	1513	68	73	> 20E3[b]	> 20E3[b]	> 20E3[b]
1^Y	**A**	2/3	**IV**	1.55	5,89E-10	1,4E-11	2,78E-11	7,4E-12	972	51	55	> 20E3[b]	> 20E3[b]	> 20E3[b]
1^Y	**A**	2/3	**III**	1.45	5,79E-10	3,0E-12	(2,26E-12)[e]	(4,5E-12)[e]	1013	11	12	(> 20E3[b])[e]	(> 20E3[b])[e]	(> 20E3[b])[e]
1^Y	**A**	1	**I**	1.75	5,29E-10	2,2E-11	(1,37E-11)[e]	(4,1E-11)[e]	1238	110	127	(> 20E3[b])[e]	(> 20E3[b])[e]	(> 20E3[b])[e]
1^Y	**A**	1	**IIa**	1.62	4,92E-10	2,8E-11	(1,26E-12)[e]	(3,7E-11)[e]	1461	173	210	(> 20E3[b])[e]	(> 20E3[b])[e]	(> 20E3[b])[e]
1^Y	**A**	1	**IV**	1.55	5,69E-10	2,6E-10	(1,21E-13)[e]	(3,9E-10)[e]	1051	581	3280	(> 20E3[b])[e]	(> 20E3[b])[e]	(> 20E3[b])[e]
1^Y	**A**	1	**III**	1.45	6,13E-10	7,9E-11	(7,28E-12)[e]	(3,3E-10)[e]	891	207	322	(> 20E3[b])[e]	(> 20E3[b])[e]	(> 20E3[b])[e]
1^Y	**A**	1D	**IV**	1.54	5,86E-10	3,1E-12	---	---	987	11	12	---	---	---
1^Y	**A**	1D	**III**	1.45	5,90E-10	1,0E-12	---	---	970	4	4	---	---	---
1^Y	**B**	1/3	**1**	1.96	2,11E-10	4,5E-11	1,64E-09	3,4E-10	11689	4576	10310	121	35	67
1^Y	**B**	1/3	**I**	1.74	3,74E-10	4,8E-11	2,91E-09	9,0E-10	2781	695	1104	43	16	40
1^Y	**B**	1	**I**	1.76	3,87E-10	6,4E-11	1,57E-09	1,1E-10	2560	778	1416	132	16	20
1^Y	**B**	1	**IIa**	1.63	5,05E-10	1,2E-10	1,83E-09	1,2E-09	1379	513	1166	99	57	607
1^Y	**B**	1	**IIIa**	1.47	5,27E-10	5,3E-11	2,53E-09	7,0E-11	1251	244	346	55	3	3
1^Y	**B**	1T	**Ia**	1.74	2,60E-10	1,4E-11	1,85E-08	2,2E-10	6877	878	1076	> 20E3[c]	> 20E3[c]	> 20E3[c]
1^Y	**B**	1T	**III**	1.46	3,76E-10	1,1E-10	9,97E-10	4,1E-10	2755	1236	3626	319	158	672
3	none	0	**3**	1.39	7,70E-10	4,2E-12	---	---	545	6	6	---	---	---
3	**A**	1	**V**	1.89	1,24E-09	8,0E-11	4,51E-10	1,3E-11	208	24	29	1791	113	124
3	**A**	1	**IV**	1.55	5,83E-10	3,4E-11	1,15E-10	4,5E-11	997	118	144	> 20E3[b]	> 20E3[b]	> 20E3[b]

[a] **A** = $[Ph_3C][B(C_6F_5)_4]$; **B** = $[PhNMe_2H][B(C_6F_5)_4]$, equivalents given in x per trimer = Y center = x/3 per Y atom, D indicates decantation, T indicates a prolonged prereaction time of 6 h. [b] Droplets of second phase.[c] Coordination polymer. [d]s-Values represent the errors of the respective fit. [e] Accuracy limited as the error of the fit exceeds D.

5. Possible Reaction Mechanism for the Formation of the Degradation Product 2

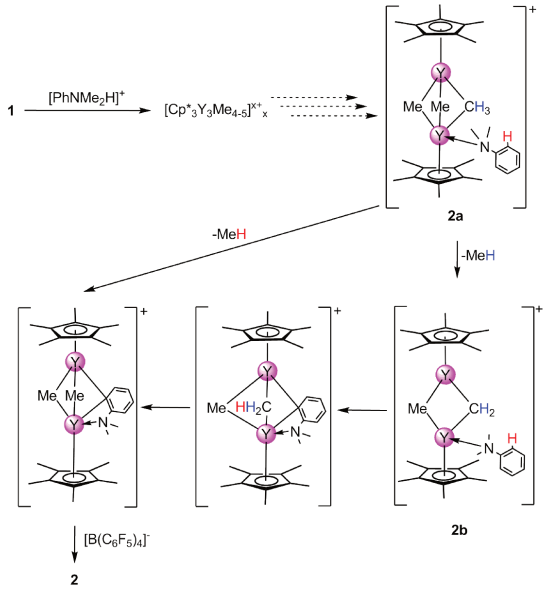

Scheme S1. Two possible mechanisms for the formation of $[(Cp^*Y)_2Me_2(N(Me)_2(C_6H_4)]_n[B(C_6F_5)_4]_n$ **(2)** from $[Cp^*YMe_2]_3$ ($\mathbf{1^Y}$) and **B** over time.

SUPPORTING INFORMATION

6. References

[1] W. J. Evans, R. Anwander, J. W. Ziller, *Organometallics* **1995**, *14*, 1107-1109.
[2] A. Fischbach, R. Anwander, *Adv Polym Sci* **2006**, *204*, 155-281.
[3] A. Fischbach, A.; M. G. Klimpel, M. Widenmeyer, E. Herdtweck, W. Scherer, R. Anwander, *Angew. Chem. Int. Ed.* **2004**, *43*, 2234-2239; *Angew. Chem.* **2004**, *116*, 2284-2289.
[4] C. O. Hollfelder, L. J. Jende, D. Diether, T. Zelger, R. Stauder, C. Maichle-Mössmer, R. Anwander, *Catalysts* **2018**, *8*, 61.
[5] M. Zimmermann, K. W. Törnroos, R. Anwander, *Angew. Chem. Int Ed.* **2008**, *47*, 775-778; *Angew. Chem.* **2008**, *120*, 787-790
[6] H. M. Dietrich, C. Zapilko, E. Herdtweck, R. Anwander, *Organometallics* **2005**, *24*, 5767-5771.
[7] H. M. Dietrich, H. Grove, K. W. Törnroos, R. Anwander, *J. Amer. Chem. Soc.* **2006**, *128*, 1458-1459.
[8] V. K. Srivastava, M. Maiti, R. V. Jasra, *Eur. Polym. J.* **2011**, *47*, 2342-2350.
[9] COSMO v. 1.61, Bruker AXS Inc., Madison, WI, **2012**.
[10] *APEX 2 v. 2012.10_0*, Bruker AXS Inc., Madison, WI, **2012**.
[11] SAINT v. 8.37A, Bruker AXS Inc., Madison, WI, **2015**.
[12] L. Krause, R. Herbst-Irmer, G. M. Sheldrick, D. Stalke, *J. Appl. Cryst.* **2015**, *48*, 3-10.
[13] G. M. Sheldrick, *Acta Cryst. A* **2015**, *71*, 3-8.
[14] C. B. Hübschle, G. M. Sheldrick, B. Dittrich, *J. Appl. Cryst.* **2011**, *44*, 1281-1284
[15] L. Farrugia, WinGX and ORTEP for Windows: an update. *J. Appl. Crystallogr.* **2012,** *45*, 849-854.
[16] M. Zimmermann, K. W. Törnroos, H. Sitzmann, R. Anwander, *Chem Eur. J.* **2008**, *14*, 7266-7277.
[17] A. Fernández-Barbero, A. Fernández-Nieves, I. Grillo, E. López-Cabarcos, *Phys. Rev. E* **2002**, *66*, 051803.
[18] J. J. Crassous, A. Wittemann, M. Siebenbürger, M. Schrinner, M. Drechsler, M. Ballauff, *Coll. Polym. Sci.* **2008**, *286*, 805-812.
[19] P. J. Flory, J. J. Rehner, *J. Chem. Phys.* **1943**, *11*, 521-526.
[20] J. M. G. Cowie, *Polymers: Chemistry and Physics of Modern Materials*; 2 ed.; Blackie Academic and Professional, an imprint of Chapman & Hall: London UK, 1991.
[21] P. J. Flory, W. R. Krigbaum, *J. Chem. Phys.* **1950**, *18*, 1086-1094.
[22] A. F. M. Barton, *Handbook of Polymer-Liquid interaction parameters and solubility parameters*; CRC Press LCC: Boca Raton/FL, London, New York, Washington D.C., 1990.
[23] A. D. Horton, *Organometallics* **1996**, *15*, 2675-2677.
[24] A. D. Horton, J. de With, A. J. van der Linden, H. van de Weg, *Organometallics* **1996**, *15*, 2672-2674.
[25] E. O. Stejskal, J. E. Tanner, *J. Chem. Phys.* **1965**, *42*, 288-292.
[26] W. S. Price, *Conc. Mag. Res.* **1997**, *9*, 299-336.
[27] W. S. Price, *Conc. Mag. Res.* **1998**, *10*, 197-237.
[28] A. Einstein, *Ann. Physik* **1905**, *322*, 549-560.
[39] R. Evans, Z. Deng, A. K. Rogerson, A. S. McLachlan, J. J. Richards, M. Nilsson,G. A. Morris, *Angew. Chem. Int Ed.* **2013**, *52*, 3199-3202.) *Angew. Chem.* **2013**, *125*, 3281-3284.

Appendix A

Curriculum Vitae

Curriculum Vitae

Personal Details

Name:	Hollfelder, Christoph Otto
Date of Birth:	June 29th, 1984
Place of Birth:	Forchheim (Oberfranken)
Nationality:	German

Education

Sept. 1990–July 1994	St. Anna Grundschule Forchheim
Sept. 1994–June 2003	Ehrenbürg Gymnasium Forchheim, Specialization on Chemistry and Physics Allgemeine Hochschulreife
Sept. 2003–June 2004	Civil Service at ASB Forchheim
Oct. 2004–Apr. 2010	Study of Chemistry (Diplom), University of Bayreuth
Sept. 2005–Oct. 2005	BASF AG, Ludwigshafen am Rhein, Germany, Internship position
Oct. 2006:	Vordiplom
Oct. 2006–Apr.2010	Main Studies of Chemistry (Diplom), University of Bayreuth Specialization: Macromolecular Chemistry
Aug. 2007–June 2008	Lunds University, Internship Position, Sweden ERASMUS Fellowship
Oct. 2009–Apr. 2010	Diploma Thesis: “New esterbased molecular glasses for photolithography” (Prof. Dr. H.-W. Schmidt)
Apr. 2010:	Diploma
Nov. 2010–May 2019	Promotion: “Polymerization Catalysis of Rare-Earth Metal Alkylaluminates and Dialkyls – A Systematic Study” (Prof. Dr. R. Anwander)